



THESE DE DOCTORAT EN CO-TUTELLE INTERNATIONALE DE

L'UNIVERSITE DE BRETAGNE OCCIDENTALE
COMUE UNIVERSITE BRETAGNE LOIRE
ECOLE DOCTORALE N° 598

Sciences de la Mer et du littoral

Spécialité : Chimie marine

AVEC L'UNIVERSITE DE TASMANIE

INSTITUT D'ETUDES MARINES ET ANTARCTIQUES

Spécialité : Sciences Marines et Antarctiques

Par

Manon TONNARD

Etude du Cycle Biogéochimique du Fer : Distribution et spéciation dans l'Océan Atlantique Nord (GA01) et l'Océan Austral (Glpr05) (GEOTRACES)

Thèse présentée et soutenue à l'Institut Universitaire Européen de la Mer, Technopôle Brest-Iroise, Rue Dumont d'Urville, 29280 Plouzané, le 6 Juillet 2018

Unité de recherche : Laboratoire des sciences de l'Environnement MARin - UMR 6539 (LEMAR)
et Centre de Recherche Coopérative sur le Climat et les Ecosystèmes Antarctiques

Rapporteurs avant soutenance :

Cécile GUIEU

Directrice de Recherche CNRS, Laboratoire d'Océanographie de Villefranche-sur-Mer (LOV), UMR 7093, CNRS, Université Pierre et Marie Curie, Observatoire Océanologique de Villefranche-sur-Mer

Christoph VÖLKER

Docteur, Alfred-Wegener-Institut Helmholtz-Zentrum für Polar-und Meeresforschung, Germany

Composition du Jury :

François LACAN

Directeur de Recherche CNRS, Laboratoire d'Etudes en Géophysique et Océanographie Spatiales (LEGOS), UMR 5566, CNRS/IRD/CNES/UPS, Université de Toulouse, Observatoire Midi-Pyrénées
Président du Jury

Cécile GUIEU

Directrice de Recherche CNRS, Laboratoire d'Océanographie de Villefranche-sur-Mer (LOV), UMR 7093, CNRS, Université Pierre et Marie Curie, Observatoire Océanologique de Villefranche-sur-Mer

Christoph VÖLKER

Docteur, Alfred-Wegener-Institut Helmholtz-Zentrum für Polar-und Meeresforschung, Germany

Julia UITZ

Docteur, Laboratoire d'Océanographie de Villefranche-sur-Mer (LOV), UMR 7093, CNRS, Université Pierre et Marie Curie, Observatoire Océanologique de Villefranche

Simon USSHER

Professeur agrégé de Chimie Marine et Analytique, School of Geography, Earth and Environmental Sciences, University of Plymouth, England

Géraldine SARTHOU

HDR, Directrice de Recherche CNRS, Laboratoire des Sciences de l'Environnement MARin (LEMAR), UMR 6539, CNRS/IUEM/IRD/Ifremer, Université de Bretagne Loire, Brest, Directrice de thèse

Andrew R. BOWIE

Professeur agrégé, Antarctic Climate & Ecosystems Cooperative Research Centre (ACE-CRC), Institute for Marine and Antarctic Studies (IMAS), University of Tasmania, Hobart AUS (TAS), Directeur de thèse

Hélène PLANQUETTE

Chargée de Recherche CNRS, Laboratoire des Sciences de l'Environnement MARin (LEMAR), UMR 6539, CNRS/IUEM/IRD/Ifremer, Université de Bretagne Loire, Brest
Co-directrice de thèse

Invité

Pier Van der MERWE

Docteur, Antarctic Climate & Ecosystems Cooperative Research Centre (ACE-CRC), University of Tasmania, Hobart AUS (TAS), Co-directeur de thèse



Statements and declarations

Declaration of Originality

This thesis contains no material which has been accepted for a degree or diploma by the University or any other institution, except by way of background information and duly acknowledged in the thesis, and to the best of my knowledge and belief no material previously published or written by another person except where due acknowledgement is made in the text of the thesis, nor does the thesis contain any material that infringes copyright.

Authority of Access

This thesis may be made available for loan and limited copying and communication in accordance with the Copyright Act 1968.

Statement regarding published work contained in the thesis

The publishers of the papers comprising Chapters 3 to 5 hold the copyright for that content, and access to the material should be sought from the respective journals. The remaining non published content of the thesis may be made available for loan and limited copying and communication in accordance with the Copyright Act 1968.

Statement of co-authorship

The following people and institutions contributed to the publication of work undertaken as part of this thesis:

Candidate	Manon Tonnard	ACE-CRC/IMAS - University of Tasmania LEMAR/IUEM, CNRS UMR 6539 - Université de Bretagne Loire
Author 1	Géraldine Sarthou, Supervisor	LEMAR/IUEM, CNRS UMR 6539 - Université de Bretagne Loire
Author 2	Andrew R. Bowie, Supervisor	ACE-CRC/IMAS - University of Tasmania
Author 3	Hélène Planquette, Co-Supervisor	LEMAR/IUEM, CNRS UMR 6539 - Université de Bretagne Loire
Author 4	Pier van der Merwe, Co-Supervisor	ACE-CRC - University of Tasmania
Author 5	Morgane Gallinari	LEMAR/IUEM, CNRS UMR 6539 - Université de Bretagne Loire
Author 6	Florianne Desprez de Gésincourt	LEMAR/IUEM, CNRS UMR 6539 - Université de Bretagne Loire
Author 7	Yoan Germain	Laboratoire Cycles Géochimiques et ressources, Ifremer
Author 8	Arthur Gourain	Ocean Sciences Department, School of Environmental Sciences - University of Liverpool
Author 9	Marion Benetti	Institute of Earth Sciences - University of Iceland LOCEAN, CNRS UMR 7159, IRD, MNHN - Sorbonne Universités
Author 10	Gilles Reverdin	LOCEAN, CNRS UMR 7159, IRD, MNHN - Sorbonne Universités
Author 11	Paul Tréguer	LEMAR/IUEM, CNRS UMR 6539 - Université de Bretagne Loire
Author 12	Julia Boutorh	LEMAR/IUEM, CNRS UMR 6539 - Université de Bretagne Loire
Author 13	Marie Cheize	LEMAR/IUEM, CNRS UMR 6539 - Université de Bretagne Loire Laboratoire des cycles Géochimiques –Centre Ifremer Bretagne
Author 14	Jan-Lukas Menzel Barraqueta	GEOMAR Helmholtz-Zentrum für Ozeanforschung
Author 15	Leonardo Pereira Contreira	Fundação Universidade Federal do Rio Grande (FURG)
Author 16	Rachel Shelley	Dept. Earth, Ocean and Atmospheric Science - Florida State University School of Geography, Earth and Environmental Sciences - University of Plymouth LEMAR/IUEM, CNRS UMR 6539 - Université de Bretagne Loire
Author 17	Pascale Lherminier	Laboratoire d'Océanographie Physique et Spatiale (LOPS)/IUEM/Ifremer/CNRS/IRD - Université de Bretagne Loire
Author 18	Anne Donval	LEMAR/IUEM, CNRS UMR 6539 - Université de Bretagne Loire
Author 19	Luis Lampert	Laboratoire d'Ecologie Pélagique – Ifremer
Author 20	Hervé Claustre	Laboratoire d'Océanographie de Villefranche-sur-Mer (LOV), CNRS UMR 7093 - Université Pierre et Marie Curie
Author 21	Celine Dimier	Laboratoire d'Océanographie de Villefranche-sur-Mer (LOV), CNRS UMR 7093 - Université Pierre et Marie Curie
Author 22	Joséphine Ras	Laboratoire d'Océanographie de Villefranche-sur-Mer (LOV), CNRS UMR 7093 - Université Pierre et Marie Curie
Author 23	Raphaëlle Sauzède	Laboratoire d'Océanographie de Villefranche-sur-Mer (LOV), CNRS UMR 7093 - Université Pierre et Marie Curie
Author 24	Lorna Foliot	Laboratoire des Sciences du Climat et de l'Environnement, Gyf-sur-Yvette, France
Author 25	Kathrin Wuttig	ACE-CRC - University of Tasmania
Author 26	Thomas Holmes	ACE-CRC/IMAS - University of Tasmania
Author 27	Ashley Townsend	Central Science Laboratory - University of Tasmania
Author 28	Zanna Chase	IMAS - University of Tasmania
Author 29	Lavenia Ratnarajah	Ocean Sciences Department, School of Environmental Sciences - University of Liverpool

Author details and their roles:

Paper 1 – Tonnard, M., Planquette, H., Bowie, A. R., van der Merwe, P., Gallinari, M., Desprez de Gésincourt, F., Germain, Y., Gourain, A., Benetti, M., Reverdin, G., Tréguer, P., Boutorh, J., Cheize, M., Menzel Barraqueta, J. L., Pereira-Contreira, L., Shelley, R., Lherminier, P. and Sarthou, G. *Dissolved iron in the North Atlantic Ocean and Labrador sea along the GEOVIDE section (GEOTRACES section GA01)* (submitted to Biogeosciences),

Located in Chapter 3

Candidate contributed to the statistical analysis of the data set and the writing up of the manuscript. Authors 1, 2, 3 and 4 contributed to the preparation of manuscript and authors 1 and 3 also contributed to DFe sample collection. Authors 5, 6 and 7 contributed to the DFe analysis on the seaFAST-picoTM SF-ICP-MS. Author 8 contributed to the analysis of Particulate Fe data and their interpretation. Authors 9 and 10 contributed to the estimation of the sea-ice melting, sea-ice formation and meteoric water fractions and their interpretation. Author 11 and 5 contributed to the analysis of the major nutrients. Authors 12, 13, 14, 15, 16 contributed to DFe sample collection, in addition author 16 contributed to the analysis of the aerosols and their interpretation. Author 17 contributed to the interpretation of water mass circulation and physical processes. Author 1 and 17 were PIs of the GEOVIDE voyage.

Paper 2 – Tonnard, M., Donval, A., Lampert, L., Tréguer, P., Bowie, A. R., van der Merwe, P., Planquette, H., Claustre, H., Dimier, C., Ras, J. and Sarthou, G., *Phytoplankton assemblages in the North Atlantic Ocean and in the Labrador Sea along the GEOVIDE section (GEOTRACES section GA01) determined by CHEMTAX analysis from HPLC pigment data: from an assessment of the community structure, succession and potential limitation to broader implication* (in prep.),

Located in Chapter 4

Candidate contributed to the statistical analysis of the DFe data set and the writing up of the manuscript. Authors 1, 2, 3 and 4 contributed to the preparation of manuscript and authors 1 and 3 also contributed to DFe sample collection. Author 11 and 5 contributed to the analysis of the major nutrients. Authors 18 and 19 contributed to the building of the initial pigment matrix used in the CHEMTAX model. Authors 23, 24 collected the pigment samples, while authors 20, 21, 22 and 23 contributed to their analysis by HPLC.

Paper 3 – Tonnard, M., Wuttig, K., Holmes, T., van der Merwe, P., Townsend, A., Sarthou, G., Planquette, H., Chase, Z., Ratnarajah, L. and Bowie, A. R., *Dissolved and soluble Fe-binding organic ligands near the Kerguelen Archipelago (B-transect) and in the vicinity of Heard and McDonald Islands (HEOBI voyage – Glpr05)* (in prep.),

Located in Chapter 5

Candidate contributed to the soluble Fe (SFe), soluble Fe-binding organic ligand (SLt), DFe and dissolved Fe-binding organic ligand (DLt) sample collection, the analysis of SFe on the seaFAST-picoTM and SLt and DLt on a voltammeter, statistical analysis of the data set, and the writing up of the manuscript. Authors 1, 2, 3, 4, 25 contributed to the preparation of manuscript Authors 2, 4, 25, 26, 28 and 29 contributed to DFe, SFe, DLt and SLt sample collection. In addition, authors 4 and 25 contributed to the analysis of SFe, SLt, DFe and DLt and author 26 to the analysis of DFe. Author 27 contributed to the analysis of the DFe and SFe on the SF-ICP-MS.

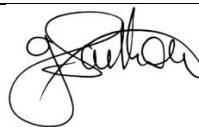
We the undersigned agree with the above stated “proportion of work undertaken” for each of the above published (or submitted) peer-reviewed manuscripts contributing to this thesis:

Signed **Candidate** Manon Tonnard

Manon TONNARD



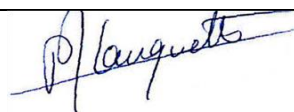
Author 1 Géraldine Sarthou



Author 2 Andrew R. Bowie

Andrew Bowie

Author 3 Hélène Planquette



Author 4 Pier van der Merwe



Author 5 Morgane Gallinari



Author 6 Florianne Desprez de Gésincourt



Author 8 Arthur Gourain



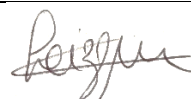
Author 9 Marion Benetti

Author 10 Gilles Reverdin

Author 11 Paul Tréguer

Author 12 Julia Boutorh

Author 13 Marie Cheize



Author 14 Jan-Lukas Menzel Barraqueta

Author 15 Leonardo Pereira Contreira

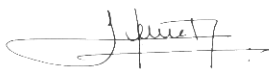
Author 16 Rachel Shelley



Author 17 Pascale Lherminier

Author 18 Anne Donval

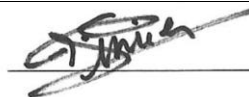
Author 19 Luis Lampert



Author 20 Hervé Claustre



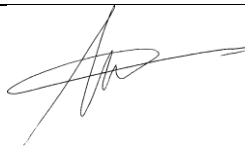
Author 21 Cecile Dimier



Author 22 Joséphine Ras

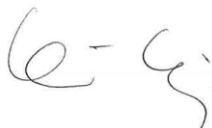


Author 23 Raphaëlle Sauzède



Author 24 Lorna Foliot

Author 25 Kathrin Wuttig



Author 26 Thomas Holmes



Author 27 Ashley Townsend



Author 28 Zanna Chase



Author 29 Lavenia Ratnarajah



Supervisor and Head of School Declaration

I the undersigned agree with the above stated “proportion of work undertaken” for each of the above published (or submitted) peer-reviewed manuscripts contributing to this thesis.

Signed

Head of School

Institute for Marine and Antarctic Studies

University of Tasmania

Date

Acknowledgements

I first want to express my sincere acknowledgements to the jury members who agreed on evaluating my work: thank you very much Cécile Guieu and Christoph Völker for reviewing the thesis, thanks to Simon Ussher, Julia Uitz and François Lacan for examining my work. I would also like to acknowledge Catherine Jeandel and Alessandro Tagliabue who followed my work during my thesis comity and who gave me advices of great value, that allow me to explore new directions.

Throughout these three years and a half (a bit more), I have had the chance to join two diverse and very interesting groups of individuals with years of experience and good advices: thank you so much Géraldine, Hélène, Andy and Pier. Words cannot express how thankful I am, I learned so much with you. I realise the significant effort you have made in order to bring this thesis until the end; you never let me down. Over and above the fact that you gave me an optimal monitoring, I had the pleasure to meet wonderful human beings, gifted with empathy, who continuously supported me throughout the thesis. I know there have been heaps of up and down and sometimes communication was hard, but what I keep in mind is how amazing was this adventure and that I am pleased I had the chance to work with you all, all this wouldn't have happened without you. Big thanks also to Delphine, you have been there for me, supporting me and cheering me up when I needed it.

This project could not have been accomplished without the help of collaborators. Thank you Catherine Pradoux for the resin you sent me at the very beginning of my thesis. Thanks a lot Justine Louis, I know you were at the very end of your PhD thesis and that time was ticking for you but you took the time to introduce me to the people in charge of the DYFAMED project. Speaking of DYFAMED, thank you so much Grigor Obolensky for lending me your workshop and especially for your help to make the Asti pumps working; thank you also to Emilie Diamond, Laurent Coppola, Vincenzo Vellucci, Foucaut Tachon, and the Breizh captain Joël Perrot and his crew from the Laboratory of Oceanography of Villefranche-sur-Mer, you guys have all been a very big help to me. I would also like to thank all the people from the HEOBI voyage, that was my first big oceanographic cruise and I still struggle believing I have been to Heard and McDonald Islands, I will never forget this amazing experience. I am highly grateful to Brett Muir, Michael Watson and Lisa Woodward for your support during the voyage, and Roderick, Brendan, Thomas, Gennadiy, Sam, Ian, Damian, Shane, Keith, Matt, Cassandra, Emma, Jonathan, Dean, Darren, Murray, Matthew, Kel and Ryan for your valuable help aboard it was great working with you. Marie Cheize, thank you so much for your worthwhile feedbacks and practice training on the FIA-CL system, thanks to you it has no more secret for me. I also wish to thank you for your patience in explaining me the voltammetry, same as Aridane Gonzales, Hannah Whitby, Kathrin Wuttig, Kristen Buck, Peter Croot, Dario Omanovic, Delphine Lannuzel and Loes Gerringa and I sincerely apologize for plaguing you with heaps of questions. Melanie East thank you so much for organizing everything within the clean lab team, you made things so easier for everybody. I was pleased to work with you, Anne Donval and Luis Lampert, thank you for sharing your phytoplankton knowledge with me and to manage finding time for me. I would like to show appreciation to Pascale Lherminier, Marion Benetti and Rachel Shelley for your contribution, your patience and the scientific discussions around the GEOVIDE data, and to Morgane, Floriane and Yoan for your amazing job with DFe data from GEOVIDE. A big thank to Yves, Gene, Anne-Sophie, Alain, Sonia, Celine for your help with the paperwork, orders and at fixing issues at the LEMAR, and to Pam, Wen, Claire, Toby and Anthony at the IMAS. Thank you everyone for guiding me in the right direction, for your warm welcome among the different laboratories, I am happy I met you; I am indebted to you.

And then, the friends. The one I met during the thesis trough the diverse accommodations I had: first St-Yves housemates, Sergii, Nico, Andrea, Pierre-Yves, Matthieu and Akim we had heaps of fun in this house, living 30 m far from the sea, our holidays to Villach with Dima and Valeri, the vieilles charrues, trip to Crozon, the sound system, hope to see you soon guys ;-); Nico, Simon, Fabio, Maia, Quentin thank you for your warm welcome in Villefranche-sur-Mer that was great to see you after all this time; second St-Yves housemates, Mathilde and Max the homemade beer was really tasty, Hobart CBD housemates, I didn't stay long but that was fun; first Battery Point and Ashfield Street housemates Jorge, Fernando, Lara, Paolo, Jazz, Maria that was intense and delightful ☺; Duke Street housemates : Julie, Michal, Barrett, Dani, Thibaut, Jay, Critina, Chris not to mention the doggy's Wicket and Robyn, I am sad we had to move out special thanks to our gardener in chief Barrett; and finally to my last Battery Point housemates Helene and Martin and Eddy. The one who pushed me to do a bit of sport: Andreas thanks a lot for bringing me out, the kayaking, the fishing, the drinking and especially the eating after the fishing were really great. Thanks to the volley ball team: Jay, Julie, Sandra,

Claudio, Benoit, Seb, Clothilde, Cris, Mana, well, we have been the worst players of the competition but that was so much fun. The one I met at conferences: Thanks a lot to the all the Goldschmidt conference team and to all the GEOTRACES Summer school team, without you it would not have been the same. Heaps of remembers and crazy stories: long-live to absinthe☺. The one who never say no for going out and met around a fire, a pinte, a band of music, a petanque, or *bailar a la musica Latina* ...; thanks to all the friends from the IMAS and the LEMAR, Nina, Manu, Arthur, Emilie, Axel, Matthieu, Clemence, Garis, Fanny, Romain, Malwenn, Julia, Gaspard, Romain, Yannick, Delphi, Tom, Sally, Nono, Habacuc, Laurent, Lara, Fernando, Laila, Pauline, Bruce, Helene, Martin, Manu, Camilla, Dani, Julie, Jay, Morgane, Gwen, Patricia, Florian, Luis, Christine, Cristina, Alessandro, Emiliano, Vero, Sandra, Ole, Tina, Sahan, Seb, Claire, Seb, Seb, Julien, Maika, Anicee, thanks for being yourselves. And finally, the “the brezhoneg semi-salted butter”: Jo and Lena, I am so sorry I missed your wedding, just one week short...I was so disappointed I could not make it. I was there for your wedding Guillaume and Marlene, I will remember these beautiful days for a long time, Guigui and Max thanks for your “welcome Rhum au lard”. Now that the PhD thesis is over I am sure we can start making a business out of it, well in Brittany I have no doubt but elsewhere, I am not sure hi hi hi! Cap’tain Clement and Aurelie, hold up the steering bar and hold up the wind! Helene and Maxou thank you so much for everything, I booked my plane ticket for San Francisco, Pierre-Yves le S. thanks for lively discussions around a teapot, thanks to Loic, Steph, Morgane, Matth G., Matth. R., Nico, Caro, Regis, Boris, Gui, Steph, Lucie, Get, Hugo, Lionel, ..., although I have not been there for all of you during the thesis, I promised to that from now, you are my priority number one. You will see me so often that you will be sick of me hi hi hi!!!

Last but not least, thanks to all my family for everything. Mom and dad, you have done so much for me, I missed my words to express how grateful I am. Huge thoughts to Ladda, Louis, Maceo, “ma reine” Marie-Annick, Loic, Fanny, Flo, Sylvain, Gael, Jerome, Anne, Laouen, Ewann, in September I will visit you in Guadalupe Paty and Andala and to all my other cousins we are a huge family sorry I won’t write the name of everybody... and to all my uncles and aunts. I dedicate this manuscript to my brother, Matthieu, you have truly been a pillar of strength for me and my grand-parents Renee and Gilbert, my source of inspiration.

yec'hed mat d'an holl, hemañ zo'vont da goll !

Publications

Tonnard, M., Planquette, H., Bowie, A. R., van der Merwe, P., Gallinari, M., Desprez de Gésincourt, F., Germain, Y., Gourain, A., Benetti, M., Reverdin, G., Tréguer, P., Boutorh, J., Cheize, M., Menzel Barraqueta, J. L., Pereira-Contreira, L., Shelley, R., Lherminier, P. and Sarthou, G. *Dissolved iron in the North Atlantic Ocean and Labrador sea along the GEOVIDE section (GEOTRACES section GA01)* (submitted) Biogeosciences

Yang, L., Nadeau, K., Meija, J., Grinberg, P., Pagliano, E., Ardini, F., Grotti, M., Schlosser, C., Streu, P., Achterberg, E. P., Sohrin, Y., Minami, T., Zheng, L., Wu, J., Chen, G., Ellwood, M. J., Turetta, C., Aguilar-Islas, A., Rember, R., Sarthou, G., **Tonnard, M.**, Planquette, H., Matoušek, T., Crum, S. and Mester, Z., *Inter-laboratory study for the certification of trace elements in seawater certified reference materials NASS-7 and CASS-6*, (2018) Analytical and Bioanalytical Chemistry.

Tonnard, M., Donval, A., Lampert, L., Tréguer, P., Bowie, A. R., van der Merwe, P., Planquette, H., Claustre, H., Dimier, C., Ras, J. and Sarthou, G., *Phytoplankton assemblages in the North Atlantic Ocean and in the Labrador Sea along the GEOVIDE section (GEOTRACES section GA01) determined by CHEMTAX analysis from HPLC pigment data: from an assessment of the community structure, succession and potential limitation to broader implication* (in prep.).

Tonnard, M., Wuttig, K., Holmes, T., van der Merwe, P., Townsend, A., Sarthou, G., Planquette, H., Chase, Z., Ratnarajah, L. and Bowie, A. R., *Dissolved and soluble Fe-binding organic ligands near the Kerguelen Archipelago (B-transect) and in the vicinity of Heard and McDonald Islands (HEOBI voyage – GIp05)* (in prep.) Frontiers.

Holmes, T., Wuttig, K., Chase, Z., van der Merwe, P., Townsend, A. T., Schallenberg, C., **Tonnard, M.** and Bowie, A. R., *Iron availability influences nutrient drawdown in the Heard and McDonald Island region, Southern Ocean* (in prep.) Marine Chemistry.

Conferences & Summer Schools

Wuttig, K., Holmes, T., van der Merwe, P., Chase, Z., Lupton, J., Gault-Ringold, M., Schallenberg, C., **Tonnard, M.**, Townsend, A. and Bowie, A. R. (2018) *Tales of volcanoes and glaciers: Trace elements around Heard and McDonald Islands on the Kerguelen Plateau in the Indian Sector of the Southern Ocean*, Ocean Science Meeting, 11.-16.02.2018, Portland, Oregon, USA. (poster)

Whitby, H., Planquette, H., Cheize, M., Menzel Barraqueta, J. L., Shelley, R. U., Boutorh, J., Pereira Contreira, L., **Tonnard, M.**, Gonzalez, A. G., Bucciarelli, E. and Sarthou, G. (2018) *Iron-binding Humic Substances Along the GEOVIDE Transect in the North Atlantic (GEOTRACES, GA01, 2014)*, Ocean Science Meeting, 11.-16.02.2018, Portland, Oregon, USA. (poster)

Tonnard, M., Planquette, H., Bowie, A. R., van der Merwe, P., Gallinari, M., Desprez de Gesincourt, F., Germain, Y., Gourain, A., Benetti, M., Reverdin, G., Treguer, P., Boutorh, J., Cheize, M., Menzel Barraqueta, J.-L., Pereira-Contreira, L., Shelley, R., Lherminier, P. and Sarthou, G., (2017) *Dissolved Fe in the north Atlantic Ocean and Labrador Sea along the GEOVIDE section (GEOTRACES GA01)*, GEOVIDE Workshop, 18.-19.12.2017, Brest, France (oral presentation)

Van der Merwe, P., Wuttig, K., Holmes, T., **Tonnard M.**, Chase, Z., Trull, T. and Bowie, A. R. (2017) *Characterising the particulate trace metal pool near hydrothermal active Heard and McDonald Islands, Southern Ocean, Kerguelen Symposium*, 13.-15.11.2017, Hobart, Australia (oral presentation)

Obernosterer, I., Blain, S., Bowie, A. R., van der Merwe, P., Holmes, T., **Tonnard., M.** and Trull, T. (2017) *Role of particle-attached bacteria in rendering iron and carbon bioavailable*, Kerguelen Symposium, 13.-15.11.2017, Hobart, Australia (oral presentation)

Tonnard, M., Gonzalez, A. G., Whitby, H., Sarthou, G., Planquette, H., van der Merwe, P., Boutorh, J., Cheize, M., Gallinari, M., Lherminier, P., Menzel Barraqueta, J.-L., Pereira Contraira, L., Shelley, R., Tréguer, P. and Bowie, A. R. (2017) *Dissolved iron distribution and organic speciation along the GEOVIDE transect in the North Atlantic Ocean and Labrador Sea (GEOTRACES, GA01, 2014)*, GEOTRACES Summer School, 20.-27.08.2017, Brest, France (poster)

Tonnard, M., Gonzalez, A.G., Whitby, H., Bowie, A.R., van der Merwe, P., Planquette, H., Boutorh, J., Cheize, M., Menzel Barraqueta, J.-L., Pereira Contreira, L., Shelley, R. and Sarthou, G. (2017) *Iron-Binding Ligands in the North Atlantic Ocean and Labrador Sea along the GEOVIDE Section (GEOTRACES GA01)*, Goldschmidt Conference, 2017 13.-18.08.2017, Paris, France (oral presentation)

Zanna, C., Bowie, A. R., Blain, S., Holmes' T., Rayner, M., Sherrin, K., **Tonnard, M.** and Trull, T. W. (2016) *Late summer distribution and stoichiometry of dissolved N, Si and P in the Southern Ocean near Heard and McDonald Islands on the Kerguelen Plateau*, AGU Fall Meeting, 12.-16.12.2016, San Francisco, USA (poster)

Tonnard, M., Planquette, H., Bowie, A. R., van der Merwe, P., Gallinari, M., Desprez de Gesincourt, F., Germain, Y., Gourain, A., Benetti, M., Reverdin, G., Treguer, P., Boutorh, J., Cheize, M., Menzel Barraqueta, J.-L., Pereira-Contreira, L., Shelley, R., Lherminier, P. and Sarthou, G., (2016) *Biogeochemical cycle of iron in open ocean: case of the North Atlantic Ocean (GEOVIDE voyage, GEOTRACES-GA01)*, ACE Chit-Chat, 08.12.2016, Hobart, Australia (oral presentation)

Tonnard, M., Wuttig, K., Holmes, T., van der Merwe, P., Townsend, A., Sarthou, G., Planquette, H., Chase, Z., Ratnarajah, L., Schallenberg, C. and Bowie, A. R. (2016) *Iron organic speciation in the vicinity of Heard and McDonald Islands*, HEOBI Workshop, 17-18.11.2016, Hobart, Australia (oral presentation)

Tonnard, M., Sarthou, G., Planquette, H., van der Merwe, P., Boutorh, J., Cheize, M., Menzel Barraqueta, J.-L., Pereira Contreira, L., Shelley, R. and Bowie, A. R. (2015) *Dissolved iron along the GEOVIDE section (GEOTRACES GA01)*, Goldschmidt Conference, 16.-21.08.2015, Prague, Czech Republic (poster)

Table of Content

Chapter 1: General Introduction	31
<u>1.1 The physical carbon pump</u>	<u>34</u>
<u>1.2 The biological carbon pump</u>	<u>36</u>
<u>1.2.1 Photosynthesis.....</u>	<u>36</u>
<u>1.2.2 Carbonate counter pump.....</u>	<u>37</u>
<u>1.2.3 Phytoplankton bloom dynamic</u>	<u>38</u>
<u>1.2.4. Export of particulate organic matter</u>	<u>39</u>
<u>1.2.5. Remineralisation: grazing and microbial activity</u>	<u>40</u>
<u>1.2.6 Nutrient controls</u>	<u>41</u>
<u>1.2.6.1 Macronutrients</u>	<u>42</u>
<u>1.2.6.2 Micronutrients</u>	<u>43</u>
<u>1.2.6.3 Response of the phytoplankton community to the availability of nutrients.....</u>	<u>47</u>
<u>1.3. The GEOTRACES program</u>	<u>48</u>
<u>1.4. Physico-chemical speciation of Fe.....</u>	<u>50</u>
<u>1.4.1 Physical speciation.....</u>	<u>50</u>
<u>1.4.1.1 Particulate pool.....</u>	<u>51</u>
<u>1.4.1.2 Dissolved pool.....</u>	<u>53</u>
<u>1.4.1.3 Soluble and colloidal pools</u>	<u>54</u>
<u>1.4.2 Chemical speciation.....</u>	<u>55</u>
<u>1.4.2.1 Redox speciation</u>	<u>55</u>
<u>1.4.2.2 Organic speciation.....</u>	<u>57</u>
<u>1.5 Biogeochemical cycle of Fe.....</u>	<u>64</u>
<u>1.5.1 External sources of Fe.....</u>	<u>64</u>

<u>1.5.1.1 Atmospheric deposition</u>	64
<u>1.5.1.2 Riverine inputs</u>	66
<u>1.5.1.3 Sediment inputs</u>	66
<u>1.5.1.4 Hydrothermalism</u>	67
<u>1.5.1.5 Glaciers, icebergs and melting sea ice</u>	68
<u>1.5.1.6 Submarine groundwater discharge</u>	70
<u>1.5.2 Regenerated sources of Fe</u>	70
<u>1.6 Summary of literature review</u>	71
<u>1.7 Study areas and thesis goals</u>	72
<u>1.7.1 The North Atlantic Ocean</u>	72
<u>1.7.2 The Kerguelen Plateau (Indian sector of the Southern Ocean)</u>	75
<u>1.7.3. Objectives and thesis outline</u>	77
Chapter 2: Material and Methods	80
<u>2.1 Ultra-clean conditions</u>	85
<u>2.1.1 Laboratory practices</u>	86
<u>2.1.2 Pre-cruise cleaning procedure</u>	86
<u>2.1.2.1 GO-FLO bottles</u>	87
<u>2.1.2.2 Niskin bottles</u>	87
<u>2.1.2.3 Sampling bottles</u>	87
<u>2.2 Sample collection</u>	89
<u>2.2.1 GEOVIDE voyage</u>	89
<u>2.2.1.1 Location</u>	90
<u>2.2.1.2 Equipment used for sample collection</u>	90
<u>2.2.1.3 Sample treatment before shore-based analysis</u>	91
<u>2.2.2 HEObi voyage</u>	91

2.2.2.1 Location.....	91
2.2.2.2 Equipment used for sample collection	93
2.2.2.3 Sample treatment before shore-based analysis	93
2.3 Statistical Methods.....	94
2.4 Analytical techniques.....	95
2.4.1 Calibration seawater.....	96
2.4.1.1 GEOVIDE standard reference seawater (LEMAR).....	96
2.4.1.2 HEOBI standard reference seawater (IMAS).....	96
2.4.2 Dissolved iron (DFe) analysis.....	97
2.4.2.1 Principle of analysis	97
2.4.2.2 Reagent preparation.....	100
2.4.2.3 Precision, accuracy and reproducibility	101
2.4.3 Fe-binding organic ligand analysis	104
2.4.3.1 Principle of analysis	104
2.4.3.2 Material, reagents and sample preparation.....	105
2.4.3.3 Theory of competitive ligand equilibration and adsorptive cathodic stripping voltammetry (CLE-AdCSV) using TAC as artificial ligand.....	108
2.4.3.4 Determination of Fe-binding ligand characteristics	109
2.4.3.5 Detection limit and TAC contamination	111
2.4.4 Pigment analysis	111
2.4.4.1 HPLC principle of analysis	112
2.4.4.2 Pigment based phytoplankton size classes	114
2.4.4.3 CHEMTAX model	114
2.4.5 Ancillary measurements.....	125
Chapter 3: Dissolved Iron Distribution in the North Atlantic Ocean.....	127
<u>Abstract</u>	130

<u>3.1 Introduction</u>	131
<u>3.2 Material and methods</u>	134
<u>3.2.1 Study area and sampling activities</u>	134
<u>3.2.2 DFe analysis with SeaFAST-picoTM</u>	136
<u>3.2.3 Meteoric water and sea ice fraction calculation</u>	137
<u>3.2.4 Ancillary measurements and mixed layer depth determination</u>	138
<u>3.2.5 Statistical analysis</u>	139
<u>3.2.6 Water mass determination and associated DFe concentrations</u>	139
<u>3.2.7 Database</u>	139
<u>3.3 Results</u>	140
<u>3.3.1 Hydrography</u>	140
<u>3.3.2 Ancillary data</u>	143
<u>3.3.2.1 Nitrate</u>	143
<u>3.3.2.2 Chlorophyll-<i>a</i></u>	143
<u>3.3.3 Dissolved Fe concentrations</u>	144
<u>3.3.4 Fingerprinting water masses</u>	144
<u>3.4 Discussion</u>	147
<u>3.4.1 High DFe concentrations at stations 1 and 17</u>	148
<u>3.4.2 DFe and hydrology keypoints</u>	148
<u>3.4.2.1 How do air-sea interactions affect DFe concentration in the Irminger Sea</u>	148
<u>3.4.2.2 Why don't we see a DFe signature in the Mediterranean Overflow Water (MOW)?</u>	149
<u>3.4.2.3 Fe enrichment in the Labrador Sea Water (LSW)</u>	150
<u>3.4.2.4 Enhanced DFe concentrations in the Irminger Sea Bottom Water</u>	152

3.4.2.5 Reykjanes Ridge: Hydrothermal inputs or Fe-rich seawater?	153
3.4.3 What are the main sources of DFe in surface waters?	154
3.4.3.1 Tagus riverine inputs	154
3.4.3.2 High latitude meteoric water and sea-ice processes	156
3.4.3.3 Atmospheric deposition	158
3.4.4 Sediment input	160
3.4.5 How does biological activity modify DFe distribution?	162
3.5 Conclusion	166
3.6 Acknowledgements	167
3.7 References	168
3.8 Supplementary material	178
Chapter 4: Assessment of Nutrient Limitation(s) of phytoplankton organisms in the North Atlantic Ocean	207
Abstract	210
4.1 Introduction	211
4.2 Material and methods	212
4.3 Results	212
4.3.1 Temporal variability and general pattern of total chlorophyll-<i>a</i> concentrations	212
4.3.2 Hydrological features of the habitat	214
4.3.3 Nutrient concentrations and distributions	215
4.3.4 Phytoplankton size class distributions	219
4.3.5 Phytoplankton functional class distributions	221
4.3.5.1 Phytoplankton functional class concentrations	221
4.3.5.2 Percentage of phytoplankton classes	222
4.4 Discussion	225

4.4.1 Differences of size classes determination by CHEMTAX and Uitz et al. (2006) analysis	225
4.4.2 Potential nutrient limitation	226
4.4.2.1 Relationship between nutrients and organic matter remineralisation	226
4.4.2.2 Using tracers to assess potential limitation	226
4.4.3 Trophic status of regions	229
4.4.4 Statistical correlations of nutrients with physical and biological parameters (CCA)	233
4.4.4.1 NASTE province: Eastern West European Basin and Iberian Margin	233
4.4.4.2 NADR province: Western West European Basin and Iceland Basin	243
4.4.4.3 ARCT province (i.e. Irminger and Labrador Seas and Greenland and Newfoundland coastal stations, stations 40-78)	246
4.5 Conclusion	251
Chapter 5: Fe-Binding Organic Ligands and Bioavailability over the Kerguelen Plateau	255
Abstract	257
5.1 Introduction	258
5.2 Material and method	262
5.3 Results	262
5.3.1 Hydrography	262
5.3.2 Soluble Fe and dissolved and soluble Fe-binding organic ligands	264
5.3.2.1 Soluble Fe concentrations	264
5.3.2.2 Soluble and dissolved Fe-binding organic ligand concentrations and conditional stability constants	265
5.4 Discussion	270
5.4.1 Size partitioning of dissolved Fe and Fe-binding ligands	271
5.4.1.1 The reference station	271
5.4.1.2 What controls DFe concentrations?	271

5.4.2 Possible sources of dissolved and soluble Fe-binding organic ligands (B-transect and R18)	273
5.4.2.1 Biological component as a source of Fe-binding organic ligands	275
5.4.2.2 Sediment as a source of Fe-binding organic ligands	278
5.4.3 Comparison between the different areas	279
5.4.3.1 Dissolved fraction	279
5.4.3.2 Impact for Fe physical and organic speciation	284
5.4.3.3 Potential effects for the phytoplankton community	285
5.5 Conclusion	286
Chapter 6:Conclusions and perspectives	288
6.1 Synthesis of the main results	290
6.1.1 The North Atlantic Ocean: DFe, macronutrient and pigment distribution	290
6.1.2 The Southern Ocean: Fe-binding organic ligands and primary production	295
6.1.3 Linking both study areas	298
6.2 Implications and perspectives	299
 French summary	 303
 Apendices	 330
A – Chapter 2	331
B – Chapter 3	347
C – Chapter 4	350
D – Chapter 5	360
 References	 362

List of figures

Figure 1.1: The four ocean carbon pumps. Figure from Legendre et al. (2015).

Figure 1.2: Simplified view of the biological carbon pump (from S. Hervé, IUEM).

Figure 1.3: Patterns of nutrient limitation with backgrounds indicating the annual averages surface concentrations of A) nitrate (scaled by the mean N:P ratio of organic matter, i.e. 16) and B) phosphate in $\mu\text{mol L}^{-1}$. From Moore et al., (2013).

Figure 1.4: Figure illustrating the major sources (in blue) and processes (in red) influencing the distribution of the TEIs. From GEOTRACES Science Plan.

Figure 1.5: The GEOTRACES plan, the black lines symbolizing the cruises completed during the international polar year, the yellow lines cruises completed and the red lines, cruises to be done. Map from the GEOTRACES website (www.geotraces.org).

Figure 1.6: The components of particulate and dissolved iron pools (including the soluble and colloidal components) and the role of inorganic and organic components (adapted from Tagliabue et al., 2017).

Figure 1.7: Schematic depiction of the biological carbon pump, emphasizing the important particle dynamics processes. From Lam and Marchal (2015).

Figure 1.8: Schematic of iron-binding ligand cycling in the ocean. From Buck et al. (2016).

Figure 1.9: Examples of organic-iron binding ligand identities in seawater. The heme analog is siroheme, a relatively soluble iron-containing heme complex. From Buck et al. (2016).

Figure 1.10: Ligand distribution as determined by the model of Völker and Tagliabue (2015) and *in-situ* measurements plotted as dots using the same color coding.

Figure 1.11: A revised representation of the major processes in the ocean iron cycle, with emphasis on the Atlantic Ocean. From Tagliabue et al. (2017).

Figure 1.12: Map of the circulation scheme, the major topographical features, main basins, currents and main water masses of the North Atlantic Ocean. From Daniault et al. (2016).

Figure 1.13: Schematic of the geostrophic circulation over and around the Kerguelen Plateau during KEOPS. From Park et al. (2008b).

Figure 2.1: Historical perspective of the change in the range and average concentrations of dissolved Fe in the open ocean. From Blain and Tagliabue (2016).

Figure 2.2: Map of the GEOTRACES GA01 voyage track plotted on bathymetry as well as the major topographical features and main basins.

Figure 2.3: Pictures (from Helene Planquette) of (from the left to the right) Trace Metal Clean Rosette, Marie Cheize and Julia Boutorh sampling for trace metals and acidifying samples, 0.45 μm polyethersulfone filters (Supor®).

Figure 2.4: Location of the stations sampled during the HEOBI voyage using the Trace Metal Clean Rosette (modified from Thomas Holmes).

Figure 2.5: Pictures (from Peter Harmsen) of (from the left to the right) Kathrin Wuttig, the Trace Metal Clean Rosette in its protective coat before deployment, Andy R. Bowie and Manon Tonnard; Zanna Chase and Manon Tonnard sampling for trace metals through 0.2 μm Pall Acropak (Supor®) capsule filters.

Figure 2.6: Schematic of the off-line flow injection systems used at the IMAS showing solution flow paths during A) filling of sample and buffer loops, B) loading of buffered sample onto the column, C) column rinsing and conditioning, and D) elution of trace metals (modified from Rapp et al., 2017).

Figure 2.7: Schematic of the voltammetric cell and electrochemical process involved during analysis (modified from Cheize, 2012).

Figure 2.8: Schematics of A) potential variation at the working electrode surface as a function of time during the adsorptive cathodic stripping voltammetry (adapted from Wang, 2006), B) sample preparation before analysis, C) plot of the current intensity as a function of the potential applied for different Fe standard addition and D) plot of the reduction peak height as a function of total Fe concentration for a UV-digested seawater and a seawater that contains natural Fe-binding organic ligands (adapted from Cheize, 2012).

Figure 2.9: Distribution of the groups determined on the output of a Principal Component Analysis.

Figure 3.1: Map of the GEOTRACES GA01 voyage plotted on bathymetry as well as the major topographical features and main basins.

Figure 3.2: Parameters measured from the regular CTD cast represented as a function of depth for GA01 section for A) Dissolved Oxygen (O_2 , $\mu\text{mol kg}^{-1}$), B) Salinity and C) Temperature ($^{\circ}\text{C}$).

Figure 3.3: Contour plot of the distribution of dissolved iron (DFe) concentrations in nmol L^{-1} along the GA01 voyage transect: upper 1000 m (top) and full depth range (bottom).

Figure 3.4: Vertical profiles of dissolved iron (DFe, black dots, solid line), particulate iron (PFe, black open dots, dashed line, Gourrain et al., in prep.) and dissolved aluminium (DAI, grey dots, Menzel Barraqueta et al., 2018) at Stations 2 (A), and 4 (B) located above the Iberian shelf, Station 56 (C), Stations 53 (D) 53 and Station 61 (E) located above the Greenland shelf and Station 78 (F) located above the Newfoundland shelf.

Figure 3.5: Plot of dissolved iron (DFe, black circles) and dissolved aluminium (DAI, white circles, Menzel Barraqueta et al., 2018) along the salinity gradient between stations 1, 2, 4, 11 and 13 with linear regression equations.

Figure 3.6: Plot of dissolved Fe (DFe) Turnover Times relative to Atmospheric Deposition (TTADs) calculated from soluble Fe contained in aerosols estimated from a two-stage sequential leach (UHP water, then 25% HAC, Shelley et al., this issue).

Figure 3.7: Section plot of the Fe^* tracer in the North Atlantic Ocean with a remineralization rate ($R_{\text{Fe:N}}$) of $0.05 \text{ mmol mol}^{-1}$ from surface to 225 m depth.

Figure 4.1: A) Map of the GEOTRACES GA01 voyage track plotted on bathymetry as well as the major topographical features and main basins. B) Satellite Chlorophyll-*a* concentrations (MODIS Aqua from <http://oceancolor.gsfc.nasa.gov>), in units of mg m^{-3} , before and during the GEOVIDE voyage (from March to June 2014). C) Contour plot of the measured total chlorophyll-*a* concentrations (TChl-*a*, mg m^{-3}) for the GEOVIDE voyage transect.

Figure 4.2: The section represents the whole voyage track from station 2 to station 78 (total of 33 stations, note that stations 44 and 46 occupied the same location). Parameters collected from the regular CTD cast: temperature (A), salinity (B), dissolved O_2 (C) and pH at 25°C (D) are represented as a function of depth.

Figure 4.3: The section represents the whole voyage track from station 2 to station 78 (total of 33 stations). Nutrients collected from the regular CTD cast [Si(OH)_4 (A), NO_2^- (B), $\text{NO}_x = \text{NO}_2^- + \text{NO}_3^-$ (C)], and from the Trace Metal Rosette (TMR) cast [DFe (D)] are represented as a function of depth.

Figure 4.4: Dissolved macronutrient (NO_x , Si(OH)_4) ratio (i.e. $\text{NO}_x:\text{Si(OH)}_4$) as a function of depth.

Figure 4.5: GEOVIDE voyage cross sections of in situ TChl-*a* concentrations in mg m^{-3} (A-C) and percentages (D-F) associated to the pico-, nano-, and micro-phytoplankton size classes using Uitz et al. (2006) formulae.

Figure 4.6: A) Plot of integrated total Chlorophyll-*a* (TChl-*a*) concentrations (in green, from 0 to 150 m depth) along the GEOVIDE section. B) Stacked bars averaged per basins and depth range (0-25: from 0 to 25, 25-50: from 25 to 50, 50-100: from 50 to 100 m and 100-200: from 100 to 200 m depth) of the concentration of the main phytoplankton classes as determined by CHEMTAX.

Figure 4.7: Box and whisker diagram averaged per basins (0-200 m depth) (A) and stacked bars averaged per basins and depth range (0-25: from 0 to 25, 25-50: from 25 to 50, 50-100: from 50 to 100 m and 100-200: from 100 to 200 m depth) (B) of the percentage of the main phytoplankton classes as determined by CHEMTAX. Note that the colour coding is common to both plots.

Figure 4.8: Comparison between the phytoplankton size class as determined by CHEMTAX and by Uitz et al. (2006) formulae for the micro-phytoplankton (A), the nano-phytoplankton (B) and the pico-phytoplankton (C).

Figure 4.9: Sections of the tracers Si^* (A) and Fe^* (B) represented as a function of depth. Negative values indicate potential growth limiting nutrients while positive values indicate an excess of $\text{Si}(\text{OH})_4$ or DFe after complete biological uptake of NO_3^- .

Figure 4.10: Relationship between the Chl-*a* concentration integrated from 0 to 150 m depth and the fraction of A) micro-phytoplankton, B) nano- and pico-phytoplankton, C) nano-phytoplankton and D) pico-phytoplankton.

Figure 4.11: Plots of canonical correspondence analysis (CCA) and Pearson correlation with level of significance (i.e. ***, p-value < 0.001; **, p-value = [0.001 ; 0.01]; *, p-value = [0.01 ; 0.05]) for A) nutrients (NO_3^- , NO_2^- , Si and DFe) defined as objects and physical (salinity, temperature and pH) and biological (fractions of pico-, nano-, and micro-phytoplankton) parameters; and phytoplankton functional-classes (Diatoms, Dinophytes, Pelagophytes, Haptophytes-6, Haptophytes-8, Cryptophytes, Cyanobacteria, Prasinophytes and Chlorophytes) defined as objects with nutrients (NO_3^- , NO_2^- , Si, DFe, Si^* , Fe^* , $\text{NO}_x\text{:Si}$) and physical (salinity, temperature, pH and z:Zeu) parameters for B) the NASTE province (stations 1-19), C) the NADR province (stations 19-38) and D) the ARCT province (stations 40-78).

Figure 4.12: Histograms of fractional drawdown ((winter – spring)/winter) of NO_3^- and Si for A) winter mixed layer depth and C) spring mixed layer depth and histograms of NO_3^- :Si ratios for B) winter mixed layer depth and D) summer mixed layer depth, for stations 1 to 19 located at the Iberian Margin and within the eastern part of the West European Basin. Black dashed line represents the optimal diatom N:Si uptake ratio.

Figure 4.13: Schematic of the potential limitations of the spring bloom in the North Atlantic Ocean along the GEOVIDE section.

Figure 5.1: Schematic of total chlorophyll-*a* (TChl-*a*) concentrations (green) at the sampling period of the HEOBI voyage on top of the main circulation features as in Park et al. (2008b) (D. Alain and S. Hervé, IUEM).

Figure 5.2: Section plots along the B-transect for A) potential temperature (θ), B) salinity and C) dissolved oxygen (O_2).

Figure 5.3: The partitioning (when available) of iron (Fe) and Fe-binding organic ligand characteristics in the dissolved (DFe, <0.2 μm , solid circles and lines, data from Holmes et al., in prep.), soluble (SFe, <10 kDa, open circles, solid lines), and colloidal (CFE, 10 kDa – 0.2 μm , open circles, dashed lines) as a function of depth for A) the reference R18, B) B-transect B9, C) Heard Island H23 and D) McDonald Island M25.

Figure 5.4: Linear relationships between A) dissolved iron (DFe, data from Holmes et al., in prep.) and soluble Fe (SFe) concentrations, B) inorganic DFe and SFe (DFe^* and SFe^* , respectively) and C) SFe and the reactivity of DLt ($\log \alpha$).

Figure 5.5: Box and whisker diagram of A) Fe concentrations (data from Holmes et al., in prep.), B) total Fe-binding organic ligand concentrations (Lt), C) the reactivity of Lt ($\log \alpha$), D) the inorganic Fe concentrations (Fe^*) and E) the conditional stability constant ($\log K^*$, with respect to Fe^{3+}) for the dissolved Fe fraction, and F) the fluorescence (in units of $\text{mg TChl-}a \text{ m}^{-3}$), G) silicates ($\mu\text{mol L}^{-1}$), H) nitrates ($\mu\text{mol L}^{-1}$), I) dissolved manganese (in nmol kg^{-1}) data from Wuttig et al., in prep.) and J) Apparent Oxygen Utilization (AOU, ($\mu\text{mol kg}^{-1}$)), as a function of the different water masses determined at the B-transect.

Figure 5.6: Plot of A) dissolved iron (DFe), B) Fe-binding organic ligand (Lt), C) conditional stability constant ($\log K'$) and D) reactivity of Lt (\log) as a function of depth for B9 from this study and B5 from Gerringa et al. (2008).

Figure 5.7: Box and whisker diagram of A) iron (Fe) concentrations, B) total Fe-binding organic ligand concentrations (Lt), C) conditional stability constants ($\log K'$, with respect to Fe^{3+}), D) the reactivity of ligands ($\log \alpha$), E) excess Fe-binding organic ligands (L'), F) $[L']:[\text{Fe}]$ ratio, G) inorganic Fe (Fe'), and H) the percentage of Fe bound to Fe-binding organic ligands, and G) as a function of Fe fractions D (dissolved) C (colloidal) and S (soluble) for the B-transect (in blue), the reference stations (in green), Heard Island (in yellow) and McDonald Island (in purple).

Figure 5.8: Conceptual schematic of the main finding at Heard and McDonald Islands stations and the B-transect and R18 stations (D. Alain and S. Hervé, IUEM). (DFe data from Holmes et al., in prep., PFe data from van der Merwe et al., in prep.; pigment data from Wojtasiewicz et al., in prep., bacteria picture courtesy from S. Blain).

Figure 6.1 : Scatter plot of stations sampled in the West European Basin (purple), in the Iceland Basin (blue), in the Irminger Sea (green) and in the Labrador Sea (red) from past studies (open circles) and this study (triangles).

Figure 6.2: A) Map of the GEOTRACES GA01 voyage plotted on bathymetry as well as the major topographical features, main basins and corresponding Longhurst provinces. B) Summary of DFe supplies, main phytoplankton classes and potential limitation(s) within the North Atlantic Ocean.

Figure 6.3: A) Location of the stations sampled during the HEOBI voyage using the Trace Metal Clean Rosette (modified from Thomas Holmes). B) Conceptual schematic of the main finding at Heard and McDonald Islands stations and the B-transect and R18 stations (D. Alain and S. Hervé, IUEM). (DFe data from Holmes et al., in prep., PFe data from van der Merwe et al., in prep.; pigment data from Wojtasiewicz et al., in prep., bacteria picture courtesy from S. Blain).

Figure 6.4: Idea of an experimental setup for on-board incubations amended with aerosols and margin particles.

List of tables

Table 1.1: Common metalloproteins present within marine phytoplankton. Adapted from Twining and Baines (2013).

Table 2.1: SAFe S, GSP and NASS-7 dissolved iron concentrations (DFe, nmol L⁻¹) determined by the SeaFAST-picoTM and their consensus (SAFe S, GSP) and certified (NASS-7) DFe concentrations.

Table 2.2: SAFe S, SAFe D1, GSP, GSC and NASS-6 dissolved iron concentrations (DFe, nmol L⁻¹) determined by the SeaFAST-picoTM and their consensus (SAFe S, SAFe D1, GSP, GSC) and certified (NASS-6) DFe concentrations.

Table 2.3: Metric performances of the HPLC analysis.

Table 2.4: Selection of pigments and their associated taxonomic significance for the CHEMTAX model.

Table 2.5: Literature review referring all works realized in the covered area within the North Atlantic Ocean, special attention was given to studies using CHEMTAX method.

Table 2.6: Initial pigment ratio matrices [F₀] for CHEMTAX model.

Table 2.7: Output matrices for the seven different groups determined by a Principal Component Analysis (PCA) from the CHEMTAX model.

Table 3.1: Station number, date of sampling (in the DD/MM/YYYY format), size pore used for filtration (µm), station location, mixed layer depth (m) and associated average dissolved iron (DFe) concentrations, standard deviation and number of samples during the GEOTRACES GA01 transect.

Table 3.2: SAFe S, GSP and NASS-7 dissolved iron concentrations (DFe, nmol L⁻¹) determined by the SeaFAST-picoTM and their consensus (SAFe S, GSP) and certified (NASS-7) DFe concentrations.

Table 3.3: Averaged DFe:DAI (Menzel Barraqueta et al., 2018) and PFe:PAI (Gourain et al., in prep.) ratios reported per margins below 100 m depth.

Table 5.1: Concentrations of soluble iron (SFe), colloidal Fe (CFe), dissolved Fe (DFe, data from Holmes et al., in prep.), total particulate Fe (PFe, data from Van der Merwe et al., in prep.), and SFe:DFe, CFe:DFe, SFe:CFe, PFe labile:PFe_{total}, DFe:PFe ratios for the reference station and stations located nearby McDonald and Heard Islands.

Table 5.2: Median concentrations of soluble, colloidal and dissolved Fe, total Fe-binding organic ligands (Lt), [Lt]:[Fe] ratios, the conditional stability constant of Lt (log K', with respect to Fe³⁺), the reactivity of Lt (log α), inorganic Fe (Fe'), and the percentage of Fe bound to Lt for the reference, B-transect, Heard Island and McDonald Island stations and for different depth ranges.

Table 5.3: Comparison of median ligand characteristics for the different water masses determined for the B-transect (t-test).

Table 5.4: Comparison of median ligand characteristics within A) the dissolved, B) the colloidal and C) the soluble fractions for the four different areas when data were available, i.e. the reference station, the B-transect stations, Heard Island stations and McDonald Island stations (t-test).

Chapter 1:

General Introduction

Chapter 1: General introduction

Table of Contents

1.1 The physical carbon pump	34
1.2 The biological carbon pump	36
1.2.1 Photosynthesis	36
1.2.2 Carbonate counter pump	37
1.2.3 Phytoplankton bloom dynamic	38
1.2.4. Export of particulate organic matter	39
1.2.5. Remineralisation: grazing and microbial activity	40
1.2.6 Nutrient controls	41
1.2.6.1 Macronutrients	42
1.2.6.2 Micronutrients	43
1.2.6.3 Response of the phytoplankton community to the availability of nutrients	47
1.3. The GEOTRACES program	48
1.4. Physico-chemical speciation of Fe	50
1.4.1 Physical speciation	50
1.4.1.1 Particulate pool	51
1.4.1.2 Dissolved pool	53
1.4.1.3 Soluble and colloidal pools	54
1.4.2 Chemical speciation	55
1.4.2.1 Redox speciation	55
1.4.2.2 Organic speciation	57
1.5 Biogeochemical cycle of Fe	64

<u>1.5.1 External sources of Fe</u>	64
<u>1.5.1.1 Atmospheric deposition</u>	64
<u>1.5.1.2 Riverine inputs</u>	66
<u>1.5.1.3 Sediment inputs</u>	66
<u>1.5.1.4 Hydrothermalism</u>	67
<u>1.5.1.5 Glaciers, icebergs and melting sea ice</u>	68
<u>1.5.1.6 Submarine groundwater discharge</u>	70
<u>1.5.2 Regenerated sources of Fe</u>	70
<u>1.6 Summary of literature review</u>	71
<u>1.7 Study areas and thesis goals</u>	72
<u>1.7.1 The North Atlantic Ocean</u>	72
<u>1.7.2 The Kerguelen Plateau (Indian sector of the Southern Ocean)</u>	75
<u>1.7.3. Objectives and thesis outline</u>	76

The estimated global oceanic carbon sink estimate is of $2.7 \pm 0.5 \text{ PgC.yr}^{-1}$ (Le Quéré et al., 2013), representing about 30% of annual atmospheric fuel emissions, highlighting the central role of the ocean in the global climatic system.

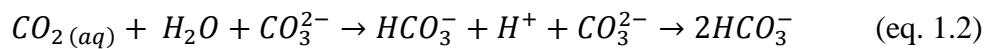
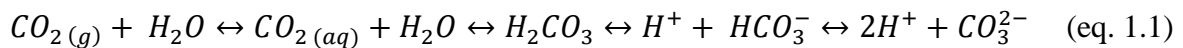
At the air-sea interface, the diffusion of atmospheric CO_2 in the ocean is enhanced by the difference of CO_2 partial pressure ($\Delta p\text{CO}_2$) between the ocean and the atmosphere. The solubility and distribution of the CO_2 within the oceans depend not only on many physico-chemical factors such as temperature, salinity or the turbulence regime, but also on biotic factors (photosynthesis, calcification). Once the CO_2 is dissolved within surface waters, it is then transported horizontally and vertically throughout the oceanic layers by three main processes i) the **physical carbon pump**, ii) the **organic carbon pump** and iii) the **carbonate counter pump** (Volk and Hoffert, 1985), the two last processes being gathered under the name of the biological carbon pump. More recently, additional concepts such as the microbial carbon pump and the lithogenic carbon pump (not detailed here) have been introduced into this general scheme (Bressac et al., 2014; Legendre et al., 2015; Terner et al., 2009). All these processes are responsible for the heterogeneous vertical distribution of DIC in the ocean that results in a strong gradient of approximately $300 \mu\text{mol kg}^{-1}$ between the surface and the deep ocean.

1.1 The physical carbon pump

The physical carbon pump includes two physico-chemical processes:

- the adsorption of CO_2 at the air-sea interface controlled by a thermodynamic equilibrium (i.e. the solubility pump) and
- its vertical transport in the ocean through the global thermohaline circulation.

Once in seawater, the atmospheric gaseous CO_2 is transformed into dissolved inorganic carbon (DIC), which includes the following forms: the non-dissociated form ($\text{CO}_{2(aq)}$), the carbonic acid (H_2CO_3 , i.e. the hydrated form), the bicarbonate ions (HCO_3^-) and the carbonate ions (CO_3^{2-}). CO_2 is a weak acid and when it dissolves, it reacts with water to form carbonic acid, which dissociates following equations 1.1 and 1.2 (Denman et al., 2007).



The CO₂ absorption increases the ocean acidity by adding H⁺ ions in solution, which resulted in a decrease of the sea surface pH by about 0.1 pH units since the beginning of the industrial revolution (Caldeira and Wickett, 2003).

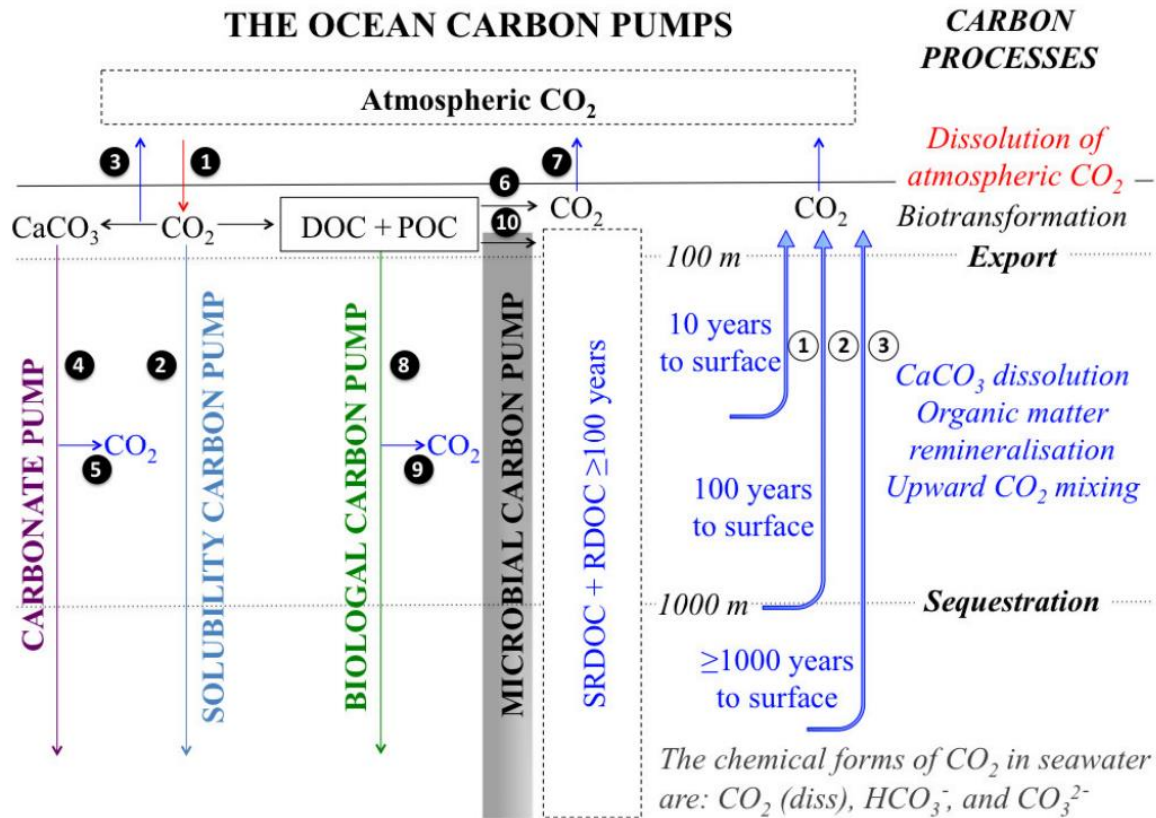


Figure 1.1: The four ocean carbon pumps: The solubility pump, i.e., the dissolution of atmospheric CO₂ in surface waters (1), followed by deep mixing of the CO₂-rich water and sequestration (2); The carbonate pump, i.e., the bio-precipitation of CaCO₃ (or PIC) in the upper water column which is accompanied by the release of CO₂ (3), followed by the sinking of bio-mineral particles to depth where their carbon is sequestered (4); The biological pump, i.e., the photosynthetic uptake of carbon by phytoplankton and its transformation by the food web in the euphotic zone, including respiration (6) and loss to the atmosphere (7), followed by transfer of particulate organic carbon (POC) into deep waters where it is sequestered (8). During the downward transit from 100 to 1000m, CO₂ is released in the water column by dissolution of part of sinking CaCO₃ (5) and remineralisation of part of the POC that is transferred to depth (9). The production of recalcitrant DOC (RDOC) and semi-refractory DOC (SRDOC) with a life time ≥ 100 years (i.e., DOC>100) presumably by microbial activity, will sequester ocean carbon because their lifetimes are ≥ 100 years (10). The small numbers in full circles identify arrows in the figure. Figure from Legendre et al. (2015).

The solubility pump is a mechanism that controls the adsorption or the outgassing of gaseous CO₂ that is modulated by air-sea CO₂ exchange as a function of CO₂ solubility (itself an inverse function of temperature), the difference of CO₂ partial pressure between the surface ocean and the atmosphere, and the gas transfer coefficient (Takahashi et al., 2002; Weiss, 1974). Cold and denser water masses from high latitudes sinks, then spreads at depth towards the equator, this sink being particularly important at high latitudes where deep water

formation takes place such as the Subpolar North Atlantic (Karleskind et al., 2011) and the Subantarctic Southern Ocean (Sallée et al., 2012). Warmer waters originating from low latitudes then compensate the water deficit at the surface. The coupling between CO₂ adsorption and thermohaline circulation will transfer carbon to the deep ocean in cold areas of the globe while tropical areas will favour a degassing of CO₂. The time scales to which the DIC is exchangeable with the atmosphere depend on the depth at which the DIC is transported via the circulation. Indeed, the DIC can be sequestered in the ocean from weeks in the surface to centuries at 3000 m depth.

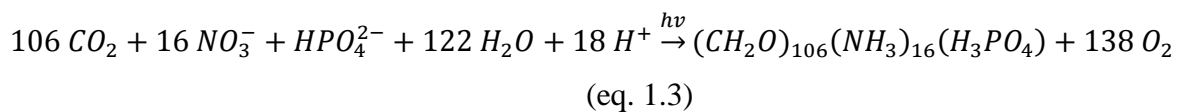
1.2 The biological carbon pump

The biological pump is a suite of biologically mediated processes that consist of surface transformation of DIC into dissolved organic carbon (DOC) and particulate organic carbon (POC), with the subsequent sinking and remineralisation of this organic matter. The DOC oceanic stock is the net result of autotrophic production by marine phytoplankton and heterotrophic microbial remineralisation (Hansell, 2001) (Fig. 1.1).

The observed gradients of DIC and DOC highlight the fundamental role of biology in the vertical distribution of carbon stocks in the ocean, which determines the time scales over which oceanic and atmospheric reservoirs interact and thus partly regulates the atmospheric CO₂ content (Kwon et al., 2009).

1.2.1 Photosynthesis

The biological carbon pump is governed by photosynthesis processes realized by micro-organisms, including all photo-autotroph planktonic organisms, mainly unicellular (Falkowski et al., 2003) convert the DIC and dissolved mineral matter into particulate organic matter (POM, e.g. sugars) and biominerals (e.g. calcite, CaCO₃, for coccolithophores; opal, BSiO₂, for diatoms). This carbon fixation, also defined as primary production (PP), fuels the flux of POC and is limited by the availability of light and nutrients and thus only occurs in ocean where solar radiation penetrates (i.e. the euphotic layer) (eq. 1.3, Fig. 1.2).



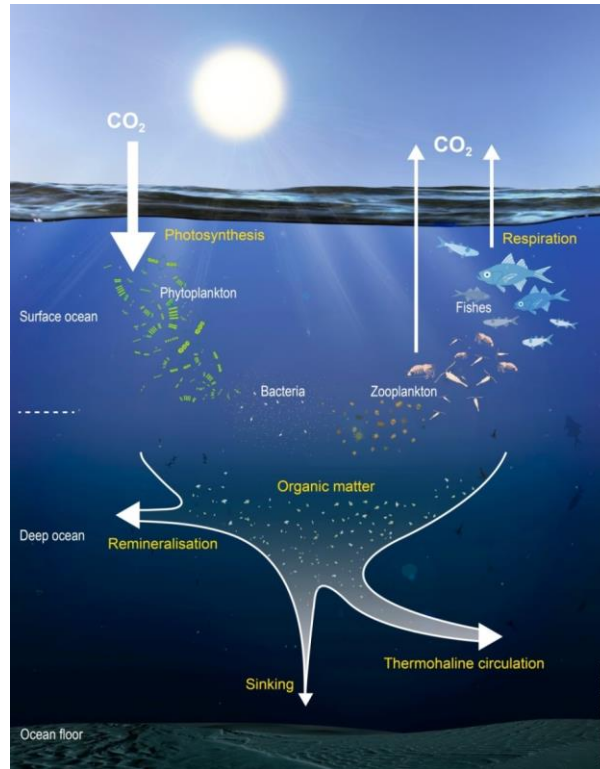
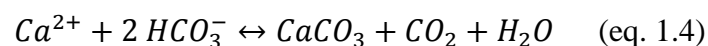


Figure 1.2: Simplified view of the biological carbon pump (from S. Hervé, IUEM).

In the absence of the biological carbon pump, atmospheric CO_2 concentration would increase by approximately 50% (200 ppmv, e.g. Boyd, 2015; Parekh et al., 2006; Sanders et al., 2014), a considerable fraction compared to present days ~ 400 ppmv. Therefore, through the biological carbon pump, ocean plays a key role in the functioning of the carbon cycle at the global scale.

1.2.2 Carbonate counter pump

Another important process that removes DIC within the upper layer of the water column involves the formation of PIC via the precipitation of CaCO_3 (eq. 1.4). Many species through a broad range of trophic levels are able to precipitate CaCO_3 (e.g. calcite or aragonite) in order to form a protective coating or shell, including some phytoplankton taxa such as coccolithophorid cells and calcareous dinophytes as well as other marine organisms (corals, foraminifera, mollusk and crustacean). However, when the PIC is exported to the deep ocean, i.e. below the lysocline, it dissolves, being responsible for a third of the vertical DIC gradient.



Although the calcification process in the mixed layer decreases DIC and therefore alkalinity, it is counter balanced by the production of carbonic acid, which increases the concentration of CO_2 in seawater initiating a diffusive flux of CO_2 from the ocean to the atmosphere (Frankignoulle et al., 1994) (eq. 1.4). Estimations of switching-off the calcification in the ocean suggest that it would lead to a 40 ppmv decrease in atmospheric $p\text{CO}_2$ (Wolf-Gladrow et al., 1999). However, in calcium carbonate dominated regions, a higher fraction of the organic matter is exported to the deep ocean ballasted by the CaCO_3 (Francois et al., 2002).

1.2.3 Phytoplankton bloom dynamic

Sverdrup (1953) suggested that blooms are caused by enhanced growth rates in response to improved light, temperature, stratification conditions and availability of nutrients because of winter mixing thus enabling the initiation of the spring bloom. The first phytoplankton organisms to take advantage of such conditions and to bloom are the micro-phytoplankton, which are then succeeded by a mixture of size-classes and functional groups depending of the resources. The bloom termination will thus result from nutrient depletion, higher grazing pressure and/or decreasing light quality.

Although the critical depth hypothesis explains the spring-summer bloom, it does not explain the vernal bloom. Several hypotheses have been advanced. For example, Behrenfeld (2010) reported that winter physical forcing could modulate the prey-predator relationship via the deepening of the Mixed Layer Depth (MLD) that dilutes phytoplankton in a higher volume and thus limits zooplankton predation rate. This dilution-recoupling hypothesis can thus explain a vernal accumulation of the phytoplankton biomass. Furthermore, Lindemann and St. John (2014) highlighted that phytoplankton have the ability to regulate their respiration rate to obscurity, which will thus reduce losses within the vernal mixed layer. As a result, there is no relationship between the accumulation rate and the growth rate, as biomass can accumulate within deep mixed layer despite a low growth rate. Physical processes such as meso- and sub-mesoscale features (i.e. eddies, upwellings, fronts) can also greatly influence the bloom dynamic by restratification of the deep mixed layer within a timescale of days while the heat fluxes are still negative (Boccaletti et al., 2007; Fox-Kemper et al., 2008). Indeed, eddies developing within horizontal density gradients could lead to the horizontal transport of denser water masses under lighter water masses, which thus stays at the surface. Similarly, wind can also strengthen or lower the restratification through the Ekman transport (Mahadevan et al., 2010).

Diffusion and advection can reintroduce nutrients in the euphotic layer and fuel the primary production (Benitez-Nelson et al., 2000). Lacour et al. (in prep.) reported that the alternation between convective mixing and restratification could lead to episodic carbon export of organic matter produced in surface resulting from the remnant layer, which is the layer included between the depth of a recent mixing and the depth of a past mixing. All these different features that either bring pulses of new nutrients towards the euphotic layer and the dynamic of the mixed layer, explain part of the spatial variability of phytoplankton biomass (Mahadevan et al., 2012; McGillicuddy et al., 2003) and of POC export (Guieu, 2005; Karleskind et al., 2011; Waite et al., 2016).

1.2.4. Export of particulate organic matter

POC and more generally, POM, generated through primary production becomes available for the heterotroph oceanic ecosystem. It constitutes the basis of the marine trophic web and it is further exported towards the deep ocean as dead organisms and faecal pellets sink. The magnitude of the POM export and therefore of the associated nutrients depends on many parameters: 1) The nutrient availability that will drive part of the bloom magnitude and the taxonomic composition of the phytoplankton community, 2) the amount of suspended biomineral and lithogenic particles, 3) organic particles (other than phytoplankton cells) excreted by either phytoplankton, bacteria or higher trophic levels as faeces.

The size structure of the phytoplankton community with higher export related to greater size of sinking phytoplankton cells (Alldredge and Silver, 1988; Guidi et al., 2009) and the density and shape of the phytoplankton cells have been shown to influence the efficiency of the POM export (Klaas and Archer, 2002). Indeed, incorporation of biogenic silica (BSiO_2) or calcite (CaCO_3) into aggregates increases the excess density of suspended particles leading to higher sinking velocity (Honjo, 1996) with a faster transfer to deep ocean when POM is ballasted by calcite (Francois et al., 2002). However, due to their important density relative to seawater, these organisms, especially diatoms, increase their surface area relative to their volume to slow their export and to remain suspended for a longer time in the euphotic layer. Although, non-silicified and non-calcified organisms are barely heavier than seawater ($\sim 1.05 \text{ g cm}^{-3}$), such adaptive strategies are not limited to silicifying organisms (Padisák et al., 2003). An additional process that affect the POM export is the amount of terrigenous material (e.g. dust, clays), which ballast effect is intermediate compared to CaCO_3 and BSiO_2 or even lower than BSiO_2 and greatly depends on the sources and mineralogy of lithogenic particles (Klaas and Archer, 2002).

POM export is also strongly influenced by the property of the dissolved organic matter (DOM). Bacteria and some phytoplankton taxa (e.g. coccolithophores, diatoms) are able to produce such dissolved gel-like molecules that can trigger the transparent exopolymer particles (TEP) production (Deng et al., 2016; Long and Azam, 1996; Mari et al., 2005). These gel-like substances might undergo fast organic matter aggregation in a time-scale of minutes to hours to move from the colloidal to the particulate phase as TEP (e.g. Baalousha et al., 2006; Verdugo et al., 2004). The highly adhesive property of these TEP give them the ability to trap any particles (living, Dam and Drapeau, 1995; organic, mineral; Ebersbach et al., 2014) and thus affect POM and PIC exports (Burd et al., 2016; Mari et al., 2016; Passow, 2002) via aggregation mechanisms.

Finally, the secondary producers such as zooplankton contribute to the export of particulate material by excreting faecal pellets that sink as fast as $\sim 100 \text{ m d}^{-1}$ (e.g. De La Rocha and Passow, 2007; Laurenceau-Cornec et al., 2015; Turner, 2002). These organisms can also actively carry the organic matter out of the euphotic layer to mesopelagic depths through their diel migration. Indeed, the prey consumed during the night can be resuspended as faecal pellets deeper in the water column during the day, contributing from few to 70% of the POC flux (Jonasdottir et al., 2015; Steinberg et al., 2000).

Although the growth rate of individual cells may depend on nutrient availability and aggregation processes, the net growth rate of the cell population is also profoundly influenced by other loss processes led by zooplankton and bacterial activities in the euphotic layer and in the mesopelagic zone that regenerate POM into DOM.

1.2.5. Remineralisation: grazing and microbial activity

Phytoplankton and phytodetrital aggregates (including TEP), namely the marine snow, constitute the food source of micro- and meso-zooplankton (Turner, 2015). Zooplankton grazing will lead to the fragmentation of these large sinking particles into smaller less-sinking particles, to the production of DOM. DOM is formed by excretion or as a result of leaching from faecal pellets and by loss of cell contents from prey during handling (Lampert, 1978), whereas DIC is formed through respiration (Steinberg et al., 2000). Therefore, the flux of POM can be mitigated by zooplankton grazing (Steinberg et al., 2008), which accounts for 7-66% of the loss of sinking POC in the bathypelagic layer (Burd et al., 2010) through coprophagy, coprorhexy and coprochaly (Belcher et al., 2016). However, the recycling of POM by zooplankton grazing will release, similarly as for carbon, dissolved nutrients back to the water column. Interestingly, it has been reported by Giering et al. (2012)

that zooplankton regeneration increased the recycling of Fe relative to N, accounting for 30 to 100% of the total Fe supply to the euphotic zone (Bowie et al., 2001; Sarthou et al., 2008; Strzepek et al., 2005) in forms that are directly bioavailable (Dalbec and Twining, 2009; Nuester et al., 2014), which thus may have huge implication in HNLC areas. However, particle degradation in seawater is mainly achieved by prokaryotes (i.e. heterotrophic *Bacteria* and *Archaea*) within the mesopelagic zone, being responsible for 70-95% of the estimated remineralisation (Giering et al., 2014). This microbial loop is regulated by the release of DOC from zooplankton activities, enzymatic solubilisation, mechanical disaggregation and temperature (e.g. Belcher et al., 2016; Giering et al., 2014; Steinberg et al., 2008). Particle-attached bacteria solubilize POC into DOC which is either directly respired by them or by free-living bacteria in the mesopelagic zone (Turley and Mackie, 1994).

Therefore, the majority of the POM formed in the euphotic layer is recycled and only 0.02% is trapped in oceanic sediments and stored for time scales of millions of years (Bopp and Le Quéré, 2009). Hence, it appears that essential elements are rapidly recycled through the biota at the surface and more slowly during vertical transport in the water column (Morel and Price, 2003). As a result of the processes described in the previous sections, i.e. phytoplankton uptake, POM export, recycling, most essential dissolved trace metals are depleted at the surface, and show enhanced concentrations in the mesopelagic zone with important variability depending on their sources and on the phytoplankton composition.

1.2.6 Nutrient controls

The rapid attenuation of light with depth restricts the growth of the oceanic photoautotrophic microbes, i.e. phytoplankton, to a thin layer. Within this layer, phytoplankton must obtain, besides light and inorganic carbon, chemical forms of essential elements (termed nutrients) to be able to conduct photosynthesis. The availability of these nutrients in the upper ocean frequently limits the activity and abundance of these organisms (Moore et al., 2013). Because phytoplankton groups differ from their nutrient requirement or strategies to uptake nutrients, nutrient availability shapes and structures the phytoplankton community (Twining and Baines, 2013). Among these nutrients, two categories are usually distinguished, based on their concentration in seawater, namely the macro- ($\mu\text{mol L}^{-1}$) and micro- (fmol L^{-1} to nmol L^{-1}) nutrients.

1.2.6.1 Macronutrients

Alfred Redfield first drew attention to the co-variability of dissolved nitrate (NO_3^-) and phosphate (PO_4^{3-}) in the ocean interior, and the similarity of this ratio to N:P ratios within POM and cellular material (Redfield, 1934). Since then, the “Redfield ratios” of 106C:16N:1P are employed as a key stoichiometric concept in ocean biogeochemistry (Anderson and Sarmiento, 1994; Deutsch et al., 2007). However, it has long been recognized that there is considerable variability in the stoichiometric ratios for all elements within cellular material (e.g. Geider and La Roche, 2002; Sterner and Elser, 2002). This variability is likely due to the different forms of N and P that are available to the phytoplankton community in the ocean, and to the different mechanisms and processes that will induce the uptake of these nutrients by phytoplankton.

Dissolved inorganic phosphorus (DIP) is only present in seawater under the phosphate form and varies from < 0.1 to $3.0 \mu\text{mol L}^{-1}$. Phosphorus is primarily delivered to the ocean through continental weathering via riverine input, submarine groundwater discharge and dust deposition (including aerosols, volcanic ash and mineral dust) in the dissolved and particulate phases (e.g. Paytan and McLaughlin, 2007). However, ~99% of particulate P from riverine input is retained within the continental shelf and is thus of minor importance for open ocean waters compared to other sources. Additional sources of phosphorus are the melting of ice sheets (e.g. Hawkings et al., 2016) and potentially sea ice melt for high-latitude regions. The dominant sink of P is deposition and burial in marine sediment after transformation from dissolved to particulate phases (Paytan and McLaughlin, 2007).

Although dissolved inorganic nitrogen (DIN) exists under a variety of forms (i.e. ammonium, NH_4^+ ; nitrite, NO_2^- ; nitrous oxide, N_2O ; oxide, NO and dinitrogen, $\text{N}_{2(\text{g})}$), it is mainly present in the marine system as nitrate (NO_3^-) and is brought to the ocean by rivers, atmospheric deposition and by equilibrium between atmospheric N_2 and dissolved N_2 . All these forms of nitrogen can switch from one form to another one by biological processes, such as denitrification, nitrification and N_2 -fixation (Gruber and Sarmiento, 1997). However, most of these biological interconversions are either energy-yielding (e.g. nitrification) or energy-demanding (e.g. nitrogen fixation) (Karl et al., 2002).

Silicic acid ($\text{Si}(\text{OH})_4$), unlike N and P, is only essential for some phytoplankton taxa, namely diatoms, silicoflagellates and radiolarians to build up their protective coating made of biogenic silica (BSiO_2). This nutrient is essentially brought to the ocean by rivers (Tréguer and De La Rocha, 2013) and can reach up to $170 \mu\text{mol L}^{-1}$. In the world ocean, 56% of the

BSiO₂ is recycled in the euphotic layer and only 3% reaches the seafloor due to its dissolution (Tréguer and De La Rocha, 2013).

The two main macronutrients, N and P, exhibit a huge range of concentrations between and within the different ocean basins. In some areas of the ocean, the concentrations of N and P are so low, that these areas are considered as nutrient deserts and classified as oligotrophic, such as the subtropical Sargasso Sea (e.g. Moore et al., 2009; Moore et al., 2013; Wu and Boyle, 2002). In contrast, the Southern Ocean as well as both the North of the Pacific Ocean are all N- and P-replete (e.g. Moore et al., 2013). Despite the surplus of nutrients for primary producers, chlorophyll-*a* concentrations, a tracer of the phytoplankton biomass, within these areas, remain very low. These regions of the world's oceans are called High Nutrient Low Chlorophyll (HNLC) areas and represent about 25% of the ocean (de Baar et al., 1999).

1.2.6.2 Micronutrients

Fe has been recognized as a limiting element of ocean productivity (e.g. Boyd et al., 2000; Martin et al., 1994; 1988; 1990), being involved in photosynthesis and respiration processes (Morel et al., 2003; Raven et al., 1999). Indeed, Martin and Fitzwater (1988) were the first to conduct deck incubation experiments with seawater from the subarctic Pacific Ocean, one of the three HNLC regions and demonstrated that the addition of only nanomolar concentrations of dissolved Fe to surface water enhanced the chlorophyll concentrations and led to the complete consumption of major nutrients. They concluded their article postulating that the observations made in subarctic Pacific waters may also be true in the Southern Ocean, another HNLC region and speculated that Fe limitation of Southern Ocean phytoplankton was relieved during ice ages by enhanced dusts inputs as suggested by the aluminium (Al) and Fe contents in ice cores collected in Antarctica. In a second paper, Martin (1990) confirmed that ocean productivity is limited by Fe deficiency in the Southern Ocean and Equatorial Pacific. Since 1993, Martin's hypothesis continued to be investigated with the study of high-scale natural and artificial fertilization of ocean HNLC areas (Bakker et al., 2005; Blain et al., 2007; Boyd et al., 2007; de Baar et al., 2005). Martin was a scientist with strong ideas that changed forever how scientists regard the Earth's oceans.

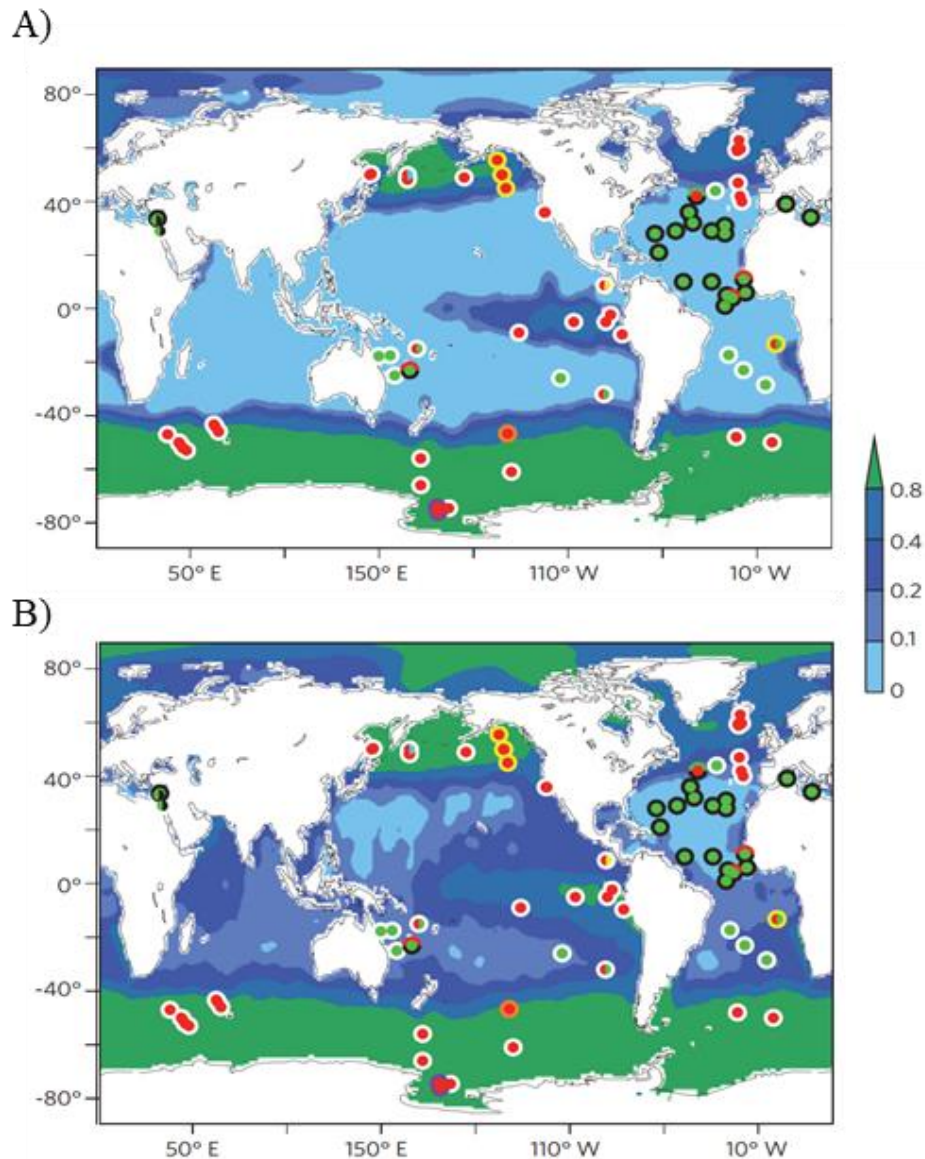


Figure 1.3: Patterns of nutrient limitation with backgrounds indicating the annual averages surface concentrations of A) nitrate (scaled by the mean N:P ratio of organic matter, i.e. 16) and B) phosphate in $\mu\text{mol L}^{-1}$. Circles indicate the primary (central circles) and secondary (outer circles) limiting nutrients as inferred from chlorophyll and/or primary productivity increases following artificial amendment of: N (green), P (black), Fe (red), Si (orange), Co (yellow), Zn (cyan) and vitamin B12 (purple). Divided circles indicate potentially co-limiting elements. From Moore et al. (2013).

The significant growth of research on marine iron biogeochemistry in the past 35 years was triggered by the two seminal publications of Martin (and collaborators) in the late 1980s (Martin and Fitzwater, 1988; Martin, 1990). The importance of Fe is due to how Fe is required for numerous metabolic processes and playing a particularly important role in photosynthesis electron transport (Geider et al., 1993).

Iron is also required in the process of nitrogen fixation, as part of the metalloenzyme nitrogenase, and consequently plays a co-limiting role of primary production (Mills et al., 2004; Moore et al., 2009; Moore et al., 2001). Moreover, Fe is used in the formation of

superoxide dismutase (SOD), an enzyme involved in cell-defence processes against reactive oxygen species (Wolfe-Simon et al., 2005), nitric and nitrous oxide reductases, in the conversion of hydrogen peroxide to water and disproportionation of superoxide to hydrogen peroxide and O₂ as well as in the nitrate and nitrite reductase (Sunda, 1989; Twining and Baines, 2013, Table 1.1). Due to its role in multiple critical biochemical processes, it was shown that low levels of this micronutrient could limit primary productivity in about 50% of the World's ocean (Boyd and Ellwood, 2010; Moore et al., 2009; Moore et al., 2006) (Fig. 1.3). Therefore, Fe plays a crucial key role in oceanic and atmospheric carbon cycles and better understanding the biogeochemical cycle of Fe will allow a better understanding of the carbon cycle. However, the impact of Fe fertilization in terms of organic carbon export and storage efficiency is still poorly constrained (e.g. Martin et al., 2013; Smetacek et al., 2012).

Therefore, Fe has been the cornerstone of the investigation on trace metal requirements for phytoplankton. However, other trace metals are key nutrients for phytoplankton. Overall, the metal phytoplankton cell quotas are driven by biochemical demand, i.e. the more the metals are involved in processes, the more they will abound in cells, with the following generalized metal abundance ranking: $Fe \approx Zn > Mn \approx Ni \approx Cu \gg Co \approx Cd > Mo$ (Twining and Baines, 2013). In a similar manner as Fe, Zinc (Zn) is involved in a plethora of cell functions such as carbon uptake, acquisition of dissolved organic phosphorus (Morel and Price, 2003), it is also used as cofactor for nucleic acid transcription and repair proteins (Twining and Baines, 2013) (Table 1.1). Conversely, other trace metals seem to have more specific and limited roles but have not been studied as extensively as Fe. For example, metals such as Mn (Peers and Price, 2004; Wolfe-Simon et al., 2006), Cu or Ni (Ho, 2013; Nuester et al., 2012) are also used as co-factors in SOD (Wolfe-Simon et al., 2005). Cobalt (Co) is present at the core of vitamin B12 (Bertrand et al., 2007), which is synthesised by prokaryotes and assimilated by eukaryotic phytoplankton (Croft et al., 2005). Co is also present in the active site of carbonic anhydrase enzyme, as well as Zn and Cd, and is thus involved in the carbon uptake (e.g. Morel et al., 1994; Price and Morel, 1990; Yee and Morel, 1996). Consequently, the acquisition of major nutrients is not independent of the availability of trace metals, catalysing their transformation for uptake.

Table 1.1: Common metalloproteins present within marine phytoplankton. Adapted from Twining and Baines (2013).

Metal	Protein(s)	Function(s)
Fe (iron)	Cytochromes	Electron transport in photosynthesis and respiration
	Ferredoxin	Electron transport in photosynthesis and N fixation
	Other Fe-S proteins	Electron transport in photosynthesis and respiration
	Nitrate and nitrite reductase	Conversion of nitrate to ammonia
	Chelatase	Porphyrin and phycobiliprotein synthesis
	Nitrogenase	N fixation
	Catalase	Conversion of hydrogen peroxide to water
	Peroxidase	Reduction of reactive oxygen species
	Superoxide dismutase	Disproportionation of superoxide to hydrogen peroxide and O ₂
Zn (zinc)	Carbonic anhydrase	Hydration and dehydration of carbon dioxide
	Alkaline phosphatase	Hydrolysis of phosphate esters
	RNA polymerase	Nucleic acid replication of carbon dioxide
	tRNA synthetase	Synthesis of tRNA
	Reverse transcriptase	Synthesis of single-stranded DNA from RNA
	Carboxypeptidase	Hydrolysis of peptide bonds
	Superoxide dismutase	Disproportionation of superoxide to hydrogen peroxide and O ₂
Mn (manganese)	O ₂ -evolving enzyme	Oxidation of water during photosynthesis
	Superoxide dismutase	Disproportionation of superoxide to hydrogen peroxide and O ₂
	Arginase	Hydrolysis of arginine to ornithine and urea
	Phosphotransferases	Phosphorylation reactions
Ni (nickel)	Urease	Hydrolysis of urea
	Superoxide dismutase	Disproportionation of superoxide to hydrogen peroxide and O ₂
Cu (copper)	Plastocyanin	Photosynthesis electron transport
	Cytochrome oxidase	Mitochondrial electron transport
	Ascorbate oxidase	Ascorbic acid oxidation and reduction
	Superoxide dismutase	Disproportionation of superoxide to hydrogen peroxide and O ₂
	Multicopper ferroxidase	High-affinity transmembrane Fe transport
Co (cobalt)	Vitamin B12	C and H transfer reactions
Cd (cadmium)	Carbonic anhydrase	Hydration and dehydration of carbon dioxide
Mo (molybdenum)	Nitrate reductase	Conversion of nitrate to ammonia
	Nitrogenase	N ₂ -fixation
V (vanadium)	Nitrogenase	N ₂ -fixation

1.2.6.3 Response of the phytoplankton community to the availability of nutrients

“It is a recognized principle of ecology that the interactions of organisms and environment are reciprocal. The environment not only determines the conditions under which life exists, but the organisms influence the conditions prevailing in their environment.” (Redfield, 1958)

“This two way interaction... has a profound influence on the biogeochemistry of the ocean...” (Sunda, 2012).

The availability of nutrients shapes the phytoplankton community structure. Indeed, phytoplankton taxa do not have the same requirement for all nutrients and are not all able to uptake the different chemical forms one nutrient can take. Although all phytoplankton taxa are capable of photosynthesis and respiration, most of the other biological functions are taxon-specific. In addition, some phytoplankton taxa have developed adaptive behaviour as a response to nutrient availability. Therefore, it is more likely that limitation of one nutrient or co-limitation will affect the phytoplankton community structure.

There is a clear relationship between the trophic status of a water body and the size class distributions of algal assemblages and therefore of the taxonomic composition (Claustre, 1994; Uitz et al., 2006). Among the phytoplankton community, three size-classes (micro-, nano- and picoplankton) have been distinguished representative of algal functional groups. Indeed, picoplankton (0.7 – 2 μm) are preferentially associated with the presence of regenerated forms of nutrient, i.e. recycled within the euphotic zone, whereas microplankton (20 – 200 μm , e.g. large diatoms) are more involved in new production, i.e. when nutrient inputs from outside the euphotic zone become available (e.g. upwelling of nutrients, riverine inputs) (e.g. Eppley and Peterson, 1979; Malone et al., 1980). A good example of how the available chemical form of a specific nutrient, which depends on its sources, affect phytoplankton size-classes is nitrogen.

Among co-limitations, three categories based on their mathematical formulations and visualization were distinguished (Saito et al., 2008). Type I co-limitation involves two independent nutrients. A typical example of this is N-limitation of some taxa due to decreasing N:P ratios, thus favouring the development of N_2 -fixers and concomitantly the P-limitation of the N_2 -fixers (Benitez-Nelson, 2000). Type-II co-limitation involves the biochemical substitution of a nutrient for another. Indeed, the replacement of one essential element by another may be a common occurrence in marine plankton. For example, the replacement of Zn by Cd or Co have been observed in the carbonic anhydrase, the metalloprotein responsible of C uptake, of some eukaryotic species (Morel et al., 1994; Sunda

and Huntsman, 1995b). Type III co-limitation is the biochemical dependency of nutrients, where the ability to acquire one nutrient is dependent upon the sufficient supply of another, which is the case of Zn and C in the carbonic anhydrase (Price and Morel, 1990) or of Zn and P in the alkaline phosphatase (Shaked et al., 2006), which allows phytoplankton to acquire P from organic compounds. Whilst some nutrients can limit phytoplankton community as they are bioessential, some of them are toxic. Cu is an example of an essential trace metal, but that can be toxic to some phytoplankton taxa at relatively high concentrations (e.g. *Synechococcus*; Brand et al., 1986).

To sum up, phytoplankton organisms control the chemistry and cycling of biologically important trace metals in the sea, as different phytoplankton taxa and functional groups have different biological requirements for growth (e.g. Buitenhuis et al., 2008; Saito et al., 2010; Sarthou et al., 2005) leading to differences in intracellular nutrient quota and drawdown (e.g. Arrigo et al., 1999; de Baar et al., 1997; Ho et al., 2003; Quigg et al., 2003; Quigg et al., 2011; Twining and Baines, 2013; Twining et al., 2004a). The metals control in part the growth of the organisms and major nutrient cycling such as C and N.

1.3. The GEOTRACES program

Despite the recognized importance of trace elements in the ocean, the ability to exploit knowledge of their specific characteristics is limited by uncertainty regarding their sources, sinks, internal cycling and chemical speciation and by the lack of standardise sampling protocols across labs (Anderson et al., 2014). Therefore, to address these challenges an expert committee suggested in 2000 a new international program named the GEOTRACES program.

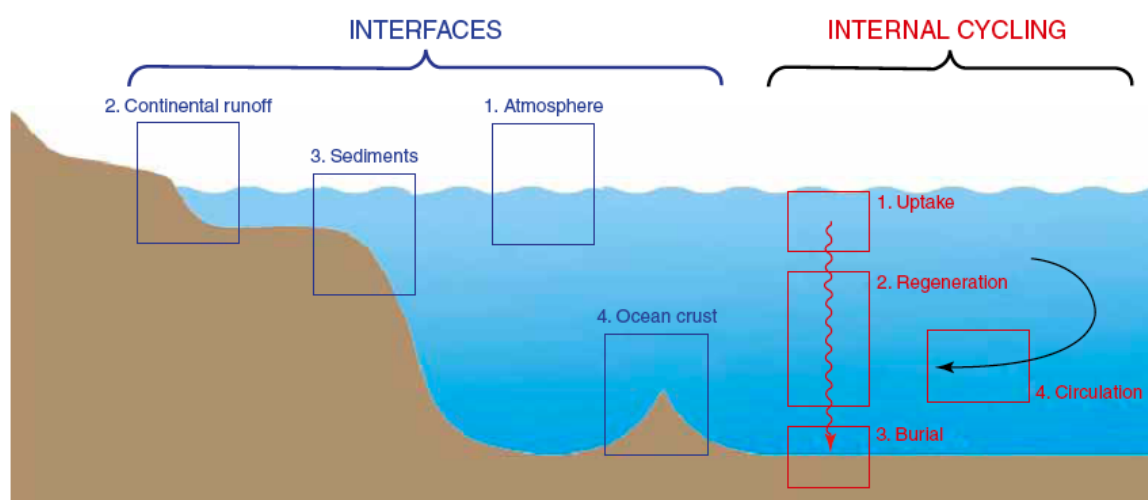


Figure 1.4: Figure illustrating the major sources (in blue) and processes (in red) influencing the distribution of the TEIs. From GEOTRACES Science Plan.

GEOTRACES aims at understanding the biogeochemical cycles of key trace elements and their isotopes (TEIs), identifying processes and quantifying fluxes that control TEIs large-scale distributions in important oceanic basins, assessing the sensitivity of these distributions in environmental conditions impacted by climate change, identifying proxies of the past environment and anticipating the response of biogeochemical cycles to global change (www.geotraces.org). To do so, one has to determine the processes and sources influencing TEIs distributions, define fluxes at four interfaces (ocean and continental runoff, sediments, atmosphere and ocean crust) and characterize four types of internal cycling (uptake, regeneration, burial and circulation, Fig. 1.4). In 2007, preliminary sampling occurred during the international polar year, in 2008, the first inter-calibrations were achieved and the data management started (see Chapter 2). The year 2010 marked the beginning of the initial sections and process studies with a main focus on (i) trace metal bioavailability, (ii) Redfieldian concepts of trace metal stoichiometry, (iii) the high-resolution distribution of trace metal, (iv) trace metal ligand composition and their role in their cycling, (v) the role of particle dynamics in trace metal cycles, (vi) the estimation of their fluxes and finally (vii) the discrimination between preformed and regenerated trace metal. Nowadays, synthesis begins, cruises continue. So far, in the frame of the GEOTRACES program, 100 cruises have been completed (Fig. 1.5) with the help of 17 nations and allow the publication of more than 900 articles.

*“organize **collaboration** to achieve objectives not attainable by a single lab – or even by a single nation”*

(Bob Anderson, at the first GEOTRACES summer school, Plouzané, 2017)

The GEOTRACES’ biggest appeal lying in these words.

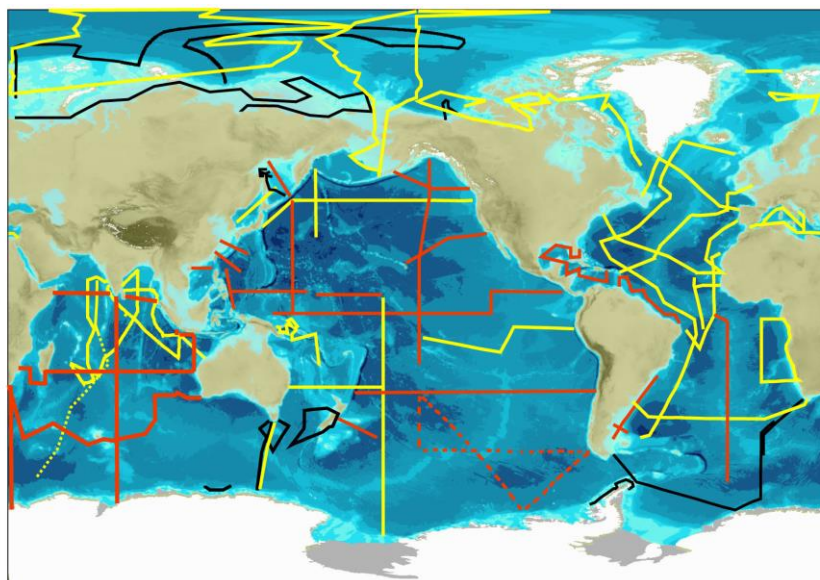


Figure 1.5: The GEOTRACES plan, the black lines symbolizing the cruises completed during the international polar year, the yellow lines cruises completed and the red lines, cruises to be done. Map from the GEOTRACES website (www.geotraces.org).

This thesis work falls within the GEOTRACES program, with a participation to two dedicated cruises (see section 1.6). Iron being the core element of this thesis, from now, we will only focus on Fe regardless other trace metals.

1.4. Physico-chemical speciation of Fe

The speciation of a chemical element corresponds to its distribution among its different physico-chemical species. The interaction of Fe with the marine food web depends greatly on its physical (soluble/colloidal/particulate) and chemical (organic/inorganic and redox) speciation (Fig. 1.6).

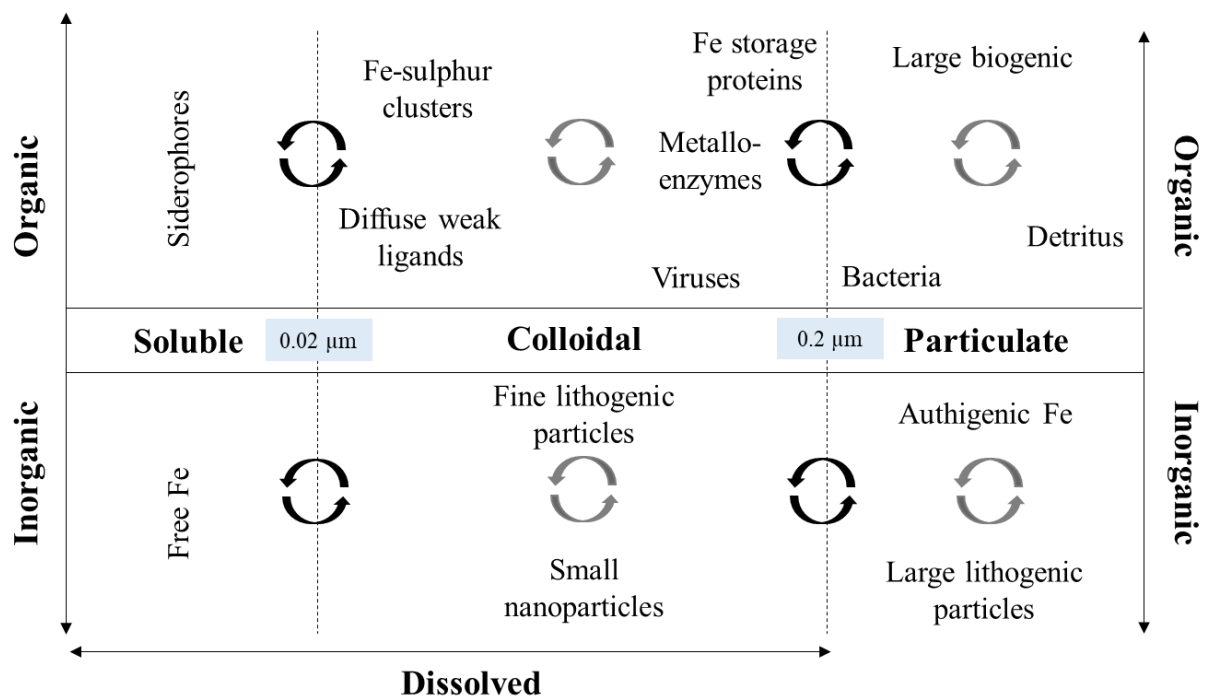


Figure 1.6: The components of particulate and dissolved iron pools (including the soluble and colloidal components) and the role of inorganic and organic components (adapted from Tagliabue et al., 2017).

1.4.1 Physical speciation

In the ocean, the physical speciation of Fe relies on separating the particulate Fe (PFe, which remains on a 0.2 - 0.45 μm filter, from the filtrate (dissolved Fe or DFe) (Bruland et al., 1994; Gordon et al., 1998a; Martin et al., 1989). The dissolved pool is composed of both soluble Fe (SFe, $< 0.02 \mu\text{m}$ or 10 kDa), and colloidal Fe (10 kDa or $0.02 \mu\text{m} < \text{CFe} < 0.2 \mu\text{m}$) operational size fractions (Wu et al., 2001).

1.4.1.1 Particulate pool

In the ocean, the pool of Fe is dominated by the particulate fraction (de Baar and de Jong, 2001). Marine particles exist in a continuous spectrum of sizes, but they can be operationally grouped into small colloids, a small size fraction (0.45 or 0.8 μm to 53 μm) and a large size fraction ($> 53 \mu\text{m}$). Although small colloids are light enough as not to quickly settle without further aggregation (Buffle et al., 1998), the two larger size fractions of particles (i.e. $> 0.45 \mu\text{m}$) present a molecular mass of more than 10^6 kDa (Lead and Wilkinson, 2007). The large size fraction of particles is more likely to sink vertically due to their density and consequently, has a shorter residence time (days to weeks) and contributes to most of the vertical particle flux (Lam and Marchal, 2015). The small size fraction corresponds to suspended particles which are less likely to sink, therefore their residence in the water column is relatively long (months) and they constitute most of the total particle mass (Bishop et al., 1977; Bishop et al., 1978; Bishop et al., 1985; Bishop et al., 1986; Bishop and Wood, 2008; Lam and Bishop, 2007). Advection by currents affect their transport. Aggregation and disaggregation processes that lead to the packaging of small particles and to the breakdown of large particles into small particles, respectively, can either be abiotic (e.g. from physical coagulation and from shear stress, respectively) and biologically mediated (e.g. from zooplankton faecal pellet production and from zooplankton fragmentation, respectively) (Fig. 1.7). Overall, the vertical distribution of particles is characterized by a surface maximum sustained by primary production, which decreases exponentially with depth. Some regions are characterized by strong intermediate and/or bottom nepheloid layers, resulting in profiles with surface and near-bottom maxima and a clear-water minimum in the 2000 – 3000 m depth range (e.g. Biscaye and Eittrheim, 1977; Brewer et al., 1976; Jeandel et al., 2015; Ohnemus and Lam, 2015).

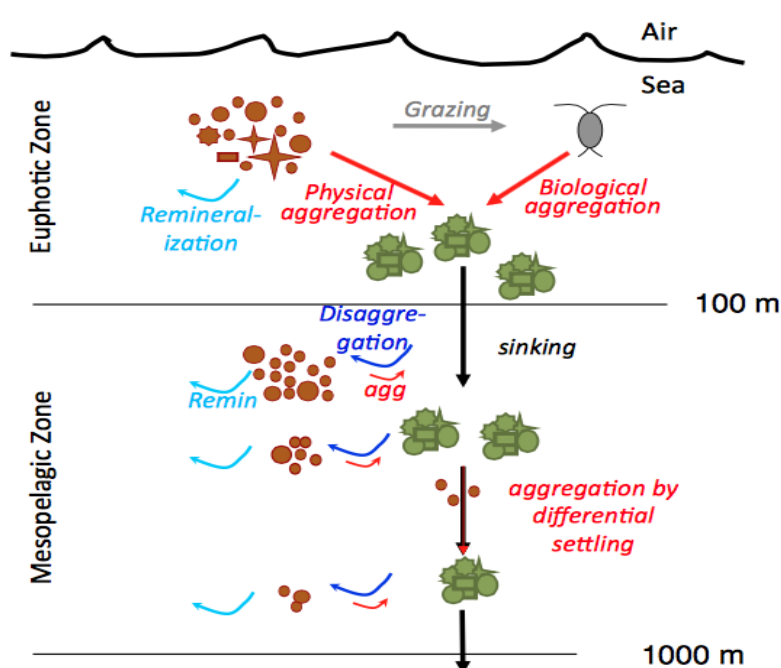


Figure 1.7: Schematic depiction of the biological carbon pump, emphasizing the important particle dynamics processes: aggregation (red arrows), sinking (black arrows), disaggregation (dark blue arrows), and remineralisation (light blue arrows). Particles in the small, suspended size fraction (brown) comprise phytoplankton, authigenic particles, and lithogenic particles. They do not sink or sink very slowly. Particles in the large, sinking size fraction (green) comprise faecal material and aggregates of smaller particles and do sink. Aggregation can be abiotic (physical) or mediated by zooplankton packaging through faecal pellet production (biological). Disaggregation can result, for example, from shear stress or can be biologically mediated. In this conceptual model, particles in the suspended size fraction (brown) decrease with depth because of remineralisation. From Lam and Marchal (2015).

The origin of the PFe pool to the ocean is an heterogeneous mix of either externally derived lithogenic material (i.e. alumina-silicates), transported to the ocean through erosion of continents, by rivers or by atmospheric deposition (Collier and Edmond, 1984; Duce et al., 1991; Duce and Tindale, 1991) or internally produced in the water column by marine biological activity including intra and extra-cellular Fe of living organisms as well as detrital material such as dead phytoplankton and faecal pellets and corresponding to the biogenic fraction of Fe or by authigenic precipitation of minerals (i.e. Fe and Mn oxyhydroxides) (Fowler and Knauer, 1986; Heller et al., 2017; Jeandel et al., 2015; Morel and Price, 2003; Revels et al., 2015; Tebo et al., 2004) which will each contain different coordination sites to bind Fe (Stumm, 1992). A large part of the lithogenic PFe is embedded in crystal matrices which are virtually inert due to their high thermodynamic stability (Wells et al., 1983) and therefore are not considered as bioavailable. The labile fraction, operationally defined as the acid leachable phase of total PFe (Berger et al., 2008), is more prone to be bioavailable to organisms (Frew et al., 2006; Kuma and Matsunaga, 1995) through reductive or non-reductive dissolution processes, transferring Fe from the particulate phase into the dissolved phase (Abadie et al., 2017; Homoky et al., 2016). Few micro-organisms are able to directly uptake particulate Fe, which is basically only the case of phytoplankton capable of phagotrophy (so-called mixotrophic species) as they bear a pseudopod which allow them to

engulf cellular content of other micro-organisms such as diatoms (Jacobson and Anderson, 1986) and bacteria (Maranger et al., 1998). In addition, PFe can also be remobilised by other phytoplankters such as the cyanobacteria *Trichodesmium* through an effective dissolution of particles (Rubin et al., 2011).

PFe concentrations vary considerably throughout the water column and between oceanic basins. However, this pool has received less attention than the dissolved, and as a result, is still rather unconstrained.

1.4.1.2 Dissolved pool

Dissolved Fe distribution is shaped by a combination of processes: external and internal inputs (see Section 1.5) and removal processes superimposed upon physical mixing and advection in the ocean basins. DFe exhibits a hybrid type behaviour demonstrating both nutrient-type (or recycled) profile shapes as well as scavenged-type (Bruland et al., 1994; Whitfield and Turner, 1987). Like major nutrients (nitrate, phosphate and silicic acid), DFe is depleted in remote oceanic surface ocean waters due to biological uptake or passive scavenging onto particles and appears to be regenerated at depth due to remineralization of both lithogenic and biogenic particles as part of the major biogeochemical cycles associated with plankton productivity (Blain et al., 2008a; Johnson et al., 1997a; Johnson et al., 1997b; Martin and Gordon, 1988; Sarthou et al., 2008). While affected by this kind of processes, DFe vertical profiles will exhibit surface water depletion and lower concentrations in younger intermediate waters than the concentration in older water masses. In contrast, in less productive waters of the oligotrophic central gyres, particularly in areas of high dust inputs, DFe can exhibit surface-water maxima highlighting its external sources and concentration loss along global thermohaline circulation more indicative of scavenged-type element (Bruland and Lohan, 2004; Bruland et al., 1994; Johnson et al., 1997a; Measures et al., 2008; Sarthou et al., 2007). However, while nutrient-type metals, with their relatively long oceanic residence times (e.g. $\sim 51,000$ years for zinc), tend to increase in concentration in deep waters of the ocean as the latter age, DFe concentrations vary with depth between oceanic basins as well as within the same oceanic basin. For example, Rijkenberg et al. (2014) reported overall decreasing DFe concentrations with depth (from 0.80 to 0.40 nmol L^{-1}) and lower variability ($\sim 0.20 \text{ nmol L}^{-1}$) compared to the DFe concentrations from the twilight zone ($\sim 0.40 \text{ nmol L}^{-1}$) in the west Atlantic Ocean, while DFe concentrations seemed to increase with depth in the different basins of the Southern Ocean varying from 0.40 to 0.70 nmol L^{-1} (Tagliabue et al., 2012). The DFe variability throughout the water column is likely due to its short residence

time, estimated to be ~ 200 years based on dust deposition alone as major Fe source, and appears to be controlled by three key processes: remineralization from the rain of both lithogenic and biogenic particles from above, particle scavenging (Johnson et al., 1997a) and organic speciation (Johnson et al., 1997b).

1.4.1.3 Soluble and colloidal pools

Within the DFe fraction soluble Fe (SFe, < 0.02 μm or 10 kDa), and colloidal Fe (10 kDa or 0.02 μm < CFe < 0.2 or 0.45 μm) pools (Wu et al., 2001) are still poorly studied and constrained. Indeed, colloids are compounds defined as solid phase entities that are operationally included in the dissolved size fraction. However, they retain their status as particles because they are physically distinct from the fluid via a surface boundary. Because of their diminutive size, colloids remain suspended until they aggregate to a size experiencing significant gravitational settling. Colloids thus serve the important role of transporting material between the dissolved and sinking particulate phases, thereby coupling two of the scavenging processes: a rapid initial adsorption of SFe onto colloid material in solution, followed by a slow aggregation of the colloids into particulate material of filterable size (Honeyman and Santschi, 1989). Colloids have been shown to contribute from 0 to 90% of total DFe across the global ocean and includes both inorganic (i.e. fine lithogenic particles and small nanoparticles) and organic species (see section 4.2.2) such as humic substances, exopolysaccharides, transparent exopolymers or Fe nanoparticles (as small as 5-60 Fe atoms per colloid) (Bergquist et al., 2007; Boye et al., 2010; Chever et al., 2010; Cullen et al., 2006; Fitzsimmons and Boyle, 2014a; Kondo et al., 2008; Nishioka et al., 2001; Schlosser and Croot, 2008; Ussher et al., 2010; Wu et al., 2001; Wu and Luther, 1994). The colloidal phase can be directly measured using flow field-flow fractionation (e.g. Stolpe et al., 2010) but is usually operationally defined as the subtraction of the soluble phase, determined by ultra-filtration, from the dissolved phase (eq. 1.5):

$$CFe = DFe - SFe \quad (\text{eq. 1.5})$$

SFe includes the free species Fe^{2+} and Fe^{3+} , the inorganic species $\text{Fe(II)}'$ and $\text{Fe(III)}'$ as well as species organically bound to ligands of low molecular mass (e.g. siderophores) (see section 1.4.2.2).

Incubation studies have shown that while a limited number of CFe forms are highly bioavailable (such as exopolymeric saccharide Fe complexes, Hassler et al., 2011a), SFe is typically more bioavailable and is taken into the cell much faster than CFe which requires first a dissociation from the colloid into the soluble phase before being taken into the cell

(Chen et al., 2003; Chen and Wang, 2001; Wang and Dei, 2003). Crystalline inorganic CFe (such as nanoparticulate Fe oxyhydroxide) generally has low bioavailability to marine phytoplankton (Rich and Morel, 1990; Wells et al., 1983), although freshly precipitated amorphous CFe nanoparticles have been found to be somewhat bioavailable to coastal species (Kuma and Matsunaga, 1995). SFe and CFe undergo different sinks with SFe experiencing sorption or desorption and CFe experiencing aggregation or disaggregation, consequently, the two dissolved phases may have inherently different residence times.

To sum up, the mass balances for Fe when considering its physical distribution can be described as:

$$Fe_{total} = PFe + CFe + SFe \quad (\text{eq. 1.6})$$

1.4.2 Chemical speciation

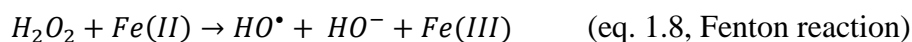
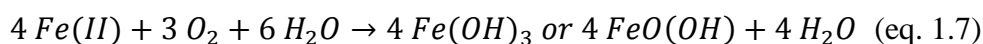
Another way of addressing Fe speciation in the ocean is based on chemical characteristics, including the redox and the organic/inorganic speciation. Both of them help understanding the fate of Fe in seawater by giving information on its stability, kinetics and bioavailability.

1.4.2.1 Redox speciation

Under most natural conditions, Fe is found in the +(II) and +(III) oxidation states and forms salts with the majority of common anions. Within the Fe redox couple Fe(III)/Fe(II) characterized by the standard potential $E^0 = 0.771 \text{ V}$, Fe(II) is the reduced form and Fe(III) is the oxidized form and are called ferrous and ferric compounds, respectively. The inorganic species gather hydrolysed species and species complexed to inorganic ligands: Fe(II)' and Fe(III)'.

In aerated aqueous solutions at circumneutral pH, the $\text{Fe}(\text{H}_2\text{O})_6^{3+}$ cation is hydrolysed to form polynuclear oxy-hydroxides. The Fe(III)' species include, ordered from most to least concentrated in seawater at pH 8, $\text{Fe}(\text{OH})_3$, $[\text{Fe}(\text{OH})_4]^-$, $[\text{Fe}(\text{OH})_2]^+$, Fe^{3+} and for the less widespread, $[\text{FeCl}]^{2+}$, $[\text{FeCl}]^+$, FeF_2^+ , FeF_3 , FeSO_4^+ and $\text{Fe}(\text{OH})^{2+}$ (de Baar and de Jong, 2001). In oxic conditions, Fe(III)' is thermodynamically stable but highly insoluble (10 pmol.L^{-1}) as reported by Liu and Millero (1999) for Fe(III)' hydroxide in 0.7 M NaCl (pH 8.1, 25°C) and in seawater (Liu and Millero, 2002). Indeed, with time, Fe(III)' oxyhydroxides dehydrate and progressively crystallize into Fe(III)' oxides, thus decreasing their solubility.

Fe(III)' most refractory forms, Fe(III)' oxyhydroxides, are therefore less and less bioavailable for phytoplankton (Kuma and Matsunaga, 1995; Wells and Mayer, 1991a). The rest of its forms being highly reactive, Fe(III) is easily adsorbed onto surface particles (lithogenic and biogenic) and is consequently, quickly removed from the water column by particle settling. The Fe(II)' species gather, still ordered from most to least concentrated in seawater at pH 8, Fe^{2+} , $[\text{Fe}(\text{CO}_3)]$, $[\text{FeOH}^+]$, FeHCO_3^+ , $[\text{Fe}(\text{CO}_3)_2]^{2-}$ and $\text{Fe}(\text{OH})_2$ (de Baar and de Jong, 2001). The solubility of Fe(II) greatly exceeds that of Fe(III) in seawater but is not stable in oxic environment and $\text{pH} > 5$. It promptly oxidizes into Fe(III) due to the presence of either dioxygen (O_2 , eq. 1.7) or hydrogen peroxide (H_2O_2 , eq. 1.8) (Gonzalez-Davila et al., 2005; Millero and Sotolongo, 1989; Millero et al., 1987; Santana-Casiano et al., 2006; Santana-Casiano et al., 2004).



Hence, oxic aqueous solutions at seawater pH are predicted to contain negligible Fe(II) at equilibrium (Stumm and Morgan, 1996). The occurrence of Fe(II) at detectable levels in such oxygenated seawater requires, therefore, continuous inputs and slow oxidation. The oxidation of Fe(II) also greatly depends on the ionic strength (Millero and Izaguirre, 1989) and on the temperature (Millero and Sotolongo, 1989) of seawater. However, when the oxidation of organic material reduces oxygen concentrations at levels typical of suboxic or anoxic environments, Fe(II) is stable (Gledhill and van den Berg, 1995; O'Sullivan et al., 1991) and can be found at mmol L^{-1} concentrations and its solubility will then depend upon the precipitation of Fe(II)-sulfide from the redox couple sulfate/sulphide (Blain and Tagliabue, 2016). Accordingly, significant Fe(II) concentrations can be found near hydrothermal vent systems (Breitbarth et al., 2010), sediments (Coleman et al., 1993; Pakhomova et al., 2007), oxygen minimum zones (Kondo and Moffett, 2015; Kremling, 1983; Vedamati et al., 2014), rainwater (Kieber et al., 2003) and snow (Zhuang et al., 1995). The production mechanism of Fe(II) within the water column are mainly linked to photochemical reduction processes occurring within surface waters of the ocean (Barbeau et al., 2001; Wells and Mayer, 1991b). It also seems that Fe(II) is produced through the activation of Fe biological uptake mechanisms (Chase and Anderson, 2004; Kustka et al., 2005; Maldonado et al., 2001; Maldonado and Price, 1999; Rose et al., 2005).

The fact that DFe concentrations, despite being low, were observed above its inorganic solubility limit has been attributed to the presence of natural organic ligands (Johnson et al., 1997b; Liu and Millero, 2002). For over 20 years now, it is known that more than 99 % of

this fraction is bound to organic ligands (Rue and Bruland, 1995). Organic ligands avoid Fe precipitation and hydrolysis at the pH of seawater by increasing its solubility through an equilibrium between free and complexed forms of Fe that favours complexation with strong ligands due to the chelate effect. This in turn may increase its residence time in the surface of the ocean (Boyd and Ellwood, 2010; Gledhill and Buck, 2012; Hunter and Boyd, 2007). Moreover, organic ligands may increase Fe bioavailability, thus playing a key role in its oceanic biogeochemical cycle (Hassler et al., 2011a; Maldonado and Price, 1999).

1.4.2.2 Organic speciation

The existence and the importance of total dissolved Fe-binding organic ligand (DLt) in the biogeochemical cycle of Fe has been recognized since 1994 (Gledhill and Van Den Berg, 1994). The main result was that 99% of DFe measured in the upper 1000m in the Northeast Atlantic Ocean was bound to natural organic ligands. Further studies confirmed their ubiquity throughout the water column (e.g. Boye et al., 2001; Gerringa et al., 2008; Gledhill and Buck, 2012; Rue and Bruland, 1995; Van den Berg, 1995; Wu and Luther, 1995).

Iron organic speciation is assessed using voltammetry technics which enable the quantification of DFe (or SFe, or CFe) concentration, the total DLt (or SLt, or CLt) and their associated conditional stability constants ($K'_{FeL_i,Fe'}^{cond}$ or $K'_{FeL_i,Fe^{3+}}^{cond}$; reported either with respect to $[Fe'(III)]$, hereafter $[Fe']$, or $[Fe^{3+}]$, respectively) expressing ligand affinity to Fe,

$$\text{i.e. } K'_{FeL_i,Fe'}^{cond} = \frac{[FeL_i]}{[Fe'][L'_i]} \quad (\text{eq. 1.9})$$

where $[Fe']$ represents all the inorganic species of DFe(III) (see Section 1.3.1.1). $K'_{FeL_i,Fe'}^{cond}$ can be converted to $K_{FeL_i,Fe^{3+}}^{cond}$ (conditional stability constant with respect to Fe^{3+}) using the inorganic side reaction coefficient ($\alpha'_{Fe} = [Fe']/[Fe^{3+}]$) as follow:

$$K_{FeL_i,Fe^{3+}}^{cond} = \alpha'_{Fe} K'_{FeL_i,Fe'}^{cond} \quad (\text{eq. 1.10})$$

In this thesis, $\alpha'_{Fe} = 10^{10}$ at pH 8 was used (Hudson et al., 1992; Kuma et al., 1996; Liu and Millero, 2002; Millero, 1998; Sunda and Huntsman, 2003). The measured conditional stability constant operationally defines the ligand class to which it belongs.

These classes have been separated into four classes: the first class (L_1) corresponds to a $\log K'_{FeL_i, Fe'}^{cond} > 12$; the second class (L_2) corresponds to a $\log K'_{FeL_i, Fe'}^{cond} = 11-12$, the third class (L_3) corresponds to a $\log K'_{FeL_i, Fe'}^{cond} = 10-11$, and the fourth class (L_4) corresponds to a $\log K'_{FeL_i, Fe'}^{cond} < 10$. They refer to the strong, intermediate and weak (L_3 and L_4) ligand classes, respectively (Gledhill and Buck, 2012). In the meantime, it has also been recommended to report excess ligand concentrations ($[L']=[L]-[DFe]$) as a proxy for ligand under saturation (e.g. Boye et al., 2001; Rijkenberg et al., 2008; Witter et al., 2000; Witter and Luther, 1998; Wu and Luther, 1995). Consequently, the mass balance from a chemical perspective might be described as:

$$Fe_{total} = Fe' + FeL + Fe_{inert} \quad (\text{eq. 11})$$

Where Fe_{inert} represents the Fe fraction bound up in matrices that are essentially non-labile (Gledhill and Buck, 2012).

Distribution of Fe-binding ligands in the marine environment

While DLt are present seemingly everywhere, from surface to deep waters of the coastal and open ocean, there are some distinguishable trends in their distributions and thermodynamic characteristics (Gledhill and Buck, 2012). In most cases, ligand concentrations were measured in excess of DFe concentrations (Gledhill and Buck, 2012), with the highest and the most variable ligand concentrations relative to DFe observed in the surface ocean (e.g. Boye et al., 2001; Gerringa et al., 2008; Rue and Bruland, 1995; Van den Berg, 1995; Wu and Luther, 1995), often with stronger stability constants (Bruland and Rue, 2001; Hunter and Boyd, 2007). In contrast, the deep ocean exhibited more or less constant profiles often close to saturation (Boye et al., 2006; Boye et al., 2010; Boye et al., 2001; Ibanmami et al., 2011; Nolting et al., 1998; Rue and Bruland, 1995; Van den Berg, 1995), with the presence of L_1 -type in the top hundred meters of the water column and the L_2 -type throughout the water column (Cullen et al., 2006; Ibanmami et al., 2011; Rue and Bruland, 1995, 1997). L_3 -type was reported to be relatively constant down to ~ 500 m depth with a slight minimum in surface waters (Bundy et al., 2016) and has been reported to be the result of particulate organic matter remineralization by the heterotrophic community (Boyd et al., 2010). L_4 -type ligands are presumed to stay in the water column only under certain conditions and on a certain timescale. Although they have been reported to be produced

during biological incubation experiment, yet they have not been identified in the water column but received less attention than L_1 - and L_2 -type ligands (Bundy et al., 2016).

Within the surface layer, it has been shown that the highest DLt concentrations (Fig. 1.8) were often associated with the chlorophyll biomass maxima (Boye et al., 2006; Boye et al., 2001; Buck and Bruland, 2007; Croot et al., 2004; Gerringa et al., 2008; Gerringa et al., 2006; Ibisani et al., 2011; Rue and Bruland, 1995; Tian et al., 2006; Van den Berg, 1995, 2006; Wagener, 2008) and to low DFe concentrations, consequently linking the production of Lt to biological uptake of Fe in Fe-limited areas (e.g. Buck and Bruland, 2007). The excess of DLt without any chlorophyll biomass maxima, for its part, may alternatively be the remnants of previous blooms as demonstrated by Sato et al. (2007) due to the presence of grazers (Fig. 1.8). It could also be the result of, depending on the study area, wet or dry atmospheric inputs (Gerringa et al., 2007; Kieber et al., 2001) as DFe and DLt are both present in clouds (Boutorh et al., 2017) and in rainwater (Cheize et al., 2012), though dust deposition can lead to a reduction in excess ligand (Rijkenberg et al., 2008) (Fig. 1.8). DLt have also been shown to be delivered to surface by sea ice melting (Lannuzel et al., 2015), river plumes (Buck et al., 2007; Kondo et al., 2007; Powell and Wilson-Finelli, 2003; Slagter et al., 2017) and with bacteria through the remineralisation of particles regardless of their nature (Vraspir and Butler, 2009) (Fig. 1.8).

Anomalously high excess ligand concentrations in some specific environment such as shelf and bottom boundary layers (Fig. 1.8) have been reported and can even be higher than in most of surface waters (Batchelli et al., 2010; Boye et al., 2003; Buck et al., 2007; Croot and Johansson, 2000; Gerringa et al., 2008; Gobler et al., 2002; Johnson et al., 2007; Kondo et al., 2007). Recently, Gerringa et al. (2017) highlighted the presence of L' associated to high DFe concentrations from a mud-volcano, in addition to the hydrothermal source of ligands highlighted by Bennett et al. (2008). Hydrothermal DFe was shown to be transported about 4,300 km from its hotspot source (e.g. Southern East Pacific Rise, Fitzsimmons et al., 2017; Resing et al., 2015). Such behaviour was unexpected regarding Fe chemistry in seawater (see Section 3.2.1) and complexation of DFe to strong DLt was proposed as one explanation (Tagliabue et al., 2014a, see Section 1.5.4 for other explanation) and have been demonstrated to be part of the strong (L_1) ligand type (Buck et al., 2018; Buck et al., 2015; Fitzsimmons et al., 2017). However, within the hotspot, ligands are rather saturated with DFe resulting in relatively high DFe' concentrations (Buck et al., 2018; Buck et al., 2015; Gerringa et al., 2017).

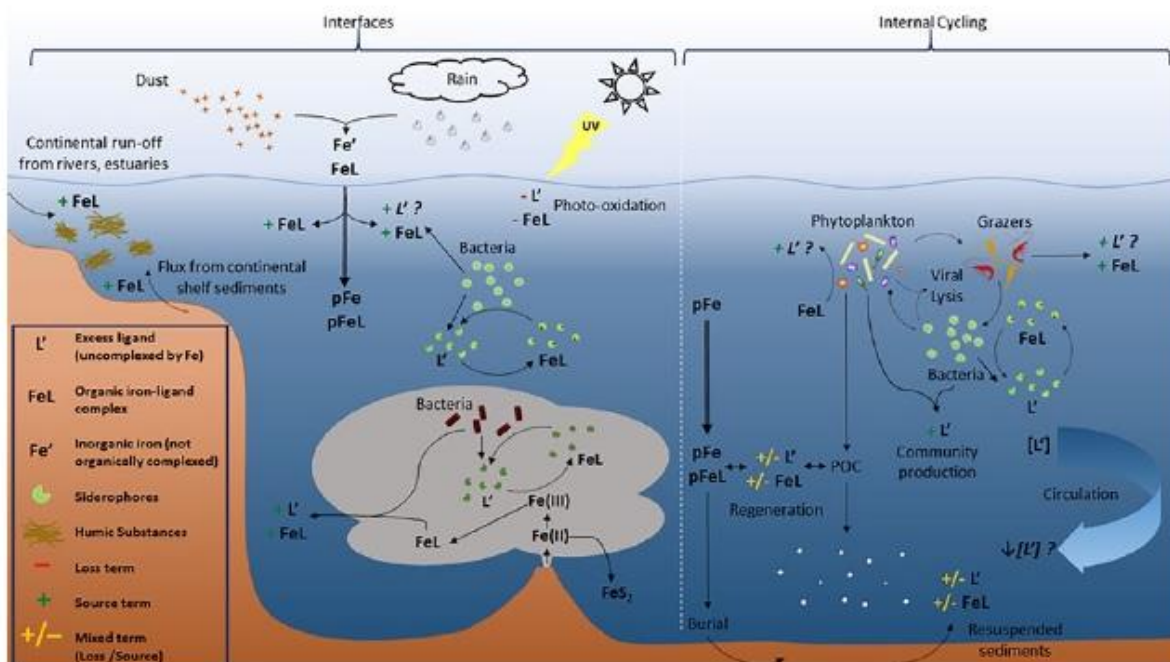


Figure 1.8: Schematic of iron-binding ligand cycling in the ocean. From Buck et al. (2016).

The study of the organic speciation of the soluble and colloidal fractions demonstrated that the soluble component seems to exhibit much higher concentrations than the colloidal component (Boye et al., 2010; Cullen et al., 2006; Kondo et al., 2008; Thuróczy et al., 2010), soluble Fe-binding organic ligands (SLt) being more concentrated in the surface layer, colloidal Fe-binding organic ligands (CLt) closer to saturation throughout the water column (Gledhill and Buck, 2012; and references therein). Kondo et al. (2008) highlighted, during an artificial fertilization experiment (SEEDS II) that while the excess DLt was decreasing due to the addition of Fe, which saturated the ligands, excess of soluble ligand concentrations was increasing in the soluble fraction during the bloom decline.

Nature of Fe-binding organic ligands

The origin of these organic ligands is either directly produced from bacteria and phytoplankton (e.g. porphyrins, siderophores, domoic acid) in the ocean, or as a result of cell lysis or grazing and/or have a terrestrial origin (i.e. humic substances). Siderophores (Fig. 1.9) are produced by bacteria, and a wide range have been identified in seawater using mass spectrometric techniques (Boiteau et al., 2013; Mawji et al., 2011; Mawji et al., 2008b; Velasquez et al., 2011) and have been shown to incorporate low molecular weight hydroxamate-, catecholate-, and/or a α -hydroxy carboxylate-binding subunits arranged in different architectures (Barbeau et al., 2003). Porphyrins (Fig. 1.9), which include

chlorophylls and its degradation products (i.e. phaeophytin, hemes and vitamin B12), are produced by almost all organisms via a well conserved tetrapyrrole biosynthesis pathway (Mochizuki et al., 2010). Although, they function as prosthetic groups in proteins and are useful for their ability to absorb light, transfer electrons, and bind oxygen their production are tightly controlled as they cause oxidative stress if present in excess of their proteins (Mochizuki et al., 2010). They bind Fe(III) spontaneously but they present a low solubility at seawater pH (Rijkenberg et al., 2006; Schlosser and Croot, 2008). Domoic acid (DA), a toxin for higher trophic level produced by the diatom *Pseudo-nitschia*, is also able to bind Fe but with low affinity ($K_{FeDA,Fe}^{cond} = 8.7$, Rue and Bruland, 2001). Humic substances (HS, Fig. 1.9) are also a big part of the ligand pool if not the main part. Their composition is dominated by polyphenol and carboxylic and/or benzoic acids (Buffle, 1990). They are divided into two groups depending on their solubility: fulvic acids being soluble at pH 1 and humic acids precipitating at the same pH, but present similar stability constant ($K_{FeHS,Fe}^{cond}$ 10.6 and 11.1, respectively) with concentrations as high as the $\mu\text{g HS L}^{-1}$ (Laglera et al., 2007; Laglera and van den Berg, 2009; Whitby et al., 2018). Quite recently, it has been demonstrated that saccharides, including exopolysaccharides (EPS), are also part of the ligand pool as they complex Fe which is then directly bioavailable for phytoplankton organisms (Hassler et al., 2011a; Hassler and Schoemann, 2009). Hassler et al. (2011a) highlighted that only 1 nmol L⁻¹ of EPS is enough to solubilize Fe principally in the colloidal phase.

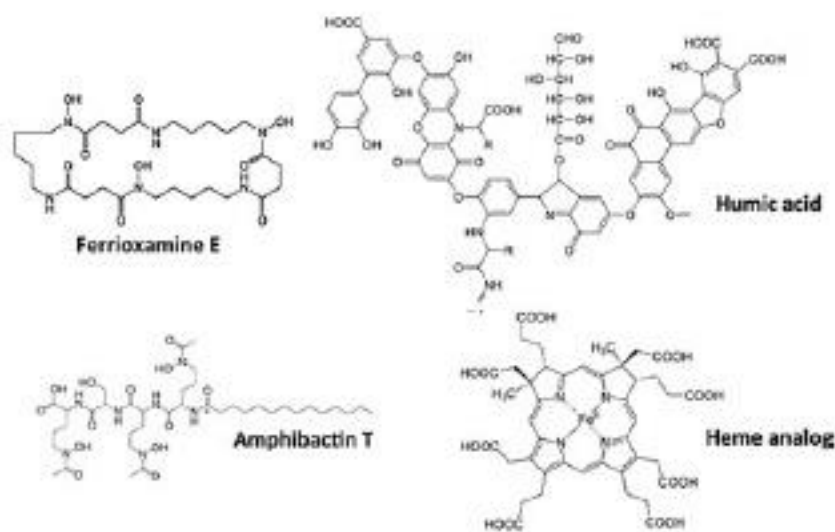


Figure 1.9: Examples of organic-iron binding ligand identities in seawater. The heme analog is siroheme, a relatively soluble iron-containing heme complex. From Buck et al. (2016).

Link between biological activity and ligand concentrations

As aforementioned, many field studies have commonly found highest L' concentrations within and around the biomass maxima (e.g. Rue and Bruland, 1995; Van den Berg, 1995, 2006). However, the direct link between organically bound Fe and its reductive assimilation has only been revealed for some phytoplankton taxa (Hutchins et al., 1999; Maldonado et al., 2005) (Maldonado and Price, 2001; Shaked et al., 2005).

Marine heterotrophic and phototrophic bacteria exude siderophores, that is to say high Fe affinity molecules (Homann et al., 2009; Ito and Butler, 2005; Martinez and Butler, 2007; Martinez et al., 2003; Martinez et al., 2000), to tackle the Fe-depleted conditions within their environment and to adsorb the Fe-siderophore complexes. It is known that many microorganisms are able not only to utilize their own siderophores, but also to assimilate siderophores from numerous other bacteria (Wilhelm and Trick, 1994). If the adsorption of these complexes are not bacteria species-specific (Stintzi et al., 2000), it does not mean that they are all bioavailable for phytoplankton species. Indeed, Hutchins et al. (1999) reported that Fe(III)-siderophore complexes seem to be more readily available to the prokaryotic phytoplankton community, while Fe(III)-porphyrin complexes are more readily available to the eukaryotic diatoms. Eukaryotic diatoms are not known to have the receptors sites to assimilate Fe(III)-siderophores directly, but they can utilize cell surface reductase systems to reduce the Fe(III) bound to the siderophore, and the resulting Fe(II) can either dissociate and become available (as Fe(II)') or can be reoxidized to Fe(III)' and become available for assimilation (Maldonado and Price, 2001). It has also been shown by Barbeau et al. (2003) that α -hydroxy carboxylate groups are stable as uncomplexed acids, but when coordinated to Fe(III) they undergo light-induced ligand oxidation and reduction of Fe(III) to Fe(II). However, these photoreduction processes are strongly dependent on the identity of the FeL (Barbeau et al., 2003; Rijkenberg et al., 2006). After the breaking down of the siderophore ligands induced by light, photo-degradation products are generated and exhibit weaker conditional stability constants similar to the L₂ class of ligands observed in surface waters which are more readily available for phytoplankton than the original Fe(III)-siderophore (Barbeau et al., 2001; Rue and Bruland, 1995).

In summary, although ligands have been found to be ubiquitous compounds throughout the water column, their respective classes determined as a function of their strength are dependent on their sources and are thus localised at specific depth-ranges. Modelling studies have highlighted the importance of organic ligands in determining the

thermodynamic solubility of Fe and have showed that variations in organic ligand concentrations and stability constants influence the residence time and potential bioavailability of Fe (Tagliabue et al., 2009; Tagliabue et al., 2017; Tagliabue and Volker, 2011). Finally, Völker and Tagliabue (2015) used a model in which ligands were produced from organic matter remineralisation and phytoplankton processes, and lost through bacterial and photochemical degradation, aggregation and through phytoplankton uptake. With their model, aimed at linking *in-situ* measurements to obtain a broader view of large-scale processes, they were able to reproduce the decreasing ligand concentrations along the conveyor belt circulation in the deep ocean, the Southern Ocean lower surface and subsurface concentrations and the enhanced ligand concentrations in the mesopelagic area compared to the abyssal ocean. Although large-scale processes and more specifically open-ocean data were well represented by the model, surface (0-50 m) data and ocean-land boundaries were still poorly constrained (Fig. 1.10).

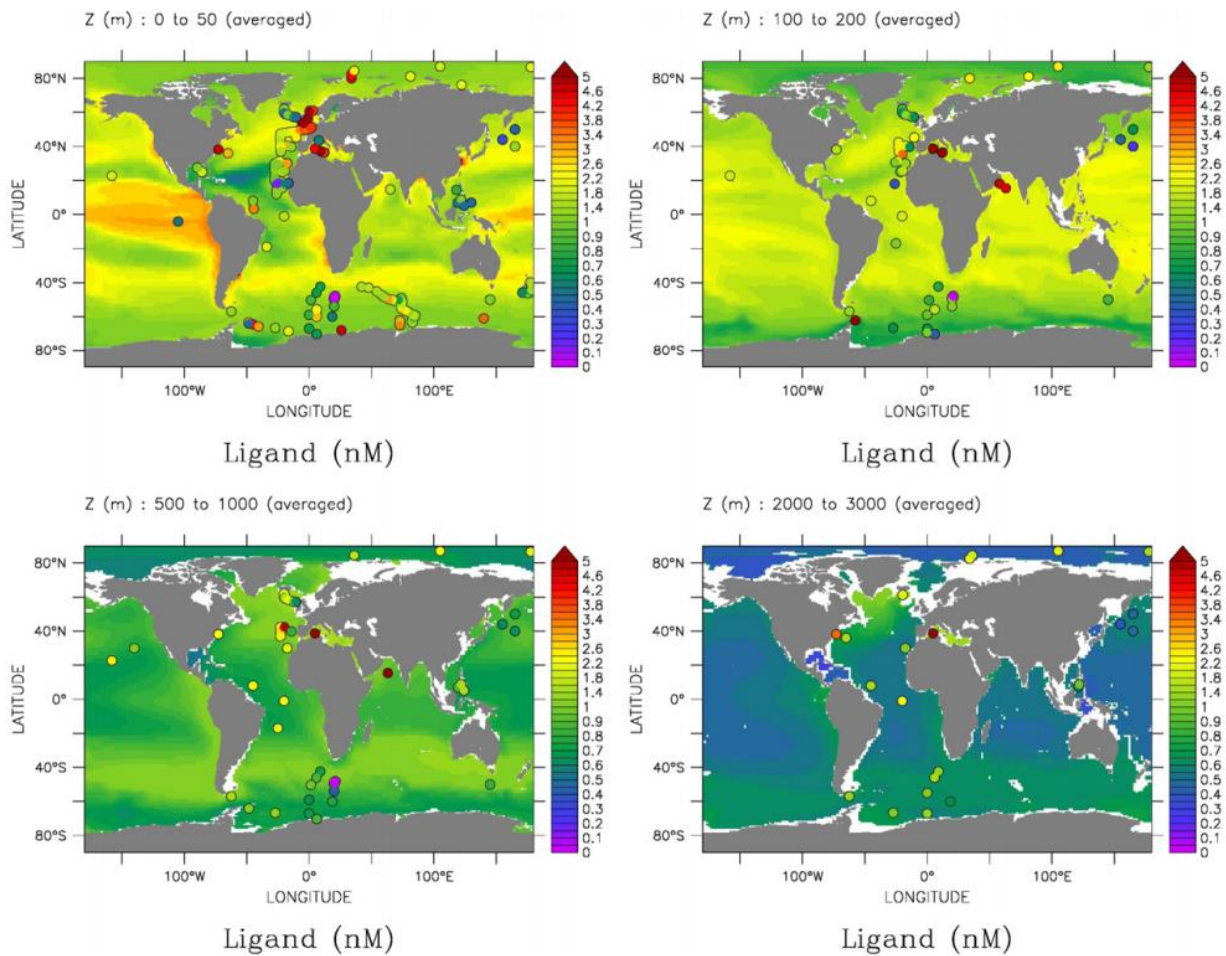


Figure 1.10: Ligand distribution as determined by the model of Völker and Tagliabue (2015) and *in-situ* measurements plotted as dots using the same color coding.

1.5 Biogeochemical cycle of Fe

In the following section, the different sources and processes shaping the biogeochemical cycle of Fe are detailed below (Fig. 1.11).

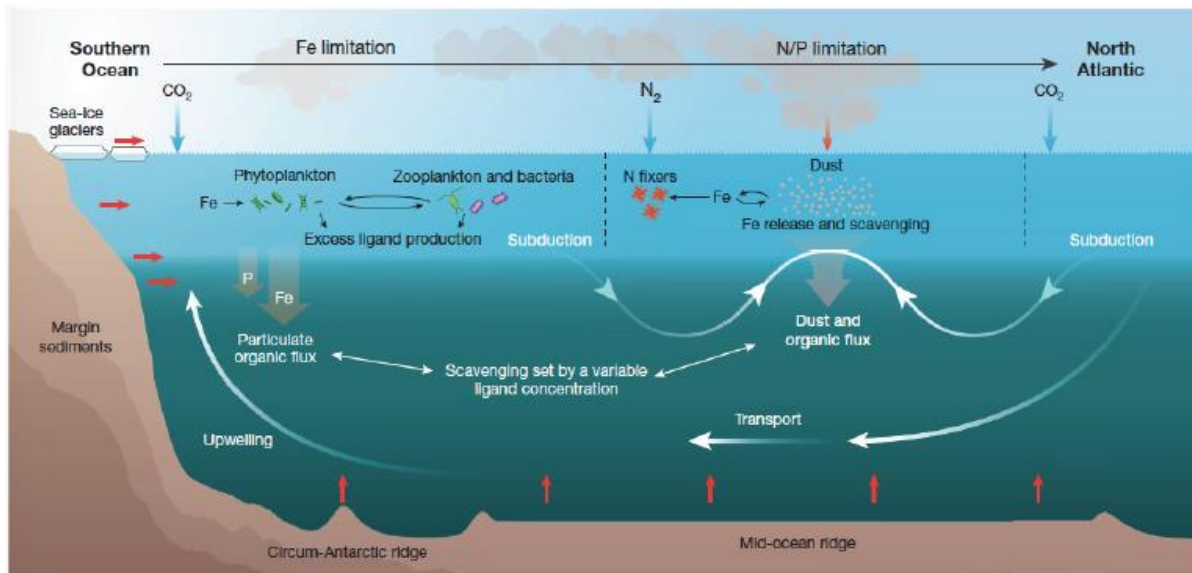


Figure 1.11: A revised representation of the major processes in the ocean iron cycle, with emphasis on the Atlantic Ocean. They draw attention to a broad meridional contrast between the iron-limited Southern Ocean and the major nutrient-limited low-latitude regimes. Dust remains dominant in the low latitudes, but continental margin and upwelled hydrothermal sources + winter entrainment are more important in the Southern Ocean. Flexible iron uptake and biological cycling, along with the production of excess iron-binding ligands, dominate the Southern Ocean, whereas nitrogen fixation occurs in the low latitudes (although this process can also be restricted by lack of iron outside of the north Atlantic subtropical gyre). The particulate organic iron flux is decoupled from that of phosphorus at high latitudes and the flux of lithogenic material is important at low latitudes influenced by dust. Subduction of excess organic iron binding ligands from the Southern Ocean has a remote influence on the interior ocean at low latitudes. From Tagliabue et al. (2017).

1.5.1 External sources of Fe

In the ocean, DFe is scavenged on particles (see Section 1.4.1.2), which can be further lost from the water column due to sediment burial. Therefore, external sources of Fe are crucial to counter-balance losses. In this section, the main external sources of Fe to ocean are presented in relation to their bioavailability.

1.5.1.1 Atmospheric deposition

Although atmospheric deposition accounts for only 2% of the column integrated Fe inventory (Tagliabue et al., 2014a), it is the main source of DFe to the open ocean surface waters, especially at low latitude and in the Atlantic Ocean (e.g. Duce and Tindale, 1991; Jickells et al., 2005; Ussher et al., 2013). This external source of Fe includes two main

origins, namely desert dust deposition and combustion that represent 95 and 5% of the global atmospheric Fe cycle, respectively (Mahowald et al., 2009).

Fe dust supply is primarily controlled by the uplift of dust from terrestrial systems, whose main source regions are characterized by enhanced soil aridity. Hence, the source regions are predominantly located in North Africa, the Arabian Peninsula, Central Asia, China, Australia and Southern Africa (Ginoux et al., 2012; Mahowald et al., 2005). The uplift of dust is sensitive to local conditions such as local wind speeds and humidity that needs to exceed a threshold velocity to transport soil grains horizontally (Prospero, 2002). Once aerosols reach the upper atmosphere they can be transported over long distances depending on the rate of gravitational settling and the particle size (Kallos et al., 2006; Maring et al., 2003). During this transport, dust is exposed to unique chemical conditions that modify its speciation and solubility (Hand et al., 2004). Fe deposition to the ocean is then a function of dry and wet (including rain and snow) deposition with Fe on larger particles assumed to fall closer to the source (Jickells et al., 2005) and to be less soluble (~1%) than the Fe associated with finer particles transported farther away (10-40%) (Fan et al., 2006).

Although atmospheric deposition represents a huge part of the external sources of Fe the extent to which this Fe is bioavailable is still poorly constrained. The fractional solubility of aerosol trace metals is dependent on a number of factors, such as aerosol type (mineral dust, industrial emissions, sea salt, volcanic), particle size (finer particles are generally more soluble than coarse ones), or atmospheric processes (Baker and Croot, 2010). This solubility can vary from 0% to 100% (e.g. Shelley et al., 2018). After contact with seawater, Fe from atmospheric particles will undergo rapid dissolution with the vast majority of dissolvable Fe mobilised within the first few minutes (Desboeufs et al., 2005; Mackey et al., 2015). After this time lapse, Fe is more prone to be scavenged onto particles.

Recently, it has been suggested that the amount of atmospheric organic acids control the binding of soluble aerosol Fe with organic ligands once the Fe equilibrates in seawater with over 95% of the soluble Fe potentially able to bind to marine organic ligands (e.g. Fishwick et al., 2014; Meskhidze et al., 2017). On the other hand, many studies argued that the aerosol trace metal fractional solubility is driven by the amount of DOM in seawater (Bressac and Guieu, 2013; Bressac et al., 2014; Desboeufs et al., 2014; Paris and Desboeufs, 2013; Wagener et al., 2008). High and fresh DOM conditions induce a negative feedback on DFe concentrations through rapid formation of aggregates, whereas low DOM conditions allow a transient increase in DFe concentrations before being removed by adsorption onto settling particles (Bressac and Guieu, 2013).

1.5.1.2 Riverine inputs

Rivers carry with them large quantities of Fe in both the dissolved and particulate fractions but mainly in the form of suspended sediments (de Baar and de Jong, 2001; Poulton and Raiswell, 2002). They are of great importance at a regional scale with stronger Fe supply from low-latitude Atlantic and northern Indian oceans (Gaillardet et al., 2014) with average DFe concentrations of 720 nmol L^{-1} in freshwaters and a DFe input to estuaries of $0.47 \text{ Gmol yr}^{-1}$ (de Baar and de Jong, 2001). More recently, Chester and Jickells (2012) re-evaluated the river Fe supply to be of 4.2 Gmol yr^{-1} . However, due to the salinity gradient, the majority of this DFe flocculates and is removed to the particulate phase within estuaries (Sholkovitz, 1978). Interestingly, this PFe has been reported by Berger et al. (2008) and by Buck et al. (2007) to be rich in labile Fe thus potentially constituting an additional source of DFe to the coastal zone. Indeed, rivers have been reported to be highly concentrated with Fe-binding organic ligands, especially humic substances (Slagter et al., 2017) and even the presence of strong L_1 -type ligand have been reported to be correlated to DFe concentrations (Buck et al., 2007). Moreover, Krachler et al. (2005) reported that terrigenous fulvic-iron complexes originating from weathering processes occurring in the soils upstream can act as natural ocean fertilizer with important amount of bioavailable Fe (up to $480 \mu\text{g L}^{-1}$). Thus, the influence of river-derived Fe on oceanic concentrations greatly depends on its organic speciation that can stabilize river Fe in the dissolved form over long distances (Krachler et al., 2015; Laglera and van den Berg, 2009).

1.5.1.3 Sediment inputs

Fe flux from sediments, including sediment resuspension events and associated pore-water release, lead to high DFe concentrations in coastal waters (Blain et al., 2008c; Chase et al., 2005; Elrod et al., 2004; Hatta et al., 2015; Lohan and Bruland, 2008; Measures et al., 2013) and could be as large as the atmospheric inputs (Moore and Braucher, 2008). Two processes supply DFe from the sediment to the benthic boundary layer (BBL), reductive and non-reductive dissolution (Conway and John, 2014; Homoky et al., 2013; Radic et al., 2011).

Continental shelves receive large amounts of organic material and thus early diagenesis processes occur. Indeed, remineralisation can lower sediment oxygen concentrations, promoting reductive dissolution of PFe oxyhydroxides to DFe that can then diffuse across the sediment water interface as DFe(II) colloids (Homoky et al., 2011). Such processes will not lead to further transport of DFe moving to more oxygenated water masses

due to back precipitation, unless complexation with Fe-binding organic ligands occurs (Batchelli et al., 2010; Gerringa et al., 2008). Although Fe(III) is one of the dominant terminal electron acceptors for organic carbon metabolism (Kostka et al., 1999), in sulfate-rich areas, sulfate becomes the dominant oxidant and thus Fe precipitates as iron sulphides (FeS and FeS₂) (Moeslund et al., 1994). Other processes involving early diagenesis of sediments and the release of Fe(II) includes bioturbation that is dependent on the oxygen levels of overlaying bottom water (Severmann et al., 2010). The non-reductive dissolution of sediment is the dissolution of particles after resuspension that is favoured in oxic BBL with low organic matter degradation and/or low Fe oxides (Homoky et al., 2013; Radic et al., 2011).

These two processes exhibit differences in their DFe supply. Indeed, Conway and John (2014) reported that non-reductive dissolution of sediments from the North American Margin was about 5 times higher than the reductive dissolution of African sediments. Finally, PFe has been shown to be elevated in nepheloid layers which could constitute a substantial source of DFe. Although DFe inputs from nepheloid layers have been evidenced, the processes solubilizing the PFe are still poorly constrained (Cheize et al., under review; Laes et al., 2007; Lam et al., 2015; Revels et al., 2015). Nonetheless, the transport of water masses, which interacted with the BBL, by lateral advection or vertical mixing extends beyond areas directly influenced by sediment resuspension (de Baar et al., 1995; Lam and Bishop, 2008) and sediment sources have been estimated to be the most important source of Fe, accounting for ~74% of the oceans Fe inventory (Tagliabue et al., 2014a).

1.5.1.4 Hydrothermalism

Although mid-ocean ridges and back arc basins are commonly enriched in DFe, the extreme conditions prevailing in such features compared to surrounding waters lead to the precipitation of Fe as solid minerals (German et al., 1991). Indeed, the rock-fluid interactions associated to the extreme temperatures and low pH, enable the enrichment of DFe within the vent fluids by 10⁶:1 (German and Seyfried, 2014) with concentrations ranging from < 2 to 26,000 µmol L⁻¹ (e.g. Elderfield and Schultz, 1996; Gallant and Von Damm, 2006; Holmes et al., 2017). Once the vent fluid escapes the chimney, the plumes entrains ambient seawater and Fe-sulfides precipitate as a result of oxidation, rapid cooling of hot water and increase in pH (see Holmes et al., 2017 and reference therein). Therefore, it was originally assumed that hydrothermal supply had only little impact on Fe ocean inventories.

In the past decades, observations and modelling of abyssal ocean Fe inventory concluded that hydrothermal Fe supply necessitates a longer residence time (e.g. Boyle et al., 2005; Klunder et al., 2011; Tagliabue et al., 2010), and should be investigated in more detail with dedicated process studies (German et al., 2016). The mechanism responsible for the stabilization of DFe within the plume as it mixes with surrounding waters have been inferred to the formation of complexes with organic ligands (e.g. Bennett et al., 2008; Buck et al., 2018; Fitzsimmons et al., 2017; Sander and Koschinsky, 2011; Statham et al., 2005, see Section 1.4.2.2) or transport by nanoparticles (Gartman et al., 2014; Yucel et al., 2011). Hydrothermal DFe stabilized by the former mechanism has been shown to persist for thousands of kilometres from the source (Buck et al., 2018; Fitzsimmons et al., 2017; Resing et al., 2015) thus increasing the probability to reach surface waters, enhance the primary production and impact carbon export not only in areas where the hydrothermal system is located in shallow or upwelled waters (Fitzsimmons et al., 2014; Wurl et al., 2011). Hydrothermal inputs of DFe along mid-ocean ridges and back arc basins have recently been re-estimated to account for ~ 23% of the inventory of Fe in the ocean (Tagliabue et al., 2014a) and to support ~15-30% of the export production south of the Antarctic Polar Front (Resing et al., 2015).

1.5.1.5 Glaciers, icebergs and melting sea ice

In high latitudes, additional sources of Fe must be considered. Indeed, within the Arctic and the Antarctic, glacial melting, icebergs and sea ice have been shown to deliver substantial amounts of DFe (e.g. Bhatia et al., 2013; Lannuzel et al., 2016b; Raiswell, 2011; Raiswell et al., 2008; Shaw et al., 2011; Smith Jr. et al., 2007).

The Fe originating from the melting of glaciers comes from the mechanical and chemical weathering of sediments underneath glaciers (Raiswell et al., 2006), it can also be entrained into the glacier after snow deposition (i.e. extraterrestrial and dust) (e.g. Bintanja and van de Wal, 2008; Fischer et al., 2007) and/or from a marine source for ice shelves (e.g. Schoof, 2007). Many studies investigated the role of these meltwaters from the Greenland ice sheet in delivering Fe to coastal waters. All the studies agreed on the ability of glacial meltwater from Greenland Ice Sheet to deliver DFe and CFe (Bhatia et al., 2013; Hawkings et al., 2014; Schroth et al., 2014; Statham et al., 2008). Recently, Schroth et al. (2014) pointed to the fact that although ice sheets exhibit higher Fe concentrations than in the underlying seawater, the extent to which these Fe concentrations can actually fertilize

seawater was overestimated due to removal processes at the interface between non-saline glacial meltwater and seawater, but were nonetheless a significant source to watersheds. This discovery emphasized the potential role of CFe in fertilizing coastal waters with the study carried out by Hawkings et al. (2014) who reported that Greenland ice sheet is enriched in Fe which is dominated by a highly reactive potentially bioavailable nanoparticulate suspended sediment fraction (0.02 - 0.45 μm , CFe). These particles released from the Greenland meltwater are likely maintained in the euphotic zone due to the buoyancy of the meltwater plume and the potential photochemical degradation of these nanoparticles (Bhatia et al., 2013). In the Southern Ocean, Gerringa et al. (2012) reported that the Pine Island Glacier meltwaters supplied high DFe, up to 150 km away from the glacier that were sustained by Fe-binding organic ligands (Gerringa et al., 2012) in a bioavailable form resulting in a dense phytoplankton bloom (Alderkamp et al., 2012).

Free drifting icebergs originate from ice sheets and thus are often rich in terrigenous material and potentially in Fe (Lin et al., 2011; Lin and Twining, 2012; Smith Jr. et al., 2007). Lin and Twining (2012) reported relatively high concentrations of Fe-binding organic ligands within icebergs compared to remote seawater, thus reducing Fe loss by scavenging. Therefore, during their equatorward transport, icebergs can potentially export Fe from the ice sheet into open ocean waters while they melt. Although these sources (melting ice sheet and icebergs) are still poorly constrained, estimates suggest an overall highly reactive Fe oxide flux of $14 \pm 11 \text{ Tg yr}^{-1}$, including $7 \pm 6 \text{ Tg yr}^{-1}$ from icebergs to the ocean (Raiswell et al., 2006).

Janssens et al. (2016) reported that DFe and PFe begin to accumulate in sea ice as soon as it forms compared to underlying seawater. As the sea ice forms the incorporation of DFe and PFe will strongly depend on the microstructure and texture of the sea ice, with impurities rejected more efficiently in columnar ice than in granular ice due to slower formation (Petrich and Eicken, 2010) thus impacting the speciation of Fe (Lannuzel et al., 2010). Previous studies highlighted that the particulate phase dominates the Fe pool in both fast ice (de Jong et al., 2013; Grotti et al., 2005; Lannuzel et al., 2014; van der Merwe et al., 2011) and pack ice (Janssens et al., 2016; Lannuzel et al., 2016a; Lannuzel et al., 2008). During springtime, the melting of sea ice releases Fe and organic matter such as EPS (Krembs et al., 2002; Lannuzel et al., 2015; van der Merwe et al., 2009) likely due to the bacterial activity within sea ice (Junge et al., 2004), which may increase Fe solubility and bioavailability in seawater (Hassler et al., 2011d; van der Merwe et al., 2009) or that might undergo organic matter aggregation (e.g. Baalousha et al., 2006; Verdugo et al., 2004).

Indeed, Lannuzel et al. (2008) reported that 70% of the DFe is lost in 10 days either because of phytoplankton uptake or scavenging onto particles. Although Fe from sea ice melting is not technically a new source of Fe, recently Genovese et al. (2018) reported that ligands from pack ice are not saturated in Fe and consequently these L' may help solubilizing free or newly formed Fe in surface waters.

1.5.1.6 Submarine groundwater discharge

Submarine groundwater discharge is the flow of water through the sediments and continental margins that comprises terrestrial water mixed with seawater that has infiltrated coastal aquifers between land and coastal ocean (Moore, 2010). As groundwater passes through the sediments, submarine ground waters have high Fe concentrations (Moore, 2010). Large-scale budgets suggested that the magnitude of submarine groundwater discharge is about three to four times the riverine input (Kwon et al., 2014), and highly enriched in DFe (Rodellas et al., 2014).

1.5.2 Regenerated sources of Fe

The internal cycling of Fe (i.e. its regenerated sources) includes the release of Fe from a biotic pool such as heterotrophic bacteria, grazers and viruses. It has been highlighted that a high fraction of regenerated Fe was necessary to support the total production measured in the euphotic zone (Fung et al., 2000; Landry et al., 1997).

Boyd et al. (2010) reported that heterotrophic bacteria mobilize more than 25% PFe d⁻¹ in surface waters compared to less than 2% PFe d⁻¹ at depth (from surface mixed layer to 1000 m depth). These differences were explained by the nature of the PFe with biogenic PFe being the main source of both DFe and ligands compared to lithogenic PFe (Boyd et al., 2010). Conversely, Sarthou et al. (2008) reported that regenerated Fe was increased by 48% in the presence of copepods and was released in the form of inorganic species and/or bound to freely soluble organic ligands above the Kerguelen Plateau. However, in this area where external supplies are intense, regenerated Fe only accounted for 49% of total Fe which was much less than that reported by Boyd et al., 2005 (i.e. 90%) in HNLC waters of the Southern Ocean. Interestingly, the biotic Fe pools have been shown by Boyd et al. (2015) to be relatively constant in HNLC subantarctic and subtropical high-Fe waters, likely highlighting that recycling of Fe may compensate the decrease in the external Fe supply.

Although micro- and meso-zooplankton have been demonstrated to be key players of the remineralisation in the surface layer (Barbeau et al., 1996; Hutchins and Bruland, 1994),

it seems that the most important source of regenerated Fe is viral activity as reported by Poorvin et al. (2004). Indeed, the authors reported that viral activity satisfies almost the full phytoplankton Fe demand (i.e. ~ 90% of their need) from virus-mediated lysis of bacterioplankton alone delivering organically complexed Fe. These virus-mediated organic complexes released during cell lysis were reported by Mioni et al. (2005) to be 1000 times more bioavailable and efficiently assimilated by bacterial cells than Fe(III)'. However, it has been highlighted that most of the virus abundance in the ocean is localised within the first hundred meters of the water column (e.g. Cochlan et al., 1993; Culley and Welschmeyer, 2002). Conversely, micro- and meso-zooplankton distributions are not restricted to surface waters and thus may also contribute to Fe remineralization in deep waters (Blain and Tagliabue, 2016).

Regenerated sources of Fe have the effect of modulating the Fe chemical forms by either releasing dissolved organically complexed Fe from intracellular Fe or by increasing the lability and the bioavailability of Fe-colloids and PFe delivered from external sources.

1.6 Summary of literature review

In the above sections, we have seen the multiple pathways through which DFe is delivered to the water column as new (Section 1.5.1) or as regenerated (Sections 1.2.5 and 1.5.2). DFe can be released from hydrothermal vents, rivers, glaciers, sea ice, snow, wet or dry atmospheric deposition (including rainwater), clouds, sediments (including benthic nepheloid layers, sediment pore waters and through reductive and non-reductive dissolution processes). Deeper sources, enriched in DFe play an important role in the carbon cycle as they can be entrained, upwelled into surface waters through the influence of winds and/or thermohaline circulation and/or eddies thus naturally fertilizing phytoplankton communities present in the surface. DFe can also be regenerated in the water column through bacterial remineralization and grazing. All these sources seemed to not only deliver DFe but also Fe-binding organic ligands (Fig. 1.11). Insights on the organic speciation of Fe within its different phases will allow us to assess the degree to which iron might be available.

Particle dynamics and their propensity to be remineralized are adding another degree of complexity to the Fe biogeochemical cycle. Depending on their nature (biogenic vs. lithogenic), particles can indeed supply both DFe and ligands, or scavenge DFe and ballast biogenic PFe (Boyd et al., 2010). Moreover, particle impact is also dependent on the bacteria

community structure (particle-attached vs. free-living bacteria), with potentially particle-attached bacteria playing a main role in the release of both DFe and ligands (Obenosterer et al., in prep.). Also, whether DFe is present as mostly CFe or SFe will also influence the organic speciation with ligands, and the ligands themselves. Depending on their origin, molecular structure and kinetics will affect how the biota acquire Fe and in turn, will determine the fate of DFe.

Although much progress has been made in understanding how iron links to wider biogeochemical cycles, the processes that affect the sources and sinks of DFe in the ocean depend themselves on the reactivity of Fe, which seems to be driven by the concentrations and physical speciation of ligands. Chemical reactivity will modulate the dissolution of PFe (Cheize et al., under review) and the propensity of different forms of iron to be organically complexed or transferred to particulate pools via scavenging and colloidal aggregation.

1.7 Study areas and thesis goals

This thesis work is focusing on two contrasted regions: the North Atlantic Ocean and the Kerguelen Plateau located in the Indian sector of the Southern Ocean. Their main characteristics are described in the following sections but detailed in Chapters 3, 4 (North Atlantic), and 5 (Kerguelen plateau), while the specific objectives of this work will end this introduction.

1.7.1 The North Atlantic Ocean

The surface water properties of the world's oceans drive the thermohaline circulation and involves the northward flow of warm and salty surface waters from the subtropics into the North Atlantic Ocean via the North Atlantic Current (NAC) that mixes with cold and fresher waters originating from the Arctic and transported through the East Greenland (EGC) West Greenland (WGC) and Labrador (LC) currents (Emery, 2001) (Fig. 1.12). The mixing of these two contrasted different water masses leads to a density increase resulting in their deep convection and subsequent southward transport, which represents the so-called Atlantic Meridional Overturning Circulation (AMOC) (Fig. 1.12). The AMOC is thus responsible for transporting large amounts of water, heat, salt, carbon, nutrients and other substances around the globe (Marshall et al., 2001). The variability of the AMOC contributes substantially to sea surface temperature (SST) and sea ice fluctuations in the North Atlantic (Jungclauss et al., 2005). Its strength is related to the convective activity in the deep-water formation regions,

most notably the Labrador Sea, and the time varying control on the freshwater export from the Arctic to the convection sites modulates the AMOC (Jungclauss et al., 2005). Fluctuations in any of these components might therefore affect the AMOC and hence variability in the carbon export. Indeed, the North Atlantic Ocean, despite covering only 15% of the global ocean area, has been shown by Sabine et al. (2004) to be one of the largest storage of anthropogenic CO₂ absorbing up to 23% of global oceanic anthropogenic CO₂ through not only the physical carbon pump but also through the biological carbon pump. The North Atlantic Ocean is known for its pronounced spring phytoplankton blooms in response to upwelling or water column stratification (Bury et al., 2001; Henson et al., 2009; Savidge et al., 1995). Within the nutrient-poor waters from the subtropical gyre, the phytoplankton growth has been shown to be N and P-co-limited (e.g. Moore et al., 2008). The extensive studies conducted through the Continuous Plankton Recorder (CPR) have highlighted the relationship between the North Atlantic Oscillation (NAO) and the phytoplankton dynamics of the central North Atlantic Ocean (Barton et al., 2003). The NAO is associated to a change in the westerlies, with in the case of a negative NAO phase weak westerlies resulting in a north-westward displacement of the subarctic front (SAF), and vice versa (Bersch et al., 2007). Thus, depending on the location of the SAF, phytoplankton communities from the central North Atlantic Ocean will be more or less prompt to light or nutrient limitation. In the subpolar gyre, the intense winter mixing fuels the surface waters with nutrient. However, once the water column stratifies and phytoplankton are released from light limitation, the subpolar gyre has been shown to become N or (and) Fe-(co)-limited in the Iceland Basin and the Irminger Sea (e.g. Nielsdóttir et al., 2009; Painter et al., 2014; Sanders et al., 2005). In the case of Fe limitation, this results in the formation of the seasonal high-nutrient, low chlorophyll (HNLC) conditions in the subpolar gyre, especially in the Irminger Sea and Iceland Basin. Although many studies investigated the distribution of DFe in the North Atlantic Ocean, much of this work was restricted to the upper layers (< 1000 m depth) or to one basin. Consequently, the pathways through which DFe is delivered to seawater and removed from the water column (see Chapter 3) as well as how Fe in relation to other nutrients, limits phytoplankton organisms and consequently the structure of the phytoplankton community (see Chapter 4), are still poorly constrained in this region.

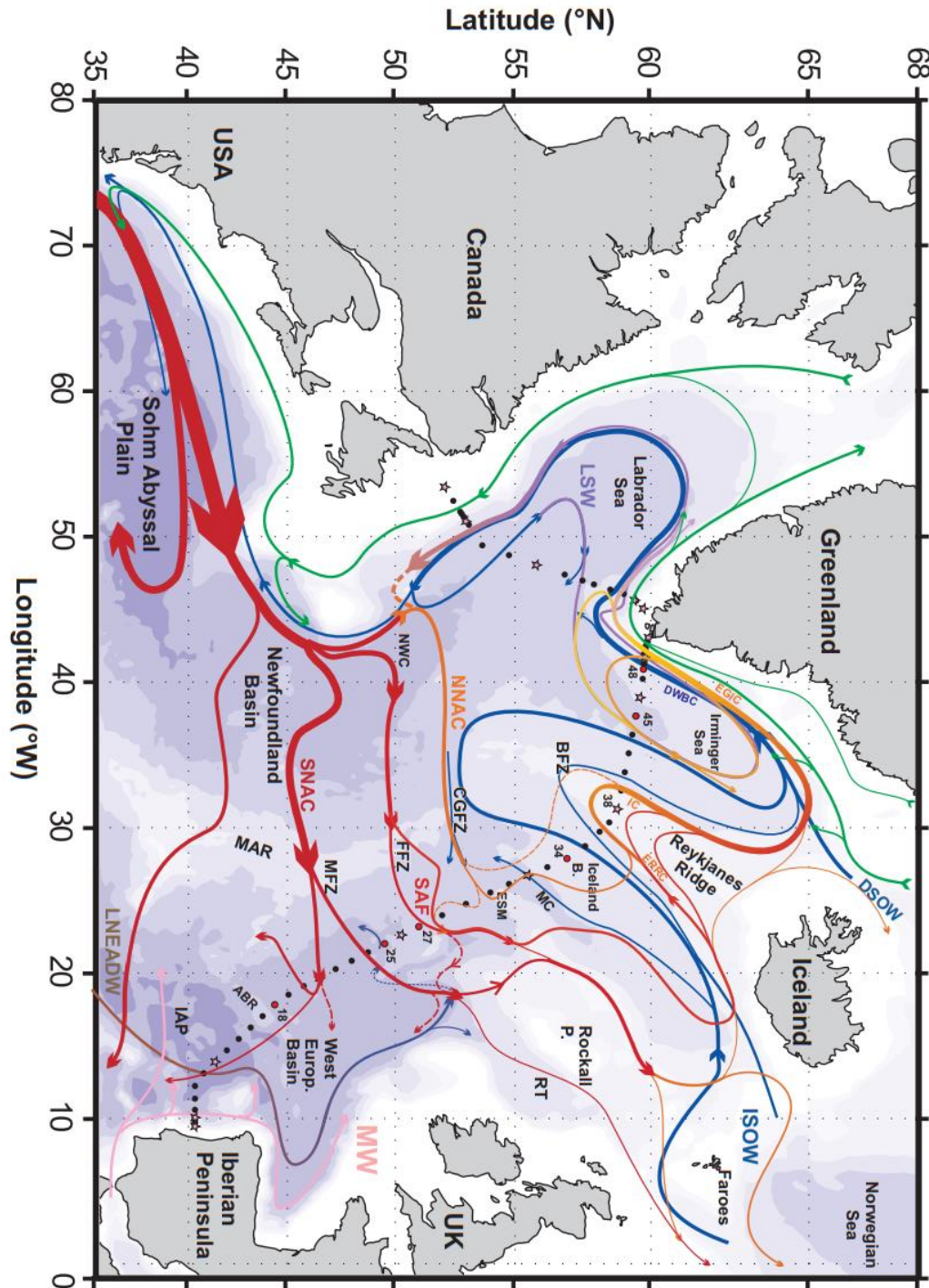


Figure 1.12: Map of the circulation scheme, the major topographical features, main basins, currents and main water masses of the North Atlantic Ocean. The GEOVIDE cruise track (black dots) is superimposed over the main water masses and currents present in the area. The different colors display the different characteristics: Red, Warm and salty surface currents, which turn into Yellow mid depth currents with lower temperature and salt content. Blue, refers to fresh cold return waters. Green, refers to shelf edge boundary currents and purple refers to the newly formed Labrador Sea Water. EGC: East Greenland Current (green), WGC: West Greenland Current (green), LC: Labrador Current (green), NAC: North Atlantic Current (red), MW: Mediterranean Water (pink), LSW: Labrador Sea Water (purple), ISOW: Iceland-Scotland Overflow Water (blue), DSOW: Denmark Strait Overflow Water (blue), DWBC: Deep Western Boundary Current (blue), NEADW: North East Atlantic Deep Water (brown), CGFY: Charlie-Gibbs Fracture Zone, BFZ: Bight Fracture Zone, IAP: Iberian Abyssal Plain, MAR: Mid Atlantic Ridge. From Daniault et al. (2016).

1.7.2 The Kerguelen Plateau (Indian sector of the Southern Ocean)

The Southern Ocean, like the North Atlantic Ocean, has been shown to be an important global sink for atmospheric CO₂ (Gruber et al., 2009; Lenton et al., 2013; Sarmiento et al., 2010). However, in this area, Pasquer et al. (2015) highlighted that the air-sea exchange of CO₂ is driven by thermodynamical conditions, while biological activity is only responsible for a modest fraction of the carbon sink. Indeed, the Southern Ocean is the largest HNLC region of the three main oceanic systems. Despite being an overall low productive ocean region, some areas of the Southern Ocean are very productive. Indeed, high levels of living biomass were noticed in the wake of the Southern Ocean islands. The bloom above the Kerguelen Plateau (Fig. 1.13) being among the largest (Morris and Charette, 2013). This phenomenon was called the “Island mass effect” by Hart (1942). He was the first to mention that the release of an oligo-element such as Fe from the island was likely the cause of the observed biomass. About half a century later, the study carried out during the ANTARES3/F-JGOFS cruise reported elevated chlorophyll-*a* associated with enhanced DFe concentrations, thus confirming the hypothesis of an Fe limitation of the Southern Ocean phytoplankton community relieved by island inputs (Blain et al., 2001; Bucciarelli et al., 2001). The Kerguelen Ocean and Plateau Compared Study (KEOPS) revealed intense phytoplankton biomass over the Kerguelen Plateau (Uitz et al., 2009) and very low surface DFe concentrations ($\sim 0.1 \text{ nmol L}^{-1}$) throughout the study area. However, there was a DFe enrichment at the stations located on the plateau compared to off-plateau stations (Blain et al., 2008c). The process responsible for the upward transfer of the DFe from the Plateau was diapycnal mixing enhanced by internal wave activity (Park et al., 2008a), thus providing Fe for the phytoplankton community but not enough to match the phytoplankton demand. Indeed, Sarthou et al. (2008) reported that about half of the biogenic PFe was regenerated above the plateau. In addition, Park et al. (2008b) highlighted a long water-mass residence time of several months above the plateau due to weak currents, thus avoiding the loss of DFe through advection. DFe losses through scavenging were expected to be minimum due to the high excess ligand concentrations found in the whole study area (Gerringa et al., 2008). However, the intensity and the location of the bloom presented interannual variabilities, with the highest chlorophyll concentrations not always associated to the shallowest depths as well as some region of the plateau exhibiting low chlorophyll concentrations all year round (Mongin et al., 2008). Although DFe has clearly been highlighted as the main parameter

controlling the phytoplankton bloom over the Kerguelen Plateau, its bioavailability and thus its chemical and physical speciation are still not understood.

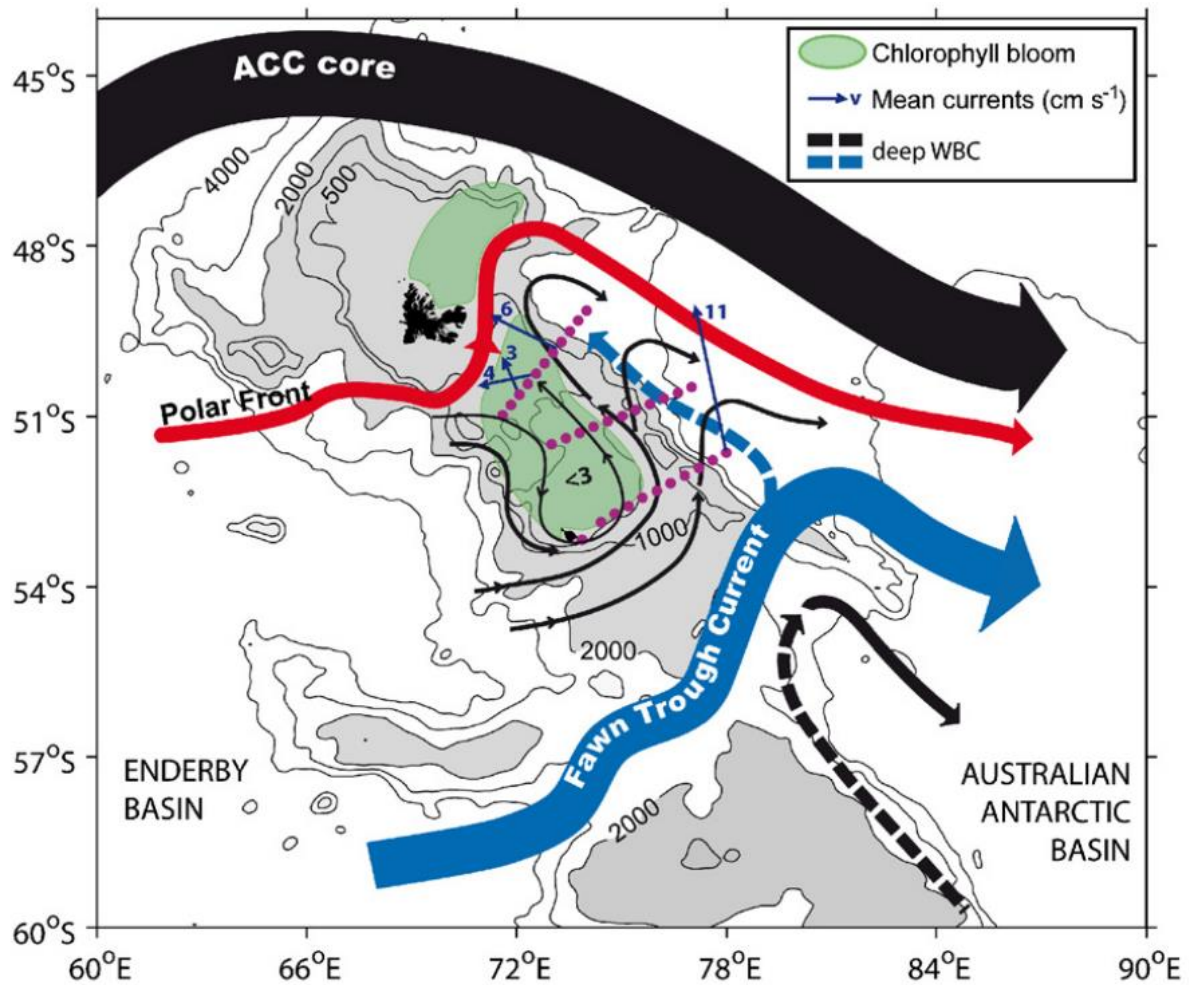


Figure 1.13: Schematic of the geostrophic circulation over and around the Kerguelen Plateau during KEOPS from Park et al. (2008b) with thin blue arrows representing mean current vectors over the upper 500 m layer, thin black arrows stressing area of a sluggish flow, discontinuous bold lines representing subsurface western boundary currents, red arrow representing the Polar Front and in green areas of annual chlorophyll bloom. Note that purple dots correspond to stations sampled during KEOPS.

1.7.3. Objectives and thesis outline

The GEOTRACES program highlighted that the biogeochemical cycle and distribution of DFe emerges as unique to that of other nutrients (Tagliabue et al., 2016). Despite recent effort from the scientific community in the frame of the GEOTRACES program, the Fe cycle is still poorly constrained. Indeed, a large disparity in the residence times for Fe across different models was found, which clearly reflects the complexity of properly representing the Fe cycle. Models that successfully reproduce observed features are those including emerging insights into new sources and cycling pathways of Fe. This clearly highlights that although 30 years of research have been carried out on Fe cycle, there has still some learning to do on both Fe sources and especially the magnitude of its scavenging losses. Good examples demonstrating that a lot of questions still need to be answered and that we need to continue research on the Fe cycle are i) the recent finding about strong hydrothermal iron sources (e.g. Resing et al., 2015) challenging the long-standing view, which considered these sources to be negligible (Elderfield and Schultz, 1996), ii) the debate persisting on the importance of organic ligands in explaining the Fe biogeochemical cycle with the fact that if organic ligands are ubiquitous compounds how could they explain the distribution of DFe. Recent advances on this topic showed that modelling Fe-binding organic ligands prognostically, as opposed to assuming a uniform ligand concentration, leads to a more nutrient-like profile of Fe that is in better accordance with field data (Völker and Tagliabue, 2015). This points out that organic ligand residence time in the water column and their loss terms are still poorly constrained and that we need to continue to build knowledge of the sources, sinks and characteristics of organic ligands in the oceans (Lohan et al., 2015). Finally, only few papers refer to the link between all nutrient distributions taken together with phytoplankton assemblages (e.g. Hassler et al., 2012). This should be done systematically to gain further insight into their potential control on phytoplankton biomass and to assess the main limiting nutrients in the world's ocean. This will allow us to potentially predict the phytoplankton class that will be present in a specifically nutrient-(co)-limited environment. Hence, improving our understanding of the oceanic Fe cycle and its sensitivity to changing environmental conditions and the control of macro- and micro-nutrients on phytoplankton communities will improve projections of ocean's response to climate change.

In order to address certain of these key questions, the objectives of this thesis, as part of the GEOTRACES program, revolve around three scientific questions: 1) What are the distributions, sources, and sinks of dissolved iron within two specified study regions? 2)

Within these regions, what is the link between the phytoplankton community structure and dissolved iron concentrations? 3) How does the organic speciation of dissolved iron affect its concentration and bioavailability for the phytoplankton community? These three questions were investigated in two contrasting areas presented above: the North Atlantic Ocean (GEOVIDE, GA01 GEOTRACES voyage, PIs G. Sarthou and P. Lherminier) and the Southern Ocean (HEOBI, GIp05 GEOTRACES voyage, PIs A. Bowie, T. Trull, Z. Chase). Both these science voyages were approved by the GEOTRACES program.

The layout of this manuscript is as follows:

- Chapter 2: In this chapter, the specifics of trace metal work are described. The different methods used in this thesis are presented as well as statistical methods.
- Chapter 3: This chapter presents the results of DFe in the North Atlantic Ocean and in the Labrador Sea along the GEOVIDE section. This chapter is in a form of a submitted manuscript to Biogeosciences Discussions.
- Chapter 4: This chapter focuses on the phytoplankton assemblage distribution in the North Atlantic and Labrador Sea along the GEOVIDE section as determined by the CHEMTAX model from HPLC pigment data. The aim of this manuscript in preparation, is to understand the link between physical forcing and phytoplankton distributions.
- Chapter 5: This chapter mainly focuses on Fe-binding organic ligands. It will explore the link between organic ligands and the biology in the Southern Ocean and aims at better constraining their characteristics. This will be submitted to Marine Chemistry.
- Chapter 6: The last chapter of this thesis summarizes the information given in chapters 3, 4 and 5. Chapter 6 also suggests future directions for international programs and new perspectives.

Chapter 2:

Material and Methods

Chapter 2 - Material and Methods

Table of Contents

2.1 Ultra-clean conditions	85
2.1.1 Laboratory practices	86
2.1.2 Pre-cruise cleaning procedure	86
2.1.2.1 GO-FLO bottles	87
2.1.2.2 Niskin bottles	87
2.1.2.3 Sampling bottles	87
2.2 Sample collection	89
2.2.1 GEOVIDE voyage	89
2.2.1.1 Location	90
2.2.1.2 Equipment used for sample collection	90
2.2.1.3 Sample treatment before shore-based analysis	91
2.2.2 HEObI voyage	91
2.2.2.1 Location	91
2.2.2.2 Equipment used for sample collection	93
2.2.2.3 Sample treatment before shore-based analysis	93
2.3 Statistical Methods	94
2.4 Analytical techniques	95
2.4.1 Calibration seawater	96
2.4.1.1 GEOVIDE standard reference seawater (LEMAR)	96
2.4.1.2 HEObI standard reference seawater (IMAS)	96
2.4.2 Dissolved iron (DFe) analysis	97
2.4.2.1 Principle of analysis	97

<u>2.4.2.2 Reagent preparation</u>	100
<u>2.4.2.3 Precision, accuracy and reproducibility</u>	101
<u>2.4.3 Fe-binding organic ligand analysis</u>	104
<u>2.4.3.1 Principle of analysis</u>	104
<u>2.4.3.2 Material, reagents and sample preparation</u>	105
<u>2.4.3.3 Theory of competitive ligand equilibration and adsorptive cathodic stripping voltammetry (CLE-AdCSV) using TAC as artificial ligand</u>	108
<u>2.4.3.4 Determination of Fe-binding ligand characteristics</u>	109
<u>2.4.3.5 Detection limit and TAC contamination</u>	111
<u>2.4.4 Pigment analysis</u>	111
<u>2.4.4.1 HPLC principle of analysis</u>	112
<u>2.4.4.2 Pigment based phytoplankton size classes</u>	114
<u>2.4.4.3 CHEMTAX model</u>	114
<u>2.4.5 Ancillary measurements</u>	125

Preamble

In this chapter, “ultra-clean conditions” that are required for the study of trace metals are presented at first. Then, the sampling techniques and the different storage conditions of the two study areas (i.e. North Atlantic Ocean and the Southern Ocean) are presented. Finally, analytical methods for the determination of dissolved iron (i.e. seaFAST-picoTM SF-ICP-MS), organic speciation (i.e. voltammetry) and pigment analysis (i.e. HPLC and CHEMTAX model) are described as well as the statistical methods.

The sample collection during GEOVIDE and HEOBI and their analysis were performed thanks to the contribution of many persons:

During GEOVIDE

- The DFe samples were collected by H       Planquette, Julia Boutorh, Marie Cheize, Jan-Lukas Menzel Barraqueta, Leonardo Pereira-Contreira and Rachel Shelley; and were analysed via the seaFAST-picoTM SF-ICP-MS by Morgane Gallinari, H       Planquette, G       Sarthou, Floriane Desprez de G         and Yoan Germain.
- The pigment samples were collected by Rapha     Sauz     and Lorna Foliot, analysed via HPLC by Herv     Claustre, Celine Dimier, Rapha     Sauz     and Jos         Ras and were ran in CHEMTAX by myself with the valuable help from Anne Donval and Luis Lampert.
- The nutrients were collected by Manon Le Goff, Emilie Grossteffan, and analysed via segmented flow analysis by Morgane Gallinari, Manon Le Goff, Emilie Grossteffan and Paul Tr        .
- The Fe organic speciation samples were collected by H       Planquette, Julia Boutorh, Marie Cheize, Jan-Lukas Menzel Barraqueta, Leonardo Pereira-Contreira and Rachel Shelley; and were analysed via voltammetry by Aridane G. Gonzales, Hannah Whitby and I.

During HEOBI

- The DFe, SFe, DLt and SLt samples were collected by Kathrin Wuttig, Pier van der Merwe, Thomas Holmes, Zanna Chase, Lavenia Ratnarajah, Andrew R. Bowie and I.

- The DFe samples were analysed via the seaFAST-picoTM SF-ICP-MS by Thomas Holmes, Kathrin Wuttig, Pier van der Merwe, Ashley Townsend and Christina Schallenberg, while the SFe samples were analysed similarly by Kathrin Wuttig, Pier van der Merwe, Ashley Townsend, Delphine Lannuzel, Luis Paulo Duprat and I.
- The soluble and dissolved Fe organic speciation samples were analysed by myself with the valuable help from Kathrin Wuttig, Pier van der Merwe and Hannah Whitby.

2.1 Ultra-clean conditions

Marine analytical chemists interested in trace metals face a challenge: the measurement of very low concentrations (in the range of picomolar to nanomolar) in a complex matrix (seawater) with ubiquitous risk of contamination for many of the studied elements. A historical survey of the DFe concentrations in open ocean seawater reported in the literature since 1935 shows that the concentration of DFe covers four orders of magnitude (Fig. 2.1). Recent data has shown this is not a true representation (Blain and Tagliabue, 2016).

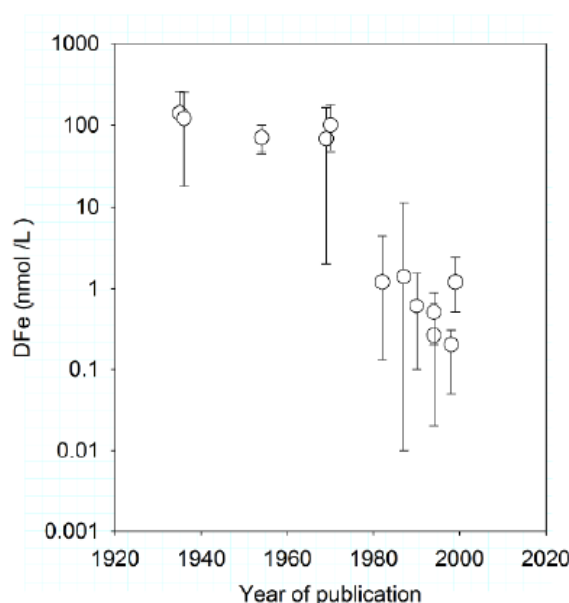


Figure 2.2: Historical perspective of the change in the range and average concentrations of dissolved Fe in the open ocean (from Blain and Tagliabue, 2016).

It was only in 1980s, that the first clean measurements of DFe were performed and revealed oceanographically consistent distributions, but only for a few stations (1982-1989, MLML group; Gordon et al., 1982; Martin, 1990; Martin et al., 1990; Martin and Gordon, 1988; Martin et al., 1991). This starting point led to the birth of many international collaborations whose emphasis was on the entire spectrum of activities related to trace metal measurements, ranging from sampling, filtration, storage and analysis. In the absence of any certified reference material for trace metal analysis at low concentrations, a project was developed to sample a large volume of homogenized surface and deep open-ocean seawater, aimed at providing 500 mL reference material to worldwide researchers investigating the chemistry of trace metals worldwide. From this broad goal, three specific scientific voyages for “standardisation and intercalibration” were achieved in the frame of three international programs: IRONAGES, Sampling and Analysis of Iron (SAFe) and GEOTRACES. The first large-scale international intercomparison was carried out in 2000 and referred to low iron

samples taken from the surface Atlantic Ocean (Bowie et al., 2006). The second voyage occurred in 2004, in the North Pacific, during which one surface (SAFe S, 2 m depth) and two deep (SAFE D1 and SAFe D2, 1000 m depth) open-ocean seawater samples were collected as reference material (Johnson et al., 2007; Lohan et al., 2006). In 2008, the GS and GD GEOTRACES seawater samples were collected in surface and deep open-ocean waters, respectively, from the North Atlantic BATS crossover station off Bermuda. Finally, in 2009, the North Pacific voyage sampled two surface seawater sites, the GSP water from the SAFe site and the GSC water from Santa Barbara Channel during bloom conditions. These international inter-calibrations have made possible the establishment of standardized procedures to collect trace metal seawater samples and to improve both the storage conditions and the analysis of samples.

All these new protocols are listed and detailed in a common document: the GEOTRACES cookbook (Cutter et al., 2017) which has already been updated twice since its first edition in 2010 and was written by the GEOTRACES Standards and Intercalibration (S&I) Committee. The reference material collected during the two international inter-calibrations are still reported in publications today and their values are constantly updated.

2.1.1 Laboratory practices

As iron is an ubiquitous element on Earth (~5.6 % by weight) and because it is present in trace concentrations in the open ocean ($< 1 \text{ nmol L}^{-1}$), it is important to take special care in handling samples, in the cleanliness of the laboratory environment, air quality and the required tools in order to avoid contamination. As a consequence, laboratory work was undertaken during both science voyages within a containerised clean laboratory under high efficiency particulate air (HEPA) conditions, and in clean rooms at both laboratories (i.e. Laboratoire des sciences de l'Environnement MARin (LEMAR - UMR 6539) and the Institute for Marine and Antarctic Studies (IMAS) under an ISO class 5 laminar flow hood for the handling of all samples and reagents.

2.1.2 Pre-cruise cleaning procedure

Prior to the cruise, and according to the GEOTRACES approved methods handbook (www.geotraces.org, Cutter et al., 2017) all the material used was cleaned with different protocols, depending of their final use.

2.1.2.1 GO-FLO bottles

Teflon-coated GO-FLO bottles (General Oceanics), used to collect seawater, were first disassembled, including viton o-rings. All o-rings were switched to silicone ones, then were wiped cleaned with isopropyl alcohol to remove remaining oil/grease and contaminants from manufacturing. The o-rings grooves were also wiped with isopropyl alcohol. GO-FLO's top air-bleed valve were replaced with a Swagelok fitting to allow pressurization with clean dinitrogen (Air Liquide), and their sample valve were replaced with a Teflon plug valve. Then, GO-FLO bottles were reassembled, filled with 5% (v/v) aqueous Decon detergent for one day, rinsed seven times with deionized water (DIW) thoroughly until all traces of detergent were removed and three times with ultrapure water (resistivity of 18.2 M Ω ·cm at 25 °C, UHPW hereafter). The bottles were then rinsed with 250-mL of isopropyl alcohol (Cutter and Bruland, 2012), followed by three rinses with DIW and three additional rinses with Milli-Q. They were then filled with 0.1 M HCl (Suprapur[®] Merck) for one day, and emptied out through the spigot to rinse it, rinsed five times with UHPW, and finally filled with UHPW for more than one day before use. They were also thoroughly flushed with seawater at a test station prior to use at the first official sampling station.

2.1.2.2 Niskin bottles

Niskin bottles used to collect seawater for trace metal during the HEOBI voyage were first tooth-brushed with 2% (v/v) aqueous Decon detergent and left in this solution for one day, rinsed with DIW thoroughly and three times with UHPW. Niskin bottles were then filled with 5% (v/v) hydrochloric acid (HCl, instrument grade, Seastar[™] chemicals) for two days and then rinsed five times with UHPW. Finally, they were flushed at sea with open ocean seawater and blank tested with on-board Flow Injection Analysis with Chemiluminescence detection (FIA-CL) prior to use at the first official sampling station.

2.1.2.3 Sampling bottles

Low-density polyethylene (LDPE, Nalgene) bottles used to sample for DFe (60mL) and organic speciation (125 mL) during GEOVIDE. DFe samples were then subsampled in acid-cleaned 30mL LDPE bottles for SeaFAST-pico[™] analyses. LDPE bottles were soaked in about 5% (v/v) aqueous Decon detergent for a week and then rinsed four times with DIW, followed by three rinses with UHPW (Milli-Q). Bottles were subsequently filled for a month with 6 M HCl (reagent grade) and submerged in a 2 M HCl (reagent grade) bath, then rinsed

five times with UHPW. The final step consisted of filling the LDPE bottles with 0.1 M HCl (Merck, Ultrapur®) prior to use.

DFe, SFe, DLt and SLt and polypropylene (PP) tubes and their caps used to pour HEOBI samples and to collect them after preconcentration on the seaFAST-picoTM unit were cleaned in the same way. LDPE bottles and PP tubes were soaked in about 5% (v/v) aqueous Decon detergent for a week and then rinsed four times with reverse osmosis water (ROW) followed by three rinses with UHPW (Milli-Q). Bottles and tubes were subsequently filled for a month with 6 M HCl (reagent grade) and submerged in a 2 M HCl (reagent grade) bath, then rinsed five times with UHPW. The final step consisted of filling the LDPE bottles with 1 M HCl (Merck, Suprapur®), while PP tubes and caps were dried under a laminar flow hood prior to use. Finally, for DFe sampling, LDPE-bottles were rinsed again five times with UHPW (Milli-Q) under clean air and filled with 2‰ (v/v) HCl (Merck, Ultrapur®). Lt sampling LDPE-bottles, as opposed to DFe sampling bottles, were stored with UHPW (Milli-Q) for at least a month. The pH plays a key role in the determination of organic speciation analytical technique and for this reason, it is important that all the material used for Lt determination was free of traces of acid.

Polytetrafluoroethylene (PTFE, Teflon ®) and Fluorinated ethylene propylene (FEP, Teflon ®) bottles were used to prepare reagents. PTFE and FEP bottles were soaked for one day in about 2% (v/v) aqueous Decon detergent, rinsed seven times with DIW, three times with UHPW (Milli-Q), soaked for one day in 6 M HCl (reagent grade), subsequently rinsed five times with UHPW (Milli-Q). Bottles were then filled with 1M nitric acid (HNO₃, Merck, Suprapur ®) for five hours at 100°C, rinsed five times with UHPW (Milli-Q), filled with UHPW (Milli-Q) for five hours at 80°C and finally rinsed five times with UHPW (Milli-Q) prior to use.

Savillex® Teflon vials were used to aliquot Fe standards, TAC and EPPS buffer, in which direct pipetting was done as well as for the preparation of voltammetric titrations. New Savillex vials and caps were soaked in about 2% (v/v) aqueous Decon detergent for a week and then rinsed three times with UHPW (Milli-Q). Vials and caps were then boiled in 50% (v/v) HCl (Merck, Suprapur®) for two hours, followed by first the UHPW (Milli-Q) rinsing of the whole bulk one time and individually three times. Finally, each capped vial was filled with about 10% of their volume capacity with a solution made of 50% (v/v) HNO₃ (Merck, Suprapur ®) and 10% (v/v) hydrofluoric acid (HF, Merck, Suprapur ®) for four hours at

120°C and subsequently rinsed three times with UHPW (Milli-Q), left for about a month in UHPW (Milli-Q) and re-rinsed three times with UHPW (Milli-Q) prior to use.

Note that all pipette tips (10-200 μL ; 100-1000 μL ; 1-5 mL and 1-10 mL) used during this thesis were cleaned just prior to use by pipetting three times a solution of 10% (v/v) aqueous HCl (Merck, Suprapur®) and three times UHPW (Milli-Q) from two different bottles (to remove all traces of acid).

2.2 Sample collection

In the following sections, the sampling location, the equipment used and the treatment before shore-based analysis are detailed for the two science voyages that occurred in the North Atlantic Ocean (GEOVIDE) and in the Southern Ocean (HEOBI).

2.2.1 GEOVIDE voyage

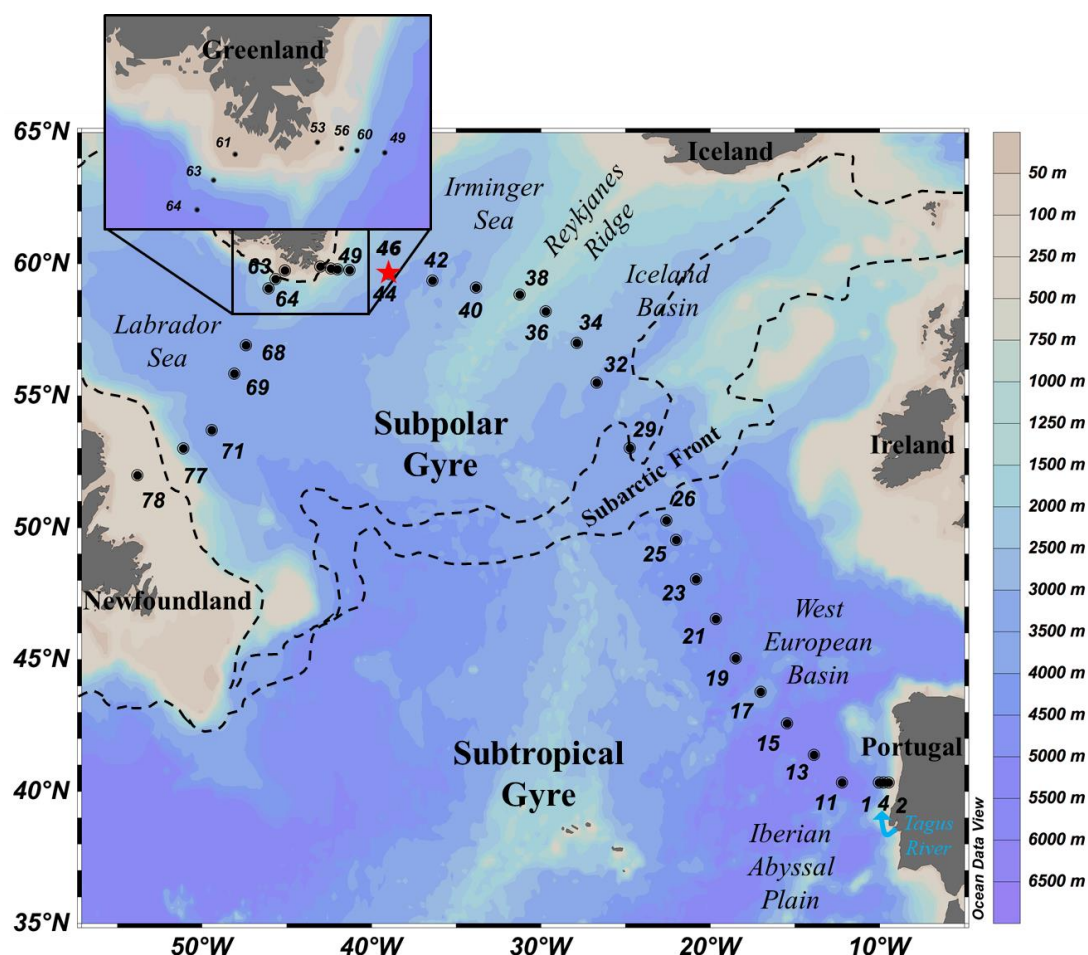


Figure 2.2: Map of the GEOTRACES GA01 voyage track plotted on bathymetry as well as the major topographical features and main basins. Crossover station with the GEOTRACES GA02 voyage is shown as a red star. (Ocean Data View (ODV) software, version 4.7.6, R. Schlitzer, <http://odv.awi.de>, 2016).

2.2.1.1 Location

Samples were collected during the GEOVIDE (GEOTRACES-GA01 section) oceanographic voyage from 15 May 2014 (Lisbon, Portugal) to 30 June 2014 (St. John's, Newfoundland, Canada) aboard the N/O *Pourquoi Pas?* (Fig. 2.2). The study was carried out along the OVIDE line (<http://www.umar-lops.fr/Projets/Projets-actifs/OVIDE>) which has been sampled every two years since 2002 in the North Atlantic (e.g. Mercier et al., 2015) and in the Labrador Sea.

In total, 32 stations were occupied for trace metal sampling, and samples were usually collected at 22 depths, except at shallower stations close to the Iberian, Greenland and Canadian shelves where fewer samples (between 6 and 11) were collected.

In total, 33 stations were occupied along this transect over 1- to 4-day periods between sites for the pigment samples, which were collected at about 10 depths ranging from 5 to 203 m depth, except at shallower stations close to the Iberian (station 2 and 4, n = 8 and 5, maximum depth 141 and 197 m, respectively) and Greenland (station 53 and 61, n = 8 and 10, maximum depth 157 and 119 m, respectively) margins where fewer samples were collected. The samples were collected from night and day CTD casts.

2.2.1.2 Equipment used for sample collection

Samples were collected using the French-national ultra-clean sampling device. This consisted of a trace metal clean polyurethane powder-coated aluminium frame rosette (hereafter referred to as TMR, see Fig. 2.3) equipped with twenty-two 12L, externally closing, Teflon-lined, GO-FLO bottles (General Oceanics) and attached to a Kevlar[®] line, as described above. Potential temperature (θ), salinity (S), dissolved oxygen (O_2) and beam attenuation data were retrieved from the CTD sensors (CTD SBE911 equipped with a SBE-43). Salinity and oxygen data were calibrated using analysis of discrete samples with a salinometer (Guildline) and the Winkler method (Carpenter, 1965), respectively. Note that Teflon[®] tubing used to connect the filter holders or cartridges to the GO-FLO bottles were washed in an acid-bath (10% v/v HCl, Suprapur[®], Merck) for at least 12 h and rinsed three times with UHPW prior to use. To avoid ship contamination of surface waters, the shallowest sampling depth was 15 m at all stations.

The additional samples for pigment analysis were collected using the classic CTD-rosette system equipped with twenty-four 12L Niskin bottles.



Figure 2.3: Pictures (from Helene Planquette) of (from the left to the right) Trace Metal clean Rosette, Marie Cheize and Julia Boutorh sampling for trace metals and acidifying samples, 0.45 μm polyethersulfone filters (Supor[®]).

2.2.1.3 Sample treatment before shore-based analysis

After TMR recovery, GO-FLO bottles were immediately transferred into a clean container (Fig. 2.3) equipped with a class 100 laminar flow hood. Samples were either taken from the filtrate of particulate samples (collected on polyethersulfone filters, 0.45 μm Supor[®], see Gourain et al., submitted; Fig. 2.3) or after filtration on 0.2 μm filter cartridges (Sartorius SARTOBRAN[®] 300) (see Chapter 3 and 5 for DFe and FeL sample details, respectively) under a slight pressurisation (0.2 bar; filtered (Acrovent) N₂ (Air Liquide)). The sampling bottles were rinsed 3 times with about 30% of their capacity and then filled and stored in acid-cleaned 60 mL and 125 mL LDPE bottles for DFe and dissolved trace metal (DTM) samples, respectively. DFe and DTM samples were then acidified to \sim pH 1.7 with 2 ‰ (v/v) HCl (Merck, Ultrapur[®]) under a class 100 laminar flow hood in the clean container, double bagged, and stored at ambient temperature.

The pigment samples were vacuum filtered through 25 mm diameter *Whatman* GF/F glass fibre filters (0.7 μm particle retention size). Typically, 2.325 L were sampled, except at stations 53, 60, 61, 68, 71 and 77, where 1.295-2.265 L were filtered in surface waters. Filters were immediately stored in liquid nitrogen then at -80°C until analysis on land.

2.2.2 HEOBI voyage

2.2.2.1 Location

During the HEOBI voyage (GEOTRACES process study GIpr05), samples were collected aboard R/V *Investigator* from 8th January (Fremantle, Western Australia) to 27th

February (Hobart, Tasmania) 2016 around Heard and McDonald Islands on the Kerguelen Plateau in the Indian sector of the Southern Ocean (Fig. 2.4). In total, 11 stations were collected for DLt (and DFe) samples and 6 stations for SLt and SFe at 2 to 12 depths. The sampling consisted in a repetition of the B-transect occupied during the KEOPS voyage (Blain et al., 2008c; Gerringa et al., 2008) and additional samples were collected around Heard and McDonald Islands. Note that CTD casts were conducted at the same locations.

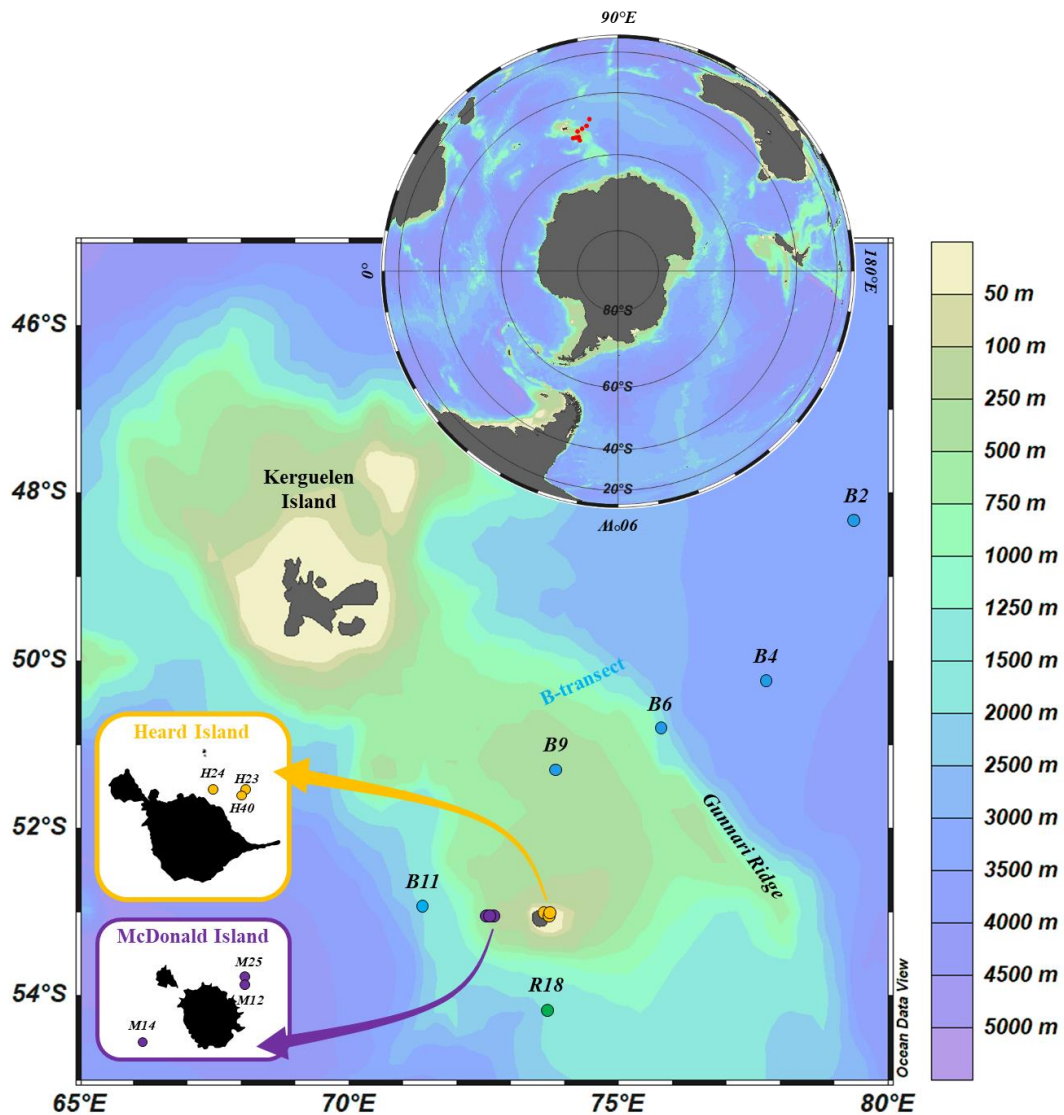


Figure 2.4: Location of the stations sampled during the HEOBI voyage using the Trace Metal Clean Rosette (modified from Thomas Holmes). Heard and McDonald Islands are shown in the inset, in yellow and purple, respectively, the reference station (R18) is represented in green. Transect B, in blue, follows the Kerguelen Ocean and Plateau Compared Study (KEOPS) transect B.

2.2.2.2 Equipment used for sample collection

The seawater samples were taken from twelve acid-cleaned 12-L Niskin bottles manufactured with an internal Teflon[®] coating deployed using the Australian Marine National Facility TMR-powder coated aluminium frame attached to a Kevlar line (Fig. 2.5). The CTD package consisted of a Seabird SBE9 underwater unit, an SBE3 temperature sensor, an SBE4 conductivity sensor, a Wetlabs C-Star transmissometer and an SBE43 dissolved oxygen sensor. Similarly as for the GEOVIDE voyage, Teflon[®] tubing used to connect the cartridges to the Niskin bottles were washed in an acid-bath (10% v/v HCl, Suprapur[®], Merck) for at least 12 h and rinsed three times with UHPW prior to use.



Figure 2.5: Pictures (from Peter Harmsen) of (from the left to the right) Kathrin Wuttig, the Trace Metal Clean Rosette in its protective coat before deployment, Andy R. Bowie and Manon Tonnard; Zanna Chase and Manon Tonnard sampling for trace metals through 0.2 µm Pall Acropak (Supor®) capsule filters.

2.2.2.3 Sample treatment before shore-based analysis

Once recovered, the Niskin bottles were transferred into a trace metal clean containerised laboratory for sub-sampling and sample processing (Fig. 2.5). All sample manipulation was conducted under ISO 5 HEPA filtered air within the containerised clean room. All samples were collected in LDPE bottles. The dissolved fraction (i.e. DFe and DLt samples) was filtered through Pall Acropak (Supor®) capsule filters (0.2 µm with 0.8 µm pre-filter, Fig. 2.5), while the soluble fraction (i.e. SFe and SLt) was collected off line using a

peristaltic pump through Anotop cartridges (0.02 μm , Whatman) from the dissolved fraction. Both filters and cartridges were acid cleaned and then flushed with the seawater sampled and LDPE bottles were rinsed by a third of their volume capacity with the seawater sampled prior to collect samples. All the filtered samples for DFe and SFe analysis were immediately acidified with HCl (pH 1.8, 2 ‰ v/v 12M HCl, SeastarTM, Baseline®) under a class 100 laminar flow hood in the clean container. All the filtered samples for DLt and SLt were immediately frozen at -20°C. All samples were then double bagged and stored in the dark prior to shore-based analysis.

2.3 Statistical Methods

All statistical approaches were performed using the R statistical software (R development Core Team 2012). For all the results, p-values were calculated against the threshold value alpha (α), that we assigned at 0.05, corresponding to a 95% level of confidence. For all data sets, first Shapiro-Wilk tests were performed to assess the normality of the data, if normality was not confirmed (p-value < 0.05), non-parametric tests were thus performed due to the non-compliance of normality after log-transformation of data. To compare two independent groups, t-tests were performed in case of normality, while Wilcoxon tests were performed in case of non-normality. In Chapter 3, the pore size used for filtration (i.e. 0.2 or 0.45 μm , see Section 2.2.1.3) was tested between stations while swapping between both filtration techniques for samples paired by depth with an alternative hypothesis signed depending on the pore size used.

To compare more than two independent groups, ANOVA were performed in case of normality, while Kruskal-Wallis tests were performed in case of non-normality. In Appendix A, the normality of data allowed to compare more than two groups with several dependant variables thanks to a MANOVA. The relationships between two groups were assessed by a Pearson correlation, in case of normality of the data, or by a Spearman correlation in case of non-normality. Note that throughout the thesis when p-values are reported the tests performed are specified.

Large data sets (> 500 samples) were explored using Principal Component Analysis (PCA, R packages “FactoMineR” and “factoextra”) when variables were quantitative. The components that were selected had a proportion of variance higher than that of average (in our cases, 2). Note that to avoid misinterpretation, the \cos^2 , indicative of the good representation of the variables or individuals in the 2D-plan, were coded as a function of

transparency (i.e. not represented if $\cos^2 < 0.5$). Note that to annihilate the effect of the difference of units or of the measuring scales of each variable to the variance, variables were scaled (i.e. centered around the average and reduced by the standard deviation of each variable and for a single sample), thus giving the same importance to all of them. In Chapter 4 and 5, clustering analyses were performed on the outputs of the PCA using the gap statistic and k-mean methods for estimating the optimal number of groups.

Finally, Canonical Correspondence Analysis (CCA, R package “vegan”, Oksanen et al., 2010) was used to constrain a set of objects by explanatory variables whose requirement is that the samples are independent (e.g. Torondel et al., 2016). In our case, a first CCA was performed to constrain nutrients by physical and phytoplankton size class, highlighting three different groups corresponding to the following Longhurst (2007) provinces: North Atlantic Subtropical East (NASTE), North Atlantic Drift (NADR) and Atlantic Arctic (ARCT). Three other CCAs were performed to constrain phytoplankton species by physico-chemical variables per Longhurst areas. Note that the explanatory variables were selected after an automatic model building based on Akaike Information Criterion (AIC) and with permutation tests (step A function), an automatic model building based on permutation p-values (ordistep A function), a manual model building define first as the maximal model scope and secondly as an empty model to start with. The significance of the variables of these four models were tested based on a permutational multivariate analysis of variance using distance matrices with pseudo-*F* ratios (adonis A function) and the selected variables were used to built the final model that was tested by an ANOVA like permutation test for CCA to assess the significance of constraints (anova.cca A function).

All sections and surface layer plots were prepared using Ocean Data View (Schlitzer, 2016). Other plots were realized either using R software (R packages “ggplot2”, “grid” and “extrafont”) or Excel (Microsoft).

2.4 Analytical techniques

In this section, the different calibration seawater and analytical techniques used during this thesis are presented, including the seaFAST-picoTM SF-ICP-MS, the voltammetry and the HPLC.

2.4.1 Calibration seawater

In both laboratories, seaFAST-picoTM calibration curves were performed on in-house standard reference seawater matrices. Three in-house standard reference seawater matrices (i.e. GEOVIDE#1, GEOVIDE#2 and GEOVIDE#3) were used at the LEMAR and two in-house standard reference seawater matrices (i.e. HEOBI#1 and HEOBI#2) were used at the IMAS. These seawater matrices were also used in voltammetry to assess the artificial ligand contamination and the sensitivity of the device after UV-digestion of the matrices.

2.4.1.1 GEOVIDE standard reference seawater (LEMAR)

The GEOVIDE seawater matrices (referred hereafter as GEOVIDE#1, GEOVIDE#2 and GEOVIDE#3) were collected with a towed fish at around 2-3 m deep, were filtered in-line inside a clean container through a 0.2 μm pore size filter capsule (Sartorius SARTOBRAN[®] 300) and were stored unacidified in 20-30 L LDPE carboys (NalgeneTM). All the carboys (NalgeneTM) were acid-cleaned the same way as for the sampling bottles of DFe (see Section 1.2.3) and were pre-rinsed with 6 to 9 L of seawater before sampling. These seawater samples have a DFe concentration of GEOVIDE#1 = $0.22 \pm 0.06 \text{ nmol L}^{-1}$ (n = 30), GEOVIDE#2 = $0.96 \pm 0.13 \text{ nmol L}^{-1}$ (n = 39) and GEOVIDE#3 = $0.42 \pm 0.07 \text{ nmol L}^{-1}$ (n = 84).

2.4.1.2 HEOBI standard reference seawater (IMAS)

The HEOBI seawater matrices (referred hereafter as HEOBI#1 and HEOBI#2) were collected with the TMR at station R18 (54° 10'S, 73° 40'E) by combining 8 bottles fired between 48-83m and was filtered inside a clean container through Pall Acropak (Supor[®]) capsule filters (pore size 0.2 μm). This seawater was stored in 50 L LDPE carboys (NalgeneTM). All the carboys were acid-cleaned the same way as for the sampling bottles of DFe (see Section 1.2.3) and were pre-rinsed before sampling. These seawater matrices which were stored acidified (2% v/v HCl 11M, SeastarTM Baseline[®]), have a DFe concentration of HEOBI#1 = $0.19 \pm 0.05 \text{ nmol L}^{-1}$ (n = 9) and HEOBI#2 = $0.10 \pm 0.04 \text{ nmol L}^{-1}$ (n = 25).

2.4.2 Dissolved iron (DFe) analysis

The DFe concentrations from the GEOVIDE voyage were analysed at the LEMAR by the seaFAST-picoTM (ESI, Elemental Scientific, USA) coupled to a Sector Field Inductively Coupled Plasma Mass Spectrometry (SF-ICP-MS, Thermo Fisher Scientific, Inc.). Note that the same data set was also analysed by flow injection analysis with chemiluminescence detection (FIA-CL) in the land-based LEMAR laboratory after a method development using the Toyopearl resin, which is summarised in Appendix A. The DFe and SFe concentrations from the HEOBI voyage were analysed at the IMAS by seaFAST-picoTM coupled to SF-ICP-MS. Note that the two seaFAST-picoTM SF-ICP-MS used in the different laboratories present slight differences, which are stated below.

2.4.2.1 Principle of analysis

This technique involves a pre-concentration step of the trace metals present in the seawater matrix on a Nobias resin column and their detection by SF-ICP-MS, thus allowing their simultaneous quantification. The Nobias PA1-chelate contains ethylenediaminetriacetic (EDTRiA) acid and iminodiacetate (IDA) functional groups on a hydrophilic methacrylate resin. The method used at the LEMAR allows the interference-free determination of Mn, Co, Zn, Cu, Pb and Fe, while at the IMAS the method allows the interference-free determination of Mn, Co, Zn, Cu, Pb, Ti, Cd, Ni, Ga, V and Fe. Note that the describing of the seaFAST-picoTM unit and of the SF-ICP-MS instrumentation and settings are fully described in Lagerström et al. (2013), Rapp et al. (2017) and Wuttig et al. (subm.). In the following section, a summary of the general principles used in both labs is described.

At the LEMAR (online preconcentration)

The seaFAST-picoTM unit (Fig. 2.6) is equipped with a HEPA filter under which the samples placed in 30mL acid-cleaned LDPE bottles (NalgeneTM) are located (for cleaning procedure refer to Section 2.1.2.3). All analyses were performed online meaning that the preconcentration step on the seaFAST-picoTM unit was directly followed by the detection on the SF-ICP-MS as they were connected to each other. The manifold allows for a preconcentration factor of 50 and the column is eluted for 170 seconds with the eluent directly through the PFA nebulizer. The eluent was spiked with 1ppb ¹¹⁵Indium (¹¹⁵In, see Section 2.3.2.2 for preparation detail) in order to correct for the instrument drift. Three UHPW blanks were run at the beginning of the sequence. Then, a six-point calibration curve

which was prepared gravimetrically by standard additions of the mixed element standard to the in-house standard (i.e. GEOVIDE#1, GEOVIDE#2 or GEOVIDE#3) was ran at the beginning, the middle and the end of each run. GSP and GSC seawater were also run.

At the IMAS (offline preconcentration)

The main difference was the use of the seaFAST-picoTM on-line with the SF-ICP-MS at the LEMAR versus off-line at the IMAS (Fig. 2.6). Consequently, the 750 μL of eluent were collected into 5mL-acid-cleaned PP tubes (for cleaning procedure refer to Section 2.1.2.3) via the probe prior to analysis of the trace metal concentrations by the SF-ICP-MS (CSL at UTAS, Wuttig et al., in prep.). A preconcentration run on the seaFAST-picoTM consisted of 2 times 3 replicates of UHPW blanks, 1 replicate of a four-point internal calibration curve (0, 1, 5 and 10 ppb final eluted concentration) prepared by standard additions of the multi-element standard to the acidified in-house standard (HEOBI#1 or HEOBI#2) 2‰ (v/v) HCl (11M, SeastarTM Baseline®), 3 replicates of the zero standard addition, the reference and certified seawater matrices and the samples. An external calibration curve (i.e. no preconcentration step) was also prepared for the SF-ICP-MS to allow quantification of the percentage of recovery of the Nobias column. The external calibration curve consisted of a four-point calibration curve (0, 1, 5 and 10 ppb) prepared in HNO₃ 10% (v/v) (16M, SeastarTM, Baseline®) with UHPW and spiked with 1 mL L⁻¹ Rhodium (Rh, PlasmaCAL calibration standards) to correct for sensitivity changes on the SF-ICP-MS and evaporation on the seaFAST-picoTM. For each SF-ICP-MS run at least one Mo standard of 10 ppb was analysed to correct for any contribution of MoO⁺ interference in the measured Cd signal. In-between each standard analysis, each depth profile and at the end of the analysis two rinses and one Quality Check (QC, see Section 3.2.2.2 for preparation detail) were analysed to check for SF-ICP-MS blanks and for instrumental drifts over the 7-8 hours of the run, respectively.

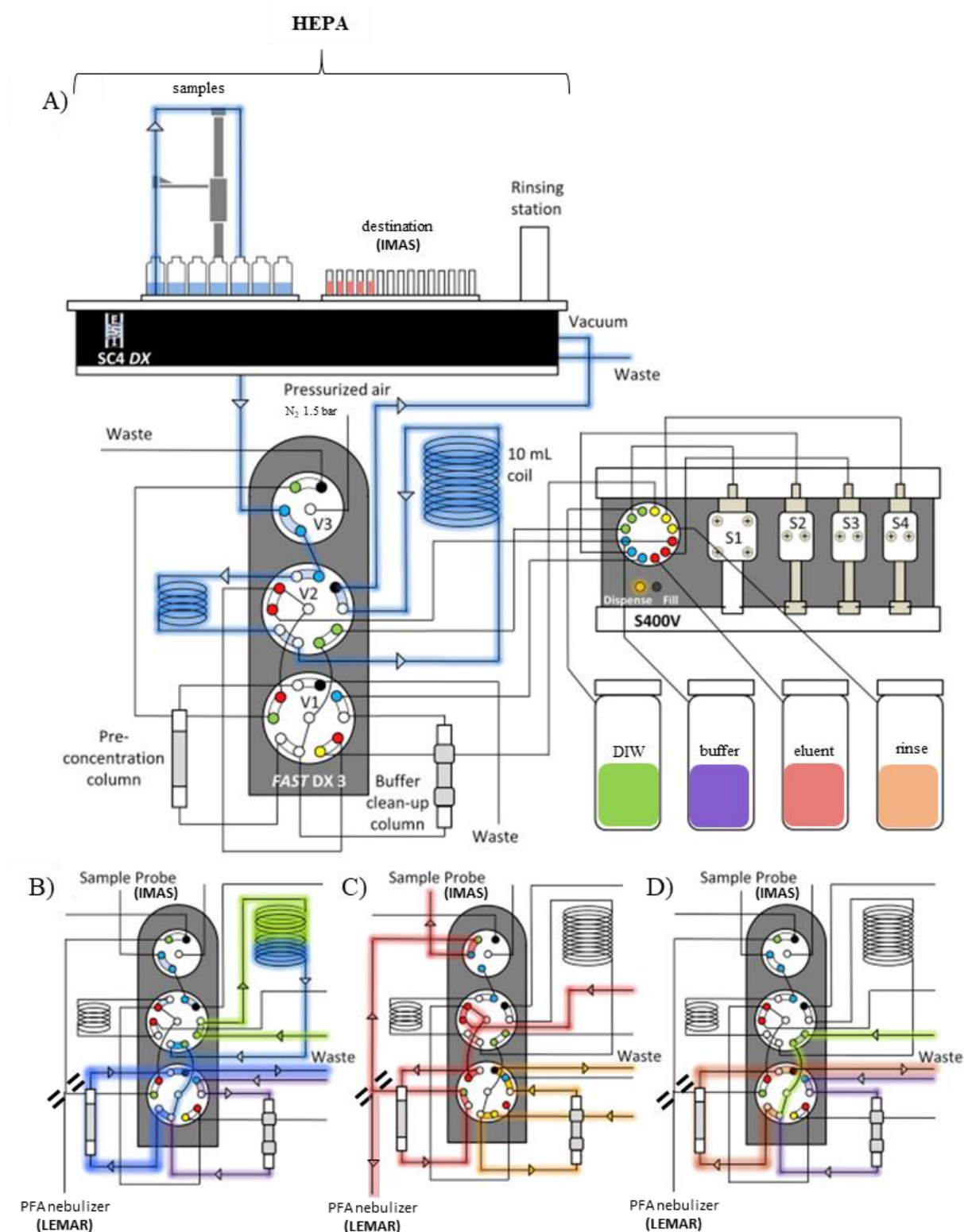


Figure 2.6: Schematic of the off-line flow injection systems used at the IMAS showing solution flow paths during A) filling of sample and buffer loops, B) loading of buffered sample onto the column, C) column rinsing and conditioning, and D) elution of trace metals. Note that V1 to V3 refer to the three valves and that S1 to S4 refer to the four syringes (modified from Rapp et al., 2017).

2.4.2.2 Reagent preparation

UHPW was used on a daily basis to prepare the following reagents in acid cleaned LDPE, FEP or PTFE bottles (see Section 2.1.2.3 for cleaning procedure):

At the LEMAR (online system)

The ammonium acetate buffer – An acetic acid-ammonium acetate buffer (CH_3COO^- and NH_4^+) was made of 140 mL acetic acid (> 99% NORMATOM® - VWR chemicals) and ammonium hydroxide (25%, Merck Suprapur®) in 500 mL PTFE bottles and was adjusted to $\text{pH } 6.0 \pm 0.2$ for the on-line pH adjustment of the samples.

The eluent – The elution acid was made of 1.4 M nitric acid (HNO_3 , Merck Ultrapur®) in UHPW (Milli-Q) by a 10-fold dilution and spiked with $1 \mu\text{g L}^{-1} \text{ }^{115}\text{In}$ (SCP Science calibration standards) to allow for drift correction.

Rinsing and carrier solutions – Autosampler and column rinsing solutions were made of HNO_3 2.5% (v/v) (Merck Suprapur®) in Milli-Q water. The carrier solution driven by the syringe pumps to move the sample and buffer through the flow injection system was made in the same way.

Standard solution – Mixed element standard solution was prepared gravimetrically using high purity standards (Fe, Mn, Cd, Co, Zn, Cu, Pb; SCP Science calibration standards) in HNO_3 3% (v/v) (Merck Ultrapur®).

At the IMAS (offline system)

For the seaFAST-picoTM preconcentration system

The ammonium acetate buffer – A 4 M acetic acid-ammonium acetate buffer (CH_3COO^- and NH_4^+) was made of 280 mL of acetic acid (18M, SeastarTM, Baseline®) and 384 mL ammonia solution (11M, SeastarTM, Baseline®) made up to 1L with UHPW and was adjusted to $\text{pH } 6.1 \pm 0.1$ for the pH adjustment of the samples.

The eluent and carrier – The elution and carrier acid was made of 106 mL HNO_3 (16M, SeastarTM, Baseline®) made up to 1L with UHPW. The eluent was spiked with 1 mL L^{-1} rhodium (^{103}Rh , QCD Analysts, Spring Lake, USA).

Rinsing solutions – Autosampler, column rinsing solutions and carrier solution were made of HNO_3 2% (v/v) (16M, SeastarTM, Baseline®) in UHPW and in 4L batches.

Standard solution (internal calibration) – Mixed element standard solution was prepared gravimetrically using high purity standards (Fe, Mn, Co, Zn, Cu, Pb, Ti, Cd, Ni, Ga, V;

PlasmaCAL calibration standards) in HNO₃ 2‰ (v/v) (16M, SeastarTM, Baseline®) with UHPW. For the 40x preconcentration matrix-matched standards were prepared using 39 mL of acidified 2‰ (v/v) HCl (11M, SeastarTM, Baseline®) in-house HEOBI#1 or #2 and 1 mL of multi-element standard solution (0, 1, 5, 10 µg L⁻¹) in 2‰ (v/v) (16M, SeastarTM, Baseline®) and treated as samples, thus leading to the same matrix as for the external calibration after pre-concentration.

For the ICP-MS analysis

Rinse solution – Daily 2-3L rinse acid were made of 10% HNO₃ (v/v) (16M, SeastarTM, Baseline®) completed to 1L with UHPW.

Standard solution (external calibration) – Mixed element standard solution was prepared gravimetrically using high purity standards (Fe, Mn, Co, Zn, Cu, Pb, Ti, Cd, Ni, Ga, V; PlasmaCAL calibration standards) in HNO₃ 10% (v/v) (16M, SeastarTM, Baseline®) with UHPW and spiked with 1 mL L⁻¹ rhodium (¹⁰³Rh, QCD Analysts, Spring Lake, USA) to allow for drift correction. Note that samples were not UV-digested, therefore, for dissolved Co and Cd concentrations correspond to their labile fraction, namely the fraction of dissolved that is not bound by strong organic ligands (Lagerström et al., 2013).

Rinses – The rinses were prepared in the same way of the 0 ppb standard, 0 ppb standard in 10% HNO₃ (v/v) (16M, SeastarTM, Baseline®) with UHPW spiked with Rh 1mL L⁻¹.

QCs – The QCs were prepared in the same way of the 1 ppb standard, 1 ppb standard in 10% HNO₃ (v/v) (16M, SeastarTM, Baseline®) with UHPW spiked with Rh 1mL L⁻¹.

2.4.2.3 Precision, accuracy and reproducibility

Sample concentrations and procedural blanks were calculated from In and Rh-normalized data at the LEMAR and IMAS, respectively. For both seaFAST-picoTM SF-ICP-MS analytical techniques, data were blank-corrected by subtracting an average acidified UHPW blank that was pre-concentrated on the seaFAST in the same way as the samples and seawater standards. The detection limit for a given run was calculated as 3 times the standard deviation of the acidified UHPW blanks.

At the LEMAR

Precision was assessed through the standard deviation of replicate samples (every 10th sample was a replicate, i.e. 6 replicates), accuracy was determined from analysis of consensus (SAFe S, GSP) and certified (NASS-7) seawater matrices and repeatability was

assessed through the average of the in-house standard GEOVIDE seawater, the UHPW blanks all runs together (Table 2.1). The reference seawater averaged: $S = 0.10 \pm 0.01 \text{ nmol L}^{-1}$ ($n = 12$). The GSP seawater matrix averaged 0.16 ± 0.04 ($n = 15$). The certified NASS-7 seawater matrix averaged $6.7 \pm 1.7 \text{ nmol L}^{-1}$ ($n = 12$), for a certified DFe concentration of $6.3 \pm 0.5 \text{ nmol L}^{-1}$ (<https://www.nrc-cnrc.gc.ca>). The in-house standards used for the seaFAST calibration averaged GEOVIDE#1 = $0.22 \pm 0.06 \text{ nmol L}^{-1}$ ($n = 30$), GEOVIDE#2 = $0.96 \pm 0.13 \text{ nmol L}^{-1}$ ($n = 39$) and GEOVIDE#3 = $0.42 \pm 0.07 \text{ nmol L}^{-1}$ ($n = 84$), the UHPW blanks averaged $0.08 \pm 0.09 \text{ nmol L}^{-1}$ ($n = 17$) and the detection limit was on average $0.05 \pm 0.05 \text{ nmol L}^{-1}$ ($n = 17$).

Table 2.1: SAFe S, GSP and NASS-7 dissolved iron concentrations (DFe, nmol L⁻¹) determined by the SeaFAST-picoTM and their consensus (SAFe S, GSP; <https://websites.pmc.ucsc.edu/~kbruland/GeotracesSaFe/kwbGeotracesSaFe.html>) and certified (NASS-7; https://www.nrc-cnrc.gc.ca/eng/solutions/advisory/crm/certificates/nass_7.html) DFe concentrations. Note that yet no consensual value is reported for the GSP seawater.

Seawater used for calibration	SeaFAST-pico TM DFe values (nmol L ⁻¹)				reference or certified DFe values (nmol L ⁻¹)		
	Average	SD	n		Average	SD	
SAFe S	0.100	± 0.006	2		0.095	± 0.008	
GSP	0.16	± 0.04	15		NA	\pm	NA
NASS-7	6.7	± 1.7	12		6.3	± 0.5	

At the IMAS

Precision was assessed through the standard deviation of QCs and of HEOBI#2 seawater replicates within the same run, accuracy was determined from analysis of consensus (SAFe S, GSP, GSC, SAFe D1), certified (NASS-6) (Table 2.2) and in-house standard HEOBI#1 seawater matrices and repeatability was assessed through the average of the QCs, UHPW blanks and HEOBI#2 seawater all runs together (Fig. 2.17B and D). The precision was 2% for the QCs and 30% for the HEOBI#2. The reference seawater matrices averaged: $S = 0.13 \pm 0.01 \text{ nmol L}^{-1}$ ($n = 2$), $D1 = 0.73 \pm 0.01 \text{ nmol L}^{-1}$ ($n = 2$). The GSP and GSC seawater matrices averaged 0.14 ± 0.06 ($n = 10$) and 1.8 ± 0.1 ($n = 10$), respectively. The certified NASS-6 seawater matrix averaged $NASS-6 = 9.5 \pm 0.5 \text{ nmol L}^{-1}$ ($n = 13$), for a certified DFe concentration of $8.9 \pm 0.8 \text{ nmol L}^{-1}$ (<https://www.nrc-cnrc.gc.ca>). The in-house standards averaged $HEOBI\#1 = 0.15 \pm 0.06 \text{ nmol L}^{-1}$ ($n = 20$). Throughout the runs the QCs (DFe = 17.9 nmol L^{-1}) averaged $18.2 \pm 0.5 \text{ nmol L}^{-1}$ ($n = 28$), the in-house standards used for

the seaFAST calibration averaged $\text{HEOBI\#2} = 0.10 \pm 0.06 \text{ nmol L}^{-1}$ ($n = 46$), the UHPW blanks averaged $0.03 \pm 0.02 \text{ nmol L}^{-1}$ ($n = 30$) and the detection limit was on average $0.03 \pm 0.03 \text{ nmol L}^{-1}$ ($n = 15$).

Table 2.2: SAFe S, SAFe D1, GSP, GSC and NASS-6 dissolved iron concentrations (DFe, nmol L⁻¹) determined by the SeaFAST-pico™ and their consensus (SAFe S, SAFe D1, GSP, GSC; <https://websites.pmc.ucsc.edu/~kbruland/GeotracesSaFe/kwbGeotracesSaFe.html>) and certified (NASS-6; https://www.nrc-cnrc.gc.ca/eng/solutions/advisory/crm/certificates/nass_6.html) DFe concentrations. Note that yet no consensual value is reported for the GSP nor GSC seawater samples.

Seawater used for calibration	SeaFAST-pico™ DFe values (nmol L ⁻¹)				reference or certified DFe values (nmol L ⁻¹)		
	Average	SD	n		Average	SD	
SAFe S	0.13	± 0.01	2		0.095 ± 0.008		
SAFe D1	0.73	± 0.01	2		0.69 ± 0.04		
GSP	0.14	± 0.06	10		NA ± NA		
GSC	1.8	± 0.1	10		NA ± NA		
NASS-6	9.5	± 0.5	13		8.9 ± 0.8		

2.4.3 Fe-binding organic ligand analysis

Competing ligand exchange adsorptive cathodic stripping voltammetry (CLE-AdCSV) was employed for the determination of Fe-binding organic complexation of the HEOBI samples that are discussed in Chapter 5.

2.4.3.1 Principle of analysis

Voltammetry analytical techniques are based on the measurement of a current as the potential is varied. The method detects charge transfer processes, which in case of Fe concerns the reduction of Fe(III) into Fe(II) between an electrode (i.e. mercury (Hg) working electrode) and an electrolyte (i.e. the sample) (Fig. 2.7). The voltammetry uses a three-electrode setup consisting of a working electrode, a reference electrode and an auxiliary electrode to measure the Fe-binding organic ligand concentrations (in Equivalent of nmol L^{-1} of Fe, Eq of nmol L^{-1} Fe) and strength.

The whole voltammetric cell is under dry ultra-high-purity grade N_2 gas (Supagas® or BOC®) pressure. This allows on one hand, the removal of dissolved O_2 from the sample that can interfere with the signal (Fig. 2.7, 1), and on the other hand the formation of a new Hg drop at the large static Hanging Mercury Drop Electrode (HMDE, Fig. 2.7, 2) for each measurement. The reference electrode (Fig. 2.7, 3) is made of a double junction Ag/saturated silver chloride (AgCl) with a salt bridge filled with 3 M potassium chloride (KCl) solution. Finally, the auxiliary electrode (Fig. 2.7, 4) made of glassy carbon rod, also called counter electrode, carries out the signal acquisition. Once a new Hg drop is formed, the acquisition of a measurement consists of two steps: the deposition and the cathodic stripping phases.

During the deposition step, also called pre-concentration phase, the potentiostat sets a potential coinciding with the stirrer starting up (Fig. 2.7, 5), which both enables the migration and the convection flow of the complexes towards the HMDE surface. The chemical species, to be adsorbed onto the Hg drop, needs to be soluble in Hg, which is not the case of Fe (low solubility in Hg, Van den Berg, 1984; Wang and Mahmoud, 1987). Therefore, to allow the measurement of sub-nanomolar Fe concentrations an artificial electroactive ligand is added to the seawater matrix that chelates Fe. The presence of this artificial ligand (L_A , Fig. 2.7) will also avoid the formation of intermetallic complexes (e.g. Fe-Mn) that could interfere with the analysis. The measurement of a complex reduction and not of a chemical species is called adsorptive voltammetry.

The cathodic stripping phase follows the pre-concentration phase and consists of sweeping towards more negative (cathodic) potentials from the potential set during the pre-concentration phase. In the case of Fe, this enables the reduction of the artificial complexes formed $\text{Fe}^{3+}\text{L}_\text{A}$ (Fig. 2.7) and the subsequent stripping of the analyte that takes off electrons ($\text{Fe}^{3+}\text{L}_\text{A} + \text{e}^- \rightarrow \text{Fe}^{2+}\text{L}_\text{A}$) measured as a depletion in the current (i.e. peak height) via the glassy carbon electrode (Fig. 2.8A). Concomitantly, the stirring is stopped throughout the stripping phase to allow the deposited material to distribute more evenly in the mercury drop. The acquired signal is therefore the current intensity as a function of the potential (Fig. 2.8A). The potential of the reduction peak is specific of the chemical species and of the method used.

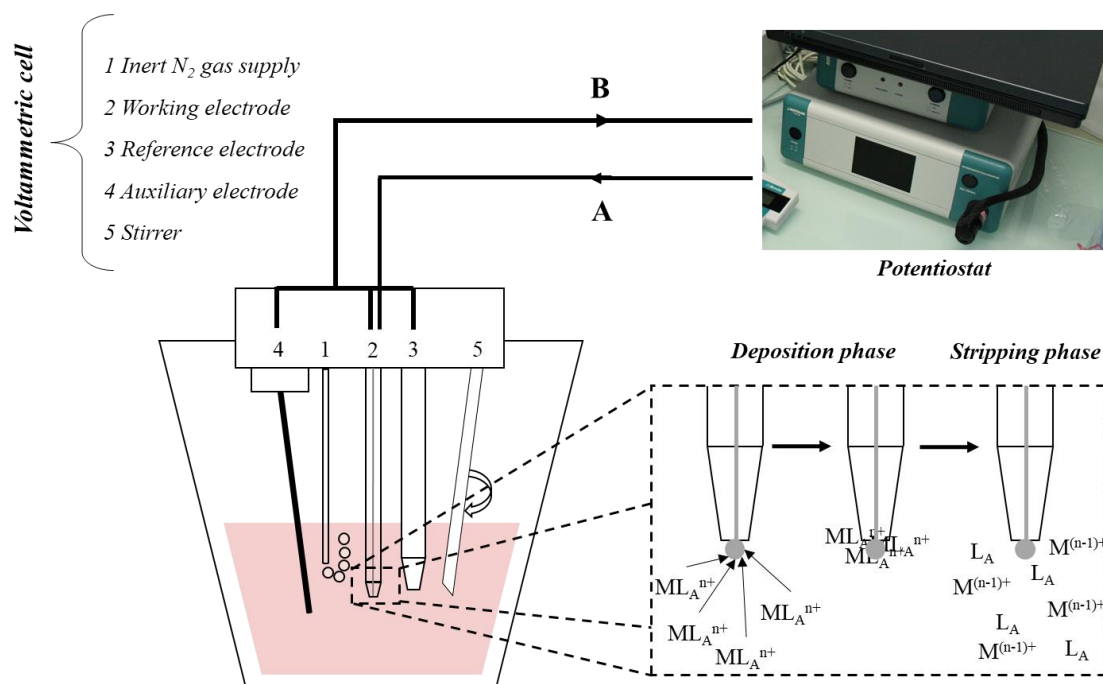


Figure 2.7: Schematic of the voltammetric cell and electrochemical process involved during analysis. A corresponds to the potential imposed by the potentiostat and B to the current measured. The frame represents the reduction reaction of artificial metallic complexes in adsorptive cathodic stripping voltammetry (AdCSV). (Modified from Cheize, 2012).

2.4.3.2 Material, reagents and sample preparation

Material

The equipment consisted of a μ Autolab Type III potentiostat and a 663 VA Stand (Metrohm[®], France) controlled by the NOVA 2.0 software (Metrohm, Autolab). Samples were stirred using the inbuilt Teflon[®] stirring rod (1500 rpm) of the VA 663 Stand. All

equipment was protected against electrical noise by a current filter (Fortress 750, Best Power).

Reagents

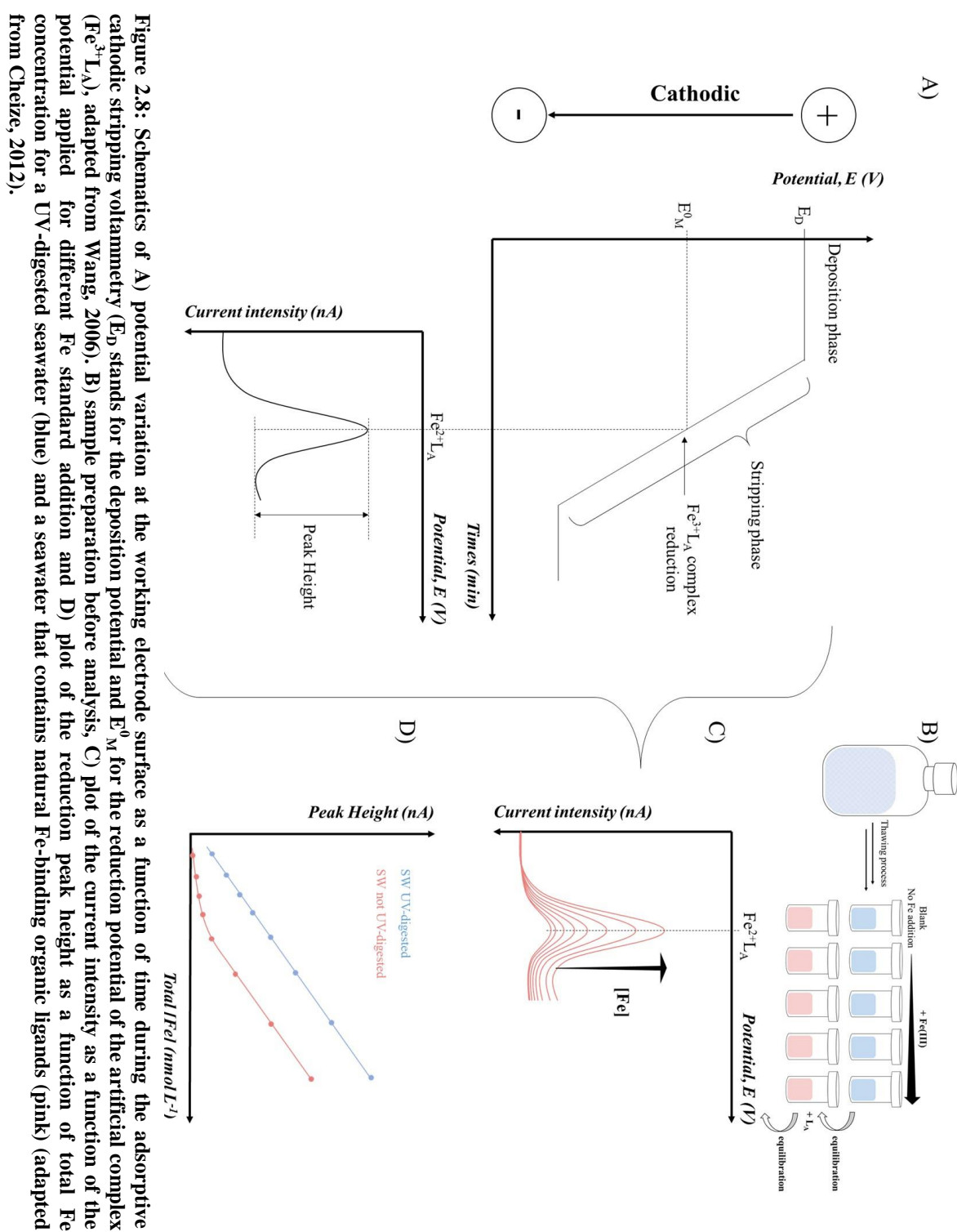
The method employed was the one from Croot and Johansson (2000) using the 2-(2-Thiazolylazo)-*p*-cresol (TAC, Aldrich) as the competing ligand. A fresh 0.01 M stock solution of the artificial ligand (TAC, Aldrich) in methanol (CH₃OH, HPLC grade, 99.9%, Fluka) was prepared weekly and stored in the fridge at 4°C, no purification was performed. The buffer 3-[4-(2-hydroxyethyl)-1-piperazinyl]-propanesulfonic acid (EPPS, 99% Sigma, 1M) was prepared in ammonium (NH₄OH, SeastarTM Baseline®, 1M) and the pH was adjusted to 8.05 using either HCl or NH₃ (SeastarTM Baseline®). The buffer was purified three times on an 8-hydroxyquinoline (8-HQ) resin. Before reagent purification, the resin was pre-cleaned with 500 mL of 0.5 M HCl (SeastarTM Baseline®), and rinsed thoroughly with 500 mL of UHPW using a peristaltic pump. Iron standard solutions were prepared by dilution of a commercial solution of FeCl₃·6H₂O (Carlo Erba Reagenti) into UHPW acidified at 0.1 % (v/v) with HCl (SeastarTM Baseline®). A first solution, F1, was prepared gravimetrically to a final concentration of 0.1 M. Then F2 and F3 solutions were prepared by adding respectively 500 and 50 µL of the F1 solution to 50 mL of acidified UHPW to a final concentration of 1 µM and 100 nM respectively. These standard solutions were prepared fortnightly.

Sample preparation for titration

Once the sample bottle is defrosted at ambient temperature, fourteen aliquots of 10 mL were distributed to lidded Teflon[®] vials (Savillex, see Section 2.1.2.3 for cleaning procedure) for the titrations (Fig. 2.8B). Note that before and after each titration vials were rinsed 5 times with UHPW and were left for a day in UHPW prior to use. Samples were prepared according to the Croot and Johansson (2000) method and titrated with spikes of Fe(III) standard solutions to final concentrations of 0, 0, 0, 0.2, 0.4, 0.6, 0.8, 1, 1.5, 2, 4, 6, 8 and 10 nmol L⁻¹ for DLt samples and of 0, 0, 0, 0, 0.1, 0.2, 0.4, 0.6, 0.8, 1, 2, 4, 6, 8 for SLt samples (Fig. 2.8B). After equilibration, the concentration of Fe(TAC)₂ within the samples was measured using the method fully described by Croot and Johansson (2000).

Once the aliquots analysed, increasing peak heights are obtained for higher Fe additions (Fig. 2.8C). While representing the peak height as a function of the total Fe concentration (i.e. the Fe present in the sample + Fe(III) standard addition), two slopes are observed in case of the presence of natural Fe-binding organic ligands (Fig. 2.8D, pink

curve). The first slope corresponds to the gradual saturation of the excess natural ligands in Fe with Fe standard addition, thus limiting the complexation of the artificial ligand with Fe. Consequently, the reduction of the artificial complexes is lower until the Fe addition corresponds to the Fe saturation of natural ligands, after which concentration, the artificial ligand is able to complex with Fe without any competition thus leading to a linear curve, i.e. the second slope (i.e. S , the sensitivity), identical as the one for a UV-digested seawater. Indeed, in case of UV-digestion of the seawater, all the natural Fe-binding organic ligands are destroyed and thus a linear curve is obtained between the peak height and the total Fe concentration (Fig. 2.8D, blue line).



2.4.3.3 Theory of competitive ligand equilibration and adsorptive cathodic stripping voltammetry (CLE-AdCSV) using TAC as artificial ligand

The principle of measuring the binding characteristics of Fe-binding organic ligands is extensively described (e.g. Croot and Johansson, 2000; Gledhill and Buck, 2012; Gledhill and Van Den Berg, 1994). Briefly, the CLE phase entails the formation of an equilibrium between the natural Fe(III)-complexing ligands and a known quantity of an artificial competing ligand, which forms an electroactive complex with Fe. This electroactive complex is defined by a known conditional stability constant (i.e. $K_{Fe(TAC)_2, Fe^{3+}}^{cond}$). In the AdCSV phase, the Fe-TAC complex formed during equilibration is adsorbed potentiostatically onto the hanging Hg drop electrode and subsequently reduced during a cathodic potential scan. The reduction current measured from the adsorbed Fe-TAC complex is then used to calculate the ligand concentrations and stability constants of the natural Fe(III)-complexing ligands.

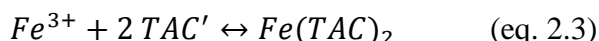
In the absence of an artificial competing ligand, the mass balance formed between all the Fe species in ambient seawater can be represented as in equation 2.1:

$$[Fe_T] = \sum_i [Fe'] + \sum_i [FeL_i] \quad (\text{eq. 2.1})$$

where $\sum_i [Fe']$ represents the sum of all inorganic Fe species and complexes ($\sum_i [Fe'] = [Fe^{3+}] \times (1 + \sum_{j=1}^2 K_j' [L_{inorg}^-])$), and $\sum_i [FeL_i]$ represents the sum of all Fe complexes formed with the different classes of natural organic ligands. Upon the addition of TAC, the new mass balance formed with all species of Fe can be represented as in equation 2.2:

$$[Fe_T] = \sum_i [Fe'] + \sum_i [FeL_i] + \sum_i [Fe(TAC)_2] \quad (\text{eq. 2.2})$$

where $\sum_i [Fe(TAC)_2]$ is the sum of all Fe-TAC complexes formed following the addition of TAC, in equilibration with Fe^{3+} as follows:



where TAC' is the free TAC defined here as the concentration of TAC that is not bound to Fe. This equilibrium is set by a known conditional stability constant ($\beta_{Fe(TAC)_2, Fe^{3+}}^{cond}$) between Fe and TAC which is defined as in equation 2.4:

$$\beta_{Fe(TAC)_2, Fe^{3+}}^{cond} = \frac{[Fe(TAC)_2]}{[Fe^{3+}][TAC']^2} \quad (\text{eq. 2.4})$$

Since TAC is largely in excess, it is assumed that $[TAC'] = [TAC]$ and thus for $[TAC] = 10 \mu\text{M}$, $\beta_{Fe(TAC)_2, Fe^{3+}}^{cond} = 10^{22.4}$ (Croot and Johansson, 2000). Using equation 2.4 gives:

$$[Fe^{3+}] = \frac{[Fe(TAC)_2]}{\alpha_{Fe(TAC)_2}} \quad (\text{eq. 2.5})$$

with $\alpha_{Fe(TAC)_2}$, the side reaction coefficient for $Fe(TAC)_2$, defined as follows:

$$\alpha_{Fe(TAC)_2} = \beta_{Fe(TAC)_2, Fe^{3+}}^{cond} [TAC]^2 = 10^{12.4} \quad (\text{eq. 2.6})$$

According to the mass balance of Fe, equation 2.7 is obtained:

$$[FeL] = [Fe_{initial}] + [Fe_{added}] - [Fe(TAC)_2] \quad (\text{eq. 2.7})$$

where $[FeL]$ is the concentration of natural Fe-binding organic ligand complexed to Fe, $[Fe_{initial}]$ is the Fe concentration measured by SeaFAST-picoTM-Element 2 SF-ICP-MS for either the dissolved or soluble fractions; $[Fe_{added}]$ is the Fe concentration added for the titration and $[Fe(TAC)_2]$ is the concentration of Fe bound to TAC and is calculated for every Fe addition by dividing the peak height (nA) by the slope of the straight part of the titration curve (i.e. S). The slope of the method is influenced by ligand sites not yet saturated with Fe and the analytical sensitivity (S, in nA L mol⁻¹ min⁻¹) is obtained from the slope of the linear part of the titration curve, where all natural Fe(III) ligands are saturated with Fe.

2.4.3.4 Determination of Fe-binding ligand characteristics

The resulting titrations from the CLE-AdCSV analyses were interpreted using the ProMCC program (Omanović et al., 2015) that combines the Van den Berg/Ruzic (Ruzic, 1982; Van den Berg, 1984), Langmuir/Gerringa (Gerringa et al., 1995) and Scatchard (Mantoura and Riley, 1975; Scatchard et al., 1957) linearization techniques resulting in an average value for conditional stability constants ($K_{FeL, Fe^{3+}}^{cond}$, reported in Chapter 5 with respect to Fe^{3+}), total Fe-binding organic ligand concentrations ($[Lt]$) and their respective standard deviations (Buck et al., 2012). Sensitivity (S) of the voltammetric response to iron additions was determined from the slope of at least the last three titration points, and the slope that provided the best fit between the output of all interpretation techniques was typically used for the result calculations.

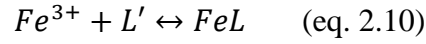
The Langmuir model (Gledhill and Van Den Berg, 1994) assumes that equilibrium between all Fe(III) species exists, all binding sites between Fe and the unknown ligand are equal and binding is reversible, as follows:

$$[FeL] = \frac{K_{FeL, Fe^{3+}}^{cond} [Fe^{3+}] [Lt]}{1 + K_{FeL, Fe^{3+}}^{cond} [Fe^{3+}]} \quad (\text{eq. 2.8})$$

where $[FeL]$ is the concentration of natural Fe-binding organic ligand complexed to Fe assuming the existence of one organic ligand, and a 1:1 coordination, $[Fe^{3+}]$ is the ionic Fe concentration, $K_{FeL, Fe^{3+}}^{cond}$ and $[Lt]$ are two unknown parameters that need to be determined (cf. eqs. 2.9, 2.10 and 2.11).

$$K_{FeL, Fe^{3+}}^{cond} = \frac{[FeL]}{[Fe^{3+}] [Lt]} \quad (\text{eq. 2.9})$$

where $K_{FeL,Fe^{3+}}^{cond}$ is the conditional stability constant of Fe^{3+} with the natural ligand, $[L']$ is the concentration of empty ligand sites, i.e. the excess ligand concentration. Assuming equilibrium as follows:



Then the ligand mass balance can be expressed as follows:

$$[Lt] = [FeL] + [L'] \quad (\text{eq. 2.11})$$

Combining equations 9 and 11 and writing it as a function of $[FeL]$ gives equation 8.

$K_{FeL,Fe^{3+}}^{cond}$ can be converted to $K_{FeL,Fe'}^{cond}$ (conditional stability constant with respect to Fe') using the inorganic side reaction coefficient ($\alpha'_{Fe} = [Fe']/[Fe^{3+}]$) as follow:

$$K_{FeL,Fe^{3+}}^{cond} = \alpha'_{Fe} K_{FeL,Fe'}^{cond} \quad (\text{eq. 2.12})$$

where $\alpha'_{Fe} = 10^{10}$ from the work of Hudson et al. (1992), Kuma et al. (1996) and Millero (1998).

The percentage of Fe occurring as organic species was calculated from:

$$[FeL]\% = \frac{[FeL] \times 100}{[Fe]} \quad \text{or} \quad (\text{eq. 2.13})$$

Finally, the side reaction coefficient of the organic ligand (α_{FeL} , referred to as α later in Chapter 5) was calculated as the product of $K_{FeL,Fe^{3+}}^{cond}$ or $K_{FeL,Fe'}^{cond}$ (referred to as K' later in Chapter 5) and L' :

$$\alpha_{FeL} = K_{FeL,Fe^{3+}}^{cond} \times [L'] = \frac{[FeL]}{[Fe^{3+}]} \quad (\text{eq. 2.14})$$

The ligand characteristics were calculated with two models, one assuming the presence of one ligand class and the other assuming the presence of two ligand classes. We were unable to calculate the ligand characteristics for the two ligand classes because either only one ligand group was present, the two different class characteristics were too close to be separated or the detection window applied was too high. Indeed, to be able to measure different ligand classes, the competing ligand must be in equilibrium with all the different classes of ligands present in the seawater sample, which can be achieved by increasing or decreasing the concentration of the competing artificial ligand added (i.e. TAC). The higher the concentration of the added artificial ligand, the higher the artificial ligand degree of competition is, and vice versa. A low detection window will enable the determination of strong and weaker class whereas, a higher detection window will only enable the determination of the stronger class of natural ligand (e.g. Ibisani et al., 2011; Rue and Bruland, 1995). Uncertainties of each parameter are computed by the fitting algorithm (fitter.dll) in the ProMCC in form of standard error (SE) and are expressed as 95%

confidence intervals by multiplying SE by the t-value (i.e. Student's t-distribution) calculated according to number of titration data points (Omanović et al., 2015).

2.4.3.5 Detection limit and TAC contamination

Every day, the sensitivity of the method was checked by Fe-standard additions (0, 0, 0, 0, 0.25, 0.50, 0.75 nmol L⁻¹ final concentration) to the low-Fe UV-digested HEOBI#2 seawater (i.e. the blank). The detection limit of the method was determined as 3 times the standard deviation of these blank measurements (calculated for each TAC batches, n = 5) and was equal to 0.04 ± 0.02 Eq of nmol L⁻¹ Fe (n=63). The cleanliness of the EPPS buffer was assessed by 1, 2 and 3 buffer addition to the 0.75 nmol L⁻¹ standard made in UV-digested HEOBI#2 seawater each time a new batch was prepared. The buffer was considered clean if three times the standard deviation of these three measurements were below the detection limit, otherwise the buffer was purified on an 8-HQ resin.

A second analysis of B2-B11 HEOBI samples revealed no significant differences between the [DLt] and log $K_{FeL,Fe^{3+}}^{cond}$ values obtained for this duplicate sample, as determined by an ANOVA (p-values > 0.1).

The chemical TAC from two batch bottles contained significant amounts of Fe, which resulted in an extra inadvertent addition of 0.09 and 0.15 nmol L⁻¹ Fe to some DLt samples (see Appendix D). Therefore, to analyse the titration data, 0.09 or 0.15 nmol L⁻¹ Fe was added to each DFe concentrations determined by Holmes et al. (in prep.). The consequence was that the standard deviation on the estimation of $K_{FeL,Fe^{3+}}^{cond}$ was larger (Gerringa et al., 2015). The artificial ligand contamination was estimated by subtracting the HEOBI#2 DFe concentration determined by seaFAST-picoTM from its DFe concentration determined in CLE-AdCSV from Fe-standard additions to UV-digested HEOBI#2 seawater. Note that the batch of TAC used for the determination of SLt sample characteristics was not contaminated.

2.4.4 Pigment analysis

During the GEOVIDE voyage, pigment samples were collected using the classic CTD at the same stations as for the TMR. All these pigments were analysed by High Performance Liquid Chromatography (HPLC, Agilent Technologies 1200) and then ran in the CHEMTAX model to estimate the composition of the phytoplankton community. Phytoplankton class distribution relative to nutrient availability is discussed in Chapter 4.

2.4.4.1 HPLC principle of analysis

The HPLC aims at determining the concentrations of phytoplankton pigments. It is a process where analytes are separated due to their varying distribution between two phases, namely a stationary and a mobile phases. This analytical technique allows the simultaneous detection of a wide range of pigments (i.e. carotenoids, chlorophylls and their degradation products). Pigments were separated and quantified following an adaptation of the method described by van Heukelem and Thomas (2001) and the analytical procedure used is described in Ras et al. (2008). The method adaptation allowed for higher sensitivity in the analysis of low phytoplankton biomass waters (see Ras et al., 2008).

Frozen filters were extracted at -20°C in 3 mL of methanol (100%), sonicated and then clarified by vacuum filtration through *Whatman* GF/F filters. The total extraction time was 2 hours. The extracts were then analysed by HPLC with a complete *Agilent Technologies* system (comprising *LC Chemstation* software, a degasser, a binary pump, a refrigerated autosampler, a column thermostat and a diode array detector) when possible on the same day as extraction. The sample extracts were premixed (1:1) with a tetrabutylammonium acetate (TBAA) buffer solution (28 mmol L^{-1}) prior to injection in the HPLC. The mobile phase was a mix between a solution (A) of TBAA 28 mmol L^{-1} :methanol (30:70, v:v) and a solution (B) of 100% methanol (i.e. the organic solvent) with varying proportions during analysis. At the beginning, the phase was principally made of mixing TBAA 28 mmol L^{-1} :methanol (30:70, v:v) and is thus polar. Consequently, the hydrophobic compounds will bind to the stationary phase. The organic solvent (i.e. methanol) concentration is then raised within the mobile phase until the hydrophobicity of the mobile phase become higher than the stationary phase; hydrophobic compounds are thus desorbed from the stationary phase, i.e. eluted. The gradient of concentration between the two solutions were as follows (t(min);%B;%A): (0;10;90), (25;95;5) and (28;95;5). The eluent is then carried towards the diode array detector that allowed for the absorption of most pigments to be detected at 450 nm, while chlorophyll-*a* and its derivatives were detected at 667 nm and bacteriochlorophyll-*a* at 770 nm. The diode array absorption spectra of each peak were used for identification purposes.

Pigment concentrations (in mg m^{-3}) were calculated according to Beer-Lambert's law (i.e. $A = \epsilon LC$) from the peak areas with an internal standard correction (Vitamin E acetate, Sigma) and an external standard calibration (DHI Water and Environment, Denmark). This method allowed the detection of 23 phytoplankton pigments. The detection limits, defined as

three times the signal:noise ratio for a filtered volume of 1 L, was 0.0001 mg.m^{-3} for total chlorophyll-*a* (TChl-*a*) and its injection precision was 0.91% (Table 2.3).

Table 2.3: Metric performances of the HPLC analysis.

Metric performances	
TChl- <i>a</i> injection precision	0.91 %
TChl- <i>a</i> accuracy (SeaHARRE-6)	3.72 %
Retention time precision	0.54 %
Calibration precision	0.4 %
Calibration accuracy	0.3 %

2.4.4.2 Pigment based phytoplankton size classes

The method developed by Uitz et al. (2006) was used to determine size classes for each sample. In this method, seven pigments are used as biomarkers of several phytoplankton taxa: fucoxanthin (Fuco), peridinin (Peri), alloxanthin (Allo), 19'-hexanoyloxyfucoxanthin (19HF) and 19'-butanoyloxyfucoxanthin (19BF), zeaxanthin (Zea), total chlorophyll-*b* (TChl-*b*). These taxa are then gathered into three size classes (micro-, nano-, picoplankton), according to the average size of the cells. The fraction of each pigments-based size class with respect to the total phytoplankton biomass is calculated as follows:

$$[20 ; 200] \mu\text{m}: f_{micro} = \frac{1.41 [Fuco] + 1.41 [Peri]}{\sum DP_w} \quad (\text{eq. 2.15a})$$

$$[2 ; 20] \mu\text{m}: f_{nano} = \frac{0.60 [Allo] + 0.35 [19BF] + 1.27 [19HF]}{\sum DP_w} \quad (\text{eq. 2.15b})$$

$$[0.7 ; 2] \mu\text{m}: f_{pico} = \frac{0.86 [Zea] + 1.01 [TChlb]}{\sum DP_w} \quad (\text{eq. 2.15c})$$

where $\sum DP_w$ is the sum of the concentration of the seven diagnostic weighted pigments:

$$\sum DP_w = 1.41[Fuco] + 1.41[Peri] + 0.60[Allo] + 0.35[19BF] + 1.27[19HF] + 0.86[Zea] + 1.01[TChlb] \quad (\text{eq. 2.16})$$

Each diagnostic pigment is associated with a coefficient, which represents an estimate of the average ratio of the TChl-*a* concentration to the diagnostic pigment concentration. These coefficients have been obtained by multiple regression analysis, performed on a global pigment database (Uitz et al., 2006). Consequently, the TChl-*a* biomass associated to each size class is derived according to:

$$[TChla]_{micro} = f_{micro} [TChla] \quad (\text{eq. 2.17a})$$

$$[TChla]_{nano} = f_{nano} [TChla] \quad (\text{eq. 2.17b})$$

$$[TChla]_{pico} = f_{pico} [TChla] \quad (\text{eq. 2.17c})$$

While solving these equations, a matrix is obtained in which TChl-*a* biomass is split into three size classes (eq. 2.15) as well as the percentage of biomass for each size class (eq. 2.17) and by samples.

2.4.4.3 CHEMTAX model

CHEMTAX (software version 195; Mackey et al., 1996) was used to reveal the presence of taxonomically distinct pigment signatures. The aim of this method is to estimate the abundance of phytoplankton classes based on pigment concentrations in various water samples and the concentration of each taxonomic group relative to TChl-*a*. As recommended by Wright and Jeffrey (2006), random variation was added to each input matrix to use

different starting points within CHEMTAX and to circumvent local minima. Random variation was generated by multiplying each cell of the initial table by a randomly determined factor F , where $F = 1 + S * (R - 0.5)$, S is a scaling factor (normally 0.7), and R is a random number between 0 and 1 generated using the Microsoft Excel RAND function (Wright and Jeffrey, 2006). Finally, the output matrices were built from the solutions presenting the smallest residual (i.e. 10%, $n = 6$, Lampert, 2014). CHEMTAX was run iteratively 500 times and the ratio limit matrix (RLM) used was fixed to a value of 500 for all the pigments except TChl-*a* for which RLM were fixed at a value of 100. This enabled each pigment:TChl-*a* ratio to change by 500% of their initial value. The degree of freedom was increased by choosing the maximum ratios reported from the literature in the covered area as recommended by Mackey et al. (1997). By adopting a high degree of freedom approach, the initial pigment ratios selected are less critical to the output. Some tests with RLM fixed at 200 were also performed with only very small differences between RLM used.

Selecting biomarker pigments

While TChl-*a* is the universal proxy for phytoplankton abundance, other pigments (e.g. carotenoids, chlorophyll-*b* and *c*,) are unique to specific phytoplankton groups (e.g. cyanobacteria, chlorophytes, diatoms), and their respective proportion to TChl-*a* is a proxy of the community composition (e.g. Gieskes et al., 1988; Jeffrey et al., 1997; Mackey et al., 1996; Prézelin et al., 2000). Among the pigments quantified by HPLC, only the following pigments were included in the chemotaxonomic analysis: chlorophyll-*c3* (*c3*), peridinin, 19BF, 19HF, fucoxanthin, prasinoxanthin, alloxanthin, violaxanthin, neoxanthin, zeaxanthin, TChl-*b*, lutein and TChl-*a* (see Table 2.4 for CHEMTAX pigment selection). Note that Chlorophyllide-*a* and phaeopigments (phaeophorbide-*a* and phaeophytine-*a*) are degradation products. Chlorophyllide-*a* is a tracer of senescent diatoms while the degradation products derived from the demetallation of chlorophyll-*a* (phaeophorbide-*a* and phaeophytine-*a*) are grazing tracers and therefore underline the presence of zooplankton. Since the two photoprotective pigments, diadinoxanthin and diatoxanthin, are so widespread taxonomically and are part of a diadinoxanthophyll cycle, they were not selected for the chemotaxonomy estimates however, their relative concentrations change rapidly with irradiance (Demers et al., 1991) and hence they are valuable indicators of light history (Claustre, 1994; Welschmeyer and Hoepffner, 1986). Note that the distribution of the selected pigments measured along the GEOVIDE section is described in Appendix C1.

Table 2.4: Selection of pigments and their associated taxonomic significance for the CHEMTAX model. Note that pigments were selected according to Roy et al. (2011, and references therein). A comparison between the flowcount (La Roche et al., in prep.; data from GEOVIDE voyage), N₂-fixation (Fonseca Batista, unpublished data) data and the percentage of cyanobacteria determined by CHEMTAX was done, as the major source of the zeaxanthin pigment in polar waters has been shown to originate from bacteria (Wright et al., 2009). However, their drift to higher latitudes is possible in the study region via the Gulf Stream (LaRoche and Breitbarth, 2005). Heterotrophic dinophytes may be dominant but are invisible to pigment analysis due to endosymbiosis processes during which they acquired chloroplast and pigments from other taxa. The only unambiguous pigment available in the data set is peridinin, which is only representative of type-1 dinophytes (e.g. *Amphidinium carterae*, Roy et al., 2011), thus dinophytes will be generally under-estimated in the output of the CHEMTAX model. Although Chlorophyll-*c* are usefull markers of chromophytes algae (Jeffrey et al., 1997), since the Chlorophyll-*c1* (c1), and -*c2* (c2) were not separated in the HPLC technique used, only Chlorophyll-*c3* (c3) was considered. Finally, as part of the diadino xanthophyll cycle, the two photoprotective pigments, diadinoxanthin and diatoxanthin, were not considered within the CHEMTAX model.

Pigments	Abbreviation	Taxonomic or biogeochemical significance
Total Chlorophyll- <i>a</i>	TChl- <i>a</i> *	Algal biomass
Fucoxanthin	Fucox	diatoms, haptophytes, pelagophytes
Zeaxanthin	Zeax	cyanobacteria, chlorophytes, prasinophytes
Peridinin	Peri	dinophytes-type 1 ‡
Neoxanthin	Neox	chlorophytes, prasinophytes
Violaxanthin	Violax	chlorophytes, prasinophytes
Zeaxanthin	Zeax	chlorophytes, prasinophytes
Lutein	Lut	chlorophytes, prasinophytes
Total Chlorophyll- <i>b</i>	TChl- <i>b</i> †	chlorophytes, prasinophytes
Prasinoxanthin	Prasinox	prasinophytes
Alloxanthin	Allox	cryptophytes
19'-hexanoyloxyfucoxanthin	19HF	haptophytes, pelagophytes
19'-butanoyloxyfucoxanthin	19BF	haptophytes, pelagophytes
Chlorophyll- <i>c3</i>	c3	haptophytes, pelagophytes

* TChl-*a* = Chl-*a* + DVChl-*a* , since DVChl-*a* was under detection limits, thus TChl-*a* only refers to Chl-*a*.

† TChl-*b* = Chl-*b* + DVChl-*b*, since DVChl-*b* was not separated from Chl-*b*, thus prochlorophytes (biomarker pigments: DVChl-*a*, DVChl-*b* and Zeax), which are part of the Cyanophyta phylum, are only considered under the general cyanobacteria term (Jeffrey and Wright, 2006).

‡ Note that algal type used within this thesis are defined according to Jeffrey et al. (1997) and Zapata et al. (2004).

Clustering the dataset

Due to the inherent variability of the dataset, prior to running the CHEMTAX model and determining the phytoplankton classes, a Principal Component Analysis (PCA) was performed on selected pigments (except for the TChl-*a*, as it explained the entire phytoplankton organism distribution) and was followed by a clustering analysis on the PCA output to gather the samples according to their intra-specific correlations, which splits the pigment data matrix [S] into seven groups (Fig. 2.9) of homogeneous pigment correlations to optimise calculus. Therefore, the groups are closer to the natural patchiness distribution of phytoplankton organisms and will help interpreting pigments regarding biogeochemical processes and water mass distributions without establishing any subjective groups. Finally, this pre-data treatment allowed the achievement of constant pigment ratios across each group of samples that are ran together in CHEMTAX, an assumption that is presumed validated prior to run CHEMTAX.

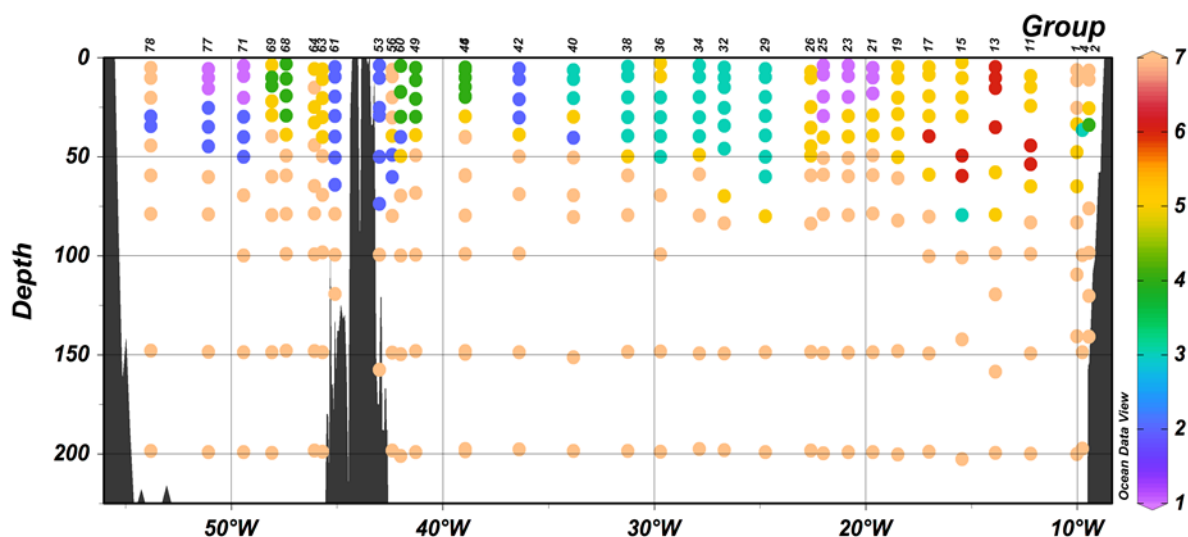


Figure 2.9: Distribution of the groups determined on the output of a Principal Component Analysis (PCA).

Initial pigment matrices [F0]

To tackle the lack of phytoplankton determination by microscopy, initial pigment ratios matrices used in the iterations for CHEMTAX were obtained combining published pigment ratio matrices from studies accomplished in the North Atlantic Ocean and the European Marine Observation and Data Network (EMODN) database¹ in the North Atlantic Ocean. Note that special attention was given to studies using the CHEMTAX method (Gibb

¹ <http://www.emodnet-biology.eu/toolbox/en/download/occurrence/explore>

et al., 2001; van de Poll et al., 2013; Veldhuis and Kraay, 2004) and that only species reported within 1° from the GEOVIDE transect were considered from the EMODN database to ensure representative species were not omitted.

All other classes previously described in the North Atlantic Ocean, including Chlorophytes, Diatoms (despite the presences of different species, cf. EMODN database), Prasinophytes, Pelagophytes and Cryptophytes, were used without any subclassification (see Table 2.5). Hence, four matrices were selected as input matrices (Table 2.6) and were ran separately to the 7 groups determined by the PCA and clustering analysis (see Table 2.7). These results are an approach of algal class chlorophyll biomass distribution obtained by chemotaxonomy and are only an estimation of the main trend of algal class compositions.

Validation of output matrices

CHEMTAX output ratios were in good agreement with the range of values observed in the literature (e.g. Gibb et al., 2001; Roy et al., 2011; van de Poll et al., 2013; Veldhuis and Kraay, 2004) except for group 2, which presented very high chlorophyll-*c3*:TChl-*a* ratio, out of the observed range for type-8-haptophytes (Table 2.7, in red) in both culture and natural assemblages and was thus unlikely plausible. Indeed, in spite of the significant correlation displayed between *c3* and both HF ($R^2 = 0.59$, p-value < 0.001) and BF ($R^2 = 0.67$, p-value < 0.001), *c3* was also strongly correlated to TChl-*b* ($R^2 = 0.70$, p-value < 0.001). However, no better resolution could be obtained for this group.

The utilization of the same pigments to determine the chlorophyte and the prasinophyte functional-classes in the matrices could lead to calculation issues in the output matrix. Indeed, while running the CHEMTAX model, the fitting step can lead to the flip-flopping of the defined pigment ratios in between classes using the same input pigments (Wright and Jeffrey, 2006). Although pigment:TChl-*a* ratios for chlorophyte and prasinophyte classes were in the range of observed values in the field (Table 2.7), their inter-class variations were very low within each output matrices. Therefore, to help distinguishing these two classes, the Lutein:TChl-*b* (L:*b*) and the Zeaxanthin:Lutein (Z:L) ratios were calculated for each group as it has been demonstrated that these ratios are generally lower for chlorophytes than for prasinophytes (Roy et al., 2011). The values reported in the literature for L:*b* ratios ranged from 0.3 to 1.77 and 0 to 0.18 0.030 mg mg⁻¹ (Schlüter and Møhlenberg, 2003) and for Z:L 0.20 to 0.35 and from 2.8 to 6.6 mg mg⁻¹ for chlorophytes and prasinophytes, respectively (field values, Roy et al., 2011, and references therein). Our results

showed good agreement with the literature data. Indeed, we found L:*b* ratios averaging $0.41 \pm 0.16 \text{ mg mg}^{-1}$ and $0.026 \pm 0.001 \text{ mg mg}^{-1}$ and Z:L ratios averaging $0.29 \pm 0.15 \text{ mg mg}^{-1}$ and $3.0 \pm 0.4 \text{ mg mg}^{-1}$ for chlorophytes and prasinophytes, respectively, if group 4 ratio is removed for the prasinophytes functional-class for the Z:L ratio. Consequently, despite the lack of taxonomic identification by microscopy, it seemed that CHEMTAX was able to estimate properly the different phytoplankton functional classes along the GEOVIDE section.

Table 2.5: Literature review referring all works realized in the covered area within the North Atlantic Ocean, special attention was given to studies using CHEMTAX method.

References	Location	Longhurst provinces	Classes observed
Lutz et al., 2003	Labrador Sea (from Labrador to Greenland shelves)	ARCT, BPLR	<i>Synechococcus</i> , chlorophytes, haptophytes, diatoms, dinophytes
Stuart et al., 2000	Labrador Sea (from South Wolf Island, Labrador, to Cape Desolation, Greenland)	ARCT, BPLR	Diatoms (Labrador shelf), haptophytes type 8 (<i>Phaeocystis pouchetii</i> , close to Greenland)
Li et al., 1995	Central North Atlantic Ocean	NASTE, GFST, NWCS	<i>Prochlorococcus</i> , <i>Synechococcus</i> , eukaryotic algae
Luo et al., 2012 (and references therein)	Global Ocean	All	Diazotroph cyanobacteria (<i>Trichodesmium</i>), unicellular diazotroph cyanobacteria (<i>Crocospaera watsonii</i>), heterocystous cyanobacteria (<i>Nostocales</i> , of the genera <i>Richelia</i> and <i>Calothrix</i> found in symbiosis within diatoms <i>Rhizosolenia</i> and <i>Hemiaulus</i> diatom frustule or as epiphytes on <i>Chaetoceros</i> diatom)
Winter et al., 2014	North Atlantic Ocean	ARCT, NADR, NASTE	Haptophytes type 6 (i.e. <i>Emiliana huxleyi</i>)
LaRoche and Breitbarth, 2005	North Atlantic Ocean	ARCT, BPLR, NWCS, GFST, NADR, NASTE, NASTW	Cyanobacteria, <i>Trichodesmium</i> , drifts to higher latitudes due to Gulf Stream
Li and Harrison, 2001	Labrador Sea and central North Atlantic Ocean	ARCT, BPLR, NWCS, GFST, NADR, NASTE, NASTW	Bacteria (ARCT, NADR, GFST), picophytoplankton (NASTE, NASW, GFST, NADR)
Tyrell et al., 2003	North East Atlantic Ocean (40-50 °N, 20 °W)	NATR, NASTE, NADR	Diazotroph cyanobacteria (<i>Trichodesmium</i>)
Feng et al., 2009	Shipboard experiments on North Atlantic phytoplankton assemblages (57.58°N, 15.32°W)	NADR/ARCT	Diatoms, coccolithophorids
Martin et al., 2011	Iceland Basin	Common border between SARC and ARCT	Diatoms
Leterme et al., 2005	North Atlantic Ocean and North Sea	NADR, SARC, ARCT, NWCS, GFST, NASTE, (BPLR)	Diatoms (<i>Rhizosolenia alata alata</i> , <i>R. hebetate semispina</i> , <i>R. styliformis</i> , <i>Thalassionema nitzschoides</i> , <i>Thalassiosira</i> spp., <i>Thalassiothrix longissima</i>), dinophytes (<i>Ceratium furca</i> , <i>C. fusus</i> , <i>C. horridum</i> , <i>C. lineatum</i> , <i>C. tripos</i>), coccolithophorids, silicoflagellates,
Gibb et al., 2001	North Eastern Atlantic Ocean (37-62 °N, 20 °W)	NASTE, NADR, SARC	Diatoms, dinophytes, haptophytes, pelagophytes, chlorophytes, cyanobacteria, cryptophytes, prochlorophytes

Table 2.5 (continued)

References	Location	Longhurst provinces	Classes observed
van de Poll et al., 2013	Subtropical, temperate and subpolar sections of North Atlantic Ocean (27-63 °N, 10-25 °W)	NATR, NASTE, NADR, SARC	Prasinophytes, dinophytes, cryptophytes, haptophytes types 6 and 8, pelagophytes, <i>Synechococcus</i> , <i>Prochlorococcus</i> , diatoms
Veldhuis and Kraay, 2004	Subtropical North Atlantic Ocean (10-40 °N, 20-50 °W)	NASTE, NASTW, NATR	Diatoms, <i>Synechococcus</i> , <i>Prochlorococcus</i> (HL & LL), dinophytes, haptophytes type 8, pelagophytes, chlorophytes, cryptophytes, prasinophytes, <i>Trichodesmium</i>
Roy et al., 2011	Global Ocean	All	All classes (pigment ratios from culture & field)
Lochte et al., 1993	JGOFS North Atlantic Bloom Experiment (47°N, 20°W, 24 th -31 st April)	NADR	diatoms (before 15 th of May) followed by haptophytes (coccolithophorids, after 15 th of May) when silicates were depleted and increased of bacteria and microzooplankton (consuming about 64% of PP)
Li, 2002	Northwestern North Atlantic Ocean (38-61°N, 42-67°W)	ARCT, BPLR, NWCS, GFST	Fall to spring transition: reduction in picoplankton (<i>Synechococcus</i>), increment in large nanoplankton (diatoms and other) and no variation in small nanoplankton (haptophytes) assemblages
Reid et al., 2007	Northwest Atlantic (Labrador Sea and Irminger basin)	ARCT	Pacific diatom <i>Neodenticula seminae</i> , consequence of regional climate warming (change in circulation between the North Atlantic and North Pacific Oceans via the Arctic as Arctic ice melts)

Table 2.6: Initial pigment ratio matrices $[F_0]$ for CHEMTAX model.

input 1	c3	perid	BF	fucox	neox	prasinox	violax	HF	allox	zeax	lutein	Tchl_b	Tchl_a
Chlorophytes	0	0	0	0	0.066	0	0.067	0	0	0.039	0.171	0.334	1
Diatoms	0	0	0	0.775	0	0	0	0	0	0	0	0	1
Dinophytes	0	1.06	0	0	0	0	0	0	0	0	0	0	1
Prasinophytes	0	0	0	0	0.063	0.245	0.054	0	0	0.058	0.021	0.704	1
Pelagophytes	0.25	0	0.8	0.365	0	0	0	0.067	0	0	0	0	1
Cryptophytes	0	0	0	0	0	0	0	0	0.379	0	0	0	1
Haptophytes	0.17	0	0.02	1.21	0	0	0	1.36	0	0	0	0	1
Cyanobacteria	0	0	0	0	0	0	0	0	0	0.59	0	0	1

input 2	c3	perid	BF	fucox	neox	prasinox	violax	HF	allox	zeax	lutein	Tchl_b	Tchl_a
Chlorophytes	0	0	0	0	0.066	0	0.067	0	0	0.039	0.171	0.334	1
Diatoms	0	0	0	0.775	0	0	0	0	0	0	0	0	1
Dinophytes	0	1.06	0	0	0	0	0	0	0	0	0	0	1
Prasinophytes	0	0	0	0	0.063	0.245	0.054	0	0	0.058	0.021	0.704	1
Pelagophytes	0.25	0	0.8	0.365	0	0	0	0.067	0	0	0	0	1
Cryptophytes	0	0	0	0	0	0	0	0	0.379	0	0	0	1
Haptophytes 6	0.175	0	0.005	0.229	0	0	0	0.47	0	0	0	0	1
Haptophytes 8	0.171	0	0.103	0.3	0	0	0	0.371	0	0	0	0	1
Cyanobacteria	0	0	0	0	0	0	0	0	0	0.59	0	0	1

input 3	c3	perid	BF	fucox	neox	prasinox	violax	HF	allox	zeax	lutein	Tchl_b	Tchl_a
Chlorophytes	0	0	0	0	0.066	0	0.067	0	0	0.039	0.171	0.334	1
Diatoms	0	0	0	0.775	0	0	0	0	0	0	0	0	1
Dinophytes	0	1.06	0	0	0	0	0	0	0	0	0	0	1
Prasinophytes	0	0	0	0	0.063	0.245	0.054	0	0	0.058	0.021	0.704	1
Pelagophytes	0.25	0	0.8	0.365	0	0	0	0.067	0	0	0	0	1
Cryptophytes	0	0	0	0	0	0	0	0	0.379	0	0	0	1
Haptophytes	0.17	0	0.02	1.21	0	0	0	1.36	0	0	0	0	1
<i>Synechococcus</i>	0	0	0	0	0	0	0	0	0	0.636	0	0	1
<i>Trichodesmium</i>	0	0	0	0	0	0	0	0	0	0.143	0	0	1

input 4	c3	perid	BF	fucox	neox	prasinox	violax	HF	allox	zeax	lutein	Tchl_b	Tchl_a
Chlorophytes	0	0	0	0	0.066	0	0.067	0	0	0.039	0.171	0.334	1
Diatoms		0	0	0.775	0	0	0	0	0	0	0	0	1
Dinophytes	0	1.06	0	0	0	0	0	0	0	0	0	0	1
Prasinophytes	0	0	0	0	0.063	0.245	0.054	0	0	0.058	0.021	0.704	1
Pelagophytes	0.25	0	0.8	0.365	0	0	0	0.067	0	0	0	0	1
Cryptophytes	0	0	0	0	0	0	0	0	0.379	0	0	0	1
Haptophytes 6	0.175	0	0.005	0.229	0	0	0	0.47	0	0	0	0	1
Haptophytes 8	0.171	0	0.103	0.300	0	0	0	0.371	0	0	0	0	1
<i>Synechococcus</i>	0	0	0	0	0	0	0	0	0	0.636	0	0	1
<i>Trichodesmium</i>	0	0	0	0	0	0	0	0	0	0.143	0	0	1

Table 2.7: Output matrices for the seven different groups determined by a Principal Component Analysis (PCA) from the CHEMTAX model. Note that only the output matrix which shows the minimum of residual for the four different input matrices is displayed and that within the best fit input matrix only the 10% best results are considered. Note also that values in bold are out of the range for phytoplankton grown in culture but within the natural phytoplankton community range and that the red italic value is both out of the range for culture and natural phytoplankton community.

Group 1	c3	perid	BF	fucoc	neox	prasinox	violax	HF	allox	zeax	lutein	Tchl_b	Tchl_a
Chlorophytes	0	0	0	0	0.077	0	0.066	0	0	0.045	0.139	0.450	1
Diatoms	0	0	0	0.824	0	0	0	0	0	0	0	0	1
Dinophytes	0	1.03	0	0	0	0	0	0	0	0	0	0	1
Prasinophytes	0	0	0	0	0.098	0.166	0.083	0	0	0.066	0.021	0.655	1
Pelagophytes	0.31	0	1.09	0.42	0	0	0	0.076	0	0	0	0	1
Cryptophytes	0	0	0	0	0	0	0	0	0.347	0	0	0	1
Haptophytes 6	0.18	0	0.006	0.29	0	0	0	0.78	0	0	0	0	1
Haptophytes 8	0.30	0	0.08	0.33	0	0	0	0.36	0	0	0	0	1
Cyanobacteria	0	0	0	0	0	0	0	0	0	0.52	0	0	1

Group 2	c3	perid	BF	fucoc	neox	prasinox	violax	HF	allox	zeax	lutein	Tchl_b	Tchl_a
Chlorophytes	0	0	0	0	0.085	0	0.079	0	0	0.039	0.186	0.394	1
Diatoms	0	0	0	0.508	0	0	0	0	0	0	0	0	1
Dinophytes	0	0.97	0	0	0	0	0	0	0	0	0	0	1
Prasinophytes	0	0	0	0	0.066	0.267	0.061	0	0	0.065	0.024	0.826	1
Pelagophytes	0.21	0	0.74	0.39	0	0	0	0.055	0	0	0	0	1
Cryptophytes	0	0	0	0	0	0	0	0	0.411	0	0	0	1
Haptophytes 6	0.34	0	0.010	0.45	0	0	0	0.84	0	0	0	0	1
Haptophytes 8	1.11		0.06	1.32	0	0	0	0.10	0	0	0	0	1
Cyanobacteria	0	0	0	0	0	0	0	0	0	0.58	0	0	1

Group 3	c3	perid	BF	fucoc	neox	prasinox	violax	HF	allox	zeax	lutein	Tchl_b	Tchl_a
Chlorophytes	0	0	0	0	0.075	0	0.065	0	0	0.043	0.068	0.437	1
Diatoms	0	0	0	0.875	0	0	0	0	0	0	0	0	1
Dinophytes	0	1.16	0	0	0	0	0	0	0	0	0	0	1
Prasinophytes	0	0	0	0	0.088	0.339	0.052	0	0	0.052	0.020	0.625	1
Pelagophytes	0.30	0	1.01	0.38	0	0	0	0.073	0	0	0	0	1
Cryptophytes	0	0	0	0	0	0	0	0	0.351	0	0	0	1
Haptophytes 6	0.24	0	0.005	0.16	0	0	0	0.82	0	0	0	0	1
Haptophytes 8	0.19	0	0.11	0.29	0	0	0	0.38	0	0	0	0	1
Cyanobacteria	0	0	0	0	0	0	0	0	0	0.54	0	0	1

Group 4	c3	perid	BF	fucoc	neox	prasinox	violax	HF	allox	zeax	lutein	Tchl_b	Tchl_a
Chlorophytes	0	0	0	0	0.066	0	0.075	0	0	0.043	0.150	0.447	1
Diatoms	0	0	0	0.932	0	0	0	0	0	0	0	0	1
Dinophytes	0	1.14	0	0	0	0	0	0	0	0	0	0	1
Prasinophytes	0	0	0	0	0.102	0.294	0.085	0	0	0.079	0.004	0.708	1
Pelagophytes	0.27	0	0.81	0.35	0	0	0	0.067	0	0	0	0	1
Cryptophytes	0	0	0	0	0	0	0	0	0.303	0	0	0	1
Haptophytes 6	0.15	0	0.004	0.23	0	0	0	0.47	0	0	0	0	1
Haptophytes 8	0.38	0	0.02	0.33	0	0	0	0.06	0	0	0	0	1
Cyanobacteria	0	0	0	0	0	0	0	0	0	0.68	0	0	1

Table 2.7 (continued)

Group 5	c3	perid	BF	fucox	neox	prasincox	violax	HF	allox	zeax	lutein	Tchl_b	Tchl_a
Chlorophytes	0	0	0	0	0.067	0	0.072	0	0	0.042	0.191	0.314	1
Diatoms	0	0	0	0.792	0	0	0	0	0	0	0	0	1
Dinophytes	0	0.90	0	0	0	0	0	0	0	0	0	0	1
Prasinophytes	0	0	0	0	0.082	0.188	0.050	0	0	0.059	0.023	0.672	1
Pelagophytes	0.25	0	1.05	0.36	0	0	0	0.064	0	0	0	0	1
Cryptophytes	0	0	0	0	0	0	0	0	0.414	0	0	0	1
Haptophytes 6	0.17	0	0.005	0.21	0	0	0	0.86	0	0	0	0	1
Haptophytes 8	0.41	0	0.12	0.33	0	0	0	0.25	0	0	0	0	1
Cyanobacteria	0	0	0	0	0	0	0	0	0	0.67	0	0	1

Group 6	c3	perid	BF	fucox	neox	prasincox	violax	HF	allox	zeax	lutein	Tchl_b	Tchl_a
Chlorophytes	0	0	0	0	0.062	0	0.095	0	0	0.041	0.250	0.414	1
Diatoms	0	0	0	0.634	0	0	0	0	0	0	0	0	1
Dinophytes	0	1.29	0	0	0	0	0	0	0	0	0	0	1
Prasinophytes	0	0	0	0	0.108	0.121	0.056	0	0	0.086	0.024	0.947	1
Pelagophytes	0.33	0	0.93	0.27	0	0	0	0.075	0	0	0	0	1
Cryptophytes	0	0	0	0	0	0	0	0	0.418	0	0	0	1
Haptophytes 6	0.24	0	0.01	0.25	0	0	0	0.45	0	0	0	0	1
Haptophytes 8	0.29	0	0.29	0.17	0	0	0	1.50	0	0	0	0	1
Cyanobacteria	0	0	0	0	0	0	0	0	0	0.72	0	0	1

Group 7	c3	perid	BF	fucox	neox	prasincox	violax	HF	allox	zeax	lutein	Tchl_b	Tchl_a
Chlorophytes	0	0	0	0	0.057	0	0.061	0	0	0.038	0.136	0.436	1
Diatoms	0	0	0	0.584	0	0	0	0	0	0	0	0	1
Dinophytes	0	1.11	0	0	0	0	0	0	0	0	0	0	1
Prasinophytes	0	0	0	0	0.059	0.251	0.062	0	0	0.063	0.019	1.115	1
Pelagophytes	0.30	0	0.85	0.42	0	0	0	0.080	0	0	0	0	1
Cryptophytes	0	0	0	0	0	0	0	0	0.385	0	0	0	1
Haptophytes 6	0.21	0	0.03	0.22	0	0	0	0.43	0	0	0	0	1
Haptophytes 8	0.26	0	0.16	0.27	0	0	0	0.39	0	0	0	0	1
Cyanobacteria	0	0	0	0	0	0	0	0	0	0.66	0	0	1

Group 6 (bis)	c3	perid	BF	fucox	neox	prasincox	violax	HF	allox	zeax	lutein	Tchl_b	Tchl_a
Chlorophytes	0	0	0	0	0.053	0	0.087	0	0	0.046	0.211	0.352	1
Diatoms	0	0	0	0.879	0	0	0	0	0	0	0	0	1
Dinophytes	0	0.89	0	0	0	0	0	0	0	0	0	0	1
Prasinophytes	0	0	0	0	0.102	0.116	0.050	0	0	0.072	0.024	0.902	1
Pelagophytes	0.43	0	0.85	0.23	0	0	0	0.081	0	0	0	0	1
Cryptophytes	0	0	0	0	0	0	0	0	0.395	0	0	0	1
Haptophytes	0.18	0	0.02	0.26	0	0	0	1.67	0	0	0	0	1
<i>Synechococcus</i>	0	0	0	0	0	0	0	0	0	0.83	0	0	1
<i>Trichodesmium</i>	0	0	0	0	0	0	0	0	0	0.15	0	0	1

2.4.5 Ancillary measurements

Nutrient samples (silicate, Si(OH)_4 ; nitrite, NO_2^- and nitrate, NO_3^- ; $\text{NO}_2^- + \text{NO}_3^- = \text{NOx}$) were obtained from the CTD casts and analysed by spectrophotometry according to Aminot and Kerouel (2007). Note that there were no phosphate (PO_4^{3-}) data available for the GEOVIDE voyage due to analytical issues. The data from the CTD casts that were deployed immediately before or after the TMR casts were used. When needed, to avoid depth mismatched between pigment and macronutrient CTD casts, the interpolated nutrient data were used (see Appendix C2). Note that the measured value was preferred to the interpolated value if the depth mismatch was lower than 5 m depth far from the pigment depth. All these data will be available on the LEFE/CYBER database ².

The mixed layer depth (Z_m) for each station was calculated using the function “calculate.mld” (part of the “rcalcofi” package, Ed Weber at NOAA SWFSC) created by Sam McClathie (NOAA Federal, 30th December 2013) for R software and where Z_m is defined as an absolute change in $\Delta\sigma_t$ ($\geq 0.125 \text{ kg m}^{-3}$) with respect to an approximately uniform region of density just below the ocean surface (Kara et al., 2000). In addition to the density criterion, the temperature and salinity profiles were inspected at each station for uniformity within this layer. When they were not uniform, the depth of any perturbation in the profile was chosen as the base of the Z_m . The depth of the euphotic layer (Z_{eu}) was calculated for each station as the depth where photosynthetic available radiation (PAR) is 1% of its surface value (Lee et al., 2007). Finally, the Z_{eu} and Z_m were compared to determined whether the water column was stratified (i.e. $Z_{eu} \geq Z_m$) or mixed (i.e. $Z_{eu} < Z_m$) (Ras et al., 2008).

² <http://www.obs-vlfr.fr/proof/php/geovide/geovide.php>

Chapter 3:

Dissolved Iron Distribution in the North Atlantic Ocean

Chapter 3: Dissolved Iron distribution in the North Atlantic

Table of Contents

Abstract	130
3.1 Introduction	131
3.2 Material and methods	134
3.2.1 Study area and sampling activities	134
3.2.2 DFe analysis with SeaFAST-picoTM	136
3.2.3 Meteoric water and sea ice fraction calculation	137
3.2.4 Ancillary measurements and mixed layer depth determination	138
3.2.5 Statistical analysis	139
3.2.6 Water mass determination and associated DFe concentrations	139
3.2.7 Database	139
3.3 Results	140
3.3.1 Hydrography	140
3.3.2 Ancillary data	143
3.3.2.1 Nitrate	143
3.3.2.2 Chlorophyll-<i>a</i>	143
3.3.3 Dissolved Fe concentrations	144
3.3.4 Fingerprinting water masses	144
3.4 Discussion	147
3.4.1 High DFe concentrations at stations 1 and 17	148
3.4.2 DFe and hydrology keypoints	148

<u>3.4.2.1 How do air-sea interactions affect DFe concentration in the Irminger Sea</u>	148
<u>3.4.2.2 Why don't we see a DFe signature in the Mediterranean Overflow Water (MOW)?</u>	149
<u>3.4.2.3 Fe enrichment in the Labrador Sea Water (LSW)</u>	150
<u>3.4.2.4 Enhanced DFe concentrations in the Irminger Sea Bottom Water</u>	152
<u>3.4.2.5 Reykjanes Ridge: Hydrothermal inputs or Fe-rich seawater?</u>	153
<u>3.4.3 What are the main sources of DFe in surface waters?</u>	154
<u>3.4.3.1 Tagus riverine inputs</u>	154
<u>3.4.3.2 High latitude meteoric water and sea-ice processes</u>	156
<u>3.4.3.3 Atmospheric deposition</u>	158
<u>3.4.4 Sediment input</u>	160
<u>3.4.5 How does biological activity modify DFe distribution?</u>	162
<u>3.5 Conclusion</u>	166
<u>3.6 Acknowledgements</u>	167
<u>3.7 References</u>	168
<u>3.8 Supplementary material</u>	178

Dissolved iron in the North Atlantic Ocean and Labrador Sea along the GEOVIDE section (GEOTRACES section GA01)

This Chapter is a manuscript that has been submitted to *Biogeosciences* and is currently under review. The supplementary material corresponding to this submitted scientific article is displayed at the end of this chapter. An additional supplementary material is available in Appendix B only for the thesis manuscript.

Authors: Manon Tonnard, Hélène Planquette, Andrew R. Bowie, Pier van der Merwe, Morgane Gallinari, Floriane Desprez de Gésincourt, Yoan Germain, Arthur Gourain, Marion Benetti, Gilles Reverdin, Paul Tréguer, Julia Boutorh, Marie Cheize, François Lacan, Jan-Lukas Menzel Barraqueta, Leonardo Pereira-Contreira, Rachel Shelley, Pascale Lherminier, Géraldine Sarthou

Abstract

Dissolved Fe (DFe) samples from the GEOVIDE voyage (GEOTRACES GA01, May-June 2014) in the North Atlantic Ocean were analysed using a SeaFAST-picoTM coupled to an Element XR SF-ICP-MS and provided interesting insights on the Fe sources in this area. Overall, DFe concentrations ranged from $0.09 \pm 0.01 \text{ nmol L}^{-1}$ to $7.8 \pm 0.5 \text{ nmol L}^{-1}$. Elevated DFe concentrations were observed above the Iberian, Greenland and Newfoundland Margins likely due to riverine inputs from the Tagus River, meteoric water inputs and sedimentary inputs. Enhanced air-sea interactions were suspected to be responsible for the increase in DFe concentrations within subsurface waters of the Irminger Sea due to deep convection occurring the previous winter, which provided iron-to-nitrate ratios sufficient to sustain phytoplankton growth. Increasing DFe concentrations along the flow path of the Labrador Sea Water were attributed to sedimentary inputs from the Newfoundland Margin. Bottom waters from the Irminger Sea displayed high DFe concentrations likely due to the dissolution of Fe-rich particles in the Denmark Strait Overflow Water and the Polar Intermediate Water. Finally, the nepheloid layers located in the different basins and at the Iberian Margin were found to act as either a source or a sink of DFe depending on the nature of particles with organic particles likely releasing DFe and Mn-particles scavenging DFe.

3.1 Introduction

The North Atlantic Ocean is known for its pronounced spring phytoplankton blooms (Henson et al., 2009; Longhurst, 2007). Phytoplankton blooms induce the capture of aqueous carbon dioxide through photosynthesis, and conversion into particulate organic carbon (POC). This POC is then exported into deeper waters through the production of sinking biogenic particles and ocean currents. Via these processes, and in conjunction with the physical carbon pump, the North Atlantic Ocean is the largest oceanic sink of anthropogenic CO₂ (Pérez et al., 2013), despite covering only 15% of global ocean area (Humphreys et al., 2016; Sabine et al., 2004) and is therefore crucial for Earth's climate.

Indeed, phytoplankton must obtain, besides light and inorganic carbon, chemical forms of essential elements, termed nutrients to be able of photosynthesis. Indeed, Fe is a key element for a number of metabolic processes (e.g. Morel et al., 2008). The availability of these nutrients in the upper ocean frequently limits the activity and abundance of these organisms together with light conditions (Moore et al., 2013). In particular, winter nutrient reserves in surface waters set an upper limit for biomass accumulation during the annual spring-to-summer bloom and will influence the duration of the bloom (Follows and Dutkiewicz, 2001; Henson et al., 2009; Moore et al., 2013; 2008). Hence, nutrient depletion due to biological consumption is considered as a major factor in the decline of blooms (Harrison et al., 2013).

The extensive studies conducted in the North Atlantic Ocean through the Continuous Plankton Recorder (CPR) have highlighted the relationship between the strength of the westerlies and the displacement of the subarctic front (SAF), (which corresponds to the North Atlantic Oscillation (NAO) index (Bersch et al., 2007)), and the phytoplankton dynamics of the central North Atlantic Ocean (Barton et al., 2003). Therefore, the SAF not only delineates the subtropical gyre from the subpolar gyre but also two distinct systems in which phytoplankton limitations are controlled by different factors. In the North Atlantic Ocean, spring phytoplankton growth is largely light-limited within the subpolar gyre. Light levels are primarily set by freeze-thaw cycles of sea ice and the high-latitude extremes in the solar cycle (Longhurst, 2007). Simultaneously, intense winter mixing supplies surface waters with high concentrations of nutrients. In contrast, within the subtropical gyre, the spring phytoplankton growth is less impacted by the light regime and has been shown to be N and P-co-limited

(e.g. Harrison et al., 2013; Moore et al., 2008). This is principally driven by Ekman downwelling with an associated export of nutrients out of the euphotic zone (Oschlies, 2002). Thus, depending on the location of the SAF, phytoplankton communities from the central North Atlantic Ocean will be primarily light or nutrient limited.

However, once the water column stratifies and phytoplankton are released from light limitation, seasonal high-nutrient, low chlorophyll (HNLC) conditions were reported at the transition zone between the gyres, especially in the Irminger Sea and Iceland Basin (Sanders et al., 2005). In these HNLC zones, trace metals are most likely limiting the biological carbon pump. Among all the trace metals, Fe has been recognized as the prime limiting element of North Atlantic primary productivity (e.g. Boyd et al., 2000; Martin et al., 1994; 1988; 1990). However, the phytoplankton community has been shown to become N and/or Fe-(co)-limited in the Iceland Basin and the Irminger Sea (e.g. Nielsdóttir et al., 2009; Painter et al., 2014; Sanders et al., 2005).

In the North Atlantic Ocean, dissolved Fe (DFe) is delivered through multiple pathways such as ice-melting (e.g. Klunder et al., 2012; Tovar-Sanchez et al., 2010), atmospheric inputs (Achterberg et al., 2018; Baker et al., 2013; Shelley et al., 2015; 2017), coastal runoff (Rijkenberg et al., 2014), sediment inputs (Hatta et al., 2015), hydrothermal inputs (Achterberg et al., 2018; Conway and John, 2014) and by water mass circulation (vertical and lateral advections, e.g. Laes et al., 2003). Dissolved Fe can be regenerated through biological recycling (microbial loop, zooplankton grazing, e.g. Boyd et al., 2010; Sarthou et al., 2008). Iron is removed from the dissolved phase by biological uptake, export and scavenging along the water column and precipitation (itself a function of salinity, pH of seawater and ligand concentrations).

Although many studies investigated the distribution of DFe in the North Atlantic Ocean, much of this work was restricted to the upper layers (< 1000 m depth) or to one basin. Therefore, uncertainties remain on the large-scale distribution of DFe in the North Atlantic Ocean and more specifically within the subpolar gyre where few studies have been undertaken, and even fewer in the Labrador Sea. In this biogeochemically important area, high-resolution studies are still lacking for understanding the processes influencing the cycle of DFe.

The aim of this paper is to elucidate the sources and sinks of DFe, its distribution regarding water masses and assesses the links with biological activity along the GEOVIDE (GEOTRACES-GA01) transect. This transect spanned several biogeochemical provinces including the West European Basin, the Iceland Basin, the Irminger and the Labrador Seas (Fig. 3.1). In doing so we hope to constrain the potential long-range transport of DFe through the Deep Western Boundary Current (DWBC) via the investigation of the local processes effecting the DFe concentrations within the three main water masses that constitute it: Iceland Scotland Overflow Water (ISOW), Denmark Strait Overflow Water (DSOW) and Labrador Sea Water (LSW).

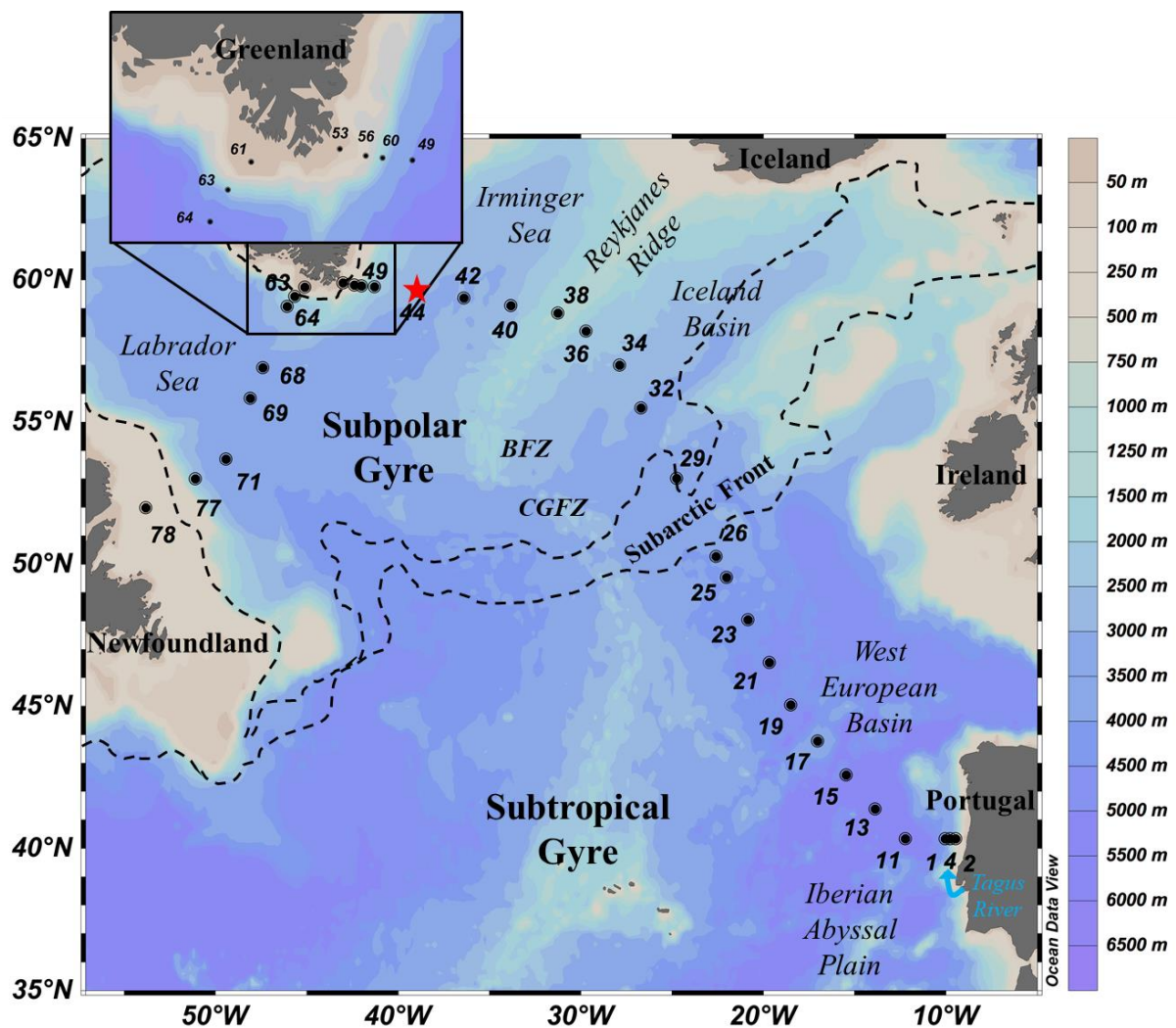


Figure 3.1: Map of the GEOTRACES GA01 voyage plotted on bathymetry as well as the major topographical features and main basins. Crossover station with GEOTRACES voyage (GA03) is shown as a red star. (Ocean Data View (ODV) software, version 4.7.6, R. Schlitzer, <http://odv.awi.de>, 2016). BFZ: Bight Fracture Zone, CGFZ: Charlie-Gibbs Fracture Zone.

3.2 Material and methods

3.2.1 Study area and sampling activities

Samples were collected during the GEOVIDE (GEOTRACES-GA01 section, Fig. 3.1) oceanographic voyage from 15 May 2014 (Lisbon, Portugal) to 30 June 2014 (St. John's, Newfoundland, Canada) aboard N/O *Pourquoi Pas?*. The study was carried out along the OVIDE line (<http://www.umr-lops.fr/Projets/Projets-actifs/OVIDE>, previously referred to as the WOCE A25 Greenland to Portugal section), and in the Labrador Sea (corresponding to the WOCE A01 leg 3 Greenland to Newfoundland section). The OVIDE line has been sampled every two years since 2002 in the North Atlantic (e.g. Mercier et al., 2015), and in the Labrador Sea (broadly corresponding to the WOCE A01 leg 3 Greenland to Newfoundland section). In total, 32 stations were occupied, and samples were usually collected at 22 depths, except at shallower stations close to the Iberian, Greenland and Canadian shelves (Fig. 3.1) where fewer samples (between 6 and 11) were collected. To avoid ship contamination of surface waters, the shallowest sampling depth was 15 m at all stations. Therefore, 'surface water samples' refers to 15m depth.

Samples were collected using a trace metal clean polyurethane powder-coated aluminium frame rosette (hereafter referred to as TMR) equipped with twenty-two 12L, externally closing, Teflon-lined, GO-FLO bottles (General Oceanics) and attached to a Kevlar[®] line. The cleaning protocols for sampling bottles and equipment followed the guidelines of the GEOTRACES Cookbook (www.geotraces.org, Cutter et al., 2017). After TMR recovery, GO-FLO bottles were transferred into a clean container equipped with a class 100 laminar flow hood. Samples were either taken from the filtrate of particulate samples (collected on polyethersulfone filters, 0.45 µm supor[®], see Gourain et al., this issue) or after filtration using 0.2 µm filter cartridges (Sartorius SARTOBRAN[®] 300) due to water budget restriction (Table 3.1). No significant difference was observed between DFe values filtered through 0.2 µm and 0.45 µm filters (p-value > 0.2, Wilcoxon test) for most stations. Differences were only observed between profiles of stations 11 and 13 and, 13 and 15. Seawater was collected in acid-cleaned 60 mL LDPE bottles, after rinsing 3 times with about 20 mL of seawater. Teflon[®] tubing used to connect the filter holders or cartridges to the GO-FLO bottles were washed in an acid-bath (10% v/v HCl, Suprapur[®], Merck) for at least 12 h and rinsed three times with Ultra High Purity Water (UHPW > 18 MΩ.cm) prior to use. Samples were then acidified to ~ pH 1.7 with HCl (Ultrapur[®] Merck, 2 ‰ v/v) under a class

100 laminar flow hood inside the clean container. The sample bottles were then double bagged and stored at ambient temperature in the dark before shore-based analyses.

Table 3.1: Station number, date of sampling (in the DD/MM/YYYY format), size pore used for filtration (μm), station location, mixed layer depth (m) and associated average dissolved iron (DFe) concentrations, standard deviation and number of samples during the GEOTRACES GA01 transect. Note that the asterisk next to station numbers refers to disturbed temperature and salinity profiles as opposed to uniform profiles.

Station	Date sampling	filtration	Latitude	Longitude	Z_m	DFe (nmol L^{-1})			
	DD/MM/YYYY	μm	$^{\circ}\text{N}$	$^{\circ}\text{E}$	m	average	SD	n	
1	19/05/2014	0.2	40.33	-10.04	25.8	1.07	\pm 0.12	1	
2	21/05/2014	0.2	40.33	-9.46	22.5	1.01	\pm 0.04	1	
4	21/05/2014	0.2	40.33	-9.77	24.2	0.73	\pm 0.03	1	
11	23/05/2014	0.2	40.33	-12.22	31.3	0.20	\pm 0.11	2	
13	24/05/2014	0.45	41.38	-13.89	18.8	0.23	\pm 0.02	1	
15	28/05/2014	0.2	42.58	-15.46	34.2	0.22	\pm 0.03	2	
17	29/05/2014	0.2	43.78	-17.03	36.2	0.17	\pm 0.01	1	
19*	30/05/2014	0.45	45.05	-18.51	44.0	0.13	\pm 0.05	2	
21	31/05/2014	0.2	46.54	-19.67	47.4	0.23	\pm 0.08	2	
23*	02/06/2014	0.2	48.04	-20.85	69.5	0.21	\pm 0.05	6	
25	03/06/2014	0.2	49.53	-22.02	34.3	0.17	\pm 0.04	2	
26	04/06/2014	0.45	50.28	-22.60	43.8	0.17	\pm 0.03	2	
29	06/06/2014	0.45	53.02	-24.75	23.8	0.17	\pm 0.02	1	
32	07/06/2014	0.2	55.51	-26.71	34.8	0.59	\pm 0.08	2	
34	09/06/2014	0.45	57.00	-27.88	25.6	NA	\pm	0	
36	10/06/2014	0.45	58.21	-29.72	33.0	0.12	\pm 0.02	1	
38	10/06/2014	0.45	58.84	-31.27	34.5	0.36	\pm 0.16	2	
40	12/06/2014	0.45	59.10	-33.83	34.3	0.39	\pm 0.05	1	
42	12/06/2014	0.45	59.36	-36.40	29.6	0.36	\pm 0.05	1	
44	13/06/2014	0.2	59.62	-38.95	25.8	NA	\pm	0	
49	15/06/2014	0.45	59.77	-41.30	60.3	0.30	\pm 0.05	2	
53*	17/06/2014	0.45	59.90	-43.00	36.4	NA	\pm	0	
56*	17/06/2014	0.45	59.82	-42.40	30.0	0.87	\pm 0.06	1	
60*	17/06/2014	0.45	59.80	-42.00	36.6	0.24	\pm 0.02	2	
61*	19/06/2014	0.45	59.75	-45.11	39.8	0.79	\pm 0.12	1	
63*	19/06/2014	0.45	59.43	-45.67	86.7	0.40	\pm 0.03	1	
64	20/06/2014	0.45	59.07	-46.09	33.9	0.27	\pm 0.06	2	
68*	21/06/2014	0.45	56.91	-47.42	26.3	0.22	\pm 0.01	1	
69*	22/06/2014	0.45	55.84	-48.09	17.5	0.24	\pm 0.02	1	
71	24/06/2014	0.45	53.69	-49.43	36.7	0.32	\pm 0.04	2	
77*	26/06/2014	0.45	53.00	-51.10	26.1	NA	\pm	0	
78	27/06/2014	0.45	51.99	-53.82	13.4	0.79	\pm 0.05	1	

Large volumes of seawater sample (referred hereafter as the in-house standard seawater) were also collected using a towed fish at around 2-3 m deep and filtered in-line inside a clean container through a 0.2 μm pore size filter capsule (Sartorius SARTOBRAN® 300) and was stored unacidified in 20-30 L LDPE carboys (Nalgene™). All the carboys were cleaned following the guidelines of the GEOTRACES Cookbook (Cutter et al., 2017). This in-house standard seawater was used for calibration on the SeaFAST-pico™ - SF-ICP-MS (see Section 3.2.2) and was acidified to \sim pH 1.7 with HCl (Ultrapur® Merck, 2 ‰ v/v) at least 24h prior to analysis.

3.2.2 DFe analysis with SeaFAST-pico™

Seawater samples were preconcentrated using a SeaFAST-pico™ (ESI, Elemental Scientific, USA) and the eluent was directly introduced via a PFA-ST nebulizer and a cyclonic spray chamber in an Element XR Sector Field Inductively Coupled Plasma Mass Spectrometry (Element XR SF-ICP-MS, Thermo Fisher Scientific Inc., Omaha, NE), following the protocol of Lagerström et al. (2013).

High-purity grade solutions and water (Milli-Q) were used to prepare the following reagents each day: the acetic acid-ammonium acetate buffer (CH_3COO^- and NH_4^+) was made of 140 mL acetic acid (> 99% NORMATOM® - VWR chemicals) and ammonium hydroxide (25%, Merck Suprapur®) in 500 mL PTFE bottles and was adjusted to $\text{pH } 6.0 \pm 0.2$ for the on-line pH adjustment of the samples. The eluent was made of 1.4 M nitric acid (HNO_3 , Merck Ultrapur®) in Milli-Q water by a 10-fold dilution and spiked with $1 \mu\text{g L}^{-1} {}^{115}\text{In}$ (SCP Science calibration standards) to allow for drift correction. Autosampler and column rinsing solutions were made of HNO_3 2.5% (v/v) (Merck Suprapur®) in Milli-Q water. The carrier solution driven by the syringe pumps to move the sample and buffer through the flow injection system was made in the same way.

All reagents, standards, samples, and blanks were prepared in acid cleaned low density polyethylene (LDPE) or Teflon fluorinated ethylene propylene (FEP) bottles. Bottles were cleaned following the GEOTRACES protocol (Cutter et al., 2017).

Mixed multi-element standard solution was prepared gravimetrically using high purity standards (Fe, Mn, Cd, Co, Zn, Cu, Pb; SCP Science calibration standards) in HNO_3 3% (v/v) (Merck Ultrapur®). A six-point calibration curve was prepared by standard additions of the mixed element standard to our acidified in-house standard and ran at the beginning, the middle and the end of each analytical session. The distribution of the trace metals other than Fe will be reported elsewhere (Planquette et al., in prep.). Final concentrations of samples and

procedural blanks were calculated from In-normalized data. Data were blank-corrected by subtracting an average acidified Milli-Q blank that were pre-concentrated on the SeaFAST-picoTM in the same way as the samples and seawater standards. Each analytical session consisted of about fifty samples and two calibrations, one at the beginning and another one at the end of each analytical session. The errors associated to each sample were calculated as the standard deviation for five measurements of low-Fe seawater samples. The mean Milli-Q blank was equal to $0.08 \pm 0.09 \text{ nmol L}^{-1}$ ($n = 17$) all analytical session together. The detection limit, calculated for a given run as three times the standard deviation of the Milli-Q blanks, was on average $0.05 \pm 0.05 \text{ nmol L}^{-1}$ ($n = 17$). Reproducibility was assessed through the standard deviation of replicate samples (every 10th sample was a replicate) and the average of the in-house standard seawater, and was equal to 17% ($n = 84$). Accuracy was determined from the analysis of consensus (SAFe S, GSP) and certified (NASS-7) seawater matrices (see Table 3.2) and in-house standard seawater ($\text{DFe} = 0.42 \pm 0.07 \text{ nmol L}^{-1}$, $n = 84$). Note that all the DFe values were generated in nmol kg^{-1} using the SeaFAST-picoTM coupled to an Element XR SF-ICP-MS and were converted to nmol L^{-1} (multiplied by a factor of 1.025 kg L^{-1}) to be directly comparable with literature.

Table 3.2: SAFe S, GSP and NASS-7 dissolved iron concentrations (DFe, nmol L^{-1}) determined by the SeaFAST-picoTM and their consensus (SAFe S, GSP; <https://websites.pmc.ucsc.edu/~kbruland/GeotracesSaFe/kwbGeotracesSaFe.html>) and certified (NASS-7; https://www.nrc-cnrc.gc.ca/eng/solutions/advisory/crm/certificates/nass_7.html) DFe concentrations. Note that yet no consensual value is reported for the GSP seawater.

Seawater used for calibration	SeaFAST-pico TM DFe values (nmol L^{-1})				reference or certified DFe values (nmol L^{-1})		
	Average	SD	n		Average	SD	
SAFe S	0.100	± 0.006	2		0.095	± 0.008	
GSP	0.16	± 0.04	15		NA	\pm	NA
NASS-7	6.7	± 1.7	12		6.3	\pm	0.5

3.2.3 Meteoric water and sea ice fraction calculation

We separated the mass contributions to samples from stations 53, 61 and 78 in Sea-Ice Melt (SIM) Meteoric Water (MW) and saline seawater inputs using the procedure and mass balance calculations that are fully described in Benetti et al. (2016). Hereafter, we describe briefly the principle. We considered two types of seawater, namely the Atlantic Water (AW) and the Pacific Water (PW). After estimating the relative proportions of AW (f_{AW}) and PW (f_{PW}) and their respective salinity and $\delta^{18}\text{O}$ affecting each samples, the

contribution of SIM and MW can be determined using measured salinity (S_m) and $\delta^{18}\text{O}$ (δO_m^{18}). The mass balance calculations are presented below:

$$f_{AW} + f_{PW} + f_{MW} + f_{SIM} = 1 \quad (\text{eq. 3.1})$$

$$f_{AW} \cdot S_{AW} + f_{PW} \cdot S_{PW} + f_{MW} \cdot S_{MW} + f_{SIM} \cdot S_{SIM} = S_m \quad (\text{eq. 3.2})$$

$$f_{AW} \cdot \delta\text{O}_{AW}^{18} + f_{PW} \cdot \delta\text{O}_{PW}^{18} + f_{MW} \cdot \delta\text{O}_{MW}^{18} + f_{SIM} \cdot \delta\text{O}_{SIM}^{18} = \delta\text{O}_m^{18} \quad (\text{eq. 3.3})$$

where f_{AW} , f_{PW} , f_{MW} , f_{SIM} are the relative fraction of AW, PW, MW, and SIM. To calculate the relative fractions of AW, PW, MW and SIM we used the following end-members: $S_{AW} = 35$, $\delta\text{O}_{AW}^{18} = +0.18\text{‰}$ (Benetti et al., 2016); $S_{PW} = 32.5$, $\delta\text{O}_{PW}^{18} = -1\text{‰}$ (Cooper et al., 1997; Woodgate and Aagaard, 2005); $S_{MW} = 0$, $\delta\text{O}_{MW}^{18} = -18.4\text{‰}$ (Cooper et al., 2008); $S_{SIM} = 4$, $\delta\text{O}_{SIM}^{18} = +0.5\text{‰}$ (Melling and Moore, 1995).

Negative sea-ice fractions indicated a net brine release while positive sea-ice fractions indicated a net sea-ice melting. Note that for stations over the Greenland Shelf, we assumed that the Pacific Water (PW) contribution was negligible for the calculations, supported by the very low PW fractions found at Cape Farewell in May 2014 (see Figure B1 in Benetti et al., 2017), while for station 78, located on the Newfoundland shelf, we used nutrient measurements to calculate the PW fractions, following the approach from Jones et al. (1998) (the data are published in Benetti et al., 2017).

3.2.4 Ancillary measurements and mixed layer depth determination

Potential temperature (θ), salinity (S), dissolved oxygen (O_2) and beam attenuation data were retrieved from the CTD sensors (CTD SBE911 equipped with a SBE-43) that were deployed on a stainless steel rosette. Nutrient and pigment samples were obtained from the stainless steel rosette casts and analysed according to Aminot and Kerouel (2007) and Ras et al. (2008), respectively. We used the data from the stainless steel rosette casts that were deployed immediately before or after our TMR casts. All these data are available on the LEFE/CYBER database (<http://www.obs-vlfr.fr/proof/php/geovide/geovide.php>).

The mixed layer depth (Z_m) for each station was calculated using the function “calculate.mld” (part of the “rcalcofi” package, Ed Weber at NOAA SWFSC) created by Sam McClathie (NOAA Federal, 30th December 2013) for R software and where Z_m is defined as an absolute change in the density of seawater at a given temperature ($\Delta\sigma_\theta \geq 0.125 \text{ kg m}^{-3}$) with respect to an approximately uniform region of density just below the ocean surface

(Kara et al., 2000). In addition to the density criterion, the temperature and salinity profiles were inspected at each station for uniformity within this layer. When they were not uniform, the depth of any perturbation in the profile was chosen as the base of the Z_m (Table 3.1).

3.2.5 Statistical analysis

All statistical approaches, namely the comparison between the pore size used for filtration, correlations and Principal Component Analysis (PCA), were performed using the R statistical software (R development Core Team 2012). For all the results, p-values were calculated against the threshold value alpha (α), that we assigned at 0.05, corresponding to a 95% level of confidence. For all data sets, non-normal distributions were observed according to the Shapiro-Wilk test. Therefore, the significance level was determined with a Wilcoxon test.

All sections and surface layer plots were prepared using Ocean Data View (Schlitzer, 2016).

3.2.6 Water mass determination and associated DFe concentrations

The water mass structure in the North Atlantic Ocean from the GEOVIDE voyage was quantitatively assessed by means of an extended Optimum Multi-Parameter (eOMP) analysis with 14 water masses (for details see García-Ibáñez et al., 2015; this issue). Using this water mass determination, DFe concentrations were considered as representative of a specific water mass only when the contribution of this specific water mass was higher than 60% of the total water mass pool.

3.2.7 Database

The complete database of dissolved Fe is available in the electronic supplement www.biogeosciences.net. Overall, 540 data points of dissolved Fe are reported, among which 511 values are used in this manuscript. The remaining 29 values (5.7% of the total dataset) are flagged as (suspect) outliers. These 29 outliers were not used in figures and in the interpretation of this manuscript. The criteria for rejection were based on the comparison with other parameters measured from the same GO-FLO sampler, and curve fitting versus samples collected above and below the suspect sample. The complete data set will be available in national and international databases (LEFE-CYBER, <http://www.obs-vlfr.fr/proof/index2.php>, and GEOTRACES <http://www.bodc.ac.uk/geotraces/>).

3.3 Results

3.3.1 Hydrography

The hydrology and circulation of the main water masses along the OVIDE section in the North Atlantic Subpolar Gyre and their contribution to the Atlantic Meridional Overturning Circulation (AMOC) have been described using an eOMP analysis by García-Ibáñez et al., (2015; this issue) and Zunino et al. (2017). For a schematic of water masses, currents and pathways, see Daniault et al. (2016). Hereafter we summarise the main features (Figs. 3.1 and 3.2).

Upper waters (~ 0 – 800 m) - The cyclonic circulation of the Eastern North Atlantic Central Water (ENACW) ($12.3 < \theta < 16^{\circ}\text{C}$, $35.66 < S < 36.2$, $241 < \text{O}_2 < 251 \mu\text{mol kg}^{-1}$) occupied the water column from 0 to ~ 800 m depth from stations 1 to 25 contributing to 60% of the water mass pool. The sharp Subarctic Front (between stations 26 and 29), caused by the northern branch of the North Atlantic Current (NAC) separated the cyclonic subpolar from the anticyclonic subtropical gyre domains at 50°N and 22.5°W . The ENACW were also encountered to a lesser extent and only in surface waters (from 0 to ~ 100 m depth) between stations 29 and 34 (contributing to less than 40% of the water mass pool). West of the Subarctic Front, Iceland SubPolar Mode Waters (IcSPMW, $7.07 < \theta < 8^{\circ}\text{C}$, $35.16 < S < 35.23$, $280 < \text{O}_2 < 289 \mu\text{mol kg}^{-1}$) was encountered from stations 34-40 (accounting for more than 45% of the water mass pool from 0 to ~ 800 m depth) and Irminger SubPolar Mode Waters (IrSPMW, $\theta \approx 5^{\circ}\text{C}$, $S \approx 35.014$) from stations 42-44 (contributing to 40% of the water mass pool from 0 to ~ 250 m depth) and stations 49 and 60 (accounting for 40% of the water mass pool down to 1300 m depth). The IcSPMW was also observed within the Subtropical gyre (stations 11-26), subducted below ENACW until ~ 1000 m depth. Stations 63 (> ~ 200 m depth) and 64 (from surface down to ~ 500 m depth) exhibited a contribution of the IrSPMW higher than 45%. Stations 44, 49 and 60, from the Irminger Sea, and 63 from the Labrador Sea were characterised by lower sea-surface salinity ranges ($S = [34.636, 34.903]$, stations 63 and 60, respectively). Subarctic Intermediate Water (SAIW, $4.5 < \theta < 6.0^{\circ}\text{C}$, $34.70 < S < 34.80$) contributed to more than 40% of the water mass pool in the Iceland Basin between the surface and ~ 400 m depth at stations 29 and 32 and throughout the water column of stations 53, 56 and 61 and from surface down to ~ 200 m depth at station 63. From stations 68 to 78 surface waters were characterized by a minimum of salinity and a maximum of oxygen ($S = 34.91$, $\text{O}_2 = 285 \mu\text{mol kg}^{-1}$, $\theta \approx 3^{\circ}\text{C}$) and corresponded to the newly formed

Labrador Sea Water (LSW). The LSW was also observed in surface waters of station 44 with a similar contribution than IrSPMW ($\sim 40\%$).

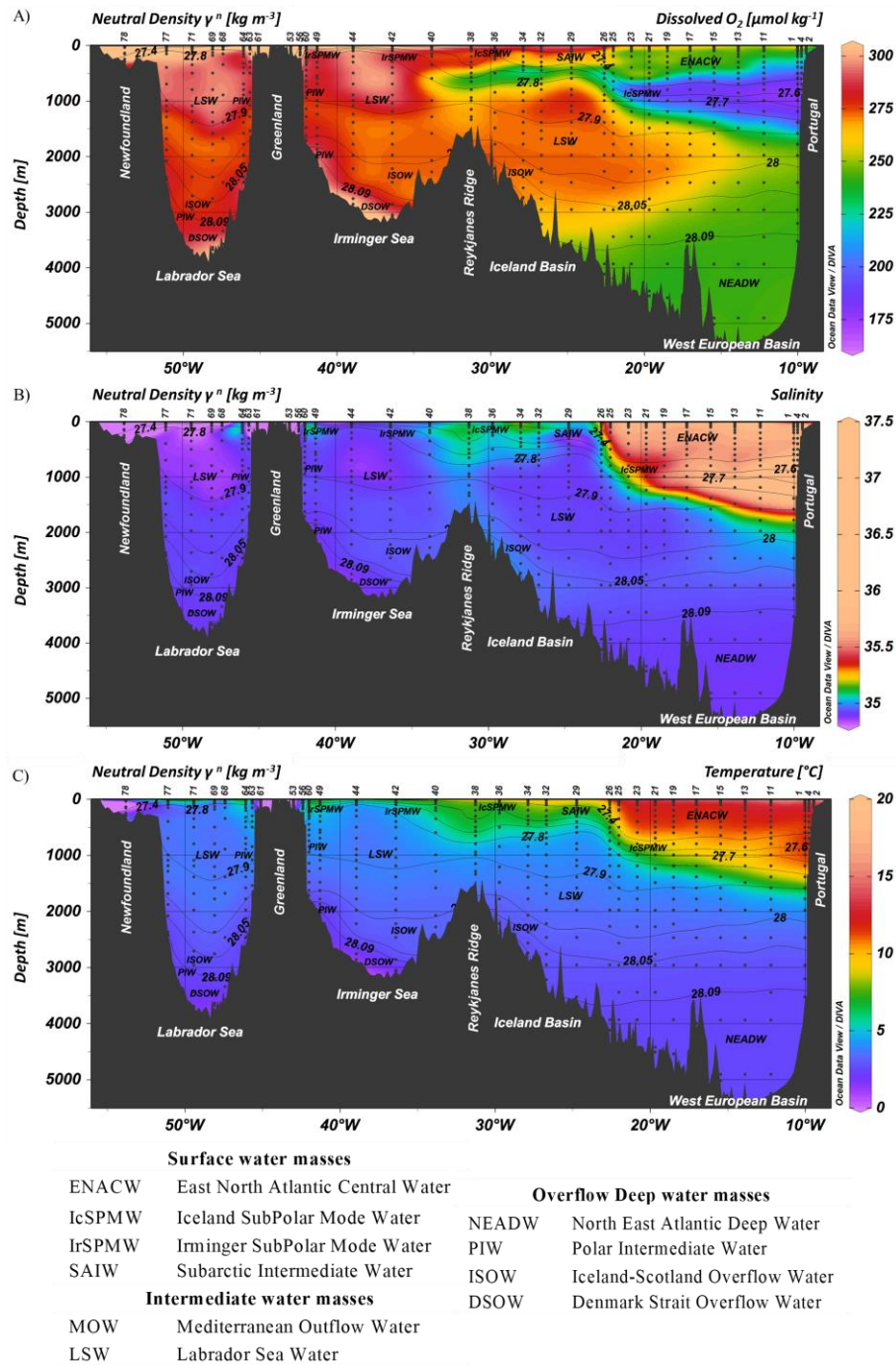


Figure 3.2: Parameters measured from the regular CTD cast represented as a function of depth for GA01 section for (A) Dissolved Oxygen (O_2 , $\mu\text{mol kg}^{-1}$), (B) Salinity and (C) Temperature ($^{\circ}\text{C}$). The contour lines represent isopycnals (neutral density, γ^n , in units of kg m^{-3}).

Intermediate waters (~ 800 – 1400 m) - The Mediterranean Outflow Water (MOW), distinguishable from surrounding Atlantic Water by its high salinity tongue (up to 36.2), a minimum of oxygen ($O_2 = 210 \mu\text{mol kg}^{-1}$) and relatively high temperatures (up to 11.7°C) was observed from station 1 to 21 between 800 and 1400 m depth at a neutral density ranging from 27.544 to 27.751 kg m^{-3} with the maximum contribution to the whole water mass pool seen at station 1 ($64 \pm 6\%$). Its main core was located at ~ 1200 m depth off the Iberian shelf from stations 1 to 11 and then gradually rising westward due to mixing with LSW within the North Atlantic subtropical gyre and a contribution of this water mass decreasing until station 21 down to 10-20%. The LSW ($27.763 < \text{neutral density} < 27.724 \text{ kg m}^{-3}$) was sourced from the SPMW after intense heat loss and led to its deep convection. During GEOVIDE, LSW formed by deep convection the previous winter was found at several stations in the Labrador Sea (68, 69, 71 and 77). After convecting, LSW splits into three main branches with two main cores separated by the Reykjanes Ridge (stations 1-32, West European and Iceland Basins; stations 40-60, Irminger Sea), and the last one entering the West European Basin (Zunino et al., 2017).

Overflows and Deep waters (~ 1400 - 5500 m) - North East Atlantic Deep Water (NEADW, $1.98 < \theta < 2.50^\circ\text{C}$, $34.895 < S < 34.940$) was the dominant water mass in the West European Basin at stations 1-29 from 2000 m depth to the bottom and is characterized by high silicic acid ($42 \pm 4 \mu\text{mol L}^{-1}$), nitrate ($21.9 \pm 1.5 \mu\text{mol L}^{-1}$) concentrations and lower oxygen concentration ($O_2 \approx 252 \mu\text{mol kg}^{-1}$) (see Sarthou et al., 2018). The core of the NEADW (stations 1-13) was located near the seafloor and gradually decreased westward. Polar Intermediate Water (PIW, $\theta \approx 0^\circ\text{C}$, $S \approx 34.65$) is a ventilated, dense, low-salinity water intrusion to the deep overflows within the Irminger and Labrador Seas that is formed at the Greenland shelf. PIW represents only a small contribution to the whole water mass pool (up to 27%) and was observed over the Greenland slope at stations 53 and 61 as well as in surface waters from station 63 (from 0 to ~ 200 m depth), in intermediate waters of stations 49, 60 and 63 (from ~ 500 to ~ 1500 m depth) and in bottom waters of stations 44, 68, 69, 71 and 77 with a contribution higher than 10%. Iceland Scotland Overflow Water (ISOW, $\theta \approx 2.6^\circ\text{C}$, $S \approx 34.98$) is partly formed within the Arctic Ocean by convection of the modified Atlantic water. ISOW comes from the Iceland-Scotland sills and flows southward towards the Charlie-Gibbs Fracture Zone (CGFZ) and Bight Fracture Zone (BFZ) (stations 34 and 36) after which it reverses its flowing path northward and enters the Irminger Sea (stations 40 and

42) to finally reach the Labrador Sea close to the Greenland coast (station 49, station 44 being located in between this two opposite flow paths). Along the eastern (stations 26-36) and western (stations 40-44) flanks of the Reykjanes Ridge, ISOW had a contribution higher than 50% to the water mass pool. ISOW was observed from 1500 m depth to the bottom of the entire Iceland Basin (stations 29-38) and from 1800 to 3000 m depth within the Irminger Sea (stations 40-60). ISOW, despite having a fraction lower than 45% above the Reykjanes Ridge (station 38), was the main contributor to the water mass pool from 1300 m depth down to the bottom. ISOW was also observed within the Labrador Sea from stations 68 to 77. Finally, the deepest part of the Irminger (stations 42 and 44) and Labrador (stations 68-71) Seas were occupied by Denmark Strait Overflow Water (DSOW, $\theta \approx 1.30^{\circ}\text{C}$, $S \approx 34.905$).

3.3.2 Ancillary data

3.3.2.1 Nitrate

Surface nitrate (NO_3^-) concentrations (García-Ibáñez et al., 2018; Pérez et al., 2018; Sarthou et al., 2018) ranged from 0.01 to 10.1 $\mu\text{mol L}^{-1}$ (stations 53 and 63, respectively). There was considerable spatial variability in NO_3^- surface distributions with high concentrations found in the Iceland Basin and Irminger Sea (higher than 6 $\mu\text{mol L}^{-1}$), as well as at stations 63 (10.1 $\mu\text{mol L}^{-1}$) and 64 (5.1 $\mu\text{mol L}^{-1}$), and low concentrations observed in the West European Basin, in the Labrador Sea and above continental margins. The low surface concentrations in the West European Basin ranged from 0.02 (station 11) to 3.9 (station 25) $\mu\text{mol L}^{-1}$. Station 26 delineating the extreme western boundary of the West European Basin exhibited enhanced NO_3^- concentrations as a result of mixing between ENACW and IcSPMW, although these surface waters were dominated by ENACW. In the Labrador Sea (stations 68-78) low surface concentrations were observed with values ranging from 0.04 (station 68) to 1.8 (station 71) $\mu\text{mol L}^{-1}$. At depth, the lowest concentrations (lower than 15.9 $\mu\text{mol L}^{-1}$) were measured in ENACW ($\sim 0 - 800$ m depth) and DSOW (> 1400 m depth), while the highest concentrations were measured within NEADW (up to 23.5 $\mu\text{mol L}^{-1}$), and in the mesopelagic zone of the West European and Iceland Basins (higher than 18.4 $\mu\text{mol L}^{-1}$).

3.3.2.2 Chlorophyll-*a*

Overall, most of the phytoplankton biomass was localised above 100 m depth with lower total chlorophyll-*a* (TChl-*a*) concentrations South of the Subarctic Front and higher at higher latitudes (see supplementary material Fig. S1). While comparing TChl-*a* maxima

considering all stations, the lowest value (0.35 mg m^{-3}) was measured within the West European Basin (station 19, 50 m depth) while the highest values were measured at the Greenland (up to 4.9 mg m^{-3} , 30 m depth, station 53 and up to 6.6 mg m^{-3} , 23 m depth, station 61) and Newfoundland (up to 9.6 mg m^{-3} , 30 m depth, station 78) margins.

3.3.3 Dissolved Fe concentrations

Dissolved Fe concentrations (see supplementary material Table S1) ranged from $0.09 \pm 0.01 \text{ nmol L}^{-1}$ (station 19, 20 m depth) to $7.8 \pm 0.5 \text{ nmol L}^{-1}$ (station 78, 371 m depth) (see Fig. 3.3). Generally, vertical profiles of DFe for stations above the margins (2, 4, 53, 56, 61, and 78) showed an increase with depth, although sea-surface maxima were observed at stations 2, 4 and 56. For these margin stations, values ranged from 0.7 to 1.0 nmol L^{-1} in the surface waters. Concentrations increased towards the bottom, with more than 7.8 nmol L^{-1} measured at station 78, approximately $1\text{--}3 \text{ nmol L}^{-1}$ for stations 2, 4, 53, and 61, and just above 0.4 nmol L^{-1} for station 56 (Fig. 3.4). Considering the four oceanic basins, mean vertical profiles (supplementary material Fig. S2) showed increasing DFe concentrations down to 3000 m depth followed by decreasing DFe concentrations down to the bottom. Among deep-water masses, the lowest DFe concentrations were measured in the West European Basin. The Irminger Sea displayed the highest DFe concentrations from 1000 m depth to the bottom relative to other basins at similar depths (Fig. 3.4 and supplementary material Fig. S2). In the Labrador Sea, DFe concentrations were low and relatively constant at about $0.87 \pm 0.06 \text{ nmol L}^{-1}$ from 250 m to 3000 m depth (Fig. S2). Overall, surface DFe concentrations were higher ($0.36 \pm 0.18 \text{ nmol L}^{-1}$) in the North Atlantic Subpolar gyre (above 52°N) than in the North Atlantic Subtropical gyre ($0.17 \pm 0.05 \text{ nmol L}^{-1}$). The upper surface DFe concentrations were generally smaller than 0.3 nmol L^{-1} , except for few stations in the Iceland Basin (stations 32 and 38), Irminger (stations 40 and 42) and Labrador (station 63) Seas, where values ranged between $0.4\text{--}0.5 \text{ nmol L}^{-1}$.

3.3.4 Fingerprinting water masses

In the Labrador Sea, IrSPMW exhibited an average DFe concentration of $0.61 \pm 0.21 \text{ nmol L}^{-1}$ ($n=14$). DFe concentrations in the LSW were the lowest in this basin, with an average value of $0.71 \pm 0.27 \text{ nmol L}^{-1}$ ($n=53$) (see supplementary material Fig. S3). Deeper, ISOW displayed slightly higher average DFe concentrations ($0.82 \pm 0.05 \text{ nmol L}^{-1}$, $n=2$).

Finally, DSOV had the lowest average ($0.68 \pm 0.06 \text{ nmol L}^{-1}$, $n=3$, see supplementary material Fig. S3) and median (0.65 nmol L^{-1}) DFe values for intermediate and deep waters.

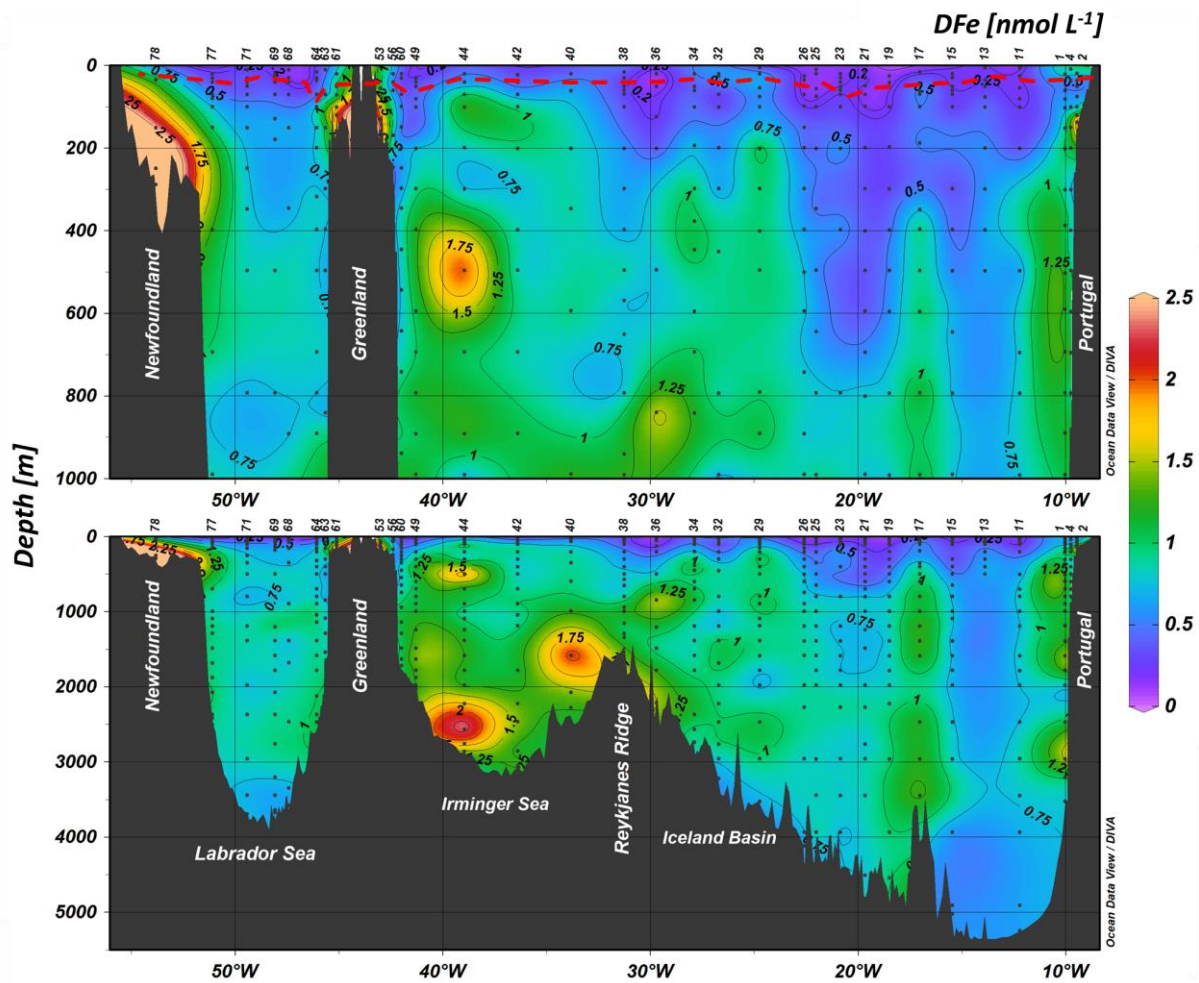


Figure 3.3: Contour plot of the distribution of dissolved iron (DFe) concentrations in nmol L^{-1} along the GA01 voyage transect: upper 1000 m (top) and full depth range (bottom). The red dashed line indicates the depth of the Surface Mixed Layer (SML). Small black dots represent collected water samples at each sampling station. (Ocean Data View (ODV) software, version 4.7.6, R. Schlitzer, <http://odv.awi.de>, 2016).

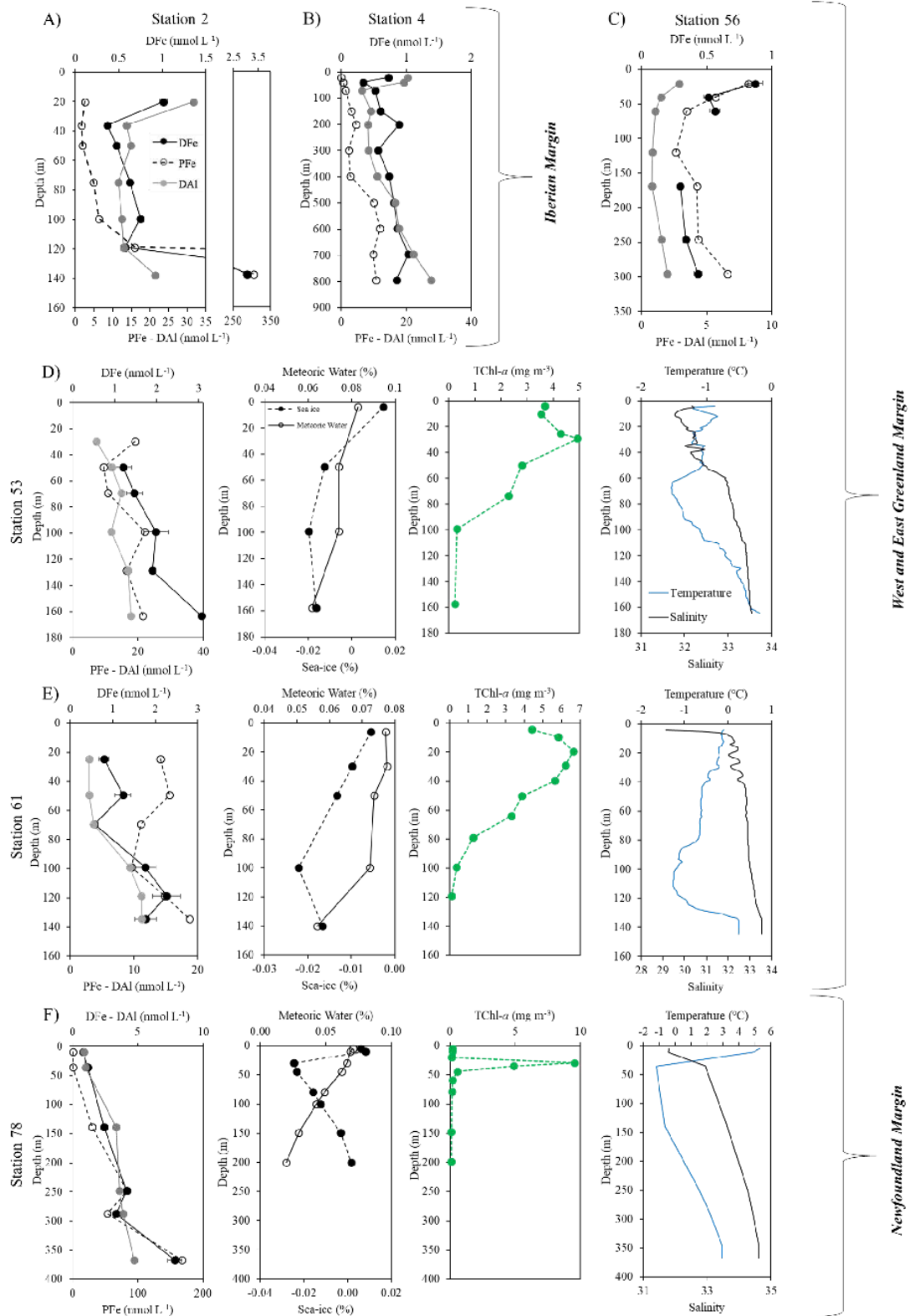


Figure 3.4: Vertical profiles of dissolved iron (DFe, black dots, solid line), particulate iron (PFe, black open dots, dashed line, Gourain et al., in prep.) and dissolved aluminium (DAI, grey dots, Menzel Barraqueta et al., 2018) at Stations 2 (A), and 4 (B) located above the Iberian shelf, Station 56 (C), Stations 53 (D) 53 and Station 61 (E) located above the Greenland shelf and Station 78 (F) located above the Newfoundland shelf. Note that for stations 53, 61 and 78, plots of the percentage of meteoric water (open dots) and sea-ice (black dots and dashed line) (Benetti et al., see text for details), Total Chlorophyll-*a* (TChl-*a*, green), temperature (blue) and salinity (black) are also displayed as a function of depth.

In the Irminger Sea, surface waters were composed of SAIW ($0.56 \pm 0.24 \text{ nmol L}^{-1}$, $n=4$) and IrSPMW ($0.72 \pm 0.32 \text{ nmol L}^{-1}$, $n=34$). The highest open-ocean DFe concentrations (up to $2.5 \pm 0.3 \text{ nmol L}^{-1}$, station 44, 2600 m depth) were measured within this basin. In the upper intermediate waters, LSW was identified only at stations 40 to 44, and had the highest DFe values with an average of $1.2 \pm 0.3 \text{ nmol L}^{-1}$ ($n=14$). ISOW showed higher DFe concentrations than in the Iceland Basin ($1.3 \pm 0.2 \text{ nmol L}^{-1}$, $n=4$). At the bottom, DSOW was mainly located at stations 42 and 44 and presented the highest average DFe values ($1.4 \pm 0.4 \text{ nmol L}^{-1}$, $n=5$) as well as the highest variability from all the water masses presented in this section (see supplementary material Fig. S3).

In the Iceland Basin, SAIW and IcSPMW displayed similar averaged DFe concentrations ($0.67 \pm 0.30 \text{ nmol L}^{-1}$, $n=7$ and $0.55 \pm 0.34 \text{ nmol L}^{-1}$, $n=22$, respectively). Averaged DFe concentrations were similar in both LSW and ISOW, and higher than in SAIW and IcSPMW ($0.96 \pm 0.22 \text{ nmol L}^{-1}$, $n=21$ and $1.0 \pm 0.3 \text{ nmol L}^{-1}$, $n=10$, respectively, see supplementary material Fig. S3).

Finally, in the West European Basin, DFe concentrations in ENACW were the lowest of the whole section with an average value of $0.30 \pm 0.16 \text{ nmol L}^{-1}$ ($n=64$). MOW was present deeper in the water column but was not characterized by particularly high or low DFe concentrations relative to the surrounding Atlantic waters (see supplementary material Fig. S3). The median DFe value in MOW was very similar to the median value when considering all water masses (0.77 nmol L^{-1} , Fig. 3.3 and supplementary material S3). LSW and IcSPMW displayed slightly elevated DFe concentrations compared to the overall median with mean values of 0.82 ± 0.08 ($n=28$) and 0.80 ± 0.04 ($n=8$) nmol L^{-1} , respectively. The DFe concentrations in NEADW were relatively similar to the DFe median value of the GEOVIDE voyage (median DFe = 0.75 nmol L^{-1} , Fig. 3.3 and supplementary material Fig. S3) with an average value of $0.74 \pm 0.16 \text{ nmol L}^{-1}$ ($n=18$) and presented relatively low median DFe concentrations (median DFe = 0.71 nmol L^{-1}) compared to other deep water masses.

3.4 Discussion

In the following sections, we will first discuss the high DFe concentrations observed throughout the water column of stations 1 and 17 located in the West European Basin (Section 3.4.1), then, the relationship between water masses and the DFe concentrations (Section 3.4.2) in intermediate (Section 3.4.2.2 and 3.4.2.3) and deep (Section 3.4.2.4 and

3.4.2.5) waters. We will also discuss the role of wind (Section 3.4.2.1), rivers (Section 3.4.3.1), meteoric water and sea-ice processes (Section 3.4.3.2), atmospheric deposition (Section 3.4.3.3) and sediments (Section 3.4.4) in delivering DFe. Finally, we will discuss the potential Fe limitation using DFe:NO₃⁻ ratios (Section 3.4.5).

3.4.1 High DFe concentrations at station 1 and 17

Considering the entire section, two stations (stations 1 and 17) showed irregularly high DFe concentrations ($> 1 \text{ nmol L}^{-1}$) throughout the water column, thus suggesting analytical issues. However, these two stations were analysed twice and provided similar results, therefore discarding any analytical issues. This means that these high values originated either from genuine processes or from contamination issues. If there had been contamination issues, one would expect a more random distribution of DFe concentrations and less consistence throughout the water column. It thus appears that contamination issues were unlikely to happen. Similarly, the influence of water masses to explain these distributions was discarded as the observed high homogenized DFe concentrations were restricted to these two stations. Station 1, located at the continental shelf-break of the Iberian Margin, also showed enhanced PFe concentrations from lithogenic origin suggesting a margin source (Gourain et al., 2018). Conversely, no relationship was observed between DFe and PFe nor transmissometry for station 17. However, Ferron et al. (2016) reported a strong dissipation rate at the Azores-Biscay Rise (station 17) due to internal waves. The associated vertical energy fluxes could explain the homogenized profile of DFe at station 17, although such waves are not clearly evidenced in the velocity profiles. Consequently, the elevated DFe concentrations observed at station 17 remain unsolved.

3.4.2 DFe and hydrology keypoints

3.4.2.1 How do air-sea interactions affect DFe concentration in the Irminger Sea?

Among the four distinct basins described in this paper, the Irminger Sea exhibited the highest DFe concentrations within the surface waters (from 0 to 250 m depth) with values ranging from 0.23 to 1.3 nmol L^{-1} for open-ocean stations. Conversely, low DFe concentrations were previously reported in the central Irminger Sea by Rijkenberg et al. (2014) (April-May, 2010) and Achterberg et al. (2018) (April-May and July-August, 2010) with DFe concentrations ranging from 0.11 to 0.15 and from ~ 0 to 0.14 nmol L^{-1} , respectively (see supplementary material Fig. S4 and Table S2). Differences might be due to the phytoplankton bloom advancement, the high remineralization rate (Lemaître et al., 2017)

observed within the LSW in the Irminger Sea (see Section 3.4.1.3) and a deeper winter convection in early 2014. Indeed, enhanced surface DFe concentrations measured during GEOVIDE in the Irminger Sea could be due to intense wind forcing events that would deepen the winter Z_m down to the core of the Fe-rich LSW.

In the North Atlantic Ocean, the warm and salty water masses of the upper limb of the MOC are progressively cooled and become denser, and subduct into the abyssal ocean. In some areas of the SubPolar North Atlantic, deep convective winter mixing provides a rare connection between surface and deep waters of the MOC thus constituting an important mechanism in supplying nutrients to the surface ocean (de Jong et al., 2012; Louanchi and Najjar, 2001). Deep convective winter mixing is triggered by the effect of wind and a pre-conditioning of the ocean in such a way that the inherent stability of the ocean is minimal. Pickart et al. (2003) demonstrated that these conditions are satisfied in the Irminger Sea with the presence of weakly stratified surface water, a close cyclonic circulation, which leads to the shoaling of the thermocline and intense winter air-sea buoyancy fluxes (Marshall and Schott, 1999). Moore (2003) and Piron et al. (2016) described low-level westerly jets centred northeast of Cape Farewell, over the Irminger Sea, known as tip jet events. These events occur when wind is split around the orographic features of Cape Farewell, and are strong enough to induce deep convective mixing (Bacon et al., 2003; Pickart et al., 2003). It has also been shown that during winters with a positive North Atlantic Oscillation (NAO) index, the occurrence of such events is favoured (Moore, 2003; Pickart et al., 2003), which was the case in the winter 2013-2014, preceding the GEOVIDE voyage as opposed to previous studies (Lherminier, pers. comm.). The winter mixed layer depth prior to the cruise reached up to 1200 m depth in the Irminger Sea (Zunino et al., 2017), which was most likely attributed to a final deepening due to wind forcing events (centred at station 44). Such winter entrainment was likely the process involved in the vertical supply of DFe within surface waters fuelling the spring phytoplankton bloom with DFe values close to those found in LSW.

3.4.2.2 Why don't we see a DFe signature in the Mediterranean Overflow Water (MOW)?

On its northern shores, the Mediterranean Sea is bordered by industrialized European countries, which act as a continuous source of anthropogenic derived constituents into the atmosphere, and on the southern shores by the arid and desert regions of north African and Arabian Desert belts, which act as sources of crustal material in the form of dust pulses (Chester et al., 1993; Guerzoni et al., 1999; Martin et al., 1989). During the summer, when

thermal stratification occurs, DFe concentrations in the SML can increase over the whole Mediterranean Sea by 1.6-5.3 nmol L⁻¹ in response to the accumulation of atmospheric Fe from both anthropogenic and natural origins (Bonnet and Guieu, 2004; Guieu et al., 2010; Sarthou and Jeandel, 2001). After atmospheric deposition, the fate of Fe will depend on the nature of aerosols, vertical mixing, biological uptake and scavenging processes (Bonnet and Guieu, 2006; Wuttig et al., 2013). During GEOVIDE, MOW was observed from stations 1 to 29 between 1000 and 1200 m depth and associated with high dissolved aluminium (DAI, Menzel Barraqueta et al., 2018) concentrations (up to 38.7 nmol L⁻¹), confirming the high atmospheric deposition in the Mediterranean region. In contrast to Al, no DFe signature was associated with MOW (Figs. 3.2 and 3.3). This feature was also reported in some studies (Hatta et al., 2015; Thuróczy et al., 2010), while others measured higher DFe concentrations in MOW (Gerringa et al., 2017; Sarthou et al., 2007). However, MOW coincides with the maximum Apparent Oxygen Utilization (AOU) and it is not possible to distinguish the MOW signal from the remineralisation one (Sarthou et al., 2007). On the other hand, differences between studies are likely originating from the intensity of atmospheric deposition and the nature of aerosols. Indeed, Wagener et al. (2010) highlighted that large dust deposition events can accelerate the export of Fe from the water column through scavenging. As a result, in seawater with high DFe concentrations and where high dust deposition occurs, a strong individual dust deposition event could act as a sink for DFe. It thus becomes less evident to observe a systematic high DFe signature in MOW despite dust inputs.

3.4.2.3 Fe enrichment in Labrador Sea Water (LSW)

As described in Section 3.3.1, the LSW exhibited increasing DFe concentrations from its source area, the Labrador Sea, toward the other basins with the highest DFe concentrations observed within the Irminger Sea, suggesting that the water mass was enriched in DFe either locally in each basin or during its flow path (see supplementary material Fig. S3). These DFe sources could originate from a combination of high export of PFe and its remineralisation in the mesopelagic area and/or the dissolution of sediment.

The Irminger and Labrador Seas exhibited the highest averaged integrated TChl-*a* concentrations (98 ± 32 mg m⁻² and 59 ± 42 mg m⁻²) compared to the West European and Iceland Basins (39 ± 10 mg m⁻² and 53 ± 16 mg m⁻²), when the influence of margins was discarded. Stations located in the Irminger (stations 40-56) and Labrador (stations 63-77) Seas, were largely dominated by diatoms (>50% of phytoplankton abundances) and displayed the highest chlorophyllid-*a* concentrations, a tracer of senescent diatom cells, likely reflecting

post-bloom condition (Tonnard et al., in prep.). This is in line with the highest POC export data reported by Lemaitre et al. (2018) in these two oceanic basins. This likely suggests that biogenic PFe export was also higher in the Labrador and Irminger Seas than in the West European and Iceland Basins. In addition, Gourain et al. (2018) highlighted a higher biogenic contribution for particles located in the Irminger and Labrador Seas with relatively high PFe:PAI ratios (0.44 ± 0.12 mol:mol and 0.38 ± 0.10 mol:mol, respectively) compared to particles from the West European and Iceland Basins (0.22 ± 0.10 and 0.38 ± 0.14 mol:mol, respectively, see Fig. 6 in Gourain et al., 2018). However, they reported no difference in PFe concentrations between the four oceanic basins (see Fig. 12A in Gourain et al., 2018) when the influence of margins was discarded, which likely highlighted the remineralisation of PFe within the Irminger and Labrador Seas. Indeed, Lemaître et al. (2017) reported higher remineralisation rates within the Labrador (up to $13 \text{ mmol C m}^{-2} \text{ d}^{-1}$) and Irminger Seas (up to $10 \text{ mmol C m}^{-2} \text{ d}^{-1}$) using the excess barium proxy (Dehairs et al., 1997), compared to the West European and Iceland Basins (ranging from 4 to $6 \text{ mmol C m}^{-2} \text{ d}^{-1}$). Therefore, the intense remineralisation rates measured in the Irminger and Labrador Seas likely resulted in enhanced DFe concentrations within LSW.

Higher DFe concentrations were, however, measured in the Irminger Sea compared to the Labrador Sea and coincided with lower transmissometry values (i.e. 98.0-98.5% vs. >99%), thus suggesting a particle load of the LSW. This could be explained by the reductive dissolution of Newfoundland Margin sediments. Indeed, Lambelet et al. (2016) reported high dissolved neodymium (Nd) concentrations (up to $18.5 \text{ pmol.kg}^{-1}$) within the LSW at the edge of the Newfoundland Margin (45.73°W , 51.82°N) as well as slightly lower Nd isotopic ratio values relative to those observed in the Irminger Sea. They suggested that this water mass had been in contact with sediments approximately within the last 30 years (Charette et al., 2015). Similarly, during GA03, Hatta et al. (2015) attributed the high DFe concentrations in the LSW to continental margin sediments. Consequently, it is also possible that the elevated DFe concentrations from the three LSW branches which entered the West European and Iceland Basins and Irminger Sea was supplied through sediment dissolution (Measures et al., 2013) along the LSW pathway.

The enhanced DFe concentrations measured in the Irminger Sea and within the LSW were thus likely attributed to the combination of higher productivity, POC export and remineralisation as well as a DFe supply from reductive dissolution of Newfoundland sediments to the LSW along its flow path.

3.4.2.4 Enhanced DFe concentrations in the Irminger Sea bottom water

Bottom waters from the Irminger Sea exhibited the highest DFe concentrations from the whole section, excluding the stations at the margins. Such a feature could be due to i) vertical diffusion from local sediment, ii) lateral advection of water mass(es) displaying enhanced DFe concentrations, and iii) local dissolution of Fe from particles. Hereafter, we discuss the plausibility of these three hypotheses to occur.

The GEOTRACES GA02 voyage (leg 1, 64PE319) which occurred in April-May 2010 from Iceland to Bermuda sampled two stations north and south of our station 44 (~ 38.95°W, 59.62°N): station 5 (~ 37.91°W, 60.43°N) and 6 (~ 39.71°W, 58.60°N), respectively. High DFe concentrations in samples collected close to the bottom were also observed and attributed to sediment inputs highlighting boundary exchange between seawater and surface sediment (Lambelet et al., 2016; Rijkenberg et al., 2014). However, because a decrease in DFe concentrations was observed at our station 44 from 2500 m depth down to the bottom (Fig. 3.3, see supplementary material Fig. S4 and Table S2), it appeared to be unlikely that these high DFe concentrations will be the result of sediment inputs, as no DFe gradient from the deepest samples to those above was observed.

Looking at salinity versus depth for these three stations, one can observe the intrusion of Polar Intermediate Water (PIW) at station 44 from GEOVIDE, which was not observed during the GA02 voyage and which contributed to about 14% of the water mass composition (García-Ibáñez et al., this issue) and might therefore be responsible for the high DFe concentrations (see supplementary material Fig. S5A). On the other hand, the PIW was also observed at station 49 (from 390 to 1240 m depth), 60 (from 440 to 1290 m depth), 63 (from 20 to 1540 m depth), 68 (3340 m depth), 69 (from 3200 to 3440 m depth), 71 (from 2950 to 3440 m depth) and 77 (60 and 2500 m depth) with similar or higher contributions of the PIW without such high DFe concentrations (maximum DFe = $1.3 \pm 0.1 \text{ nmol L}^{-1}$, 1240 m depth at station 49). However, considering the short residence time of DFe and the circulation of water masses in the Irminger Sea, it is possible that instead of being attributed to one specific water mass, these enhanced DFe concentrations resulted from lateral advection of the deep waters. Figure S5B) shows the concentrations of both DFe and PFe for the mixing line between DSOW/PIW and ISOW at station 44 and considering 100% contribution of ISOW for the shallowest sample (2218 m depth) and of DSOW/PIW for the deepest (2915 m depth), as these were the main water masses. This figure shows increasing DFe concentrations as DSOW/PIW mixed with ISOW. In addition, Le Roy et al. (2018) reported for the GEOVIDE

voyage at station 44 a deviation from the conservative behaviour of ^{226}Ra reflecting an input of this tracer centred at 2500 m depth, likely highlighting diffusion from deep-sea sediments and coinciding with the highest DFe concentrations measured at this station. Although the transmissometry data were lower at the sediment interface than at 2500 m depth, Deng et al. (2018) reported a stronger scavenged component of the ^{230}Th at the same depth range, likely suggesting that the mixture of water masses were in contact with highly reactive particles. If there is evidence that the enhanced DFe concentrations observed at station 44 coincided with lateral advection of water masses that were in contact with particles, the difference of behaviour between DFe and ^{230}Th remains unsolved. The only parameter that would explain without any ambiguity such differences of behaviour between DFe and ^{230}Th would be the amount of Fe-binding organic ligands for these samples. Indeed, although PFe concentrations decreased from the seafloor to the above seawater, this trend would likely be explained by a strong vertical diffusion alone and not necessarily by the dissolution of particles that were laterally advected.

Therefore, the high DFe concentrations observed might be inferred from local processes as ISOW mixes with both PIW and DSOW with a substantial load of Fe-rich particles that might have dissolved in solution due to Fe-binding organic ligands.

3.4.2.5 Reykjanes Ridge: Hydrothermal inputs or Fe-rich seawater?

Hydrothermal activity was assessed over the Mid Atlantic Ridge, namely the Reykjanes Ridge, from stations 36 to 40. Indeed, within the interr ridge database (<http://www.interridge.org>), the Reykjanes Ridge is reported to have active hydrothermal sites. The sites were either confirmed (Baker and German, 2004a; German et al., 1994; Olafsson et al., 1991; Palmer et al., 1995) close to Iceland or inferred (e.g. Chen, 2003; Crane et al., 1997; German et al., 1994; Sinha et al., 1997; Smallwood and White, 1998) closer to the GEOVIDE section as no plume was detected but a high backscatter was reported potentially corresponding to a lava flow. Therefore, hydrothermal activity at the sampling sites remains unclear with no elevated DFe concentrations nor temperature anomaly above the ridge (station 38). However, enhanced DFe concentrations (up to $1.5 \pm 0.22 \text{ nmol L}^{-1}$, station 36, 2200 m depth) were measured east of the Reykjanes Ridge (Fig. 3.3). This could be due to hydrothermal activity and resuspension of sunken particles at sites located North of the section and transported through the ISOW towards the section (see supplementary material Fig. S3). Indeed, Achterberg et al. (2018) highlighted at $\sim 60^\circ\text{N}$ and over the Reykjanes Ridge a southward lateral transport of an Fe plume of up to 250-300 km. In

agreement with these observations, previous studies (e.g. Fagel et al., 1996; Fagel et al., 2001; Lackschewitz et al., 1996; Parra et al., 1985) reported marine sediment mineral clays in the Iceland Basin largely dominated by smectite (> 60%), a tracer of hydrothermal alteration of basaltic volcanic materials (Fagel et al., 2001; Tréguer and De La Rocha, 2013). Hence, the high DFe concentrations measured east of the Reykjanes Ridge could be due to a hydrothermal source and/or the resuspension of particles and their subsequent dissolution.

West of the Reykjanes Ridge, a DFe-enrichment was also observed in ISOW within the Irminger Sea (Figs. 3.4 and S3). The low transmissometer values within ISOW in the Irminger Sea compared to the Iceland Basin suggest a particle load. These particles could come from the Charlie Gibbs Fracture Zone (CGFZ, 52.67°N and 34.61°W) and potentially Bight Fracture Zone (BFZ, 56.91°N and 32.74°W) (Fig. 3.1) (Lackschewitz et al., 1996; Zou et al., 2017). Indeed, hydrographic sections of the northern valley of the CGFZ showed that below 2000 m depth the passage through the Mid-Atlantic Ridge was mainly filled with the ISOW (Kissel et al., 2009; Shor et al., 1980). Shor et al. (1980) highlighted a total westward transport across the sill, below 2000 m depth of about $2.4 \times 10^6 \text{ m}^3 \text{ s}^{-1}$ with ISOW carrying a significant load of suspended sediment ($25 \mu\text{g L}^{-1}$), including a 100-m-thick benthic nepheloid layer. It thus appears that the increase in DFe within ISOW likely came from sediment resuspension and dissolution as the ISOW flows across CGFZ and BFZ.

3.4.3 What are the main sources of DFe in surface waters?

During GEOVIDE, enhanced DFe surface concentrations were observed at several stations (stations 1-4, 53, 61, 78) highlighting an external source of Fe to surface waters. The main sources able to deliver DFe to surface waters are riverine inputs, glacial inputs and atmospheric deposition. In the following sections, these potential sources of DFe in surface waters will be discussed.

3.4.3.1 Tagus riverine inputs

Enhanced DFe surface concentrations (up to $1.07 \pm 0.12 \text{ nmol L}^{-1}$) were measured over the Iberian Margin (stations 1-4) and coincided with salinity minima ($\sim <35$) and enhanced DAi concentrations (up to 31.8 nmol L^{-1} , Menzel Barraqueta et al., 2018). DFe and DAi concentrations were both significantly negatively correlated with salinity ($R^2 = \sim 1$ and 0.94 , respectively) from stations 1 to 13 (Fig. 3.5). Salinity profiles from station 1 to 4 showed evidence of a freshwater source with surface salinity ranging from 34.95 (station 1) to 35.03 (station 4). Within this area, only two freshwater sources were possible: 1) wet atmospheric deposition (4 rain events, Shelley, pers. comm.) and 2) the Tagus River, since the ship SADCP data revealed a northward circulation (P. Lherminier and P. Zunino, Ifremer

Brest, pers. comm.). Our SML DFe inventories were about three times higher at station 1 (~ 1 nmol L⁻¹) than those calculated during the GA03 voyage (~ 0.3 nmol L⁻¹, station 1) during which atmospheric deposition were about one order of magnitude higher (Shelley et al., 2018; Shelley et al., 2015), the atmospheric source seemed to be minor. Consequently, the Tagus River appears as the most likely source responsible for these enhanced DFe concentrations, either as direct input of DFe or indirectly through Fe-rich sediment carried by the Tagus River and their subsequent dissolution. The Tagus estuary is the largest in the western European coast and very industrialized (Canário et al., 2003; de Barros, 1986; Figueres et al., 1985; Gaudencio et al., 1991; Mil-Homens et al., 2009), extends through an area of 320 km² and is characterized by a large water flow of 15.5 10⁹ m³ y⁻¹ (Fiuza, 1984). Many types of industry (e.g. heavy metallurgy, ore processing, chemical industry) release metals including Fe, which therefore result in high levels recorded in surface sediments, suspended particulate matter, water and organisms in the lower estuary (Santos-Echeandia et al., 2010).

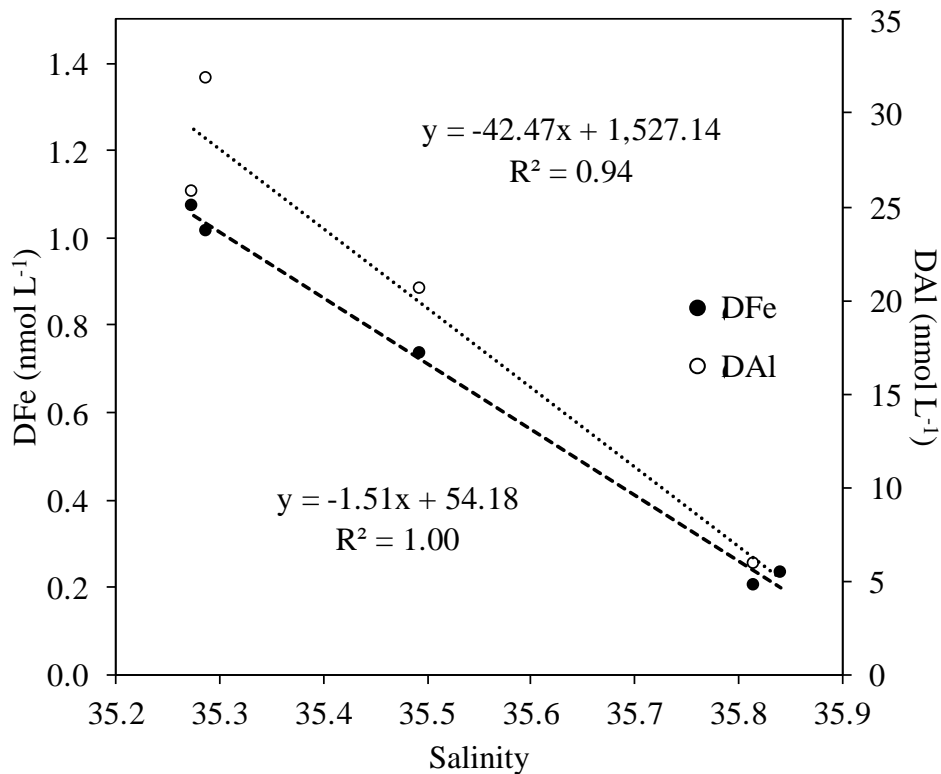


Figure 3.5: Plot of dissolved iron (DFe, black circles) and dissolved aluminium (DAI, white circles, Menzel Barraqueta et al., 2018) along the salinity gradient between stations 1, 2, 4, 11 and 13 with linear regression equations. Numbers close to sample points representing station numbers.

3.4.3.2 High latitude meteoric water and sea-ice processes

Potential sources of Fe at stations 53, 61 and 78 include meteoric water (MW, referring to precipitation, runoff and continental glacial melt), sea-ice melt (SIM), seawater interaction with shallow sediments and advection of water transported from the Arctic sourced by the Fe-rich TransPolar Drift (TPD, Klunder et al. (2012); see supplementary material Fig. S4 and Table S2). The vertical profiles of both potential temperature and salinity in the Greenland and Newfoundland Margins (station 53, 61 and 78, Fig. 3.4 D), E) and F)) highlighted the influence of fresh waters originating from the Arctic Ocean to separate surface and deeper samples at ~ 60 m (station 53) and ~ 40 m (stations 61 and 78) depth. The presence of this freshwater lens suggests that sediment derived enrichment to these surface waters was unlikely. The most plausible sources would be freshwater induced by meteoric water and sea-ice melt. Deeper in the water column, net brine release were observed at stations 53 (below 40 m depth, Fig. 3.4D) 61 (in the whole water column, Fig. 3.4E) and 78 (below 30 m depth, Fig. 3.4F). The release of brines could originate from two different processes: the sea-ice formation or the early melting of multiyear sea ice due to gravitational drainage and subsequent brine release (Petrich and Eicken, 2010; Wadhams, 2000). Indeed, during the winter preceding the GEOVIDE voyage, multiyear sea ice extended 200 km far from our Greenland stations (<http://nsidc.org/arcticseaicenews/>). In the following sections, we discuss the potential for meteoric water supply, sea-ice formation and sea-ice melting to affect DFe distribution.

3.4.3.2.1 The Greenland shelf

Considering the sampling period at stations 53 (16 June 2014) and 61 (19 June 2014), sea-ice formation is unlikely to happen as this period coincides with summer melting in both the Central Arctic and East Greenland (Markus et al., 2009). However, it is possible that the brines observed in our study could originate from sea-ice formation, which occurred during the previous winter(s) at 66°N (and/or higher latitudes). The residence time can vary from days (von Appen et al., 2014) to 6-9 months (Sutherland et al., 2009). Due to our observed strong brine signal at station 61 we suggest that the residence time was potentially longer than average. Given that the brine signal was higher at station 61 than at station 53 (which was located upstream in the EGC), we suggest that station 53 was exhibiting a freshening as a result of the transition between the freezing period toward the melting period. This would result in a dilution of the brine signal at the upstream station. Consequently, the salinity of

this brine signal may reflect sea ice formation versus melting which may have an effect on the trace metal concentration within this water (Hunke et al., 2011). The associated brine water at station 61(100 m depth) was slightly depleted in both DFe and PFe, which may be attributed to sea ice formation processes. Indeed, Janssens et al. (2016) highlighted that as soon as sea ice forms, sea salts are efficiently flushed out of the ice while PFe is trapped within the crystal matrix and DFe accumulates, leading to an enrichment factor of these two Fe fractions compared to underlying seawater. Conversely, the brine signal observed at station 53 (100 m depth) showed slight enrichment in DFe, which may be attributed to brine release during early sea ice melting and the associated release of DFe into the underlying water column as the brine sinks until reaching neutral buoyancy due to higher density.

Surface waters (from 0 to ~ 100 m depth) from station 53 and 61 were characterized by high MW fractions (ranging from 8.3 to 7.4% and from 7.7 to 7.3% , respectively, from surface to ~100 m depth, Figs. 3.5D and E). These high MW fractions were both enriched in PFe and DFe (except station 53 for which no data was available close to the surface) compared to seawater located below 50 m depth, thus suggesting a MW source. These results are in line with previous observations, which highlighted strong inputs of DFe from a meteoric water melting source in Antarctica (Annett et al., 2015). Although the ability of MW from Greenland Ice Sheet and runoffs to deliver DFe and PFe to surrounding waters has previously been demonstrated (Bhatia et al., 2013; Hawkings et al., 2014; Schroth et al., 2014; Statham et al., 2008), both Fe fractions were lower at the sample closest to the surface, then reached a maximum at ~ 50 m depth and decreased at ~ 70 m depth, for station 61 (Fig. 3.4D). The surface DFe depletion was likely explained by phytoplankton uptake, as indicated by the high TChl-*a* concentrations (up to 6.6 mg m⁻³) measured from surface to about 40 m depth, drastically decreasing at ~ 50 m depth to 3.9 mg m⁻³ (Fig. 3.4D). Hence, it seemed that meteoric water inputs from the Greenland Margin likely fertilized surface waters with DFe, enabling the phytoplankton bloom to subsist. The profile of PFe can be explained by two opposite plausible hypotheses: 1) MW inputs did not released PFe, as if it was the case, one should expect higher PFe concentrations at the surface (~25 m depth) than the one measured at 50 m depth due to both the release from MW and the assimilation of DFe by phytoplankton 2) MW inputs can release PFe in a form that is directly accessible to phytoplankton with subsequent export of PFe as phytoplankton died. The latter solution explains the PFe maximum measured at ~ 50 m depth and is thus the most plausible.

3.4.3.2.2 *The Newfoundland shelf*

Newfoundland shelf waters (station 78) were characterized by high MW fractions (up to 7%), decreasing from surface to 200 m depth (~2%). These waters were associated with a net sea-ice melting signal from the near surface to ~10 m depth followed by a brine release signal down to 200 m depth with the maximum contribution measured at ~30 m depth. Within the surface waters (above 20 m depth), no elevation in DFe, DAl nor PFe was noticed despite the low measured TChl-*a* concentrations (TChl-*a* ~ 0.20 mg m⁻³). This suggests that none of these inputs (sea-ice melting and meteoric water) were able to deliver DFe or that these inputs were minor compared to sediment inputs from the Newfoundland Margin. Surprisingly, the highest TChl-*a* biomass (TChl-*a* > 9 mg m⁻³) from the whole section was measured at 30 m depth corresponding to the strongest brine release signal. This either suggests that the brine likely contained important amounts of Fe (dissolved and/or particulate Fe) that were readily available for phytoplankton and consumed at the sampling period by potentially sea-ice algae themselves (Riebesell et al., 1991) or that another nutrient was triggering the phytoplankton bloom.

3.4.3.3 Atmospheric deposition

On a regional scale, the North Atlantic basin receives the largest amount of atmospheric inputs due to its proximity to the Saharan Desert (Jickells et al., 2005), yet even in this region of high atmospheric deposition, inputs are not evenly distributed. Indeed, aerosol Fe loading measured during GEOVIDE (Shelley et al., 2017) were much lower (up to four orders of magnitude) than those measured during studies from lower latitudes in the North Atlantic (e.g. Baker et al., 2013; Buck et al., 2010; and for GA03, Shelley et al., 2015), but atmospheric inputs could still be an important source of Fe to surface waters in areas far from land.

In an attempt to estimate whether there was enough atmospheric input to sustain the SML DFe concentrations, we calculated Turnover Times relative to Atmospheric Deposition (TTADs, Guieu et al., 2014). To do so, we made the following assumptions: 1) the aerosol concentrations are a snapshot in time but are representative of the study region, 2) the aerosol solubility estimates based on two sequential leaches are an upper limit of the aerosol Fe in seawater and 3) the water column stratified just before the deposition of atmospheric inputs, so MLD DFe will reflect inputs from above. Thus, the TTADs were defined as the integrated DFe concentrations in the SML for each station divided by the contribution of soluble Fe contained in aerosols averaged per basin to the water volume of the SML. Although, TTADs

were lower in the West European and Iceland Basins with an average of $\sim 9 \pm 3$ months compared to other basins (7 ± 2 years and 5 ± 2 years for the Irminger and Labrador Seas, respectively) (Fig. 3.6) they were about three times higher than those reported for areas impacted by Saharan dust inputs (~ 3 months, Guieu et al., 2014). Therefore, the high TTADs measured in the Irminger and Labrador Seas and ranging from 2 to 15 years provided further evidence that atmospheric deposition were unlikely to supply Fe in sufficient quantity to be the main source of DFe (see Sections 3.4.2.1 and 3.4.3.2) while in the West European and Iceland Basins they played an additional source, perhaps the main source of Fe especially at station 36 which displayed TTAD of 3 months.

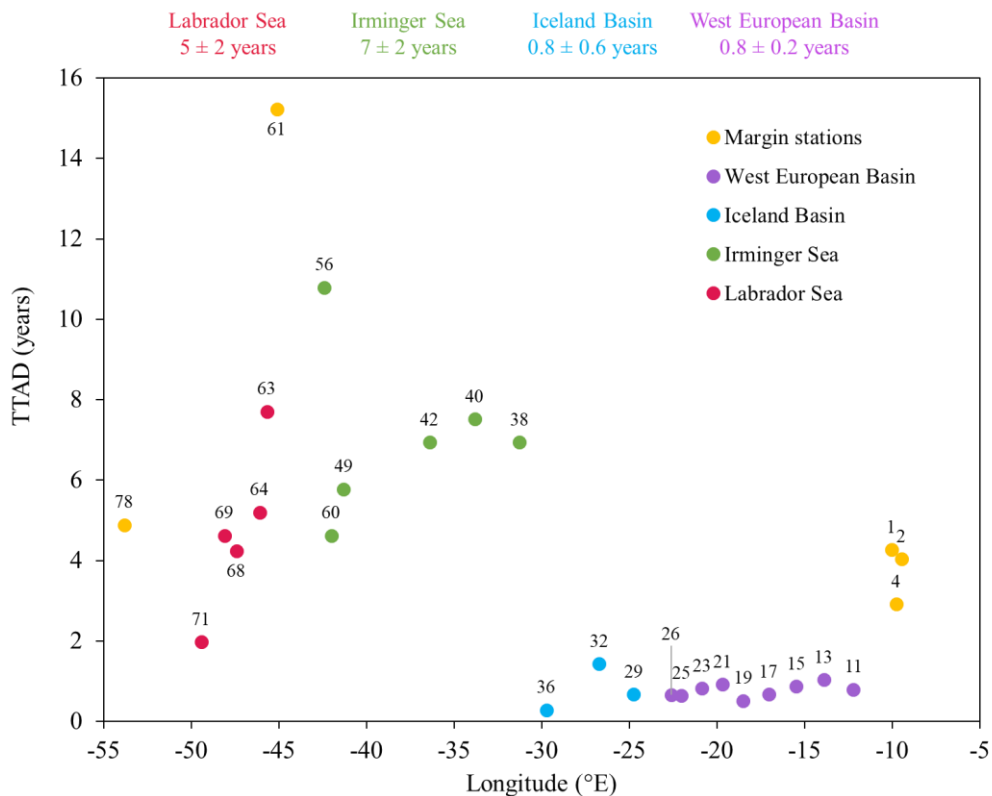


Figure 3.6: Plot of dissolved Fe (DFe) Turnover Times relative to Atmospheric Deposition (TTADs) calculated from soluble Fe contained in aerosols estimated from a two-stage sequential leach (UHP water, then 25% HAc, Shelley et al., this issue). Note that numbers on top of points represent station numbers and that the colour coding refers to different region with in yellow, margin stations; in purple, the West European Basin; in blue, the Iceland Basin; in green, the Irminger Sea and in red, the Labrador Sea. The numbers on top of the plot represent TTADs averaged for each oceanic basin and their standard deviation.

3.4.4 Sediment input

3.4.4.1 Margins:

DFe concentration profiles from all coastal stations (stations 2, 4, 53, 56, 61 and 78) are reported in Figure 3.4. To avoid surface processes, only depths below 100 m depth will be considered in the following discussion. DFe and PFe followed a similar pattern at stations 2, 53, 56, and 78 with increasing concentrations towards the sediment, suggesting that either the sources of Fe supplied both Fe fractions (dissolved and particulate) or that PFe dissolution from sediments supplied DFe. Among the different margins, the Newfoundland Margin exhibited the highest deep-water DFe concentrations. Conversely, stations 4 and 61 exhibited a decrease in DFe concentrations at the closest samples to the seafloor whereas PFe increased. DFe:PFe ratios ranged from 0.01 (station 2, bottom sample) to 0.27 (station 4, ~ 400 m depth) mol:mol with an average value of 0.11 ± 0.07 mol:mol ($n = 23$, Table 3.3), highlighting a different behaviour of Fe among margins. This could be explained by the different nature of the sediments and/or different sediment conditions (e.g. redox, organic content). Based on particulate and dissolved Fe and dissolved Al data (Gourain et al., 2018; Menzel Barraqueta et al., 2018, Table 3.3), three main different types of margins were reported (Gourain et al., 2018) with the highest lithogenic contribution observed at the Iberian Margin (stations 2 and 4) and the highest biogenic contribution at the Newfoundland Margin (station 78). These observations are consistent with higher TChl-*a* concentrations measured at the Newfoundland Margin and to a lesser extent at the Greenland Margin and the predominance of diatoms relative to other functional phytoplankton classes at both margins (Tonnard et al., in prep.). To sum up, the most biogenic sediments (Newfoundland Margin) were able to mobilise more Fe in the dissolved phase than the most lithogenic sediments (Iberian Margin), in agreement with Boyd et al. (2010) who reported greater remineralization of PFe from biogenic PFe than from lithogenic PFe based on field experiment and modelling simulations.

Table 3.3: Averaged DFe:DAI (Menzel Barraqueta et al., 2018) and PFe:PAI (Gourain et al., in prep.) ratios reported per margins. Note that to avoid phytoplankton uptake, only depth below 100 m depth are considered.

Margins	Stations #	DFe:DAI (mol:mol)			PFe:PAI (mol:mol)			DFe:PFe (mol:mol)			n
		average	±	SD	average	±	SD	average	±	SD	
<i>Iberian Margin</i>	2 and 4	0.07	±	0.03	0.20	±	0.01	0.13	±	0.09	10
<i>East Greenland Margin</i>	56 and 53	0.21	±	0.09	0.30	±	0.01	0.12	±	0.03	6
<i>West Greenland Margin</i>	61	0.18	±	0.02	0.32	±	0.01	0.14	±	0.04	3
<i>Newfoundland Margin</i>	78	1.1	±	0.41	0.31	±	0.01	0.06	±	0.02	4

3.4.4.2 Nepheloid layers:

Samples associated with high levels of particles (transmissometer < 99%) and below 500 m depth displayed a huge variability in DFe concentrations. From the entire dataset, 63 samples (~13% of the entire dataset) followed this criterion with 14 samples from the West European Basin (station 1), 4 samples from the Iceland Basin (stations 29, 32, 36 and 38), 43 samples from the Irminger Sea (stations 40, 42, 44, 49 and 60) and 2 samples from the Labrador Sea (station 69). To determine which parameter was susceptible to explain the variation in DFe concentrations in these nepheloid layers, a Principal Component Analysis (PCA) on these samples. The input variables of the PCA were the particulate Fe, Al, and particulate manganese (PMn) (Gourain et al., 2018), the DAI (Menzel Barraqueta et al., 2018) and the Apparent Oxygen Utilization (AOU) and were all correlated to DFe concentrations explaining all together 93% of the subset variance (see supplementary material Fig. S6). The first dimension of the PCA was represented by the PAI, PFe and PMn concentrations and explained 59.5% of the variance, while the second dimension was represented by the DAI and the AOU parameters, explaining 33.2% of the variance. The two sets of variables were nearly at right angle from each other, indicating no correlation between them.

The variations in DFe concentrations measured in bottom samples from stations 32, 36 (Iceland Basin), 42 and 44 (Irminger Sea) and 69 (Labrador Sea) were mainly explained by the first dimension of the PCA (see supplementary material Fig. S6). Therefore, samples characterized by the lowest DFe concentrations (stations 32 and 69) were driven by particulate Al and Mn concentrations and resulted in an enrichment of Fe within particles. These results are in agreement with previous studies showing that the presence of Mn within particles can induce the formation of Fe-Mn oxides, contributing to the removal of Fe and Mn from the water column (Kan et al., 2012; Teng et al., 2001).

Low DFe concentrations (bottom samples from stations 42 and 1) were linked to DAi inputs and associated with lower AOU values. The release of Ai has previously been observed from Fe and Mn oxide coatings on resuspended sediments under mildly reducing conditions (Van Beusekom, 1988). Conversely, higher DFe concentrations were observed for stations 44 and 49 and to a lesser extent station 60 coinciding with low DAi inputs and higher oxygen levels. This observation challenges the traditional view of Fe oxidation with oxygen, either abiotically or microbially induced. Indeed, remineralisation can decrease sediment oxygen concentrations, promoting reductive dissolution of PFe oxyhydroxides to DFe that can then diffuse across the sediment water interface as DFe(II) colloids (Homoky et al., 2011). Such processes will inevitably lead to rapid Fe removal through precipitation of nanoparticulate or colloidal Fe (oxyhydr)oxides, followed by aggregation or scavenging by larger particles (Boyd and Ellwood, 2010; Lohan and Bruland, 2008) unless complexation with Fe-binding organic ligands occurs (Batchelli et al., 2010; Gerringa et al., 2008). There exist, however, another process that is favoured in oxic benthic boundary layers (BBL) with low organic matter degradation and/or low Fe oxides, which implies the dissolution of particles after resuspension, namely the non-reductive dissolution of sediment (Homoky et al., 2013; Radic et al., 2011). In addition, these higher oxygenated samples were located within DSOW, which mainly originate (75% of the overflow) from the Nordic Seas and the Arctic Ocean (Tanhua et al., 2005), in which the ultimate source of Fe was reported by Klunder et al. (2012) to come from Eurasian river waters. The major Arctic rivers were highlighted by Slagter et al. (2017) to be a source of Fe-binding organic ligands that are then further transported via the TPD across the Denmark Strait. Hence, the enhanced DFe concentrations measured within DSOW might result from Fe-binding organic ligand complexation that were transported to the deep ocean as DSOW formed rather than the non-reductive dissolution of sediment.

3.4.5 How does biological activity modify DFe distribution?

Overall, almost all the stations from the GEOVIDE voyage displayed DFe minima in surface water associated with some maxima of TChl-*a* (see supplementary material Fig. S1). In the following section, we specifically address the question of whether DFe concentrations potentially limit phytoplankton growth. Note that macronutrients and DFe limitations relative to phytoplankton functional classes are dealt in Tonnard et al. (in prep.).

A key determinant for assessing the significance of a DFe source is the magnitude of the DFe:macronutrient ratio supplied, since this term determines to which extent DFe will be

utilised. The DFe:NO₃⁻ ratios in surface waters varied from 0.02 (station 36) to 38.6 (station 61) mmol:mol with an average of 5 ± 10 mmol:mol (see supplementary material Fig. S7). Values were typically equal or lower than 0.28 mmol mol⁻¹ in all basins except at the margins and at stations 11, 13, 68, 69 and 77. The low nitrate concentrations observed at the eastern and western Greenland and Newfoundland Margins reflected a strong phytoplankton bloom which had reduced the concentrations as highlighted by the elevated integrated TChl-*a* concentrations ranging from 129.6 (station 78) to 398.3 (station 61) mg m⁻². At the Iberian Margin, they likely reflected the influence of the N-limited Tagus River (stations 1, 2 and 4) with its low TChl-*a* integrated concentrations that ranged from 31.2 (station 1) to 46.4 (station 4) mg m⁻². The high DFe:NO₃⁻ ratios determined at those stations, which varied from 13.4 (station 78) to 38.6 (station 61) mmol:mol, suggested that waters from these areas, despite having the lowest NO₃⁻ concentrations, were relatively enriched in DFe compared to waters from Iceland Basin and Irminger Sea.

In our study, DFe:NO₃⁻ ratios displayed a gradient from the West European Basin to Greenland (supplementary material S7 and S8). This trend only reverses when the influence of Greenland was encountered, as also observed by Painter et al. (2014). The remineralisation of organic matter is a major source of macro and micronutrients in subsurface waters (from 50 to 250 m depth). Remineralisation is associated with the consumption of oxygen and therefore, Apparent Oxygen Utilization (AOU) can provide a quantitative estimate of the amount of material that has been remineralised. While no relationship was observed below 50 m depth for NO₃⁻ or DFe and AOU considering all the stations, a significant correlation was found in the Subpolar gyre when removing the influence of margins (stations 29-49, 56, 60, 63-77) ($\text{AOU} = 3.88 \text{ NO}_3^- - 39.32$, $R^2=0.79$, $n=69$, $p\text{-value} < 0.001$). This correlation indicates that remineralisation of Particulate Organic Nitrogen (PON) greatly translates into Dissolved Inorganic Nitrogen (DIN) and that NO₃⁻ can be used as a good tracer for remineralisation in the studied area. Within these Subpolar gyre waters, there was a significant correlation between DFe and AOU ($\text{AOU} = 22.6 \text{ DFe}$, $R^2=0.34$, $n=53$, $p\text{-value} < 0.001$). The open-ocean stations from Subpolar gyre also exhibited a good linear correlation between DFe and NO₃⁻ ($R^2=0.42$, $n=51$, $p\text{-value} < 0.05$). The slope of the relationship, representing the typical remineralisation ratio, was $R_{\text{Fe:N}} = 0.07 \pm 0.01 \text{ mmol mol}^{-1}$. The intercept of the regression line was $-0.4 \pm 0.2 \text{ nmol L}^{-1}$, reflecting possible excess of preformed NO₃⁻ compare to DFe in these water masses. These significant correlations allow us to use the Fe* tracer to assess where DFe concentrations potentially limit phytoplankton growth by subtracting the contribution of organic matter remineralisation from the dissolved

Fe pool, as defined by Rijkenberg et al. (2014) and Parekh et al. (2005b) for PO_4^{3-} , and modified here for NO_3^- as follow:

$$Fe^* = [DFe] - R_{Fe:N} \times [NO_3^-] \quad (\text{eq. 4})$$

where $R_{Fe:N}$ refers to the average biological uptake ratio Fe over nitrogen, and $[NO_3^-]$ refers to nitrate concentrations in seawater. Although, we imposed a fixed biological $R_{Fe:N}$ of 0.05 mmol mol^{-1} , it is important to note that the biological uptake ratio of $D\text{Fe}:\text{NO}_3^-$ is not likely to be constant. Indeed, this ratio has been found to range from 0.05 to 0.9 mmol mol^{-1} depending on species (Ho et al., 2003; Sunda and Huntsman, 1995a; Twining et al., 2004b). The ratio we choose is thus less drastic to assess potential Fe limitation and more representative of the average biological uptake of DFe over NO_3^- calculated for this study (i.e. $R_{Fe:N} = 0.07 \pm 0.01 \text{ mmol mol}^{-1}$, for Subpolar waters). Negative values of Fe^* indicate the removal of DFe that is faster than the input through remineralisation or external sources and positive values suggest input of DFe from external sources (Fig. 3.7). Consequently, figure 3.7 shows that phytoplankton communities with very high Fe requirements relative to NO_3^- ($R_{Fe:N} = 0.9$) will only be able to grow above continental shelves where there is a high supply of DFe as previously reported by Nielsdóttir et al. (2009) and Painter et al. (2014). All these results are corroborating the importance of the Tagus River (Iberian Margin, see section 3.4.2.1), glacial inputs in the Greenland and Newfoundland Margins (see section 3.4.2.2) and to a lesser extent atmospheric inputs (see section 3.4.2.3) in supplying Fe with Fe:N ratios higher than the average biological uptake/demand ratio. Figure 3.7 (see also supplementary material S7, S8, S9 and S10) also highlights the Fe limitation for the low-Fe requirement phytoplankton class ($R_{Fe:N} = 0.05$) within the Iceland Basin, Irminger and Labrador Seas. The Fe deficiency observed in surface waters (> 50 m depth) from the Irminger and Labrador Seas might be explained by low atmospheric deposition for the IcSPMW and the LSW (Shelley et al., 2017). Low atmospheric Fe supply and sub-optimal Fe:N ratios in winter overturned deep water could favour the formation of the High-Nutrient, Low-Chlorophyll (HNLC) conditions. The West European Basin, despite exhibiting some of the highest $D\text{Fe}:\text{NO}_3^-$ ratios within surface waters (see supplementary material Fig. S8), displayed the strongest Fe-depletion from 50 m depth down to the bottom, suggesting that the main source of Fe was coming from dust deposition and/or riverine inputs.

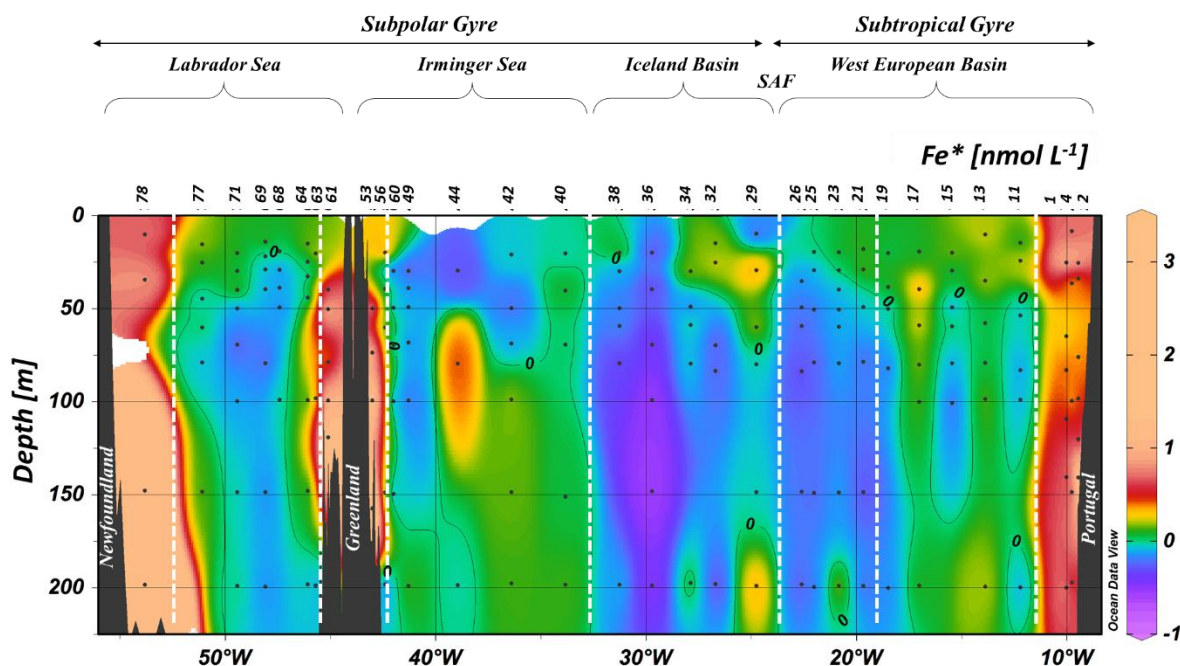


Figure 3.7: Section plot of the Fe^* tracer in the North Atlantic Ocean with a remineralization rate ($R_{\text{Fe:N}}$) of $0.05 \text{ mmol mol}^{-1}$ from surface to 225 m depth. A contour line of 0 separates areas of negative Fe^* from areas with positive Fe^* . Positive values of Fe^* imply there is enough iron to support complete consumption of NO_3^- when this water is brought to surface, and negative Fe^* values imply a deficit. See text for details.

Similarly as for the West European Basin, the pattern displayed in the surface map of DFe:NO_3^- ratios (supplementary material S8) extended to about 50 m depth, after which the trend reversed (Fig. 3.7 and supplementary material Fig. S7). Below 50 m depth, the Fe^* tracer (Fig. 3.7) was positive in the Irminger Sea and overall negative in the other basins. In the Irminger Sea positive Fe^* values were likely the result of the winter entrainment of Fe-rich LSW (see section 3.4.2.1) coinciding with high remineralised carbon fluxes in this area (station 44; Lemaître et al., 2017) (see section 3.4.2.2). The largest drawdown in DFe:NO_3^- ratios was observed between stations 34 and 38 and was likely due to the intrusion of the IcSPMW, this water mass exhibiting low DFe and high in NO_3^- (from 7 to $8 \mu\text{mol L}^{-1}$) concentrations. Similarly, the SAIW exhibited high NO_3^- concentrations. Both the IcSPMW and the SAIW sourced from the NAC. The NAC as it flows along the coast of North America receives atmospheric depositions from anthropogenic sources (Shelley et al., 2017; 2015) which deliver high N relative to Fe (Jickells and Moore, 2015) and might be responsible for the observed ranges.

3.5 Conclusion

The DFe concentrations measured during this study were in good agreement with previous studies that spanned the West European Basin. However, within the Irminger Basin the DFe concentrations measured during this study were up to 3 times higher than those measured by Rijkenberg et al. (2014) in deep waters (> 1000 m depth). This is likely explained by the different water masses encountered (i.e. the Polar Intermediate Water, ~ 2800 m depth) and by a stronger signal of the Iceland Scotland Overflow Water (ISOW) from 1200 to 2300 m depth. This corresponded to the most striking feature of the whole section with DFe concentrations reaching up to 2.5 nmol L^{-1} within the ISOW, Denmark Strait Overflow Water (DSOW) and Labrador Sea Water (LSW), three water masses that are part of the Deep Western Boundary Current and was likely the result of a lateral advection of particles in the Irminger. However, as these water masses reached the Labrador Sea, lower DFe levels were measured. These differences could be explained by different processes occurring within the benthic nepheloid layers, where DFe was sometimes trapped onto particles due to Mn-sediment within the Labrador Sea (Gourain et al., 2018) and sometimes released from the sediment potentially as a result of interactions with dissolved organic matter. Such Fe-binding organic ligands could have also been produced locally due to the intense remineralisation rate reported by Lemaître et al. (2017) of biogenic particles (Boyd et al., 2010; Gourain et al., 2018). The LSW exhibited increasing DFe concentrations along its flow path, likely resulting from sediment inputs at the Newfoundland Margin. Although DFe inputs through hydrothermal activity were expected at the slow spreading Reykjanes Ridge (Baker and German, 2004b; German et al., 1994), our data did not provide evidence of this specific source as previously suggested by Achterberg et al. (2018) at $\sim 60^\circ\text{N}$.

In surface waters several sources of DFe were highlighted especially close to land, with riverine inputs from the Tagus River at the Iberian margin (Menzel Barraqueta et al., 2018) and meteoric inputs (including coastal runoff and glacial meltwater) at the Newfoundland and Greenland margins (Benetti et al., 2016). Substantial sediment input was observed at all margins but with varying intensity. The highest DFe sediment input was located at the Newfoundland margin, while the lowest was observed at the eastern Greenland margin. These differences could be explained by the different nature of particles with the most lithogenic located at the Iberian margin and the most biogenic, at the Newfoundland margin (Gourain et al., 2018). Although previous studies (e.g. Jickells et al., 2005; Shelley et al., 2015) reported that atmospheric inputs substantially fertilized surface waters from the

West European Basin, in our study, only stations located in the West European and Iceland Basins exhibited enhanced SML DFe inventories with lower TTADs. However, these TTADs were about three times higher than those reported for Saharan dust inputs and thus atmospheric deposition appeared to be a minor source of Fe during the sampling period. Finally, there was evidence of convective inputs of the LSW to surface seawater caused by long tip jet event (Piron et al., 2016) that deepened the winter mixed layer down to ~ 1200 m depth (Zunino et al., 2017), in which Fe was in excess of nitrate and therefore, Fe was not limiting.

3.6 Acknowledgements

We are greatly indebted to the master, Gilles Ferrand, the officers and crew from the N/O *Pourquoi Pas?* for their logistic support during the GEOVIDE voyage. We would like to give a special thanks to Pierre Branellec, Michel Hamon, Catherine Kermabon, Philippe Le Bot, Stéphane Leizour, Olivier Ménage (Laboratoire d'Océanographie Physique et Spatiale), Fabien Pérault and Emmanuel de Saint Léger (Division Technique de l'INSU, Plouzané, France) for their technical expertise during clean CTD deployments as well as Emilie Grosteffan and Manon Le Goff for the analysis of nutrients. We also wanted to thank the Pôle Spectrométrie Océan (PSO, Plouzané, France) for letting us use the Element XR HR-ICP-MS. Greg Cutter is also strongly acknowledged for his help in setting up the new French clean sampling system. Catherine Schmechtig is thanked for the LEFE-CYBER database management. This work was funded by the French National Research Agency ANR GEOVIDE (ANR-13-BS06-0014) and RPDOC BITMAP (ANR-12-PDOC-0025-01), the French National Center for Scientific Research (CNRS-LEFE-CYBER), the LabexMER (ANR-10-LABX-19) and Ifremer and was supported for the logistic by DT-INSU and GENAVIR. Manon Tonnard was supported by a cotutelle joint PhD scholarship from the Université de Bretagne Occidentale (UBO-IUEM) and the University of Tasmania (UTAS-IMAS).

All dissolved iron (DFe) data are available in the supplementary material Table S1.

3.7 References

- Achterberg, E. P., Steigenberger, S., Marsay, C. M., LeMoigne, F. A., Painter, S. C., Baker, A. R., Connelly, D. P., Moore, C. M., Tagliabue, A., and Tanhua, T.: Iron Biogeochemistry in the High Latitude North Atlantic Ocean, *Scientific reports*, 8, 1-15, 10.1038/s41598-018-19472-1, 2018.
- Aminot, A., and Kerouel, R.: Dosage automatique des nutriments dans les eaux marines, Quae ed., 2007.
- Annett, A. L., Skiba, M., Henley, S. F., Venables, H. J., Meredith, M. P., Statham, P. J., and Ganeshram, R. S.: Comparative roles of upwelling and glacial iron sources in Ryder Bay, coastal western Antarctic Peninsula, *Marine Chemistry*, 176, 21-33, 10.1016/j.marchem.2015.06.017, 2015.
- Bacon, S., Gould, W. J., and Jia, Y.: Open-ocean convection in the Irminger Sea, *Geophysical Research Letters*, 30, 1246, doi:10.1029/2002GL016271, 2003.
- Baker, A. R., Adams, C., Bell, T. G., Jickells, T. D., and Ganzeveld, L.: Estimation of atmospheric nutrient inputs to the Atlantic Ocean from 50°N to 50°S based on large-scale field sampling: Iron and other dust-associated elements, *Global Biogeochemical Cycles*, 27, 755-767, 10.1002/gbc.20062, 2013.
- Baker, A. T., and German, C. R.: On the Global Distribution of Hydrothermal vent Fields, in: *Mid-Ocean Ridges*, edited by: German, C. R., Lin, J., and Parson, L. M., 2004a.
- Baker, E. T., and German, C. R.: Hydrothermal Interactions Between the Lithosphere and Oceans, in: *Mid-Ocean Ridges*, edited by: German, C. R., Lin, J., and Parson, L. M., *Geophysical Monograph Series*, AGU, 245-266, 2004b.
- Barton, A. D., Greene, C. H., Monger, B. C., and Pershing, A. J.: The Continuous Plankton Recorder survey and the North Atlantic Oscillation: Interannual- to Multidecadal-scale patterns of phytoplankton variability in the North Atlantic Ocean, *Progress in Oceanography*, 58, 337-358, 10.1016/j.pocean.2003.08.012, 2003.
- Batchelli, S., Muller, F. L. L., Chang, K. C., and Lee, C. L.: Evidence for Strong but Dynamic Iron-Humic Colloidal Associations in Humic-Rich Coastal Waters., *Environmental Science & Technology*, 44, 8485-8490, 2010.
- Benetti, M., Reverdin, G., Pierre, C., Khatiwala, S., Tournadre, B., Olafsdottir, S., and Naamar, A.: Variability of sea ice melt and meteoric water input in the surface Labrador Current off Newfoundland, *Journal of Geophysical Research Oceans*, 121, 2841-2855, doi:10.1002/2015JC011302, 2016.
- Benetti, M., Reverdin, G., Lique, C., Yashayaev, I., Holliday, N. P., Tynan, E., Torres-Valdes, S., Lherminier, P., Tréguer, P., and Sarthou, G.: Composition of freshwater in the spring of 2014 on the southern Labrador shelf and slope, *Journal of Geophysical Research: Oceans*, 122, 1102-1121, 10.1002/2016jc012244, 2017.
- Bersch, M., Yashayaev, I., and Koltermann, K. P.: Recent changes of the thermohaline circulation in the subpolar North Atlantic, *Ocean Dynamics*, 57, 223-235, 10.1007/s10236-007-0104-7, 2007.
- Bhatia, M. P., Kujawinski, E. B., Das, S. B., Breier, C. F., Henderson, P. B., and Charette, M. A.: Greenland meltwater as a significant and potentially bioavailable source of iron to the ocean, *Nature Geoscience*, 2013, 274-278, 10.1038/ngeo1746, 2013.
- Bonnet, S., and Guieu, C.: Dissolution of atmospheric iron in seawater, *Geophysical Research Letters*, 31, 10.1029/2003gl018423, 2004.

- Bonnet, S., and Guieu, C.: Atmospheric forcing on the annual iron cycle in the western Mediterranean Sea: A 1-year survey, *Journal of Geophysical Research*, 111, 10.1029/2005jc003213, 2006.
- Boyd, P. W., Watson, A. J., Law, C. S., Abraham, E. R., Trull, T., Murdoch, R., Bakker, D. C. E., Bowie, A. R., Buesseler, K. O., Chang, H., Charette, M., Croot, P., Downing, K., Frew, R., Gall, M., Hadfield, M., Hall, J., Harvey, M., Jameson, G., LaRoche, J., Liddicoat, M., Ling, R., Maldonado, M. T., McKay, R. M., Nodder, S., Pickmere, S., Pridmore, R., Rintoul, S., Safi, K., Sutton, P., Strzepek, R., Tanneberger, K., Turner, S., Waite, A., and Zeldis, J.: A mesoscale phytoplankton bloom in the polar Southern Ocean stimulated by iron fertilization, *Nature*, 407, 695-702, 2000.
- Boyd, P. W., and Ellwood, M. J.: The biogeochemical cycle of iron in the ocean, *Nature Geoscience*, 3, 675-682, 10.1038/ngeo964, 2010.
- Boyd, P. W., Ibsanmi, E., Sander, S. G., Hunter, K. A., and Jackson, G. A.: Remineralization of upper ocean particles: Implications for iron biogeochemistry, *Limnology and Oceanography*, 55, 1271-1288, 10.4319/lo.2010.55.3.1271, 2010.
- Buck, C. S., Landing, W. M., Resing, J. A., and Measures, C. I.: The solubility and deposition of aerosol Fe and other trace elements in the North Atlantic Ocean: Observations from the A16N CLIVAR/CO2 repeat hydrography section, *Marine Chemistry*, 120, 57-70, 10.1016/j.marchem.2008.08.003, 2010.
- Canário, J., Vale, C., Caetano, M., and Madureira, M. J.: Mercury in contaminated sediments and pore waters enriched in sulphate (Tagus Estuary, Portugal), *Environmental Pollution*, 126, 425-433, 10.1016/S0269-7491(03)00234-3, 2003.
- Charette, M. A., Morris, P. J., Henderson, P. B., and Moore, W. S.: Radium isotope distributions during the US GEOTRACES North Atlantic cruises, *Marine Chemistry*, 177, 184-195, 10.1016/j.marchem.2015.01.001, 2015.
- Chen, Y. J.: Influence of the Iceland mantle plume on crustal accretion at the inflated Reykjanes Ridge: Magma lens and low hydrothermal activity, *Journal of Geophysical Research*, 108, 2524, 2003.
- Chester, R., Murphy, K. J. T., Lin, F. J., Berry, A. S., Bradshaw, G. A., and Corcoran, P. A.: Factors controlling the solubilities of trace-metals from nonremote aerosols deposited to the sea-surface by the dry deposition mode, *Marine Chemistry*, 42, 107-126, 10.1016/0304-4203(93)90241-f, 1993.
- Conway, T. M., and John, S. G.: Quantification of dissolved iron sources to the North Atlantic Ocean, *Nature*, 511, 212-215, 10.1038/nature13482, 2014.
- Cooper, L. W., Whitley, T. E., Grebmeier, J. M., and Weingartner, T.: The nutrient, salinity, and stable oxygen isotope composition of Bering and Chukchi Seas waters in and near the Bering Strait, *Journal of Geophysical Research*, 102, 12,563-512,573, 1997.
- Cooper, L. W., McClelland, J. W., Holmes, R. M., Raymond, P. A., Gibson, J. J., Guay, C. K., and Peterson, B. J.: Flow-weighted values of runoff tracers ($\delta^{18}\text{O}$, DOC, Ba, alkalinity) from the six largest Arctic rivers, *Geophysical Research Letters*, 35, 1-5, 10.1029/2008GL035007, 2008.
- Crane, K., Johnson, L., Appelgate, B., Nishimura, C., Buck, R., Jones, C., Vogt, P., and Kos'yan, R.: Volcanic and Seismic Swarm Events on the Reykjanes Ridge and Their Similarities to Events on Iceland: Results of a Rapid Response Mission, *Marine Geophysical Researches*, 19, 319-338, 1997.
- Cutter, G., Casciotti, K., Croot, P., Geibert, W., Heimbürger, L. E., Lohan, M., Planquette, H., and van de Flierdt, T.: Sampling and the Sample-handling Protocols for GEOTRACES Cruises, 2017.
- Daniault, N., Mercier, H., Lherminier, P., Sarafanov, A., Falina, A., Zunino, P., Pérez, F. F., Ríos, A. F., Ferron, B., Huck, T., Thierry, V., and Gladyshev, S.: The northern North Atlantic Ocean mean circulation in the early 21st century, *Progress in Oceanography*, 146, 142-158, 10.1016/j.pocean.2016.06.007, 2016.

de Barros, M. C.: A case study of waste inputs in the Tagus estuary, in: *The role of the Oceans as a Waste Disposal Option*, edited by: Kullenberg, G., NATO ASI Series; Series C: Mathematical and Physical Sciences, 172, Springer Netherlands, 307-324, 1986.

de Jong, M. F., van Aken, H. M., Våge, K., and Pickart, R. S.: Convective mixing in the central Irminger Sea: 2002–2010, *Deep Sea Research Part I: Oceanographic Research Papers*, 63, 36-51, 10.1016/j.dsr.2012.01.003, 2012.

Dehairs, F., Shopova, D., Ober, S., Veth, C., and Goeyens, L.: Particulate barium stocks and oxygen consumption in the Southern Ocean mesopelagic water column during spring and early summer: Relationship with export production, *Deep Sea Research II*, 44, 497-516, 10.1016/S0967-0645(96)00072-0, 1997.

Deng, F., Henderson, G. M., Castrillejo, M., and Perez, F. F.: Evolution of ²³¹Pa and ²³⁰Th in overflow waters of the North Atlantic, *Biogeosciences*, 1-24, 10.5194/bg-2018-191, 2018.

Fagel, N., Robert, C., and Hilaire-Marcel, C.: Clay mineral signature of the NW Atlantic Boundary Undercurrent, *Marine Geology*, 130, 19-28, 1996.

Fagel, N., Robert, C., Preda, M., and Thorez, J.: Smectite composition as a tracer of deep circulation: the case of the Northern North Atlantic, *Marine Geology*, 172, 309-330, 2001.

Ferron, B., Kokoszka, F., Mercier, H., Lherminier, P., Huck, T., Rios, A., and Thierry, V.: Variability of the Turbulent Kinetic Energy Dissipation along the A25 Greenland–Portugal Transect Repeated from 2002 to 2012, *Journal of Physical Oceanography*, 46, 1989-2003, 10.1175/jpo-d-15-0186.1, 2016.

Figueres, G., Martin, J. M., Meybeck, M., and Seyler, P.: A comparative study of mercury contamination in the Tagus estuary (Portugal) and major French estuaries (Gironde, Loire, Rhone), *Estuarine, Coastal and Shelf Science*, 20, 183-203, 1985.

Fiuza, A.: Hidrologia e dinamica das aguas costeiras de Portugal, Ph. D., Universidade de Lisboa, Lisboa, Portugal, unpublished, 1984.

Follows, M., and Dutkiewicz, S.: Meteorological modulation of the North Atlantic Spring Bloom, *Deep Sea Research Part II: Topical Studies in Oceanography*, 49, 321-344, 2001.

García-Ibáñez, M. I., Pardo, P. C., Carracedo, L. I., Mercier, H., Lherminier, P., Ríos, A. F., and Pérez, F. F.: Structure, transports and transformations of the water masses in the Atlantic Subpolar Gyre, *Progress in Oceanography*, 135, 18-36, 10.1016/j.pocean.2015.03.009, 2015.

García-Ibáñez, M. I., Pérez, F. F., Lherminier, P., Zunino, P., Mercier, H., and Tréguer, P.: Water mass distributions and transports for the 2014 GEOVIDE cruise in the North Atlantic, *Biogeosciences*, 15, 2075-2090, 10.5194/bg-15-2075-2018, 2018.

García-Ibáñez, M. I., Pérez, F. F., Lherminier, P., Zunino, P., and Tréguer, P.: Water mass distributions and transports for the 2014 GEOVIDE cruise in the North Atlantic, *Biogeosciences*, this issue.

Gaudencio, M. J., Guerra, M. T., and Glemarec, M.: Recherches biosédimentaires sur la zone maritime de l'estuaire du Tage, Portugal: données sédimentaires préliminaires. , in: *Estuaries and Coasts: Spatial and Temporal Intercomparisons*, edited by: Elliot, M., and Ducrottoy, J. C., Olsen and Olsen, Fredensborg, 11-16, 1991.

German, C. R., Briem, J., Chin, C. S., Danielsen, M., Holland, S., James, R. H., Jonsdottir, A., Ludford, E., Moser, C., Olafsson, J., Palmer, M. R., and Rudnicki, M. D.: Hydrothermal activity on the Reykjanes Ridge: the Steinahóll vent-field at 63°06'N, *Earth and Planetary Science Letters*, 121, 647-654, 1994.

Gerringa, L. J. A., Blain, S., Laan, P., Sarthou, G., Veldhuis, M. J. W., Brussaard, C. P. D., Viollier, E., and Timmermans, K. R.: Fe-binding dissolved organic ligands near the Kerguelen Archipelago in the Southern Ocean (Indian sector), *Deep Sea Research Part II: Topical Studies in Oceanography*, 55, 606-621, 10.1016/j.dsr.2007.12.007, 2008.

Gerringa, L. J. A., Slagter, H. A., Bown, J., van Haren, H., Laan, P., de Baar, H. J. W., and Rijkenberg, M. J. A.: Dissolved Fe and Fe-binding organic ligands in the Mediterranean Sea – GEOTRACES G04, *Marine Chemistry*, 194, 100-113, 10.1016/j.marchem.2017.05.012, 2017.

Gourain, A., Planquette, H., Cheize, M., Menzel-Barraqueta, J. L., Boutorh, J., Shelley, R. U., Pereira-Contreira, L., Lemaitre, N., Lacan, F., Lherminier, P., and Sarthou, G.: particulate trace metals along the GEOVIDE section, *Biogeosciences*, 2018.

Guerzoni, S., Chester, R., Dulac, F., Herut, B., Loye-Pilot, M.-D., Measures, C., Migon, C., Molinaroli, E., Moulin, C., Rossini, P., Saydam, C., Soudine, A., and Ziveri, P.: The role of atmospheric deposition in the biogeochemistry of the Mediterranean Sea, *Progress in Oceanography*, 44, 147-190, 1999.

Guieu, C., Loye-Pilot, M. D., Benyahya, L., and Dufour, A.: Spatial variability of atmospheric fluxes of metals (Al, Fe, Cd, Zn and Pb) and phosphorus over the whole Mediterranean from a one-year monitoring experiment: Biogeochemical implications, *Marine Chemistry*, 120, 164-178, 10.1016/j.marchem.2009.02.004, 2010.

Guieu, C., Aumont, O., Paytan, A., Bopp, L., Law, C. S., Mahowald, N., Achterberg, E. P., Marañón, E., Salihoglu, B., Crise, A., Wagener, T., Herut, B., Desboeufs, K., Kanakidou, M., Olgun, N., Peters, F., Pulido-Villena, E., Tovar-Sanchez, A., and Völker, C.: The significance of the episodic nature of atmospheric deposition to Low Nutrient Low Chlorophyll regions, *Global Biogeochemical Cycles*, 28, 1179-1198, 10.1002/2014gb004852, 2014.

Harrison, W. G., Yngve Børshheim, K., Li, W. K. W., Maillet, G. L., Pepin, P., Sakshaug, E., Skogen, M. D., and Yeats, P. A.: Phytoplankton production and growth regulation in the Subarctic North Atlantic: A comparative study of the Labrador Sea-Labrador/Newfoundland shelves and Barents/Norwegian/Greenland seas and shelves, *Progress in Oceanography*, 114, 26-45, 10.1016/j.pocean.2013.05.003, 2013.

Hatta, M., Measures, C. I., Wu, J., Roshan, S., Fitzsimmons, J. N., Sedwick, P., and Morton, P.: An overview of dissolved Fe and Mn distributions during the 2010-2011 US GEOTRACES north Atlantic cruises: GEOTRACES GA03, Deep-Sea Research Part II-Topical Studies in Oceanography, 116, 117-129, 10.1016/j.dsr2.2014.07.005, 2015.

Hawkings, J. R., Wadham, J. L., Tranter, M., Raiswell, R., Benning, L. G., Statham, P. J., Tedstone, A., Nienow, P., Lee, K., and Telling, J.: Ice sheets as a significant source of highly reactive nanoparticulate iron to the oceans, *Nature communications*, 5, 1-8, 10.1038/ncomms4929, 2014.

Henson, S. A., Dunne, J. P., and Sarmiento, J. L.: Decadal variability in North Atlantic phytoplankton blooms, *Journal of Geophysical Research*, 114, 10.1029/2008jc005139, 2009.

Ho, T.-Y., Quigg, A., Finkel, Z. V., Milligan, A. J., Wyman, K., Falkowski, P. G., and Morel, F. M. M.: The elemental composition of some marine phytoplankton, *Journal of Phycology*, 39, 1145-1159, 2003.

Homoky, W. B., Hembury, D. J., Hepburn, L. E., Mills, R. A., Statham, P. J., Fones, G. R., and Palmer, M. R.: Iron and manganese diagenesis in deep sea volcanogenic sediments and the origins of pore water colloids, *Geochimica Et Cosmochimica Acta*, 75, 5032-5048, 10.1016/j.gca.2011.06.019, 2011.

Homoky, W. B., John, S. G., Conway, T. M., and Mills, R. A.: Distinct iron isotopic signatures and supply from marine sediment dissolution, *Nature Communications*, 4, 10.1038/ncomms3143, 2013.

Humphreys, M. P., Griffiths, A. M., Achterberg, E. P., Holliday, N. P., Rérolle, V., Menzel Barraqueta, J. L., Couldrey, M. P., Oliver, K. I., Hartman, S. E., and Esposito, M.: Multidecadal accumulation of anthropogenic and remineralized dissolved inorganic carbon along the Extended Ellett Line in the northeast Atlantic Ocean, *Global Biogeochemical Cycles*, 30, 293-310, doi: 10.1002/2015GB005246, 2016.

Hunke, E. C., Notz, D., Turner, A. K., and Vancoppenolle, M.: The multiphase physics of sea ice: a review for model developers, *The Cryosphere*, 5, 989-1009, 10.5194/tc-5-989-2011, 2011.

Janssens, J., Meiners, K. M., Tison, J.-L., Dieckmann, G., Delille, B., and Lannuzel, D.: Incorporation of iron and organic matter into young Antarctic sea ice during its initial growth stages, *Elementa: Science of the Anthropocene*, 4, 000123, 10.12952/journal.elementa.000123, 2016.

Jickells, T., and Moore, C. M.: The importance of atmospheric deposition for ocean productivity, *Annual Review of Ecology, Evolution, and Systematics*, 46, 481-501, 10.1146/annurev-ecolsys-112414-054118, 2015.

Jickells, T. D., An, Z. C., Andersen, K. K., Baker, A. R., Bergametti, G., Brooks, N., Cao, J. J., Boyd, P. W., Duce, R. A., Hunter, K. A., Kawahata, H., Kubilay, N., laRoche, J., Liss, P. S., Mahowald, N., Prospero, J. M., Ridgwell, A. J., Tegen, I., and Torres, R.: Global iron connections between desert dust, ocean biogeochemistry, and climate, *Science*, 308, 67-71, 2005.

Jones, E. P., Anderson, L. G., and Swift, J. H.: Distribution of Atlantic and Pacific waters in the upper Arctic Ocean: Implications for circulation, *Geophysical Research Letters*, 25, 765-768, 1998.

Kan, C. C., Chen, W. H., Wan, M. W., Phatai, P., Wittayakun, J., and Li, K. F.: The preliminary study of iron and manganese removal from groundwater by NaOCl oxidation and MF filtration, *Sustain. Environ. Res.*, 22, 25-30, 2012.

Kara, A. B., Rochford, P. A., and Hurlburt, H. E.: An optimal definition for ocean mixed layer depth, *Journal of Geophysical Research*, 105, 16,803-816, 10.1029/2000JC900072, 2000.

Kissel, C., Laj, C., Mulder, T., Wandres, C., and Cremer, M.: The magnetic fraction: A tracer of deep water circulation in the North Atlantic, *Earth and Planetary Science Letters*, 288, 444-454, 10.1016/j.epsl.2009.10.005, 2009.

Klunder, M. B., Bauch, D., Laan, P., de Baar, H. J. W., van Heuven, S. M. A. C., and Ober, S.: Dissolved iron in the Arctic shelf seas and surface waters of the Central Arctic Ocean: impact of Arctic river water and ice-melt, *Journal of Geophysical Research*, 117, 1-18, 2012.

Lackschewitz, K. S., Endler, R., Gehrke, B., Wallrabe-Adams, H.-J., and Thiede, J.: Evidence for topography- and current-controlled deposition on the Reykjanes Ridge between 59°N and 60°N, *Deep-Sea Research I*, 43, 1683-1711, 1996.

Laes, A., Blain, S., Laan, P., Achterberg, E. P., Sarthou, G., and de Baar, H. J. W.: Deep dissolved iron profiles in the eastern North Atlantic in relation to water masses, *Geophysical Research Letters*, 30, 10.1029/2003gl017902, 2003.

Lagerström, M. E., Field, M. P., Seguret, M., Fischer, L., Hann, S., and Sherrell, R. M.: Automated on-line flow-injection ICP-MS determination of trace metals (Mn, Fe, Co, Ni, Cu and Zn) in open ocean seawater: Application to the GEOTRACES program, *Marine Chemistry*, 155, 71-80, 10.1016/j.marchem.2013.06.001, 2013.

Lambelet, M., van de Flierdt, T., Crocket, K., Rehkamper, M., Katharina, K., Coles, B., Rijkenberg, M. J. A., Gerringa, L. J. A., de Baar, H. J. W., and Steinfeldt, R.: Neodymium isotopic composition and concentration in the western North Atlantic Ocean: Results from the GEOTRACES GA02 section, *Geochimica Et Cosmochimica Acta*, 177, 1-29, 2016.

Le Roy, E., Sanial, V., Charette, M. A., van Beek, P., Lacan, F., Jacquet, S. H. M., Henderson, P. B., Souhaut, M., García-Ibáñez, M. I., Jeandel, C., Pérez, F. F., and Sarthou, G.: The ²²⁶Ra–Ba relationship in the North Atlantic during GEOTRACES-GA01, *Biogeosciences*, 15, 3027-3048, 10.5194/bg-15-3027-2018, 2018.

Lemaitre, N., Planchon, F., Planquette, H., Dehairs, F., Fonseca-Batista, D., Roukaerts, A., Deman, F., Tang, Y., Mariez, C., and Sarthou, G.: High variability of export fluxes along the North Atlantic GEOTRACES section GA01: Particulate organic carbon export deduced from the ²³⁴Th method *Biogeosciences*, 1-38, 10.5194/bg-2018-190, 2018.

- Lemaître, N., planquette, H., Planchon, F., Sarthou, G., Jacquet, S., Garcia-Ibanez, M. I., Gourain, A., Cheize, M., Monin, L., Andre, L., Laha, P., Terryn, H., and Dehairs, F.: Particulate barium tracing significant mesopelagic carbon remineralisation in the North Atlantic Biogeosciences Discussions, 2017.
- Lohan, M. C., and Bruland, K. W.: Elevated Fe(II) and Dissolved Fe in Hypoxic Shelf Waters off Oregon and Washington: An Enhanced Source of Iron to Coastal Upwelling Regimes, *Environmental Science & Technology*, 42, 6462-6468, 10.1021/es800144j, 2008.
- Longhurst, A. R.: *Ecological geography of the Sea*, Second Edition ed., Elsevier Academic Press publications, Burlington, 542 pp., 2007.
- Louanchi, F., and Najjar, R. G.: Annual cycles of nutrients and oxygen in the upper layers of the North Atlantic Ocean, *Deep Sea Research Part II: Topical Studies in Oceanography*, 48, 2155-2171, 2001.
- Markus, T., Stroeve, J. C., and Miller, J.: Recent changes in Arctic sea ice melt onset, freezeup, and melt season length, *Journal of Geophysical Research*, 114, 10.1029/2009jc005436, 2009.
- Marshall, J., and Schott, F.: Open-ocean convection: observations, theory, and models, *Reviews of Geophysics*, 37, 1-64, doi: 10.1029/98RG02739, 1999.
- Martin, J.-M., Elbaz-Poulichet, F., Guieu, C., Loÿe-Pilot, M.-D., and Han, G.: River versus atmospheric input of material to the Mediterranean Sea: an overview*, *Marine Chemistry*, 28, 159-182, 1989.
- Martin, J. D., and Fitzwater, S. E.: Iron deficiency limits phytoplankton growth in the north-east Pacific subarctic, *Nature*, 331, 341-343, 1988.
- Martin, J. H., Fitzwater, S. E., and Gordon, R. M.: Iron deficiencies limits phytoplankton growth in Antarctic waters, *Global Biogeochemical Cycles*, 4, 5-12, 1990.
- Martin, J. H., Coale, K. H., Johnson, K. S., Fitzwater, S. E., Gordon, R. M., Tanner, S. J., Hunter, C. N., Elrod, V. A., Nowicki, J. L., Coley, T. L., Barber, R. T., Lindley, S., Watson, A. J., Van Scoy, K., Law, C. S., Liddicoat, M. I., Ling, R., Stanton, T., Stockel, J., Collins, C., Anderson, A., Bidigare, R., Ondrusek, M., Latasa, M., Millero, F. J., Lee, K., Yao, W., Zhang, J. Z., Friederich, G., Sakamoto, C., Chavez, F., Buck, K., Kolber, Z., Greene, R., Falkowski, P., Chisholm, S. W., Hoge, F., Swift, R., Yungel, J., Turner, S., Nightingale, P., Hatton, A., Liss, P., and Tindale, N. W.: Testing the Iron Hypothesis in Ecosystems of the Equatorial Pacific Ocean, *Nature*, 371, 123-129, 10.1038/371123a0, 1994.
- Measures, C. I., Brown, M. T., Selph, K. E., Apprill, A., Zhou, M., Hatt, M., and Hiscock, W. T.: The influence of shelf processes in delivering dissolved iron to the HNLC waters of the Drake Passage, Antarctica, *Deep Sea Research Part II: Topical Studies in Oceanography*, 90, 77-88, 10.1016/j.dsr2.2012.11.004, 2013.
- Melling, H., and Moore, R. M.: Modification of halocline source waters during freezing on the Beaufort Sea shelf: Evidence from oxygen isotopes and dissolved nutrients, *Continental Shelf Research*, 15, 89-113, 1995.
- Menzel Barraqueta, J. L., Schlosser, C., Planquette, H., Gourain, A., Cheize, M., Boutorh, J., Shelley, R. U., Pereira Contreira, L., Gledhill, M., Hopwood, M. J., Lherminier, P., Sarthou, G., and Achterberg, E. P.: Aluminium in the North Atlantic Ocean and the Labrador Sea (GEOTRACES GA01 section): roles of continental inputs and biogenic particle removal, *Biogeosciences Discussions*, 1-28, 10.5194/bg-2018-39, 2018.
- Mercier, H., Lherminier, P., Sarafanov, A., Gaillard, F., Daniault, N., Desbruyères, D., Falina, A., Ferron, B., Gourcuff, C., Huck, T., and Thierry, V.: Variability of the meridional overturning circulation at the Greenland–Portugal OVIDE section from 1993 to 2010, *Progress in Oceanography*, 132, 250-261, 10.1016/j.pocean.2013.11.001, 2015.
- Mil-Homens, M., Branco, V., Lopes, C., Vale, C., Abrantes, F., Boer, W., and Vicente, M.: Using factor analysis to characterise historical trends of trace metal contamination in a sediment core from the Tagus Prodelta, Portugal, *Water, Air, and Soil Pollution*, 197, 277-287, 2009.

Moore, C. M., Mills, M. M., Langlois, R., Milne, A., Achterberg, E. P., La Roche, J., and Geider, R. J.: Relative influence of nitrogen and phosphorus availability on phytoplankton physiology and productivity in the oligotrophic sub-tropical North Atlantic Ocean, *Limnology and Oceanography*, 53, 291-205, 2008.

Moore, C. M., Mills, M. M., Arrigo, K. R., Berman-Frank, I., Bopp, L., Boyd, P. W., Galbraith, E. D., Geider, R. J., Guieu, C., Jaccard, S. L., Jickells, T. D., La Roche, J., Lenton, T. M., Mahowald, N. M., Marañón, E., Marinov, I., Moore, J. K., Nakatsuka, T., Oschlies, A., Saito, M. A., Thingstad, T. F., Tsuda, A., and Ulloa, O.: Processes and patterns of oceanic nutrient limitation, *Nature Geoscience*, 6, 701-710, 10.1038/ngeo1765, 2013.

Moore, G. W. K.: Gale force winds over the Irminger Sea to the east of Cape Farewell, Greenland, *Geophysical Research Letters*, 30, n/a-n/a, 10.1029/2003gl018012, 2003.

Nielsdóttir, M. C., Moore, C. M., Sanders, R., Hinz, D. J., and Achterberg, E. P.: Iron limitation of the postbloom phytoplankton communities in the Iceland Basin, *Global Biogeochemical Cycles*, 23, n/a-n/a, 10.1029/2008gb003410, 2009.

Olafsson, J., Thors, K., and Cann, J. R.: A sudden cruise off Iceland, *RIDGE Events*, 2, 35-28, 1991.

Oschlies, A.: Nutrient supply to the surface waters of the North Atlantic: A model study, *Journal of Geophysical Research*, 107, 10.1029/2000jc000275, 2002.

Painter, S. C., Henson, S. A., Forryan, A., Steigenberger, S., Klar, J., Stinchcombe, M. C., Rogan, N., Baker, A. R., Achterberg, E. P., and Moore, C. M.: An assessment of the vertical diffusive flux of iron and other nutrients to the surface waters of the subpolar North Atlantic Ocean, *Biogeosciences*, 11, 2113-2130, 10.5194/bg-11-2113-2014, 2014.

Palmer, M. R., Ludford, E. M., German, C. R., and Lilley, M. D.: Dissolved methane and hydrogen in the Steinahóll hydrothermal plume, 63°N, Reykjanes Ridge, in: *Hydrothermal Vents and Processes*, edited by: Parson, L. M., Walker, C. L., and Dixon, D. R., Special Publications, Geological Society, London, 111-120, 1995.

Parekh, P., Follows, M. J., and Boyle, E. A.: Decoupling of iron and phosphate in the global ocean, *Global Biogeochemical Cycle*, 19, 2005.

Parra, M., Delmont, P., Ferragne, A., Latouche, C., Pons, J. C., and Puechmaille, C.: Origin and evolution of smectites in recent marine sediments of the NE Atlantic, *Clay Minerals*, 20, 335-346, 1985.

Pérez, F. F., Mercier, H., Vázquez-Rodríguez, M., Lherminier, P., Velo, A., Pardo, P. C., Rosón, G., and Ríos, A. F.: Atlantic Ocean CO₂ uptake reduced by weakening of the meridional overturning circulation, *Nature Geoscience*, 6, 146-152, 10.1038/ngeo1680, 2013.

Pérez, F. F., Treguer, P., Branellec, P., García-Ibáñez, M. I., Lherminier, P., and Sarthou, G.: The 2014 Greenland-Portugal GEOVIDE bottle data (GO-SHIP A25 and GEOTRACES GA01). SEANOE (Ed.), 2018.

Petrich, C., and Eicken, H.: Growth, structure and properties of sea ice, in: *Sea Ice*. 2nd ed., edited by: Thomas, D. N., and Dieckmann, G. S., Wiley-Blackwell, Oxford, U.K., 23-77, 2010.

Pickart, R. S., Straneo, F., and Moore, G. W. K.: Is Labrador Sea Water formed in the Irminger basin?, *Deep Sea Research Part I*, 50, 23-52, 2003.

Piron, A., Thierry, V., Mercier, H., and Caniaux, G.: Argo float observations of basin-scale deep convection in the Irminger sea during winter 2011–2012, *Deep Sea Research Part I: Oceanographic Research Papers*, 109, 76-90, 10.1016/j.dsr.2015.12.012, 2016.

Radic, A., Lacan, F., and Murray, J. W.: Iron isotopes in the seawater of the equatorial Pacific Ocean: New constraints for the oceanic iron cycle, *Earth and Planetary Science Letters*, 306, 1-10, 10.1016/j.epsl.2011.03.015, 2011.

- Ras, J., Claustre, H., and Uitz, J.: Spatial variability of phytoplankton pigment distribution in the Subtropical South Pacific Ocean: comparison between *in situ* and predicted data, *Biogeosciences*, 5, 353-369, 2008.
- Riebesell, U., Schloss, I., and Smetacek, V.: Aggregation of algae released from melting sea ice: implications for seeding and sedimentation, *Polar Biology*, 11, 239-248, 1991.
- Rijkenberg, M. J., Middag, R., Laan, P., Gerringa, L. J., van Aken, H. M., Schoemann, V., de Jong, J. T., and de Baar, H. J.: The distribution of dissolved iron in the West Atlantic Ocean, *PLoS One*, 9, e101323, 10.1371/journal.pone.0101323, 2014.
- Sabine, C. L., Feely, R. A., Gruber, N., Key, R. M., Lee, K., Bullister, J. L., Wanninkhof, R., Wong, C. S., Wallace, D. W. R., Tilbrook, B., Millero, F. J., Peng, T.-H., Kozyr, A., Ono, T., and Rios, A. F.: The Oceanic sink for anthropogenic CO₂, *Science*, 305, 367-371, 2004.
- Sanders, R., Brown, L., Henson, S., and Lucas, M.: New production in the Irminger Basin during 2002, *Journal of Marine Systems*, 55, 291-310, <http://dx.doi.org/10.1016/j.jmarsys.2004.09.002>, 2005.
- Santos-Echeandia, J., Vale, C., Caetano, M., Pereira, P., and Prego, R.: Effect of tidal flooding on metal distribution in pore waters of marsh sediments and its transport to water column (Tagus estuary, Portugal), *Mar Environ Res*, 70, 358-367, 10.1016/j.marenvres.2010.07.003, 2010.
- Sarthou, G., and Jeandel, C.: Seasonal variations of iron concentrations in the Ligurian Sea and iron budget in the Western Mediterranean Sea, *Marine Chemistry*, 74, 115-129, 10.1016/s0304-4203(00)00119-5, 2001.
- Sarthou, G., Baker, A. R., Kramer, J., Laan, P., Laës, A., Ussher, S., Achterberg, E. P., de Baar, H. J. W., Timmermans, K. R., and Blain, S.: Influence of atmospheric inputs on the iron distribution in the subtropical North-East Atlantic Ocean, *Marine Chemistry*, 104, 186-202, 10.1016/j.marchem.2006.11.004, 2007.
- Sarthou, G., Vincent, D., Christaki, U., Obernosterer, I., Timmermans, K. R., and Brussaard, C. P. D.: The fate of biogenic iron during a phytoplankton bloom induced by natural fertilisation: Impact of copepod grazing, *Deep Sea Research Part II: Topical Studies in Oceanography*, 55, 734-751, 10.1016/j.dsr2.2007.12.033, 2008.
- Sarthou, G., Lherminier, P., Achterberg, E. P., Alonso-Pérez, F., Bucciarelli, E., Boutorh, J., Bouvier, V., Boyle, E. A., Branell, P., Carracedo, L. I., Casacuberta, N., Castrillejo, M., Cheize, M., Contreira Pereira, L., Cossa, D., Daniault, N., De Saint-Léger, E., Dehairs, F., Deng, F., Desprez de Gésincourt, F., Devesa, J., Foliot, L., Fonseca-Batista, D., Gallinari, M., García-Ibáñez, M. I., Gourain, A., Grossteffan, E., Hamon, M., Heimbürger, L. E., Henderson, G. M., Jeandel, C., Kermabon, C., Lacan, F., Le Bot, P., Le Goff, M., Le Roy, E., Lefebvre, A., Leizour, S., Lemaitre, N., Masqué, P., Ménage, O., Menzel Barraqueta, J.-L., Mercier, H., Perault, F., Pérez, F. F., Planquette, H. F., Planchon, F., Roukaerts, A., Sanial, V., Sauzède, R., Shelley, R. U., Stewart, G., Sutton, J. N., Tang, Y., Tisnérat-Laborde, N., Tonnard, M., Tréguer, P., van Beek, P., Zurbrück, C. M., and Zunino, P.: Introduction to the French GEOTRACES North Atlantic Transect (GA01): GEOVIDE cruise, *Biogeosciences Discussions*, 1-24, 10.5194/bg-2018-312, 2018.
- Ocean Data View, <https://odv.awi.de> ODV4, version 4.7.6 (23 March 2016), access: 6 April, 2016.
- Schroth, A. W., Crusius, J., Hoyer, I., and Campbell, R.: Estuarine removal of glacial iron and implications for iron fluxes to the ocean, *Geophysical Research Letters*, 41, 3951-3958, 10.1002/2014GL060199, 2014.
- Shelley, R. U., Morton, P. L., and Landing, W. M.: Elemental ratios and enrichment factors in aerosols from the US-GEOTRACES North Atlantic transects, *Deep Sea Research*, 116, 262-272, 2015.
- Shelley, R. U., Roca-Martí, M., Castrillejo, M., Sanial, V., Masqué, P., Landing, W. M., van Beek, P., Planquette, H., and Sarthou, G.: Quantification of trace element atmospheric deposition fluxes to the Atlantic Ocean (>40°N; GEOVIDE, GEOTRACES GA01) during spring 2014, *Deep Sea Research Part I: Oceanographic Research Papers*, 119, 34-49, 10.1016/j.dsr.2016.11.010, 2017.

- Shelley, R. U., Landing, W. M., Ussher, S. J., Planquette, H., and Sarthou, G.: Characterisation of aerosol provenance from the fractional solubility of Fe (Al, Ti, Mn, Co, Ni, Cu, Zn, Cd and Pb) in North Atlantic aerosols (GEOTRACES cruises GA01 and GA03) using a two stage leach, *Biogeosciences*, 2018.
- Shor, A., Lonsdale, P., Hollister, D., and Spencer, D.: Charlie-Gibbs fracture zone: bottom-water transport and its geological effects, *Deep Sea Research*, 27A, 325-345, 1980.
- Sinha, M. C., Navin, D. A., MacGregor, L. M., Constable, S., Peirce, C., White, A., Heinson, G., and Inglis, M. A.: Evidence for accumulated melt beneath the slow-spreading Mid-Atlantic Ridge, *Philosophical Transactions of the Royal Society A*, 355, 233-253, 1997.
- Slagter, H. A., Reader, H. E., Rijkenberg, M. J. A., Rutgers van der Loeff, M., de Baar, H. J. W., and Gerringa, L. J. A.: Organic Fe speciation in the Eurasian Basins of the Arctic Ocean and its relation to terrestrial DOM, *Marine Chemistry*, 197, 11-25, 10.1016/j.marchem.2017.10.005, 2017.
- Smallwood, J. R., and White, R. S.: Crustal accretion at the Reykjanes Ridge, 61°-62°N, *Journal of Geophysical Research: Solid Earth*, 103, 5185-5201, 10.1029/97jb03387, 1998.
- Statham, P. J., Skidmore, M., and Tranter, M.: Inputs of glacially derived dissolved and colloidal iron to the coastal ocean and implications for primary productivity, *Global Biogeochemical Cycles*, 22, 1-11, 10.1029/2007GB003106, 2008.
- Sunda, W. G., and Huntsman, S. A.: Iron uptake and growth limitation in oceanic and coastal phytoplankton, *Marine Chemistry*, 50, 189-206, 10.1016/0304-4203(95)00035-p, 1995.
- Sutherland, D. A., Pickart, R. S., Peter Jones, E., Azetsu-Scott, K., Jane Eert, A., and Ólafsson, J.: Freshwater composition of the waters off southeast Greenland and their link to the Arctic Ocean, *Journal of Geophysical Research*, 114, 10.1029/2008jc004808, 2009.
- Tanhua, T., Olsson, K. A., and Jeansson, E.: Formation of Denmark Strait overflow water and its hydro-chemical composition, *Journal of Marine Systems*, 57, 264-288, 10.1016/j.jmarsys.2005.05.003, 2005.
- Teng, Z., Huang, J. Y., Fujito, K., and Takizawa, S.: Manganese removal by hollow fiber micro-filter. Membrane separation for drinking water, *European Conference on Desalination and the Environment*, Amsterdam, 28 May, 2001.
- Thuróczy, C. E., Gerringa, L. J. A., Klunder, M. B., Middag, R., Laan, P., Timmermans, K. R., and de Baar, H. J. W.: Speciation of Fe in the Eastern North Atlantic Ocean, *Deep Sea Research Part I: Oceanographic Research Papers*, 57, 1444-1453, 10.1016/j.dsr.2010.08.004, 2010.
- Tonnard, M., Donval, A., Lampert, L., Tréguer, P., Bowie, A. R., van der Merwe, P., planquette, H., Claustre, H., Dimier, C., Ras, J., and Sarthou, G.: Phytoplankton assemblages in the North Atlantic Ocean and in the Labrador Sea along the GEOVIDE section (GEOTRACES section GA01) determined by CHEMTAX analysis from HPLC pigment data, *Biogeosciences*, in prep.
- Tovar-Sanchez, A., Duarte, C. M., Alonso, J. C., Lacorte, S., Tauler, R., and Galban-Malagon, C.: Impacts of metals and nutrients released from melting multiyear Arctic sea ice, *Journal of Geophysical Research-Oceans*, 115, 10.1029/2009jc005685, 2010.
- Tréguer, P. J., and De La Rocha, C. L.: The world ocean silica cycle, *Ann Rev Mar Sci*, 5, 477-501, 10.1146/annurev-marine-121211-172346, 2013.
- Twining, B. S., Baines, S. B., Fisher, N. S., and Landry, M. R.: Cellular iron contents of plankton during the Southern Ocean Iron Experiment (SOFEX), *Deep Sea Research Part I: Oceanographic Research Papers*, 51, 1827-1850, 10.1016/j.dsr.2004.08.007, 2004.
- Van Beusekom, J. E. E.: Distribution of aluminium in surface waters of the North Sea: influence of suspended matter., in: *Biogeochemistry and Distribution of Suspended Matter in the North Sea and Implications to fisheries Biology*, edited by: Kempe, S., *Mitteilungen aus dem Geologisch-Paläontologischen Institut der Universität Hamburg, SCOPE/UNEP Sonderband*, 117-136, 1988.

von Appen, W.-J., Koszalka, I. M., Pickart, R. S., Haine, T. W. N., Mastropole, D., Magaldi, M. G., Valdimarsson, H., Garton, J., Jochumsen, K., and Krahmann, G.: The East Greenland Spill Jet as an important component of the Atlantic Meridional Overturning Circulation, *Deep Sea Research Part I: Oceanographic Research Papers*, 92, 75-84, 10.1016/j.dsr.2014.06.002, 2014.

Wadhams, P.: *Ice in the Ocean*, Gordon and Breach Science Publishers, London, UK, 2000.

Wagener, T., Guieu, C., and Leblond, N.: Effects of dust deposition on iron cycle in the surface Mediterranean Sea: results from a mesocosm seeding experiment, *Biogeosciences Discussions*, 7, 2799-2830, 2010.

Woodgate, R. A., and Aagaard, K.: Revising the Bering Strait freshwater flux into the Arctic Ocean, *Geophysical Research Letters*, 32, 10.1029/2004GL021747., 2005.

Wuttig, K., Wagener, T., Bressac, M., Dammshäuser, A., Streu, P., Guieu, C., and Croot, P. L.: Impacts of dust deposition on dissolved trace metal concentrations (Mn, Al and Fe) during a mesocosm experiment, *Biogeosciences*, 10, 2583-2600, 10.5194/bg-10-2583-2013, 2013.

Zou, S., Lozier, S., Zenk, W., Bower, A., and Johns, W.: Observed and modeled pathways of the Iceland Scotland Overflow Water in the eastern North Atlantic, *Progress in Oceanography*, 159, 211-222, 10.1016/j.pocean.2017.10.003, 2017.

Zunino, P., Lherminier, P., Mercier, H., Daniault, N., García-Ibáñez, M. I., and Pérez, F. F.: The GEOVIDE cruise in may-June 2014 revealed an intense MOC over a cold and fresh subpolar North Atlantic, *Biogeosciences*, 2017.

3.8. Supplementary material

Figure S1: Section plot of Total Chlorophyll-*a* (TChl-*a*) concentrations (mg m^{-3}) measured for the GA01 voyage. The black contour lines highlight the TChl-*a* concentrations and the white contour lines highlight the dissolved iron (DFe) concentrations. The red dashed line indicates the depth of the Surface Mixed Layer (SML) (see text for details). (Ocean Data View (ODV) software, version 4.7.6, R. Schlitzer, <http://odv.awi.de>, 2016).

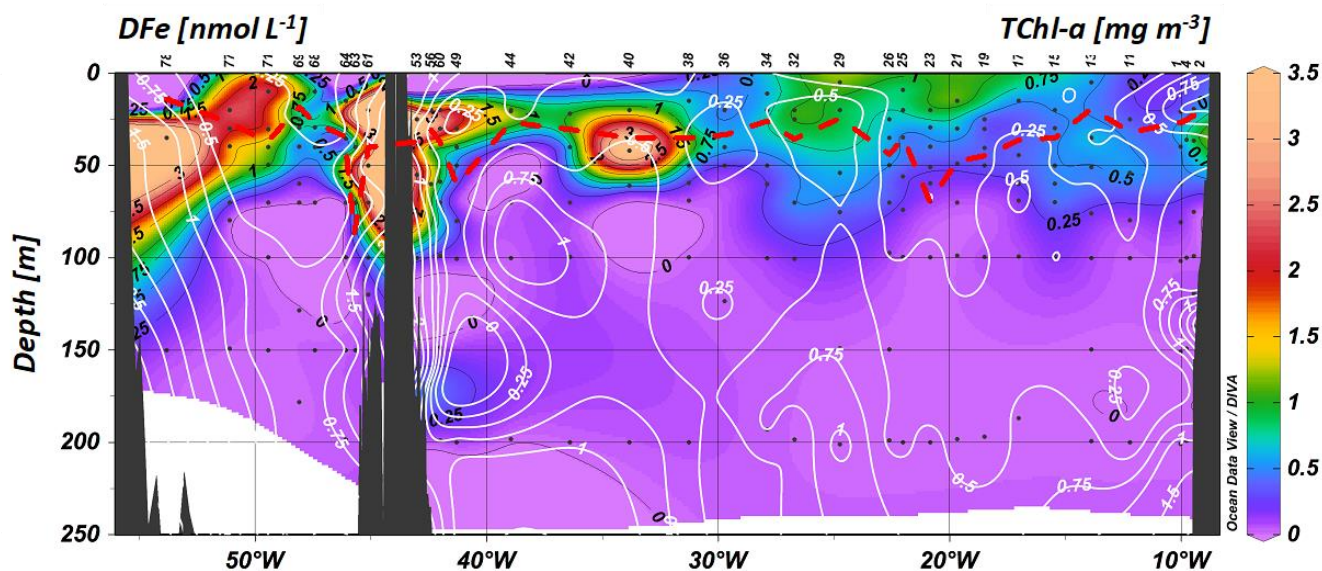


Figure S2: Mean profiles of dissolved iron (Fe) along the North Atlantic section in the West European Basin (purple), Iceland Basin (blue), Irminger Sea (green) and Labrador Sea (red) over the depth intervals: 0-100 m, 100-250 m, 250-500 m, 500-1000 m, 1000-1500 m, 1500-2000 m, 2000-3000 m, 3000-4000 m, 4000-5500 m without considering stations located above the continental plateau.

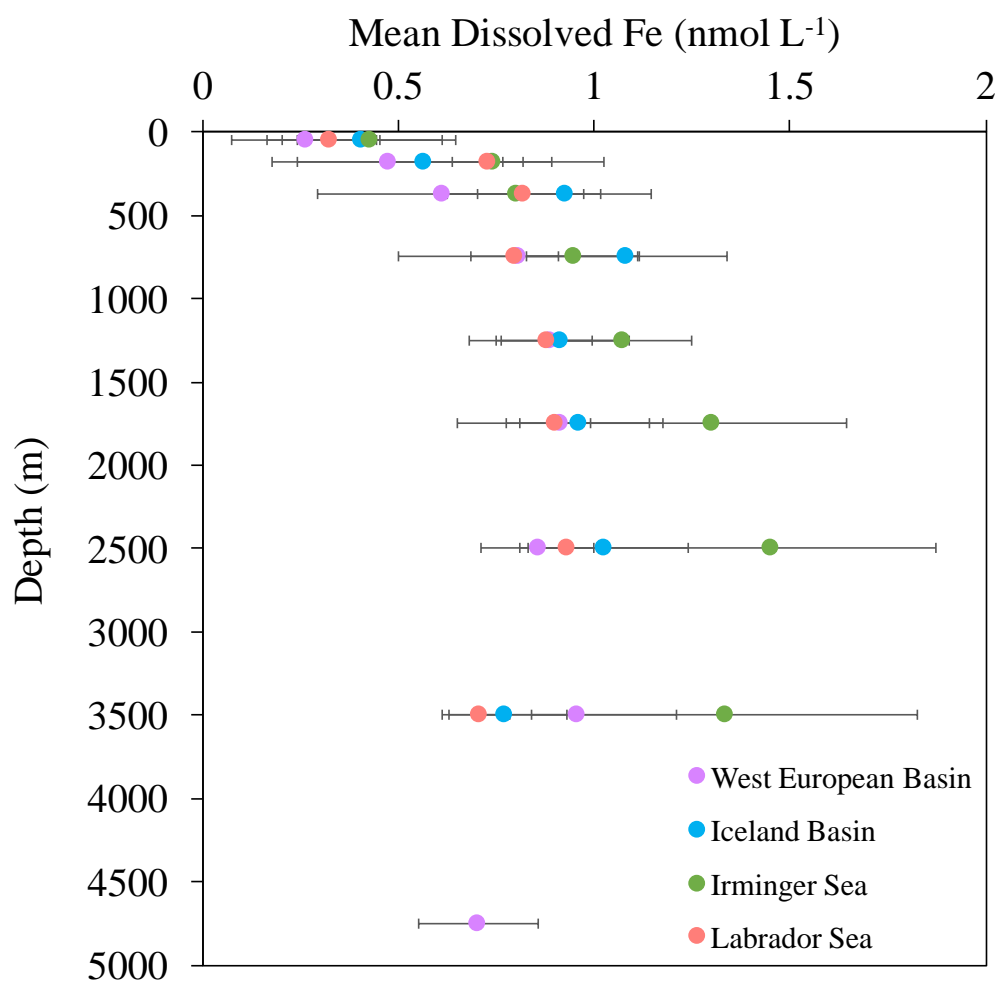


Figure S3: Box and whisker plot of dissolved iron (DFe) in nmol L^{-1} per water mass and basin. Color coding representing from West to East: the Labrador Sea (red), the Irminger Sea (green), the Iceland Basin (blue) and the West European Basin (purple). Note that stations 1 and 17 were not considered in this plot. SAIW: Sub-Arctic Intermediate Water, ENACW: East North Atlantic Central Water, IrSPMW: Irminger Sub-Polar Mode Water, IcSPMW: Iceland Sub-Polar Mode Water, MOW: Mediterranean Overflow Water, LSW: Labrador Sea Water, ISOW: Iceland-Scotland Overflow Water, DSOW: Denmark Strait Overflow Water, NEADW: North East Atlantic Deep Water.

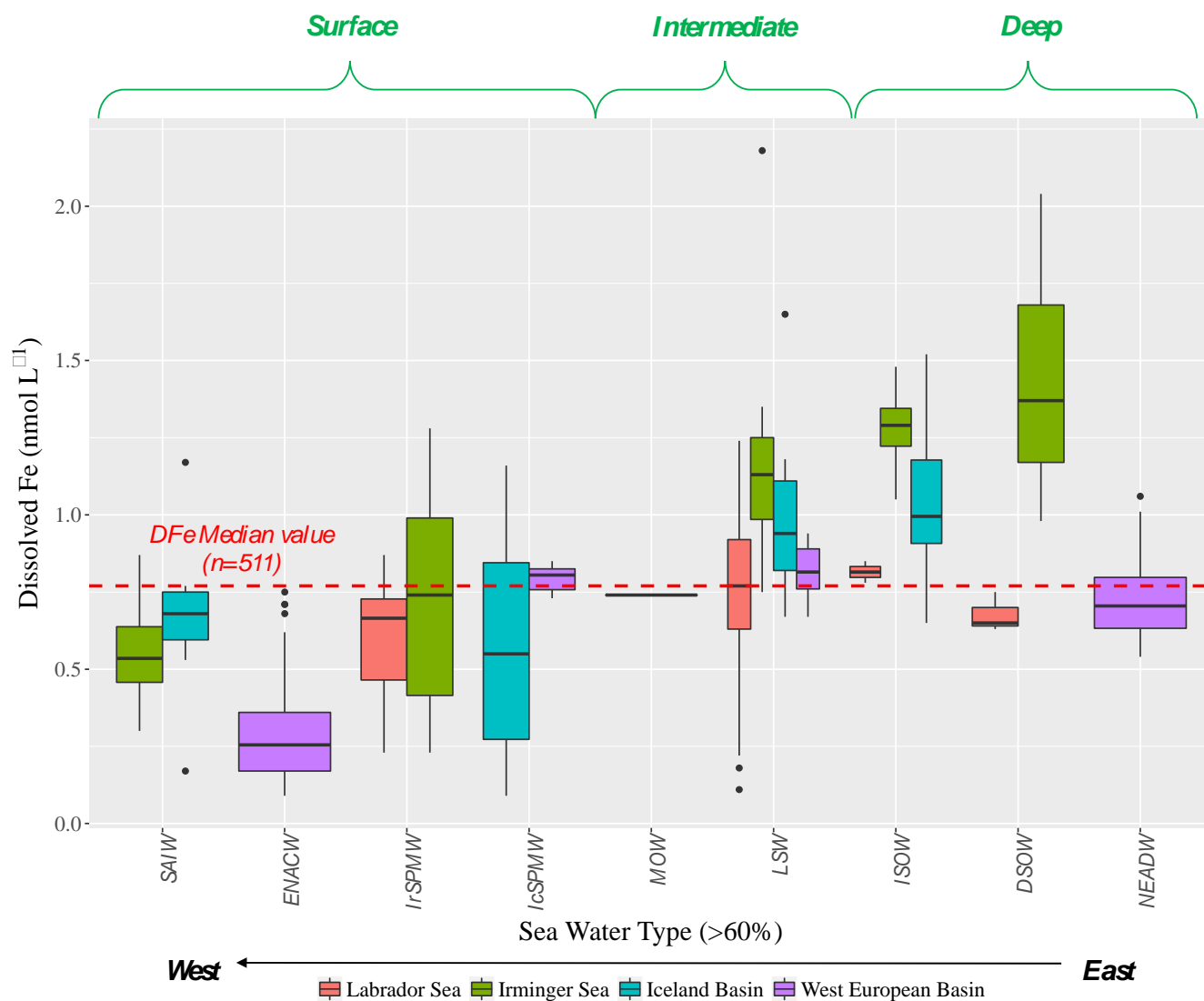


Figure S4: Surface layer of DFe concentrations, new measurements are shown in red dots (GEOVIDE voyage), while previous studies are displayed in black (Achterberg et al., 2018; Bergquist et al., 2007; Blain et al., 2004; Boye et al., 2006, 2003; de Jong et al., 2007; Gledhill et al., 1998; Hatta et al., 2015; Klunder et al., 2012; Laës et al., 2003; Martin et al., 1993; Measures et al., 2008; Mills et al., 2008; Mohamed et al., 2011; Nédélec et al., 2007; Nielsdóttir et al., 2009; Pohl et al., 2011; Rijkenberg et al., 2014; Sarthou et al., 2007, 2003; Sedwick et al., 2005; Ussher et al., 2013; Witter and Luther III, 1998; Wu and Boyle, 2002; Wu and Luther III, 1996, 1994; Wu et al., 2001).

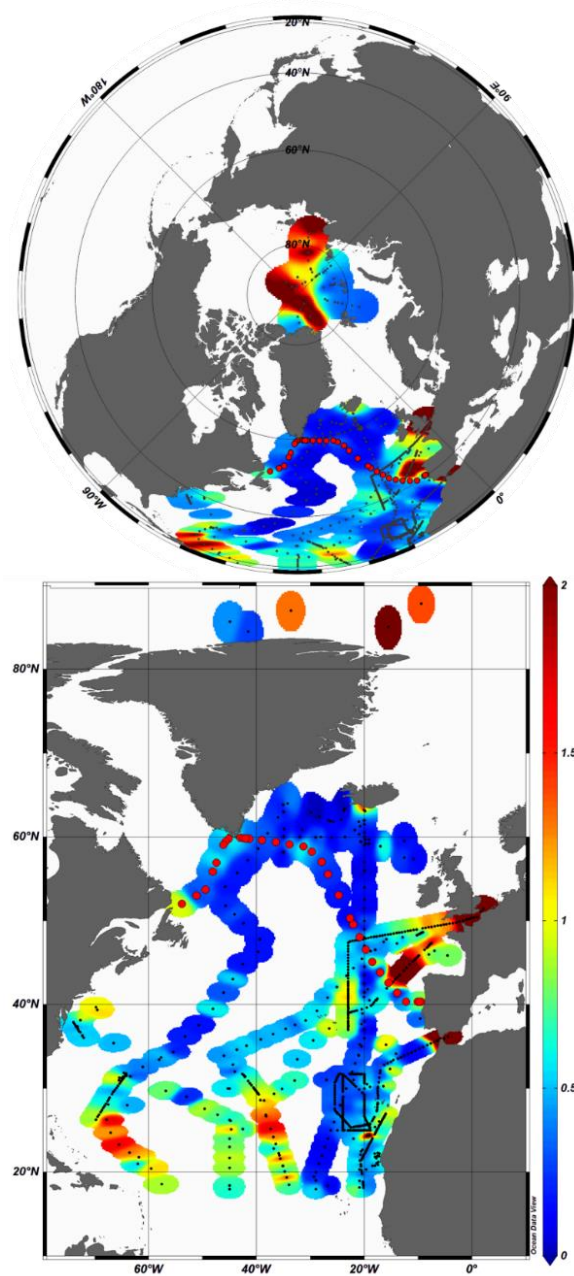


Figure S5: A) Plot of dissolved iron (DFe) concentrations as a function of the percentage of Polar Intermediate Water (PIW) contribution for open-ocean stations (stations 44, 49, 60, 63, 68, 69, 71 and 77). Station 44 highlighted in green and dashed-line representing the linear regression line between DFe concentrations and percentage of PIW contribution for all stations except station 44. B) Plot of dissolved (DFe, black dots) and particulate iron (PFe, open dots, Gourain et al., in prep.) for station 44 (from 2220 m depth to the bottom) as a function of the percentage of mixing between Iceland-Scotland Overflow Water (ISOW) as opposed to Polar Intermediate Water (PIW) and Denmark Strait Overflow Water (DSOW) (Garcia-Ibanez et al., 2015) with polynomial (DFe) and exponential (PFe) regression equations.

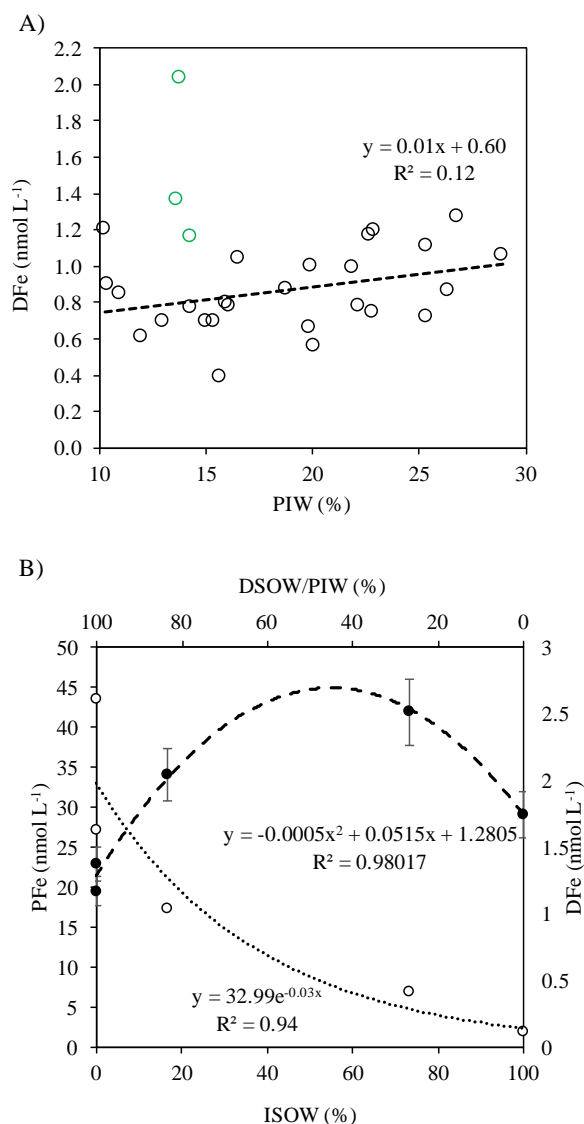


Figure S6: Plots of the first two dimensions of a Principal Component Analysis (PCA) performed on A) the following variables: Apparent Oxygen Utilization (AOU), dissolved aluminium (DAI, Menzel Barraqueta et al., 2018), particulate iron, aluminum and manganese oxides (PFe, PAI and MnO_2 , Gourain et al., in prep.) and B) for samples which presented a transmissometry lower than 99% and below 500 m depth to avoid surface processes. Note that the color coding corresponds to different water masses (contribution >60% of the whole water mass pool) with the Denmark Strait Overflow Water (DSOW) in grey, the East North Atlantic Central Water (ENACW) in yellow, the Irminger Sub-Polar Mode Water (IrSPMW) in blue, the Iceland-Scotland Overflow Water (ISOW) in green, the Labrador Sea Water (LSW) in red, the Mediterranean Overflow Water (MOW) in orange, the North East Atlantic Deep Water (NEADW) in pink and mixing of multiple water masses (NA) in white. Plots of dissolved iron (DFe) plotted as a function of distance height above the seafloor for C) the first dimension of the PCA and D) the second dimension of the PCA. Note that positive and negative values are represented in blue and red, respectively and that dot size are function of the particulate iron and manganese oxide ratios ($\text{PFe}:\text{PMnO}_2$, mol mol⁻¹).

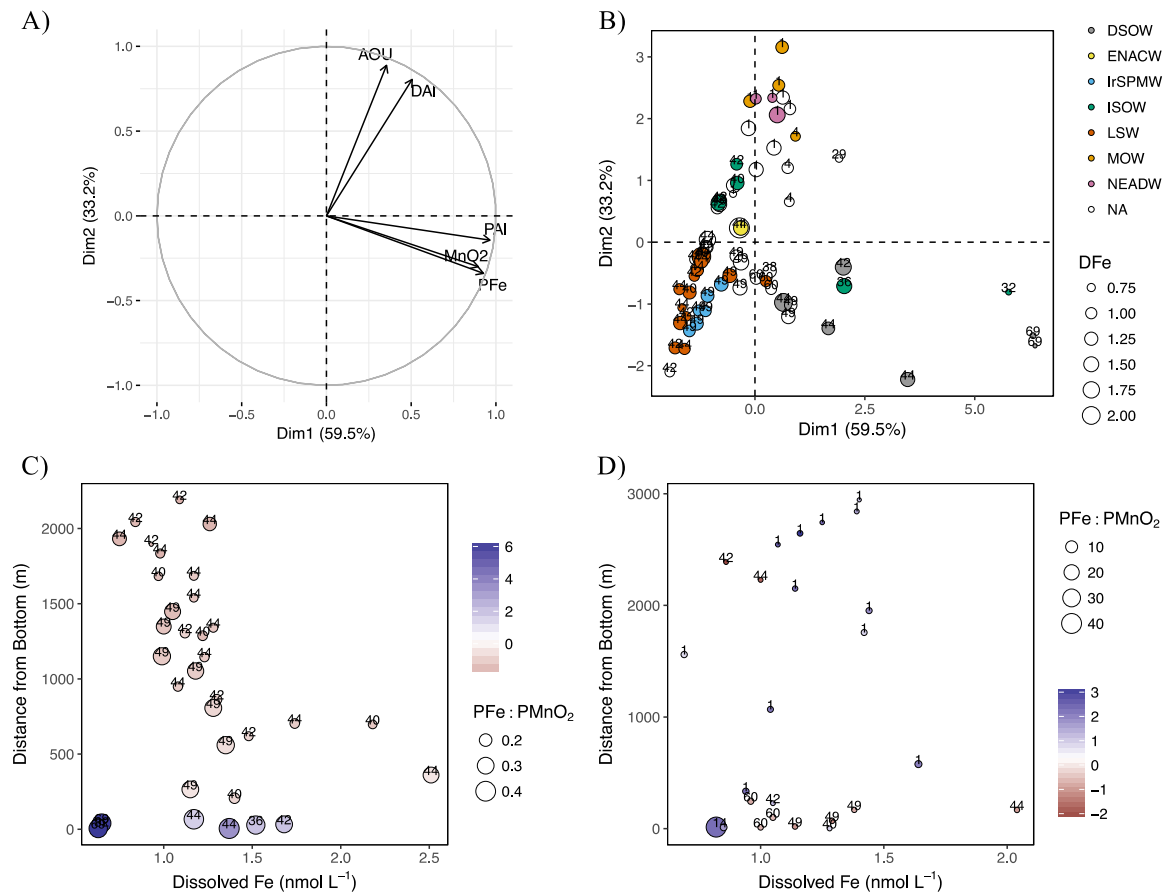


Figure S7: Vertical profiles of the DFe:NO_3^- ratio over the upper 200 m of the water column along the GEOVIDE section. Profiles from the West European Basin are plotted in black, from the Iceland Basin in grey, from the Irminger Sea in green and from the Labrador Sea in red. Stations located above the continental Plateau (stations 1, 2 and 4 from the Iberian Margin; stations 53 and 61 from the Greenland shelf; station 78 from the Newfoundland Margin) are represented with dotted lines. The vertical dashed lines (light blue) indicate lower and upper limits of phytoplankton cellular DFe:NO_3^- ratios under Fe replete conditions Ho et al., 2003; Sunda and Huntsman, 1995a; Twining et al., 2004b.

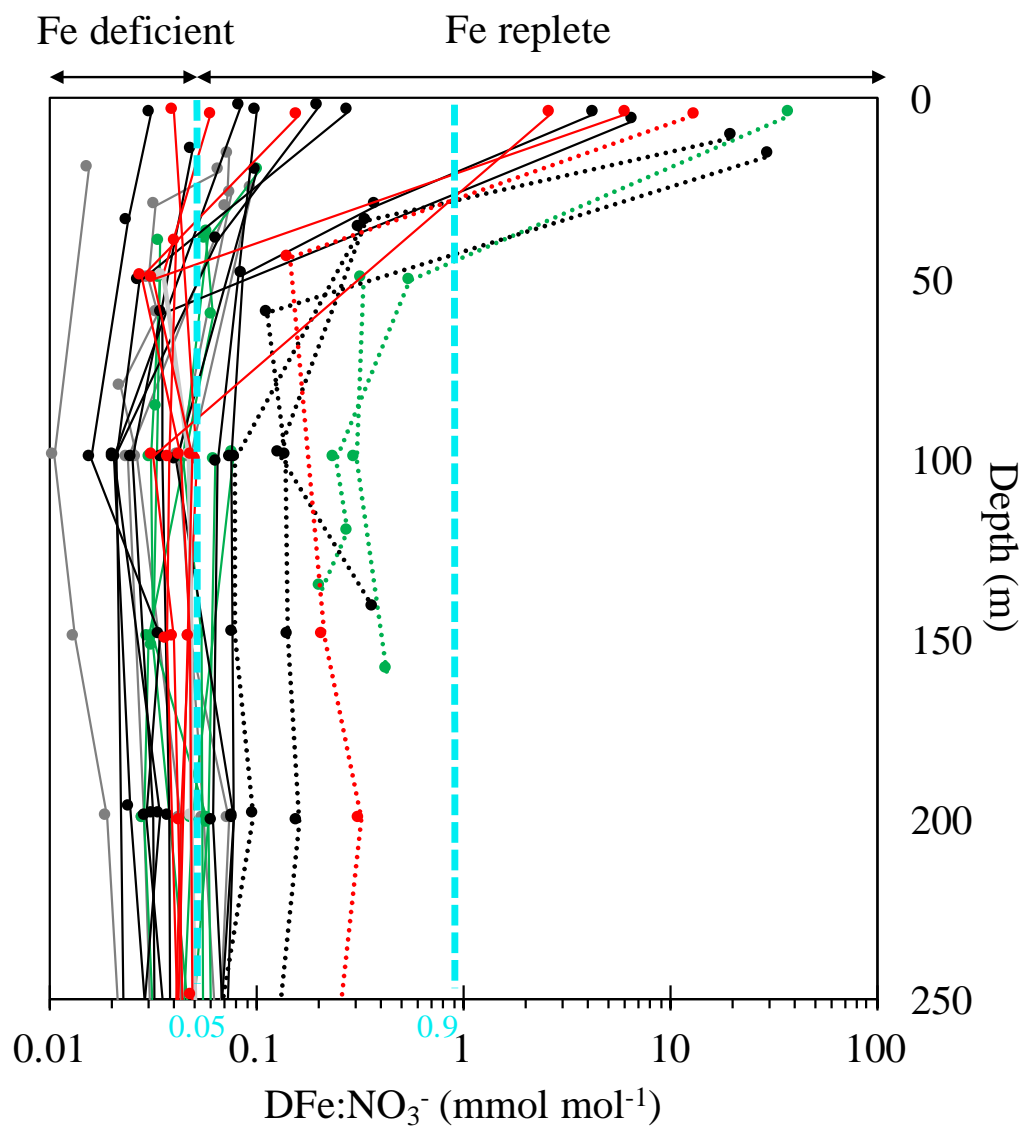


Figure S8: Surface map of the DFe:NO_3^- ratios along the GEOVIDE section.

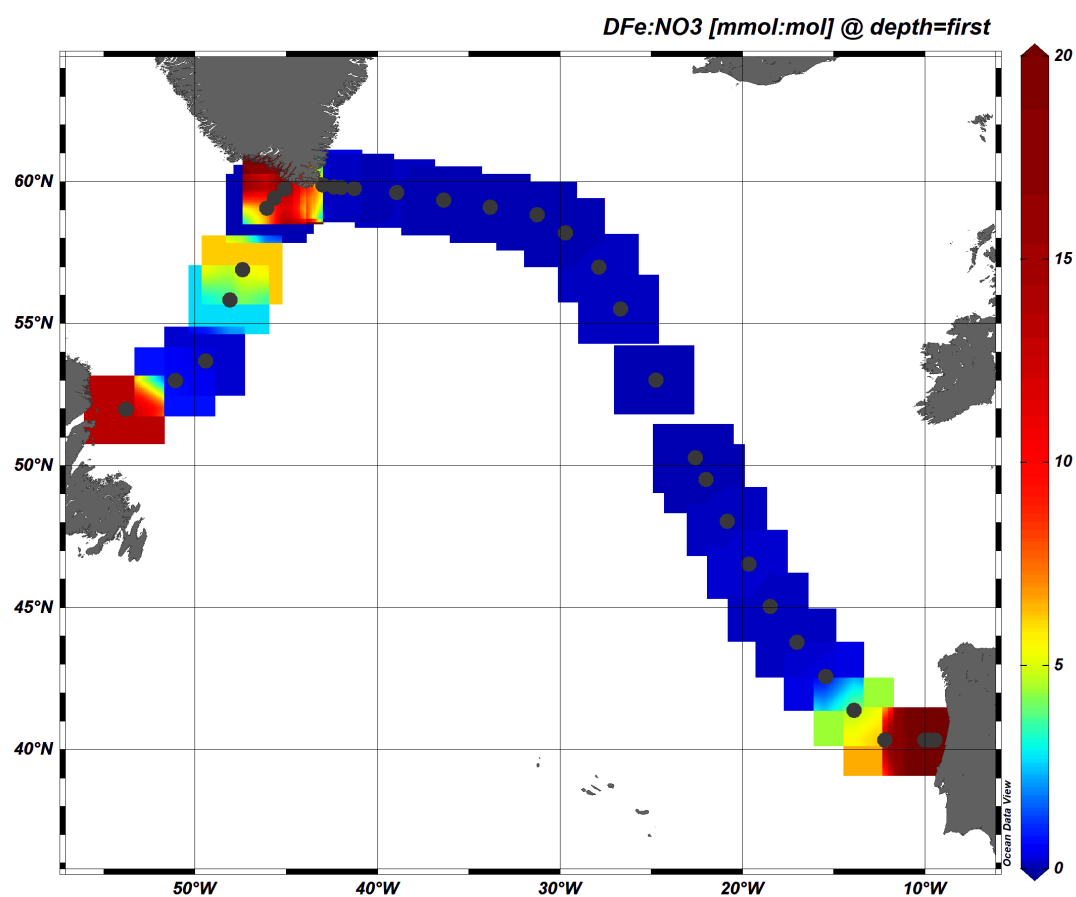


Figure S9: Section plot of the Fe^* tracer in the North Atlantic Ocean with a remineralization rate ($R_{\text{Fe:N}}$) of $0.05 \text{ mmol mol}^{-1}$ from 100 m depth to bottom waters. A contour line of 0 separates areas of negative Fe^* from areas with positive Fe^* . Positive values of Fe^* imply there is enough iron to support complete consumption of NO_3^- when this water is brought to surface, and negative Fe^* imply a deficit. See text for details.

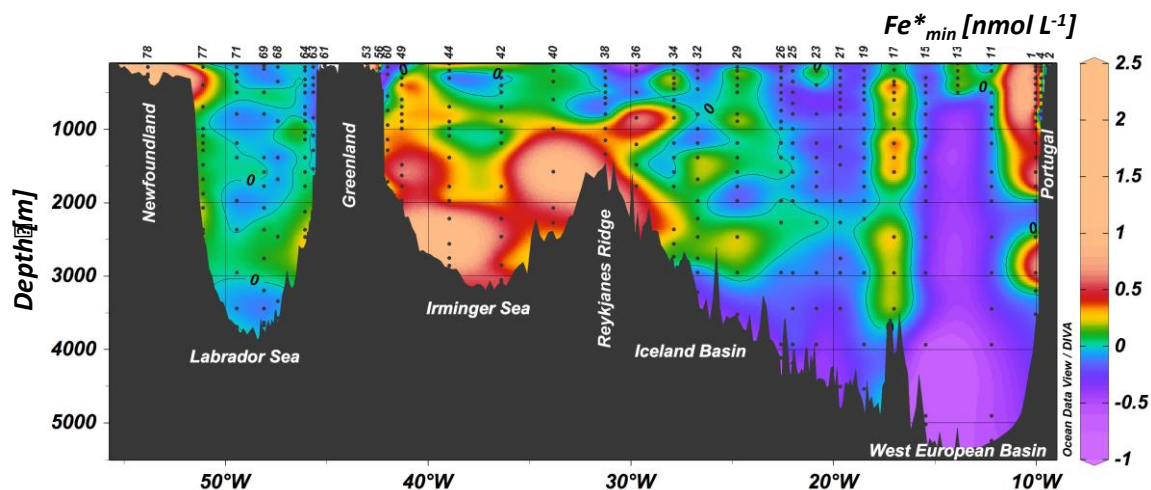


Figure S10: Box and whisker plot of Fe* in units of nmol L⁻¹ as determined per water mass and basin with a Fe:N uptake rate of 0.05. Color coding representing from West to East, the Labrador Sea (red), the Irminger Sea (green), the Iceland Basin (blue) and the West European Basin (purple). Abbreviation referring to SAIW: Sub-Arctic Intermediate Water, ENACW: East North Atlantic Central Water, IrSPMW: Irminger Sub-Polar Mode Water, IcSPMW: Iceland Sub-Polar Mode Water, MOW: Mediterranean Overflow Water, LSW: Labrador Sea Water, ISOW: Iceland-Scotland Overflow Water, DSOW: Denmark Strait Overflow Water, NEADW: North East Atlantic Deep Water.

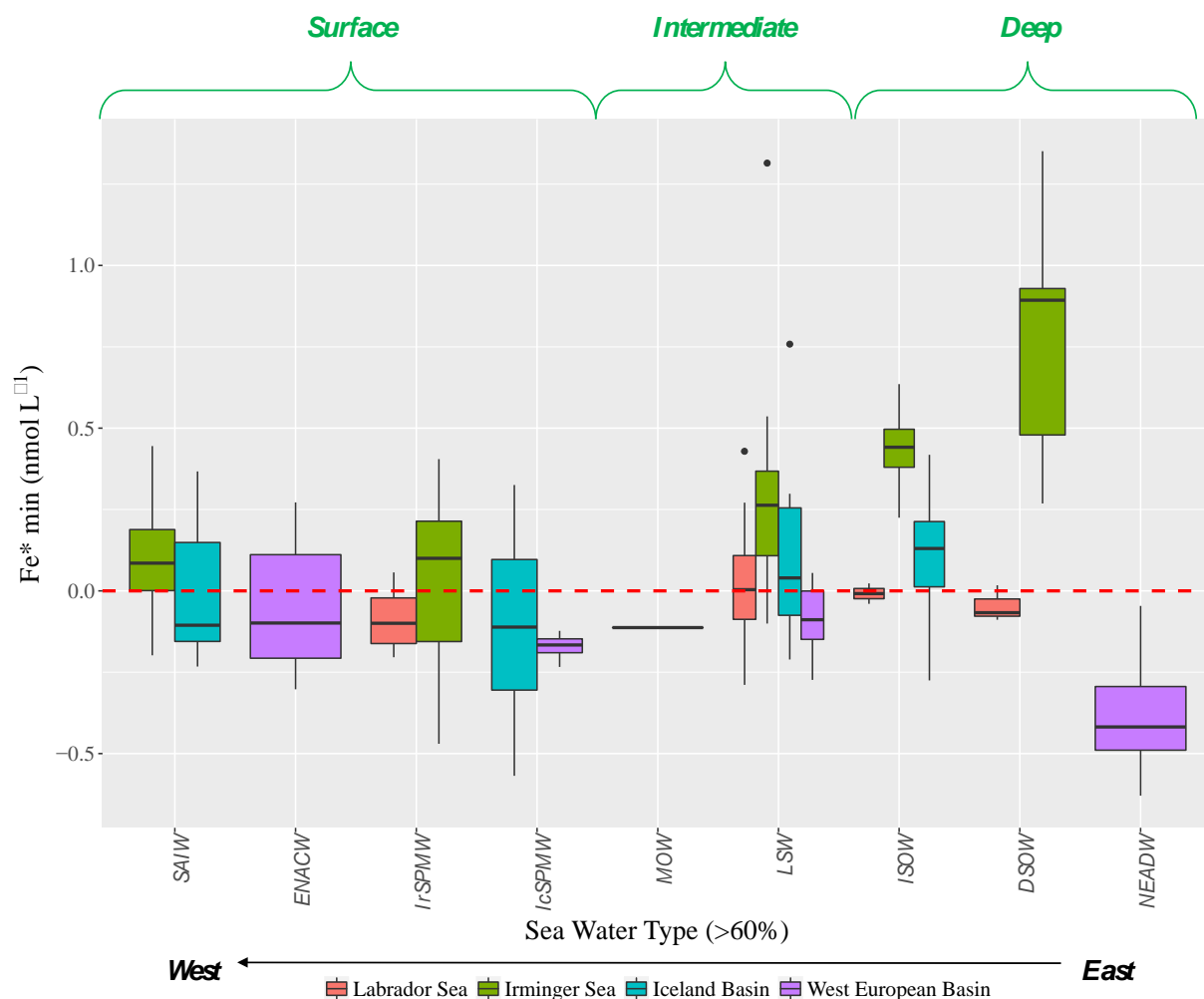


Table S2: Compilation of median dissolved iron (DFe) concentrations (min, max) for Surface (> 200 m depth), Intermediate (from 200 to 1000 m depth) and Deep (>1000 m depth) Waters in the four distinct basins of the GA01 transect and in the Arctic Ocean (data from: the British Oceanographic Data Center website <http://www.amt-uk.org/Data>, PANGAEA website <http://doi.pangaea.de/10.1594/PANGAEA.609968>, Clivar & Carbon Hydrographic Data Office website <https://cchdo.ucsd.edu/search?bbox=-75,-60,20,65> and GEOTRACES intermediate data product 2017 www.bodc.ac.uk/geotraces/data/idp2017/ and <https://webdv.awi.de/geotraces>). Bold values indicated for each depth range represent the median DFe concentrations all studies considered per basin.

Area	Time period		Fe (nmol L ⁻¹)		Filtration	Cruise	Reference
	Months	Year	range	median	µm	Name	
West European basin							
<i>surface (<200m)</i>				0.27			
	May-June	2014	0.09 - 3.0	0.24	0.2/0.45	GEOVIDE	<i>this study</i>
	May	2013	0.01 - 0.45	0.05	0.2	GA04	<i>Gerringa et al., 2017</i>
	October-November	2010	0.06 - 0.98	0.49	0.2	GA03	<i>Hatta et al., 2015</i>
	June	2005	0.35 - 0.76	0.57	0.2	AMT16	<i>Ussher et al., 2013</i>
	September	2004	0.33 - 2.6	0.49	0.2	AMT15	<i>Ussher et al., 2013</i>
	June-August	2003	0.02 - 0.25	0.08	0.4	CLIVAR-CO2	<i>Measures et al., 2008</i>
	July	2003	0.05 - 5.4	0.7	0.4	JR98	<i>Nedelec et al., 2007</i>
	October	2002	0.07 - 7.0	0.35	0.2	IRONAGE III	<i>Sarthou et al., 2007</i>
	March	2002	0.23 - 0.47	0.34	0.2	IRONAGES	<i>Laes et al., 2003</i>
	February-March	2001	0.22 - 0.64	0.4	0.2/0.45	POMME	<i>Blain et al., 2004</i>
	June	1998	0.10 - 1.5	0.71	unfiltered	AMT6	<i>Bowie et al., 2002</i>
	March	1998	0.48 - 1.6	0.82	0.2	MERLIM	<i>Boye et al., 2006; 2003</i>
	March	1998	0.34 - 5.9	1	0.2	64PE114	<i>de Jong et al., 2007</i>
	May	1989	0.08 - 0.27	0.19	0.4	Atlantis II	<i>Martin et al., 1993</i>
<i>intermediate (200-1000)</i>				0.71			
	May-June	2014	0.23 - 1.4	0.73	0.2/0.45	GEOVIDE	<i>this study</i>
	May	2013	0.10 - 0.72	0.42	0.2	GA04	<i>Gerringa et al., 2017</i>
	October-November	2010	0.38 - 1.0	0.61	0.2	GA03	<i>Hatta et al., 2015</i>

	July	2003	0.35 - 2.2	1.2	0.4	JR98	<i>Nedelec et al., 2007</i>
	March	2002	0.57 - 0.86	0.64	0.2	IRONAGES	<i>Laes et al., 2003</i>
	June	1998	0.72 - 0.83	0.81	0.2	AMT6	<i>Bowie et al., 2002</i>
	March	1998	1.1 - 1.6	1.4	0.2	MERLIM	<i>Boye et al., 2006; 2003</i>
	March	1998	1.3 - 1.9	1.6	0.2	64PE114	<i>de Jong et al., 2007</i>
	May	1989	0.26 - 0.57	0.35	0.4	Atlantis II	<i>Martin et al., 1993</i>
<i>deep (>1000)</i>				0.76			
	May-June	2014	0.53 - 1.6	0.78	0.2/0.45	GEOVIDE	<i>this study</i>
	May	2013	0.44 - 0.87	0.61	0.2	GA04	<i>Gerringa et al., 2017</i>
	October-November	2010	0.46 - 1.1	0.75	0.2	GA03	<i>Hatta et al., 2015</i>
	July	2003	1.2 - 4.4	1.6	0.4	JR98	<i>Nedelec et al., 2007</i>
	March	2002	0.67 - 1.2	0.82	0.2	IRONAGES	<i>Laes et al., 2003</i>
	June	1998	0.57 - 0.94	0.76	0.2	AMT6	<i>Bowie et al., 2002</i>
	March	1998	1.3 - 1.6	1.4	0.2	MERLIM	<i>Boye et al., 2006; 2003</i>
	March	1998	1.3 - 2.0	1.7	0.2	64PE114	<i>de Jong et al., 2007</i>
	May	1989	0.54 - 0.66	0.6	0.4	Atlantis II	<i>Martin et al., 1993</i>
Iceland Basin							
<i>surface (<200m)</i>				0.22			
	May-June	2014	0.09 - 0.75	0.34	0.2/0.45	GEOVIDE	<i>this study</i>
	July-August	2010	0.03 - 2.6	0.25	0.2	D354	<i>Achterberg et al., 2018</i>
	April-May	2010	0.11 - 2.6	0.3	0.2	D350	<i>Achterberg et al., 2018</i>
	June	2009	0.08 - 0.87	0.24	0.2	D340	<i>Mohamed et al., 2011</i>
	August-September	2007	0.04 - 0.34	0.14	0.2	D321	<i>Mohamed et al., 2011</i>
	July-September	2007	0.02 - 0.41	0.06	0.2		<i>Nielsdottir et al., 2009</i>
	June-August	2003	0.02 - 0.30	0.1	0.4	CLIVAR-CO2	<i>Measures et al., 2008</i>
	May	1989	0.06 - 0.23	0.12	0.4	Atlantis II	<i>Martin et al., 1993</i>

<i>intermediate (200-1000)</i>				0.71			
	May-June	2014	0.28 - 1.6	0.94	0.2/0.45	GEOVIDE	<i>this study</i>
	July-August	2010	0.21 - 2.7	0.73	0.2	D354	<i>Achterberg et al., 2018</i>
	April-May	2010	0.21 - 2.7	0.74	0.2	D350	<i>Achterberg et al., 2018</i>
	June	2009	0.24 - 2.23	0.63	0.2	D340	<i>Mohamed et al., 2011</i>
	August-September	2007	0.2 - 0.85	0.46	0.2	D321	<i>Mohamed et al., 2011</i>
	July-September	2007	0.07 - 0.80	0.4	0.2		<i>Nielsdottir et al., 2009</i>
	May	1989	0.17 - 0.54	0.37	0.4	Atlantis II	<i>Martin et al., 1993</i>
<i>deep (>1000)</i>				0.87			
	May-June	2014	0.63 - 1.5	0.92	0.2/0.45	GEOVIDE	<i>this study</i>
	July-August	2010	0.47 - 1.67	0.92	0.2	D354	<i>Achterberg et al., 2018</i>
	April-May	2010	0.47 - 1.9	0.77	0.2	D350	<i>Achterberg et al., 2018</i>
	June	2009	1.42 - 2.6	1.51	0.2	D340	<i>Mohamed et al., 2011</i>
	August-September	2007	0.08 - 1.5	0.71	0.2	D321	<i>Mohamed et al., 2011</i>
	May	1989	0.53 - 0.79	0.59	0.4	Atlantis II	<i>Martin et al., 1993</i>
Irminger Basin							
<i>surface (<200m)</i>				0.18			
	May-June	2014	0.22 - 3	0.55	0.2/0.45	GEOVIDE	<i>this study</i>
	July-August	2010	0 - 3.3	0.15	0.2	D354	<i>Achterberg et al., 2018</i>
	April-May	2010	0.03 - 0.97	0.11	0.2	D350	<i>Achterberg et al., 2018</i>
	April-May	2010	0.08 - 0.55	0.15	0.2	GA02	<i>Rijkenberg et al., 2014</i>
<i>intermediate (200-1000)</i>				0.47			
	May-June	2014	0.33 - 1.2	0.86	0.2/0.45	GEOVIDE	<i>this study</i>
	July-August	2010	0.03 - 1.21	0.42	0.2	D354	<i>Achterberg et al., 2018</i>
	April-May	2010	0.03 - 0.63	0.29	0.2	D350	<i>Achterberg et al., 2018</i>
	April-May	2010	0.28 - 0.69	0.48	0.2	GA02	<i>Rijkenberg et al., 2014</i>

<i>deep (>1000)</i>				0.78			
	May-June	2014	0.82 - 2.5	1.14	0.2/0.45	GEOVIDE	<i>this study</i>
	July-August	2010	0.39 - 1.01	0.7	0.2	D354	<i>Achterberg et al., 2018</i>
	April-May	2010	0.50 - 1.0	0.71	0.2	D350	<i>Achterberg et al., 2018</i>
	April-May	2010	0.65 - 0.99	0.75	0.2	GA02	<i>Rijkenberg et al., 2014</i>
<hr/>							
Labrador Basin							
<i>surface (<200m)</i>				0.33			
	May-June	2014	0.11 - 2.4	0.55	0.2/0.45	GEOVIDE	<i>this study</i>
	April-May	2010	0.05 - 0.58	0.17	0.2	GA02	<i>Rijkenberg et al., 2014</i>
<hr/>							
<i>intermediate (200-1000)</i>				0.67			
	May-June	2014	0.61 - 7.6	0.8	0.2/0.45	GEOVIDE	<i>this study</i>
	April-May	2010	0.35 - 0.87	0.55	0.2	GA02	<i>Rijkenberg et al., 2014</i>
<hr/>							
<i>deep (>1000)</i>				0.69			
	May-June	2014	0.60 - 1.1	0.85	0.2/0.45	GEOVIDE	<i>this study</i>
	April-May	2010	0.47 - 0.66	0.59	0.2	GA02	<i>Rijkenberg et al., 2014</i>
<hr/>							
Arctic Ocean							
<i>surface (<200m)</i>							
	July	2008	2.1 - 16		0.22		<i>Nishimura et al., 2012</i>
	September	2008	0.5 - 3.2		0.22	MR 08-04	<i>Nakayama et al., 2011</i>
	August - September	2007	0.10 - > 10	0.6	0.2	ARK XXII/2	<i>Klunder et al., 2012</i>
	July	2007	5.7 - 23		unfiltered	ATOS-Arctic	<i>Tovar-Sanchez et al., 2010</i>
	April-May	2007	0.8 - 3.1	1.5	0.4		<i>Aguilar-Islas et al., 2008</i>
<hr/>							
<i>intermediate (200-1000)</i>	August - September	2007	0.20 - 1.4	0.5	0.2	ARK XXII/2	<i>Klunder et al., 2012</i>
<hr/>							
<i>deep (>1000)</i>	August - September	2007	0.18 - 1.7	0.56	0.2	ARK XXII/2	<i>Klunder et al., 2012</i>
<hr/>							

Table S1: Table of dissolved iron (DFe) data for the whole GEOVIDE section. Bold characters denote stations located above the shelves. Note that QC refers to the data quality (1 = good data, 2 = questionable, 3 = bad data, were removed).

Station	Lat	Lon	Bottle	Depth	DFe			QC
(#)	(°N)	(°E)	(#)	(m)	(nmol kg-1)	(nmol L-1)	SD	(#)
1	40.333	-10.036	24	21	1.04	1.07	± 0.12	2
			22	60	0.50	0.51	± 0.06	1
			21	81	0.72	0.74	± 0.09	1
			20	102	0.82	0.84	± 0.10	1
			19	151	0.94	0.96	± 0.11	1
			18	201	1.23	1.26	± 0.15	2
			17	300	1.05	1.08	± 0.13	1
			16	387	1.28	1.31	± 0.15	1
			15	501	1.40	1.44	± 0.17	1
			14	589	1.37	1.40	± 0.16	1
			13	693	1.36	1.39	± 0.16	1
			12	792	1.22	1.25	± 0.15	1
			11	889	1.13	1.16	± 0.14	1
			10	990	1.04	1.07	± 0.12	1
			9	1185	1.18	1.21	± 0.14	1
			8	1384	1.11	1.14	± 0.13	1
			7	1582	1.40	1.44	± 0.17	2
			6	1778	1.39	1.42	± 0.17	2
			5	1976	0.67	0.69	± 0.08	1
			4	2466	1.01	1.04	± 0.12	1
			3	2957	1.60	1.64	± 0.19	2
			2	3201	0.92	0.94	± 0.11	1
			1	3521	0.80	0.82	± 0.10	1
2	40.333	-9.46	21	19	0.99	1.01	± 0.04	1
			19	37	0.36	0.37	± 0.01	1
			14	50	0.46	0.47	± 0.02	1
			13	75	0.61	0.63	± 0.02	1
			9	99	0.73	0.75	± 0.03	1
			5	119	0.56	0.57	± 0.02	1
			1	137	2.97	3.04	± 0.12	1
4	40.333	-9.767	23	21	0.71	0.73	± 0.03	2
			21	39	0.33	0.34	± 0.01	1
			19	71	0.51	0.52	± 0.02	1
			15	149	0.59	0.60	± 0.02	1

			13	200	0.87	0.89	± 0.03	2
			11	300	0.55	0.56	± 0.02	1
			9	398	0.72	0.74	± 0.03	1
			7	496	0.79	0.81	± 0.03	1
			5	596	0.84	0.86	± 0.03	1
			3	694	1.00	1.03	± 0.04	1
			1	792	0.83	0.85	± 0.03	1
11	40.333	-12.219	24	15	0.12	0.12	± 0.01	1
			23	25	0.27	0.28	± 0.02	3
			22	54	0.19	0.19	± 0.01	1
			21	80	0.18	0.18	± 0.01	1
			20	100	0.23	0.24	± 0.02	1
			19	199	0.28	0.29	± 0.02	1
			16	497	0.55	0.56	± 0.04	1
			14	695	0.74	0.76	± 0.05	1
			13	793	0.79	0.81	± 0.06	1
			12	991	0.76	0.78	± 0.05	1
			11	1188	0.72	0.74	± 0.05	1
			9	1582	0.80	0.82	± 0.06	1
			8	1779	0.75	0.77	± 0.05	1
			7	1976	0.76	0.78	± 0.05	1
			6	2466	0.73	0.75	± 0.05	1
			5	2954	0.85	0.87	± 0.06	1
			4	3445	0.77	0.79	± 0.05	1
			3	3933	0.68	0.70	± 0.05	1
			2	4904	0.63	0.65	± 0.04	1
			1	5241	0.61	0.63	± 0.04	1
13	41.383	-13.888	24	11	0.22	0.23	± 0.02	1
			23	30	0.26	0.27	± 0.03	1
			22	51	0.25	0.26	± 0.02	1
			21	75	0.35	0.36	± 0.03	1
			20	100	0.50	0.51	± 0.05	1
			19	150	0.29	0.30	± 0.03	3
			16	199	0.59	0.60	± 0.06	1
			15	298	0.60	0.62	± 0.06	1
			14	397	0.69	0.71	± 0.07	1
			13	496	0.69	0.71	± 0.07	1
15	42.581	-15.461	24	20	0.24	0.25	± 0.02	1
			23	30	0.19	0.19	± 0.02	1
			22	49	0.14	0.14	± 0.01	1

			21	60	0.32	0.33	± 0.03	2
			20	70	0.25	0.26	± 0.02	2
			19	99	0.17	0.17	± 0.02	1
			16	298	0.26	0.27	± 0.03	1
			15	397	0.34	0.35	± 0.03	1
			14	496	0.44	0.45	± 0.04	1
			13	644	0.65	0.67	± 0.07	1
			12	793	0.65	0.67	± 0.06	1
			11	989	0.74	0.76	± 0.07	1
			10	1089	0.72	0.74	± 0.07	1
			9	1384	0.60	0.62	± 0.06	1
			8	1581	0.68	0.70	± 0.07	1
			7	1779	0.70	0.72	± 0.07	1
			6	1975	0.65	0.67	± 0.06	1
			5	2466	0.71	0.73	± 0.07	1
			4	2956	0.73	0.75	± 0.07	1
			3	3932	0.56	0.57	± 0.06	1
			2	4904	0.53	0.54	± 0.05	1
			1	5020	0.57	0.58	± 0.06	1
17	43.78	-17.032	24	15	0.17	0.17	± 0.01	1
			23	30	0.88	0.91	± 0.06	3
			22	44	0.52	0.53	± 0.04	1
			21	60	0.54	0.55	± 0.04	1
			20	69	0.56	0.57	± 0.04	1
			19	99	0.54	0.55	± 0.04	1
			16	199	0.56	0.57	± 0.04	1
			15	348	0.76	0.78	± 0.05	1
			14	396	1.04	1.07	± 0.07	1
			13	496	0.96	0.98	± 0.07	1
			12	595	1.03	1.06	± 0.07	1
			11	792	1.21	1.24	± 0.08	1
			10	990	1.08	1.11	± 0.08	1
			9	1188	1.35	1.38	± 0.09	1
			8	1385	1.23	1.26	± 0.09	1
			7	1581	1.31	1.34	± 0.09	1
			4	2465	1.25	1.28	± 0.09	1
			3	2955	1.27	1.30	± 0.09	1
			2	3444	1.31	1.34	± 0.09	1
19	45.05	-18.505	24	20	0.09	0.09	± 0.01	1
			23	30	0.31	0.32	± 0.03	3

			22	40	0.17	0.17	± 0.02	1
			21	50	0.10	0.10	± 0.01	1
			20	99	0.17	0.17	± 0.02	1
			19	200	0.31	0.32	± 0.03	1
			16	298	0.23	0.24	± 0.02	1
			15	397	0.36	0.37	± 0.04	1
			14	496	0.48	0.49	± 0.05	1
			13	595	0.53	0.54	± 0.05	1
			12	793	0.71	0.73	± 0.07	1
			11	991	0.74	0.76	± 0.07	1
			10	1188	0.78	0.80	± 0.08	1
			9	1386	0.68	0.70	± 0.07	1
			8	1582	0.77	0.79	± 0.08	1
			7	1779	0.78	0.80	± 0.08	1
			6	1975	0.80	0.82	± 0.08	1
			5	2221	0.86	0.88	± 0.09	1
			4	2466	1.13	1.16	± 0.11	3
			3	2955	0.87	0.89	± 0.09	1
			2	3930	0.99	1.01	± 0.10	1
			1	4538	0.99	1.01	± 0.10	1
21	46.544	-19.672	24	19	0.17	0.17	± 0.01	1
			23	30	0.28	0.29	± 0.02	2
			22	49	0.20	0.21	± 0.01	1
			21	79	0.14	0.14	± 0.01	1
			20	99	0.17	0.17	± 0.01	1
			19	198	0.24	0.25	± 0.02	1
			16	297	0.34	0.35	± 0.02	1
			15	397	0.35	0.36	± 0.02	1
			14	496	0.35	0.36	± 0.02	1
			13	594	0.35	0.36	± 0.02	1
			12	693	0.53	0.54	± 0.04	1
			11	792	0.83	0.85	± 0.06	1
			10	989	0.79	0.81	± 0.06	1
			9	1236	0.76	0.78	± 0.05	1
			8	1482	0.74	0.76	± 0.05	1
			7	1976	0.81	0.83	± 0.06	1
			6	2269	0.88	0.90	± 0.06	1
			5	2759	0.70	0.72	± 0.05	1
			4	2955	0.88	0.90	± 0.06	1
			3	3442	0.78	0.80	± 0.05	1

23	48.039	-20.848	2	4417	1.29	1.32	± 0.09	3
			1	4506	0.71	0.73	± 0.05	1
			24	20	0.17	0.17	± 0.01	1
			23	29	0.18	0.18	± 0.01	1
			22	40	0.15	0.15	± 0.01	1
			21	50	0.18	0.18	± 0.01	1
			20	60	0.25	0.26	± 0.02	1
			19	70	0.28	0.29	± 0.02	1
			16	100	0.34	0.35	± 0.02	1
			15	199	0.73	0.75	± 0.05	1
			14	397	0.66	0.68	± 0.05	1
			13	594	0.32	0.33	± 0.02	3
			12	792	0.73	0.75	± 0.05	1
			10	1187	0.65	0.67	± 0.05	1
			9	1384	0.69	0.71	± 0.05	1
			8	1581	0.75	0.77	± 0.05	1
			7	1778	0.70	0.72	± 0.05	1
			6	1974	0.77	0.79	± 0.05	1
			5	2269	0.92	0.94	± 0.06	1
			4	2954	0.79	0.81	± 0.06	1
			3	3443	0.80	0.82	± 0.06	1
			2	3930	0.62	0.64	± 0.04	1
			1	4442	0.75	0.77	± 0.05	1
25	49.529	-22.017	24	14	0.19	0.19	± 0.02	1
			23	25	0.13	0.13	± 0.01	1
			21	49	0.14	0.14	± 0.01	1
			20	74	0.19	0.19	± 0.02	1
			19	99	0.23	0.24	± 0.02	1
			16	198	0.34	0.35	± 0.03	1
			15	346	0.38	0.39	± 0.04	1
			14	495	0.44	0.45	± 0.04	1
			13	643	0.58	0.59	± 0.06	1
			12	792	0.78	0.80	± 0.08	1
			11	990	0.92	0.94	± 0.09	1
			10	1187	0.76	0.78	± 0.08	1
			9	1386	0.87	0.89	± 0.09	1
			8	1580	0.87	0.89	± 0.09	1
			7	1778	0.79	0.81	± 0.08	1
			6	1974	0.87	0.89	± 0.09	1
			5	2563	1.07	1.10	± 0.11	3

26	50.278	-22.603	4	2955	0.84	0.86	± 0.08	1
			3	3441	0.83	0.85	± 0.08	1
			2	3930	1.03	1.06	± 0.10	1
			1	4191	0.69	0.71	± 0.07	1
			22	20	0.18	0.18	± 0.02	1
			21	34	0.15	0.15	± 0.01	1
			20	50	0.15	0.15	± 0.02	1
			19	69	0.15	0.15	± 0.02	1
			18	97	0.18	0.18	± 0.02	1
			17	150	0.43	0.44	± 0.04	1
			16	199	0.39	0.40	± 0.04	1
			15	297	0.57	0.58	± 0.06	1
			14	396	0.62	0.64	± 0.06	1
			13	496	0.82	0.84	± 0.08	1
			12	594	0.80	0.82	± 0.08	1
			11	742	0.76	0.78	± 0.08	1
			10	891	0.74	0.76	± 0.07	1
			9	989	0.83	0.85	± 0.08	1
			8	1186	0.89	0.91	± 0.09	1
			7	1384	0.83	0.85	± 0.08	1
			6	1580	0.92	0.94	± 0.09	1
			5	1974	0.90	0.92	± 0.09	1
			4	2268	0.87	0.89	± 0.09	1
			3	2953	0.75	0.77	± 0.08	1
			2	3929	0.61	0.63	± 0.06	1
			1	4116	0.63	0.65	± 0.06	1
29	53.019	-24.752	22	15	0.17	0.17	± 0.02	1
			21	25	0.75	0.77	± 0.08	2
			20	50	0.66	0.68	± 0.07	2
			19	75	0.52	0.53	± 0.05	1
			18	99	0.64	0.66	± 0.06	1
			17	149	0.71	0.73	± 0.07	1
			16	198	1.14	1.17	± 0.11	1
			15	298	1.02	1.05	± 0.10	1
			14	397	0.98	1.00	± 0.10	1
			13	495	0.95	0.97	± 0.09	1
			11	791	0.98	1.00	± 0.10	1
			10	890	1.10	1.13	± 0.11	1
			9	1087	0.99	1.01	± 0.10	1
			8	1185	0.85	0.87	± 0.09	1

			7	1382	0.92	0.94	± 0.09	1
			6	1581	0.93	0.95	± 0.09	1
			5	1776	0.71	0.73	± 0.07	1
			4	1973	0.65	0.67	± 0.06	1
			3	2464	1.09	1.12	± 0.11	1
			2	2953	0.98	1.00	± 0.10	1
			1	3522	0.69	0.71	± 0.07	1
32	55.506	-26.71	22	16	0.52	0.53	± 0.05	1
			21	26	0.64	0.66	± 0.06	1
			20	51	0.18	0.18	± 0.02	1
			19	101	0.22	0.23	± 0.02	1
			18	198	0.39	0.40	± 0.04	1
			17	298	0.49	0.50	± 0.05	1
			16	376	1.99	2.04	± 0.20	3
			15	446	0.84	0.86	± 0.08	1
			14	596	1.43	1.47	± 0.14	3
			13	691	2.02	2.07	± 0.20	3
			12	793	0.82	0.84	± 0.08	1
			11	990	0.71	0.73	± 0.07	1
			10	1186	0.67	0.69	± 0.07	1
			9	1383	1.08	1.11	± 0.11	2
			8	1532	2.53	2.60	± 0.25	3
			7	1680	1.11	1.14	± 0.11	2
			6	1974	0.92	0.94	± 0.09	1
			5	2218	0.92	0.94	± 0.09	1
			4	2464	0.97	0.99	± 0.10	1
			3	2758	1.02	1.05	± 0.10	1
			2	2952	0.71	0.73	± 0.07	1
			1	3217	0.63	0.65	± 0.06	1
34	57.004	-27.879	22	11	2.23	2.28	± 0.16	3
			21	29	0.54	0.55	± 0.04	1
			20	46	0.28	0.29	± 0.02	1
			19	60	0.53	0.54	± 0.04	1
			18	100	0.55	0.56	± 0.04	1
			17	199	0.85	0.87	± 0.06	1
			16	298	1.06	1.09	± 0.07	1
			15	377	1.01	1.04	± 0.07	1
			14	445	1.13	1.16	± 0.08	1
			13	595	0.83	0.85	± 0.06	1
			12	693	1.01	1.04	± 0.07	1

			11	841	1.15	1.18	± 0.08	1
			9	1186	0.79	0.81	± 0.06	1
			8	1383	0.87	0.89	± 0.06	1
			7	1580	0.80	0.82	± 0.06	1
			6	1777	0.88	0.90	± 0.06	1
			4	2364	1.19	1.22	± 0.08	1
			3	2561	0.91	0.93	± 0.06	1
			2	2562	0.88	0.90	± 0.06	1
			1	2733	0.97	0.99	± 0.07	1
36	58.207	-29.725	20	20	0.12	0.12	± 0.02	1
			19	39	0.09	0.09	± 0.01	1
			18	69	0.15	0.15	± 0.02	1
			16	124	0.19	0.19	± 0.03	1
			14	247	0.28	0.29	± 0.04	1
			12	494	0.69	0.71	± 0.10	1
			10	839	1.61	1.65	± 0.24	2
			8	1204	1.15	1.18	± 0.17	1
			6	1480	0.89	0.91	± 0.13	1
			4	1775	1.23	1.26	± 0.18	1
			2	2212	1.48	1.52	± 0.22	1
38	58.843	-31.267	21	20	0.46	0.47	± 0.07	2
			20	30	0.24	0.25	± 0.04	2
			19	49	0.26	0.27	± 0.04	2
			17	59	0.31	0.32	± 0.05	2
			16	69	0.27	0.28	± 0.04	2
			14	100	0.37	0.38	± 0.06	2
			12	199	0.61	0.63	± 0.09	2
			11	297	0.62	0.64	± 0.09	2
			10	397	0.62	0.64	± 0.09	2
			9	495	0.93	0.95	± 0.14	2
			8	569	0.69	0.71	± 0.10	2
			7	644	0.78	0.80	± 0.12	2
			6	792	0.69	0.71	± 0.10	2
			5	940	1.12	1.15	± 0.17	2
			4	990	1.21	1.24	± 0.18	2
			3	1149	1.08	1.11	± 0.16	2
			2	1285	0.74	0.76	± 0.11	2
			1	1337	1.23	1.26	± 0.19	2
40	59.102	-33.828	22	20	0.38	0.39	± 0.05	1
			20	37	0.56	0.57	± 0.08	1

			18	68	0.66	0.68	± 0.09	1
			16	149	0.84	0.86	± 0.12	1
			14	346	0.89	0.91	± 0.12	1
			12	593	0.95	0.97	± 0.13	1
			10	988	1.19	1.22	± 0.17	1
			8	1282	3.30	3.38	± 0.46	3
			6	1578	2.13	2.18	± 0.30	2
			4	2069	1.37	1.40	± 0.19	1
			2	2273	1.25	1.28	± 0.17	1
42	59.363	-36.397	22	20	0.35	0.36	± 0.05	1
			21	35	0.69	0.71	± 0.10	3
			20	50	0.37	0.38	± 0.05	1
			19	70	0.57	0.58	± 0.08	1
			18	99	0.97	0.99	± 0.14	1
			17	199	0.95	0.97	± 0.13	1
			16	297	0.71	0.73	± 0.10	1
			15	397	0.85	0.87	± 0.12	1
			14	495	0.78	0.80	± 0.11	1
			13	693	0.84	0.86	± 0.12	1
			12	890	1.06	1.09	± 0.15	1
			11	1038	0.82	0.84	± 0.11	1
			10	1186	0.91	0.93	± 0.13	1
			9	1383	1.69	1.73	± 0.24	3
			8	1580	2.39	2.45	± 0.34	3
			7	1777	1.09	1.12	± 0.15	1
			6	1973	1.93	1.98	± 0.27	3
			5	2217	1.27	1.30	± 0.18	1
			4	2462	1.44	1.48	± 0.20	1
			3	2854	1.02	1.05	± 0.14	1
			2	3048	1.64	1.68	± 0.23	1
			1	3078	0.96	0.98	± 0.13	1
44	59.623	-38.954	22	21	1.33	1.37	± 0.13	3
			21	31	0.54	0.55	± 0.05	1
			20	40	0.50	0.51	± 0.05	1
			19	50	1.01	1.04	± 0.10	1
			18	100	1.25	1.28	± 0.12	2
			17	198	0.80	0.82	± 0.08	1
			16	299	0.65	0.67	± 0.06	1
			15	496	2.08	2.13	± 0.21	1
			14	693	0.98	1.00	± 0.10	1

			13	891	1.23	1.26	± 0.12	1
			12	990	0.73	0.75	± 0.07	1
			11	1087	0.96	0.98	± 0.10	1
			10	1236	1.14	1.17	± 0.11	1
			9	1382	1.14	1.17	± 0.11	1
			8	1581	1.25	1.28	± 0.12	1
			7	1776	1.20	1.23	± 0.12	1
			6	1972	1.05	1.08	± 0.11	1
			5	2218	1.70	1.74	± 0.17	2
			4	2560	2.45	2.51	± 0.25	2
			3	2754	1.99	2.04	± 0.20	2
			2	2854	1.14	1.17	± 0.11	1
			1	2915	1.34	1.37	± 0.13	2
49	59.773	-41.297	22	19	0.25	0.26	± 0.02	1
			21	40	0.33	0.34	± 0.02	1
			20	61	0.42	0.43	± 0.03	1
			19	80	0.45	0.46	± 0.03	1
			18	101	0.45	0.46	± 0.03	1
			17	198	0.89	0.91	± 0.06	1
			16	297	0.96	0.98	± 0.07	1
			15	396	1.18	1.21	± 0.08	1
			14	544	1.75	1.80	± 0.12	3
			13	593	1.02	1.05	± 0.07	1
			12	693	0.98	1.00	± 0.07	1
			11	792	1.17	1.20	± 0.08	1
			10	891	0.97	0.99	± 0.07	1
			9	989	1.15	1.18	± 0.08	1
			8	1088	1.78	1.82	± 0.12	3
			7	1235	1.25	1.28	± 0.09	1
			6	1482	1.32	1.35	± 0.09	1
			5	1629	1.53	1.57	± 0.11	1
			4	1776	1.12	1.15	± 0.08	1
			3	1873	1.35	1.38	± 0.09	1
			2	1972	1.26	1.29	± 0.09	1
			1	2022	1.11	1.14	± 0.08	1
53	59.902	-43.015	16	55	1.17	1.20	± 0.12	1
			12	70	1.43	1.47	± 0.14	1
			8	100	1.93	1.98	± 0.19	1
			4	129	1.85	1.90	± 0.19	1
			1	164	2.99	3.06	± 0.30	1

56	59.823	-42.399	22	20	0.85	0.87	±	0.06	1
			20	40	0.50	0.51	±	0.03	1
			16	60	0.55	0.56	±	0.04	1
			14	119	1.84	1.89	±	0.13	3
			10	168	0.29	0.30	±	0.02	1
			6	246	0.33	0.34	±	0.02	1
			2	296	0.42	0.43	±	0.03	1
60	59.799	-42.004	22	19	0.24	0.25	±	0.02	1
			21	28	0.22	0.23	±	0.02	1
			20	38	0.84	0.86	±	0.08	3
			19	59	0.36	0.37	±	0.04	1
			18	77	0.39	0.40	±	0.04	1
			17	99	0.40	0.41	±	0.04	1
			16	149	0.45	0.46	±	0.05	1
			15	199	0.71	0.73	±	0.07	1
			14	248	0.69	0.71	±	0.07	1
			13	297	0.62	0.64	±	0.06	1
			12	345	0.79	0.81	±	0.08	1
			11	445	0.77	0.79	±	0.08	1
			10	543	0.73	0.75	±	0.07	1
			9	642	0.77	0.79	±	0.08	1
			8	741	0.86	0.88	±	0.09	1
			6	938	1.02	1.05	±	0.10	1
			5	1137	1.09	1.12	±	0.11	1
			4	1284	1.04	1.07	±	0.10	1
			3	1480	0.94	0.96	±	0.09	1
			2	1625	1.02	1.05	±	0.10	1
			1	1714	0.98	1.00	±	0.10	1
61	59.753	-45.112	12	23	0.77	0.79	±	0.12	1
			9	50	1.21	1.24	±	0.18	1
			7	70	0.56	0.57	±	0.08	1
			5	100	1.72	1.76	±	0.26	1
			3	120	2.21	2.27	±	0.33	1
			1	137	1.73	1.77	±	0.26	1
63	59.434	-45.666	12	20	0.39	0.40	±	0.03	1
			10	70	1.39	1.43	±	0.10	3
			9	99	0.68	0.70	±	0.05	1
			8	198	0.64	0.66	±	0.04	1
			7	297	0.61	0.63	±	0.04	1
			6	396	0.69	0.71	±	0.05	1

			5	495	0.64	0.66	± 0.05	1
			4	840	0.65	0.67	± 0.05	1
			3	1083	0.71	0.73	± 0.05	1
			2	1284	0.85	0.87	± 0.06	1
			1	1537	0.78	0.80	± 0.05	1
64	59.068	-46.083	22	15	0.30	0.31	± 0.04	1
			21	25	0.22	0.23	± 0.03	1
			20	35	0.26	0.27	± 0.03	1
			19	50	0.40	0.41	± 0.05	1
			18	100	0.70	0.72	± 0.08	1
			17	150	0.78	0.80	± 0.09	1
			16	198	0.79	0.81	± 0.09	1
			15	317	0.89	0.91	± 0.11	1
			14	397	0.85	0.87	± 0.10	1
			13	496	0.79	0.81	± 0.09	1
			12	693	0.81	0.83	± 0.10	1
			11	792	0.75	0.77	± 0.09	1
			10	890	0.95	0.97	± 0.11	1
			9	1038	1.03	1.06	± 0.12	1
			8	1137	0.96	0.98	± 0.11	1
			7	1383	0.93	0.95	± 0.11	1
			6	1580	0.99	1.01	± 0.12	1
			5	1776	0.92	0.94	± 0.11	1
			4	1973	2.10	2.16	± 0.25	3
			3	2120	0.98	1.00	± 0.12	1
			2	2365	0.99	1.01	± 0.12	1
			1	2464	1.05	1.08	± 0.13	1
68	56.916	-47.422	13	20	0.21	0.22	± 0.01	1
			12	29	0.11	0.11	± 0.01	1
			10	35	0.26	0.27	± 0.02	1
			9	50	0.30	0.31	± 0.02	1
			8	100	0.73	0.75	± 0.05	1
			7	345	0.62	0.64	± 0.04	1
			6	891	0.69	0.71	± 0.05	1
			5	1382	0.61	0.63	± 0.04	1
			4	1677	0.71	0.73	± 0.05	1
			3	2463	0.85	0.87	± 0.06	1
			2	3342	0.68	0.70	± 0.05	1
			1	3574	0.68	0.70	± 0.05	1
69	55.842	-48.093	22	14	0.23	0.24	± 0.02	1

			21	26	0.18	0.18	± 0.01	1
			20	30	0.22	0.23	± 0.02	1
			19	40	0.35	0.36	± 0.02	1
			18	60	0.64	0.65	± 0.04	3
			17	90	0.47	0.48	± 0.03	1
			16	128	0.62	0.64	± 0.04	1
			15	178	0.64	0.66	± 0.04	1
			14	495	0.86	0.88	± 0.06	1
			13	792	0.74	0.76	± 0.05	1
			12	1087	1.10	1.13	± 0.08	2
			10	1381	0.79	0.81	± 0.06	1
			9	1580	0.90	0.92	± 0.06	1
			8	1776	0.84	0.86	± 0.06	1
			7	2071	0.78	0.80	± 0.05	1
			6	2365	0.95	0.97	± 0.07	1
			5	2757	0.95	0.97	± 0.07	1
			4	3196	0.76	0.78	± 0.05	1
			3	3440	0.60	0.62	± 0.04	1
			2	3635	0.63	0.65	± 0.04	1
			1	3669	0.61	0.63	± 0.04	1
71	53.692	-49.433	22	20	0.28	0.29	± 0.02	1
			21	30	0.34	0.35	± 0.02	1
			20	40	0.53	0.54	± 0.04	1
			19	50	0.22	0.23	± 0.02	1
			18	60	0.33	0.34	± 0.02	1
			17	100	0.61	0.63	± 0.04	1
			16	149	0.64	0.66	± 0.04	1
			15	248	0.73	0.75	± 0.05	1
			14	347	0.79	0.81	± 0.05	1
			13	496	0.81	0.83	± 0.06	1
			12	792	0.67	0.69	± 0.05	1
			10	1187	0.81	0.83	± 0.06	1
			9	1383	0.84	0.86	± 0.06	1
			8	1678	2.17	2.23	± 0.15	3
			7	1974	0.72	0.74	± 0.05	1
			6	2366	0.78	0.80	± 0.05	1
			5	2709	1.02	1.04	± 0.07	3
			4	2952	0.83	0.85	± 0.06	1
			2	3440	0.68	0.70	± 0.05	1
			1	3689	0.73	0.75	± 0.05	1

77	53	-51.1	22	15	0.28	0.29	±	0.02	1
			21	30	0.26	0.27	±	0.02	1
			20	40	0.31	0.32	±	0.02	1
			19	60	0.55	0.56	±	0.04	1
			18	80	0.56	0.57	±	0.04	1
			17	100	0.77	0.79	±	0.05	1
			16	149	0.90	0.92	±	0.06	1
			15	396	1.21	1.24	±	0.09	2
			14	693	0.96	0.98	±	0.07	1
			13	989	0.83	0.85	±	0.06	1
			12	1088	0.87	0.89	±	0.06	1
			10	1186	0.96	0.98	±	0.07	1
			9	1285	0.95	0.97	±	0.07	1
			8	1482	0.90	0.92	±	0.06	1
			7	1679	0.95	0.97	±	0.07	1
			6	1875	0.92	0.94	±	0.06	1
			5	2072	1.01	1.04	±	0.07	1
			4	2366	0.94	0.96	±	0.07	1
			2	2415	0.93	0.95	±	0.07	1
			1	2506	0.88	0.90	±	0.06	1
78	51.989	-53.817	12	12	0.77	0.79	±	0.05	1
			9	36	1.15	1.18	±	0.08	1
			7	139	2.36	2.42	±	0.17	1
			5	248	4.02	4.12	±	0.28	1
			4	288	3.23	3.31	±	0.23	1
			1	368	7.64	7.83	±	0.53	1

Chapter 4:

Assessment of Nutrient Limitation(s) of Phytoplankton Organisms in the North Atlantic Ocean

Chapter 4: Assessment of nutrient limitation(s) of phytoplankton organisms in the North Atlantic Ocean

Table of Contents

Abstract	210
4.1 Introduction	211
4.2 Material and methods	212
4.3 Results	212
4.3.1 Temporal variability and general pattern of total chlorophyll-<i>a</i> concentrations	212
4.3.2 Hydrological features of the habitat	214
4.3.3 Nutrient concentrations and distributions	215
4.3.4 Phytoplankton size class distributions	219
4.3.5 Phytoplankton functional class distributions	221
4.3.5.1 Phytoplankton functional class concentrations	221
4.3.5.2 Percentage of phytoplankton classes	222
4.4 Discussion	225
4.4.1 Differences of size classes determination by CHEMTAX and Uitz et al. (2006) analysis	225
4.4.2 Potential nutrient limitation	226
4.4.2.1 Relationship between nutrients and organic matter remineralisation	226
4.4.2.2 Using tracers to assess potential limitation	226
4.4.3 Trophic status of regions	229
4.4.4 Statistical correlations of nutrients with physical and biological parameters (CCA) ...	233

<u>4.4.4.1 NASTE province: Eastern West European Basin and Iberian Margin</u>	233
<u>4.4.4.2 NADR province: Western West European Basin and Iceland Basin</u>	243
<u>4.4.4.3 ARCT province (i.e. Irminger and Labrador Seas and Greenland and Newfoundland coastal stations, stations 40-78)</u>	246
<u>4.5 Conclusion</u>	251

Phytoplankton assemblages in the North Atlantic Ocean and in the Labrador Sea (GEOTRACES, GA01) determined by CHEMTAX analysis: Assessment of community structure, succession and potential limitation.

This Chapter is a manuscript in preparation, the corresponding supplementary material is available in Appendix C.

Authors: Manon Tonnard, Anne Donval, Luis Lampert, Paul Tréguer, Hervé Claustre, Celine Dimier, Joséphine Ras, Raphaëlle Sauzède, Lorna Foliot, Andrew R. Bowie, Pier van der Merwe, Hélène Planquette, Géraldine Sarthou

Abstract

This study investigates the size structure and taxonomic composition of the phytoplankton spring bloom in the North Atlantic Ocean and the Labrador Sea along the GEOVIDE section (from 15 May 2014, Lisbon to 30 June 2014, St. John's). An assessment of the main potential limitations in the case of a positive North Atlantic Oscillation index is given as well as the succession of the main phytoplankton classes. Analysis of nutrient disappearance ratios suggested distinct zones in phytoplankton growth control in the study region with the most intense phytoplankton growth limitation south of 50°N. Comparison of macronutrients (NO_3^- , $\text{Si}(\text{OH})_4$) and dissolved iron (DFe) disappearance ratios, nutrient distributions, biomarker pigments used to identify dominating phytoplankton groups with CHEMTAX, photosynthetic:photoprotective pigment ratios and pigment degradation products demonstrated that south of 45°N, the diatom-dominated bloom was overall limited in silicate concentrations and N-(co)-limited closer to the Iberian margin. Between 45 and 50°N, the bloom was dominated by type-8-haptophytes and dinophytes in surface waters, while deeper waters (from 50 to 90 m depth) were dominated by type-8-haptophytes and diatoms. This area exhibited Si and Fe-(co)-limitation. The Iceland Basin bloom was dominated by type-6-haptophytes (i.e. coccolithophorids) and Fe-limited. The Irminger Sea was dominated by diatoms and displayed enhanced nutrient concentrations suggesting a top-down control of phytoplankton growth in this region and/or a light limitation rather than nutrient limitations. The Labrador Sea was potentially light and N-(co)-limited and displayed different community structure south and north of 55°N likely due to freeze-thaw cycling. Although many studies

reported a shift from diatoms to dinophytes due to increasing sea surface temperature, these results suggest that diatom were largely dominating the North Atlantic Ocean especially at high latitudes with the ongoing melting of Arctic ice. The only exception was the Iceland Basin dominated by coccolithophorids. These two classes are both known to enhance carbon export relative to other taxa due to their biomineral skeleton.

4.1 Introduction

Phytoplankton primary production is the principal engine of the biological pump. The biological pump converts aqueous CO₂ in the surface ocean into complex carbon molecules via photosynthesis and exports this fixed carbon into the deep ocean. The efficiency of the biological pump depends on the interplay between physics, chemistry and biology within the euphotic zone (Jochem and Zeitzschel, 1993). In particular, the size structure and taxonomic composition of the phytoplankton community in the open ocean are important factors in regulating sedimentation of algal cells and therefore carbon export (e.g. Bienfang, 1981; Guidi et al., 2009).

Seasonal changes in insolation and heat flux, major hydrographic features such as ocean currents and fronts (Lacour et al., 2017), as well as shorter-lived mesoscale eddies and meteorological events all structure the distribution of phytoplankton assemblages and shape their nutrient uptake across the ocean (d'Ovidio et al., 2010; Garçon et al., 2001; Sambrotto et al., 1993). In turn, the species composition and cell size structure of the phytoplankton assemblages are often characteristic of their immediate environment and its physico-chemical history (Van Oostende et al., 2017), including macro- and micro- nutrient distributions (Timmermans et al., 1998). Furthermore, phytoplankton have adapted to thrive in the range of light regimes (consistently low- or high-light conditions to highly variable conditions) and nutrient regimes (from oligotrophic to mesotrophic) that occur in the ocean.

Establishing the limiting nutrient(s) under different oceanographic conditions, and the causes and nature of such limitation, is thus an important goal for understanding feedbacks between oceanic biota and the environment (Arrigo et al., 2003). Different phytoplankton species and functional groups have different biological requirements for growth (Barcelos E Ramos et al., 2017; Buitenhuis et al., 2008; Saito et al., 2010; Sarthou et al., 2005) leading to differences in intracellular nutrient quota and drawdown (Arrigo et al., 1999; de Baar et al., 1997; Ho et al., 2003; Quigg et al., 2003; Quigg et al., 2011; Twining and Baines, 2013; Twining et al., 2004a). Among the nutrients and bioactive trace metals, iron (Fe) has received

a lot of attention during the past decades. Fe is the most important essential trace element for phytoplankton growth, and per unit of biomass, the plant cell needs more Fe than other trace elements, such as Zn, Mn and Co (Sedwick et al., 1997). In the North Atlantic Ocean, high nutrient low-chlorophyll conditions (HNLC) can occur during the spring to summer period in the Iceland Basin and Irminger Sea (Nielsdóttir et al., 2009; Sanders et al., 2005; Tonnard et al., submitted) likely due to the low Fe concentrations. This spring bloom, which is one of the most intense ones, is also characterised by a succession of phytoplankton groups (Lochte et al., 1993; Sieracki et al., 1993). It is thus the place where the seasonal growth of phytoplankton is the strongest and most variable (Harrison et al., 2013). More recently, Hatun et al., 2017 highlighted the constant decrease of Si-supply since 1990 entering the Atlantic Ocean from the Arctic. Concomitantly, Blais et al., 2017 reported a decrease of the diatom relative to taxa in the Baffin Bay as a result of sea-ice dynamic. It is thus possible that the North Atlantic phytoplankton community will undergo similar shifts as a result of different nutrient stress.

In this context, this paper presents an analysis of the distribution and potential limitation of the phytoplankton spring bloom in the North Atlantic Ocean and the Labrador Sea along the GEOVIDE section (GA01, GEOTRACES, Fig. 4.1A). In particular, we investigate the relationship between the distributions of dissolved nutrients and phytoplankton biomarker pigments, which can be used to infer phytoplankton community composition using the CHEMTAX software. This will help gain further insight into the parameters that potentially control phytoplankton biomass (Fig. 4.1.B), biodiversity, and contribution to carbon export in the upper water column (< 200 m depth).

4.2 Material and methods

(see Chapter 2)

4.3 Results

4.3.1 Temporal variability and general pattern of total Chlorophyll-*a* concentrations

The GEOVIDE voyage spanned three biogeochemical provinces (Longhurst, 2007): 1) the North Atlantic Subtropical East (NASTE) region, including the Iberian Abyssal Plain (stations 1 to 19); 2) the North Atlantic Drift (NADR) region, including the western part of the West European Basin (stations 21 to 26) and the Iceland Basin (stations 29 to 38); 3) the Atlantic Arctic

(ARCT) including the Irminger Sea (stations 40 to 60) and the Labrador Sea (stations 61 to 78) (Fig. 4.1A).

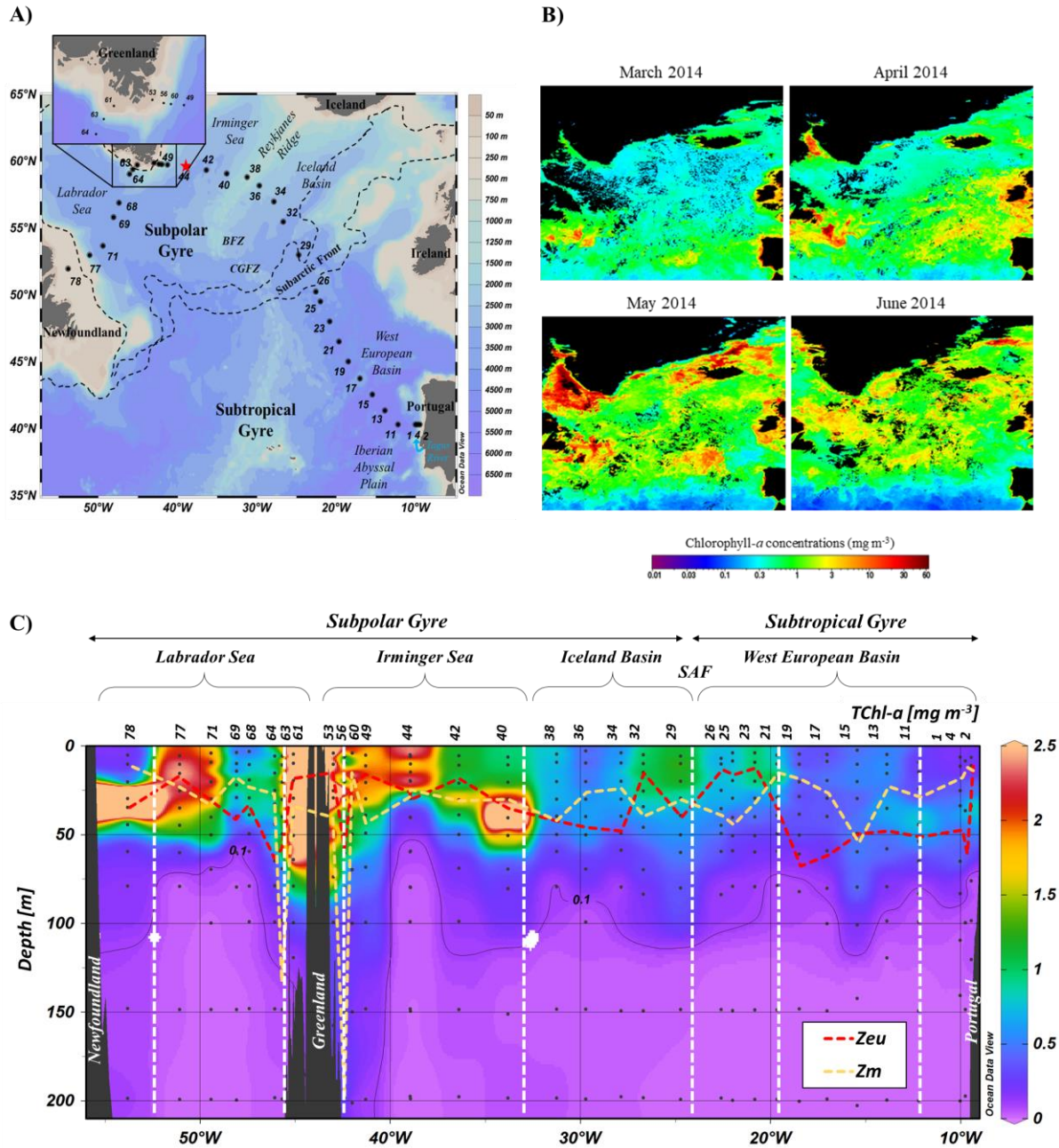


Figure 4.1: A) Map of the GEOTRACES GA01 voyage track plotted on bathymetry as well as the major topographical features and main basins. Crossover station with the GEOTRACES GA02 voyage is shown as a red star. B) Satellite Chlorophyll-a concentrations (MODIS Aqua from <http://oceancolor.gsfc.nasa.gov>), in units of mg m⁻³, before and during the GEOVIDE voyage (from March to June 2014). C) Contour plot of the measured total chlorophyll-a concentrations (TChl-a, mg m⁻³) for the GEOVIDE voyage transect. Red continuous line represents the depth of the euphotic layer (Zeu, m) and the yellow continuous line represent the depth of the mixed layer (Zm, m). Small black dots represent collected water samples at each sampling station. Note that the white dashed lines represent the main subregions.

To visualize the temporal variability of phytoplankton biomasses throughout the sampling period, the MODIS Aqua monthly mean total chlorophyll-*a* (TChl-*a*) concentrations are presented in Figure 4.1B before (March/April, Fig. 4.1B) and at the sampling time (May/June, Fig. 4.1B). Overall, the satellite data showed post-bloom conditions within the NASTE and ARCT biogeochemical provinces while the NADR province exhibited bloom conditions at the sampling period. Indeed, chlorophyll biomasses varied between 0.0024 mg m⁻³ (Station 15) and 9.6 mg m⁻³ (station 78) highlighting the intense variability observed throughout this section (Fig. 4.1C). Surface TChl-*a* concentrations were the lowest in the eastern part of the transect in the West European and the Icelandic basins and more specifically south of the Subarctic Front (0.0024 mg m⁻³ at station 15) while the highest surface (up to 100 m) values were found north of this front more specifically above the Greenland (up to 4.9 and 6.6 mg m⁻³ at station 53 and 61, respectively) and Newfoundland (up to 9.6 mg m⁻³ at station 78) margins.

4.3.2 Hydrological features of the habitat

Overall, temperature and salinity decreased from east to west and from surface to the bottom (except for Greenland and Newfoundland Margin stations). However, note that surface waters from stations 1 to 4 exhibited higher temperatures (up to ~17 °C) and lower salinities (down to 34.9). This feature was attributed to the influence of the Tagus River (e.g. Menzel Barraqueta et al., 2018; Tonnard et al., submitted). Above ~50 m depth, pH was higher (> 7.90, in logarithmic scale) in both the West European Basin and Labrador Sea than in the Iceland Basin and Irminger Sea (Fig. 4.2D). Below ~50 m depth, pH decreased from east to west and ranged from 7.68 (station 78, 138 m depth) to 7.89 (station 11, 80 m depth) (Fig. 4.2D). The O₂ concentrations increased from east to west due to the formation of the Labrador Sea Water (LSW) in the Labrador Sea and to intense mixing during winter in the Irminger Sea. A detailed description of the water masses, obtained through an extended optimum multiple parameter (eOMP) analysis can be found in García-Ibáñez et al. García-Ibáñez et al., (2015; this issue) and their circulation in Daniault et al. (2016).

The shallowest mixed layers ($Z_m < 20$ m) were observed at margin stations (except at station 61 located west of the Greenland coast), at station 21 located within the West European Basin, and at station 69 located in the Labrador Sea (Fig. 4.1C, refer to section 2.4.5 in chapter 2 for a definition of Z_m). The shallowest euphotic layers ($Z_{eu} < 20$ m) were observed at the Iberian margin (station 2), close to the Subarctic front in the West European

Basin (stations 23-26), at station 32 in the Iceland Basin, at stations 42, 49 and 60 in the Irminger Basin and stations 61 and 77 in the Labrador Sea (Fig. 4.1C, refer to section 2.4.5 in chapter 2 for a definition of Z_{eu}). The central West European Basin exhibited the deepest euphotic layers ($Z_{eu} > 50$ m) as well as stations 56 (western Irminger Sea), 63 and 64 (eastern Labrador Sea). Overall, most of the water column was stratified (i.e. $Z_{eu} \geq Z_m$) except for some stations from the West European Basin (stations 23-26), from the Iceland Basin (station 32), from the Irminger Sea (stations 42, 49, 56 and 60) and from the Labrador Sea (station 61 and 63), which was well-mixed (i.e. $Z_{eu} < Z_m$) (Fig. 4.1C).

4.3.3 Nutrient concentrations and distributions

In the following section, $Si(OH)_4$, NO_x (defined as $NO_x = NO_2^- + NO_3^-$), DFe and $NO_x:Si(OH)_4$ distribution and concentrations are described (Figs. 4.3 A-D and 4.4).

NO_x

In the Subtropical Gyre (stations 1-26), NO_x was drawdown to concentrations $< 5 \mu M$ from the surface to ~ 75 m depth. Within the Subpolar Gyre waters located in both the Iceland Basin and Irminger Sea (stations 29 to 56) concentrations began to increase, with NO_x values reaching $\sim 8 \mu mol L^{-1}$. The Greenland margins (stations 53 and 61) and Labrador Sea (stations 63-78) exhibited similar patterns as the Subtropical gyre with very low surface concentrations of NO_x ($< 5 \mu M$) except for stations 63 and 64. The nutricline start of typically varied between 11 m (station 49) and 84 m (station 26) throughout the study region and averaged 55.0 ± 16 , 56 ± 18 , 32.6 ± 17 and 42 ± 8 m depth for the West European Basin (stations 1-26, Subtropical gyre), the Iceland Basin (stations 29-38), the Irminger Sea (stations 40-60, except station 53) and the Labrador Sea (stations 63-78, except station 61), respectively.

Si(OH)₄

$Si(OH)_4$ was strongly depleted to a few $\mu mol L^{-1}$ in the upper 200 m depth of the Subtropical gyre and gradually increased from the Iceland Basin to the Irminger Sea. Greenland margins (stations 56, 53 and 61) also exhibited low $Si(OH)_4$ concentrations ($< 5 \mu M$) down to ~ 50 m depth as well as stations 68 to 77 located in the Labrador Sea. Station 78 located above the Newfoundland Margin showed the highest $Si(OH)_4$ concentrations ($> 10 \mu M$) from the whole section with decreasing concentrations from surface to depth.

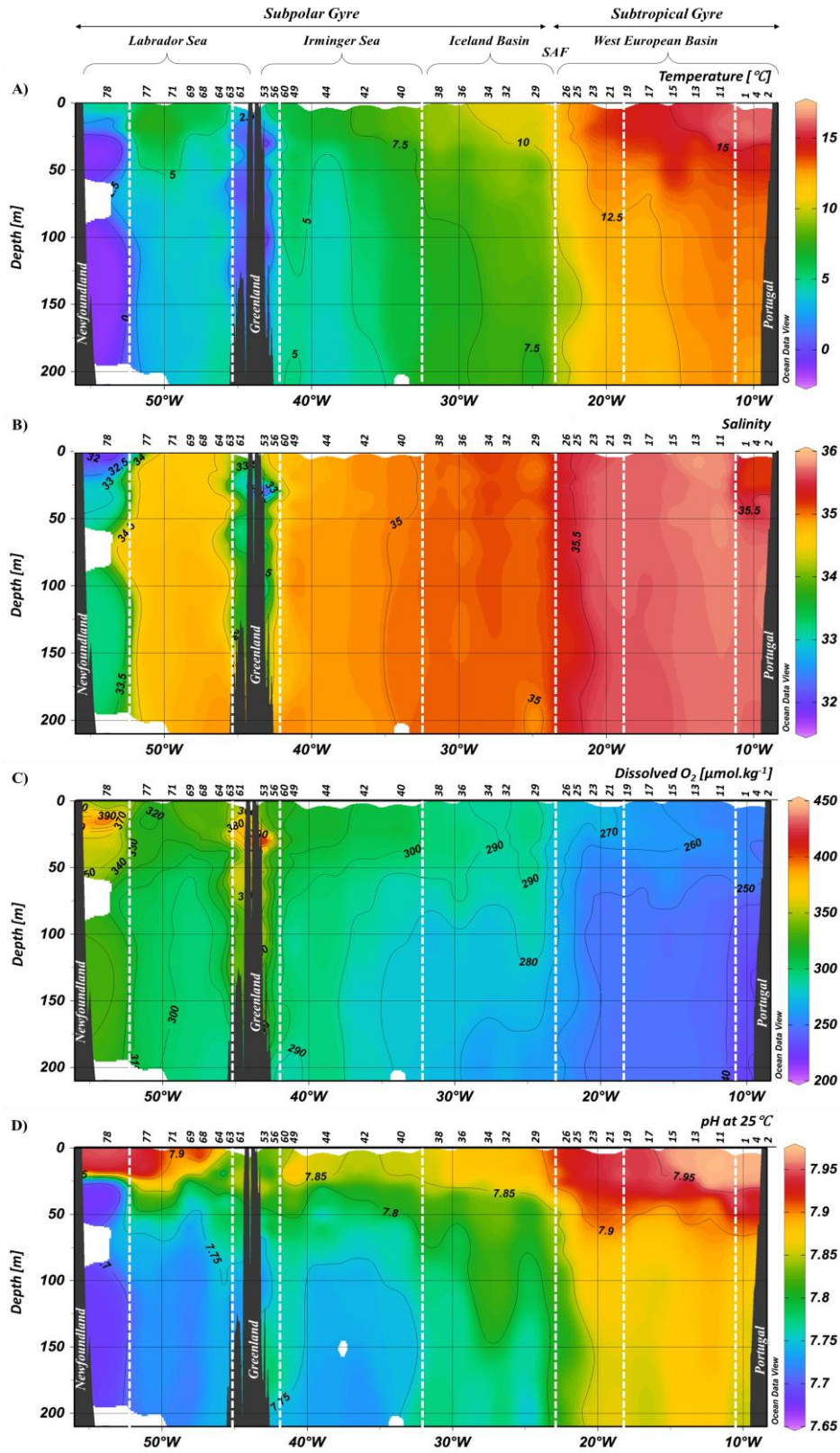


Figure 4.2: The section represents the whole voyage track from station 2 to station 78 (total of 33 stations, note that stations 44 and 46 occupied the same location). Parameters collected from the regular CTD cast: temperature (A), salinity (B), dissolved O₂ (C) and pH at 25°C (D) are represented as a function of depth. Note that the white dashed lines represent the main subregions.

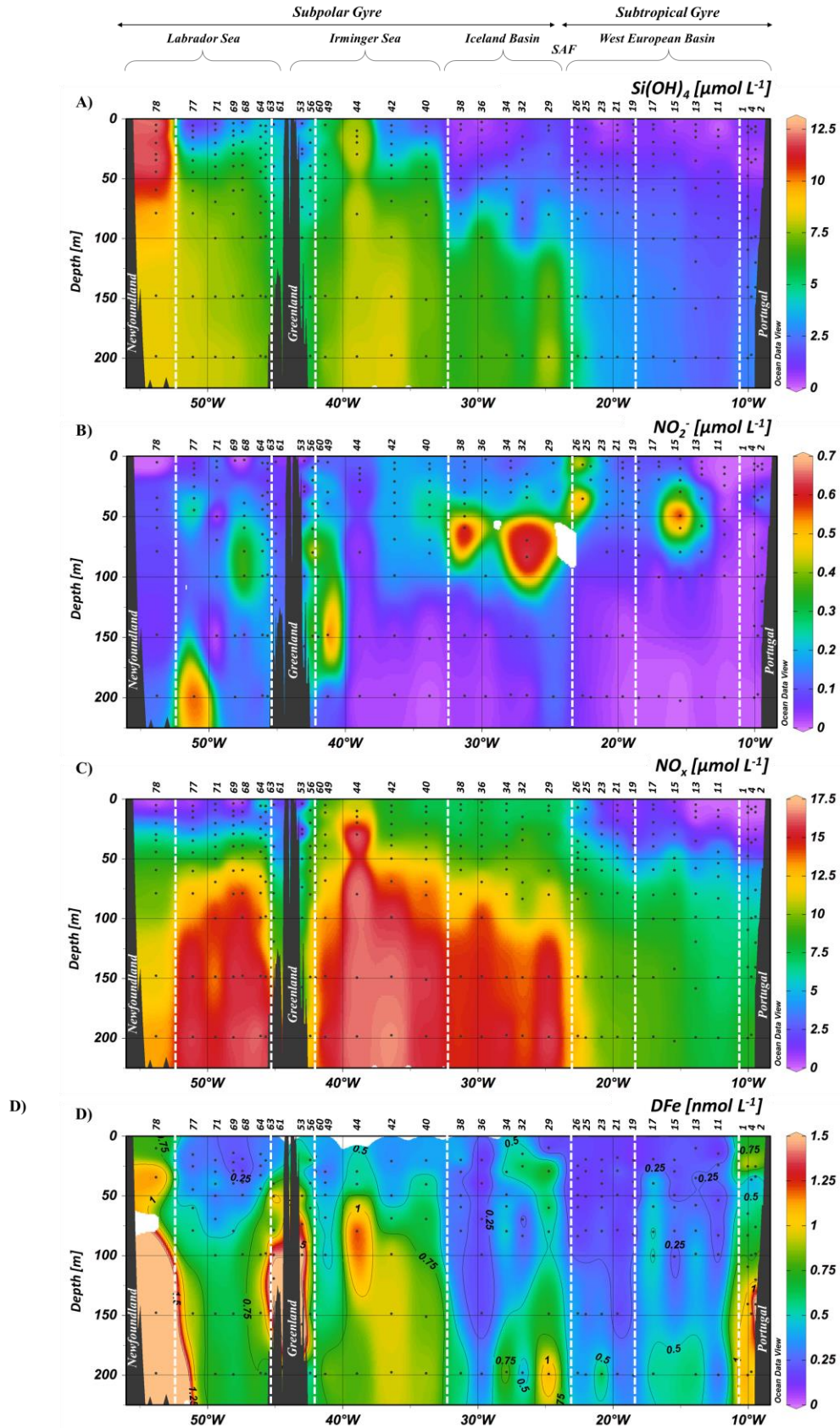


Figure 4.3: The section represents the whole voyage track from station 2 to station 78 (total of 33 stations). Nutrients collected from the regular CTD cast [Si(OH)_4 (A), NO_2^- (B), $\text{NO}_x = \text{NO}_2^- + \text{NO}_3^-$ (C)], and from the Trace Metal Rosette (TMR) cast [DFe (D)] are represented as a function of depth. Note that the white dashed lines represent the main subregions.

DFe

The DFe distribution exhibited similar pattern to that of the NOx distribution in the West European and Iceland Basins, and of Si(OH)₄ distribution within the Irminger and Labrador Seas, where minimum DFe concentrations were 0.09, 0.09, 0.23 and 0.11 nmol L⁻¹, respectively. They averaged 0.27 ± 0.15 nmol L⁻¹ (n = 56) in the West European Basin (stations 11-26), 0.43 ± 0.26 nmol L⁻¹ (n = 28) in the Iceland Basin (stations 29-38), 0.59 ± 0.28 nmol L⁻¹ (n = 34) in the Irminger Sea (stations 40-49 and 60), and 0.46 ± 0.22 nmol L⁻¹ (n = 36) in the Labrador Sea (stations 63-77). Conversely, DFe distribution from the Iberian (stations 1-4, DFe = 0.87 ± 0.61 nmol L⁻¹, n = 17), Greenland (stations 53 and 61, DFe = 1.6 ± 0.8 nmol L⁻¹, n = 9), and Newfoundland (station 78, DFe = 2.1 ± 1.5 nmol L⁻¹, n = 4) margins exhibited very different patterns than observed for macronutrients.

NOx:Si(OH)₄

NOx:Si(OH)₄ ratios (Fig. 4.4) were close to ~ 1 mol mol⁻¹ in surface waters of the Labrador Sea, above margins (Iberian Margin, West and East Greenland Margins and Newfoundland Margin) and in surface waters of the Subtropical gyre (stations 1-13). NOx:Si ratios considerably increased (up to 18.7, station 36, ~ 10 m depth) from surface down to ~ 50 m depth in the Iceland Basin (from stations 34-38). This feature will be discussed in Section 4.4.4.

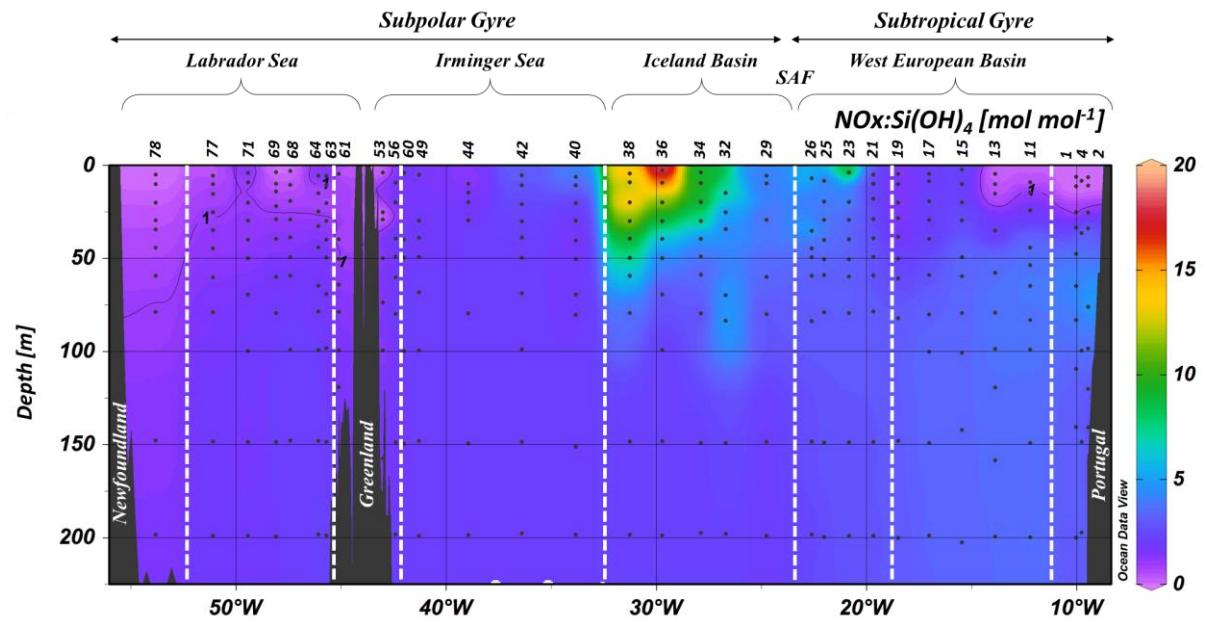


Figure 4.4: Dissolved macronutrient (NOx, Si(OH)₄) ratio (i.e. NOx:Si(OH)₄) as a function of depth. Note that the white dashed lines represent the main subregions.

4.3.4 Phytoplankton size class distributions

Phytoplankton size-class distribution, in terms of both the fraction of the total phytoplankton biomass and TChl-*a* biomass associated to each size class, is presented on Figure 4.5 (A-F).

The Pico-phytoplankton size class (Figs. 4.5A and D), was overall present along the whole transect except at Greenland and Newfoundland Margins. Concentrations higher than 0.1 mg m^{-3} were measured south of the Subarctic Front (SAF) (from stations 2 to 17, down to ~75 m depth), in the western Irminger Sea (from stations 4 to 60, down to 50 m depth) and in surface waters from the central Labrador Sea (from stations 68 to 77, above 25 m depth). In terms of biomass abundance, the pico-phytoplankton community had always the smallest contribution of all main size classes. However, it reached up to 40% of the total biomass south of the SAF (stations 11 and 13).

The Nano-phytoplankton size class (Figs. 4.5B and E), was present in the West European and Iceland Basins as well as in the central Labrador Sea above ~50 m depth. Concentrations were higher than 0.4 mg m^{-3} in the Iceland Basin and Labrador Sea. Nano-phytoplankton explained most of the TChl-*a* concentrations ($> 60\%$ of the total biomass) from stations 29 to 38, down to ~75 m and in surface waters of stations close to and above the Iberian margin (stations 1-4). Despite representing less than 50% of the total biomass in the first 210 metres of the water column from stations 1 to 19 located in the West European Basin, they represented the main size class.

Micro-phytoplankton (Figs. 4.5C and F) presented similar variations to TChl-*a* distribution, highlighting that diatoms and to a lesser extent, dinophytes, were the principal taxa with over 50% of the total biomass, at latitudes greater than 45.5°N of the GEOVIDE section. The exception to this were the surface waters (from 0 to ~75 m depth) of stations 29 to 38 where nano-phytoplankton dominated. Concentrations were higher than 2 mg m^{-3} above ~50 m depth in the Irminger Sea, Labrador Sea and at the Newfoundland margin as well as throughout the full water column of both East and West Greenland margins.

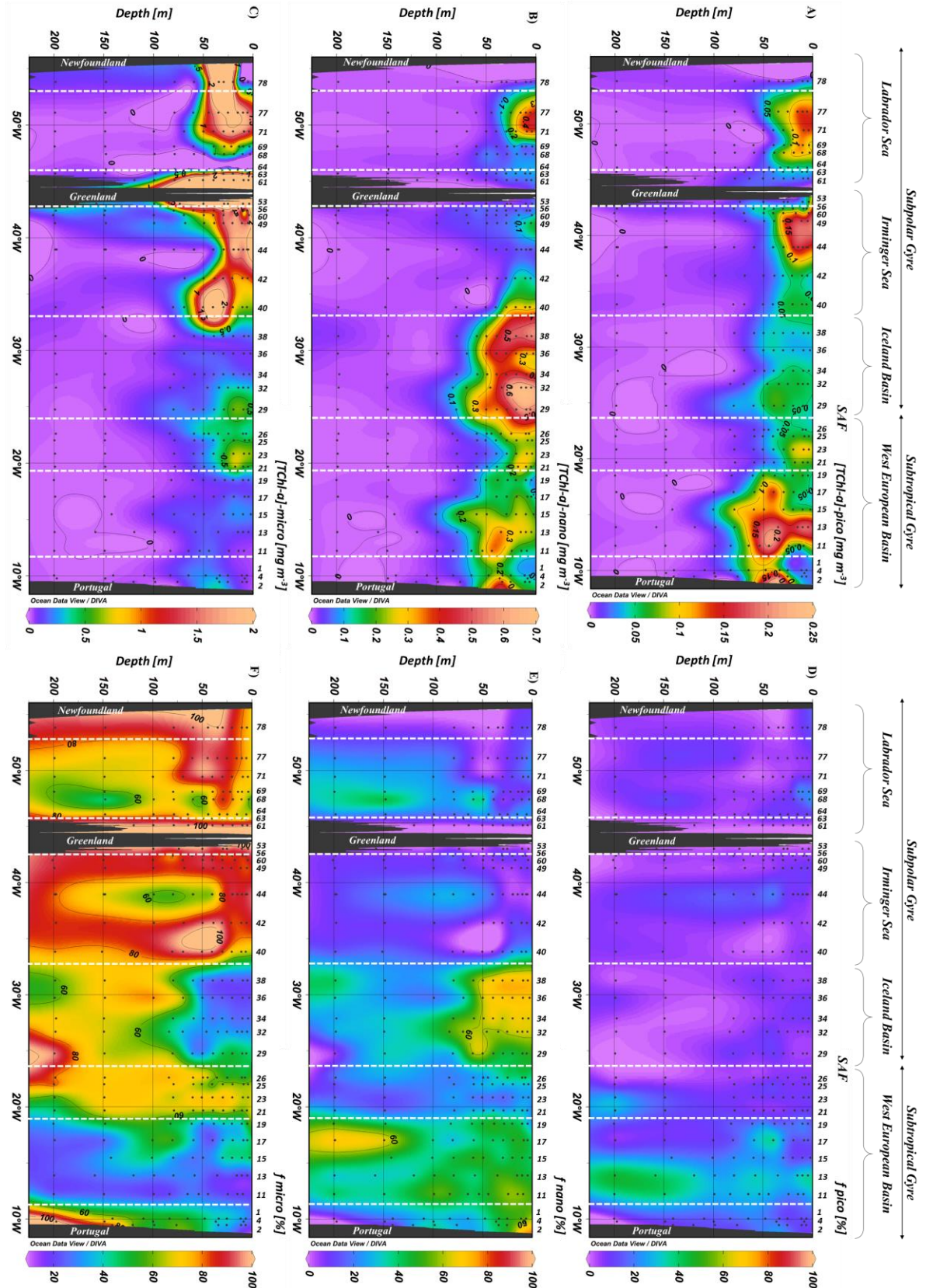


Figure 4.5: GEOVIDE voyage cross sections of in situ TChl-a concentrations in mg m^{-3} (A-C) and percentages (D-F) associated to the pico-, nano-, and micro-phytoplankton size classes using Uitz et al. (2006) formulae. Black dots represent sampling points. Note that the white dashed lines represent the main subregions.

4.3.5 Phytoplankton functional class distributions

4.3.5.1 Phytoplankton functional class concentrations

Taxonomic phytoplankton community composition, determined with CHEMTAX, is presented in Figure 4.6 (A-I) (for section plots see Appendix C3). Overall, diatoms (Fig. 4.6A) were present west of 33.5°W and down to ~100 m depth with concentrations higher than 0.5 mg m⁻³. This taxonomic class reached concentrations higher than 2 mg m⁻³ above margins (East and West Greenland and Newfoundland margins, stations 53, 61 and 78, respectively) with value as high as 9.4 mg m⁻³ at station 78 and at ~30 m depth. Dinophytes (Fig. 4.6B) were located in the western part of the West European Basin (stations 17-26) and Irminger Sea (from station 44 to 56), in the eastern part of the Iceland Basin (station 29 and 32) and in the Labrador Sea (stations 69-78) with concentrations ranging from 0.025 (station 29) to 0.280 (station 23) mg m⁻³ above ~50 m depth. Cyanobacteria (Fig. 4.6C) were mostly detected in the West European Basin, south of the Subarctic Front (stations 1-25), with concentrations as elevated as 0.12 mg m⁻³. Further north, concentrations higher than 0.02 mg m⁻³ were measured in surface waters (above 25 m depth) of the Iceland Basin (stations 34 and 38), Irminger (station 40) and Labrador (stations 68, 69 and 77) Seas, as well as at the Greenland margin (stations 53 and 61) down to 75 m depth. Haptophyte type 6 (Fig. 4.6D) and 8 (Fig. 4.6E) were broadly found above ~75 m depth and everywhere along the transect. To the East of the Greenland margin, either one type or the other was observed, except in the Labrador Sea where both types of haptophytes were cohabiting with substantial concentrations (> 0.3 mg m⁻³). Most of haptophytes type 6 (Fig. 4.6D) were located in the Iceland Basin (stations 29-38) while haptophytes type 8 (Fig. 4.6E) were located in the Irminger Sea (stations 44, 49 and 60). In the West European Basin, lower concentrations (~0.15 mg m⁻³) of both types were measured with haptophytes type 6 located above ~30 m depth and haptophytes type 8 below ~30 m depth. Pelagophytes (Fig. 4.6F) had higher concentrations (> 0.025 mg m⁻³) measured East of 33.5°W and especially in the Iceland Basin (stations 29-38, > 0.1 mg m⁻³). Chlorophytes (Fig. 4.6G) were found East of 34°W (stations 1-40) and in the Labrador Sea (stations 71 and 77) above ~50 m depth, except within the West European Basin (stations 11-17) where they were present down to 100 m depth with concentrations higher than 0.025 mg m⁻³. Prasinophytes (Fig. 4.6H) were detected in surface waters (above 50 depth) throughout the GEOVIDE section (> 0.025 mg m⁻³) except at the East and West Greenland, and Newfoundland margins where concentrations were residual (<

0.01 mg m⁻³) as well as in the top 25 m of stations 2-11 and 15-19 where they were found deeper in the water column down to ~75 m depth. Cryptophytes (Fig. 4.6I) were present from 29.5 to 46.1°W and at station 29, 71 and 77 with concentrations higher than 0.025 mg m⁻³ and broadly above 50 m depth.

4.3.5.2 Percentage of phytoplankton classes

Figure 4.7 displays the percentage of the main phytoplankton taxa averaged per basin and throughout the water column (Fig. 4.7A, for section plots see Appendix C4), as well as averaged per basin and within depth ranges (Fig. 4.7B). In the Subpolar Gyre, the highest percentage of phytoplankton classes was represented by diatoms, except for the Iceland Basin, with almost no variation regarding the distribution of the phytoplankton classes as a function of depth ranges (Fig. 4.7B). Further east of 33.5°W, in the Iceland and West European Basins as well as at the Iberian margin, haptophytes type-6 were the most abundant taxa (Fig. 4.7A). These areas coincided with the highest percentage of Pelagophytes that, conversely to haptophytes type-6 only reached 8-15% from 0 to 100 m depth. Substantial variations between classes were observed east of 33.5°W. Indeed, the percentage of diatoms with respect to other classes was increasing from surface to depth. The opposite trend was observed for the percentage of haptophytes type-6 and cyanobacteria (Fig. 4.7B). Cyanobacteria were mostly present south of the Subarctic front (Fig. 4.7A). Haptophytes type-8 constituted an important fraction of the phytoplankton community in the Labrador Sea. Interestingly, dinophytes only represented an important fraction (8-15%) of the phytoplankton community composition within the West European Basin and above 100 m depth (Fig. 4.7B). Finally, Greenland (East and West) and Newfoundland margins displayed the lowest phytoplankton class diversity (Figs. 4.7A and B). Indeed, diatoms represented from 82 to 96% of the total phytoplankton classes for deep (100-200 m) and surface (0-100 m) waters from Greenland margins and from 64 to 81% for surface (0-25 m) and deeper (100-200 m) waters from the Newfoundland margin.

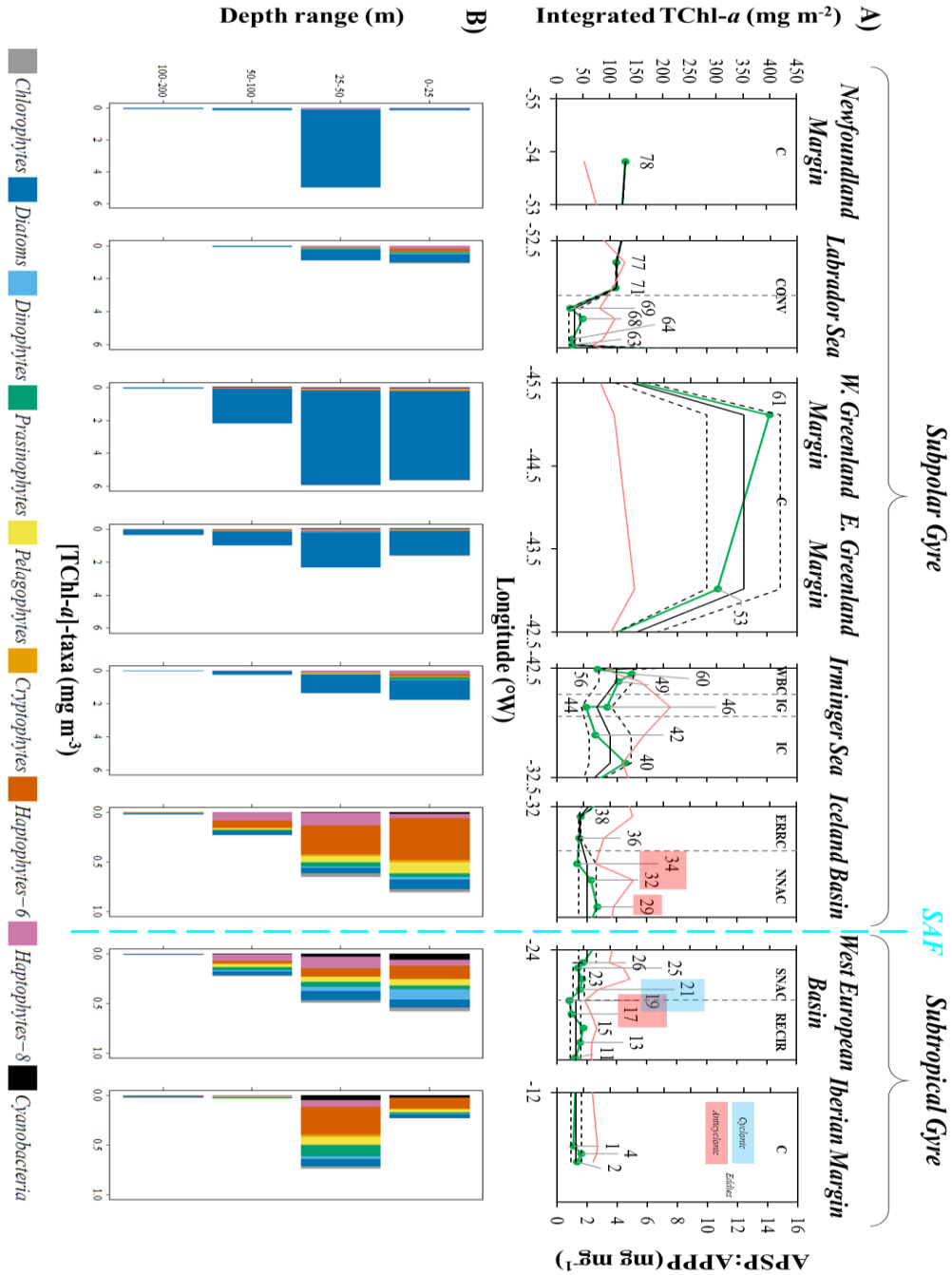


Figure 4.6: A) Plot of integrated total Chlorophyll-*a* (TChl-*a*) concentrations (in green, from 0 to 150 m depth) along the GEOVIDE section. The black continuous and dashed lines correspond to the average and standard deviation of the integrated TChl-*a* concentrations in the limits between the different components crossing the GEOVIDE section (vertical grey dashed lines), i.e. from west to east, Coastal stations (C, include Newfoundland, Greenland and Iberian Margins), Labrador Sea deep convection area (CONV: southern CONV on the left, northern CONV on the right), Western Boundary Current (WBC), Irminger Gyre (IG), Irminger Current (IC), Eastern Reykjanes Ridge Current (ERRC), northern branch of the North Atlantic current (NNAC), Subarctic Front (SAF), southern branch of the North Atlantic Current (SNAC) and the recirculation in the Iberian Abyssal Plain (RECIR). The red and blue rectangles correspond to the location of anti-cyclonic and cyclonic eddies, respectively. Note that numbers correspond to station numbers. B) Stacked bars averaged per basins and depth range (0-25: from 0 to 25, 25-50: from 25 to 50, 50-100: from 50 to 100 m and 100-200: from 100 to 200 m depth) of the concentration of the main phytoplankton classes as determined by CHEMTAX.

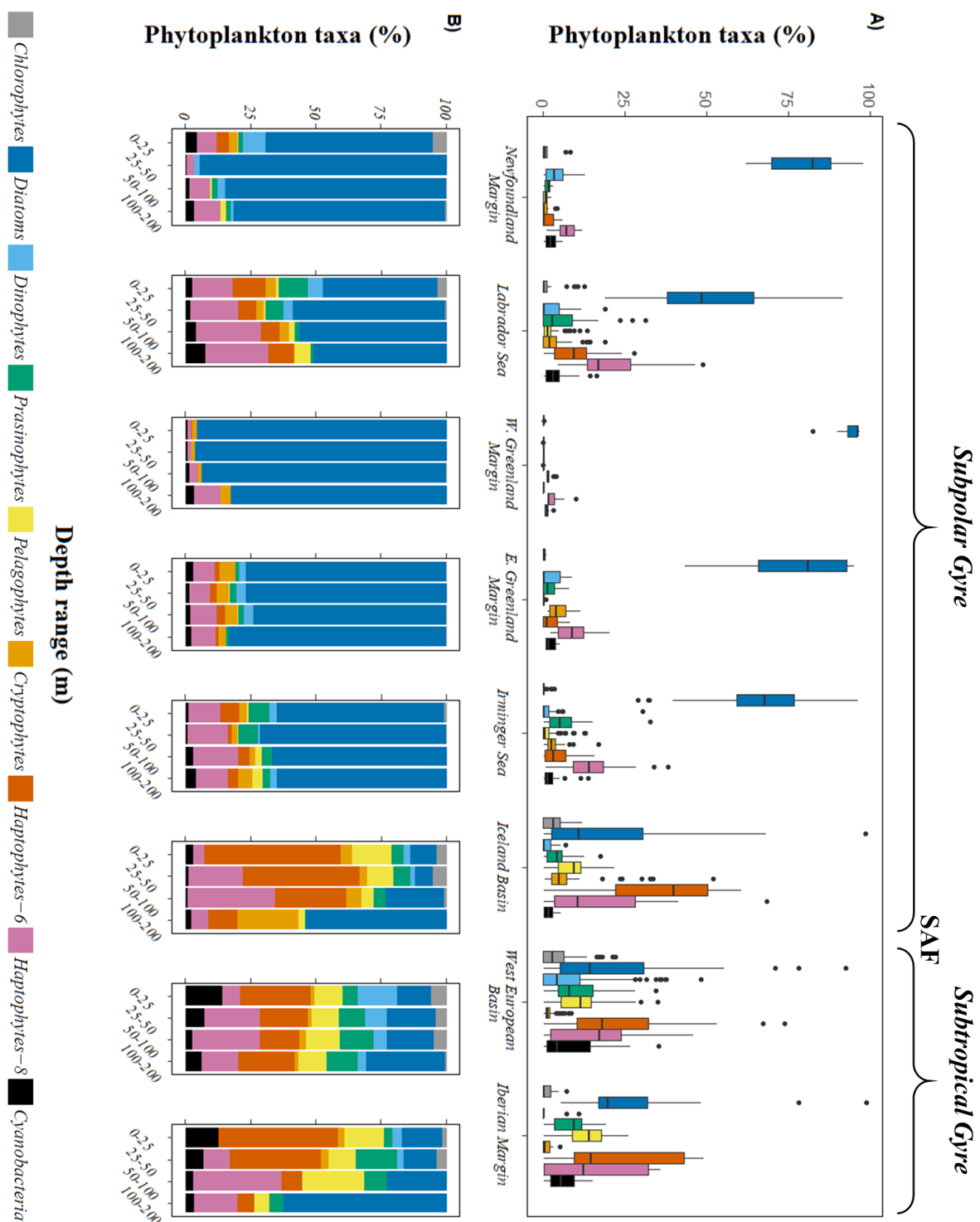


Figure 4.7: Box and whisker diagram averaged per basins (0-200 m depth) (A) and stacked bars averaged per basins and depth range (0-25: from 0 to 25, 25-50: from 25 to 50, 50-100: from 50 to 100 m and 100-200: from 100 to 200 m depth) (B) of the percentage of the main phytoplankton classes as determined by CHEMTAX. Note that the colour coding is common to both plots.

4.4 Discussion

4.4.1 Differences of size classes determination by CHEMTAX and Uitz et al. (2006) analysis

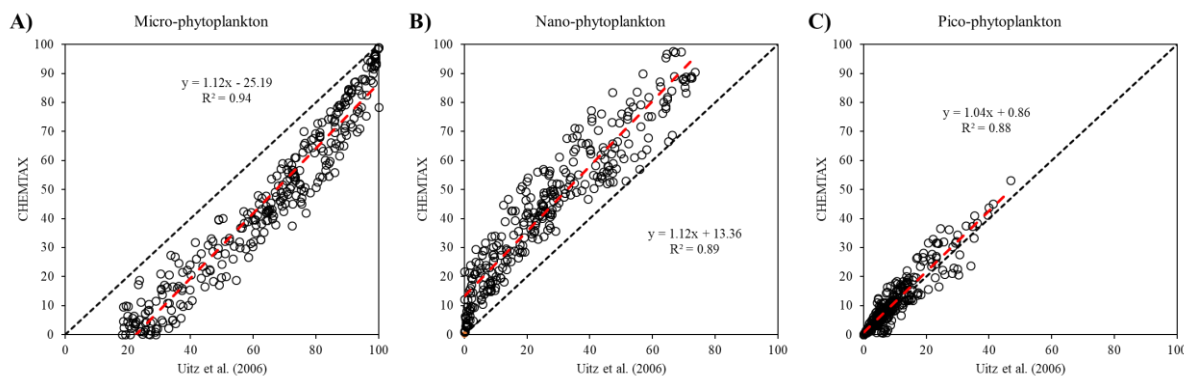


Figure 4.8: Comparison between the phytoplankton size class as determined by CHEMTAX and by Uitz et al. (2006) formulae for the micro-phytoplankton (A), the nano-phytoplankton (B) and the pico-phytoplankton (C). The black dashed represents the 1:1 ratio and the red dashed line represents the linear regression line between the phytoplankton size classes determined by CHEMTAX and by Uitz et al. (2006) formulae.

A comparison between the size classes determined by Uitz et al. (2006) formulae and by CHEMTAX was performed and the results are shown in Figure 4.8. The micro-phytoplankton size class gathered diatoms and dinophytes, the nano-phytoplankton size class was represented by pelagophytes, haptophytes and cryptophytes, while the pico-phytoplankton size class grouped cyanobacteria, chlorophytes and prasinophytes, as determined by CHEMTAX. There was an underestimation of the micro-phytoplankton (Fig. 4.8A) and an overestimation of the nano-phytoplankton (Fig. 4.8B) size classes, when comparing CHEMTAX with Uitz et al. (2006) estimations. Interestingly, differences between the two analyses in the micro-phytoplankton size class were decreasing as their relative abundance compared to other size classes increased. This mismatch can be likely explained by the fact that in the pigment-based formulae all the fucoxanthin was assigned to the diatoms, which was unlikely the case. Indeed, although fucoxanthin has been shown to well represent the diatom community (Barlow et al., 1993; Cupp, 1943; Jeffrey, 1980; Stauber and Jeffrey, 1988), many studies (Bjørnland et al., 1989; Hooks et al., 1988; Uitz et al., 2006; Vidussi et al., 2001; Wright and Jeffrey, 1987) reported the ubiquity of this pigment in many other taxa (e.g. haptophytes and pelagophytes) from the nano-phytoplankton size class, which was the case for our CHEMTAX analysis. Therefore, part of both size class mismatches were likely the result of the attribution of the fucoxanthin pigment to other taxa than just diatoms. However, none of these analyses (i.e. CHEMTAX or Uitz et al. formulae) integrated the fact that diatoms can be present in both micro- and nano-phytoplankton size classes as previously

reported by Hoffman et al. (2008; 2006). This was likely our case as highlighted by the significant correlation between CHEMTAX and Uitz et al. (2006) formulae when nano- and micro-phytoplankton were added ($[\text{nano} + \text{micro}]_{\text{CHEMTAX}} = 1.0 [\text{nano} + \text{micro}]_{\text{Uitz et al. (2006)}} \pm 0.02$, intercept = $-5 \pm 2\%$, $R^2 = 0.88$, p-value < 0.01). Finally, Figure 4.8C shows very good agreement between the two estimations of the pico-phytoplankton size class, due to unambiguous use of the pigments between the two estimates (i.e. TChl-*b* and zeaxanthin).

4.4.2 Potential nutrient limitation

4.4.2.1 Relationship between nutrients and organic matter remineralisation

The remineralisation of organic matter is a major source of macro and micronutrients in subsurface waters. Remineralisation is associated with the consumption of oxygen and therefore, Apparent Oxygen Utilization (AOU), can provide a quantitative estimate of the amount of material that has been remineralized. While no relationship was observed below 50 m depth for NO_3^- or DFe with AOU considering all the stations, a significant correlation was found in the Subpolar Gyre when removing the influence of margins (stations 29-49, 56, 60, 63-77) ($\text{AOU} = 3.88 \text{ NO}_3^- - 39.32$, $R^2=0.79$, $n=69$, p-value < 0.001) (Appendix C5). This correlation indicates that remineralisation of PON directly translates into DIN and that NO_3^- can be used as a good tracer for remineralisation in the studied area. Within these Subpolar gyre waters, there was a significant correlation between DFe and AOU ($\text{AOU} = 22.6 \text{ DFe}$, $R^2=0.34$, $n=53$, p-value < 0.001, Appendix C5). The open-ocean stations from Subpolar gyre also exhibited a good linear correlation between DFe and NO_3^- ($R^2=0.42$, $n=51$, p-value < 0.05, Appendix C5). The slope of the relationship, representing the typical remineralisation ratio, was $R_{\text{Fe:N}} = 0.07 \pm 0.01 \text{ mmol mol}^{-1}$. The intercept of the regression line was $-0.4 \pm 0.2 \text{ nmol L}^{-1}$, reflecting possible excess of preformed NO_3^- compare to DFe in these water masses. The same was concluded between NO_3^- and Si(OH)_4 ($R^2=0.69$, $n=67$, $R_{\text{N:Si}} = 1.11 \pm 0.09 \text{ mol mol}^{-1}$, intercept = $6.5 \pm 0.6 \text{ } \mu\text{mol L}^{-1}$, p-value < 0.001, Appendix C5), highlighting possible excess of preformed NO_3^- compare to Si(OH)_4 in these water masses. These significant correlations allow us to define Si^* and Fe^* tracers.

4.4.2.2 Using tracers to assess potential limitation

Si^* (Sarmiento et al., 2004) and Fe^* (Parekh et al., 2005a) tracers help assess potential limitation of Si(OH)_4 and DFe concentrations in surface waters. They are defined by

subtracting the contribution of organic matter remineralization from the silicate and dissolved Fe pools as follows (Fig. 4.9):

$$Si^* = [Si(OH)_4] - [NO_3^-] \quad (\text{eq. 4})$$

$$Fe^* = [DFe] - R_{Fe:N} \times [NO_3^-] \quad (\text{eq. 5})$$

Where $R_{Fe:N}$ is the average biological uptake ratio of dissolved iron over nitrate. Although in the following, we imposed a fixed biological $R_{Fe:N}$ of $0.05 \text{ mmol mol}^{-1}$, it is important to note that the biological uptake ratio of $DFe:NO_3^-$ is not likely to be constant. Indeed, this ratio has been found to range from 0.05 to 0.9 mmol mol^{-1} depending on species (Ho et al., 2003; Sunda and Huntsman, 1995a; Twining et al., 2004b). The ratio we choose is a conservative indicator of potential Fe limitation and more representative of the average biological uptake of DFe over NO_3^- calculated for this study (i.e. $R_{Fe:N} = 0.07 \pm 0.01 \text{ mmol mol}^{-1}$, for Subpolar waters).

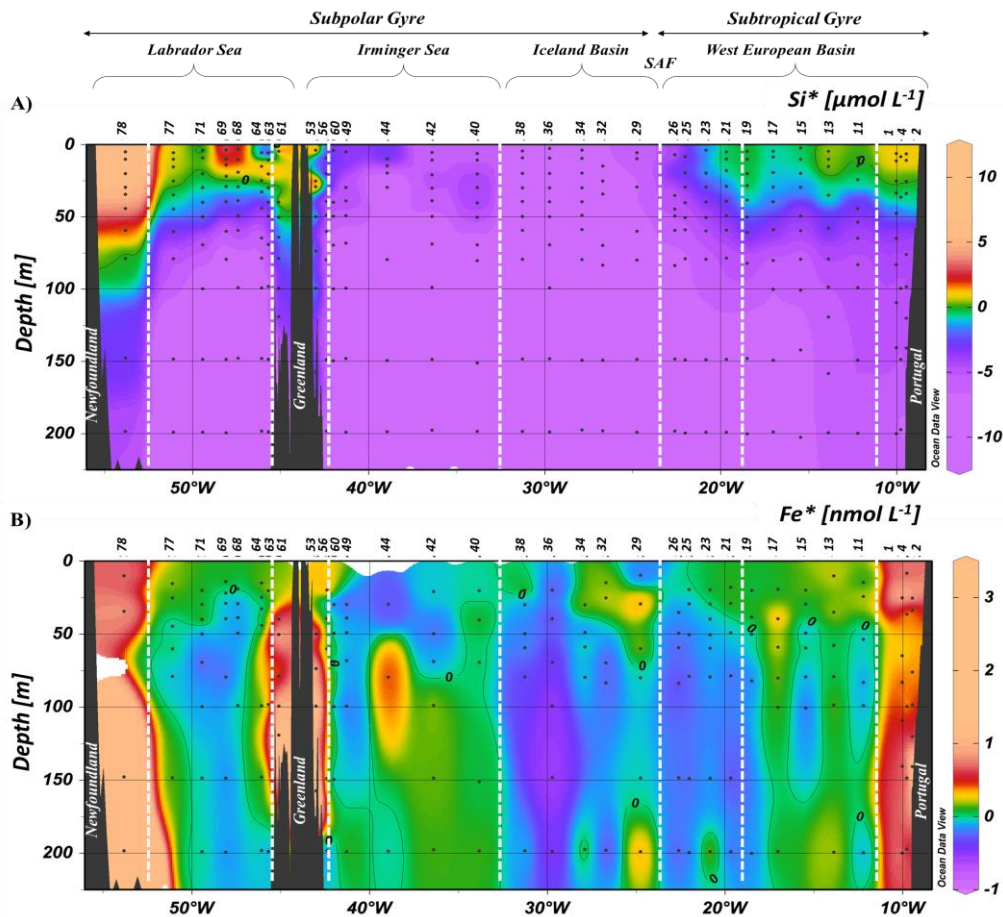


Figure 4.9: Sections of the tracers Si^* (A) and Fe^* (B), as determined by eq. 4 and eq. 5, represented as a function of depth. Negative values indicate potential growth limiting nutrients while positive values indicate an excess of $Si(OH)_4$ or DFe after complete biological uptake of NO_3^- . Note that a contour line of 0 separates areas of negative and positive Si^* and Fe^* . Note that the white dashed lines represent the main subregions.

The Si* tracer

Si* (e.g. Ellwood, 2008; Palter et al., 2010; Sarmiento et al., 2004) as an indicator of nutrient status related to the requirements of diatoms. Diatoms with adequate light and nutrients (including Fe) generally contain Si and N in a mole ratio of 1:1 (Ragueneau et al., 2000), which requires $Si^* > 0$. Also, positive Si* values indicate diatom Si sufficiency, while negative Si* point to diatom growth limitation. Positive values of Si* were found in surface waters (down to ~50 m depth) from the Subtropical Gyre (stations 1, 2, 4, 11 and 13), from the Greenland and Newfoundland Margins and from the Labrador Sea (down to 25 m depth) while negative Si* were observed from stations 15 to 49, 56 and 60 throughout the water column as well as below ~ 50 m depth for other stations. This highlights that besides surface waters of the Iberian, Greenland and Newfoundland margins (above 50 m depth), and of the Labrador Sea (above 25 m depth), diatoms were potentially $Si(OH)_4$ growth limited relative to NO_3^- , especially in the Iceland Basin and Irminger Sea.

The Fe* tracer

Negative values of Fe* potentially indicate growth limiting concentrations of DFe whereas positive values are pointing to an excess of DFe relative to the uptake of NO_3^- , implying enough Fe to support the consumption of NO_3^- (e.g. Blain et al., 2008a; Parekh et al., 2005a; Rijkenberg et al., 2014). Positive Fe* values were found where positive Si* were obtained. Moreover, a similar trend was observed in waters from the central Irminger Sea (below ~50 m depth, stations 40-44), and the Iberian Abyssal Plain (stations 1-19, throughout the water column). The sources of DFe along the GEOVIDE section were detailed by Tonnard et al. (submitted). Briefly, at margins DFe was originating from meteoric water in surface (i.e. from ice melting and precipitation at high latitudes and from the Tagus River at the Iberian margin) and deeper was released from the shelves and in the Irminger Sea was coming from air-sea interaction that entrained the Fe-replete Labrador Sea Water up to the surface. The two main surface areas (above ~ 50 m depth) exhibiting negative Fe* were the Iceland Basin (station 36) and Irminger Sea (stations 40-49), the former extending down to 210 m depth. Similarly, below ~50 m depth, the Labrador Sea (stations 68, 69 and 71), the Iceland (stations 29-38) and part of the West European (stations 11, 15 and 19-26) Basins exhibited negative Fe*.

The negative Si^* and Fe^* could either reflect post bloom conditions or lower supply of Si(OH)_4 and DFe all year round compared to NO_3^- supply in the Irminger Sea and Iceland Basin. Sanders et al. (2005) suggested that, although most NO_3^- was removed from surface seawater of the Subpolar Gyre before end of May, residual levels persisted and were likely the result of a diatom dominated bloom that became Si-limited. Similarly for DFe, Nielsdóttir et al. (2009) highlighted that the postspring bloom was Fe-limited and that the low atmospheric deposition occurring in this remote area were likely the result of this seasonal HNLC condition. These results are further discussed in Section 4.4.4 together with the phytoplankton assemblages.

4.4.3 Trophic status of regions

Knowing the trophic status of an area is of great importance in understanding the fluxes of oceanic particulate material. The fate of large diatoms and dinophytes indeed differs from that of other phytoplankton as they may sink as fast-sedimenting particles, such as copepod faecal pellets or aggregates (Fowler and Knauer, 1986; Guidi et al., 2009; Smetacek, 1985). In the ocean, large phytoplankton species are associated with nutrient replete conditions, whereas small cells dominate in oligotrophic provinces (Chisholm, 1992; Malone et al., 1980). Previous studies (Brewin et al., 2010; Brotas et al., 2013; Claustre, 1994; Uitz et al., 2006) highlighted that the trophic status of an oceanic province can be determined based on phytoplankton pigment signatures considering three indexes: the biomass ratios between micro-phytoplankton, nano-phytoplankton and pico-phytoplankton and the integrated TChl-*a* from 0 to 200 m depth. Indeed, Eppley (1992) and Sanders et al., 2005 reported that high TChl-*a* standing stocks in the ocean generally result from nitrate consumption by phytoplankton and hence serve as evidence for new production. Consequently, diatoms and dinophytes can be identified as the main contributors to new production. In contrast, cyanobacteria, prochlorophytes and small flagellates are most likely involved in systems dominated by regenerated production. Thus, diatoms and/or dinoflagellates are the taxa most suited to take rapid advantages of nitrate availability (Fogg, 1991), whereas small algae are most adapted to survive in impoverished environment.

Figure 4.10 highlights the contrasting relationships between the big size class (Fig. 4.10A) and lower size classes (Fig. 4.10B), with the big size class dominating the population at high Chl-*a* concentrations and lower size classes dominating at low Chl-*a* concentrations, in agreement with previous studies (Claustre, 1994; Sathyendranath et al., 2001). Along the

GEOVIDE transect the pico-phytoplankton size class had lower abundance compared to both micro- and nano-phytoplankton size classes (Fig. 4.10D), unlike previous model simulations, which highlighted that pico-phytoplankton dominates the population at low TChl-*a* (Brewin et al., 2010; Brotas et al., 2013). In our study, low TChl-*a* stations were dominated by nanophytoplankton. Interestingly, some stations showed contrasting trends. In particular, the bulk of the Labrador Sea stations (stations 63, 64, 68 and 69), which presented high fractions of micro-phytoplankton but low TChl-*a* concentrations, stations 29 from the Iceland Basin, which presented a high F_m -ratio but not higher TChl-*a* concentrations compared to other stations in the Iceland Basin, and Iberian margin stations (stations 2 and 4), which presented low integrated TChl-*a* concentrations.

NASTE province

Along the section, the eastern West European Basin (stations 1-19), which is part of the Iberian Abyssal Plain recirculation (RECIR, Fig. 4.7A) region, exhibited the lowest integrated TChl-*a* concentrations ($< 50 \text{ mg m}^{-2}$), and low micronutrient concentrations within the first 50 m of the water column (Fig. 4.3) likely reflecting the end of the spring-bloom (Fig. 4.1) and oligotrophic conditions (Fig. 4.10). Indeed, Lemaître et al. (2017) reported low primary production (PP, A. Roukaerts, D. Fonseca Batista and F. Deman; unpublished data) and low POC export in this region, thus confirming post-bloom conditions and a nutrient limitation of phytoplankton growth. Although the Iberian margin coastal stations displayed low integrated TChl-*a* concentrations, they were shown to be influenced by the Fe-rich Tagus River (Menzel Barraqueta et al., 2018; Tonnard et al., submitted), thus highlighting the limitation of a nutrient other than Fe. This peculiarity is further discussed in Section 4.4.4.1, in which the nutrient concentrations and the phytoplankton assemblages are directly linked via a Canonical Correspondence Analysis (CCA).

NADR province

The western part of the West European Basin and the Iceland Basin (stations 19-38) exhibited intermediate integrated TChl-*a* concentrations (ranging from 24 to 76 mg m^{-2}) and the highest PP (A. Roukaerts, D. Fonseca Batista and F. Deman; unpublished data) from the whole transect (Fig. 4.10). Unlike the NASTE province, this area of the GEOVIDE section reflected the development of the spring bloom (Fig. 4.1, see also Table 4 in Lemaître et al., 2017), which displayed characteristic transition zones located in-between the oligotrophic Subtropical Gyre to the mesotrophic/“eutrophic” Subpolar Gyre (Fig. 4.10). This area

exhibited the intertwining of well-mixed and stratified stations (Fig. 4.1), due to the circulation of the North Atlantic Current (NAC) flowing northeastward between the centre of the Iceland Basin and the Azores-Biscay Rise that was reflected in integrated TChl-*a* concentrations. Indeed, among the different areas of the NADR province, regions of high and low integrated TChl-*a* concentrations succeeded spatially. The northern branch of the NAC (NNAC, stations 29 and 32) displayed the highest integrated TChl-*a* concentrations (76 and 64 mg m⁻², respectively) compared to the southern branch of the NAC (SNAC, stations 19-25, ranging from 24 to 49 mg m⁻²) and to the eastern Reykjanes Ridge current (ERRC, stations 36 and 38, 42 and 45 mg m⁻²) regions. The SNAC region itself, exhibited higher integrated TChl-*a* concentrations than the RECIR region (Fig. 4.6A). This basin was also characterized by very low Si(OH)₄ concentrations (Fig. 4.3A), high NO_x concentrations and as a result, NO_x:Si ratios higher than 1 mol mol⁻¹ (Fig. 4.4), likely reflecting phytoplankton succession with the decline of diatoms (station 29) and the growth of the coccolithophorid community (stations 32-38), taking advantage of low Si conditions.

ARCT province

The ARCT province Stations (40-78), displayed the highest chlorophyllid-*a* concentrations, a tracer of senescent diatom cells, likely reflecting post-bloom condition (Appendix C1). This is in line with the highest POC export data reported by Lemaître et al. (2017). Although the lowest PP rates were reported for stations located in the Labrador Sea (63-69), high PP were reported for stations located in the Irminger Sea (40-60) (A. Roukaerts, D. Fonseca Batista and F. Deman; unpublished data) and to a lesser extent in the western part of the Labrador Sea (station 71-77) at the sampling period. Similarly, very high and low integrated TChl-*a* concentrations were noticed in this province (Fig. 4.6A). The coastal region (C) of the Subpolar gyre, including the Greenland and Newfoundland margins, typically displayed mesotrophic/“eutrophic” status. Although the highest TChl-*a* concentration from the whole transect was measured at the Newfoundland margin, it only concerned one depth (i.e. ~30 m depth) associated with a strong brine signal (Tonnard et al., submitted) thus likely explaining the substantially lower integrated TChl-*a* concentrations compared to the Greenland margins. The Irminger Current (IC) and Western Boundary Current (WBC) regions displayed the second highest maximum of the integrated TChl-*a* concentrations over the full section (after the C region) while, in the Irminger Gyre (IG) region lower integrated TChl-*a* concentrations were found (Fig. 4.6A). Similarly, the

Labrador Sea Water convection (CONV) region was separated in two subregions, with a northern minimum and a southern maximum (Fig. 4.6A). Although the peak of the spring bloom occurred in May, prior to sample these areas, the subregion differences with regard to the integrated TChl-*a* concentrations and trophic status were likely explained by different initiation of the bloom-timing as depicted in Figure 4.1. The first areas to bloom corresponded to regions impacted by freeze-thaw cycling, with a bloom corresponding to the melting of the sea-ice cover (cf. <http://nsidc.org/soac/sea-ice.html#seaice>, May vs. June 2014), while the bloom in other areas, seemed to be coupled to the water column stratification as depicted in Figure 4.1 with the progressive deepening of the Z_{eu} from east to west in the Labrador Sea.

It thus appears that the differences in the trophic status throughout the GEOVIDE section were directly linked to the broad circulation. This could be the result of nutrient supply from specific water masses, the turbulent regime or the relaxing of light limitation.

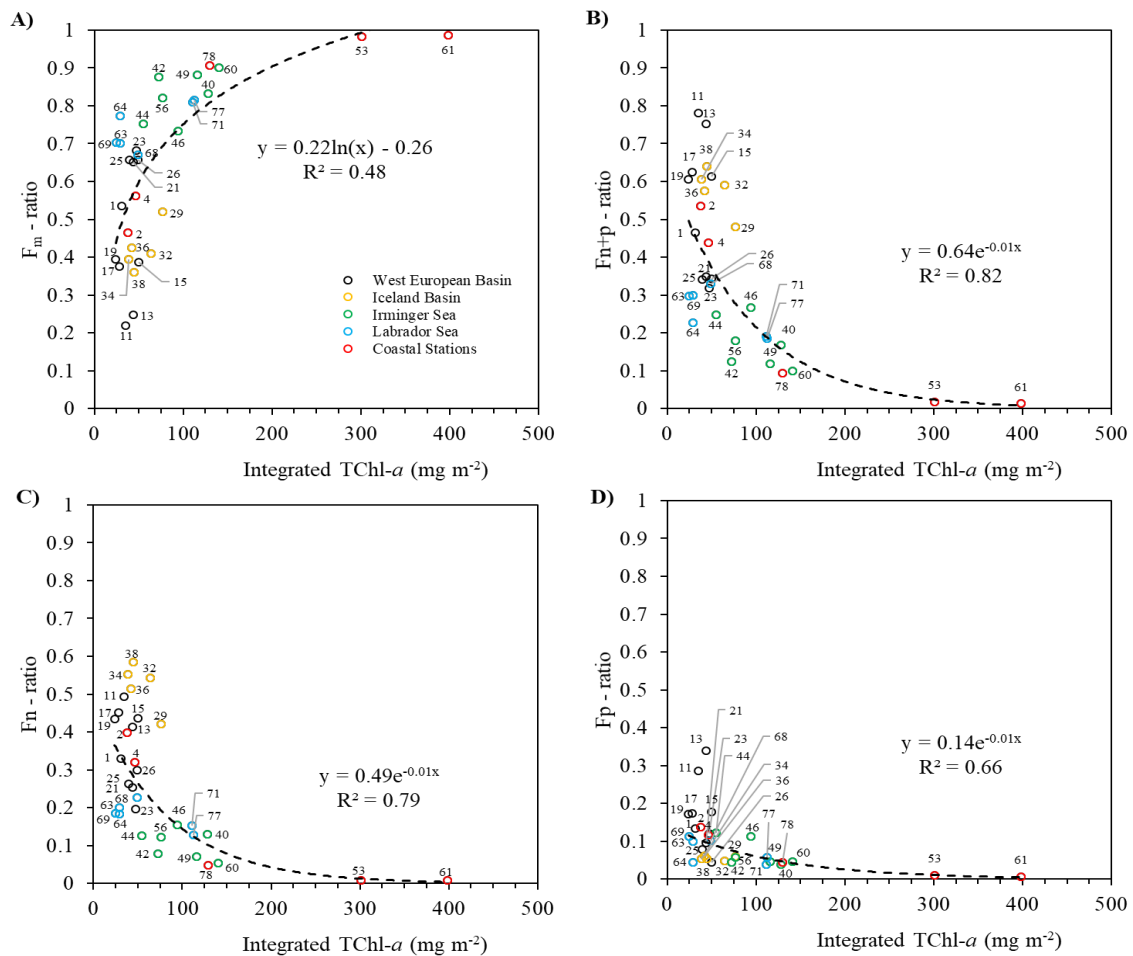


Figure 4.10: Relationship between the Chl-*a* concentration integrated from 0 to 150 m depth and the fraction of A) micro-phytoplankton, B) nano- and pico-phytoplankton, C) nano-phytoplankton and D) pico-phytoplankton.

4.4.4 Statistical correlations of nutrients with physical and biological parameters (CCA)

In the following sections, to understand phytoplankton succession and their potential limitations, different Canonical Correspondence Analyses (CCA) constraining phytoplankton classes determined by CHEMTAX by significant environmental variables (i.e. physical or chemical) were performed. The significant variables (see Chapter 2 for variable selection) are depicted in Figure 4.11 as well as the Pearson correlation coefficients between each selected variable and the associated p-value. To refine the readability of the results, they followed a first CCA whose aim was to gather broadly stations with similar nutrient patterns constrained by physical (salinity, temperature and pH) and biological (micro-, nano- and pico-phytoplankton fractions) variables. Three groups were determined and corresponded to the NASTE (stations 1-19), NADR (stations 19-38) and ARCT (stations 40-78) regions delineating the Subtropical Gyre from the meandering branches of the NAC to the Subpolar Gyre (see Appendix B6).

4.4.4.1 NASTE province: Eastern West European Basin and Iberian Margin

The CCA performed on stations located in the eastern part of the West European Basin and above 90 m depth (stations 1-19, n=26) explained 53 % of the variance with NO_3^- , z:Z_{eu} , Fe^* and temperature (p-values < 0.05) as well as Si^* variables (Fig. 4.11A, Appendix C6). Si^* was not significant in the model ANOVA-tested (Appendix C6) prior to run the CCA as the variance contained in this parameter was already explained by NO_3^- distribution ($r = -0.99$, p-value < 0.001) but was left for graphic interpretation. Dinophytes and cryptophytes phytoplankton classes were removed from the analysis as their respective abundance in this area never reached 10% and because they were more abundant in other basins.

Linking nutrient and phytoplankton classes from the NASTE province

Diatoms

At the sampling period, Diatoms were located at depths where DFe was in excess of NO_3^- as indicated with the significant positive correlation (Fig. 4.11A) between diatoms and Fe^* . Although they were not significantly correlated with the z:Z_{eu} variable (Fig. 4.11A), the lack of correlation likely emphasized that they were only present in deep samples.

Cyanobacteria and type-6 haptophytes

Surface waters from the euphotic layer ($\sim > 35$ m depth) were characterized by substantial abundances of cyanobacteria and type-6-haptophytes (i.e. Coccolithophorids). They were strongly negatively correlated to low NO_3^- concentrations and positively to both Si^* and temperature (Fig. 4.11A). However, type-6-haptophytes were only present at depth where positive Fe^* were calculated (i.e. close to the Iberian Margin). This suggests that the cyanobacteria present in these waters were diazotroph, which was confirmed by the intense N_2 -fixation rates reported by Fonseca Batista et al. (2018) at the Iberian Margin and in the eastern part of the West European Basin. While it is well known that diazotroph cyanobacteria are the main competitor in case of N-limitation (e.g. Schindler, 1977), it is very unlikely that type-6-haptophytes could benefit from such condition (Riegman et al., 2000). Indeed, type-6-haptophytes have been shown to be poor competitors for nitrate in case of N-limitation in comparison with other algae (Riegman et al., 1992; Rost and Riebesell, 2004) mostly due to their fairly low maximum uptake rate and a half-saturation constant similar or higher than those of other algae ($\sim 0.2 \mu\text{mol L}^{-1}$, Page et al., 1999). However, they have been shown to conserve high growth rate in very low N environment as a result of flexible nitrate uptake rate (Paasche, 1998; Riegman et al., 2000). The N-limited cells are smaller and overproduce coccoliths that contains 50% less organic and inorganic carbon (Muller et al., 2017) and 20% less Ca (Paasche, 1998). Such N-limitation conditions were reported to increase organic carbon (POC) fixation (Leonardos and Geider, 2005), likely resulting in enhanced POC export and higher remineralisation rates due to their inability to sink as fast as in the case of non-limiting nutrient. This would be incompatible with POC export and remineralisation rate measured during this study by Lemaître et al. (2017), as the authors reported low POC export and moderate remineralisation rate.

Another explanation of the concomitance of both cyanobacteria and type-6-haptophytes would be that they benefited from each other's presence. Indeed, Thompson et al. (2012) and Cabello et al. (2016) reported a symbiotic association between a N_2 -fixing cyanobacterium (UCYN-A) and a unicellular prymnesiophyte (e.g. *Emiliania huxleyi*). The cyanobacterium providing fixed N to the prymnesiophyte, which, in return, provides fixed C to UCYN-A, avoiding any limitation. This explanation would be more consistent with the POC remineralisation rates and export fluxes reported by Lemaître et al. (2017). An unresolved feature is the lack of correlation between cyanobacteria and Fe^* (Fig. 4.11A): previous studies (Moore et al., 2009; Sohm et al., 2011) reported that Fe-limitation controls

cyanobacterial diazotrophs distribution. Indeed, cell requirement for Fe was reported to be greater for diazotroph compared to non-diazotroph, given the requirements of the nitrogenase enzyme complex (Berman-Frank et al., 2001; Kustka et al., 2003; Raven, 1988; Rueter et al., 1992).

Type-8 haptophytes

Type-8-haptophytes were located deeper in the water column, at the depth of the euphotic layer or below, compromising between high NO_3^- concentrations and light availability (Fig. 4.11A). Riegman and Van Boekel (1996) and Schoemann et al. (2005) reported large fluctuations of the light adaptation coefficient E_k (i.e. ranging from ~ 5 to $150 \mu\text{mol quanta m}^{-2} \text{ s}^{-1}$) of type-8-haptophytes (i.e. *Phaeocystis globosa* and *P. pouchetii*), therefore highlighting their good adaptation to low light compared to other algal species. In our study, this area displayed the lowest concentrations of Phaeophorbide *a* and Phaeophytin *a*, two pigments contained within grazor faecal pellets (Ras et al., 2008), thus increasing the likelihood of the colonial form. Interestingly, type-8-haptophytes were significantly negatively correlated with Si^* (Fig. 4.11A). This suggests that they were not able to compete with diatoms when nutrient conditions were favourable for the latter. If *Phaeocystis* is able to grow faster than other algae when irradiance is low and when N and P are non-limiting (Hegarty and Villareal, 1998) or is more competitive than other phytoplankters to utilize NO_3^- as nitrogen source (Lancelot, 1995), they are not able to dominate the phytoplankton community, unless silicate concentrations are depleted (Egge and Aksnes, 1992), in which case they have been shown to dominate after a bloom of either diatoms or *Emiliania huxleyi*, thus supporting our results.

Chlorophytes, pelagophytes and prasinophytes

Finally, it seemed that chlorophytes, pelagophytes and prasinophytes were located in areas where the above-mentioned phytoplankton classes were limited by at least one parameter (i.e. N and Si for diatoms for haptophytes type 8, Hegarty and Villareal, 1998, Fe for cyanobacteria), as no significant correlation was observed between these classes and environment variables.

Nutrient drawdown and diatoms

The winter nutrient inventories (Fig. 4.12) were not estimated from the winter mixed layer depths reported by Zunino et al. (2017) as the subtropical gyre of the North Atlantic Ocean also undergoes Ekman downwelling with an associated export of nutrient out of the euphotic zone (Oschlies, 2002), which would lead to an overestimation of the winter stocks. Instead, we used the NO_3^- (3-4.5 $\mu\text{mol L}^{-1}$) and Si(OH)_4 (1.6-2.5 $\mu\text{mol L}^{-1}$) concentrations reported for winter surface waters by Leblanc (2005), which were 2 to 3 and 1 to 2 times lower than that at the base of the winter mixed layer depths reported by Zunino et al. (2017) for our study (i.e. 5.9-14.1 and 1.5-5.7 $\mu\text{mol L}^{-1}$, respectively). Therefore, to calculate winter nutrient inventories we integrated the nutrient from surface to the depth at which NO_3^- was $\sim 4.5 \mu\text{mol L}^{-1}$.

Within the NASTE province, NO_3^- and Si fractional drawdown varied from 23 (station 17) to 59% (station 1) and from 10 (station 17) to 36% (station 1), respectively (Fig. 4.12A). NO_3^- :Si ratios ranged from 3.0 (station 15) to 4.2 (station 1) mol mol^{-1} (Fig. 4.12B). Considering only the spring mixed layer stock, calculated from the density profiles, NO_3^- and Si fractional drawdown increased to almost 1 at all stations, except station 15 (Fig. 4.12C) with NO_3^- :Si ratios ranging from 3.2 (station 15) to 5.8 (station 1) mol mol^{-1} (Fig. 4.12D). Although Diatoms were not the dominant phytoplankton class at the sampling period (i.e. never exceed 20% above 75 m depth), the quasi-concomitant Si(OH)_4 and NO_3^- depletion, suggests that they were dominant in the early stage of the spring bloom. This is in agreement with previous studies that reported diatoms dominate both the first stage and the peak of the bloom (Barlow et al., 1993; Cáceres et al., 2017; Lochte et al., 1993; Sieracki et al., 1993). Therefore, diatoms were likely the main contributors of the nutrient drawdown. The eastern part of the West European Basin was largely depleted in NO_3^- and Si(OH)_4 especially for samples located above the Z_{eu} (4.1 and 4.3), with NO_x : Si(OH)_4 ratios much higher than 2 mol mol^{-1} (Fig. 4.4), highlighting a strong depletion in Si(OH)_4 concentrations relative to NO_x (see also Fig. 4.9A). Conversely, it seems that this part of the section was not limited in DFe as highlighted by overall, positive Fe^* (Fig. 4.9B). Therefore, diatoms decline was likely the result of Si-limitation, unless a micronutrient, other than DFe was more limiting than Si(OH)_4 (e.g. Zn, Lohan et al., 2002).

However, within the top 25 m depth of the water column from stations 1-13 where NO_x : Si(OH)_4 ratios were very close to the diatom optimum uptake rate (i.e. $\sim 1 \text{ mol mol}^{-1}$, Ragueneau et al., 2000), diatom abundance was very low. These stations displayed very low

Si(OH)₄ concentrations ($< 1 \mu\text{mol L}^{-1}$). Such low Si(OH)₄ concentrations were previously reported as limiting diatom growth (Brzezinski et al., 2005; Coale et al., 2004), as it is less than K_s (half-saturation constant of nutrient uptake) for Si(OH)₄ reported for laboratory-cultured diatoms (Paasche, 1973) but displayed nevertheless positive Si*. Similarly, Fe showed positive Fe* ($\sim 1 \text{ nmol L}^{-1}$) and was consequently not limiting phytoplankton growth, further supported by the high NO_x:Si ratios (Fig. 4.12B), as in case of Fe-limitation, this ratio was reported to decrease below its optimal value of 1:1 mol mol⁻¹ (Hutchins and Bruland, 1998; Takeda, 1998). Conversely, these surface waters exhibited residual NO₃⁻ concentrations ($< 0.1 \mu\text{mol L}^{-1}$) that were likely limiting diatom growth, as they were lower than the K_s of NO₃⁻ for most cultured diatom species (Eppley et al., 1969).

Interestingly, NO₃⁻:Si(OH)₄ ratios were slightly decreasing from coastal (stations 1-13) to more open-ocean stations (stations 15-19), potentially due to lower DFe supply. This would be in agreement with the DFe supply at the Iberian Margin from the Tagus River as reported by Tonnard et al. (submitted) enabling high DFe values even after the diatom bloom, likely highlighting its constant supply. On the other hand, it could also indicate a higher proportion of non-siliceous species from stations 1 to 13 than from stations 15 to 19.

In summary, surface waters from the eastern part of the West European Basin, including the Iberian margin, was separated in two sub-regions displaying nutrient limitation as follow: Si > N limitation for stations 1-13 and Fe > N / Si limitation for stations 15-19, due to the diatom bloom that occurred before the GEOVIDE voyage that lead to the predominance of both cyanobacteria and type-6-haptophytes, taking advantage of the nutrient limitation of diatoms.

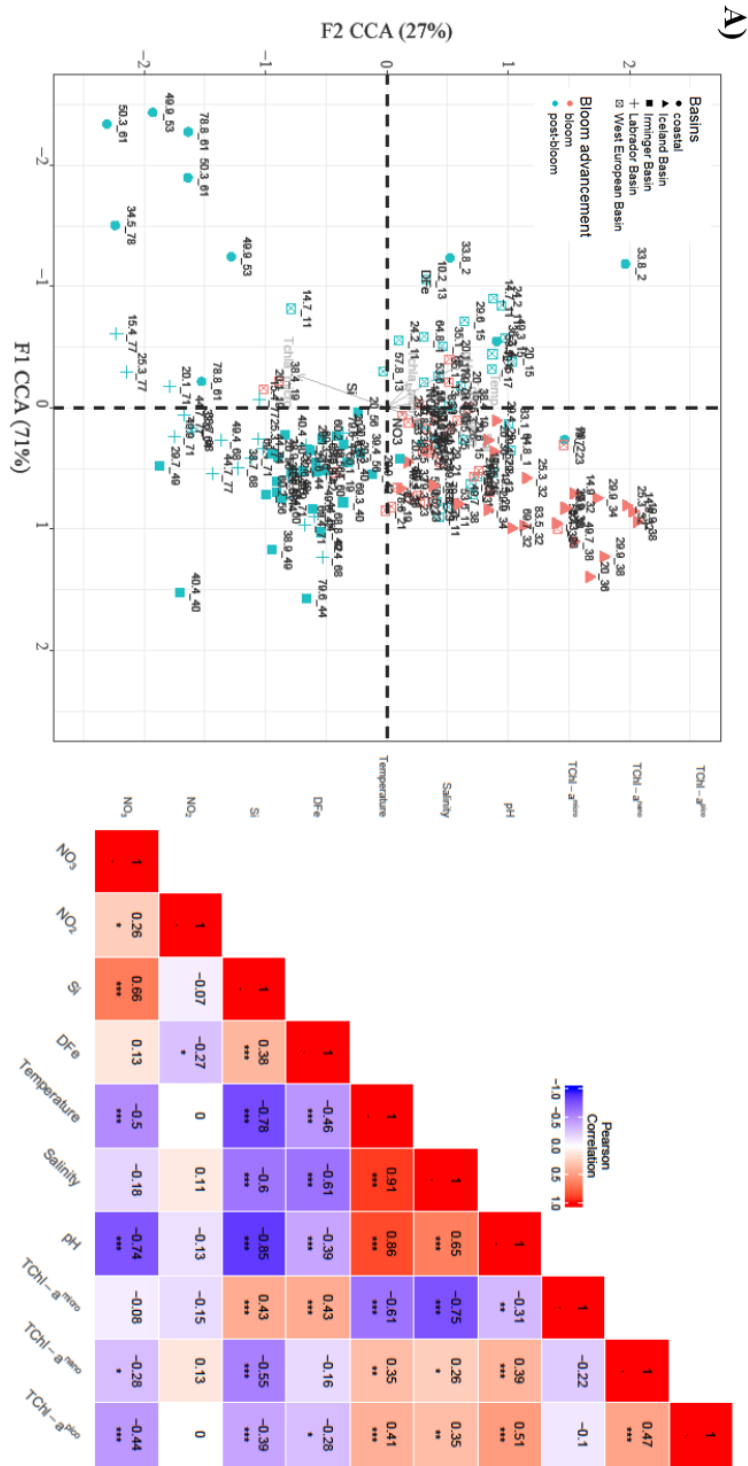
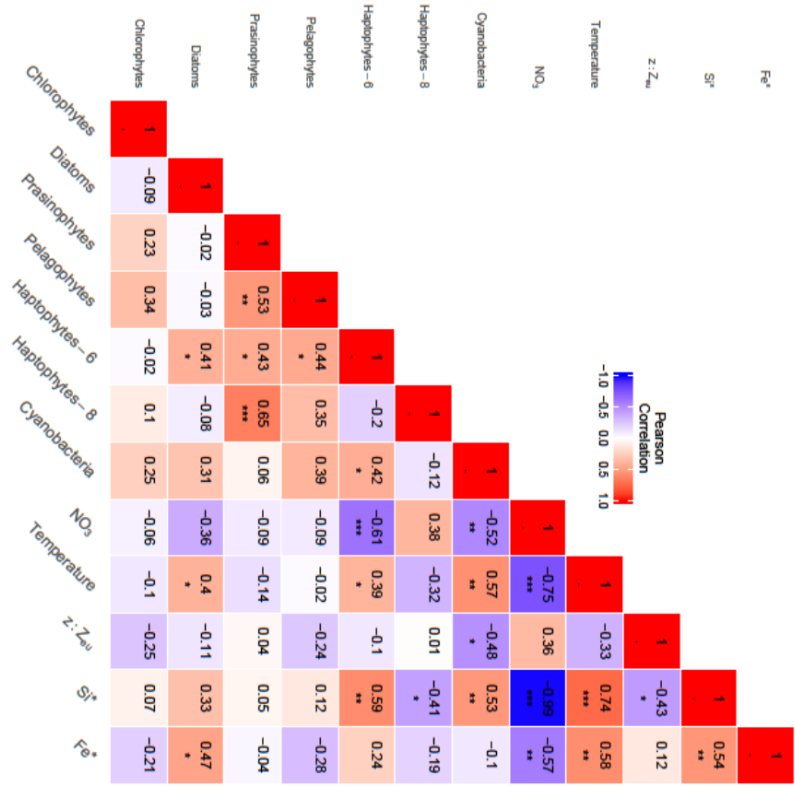
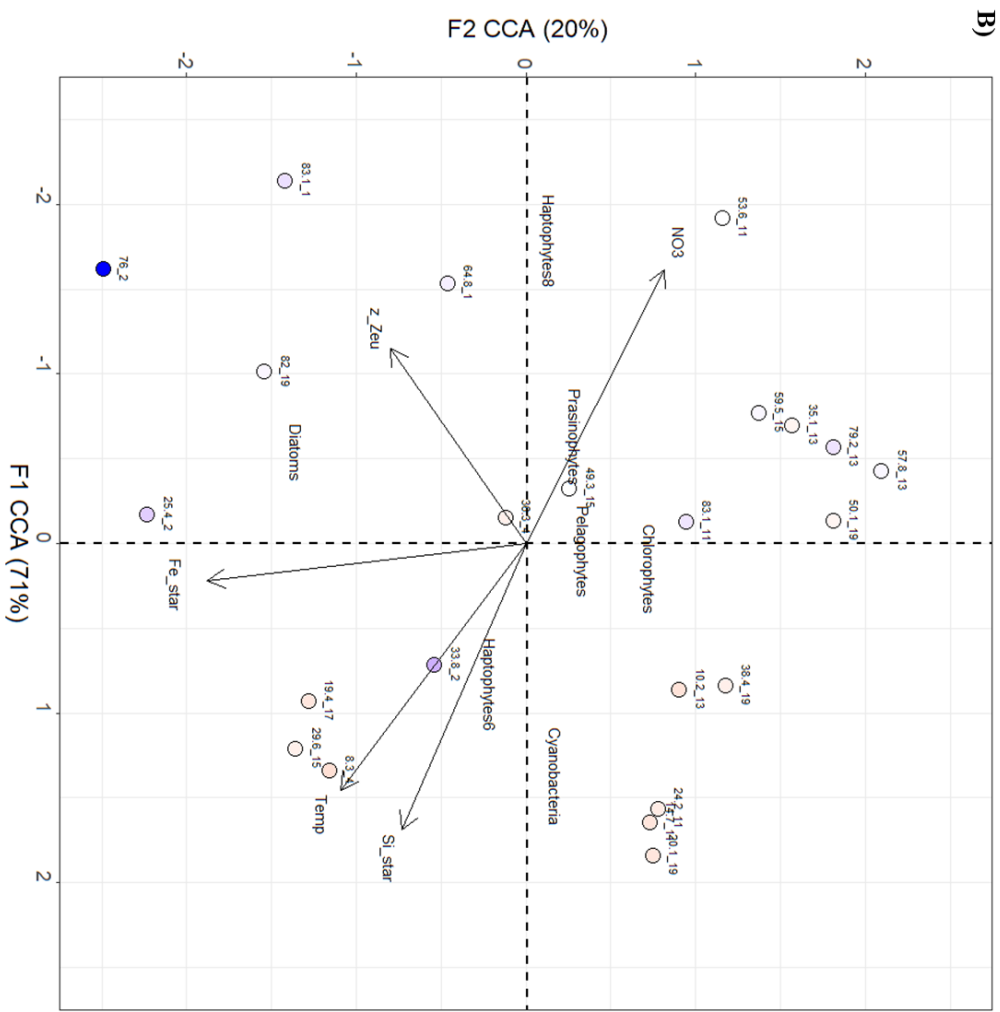
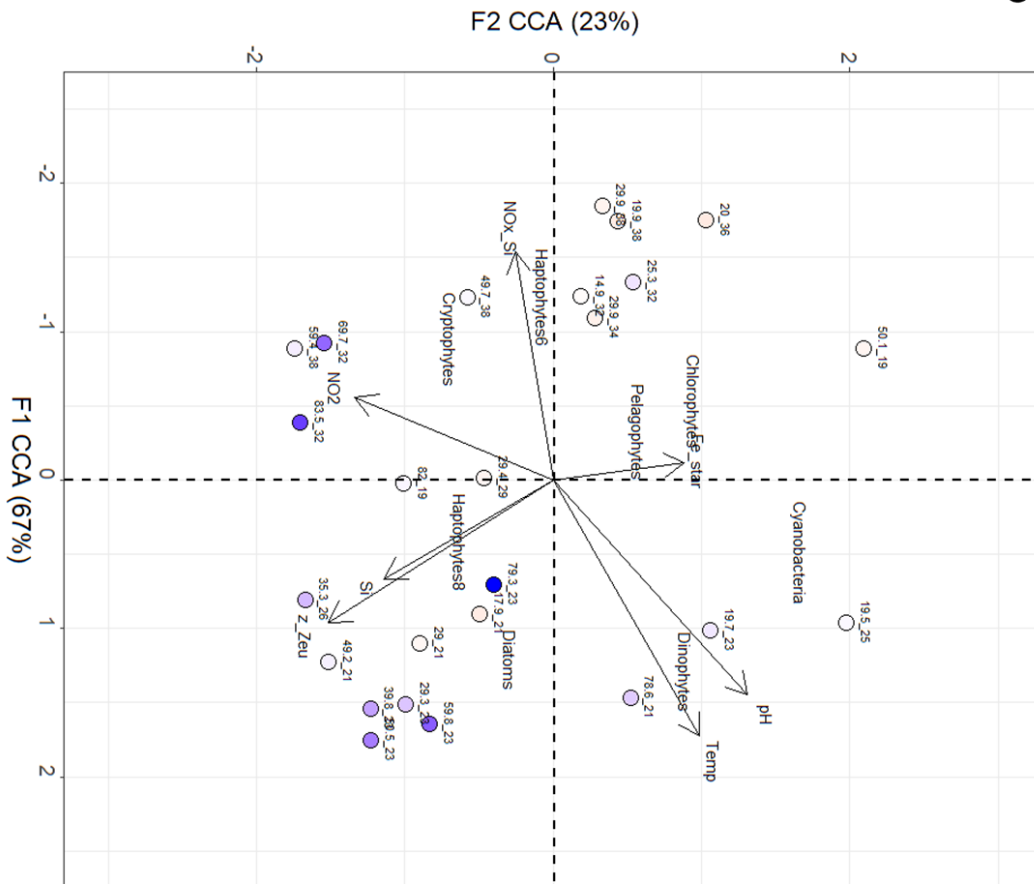


Figure 4.11: Plots of canonical correspondence analysis (CCA) and Pearson correlation with level of significance (i.e. ***, p-value < 0.001; **, p-value = [0.001 ; 0.01]; *, p-value = [0.01 ; 0.05]) for A) nutrients (NO₃⁻, NO₂⁻, Si and DFe) defined as objects and physical (salinity, temperature and pH) and biological (fractions of pico-, nano-, and micro-phytoplankton) parameters; and phytoplankton functional-classes (Diatoms, Dinophytes, Pelagophytes, Haptophytes-6, Haptophytes-8, Cryptophytes, Cyanobacteria, Prasinophytes and Chlorohytes) defined as objects with nutrients (NO₃⁻, NO₂⁻, Si, DFe, Si*, Fe*, NOx:Si) and physical (salinity, temperature, pH and z:Zeu) parameters for B) the NASTE province (stations 1-19), C) the NADR province (stations 19-38) and D) the ARCT province (stations 40-78). Note that colour coding refers on plot A to the bloom advancement (as defined by Lemaître et al. (2017) and symbols to the different basins, while for B-D, the colour coding refers to the z:Z_{eu} ratio.



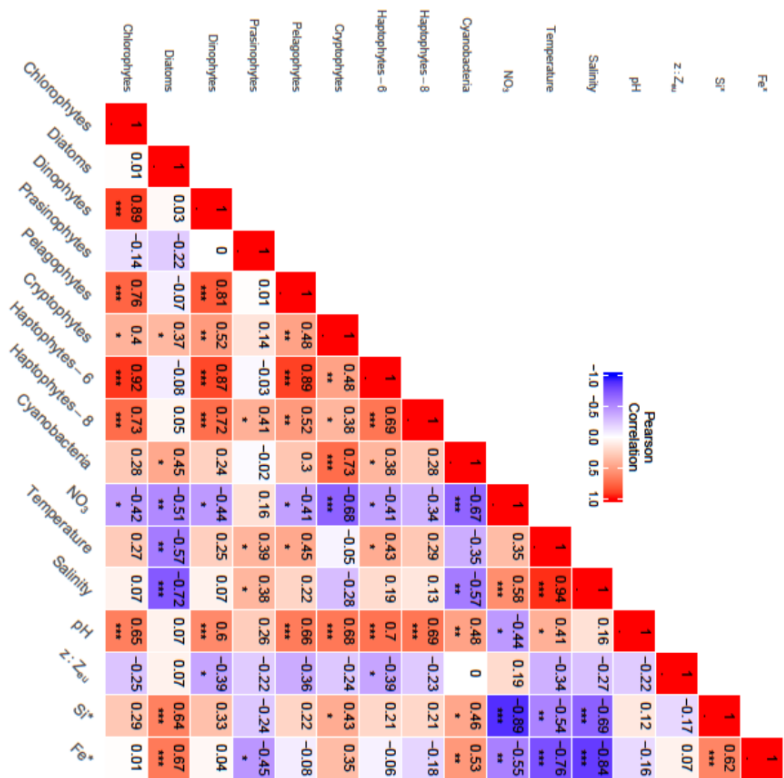
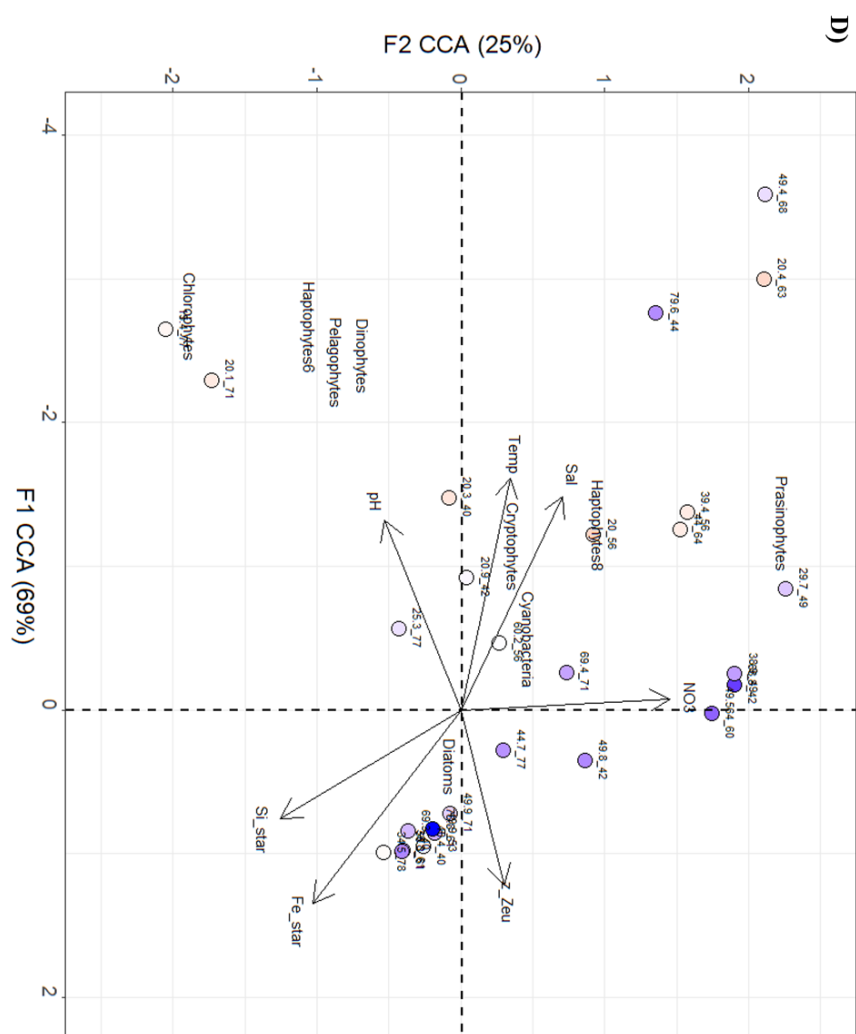
C)



Pearson Correlation

-1.0 -0.5 0.0 0.5 1.0

	Chlorophytes	Diatoms	Dinophytes	Pelagophytes	Cryptophytes	Haptophytes-6	Haptophytes-8	Cyanobacteria	NO ₂	Si	Temperature	pH	z:Zeu	Fe ³⁺	NOx:Si
Chlorophytes	1														
Diatoms	0.13	1													
Dinophytes	0.44	0.34	1												
Pelagophytes	0.65	0.01	0.13	1											
Cryptophytes	0.34	-0.23	-0.05	0.57	1										
Haptophytes-6	0.54	-0.01	-0.02	0.75	0.68	1									
Haptophytes-8	0.23	0.35	0.51	0.46	-0.08	-0.11	1								
Cyanobacteria	0.35	-0.03	0.31	0.46	0.13	0.18	-0.12	1							
NO ₂	-0.17	-0.07	-0.23	-0.27	-0.51	-0.04	0.14	-0.27	1						
Si	-0.54	-0.27	-0.39	-0.56	-0.51	-0.33	0.17	-0.52	0.1	1					
Temperature	-0.1	0.35	0.43	-0.17	-0.65	-0.31	0.29	0.44	-0.61	-0.59	1				
pH	0.11	0.45	0.58	0.04	-0.45	-0.44	0.29	-0.43	0.3	0.3	0.94	1			
z:Zeu	-0.6	-0.06	-0.2	-0.59	-0.32	-0.44	-0.09	-0.43	0.3	0.32	0.03	-0.15	1		
Fe ³⁺	0.58	0.44	0.36	0.54	0.06	0.49	0.26	0.33	-0.4	-0.32	0.16	-0.46	-0.24	1	
NOx:Si	0.21	-0.26	-0.24	0.42	0.92	0.6	-0.19	-0.04	0.14	-0.45	-0.71	-0.56	-0.24	-0.09	1



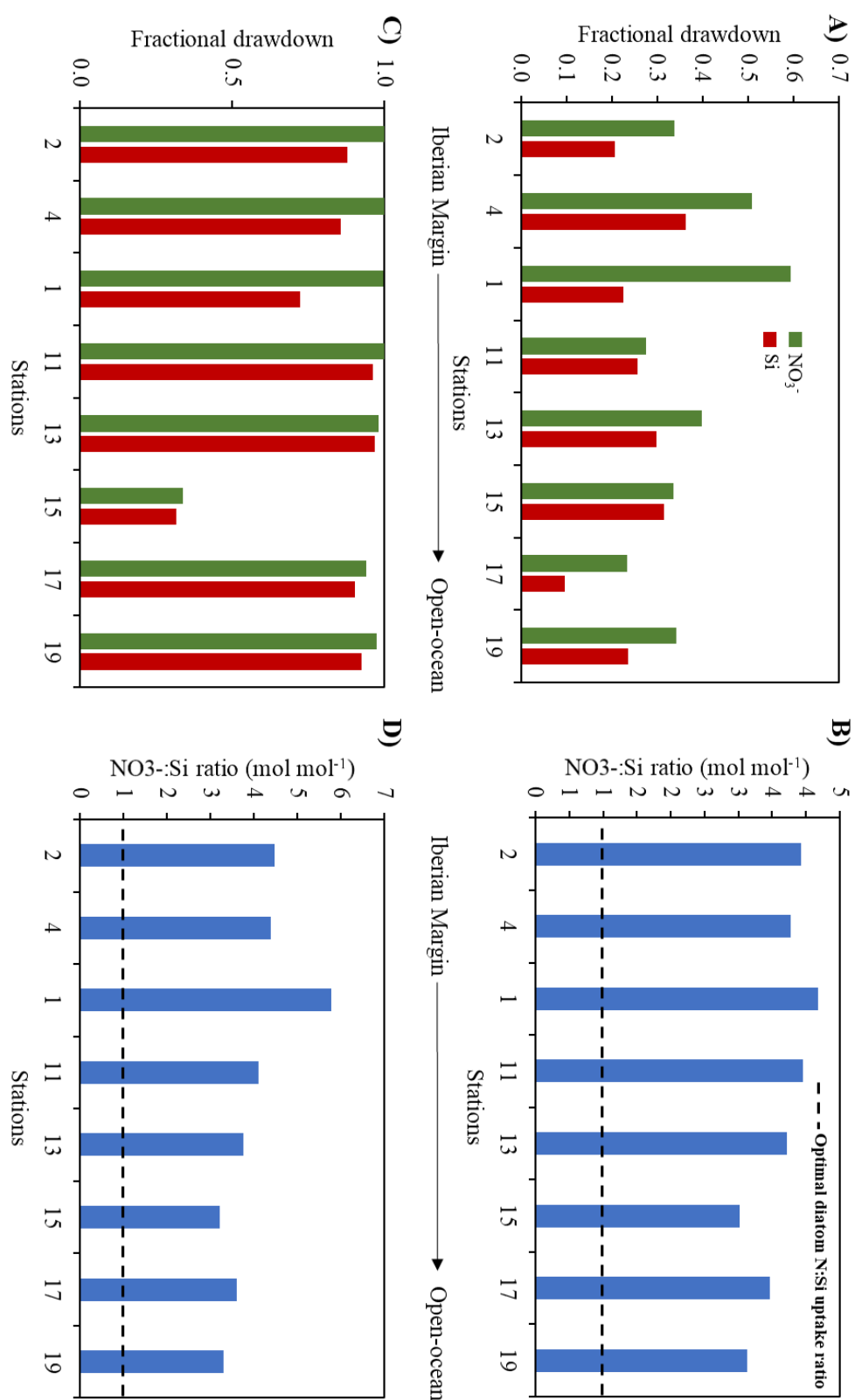


Figure 4.12: Histograms of fractional drawdown ((winter – spring)/winter) of NO₃⁻ and Si for A) winter mixed layer depth and C) spring mixed layer depth and histograms of NO₃⁻:Si ratios for B) winter mixed layer depth and D) summer mixed layer depth, for stations 1 to 19 located at the Iberian Margin and within the eastern part of the West European Basin. Black dashed line represents the optimal diatom N:Si uptake ratio.

4.4.4.2 NADR province: Western West European Basin and Iceland Basin

The CCA performed on samples located in the NADR province and above 90 m depth (stations 19-38, n=27) explained 49 % of the variance with NO_2^- , Si(OH)_4 and temperature (p-values < 0.05) as well as pH, $z:Z_{\text{eu}}$, Fe^* and NOx:Si(OH)_4 variables (Fig. 4.11B). pH, $z:Z_{\text{eu}}$, Fe^* and NOx:Si(OH)_4 were not significant in the model ANOVA-tested (Appendix C6) prior to running the CCA as the variance contained in these parameters was already explained by temperature and pH distributions (Fig. 4.11B, second panel) but were left for graphic interpretation. Prasinophytes phytoplankton class was removed from the analysis as it was not explained by the environment variables due to low ~ homogenized abundance (< 20%) in this basin (Appendix C4).

The CCA separated the phytoplankton community structure between, on one side, the SNAC (Fig. 4.11B) region on the other side, the NNAC and ERRC regions (Fig. 4.11B). The SNAC region was characterized by high pH and temperatures (Fig. 4.11B) and lower NO_3^- concentrations (Fig. 4.3C) than the NNAC and ERRC regions. The main difference was observed in the NOx:Si(OH)_4 ratios, which were much higher in the northern part of the NADR province with an average of $7.3 \pm 4.3 \text{ mol mol}^{-1}$, as opposed to $3.2 \pm 1.5 \text{ mol mol}^{-1}$, in the southern part. These ratios were especially high in the ERRC region reaching up to ~ 19 mol mol^{-1} at station 36, thus highlighting a strong Si(OH)_4 depletion relative to NO_3^- concentrations. This resulted in a shift in the phytoplankton community structure with the predominance of diatoms, dinophytes and type-8-haptophytes in the southern part and of cryptophytes, type-6-haptophytes, pelagophytes and chlorophytes in the northern part (Fig. 4.11B).

SNAC region

At the sampling period, diatoms were located at depths where DFe was in excess of NO_3^- (above 50 m depth, Fig. 4.9B) as indicated with the significant positive correlation between diatoms and Fe^* (Fig. 4.11B). It appeared that their presence removed Si(OH)_4 from the water column ($r = -0.27$, p-value > 0.1), likely highlighting that diatoms were, if not already declining, close to decline. Indeed, the strong correlation existing between diatoms and type-8-haptophytes (Fig. 4.11B) suggests that Si(OH)_4 concentrations ($0.19 - 1.9 \mu\text{mol L}^{-1}$, Fig. 4.3A) were below half-saturation constant of the diatom species present ($K_s = 0.2 - 97.4$ and $K_{\mu} = 0.02 - 8.6 \mu\text{mol L}^{-1}$, Martin-Jézéquel et al., 2000 and references therein), despite the relatively Si-enriched Atlantic Water originating from the confluence of the

Subarctic and Subtropical Waters (Hatun et al., 2017), as type-8-haptophytes are not able to dominate the bloom unless there is a Si-limitation (Egge and Aksnes, 1992; Salter et al., 2007). Conversely, instead of a diatom decline, this could highlight a shift in the diatom assemblages, from highly to slightly silicified diatoms. Although, Lemaître et al. (2017) reported lower remineralisation rates in the mesopelagic zone of this area compared to the NASTE province, in the top 100 m of the water column Phaeophytin *a* and Phaeophorbide *a* concentrations were much higher in the SNAC (up to 0.17 mg m^{-3}) than in the RECIR ($< 0.07 \text{ mg m}^{-3}$) regions (Appendix C1). These pigments, which highlight the presence of grazers, were measured in the same location as the diatoms.

Type-8-haptophytes were also significantly correlated to dinophytes (Fig. 4.11B). However, dinophytes were mainly located in surface waters as indicated by the CCA and their positive correlations with pH and temperature (Fig. 4.11B, see also Figs. 4.6B and 4.7B). Barton et al. (2015) reported that dinophytes prosper during warm, stratified conditions, and that their abundance is negatively correlated with surface wind speed, cooling, turbulence, and deeper mixed layer. Interestingly, throughout the GEOVIDE section, the maximum concentration of dinophytes was located in the SNAC region (Figs. 4.6B and 4.7B). The Z_m from the SNAC/NAC region were not different from the eastern part of the West European Basin, but the oligotrophic status of the Subtropical Gyre likely explain their absence. Furthermore, the SNAC region was characterized by very high absolute velocities ($> 0.3 \text{ m s}^{-1}$, see Fig. 8 in Zunino et al., 2017), shifting from stratified (19-21) to well-mixed stations (23-26) (Fig. 4.1C). This suggests that dinophytes benefited from the turbulence induced by the NAC, likely related to nutrient supply.

Within the NADR province, similarly to dinophytes, cyanobacteria were mainly present in the surface waters of the SNAC region as indicated by the CCA (Fig. 4.11B) and their positive correlation with pH and negative correlation with $z:Z_{eu}$ (Fig. 4.11B). However, cyanobacteria were significantly positively correlated to the pelagophytes (Fig. 4.11B), which were mainly present in the northern region (Fig. 4.6B). This can be explained by the ubiquity of cyanobacteria in the whole area (SNAC, NNAC and ERRC) and by their relatively low percentage of abundance (up to 26% and only at station 26, lower than 10% elsewhere) compared to other phytoplankton classes.

NNAC and ERRC regions

Cryptophytes, type-6-haptophytes and pelagophytes took advantage of the strong Si-depletion ($r = 0.92$, $p\text{-value} < 0.001$; $r = 0.60$, $p\text{-value} < 0.001$; $r = 0.42$, $p\text{-value} < 0.05$; respectively with $\text{NO}_x\text{:Si}$ ratios, Fig. 4.11B), which limited diatom growth in the NNAC/ERRC region (see also Fig. 4.8A). Is diatom Si-limitation the result of a pre-diatom bloom in waters upstream from the section (i.e. close to Iceland) or are waters from the NNAC/ERRC region permanently Si-limited? Figure 4.1B clearly shows that a phytoplankton bloom occurred in May 2014 (in agreement with Henson et al. (2009), i.e. mid-April – beginning of May as a mean start date) in surface waters above the Reykjanes Ridge, waters that will feed phytoplankton at stations located in the ERRC region (stations 34-38). Several studies (e.g. Hatun et al., 2017; Henson et al., 2006; Irigoien et al., 2002; Nielsdóttir et al., 2009) reported that Iceland shelf waters and the central Iceland Basin and especially waters alongside Reykjanes Ridge displayed massive diatom blooms (e.g. *Proboscia alata* and *Lauderia annulata*, in Iceland shelf waters; *Cylindrotheca closterium*, in central Iceland Basin), limited over time by Si(OH)_4 (Hatun et al., 2017; Henson et al., 2006) and Fe (Nielsdóttir et al., 2009; Tonnard et al., submitted). In addition, Hatun et al. (2017) showed clear evidence of a marked Si(OH)_4 decrease during the last 25 years in the Subpolar Gyre through decreased winter convection since 1990, a weakening and retraction of the Subpolar Gyre (including the reduction of Si-Arctic supply to the North Atlantic Ocean) and an associated increased influence of Subtropical nutrient-poor waters (i.e. Atlantic waters). This mainly means, in the case of this basin, a decrease in Si(OH)_4 supply and consequently the growth limitation of diatoms and the succession of type-6 haptophytes that dominated this area at the sampling period (Fig. 4.6). Based on our observations, it is very likely that it will result in enhanced bloom of type-6-haptophytes (i.e. Coccolithophorids, e.g. *Emiliania huxleyi*) (Giraudeau et al., 2016)

Interestingly, all the phytoplankton classes were positively correlated or related to positive Fe^* (Fig. 4.11B) indicating that Fe was clearly the nutrient shaping the distribution of phytoplankton biomass rather than indicating that Fe was not limiting phytoplankton growth. The only phytoplankton class that was not related to Fe^* was the cryptophytes, suggesting that this class displayed very low Fe requirement compared to other phytoplankton classes. Gibb et al. (2001) reported that cryptophytes were mainly located at depth in oligotrophic conditions, such as the Subtropical Gyre, suggesting that they have high nutrient requirements. However, this study shows the opposite trend with slightly higher

cryptophytes contribution to the TChl-*a* concentrations in surface waters of the Subtropical Gyre and much higher contribution at depth in the Iceland Basin. This suggests that despite their small size, which provide them with the advantage of a high surface area to volume ratio well suited to low-nutrient and low-energy conditions, they are not able to compete with other taxa and are thus located in areas where larger cells are limited. This is in line with Klaveness (1989) who reported that cryptophytes are opportunistic species. Furthermore, despite the lack of a clear relationship between cryptophytes abundances and NO_2^- ($r = 0.13$, $p\text{-value} > 0.1$), they were associated in the CCA space (Fig. 4.11B). The presence of cryptophytes has previously been associated with the uptake of reduced nitrogen (Berg et al., 2003) and it has been reported by Droop (1957) that they are not able to grow on NO_3^- as the sole source of nitrogen in culture. In this study, the highest NO_2^- concentrations were observed between 50 and 100 m depth of the ERRC/NNAC region especially at station 32, the location of an anti-cyclonic eddy (Fig. 4.6). This is in agreement with the studies of Collos (1998) and Mahadevan (2014) where enhanced NO_2^- concentrations have been shown to be related to anti-cyclonic eddies.

Finally, chlorophytes were present throughout surface waters of the NADR province ($r = -0.60$, $p\text{-value} < 0.001$, with $z:Z_{\text{eu}}$), but in low concentrations and relative abundances (Figs. 4.6 and 4.7). However, their abundance relative to TChl-*a* increased within the NNAC/ERRC region (Fig. 4.7), where they were positively correlated to pelagophytes and type-6-haptophytes (Fig. 4.11B). Such phytoplankton community structure has already been reported by Gregg and Casey (2007). The relatively low concentrations of the chlorophytes in our study area was likely explained by the fact that Coccolithophorids have a competitive advantage over chlorophytes by virtue of a greater ability to utilize nutrient at low values (Gregg and Casey, 2007).

4.4.4.3 ARCT province (i.e. Irminger and Labrador Seas and Greenland and Newfoundland coastal stations, stations 40-78)

The CCA performed on stations located in the ARCT province and above 90 m depth (stations 40-78, $n=30$) explained 58 % of the full inertia with NO_3^- , salinity, temperature and Fe^* ($p\text{-values} < 0.05$) as well as Si^* , pH and $z:Z_{\text{eu}}$ variables (Fig. 4.11C). Si^* and pH were not significant in the model ANOVA-tested (Appendix C6) prior to run the CCA as the variance contained in these parameters was already explained by NO_3^- distribution ($r = -0.89$, $p\text{-value} < 0.001$), NO_3^- ($r = -0.44$, $p\text{-value} < 0.05$) and temperature ($r = 0.41$, $p\text{-value} < 0.05$) distributions, but were left for graphic interpretation. Note that no significant correlation was

observed between $z:Z_{eu}$ and other environmental variables (Fig. 4.11C). This highlights that, besides not being significant to explain a huge proportion of the CCA inertia, $z:Z_{eu}$ was explaining part of the distribution of two phytoplankton classes (i.e. type-6-haptophytes and dinophytes, p -values < 0.05), but to a lesser extent when compared to other environmental variables. In the CCA space, diatoms were very close to the centre of both axes, meaning that their distribution was not strongly linked to environmental variables. However, they dominated all the areas from the ARCT province (Figs. 4.6B and 4.7B), except for some samples from station 68 and 69. This is in agreement with many previous studies (e.g. Barton et al., 2015; Castellani et al., 2008; Hatun et al., 2017; Henson et al., 2006; Lacour et al., 2015; Longhurst, 2007; Reid et al., 2007; Ward and Waniek, 2007), which reported their occurrence within the full ARCT province and is likely due to the inlet of Si-rich Arctic waters (Tremblay et al., 2002) through the Canadian Arctic Archipelago and the Fram Strait (Torres-Valdés et al., 2013). Their ubiquity in the ARCT province linked them strongly to almost all variables (except pH and $z:Z_{eu}$) and consequently the CCA positioned them at the centre. Indeed, diatoms were significantly positively correlated to Fe^* and Si^* as well as negatively correlated to salinity, temperature and NO_3^- (Fig. 4.11C). Although there was no significant relationship between diatoms and $z:Z_{eu}$ (Fig. 4.11C), they were the only phytoplankton class displaying a positive correlation with this parameter, highlighting that they were the only phytoplankton class located in deeper samples (but not only, see Figs. 4.6B and 4.7B). The fact that diatoms were slightly positioned on the right of the CCA plots highlights that the CCA mostly explained the distribution of diatoms within the C area. Indeed, diatom abundance neighboured 100% (eutrophic coastal stations 53, 61 and 78) (Figs. 4.11C and 4.6) within this area. The other areas, despite being also dominated by diatoms, exhibited substantial proportion of other phytoplankton classes. Indeed, the southern CONV area was characterized by important fractions of dinophytes, pelagophytes, type-6-haptophytes and chlorophytes (Figs. 4.11C, 4.6 and 4.7), while the northern CONV and the IG areas were characterized by important fractions of type-8-haptophytes, cryptophytes, prasinophytes and cyanobacteria (Figs. 4.11C, 4.6 and 4.7). Finally, the IC and the WBC areas exhibited significant fractions of Prasinophytes, type-8-Haptophytes (Figs. 4.11, 4.6 and 4.7).

Greenland and Newfoundland margins

The coastal region displayed the most positive Fe* and Si* from the whole section. Tonnard et al. (submitted) attributed the enhanced DFe concentrations measured at both the Greenland and the Newfoundland Margins to sediment inputs for deep samples and to meteoric water (including rainfall and Greenland ice sheet melting) inputs for surface samples. In addition to the Si-rich Arctic waters, many studies (Hawkings et al., 2015; Meire et al., 2016; Wadham et al., 2010) reported important Si-concentrations originating from the melting of Greenland Ice sheet. In addition, Henson et al. (2006), Ryan-Keogh et al. (2013) and Nielsdóttir et al. (2009) reported seasonal Si- and Fe-(co)-limitations of the spring phytoplankton bloom in the Irminger Sea. Therefore, such inputs were likely stimulating the growth of diatoms relative to other phytoplankton functional groups after the peak of the spring bloom, and thus likely explain the time decoupling of blooms in the Subpolar Gyre (Section 4.4.3).

Southern Labrador Sea Water convection area

Similarly, diatoms dominated other phytoplankton classes in the deeper samples from the southern CONV region (Figs. 4.6 and 4.7), while surface samples were characterized by a mix of diatoms, type-6-haptophytes, chlorophytes, dinophytes and to a lesser extent pelagophytes. Chlorophytes, dinophytes and pelagophytes were significantly positively correlated to type-6-haptophytes (Fig. 4.11C). Haptophytes have been reported to be relatively abundant in the ARCT province (Cota et al., 2003; Cota et al., 1994; Mitchell, 1992; Sathyendranath et al., 2001; Stuart et al., 2000; Winter et al., 2014) as well as Dinophytes (Barton et al., 2015; Leterme et al., 2005). In our study, type-6-haptophytes were located in surface waters of the ARCT province mainly in the southern CONV region (i.e. stations 71 and 77, Figs. 4.6 and 4.7). Their presence was also confirmed by satellite images (<https://worldview.earthdata.nasa.gov>, 19th and 28th of June 2014). In this region, they were strongly positively correlated to pH and to a lesser extent to temperature (Fig. 4.11C). Interestingly, previous studies reported that type-6-haptophytes generally succeed the diatom bloom (Falkowski et al., 2004) but are not known so far to develop concomitantly (e.g. Yücel, 2017) due to their different strategy of nutrient uptake r- vs. K-strategies for diatoms and Coccolithophorids, respectively (Margalef, 1978). Indeed, Litchman et al. (2007) reported that diatoms are opportunists, efficiently exploit resources in unstable, rarefied environments. In contrast, Coccolithophorids, possessing a high affinity for nutrients and low

resource requirements, generally grow under quiescent conditions characteristics or stratified open-ocean waters (Iglesias-Rodríguez et al., 2002). Although diatoms were susceptible to be N-limited, as indicated by positive Fe^* and Si^* in the Labrador Sea (Fig. 4.9), the lowest NO_3^- concentrations (i.e. 1.80 and 2.01 $\mu\text{mol L}^{-1}$, at stations 71 and 77, respectively) suggested that they were not limited by any nutrient at the sampling period. Indeed, half-saturation constants for uptake of NO_3^- have been reported to range from ~ 0.1 to 3.1 $\mu\text{mol L}^{-1}$ for North Atlantic pelagic diatoms (Eppley et al., 1969; Eppley and Thomas, 1969; Sarthou et al., 2005). This can be due to the marked stratification of the Labrador Sea due to substantial inputs of glacial meltwater and sea-ice melting (Benetti et al., 2017), which will then favour Coccolithophorids and dinophytes organisms rather than diatoms.

Northern Labrador Sea Water convection area

Surface waters from the northern CONV region (i.e. stations 68 and 69) were largely depleted in NO_3^- concentrations (Fig. 4.3, $\text{NO}_3^- < 0.1 \mu\text{mol L}^{-1}$). Interestingly, Stations 63 and 64 from the same region displayed relatively high nutrient concentrations (i.e. $\text{NO}_3^- = 2.30$ and 5.06 $\mu\text{mol L}^{-1}$; $\text{Si(OH)}_4 = 4.36$ and 4.47 $\mu\text{mol L}^{-1}$; $\text{DFe} = 0.40$ and 0.23 nmol L^{-1} , for stations 63 and 64, respectively) and low TChl-*a* concentrations (Fig. 4.1 and 4.6A) for the season. If nutrients are not limiting phytoplankton growth, then this could be the result of 1) intense grazing, 2) a physical forcing that entrained phytoplankton out of the euphotic layer, or 3) light-limitation of phytoplankton growth or a combination of those. The sum of Phaeophitine-*a* and Phaeophorbide-*a* concentrations were maximal in the ARTC province relative to other provinces and especially in the Labrador Sea (Appendix C1). However, stations 63-69 displayed much lower concentrations compared to neighbored stations, likely indicating a lower grazing pressure for these stations. This region is known for the deep convection of Labrador Sea Water (Lazier et al., 2002). Although it is an important feature in winter to explain a decrease in PP due to strong mixing, in spring and summer surface waters of the Labrador Sea are very stratified (Lazier et al., 2002). Therefore, it seems that neither a grazing pressure nor a physical forcing could explain such high nutrient concentrations and low TChl-*a* concentrations. Harrison and Li (2008) highlighted from the 12 year time series of the Labrador Sea Monitoring Program, that light limits primary production and phytoplankton growth much of the year, even during summer when surface irradiance is at its peak (Arteaga et al., 2014) and that from time to time nutrient limitation can be observed. An interesting pattern can be seen in Figure 4.6A, with basically low integrated TChl-*a*

concentrations where the ratios of the total photosynthetic pigments over the total photo-protective pigments (APSP:APPP) are low (Gibb et al., 2001). Stations characterized by low APSP:APPP ratios were in post-bloom conditions (i.e. low TChl-*a* concentrations), likely indicating that as solar irradiance increases, phytoplankton community is relaxed from light-limitation. Thus, at the sampling period, these stations, besides exhibiting low TChl-*a* concentrations, displayed nutrient depleted conditions. However, our data showed APSP:APPP ratios similar at stations 63 and 64 (Fig. 4.6A, red line) to the one observed in the West European Basin, thus indicating that light was not limiting. Enhanced grazing pressure at these stations is another plausible explanation. However, degradation pigments ranged from 0.01 to 0.08 mg m⁻³ at these stations and were substantially low compared to other stations of the NADR province (i.e. up to 0.93 mg m⁻³ at station 77). Therefore, the reason of relatively high nutrient concentrations remains unsolved.

Irminger Sea

The Irminger Gyre (IG) region (station 44 and 46), conversely, exhibited the highest surface macronutrient concentrations (Fig. 4.3) and the second highest surface DFe concentrations (i.e. after the C region) from the whole section. This can likely be explained by the fact that the bloom was still in development as suggested by the PP similar to the one reported for the NADR province (A. Roukaerts, D. Fonseca Batista and F. Deman; unpublished data). However, this region displayed the same phytoplankton classes and proportion than the one observed for the post-bloom stations from the northern CONV region. In addition, the IG region presented the highest APSP:APPP ratios from the whole section. Finally, the IC and WBC regions exhibited high macronutrient concentrations as well as high DFe concentrations (Fig. 4.3), suggesting that phytoplankton growth was not limited by these elements at the sampling period.

Grazing pressure of the ARCT province

In our study, it was not possible to estimate whether the grazing pressure or the nutrient limitation was responsible for the disappearance of the spring North Atlantic bloom. Both the NASTE and NADR province are known to exert a nutrient pressure on phytoplankton growth rather than a grazing pressure. Conversely, many studies (e.g. Castellani et al., 2008; Irigoien et al., 2003; Wolfe et al., 2000) reported the intense grazing occurring in both the Irminger and Labrador Seas. Our data suggest a similar pattern as Phaeophytine-*a* and Phaeophorbide-*a* concentrations were maximal in the ARCT region,

likely reflecting that the end of the bloom was a result of a high grazing pressure rather than an impoverishment in nutrients, except stations 68-69 in which diatoms were N-limited during the sampling period.

4.5 Conclusion

The aim of this paper was to first assess the limitation of the spring bloom and to constrain the succession of phytoplankton classes in the North Atlantic Ocean. All our results are summarized in Figure 4.13 and were as follows:

- (i) Surface waters from the NASTE province (i.e. the Iberian margin and the eastern part of the West European Basin), were characterized by an early bloom mostly composed of diatoms. Diatoms were N-limited from stations 1 to 13 due to the nitrate limited Tagus River supply. From stations 15 to 19, diatoms were Si-limited as a result of stratification and the downward flux of nutrient that occurs all year-round in the Subtropical Gyre. Diazotroph cyanobacteria and type-6-haptophytes in a potential symbiotic relationship succeeded the diatom bloom at stations closer to the Iberian Margin (i.e. 1-13), the type-6-haptophytes benefiting from the N-fixed by the cyanobacteria, the cyanobacteria profiting from the C fixed by the type-6-haptophytes. We suggested a Fe-limitation of both classes later in the season. Only cyanobacteria succeeded diatoms from stations 15 to 19, which likely indicated recent nutrient inputs from atmospheric sources. Similarly, these stations will presumably be Fe-limited in late spring, unless an atmospheric event occurs.
- (ii) Although the broad circulation of the NADR province resulted in three distinct areas (i.e. SNAC, NNAC and ERRC) in terms of integrated TChl-*a* concentrations, the constraining of phytoplankton distribution by physico-chemical variables separated this province in two areas: SNAC (i.e. stations 19-26) and the NNAC/ERRC (i.e. stations 29-38) areas. A bloom dominated by type-8-haptophytes and small diatoms characterized the deeper part (i.e. below ~ 50 m depth) of the southern region, while surface waters were dominated by dinophytes, which benefited from higher temperature, excess Fe relative to NO_3^- and lower grazing pressure. In this region, diatoms will be prone to Si and Fe-(co)-limitation, the rest of the community being only Fe

limited. The northern part of the NADR province was characterized by a bloom dominated by type-6-haptophytes due to a global decline in Si inputs resulting from a weakening of the Subpolar Gyre and increasing influence of Subtropical nutrient-poor waters. This bloom will be, as the season progresses, Fe-limited.

- (iii) Finally, sharp variations of integrated TChl-*a* concentrations were noticed in the ARCT province that separated six distinct areas (i.e. C, IC, IG, WBC, northern CONV and southern CONV), which were mostly explained by the broad circulation. Overall, diatoms largely dominated the full ARCT province due to the inlet of Si-rich Arctic waters through the Canadian Arctic Archipelago and to a lesser extent through Fram Strait. Greenland and Newfoundland coastal stations of the C area (stations 53, 61 and 78) were almost exclusively composed of large neritic diatoms as a result of the concomitant supply of DFe and Si from glacial meltwaters. In these northern stations, phytoplankton will likely later be light-limited. Type-6-haptophytes and dinophytes developed meanwhile the diatom bloom in surface waters of the southern CONV region (stations 71 and 77) as a result of a marked stratification, which consequently increased the grazing pressure. There, phytoplankton classes will be more subjected to N-limitation. The nitrate-impooverished surface waters of two stations from the northern CONV region (i.e. stations 68 and 69) were characterized by cyanobacteria of the *Prochlorococcus* genus. The IG region (station 44) was characterized by the same phytoplankton classes and proportion as the one observed in the northern CONV region and really high nutrient concentrations, suggesting a light-limitation of the phytoplankton community and/or eventually a top-down control. The IC and WBC region were not limited by any nutrient at the sampling period, but nutrient ratios and tracers suggest a Si and Fe-(co)-limitation, unless the grazing pressure intensified.

Many studies have reported potential shifts in the phytoplankton community structure in response to climate change, with overall a decrease in the relative abundance of the diatoms for the benefit of dinophytes due to increasing Sea Surface Temperature. Our data show that the phytoplankton community structure in the NADR province will be the most affected by the climatic system (i.e rising pCO₂ and change regarding the NAO phase) with the dominance of the coccolithophorids in the Iceland Basin; nevertheless, the North Atlantic Ocean was still largely dominated by diatoms.

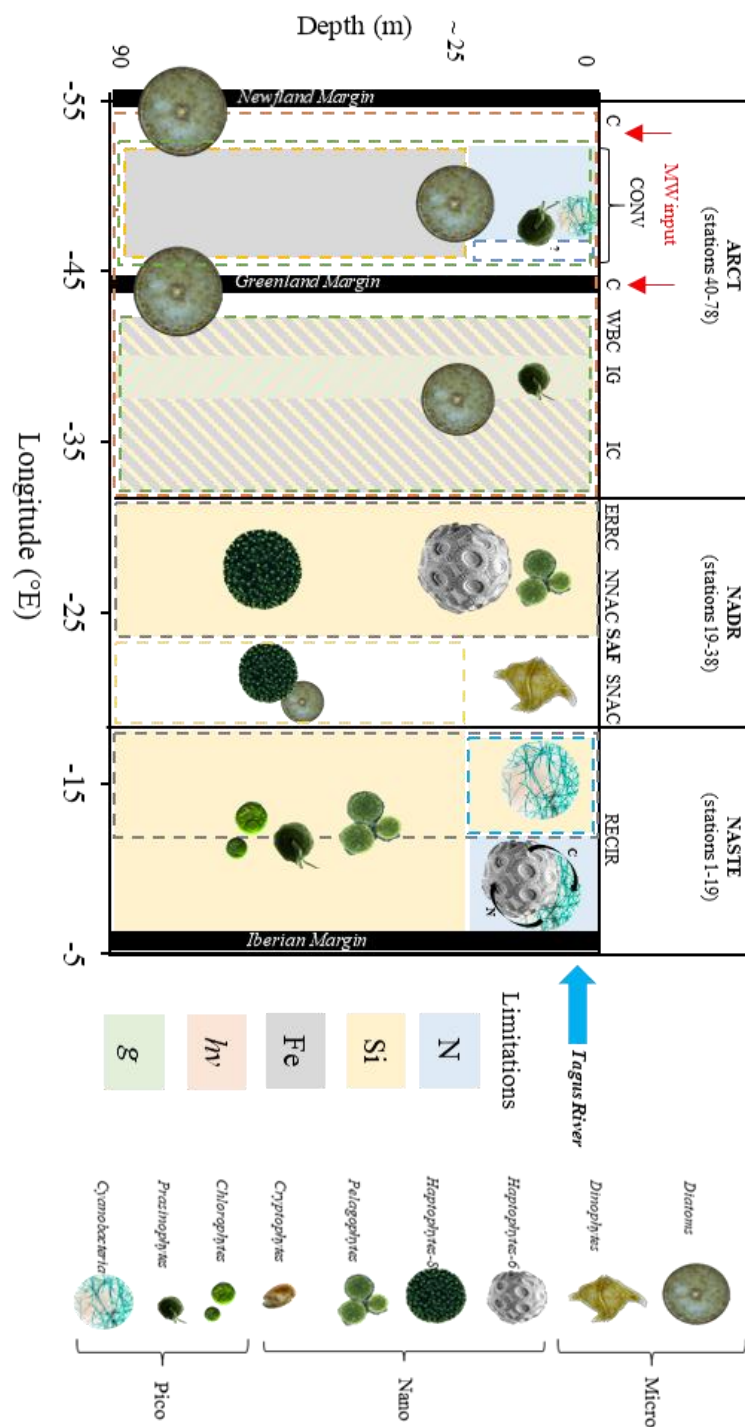


Figure 4.13: Schematic of the potential limitations of the spring bloom in the North Atlantic Ocean along the GEOVIDE section.

Chapter 5:

Fe-Binding Organic Ligands and Bioavailability over the Kerguelen Plateau

Fe-Binding Organic Ligands and Bioavailability over the Kerguelen Plateau

Table of content

Abstract	257
5.1 Introduction	258
5.2 Material and method	262
5.3 Results	262
5.3.1 Hydrography	262
5.3.2 Soluble Fe and dissolved and soluble Fe-binding organic ligands	264
5.3.2.1 Soluble Fe concentrations	264
5.3.2.2 Soluble and dissolved Fe-binding organic ligand concentrations and conditional stability constants	265
5.4 Discussion	270
5.4.1 Size partitioning of dissolved Fe and Fe-binding ligands	271
5.4.1.1 The reference station	271
5.4.1.2 What controls DFe concentrations?	271
5.4.2 Possible sources of dissolved and soluble Fe-binding organic ligands (B-transect and R18)	273
5.4.2.1 Biological component as a source of Fe-binding organic ligands	275
5.4.2.2 Sediment as a source of Fe-binding organic ligands	278
5.4.3 Comparison between the different areas	279
5.4.3.1 Dissolved fraction	279
5.4.3.2 Impact for Fe physical and organic speciation	284
5.4.3.3 Potential effects for the phytoplankton community	285
5.5 Conclusion	286

Dissolved and soluble Fe-binding organic ligands on the Kerguelen plateau and in the vicinity of Heard and McDonald Islands, Southern Ocean

This Chapter is a manuscript in preparation, the corresponding supplementary material is available in Appendix D.

Authors: Manon Tonnard, Kathrin Wuttig, Thomas Holmes, Pier van der Merwe, Ashley Townsend, Géraldine Sarthou, Hélène Planquette, Zanna Chase, Lavenia Ratnarajah, Andrew R. Bowie

Abstract

Iron-binding organic ligand samples ($n = 86$) were collected for both dissolved ($<0.2\mu\text{m}$) and soluble ($<0.02\mu\text{m}$) fractions over and off the Kerguelen plateau from January to February 2016 (HEOBI voyage, GEOTRACES Process Study GIpr05). The investigated area consisted of a repetition of the B-transect sampled during KEOPS in fall 2005 and of specific sampling locations around Heard and McDonald Islands. To understand the effect of the Kerguelen Plateau, a reference station located south of Heard and McDonald Islands was sampled for comparison. Adsorptive Differential Pulse Cathodic Stripping Voltammetry with 2-(2-Thiazolylazo)-p-cresol as the competing ligand was used to measure Fe-binding organic ligand concentrations and conditional stability constants. The concentrations of dissolved Fe-binding organic ligands ranged from 0.26 to 2.6 Eq of nmol L^{-1} Fe, with a median concentration of 0.70 Eq of nmol L^{-1} Fe and a median logarithm of conditional stability constant of 21.24 L mol^{-1} . Our results highlighted that the dissolved Fe-binding organic ligands were in excess of DFe only in the first 200 m of the reference and B-transect stations. Below this depth, and throughout the water column, they were close to or at saturation at the reference and B-transect stations, and throughout the water column around Heard and McDonald Islands. Ligand sources seemed to originate mainly from biological origins, either produced by large diatoms, as strong Fe-binding organic ligands and by bacteria as both weak and strong Fe-binding organic ligands at the reference and B-transect stations. In the vicinity of Heard and McDonald Islands, only weak ligands were measured and seemed to be also bacteria-mediated. These features resulted in marked differences in the partitioning of Fe between the reference and B-transect stations on one side and McDonald and Heard Islands on the other side. Although waters from Heard Island exhibited excess soluble ligand

concentrations, the water column of both Heard and McDonald Islands was dominated by low reactive ligands in both the dissolved and soluble phases compared to reference and B-transect stations.

Keywords: Iron, speciation, Southern Ocean, biogeochemical cycles

5.1 Introduction

The Southern Ocean is the largest high-nutrient low-chlorophyll (HNLC) region of the world (Mock and Thomas, 2008). In such areas, the phytoplankton biomass in the ocean remains fairly constant all year long and the levels of macronutrients are never significantly depleted. It has been recognized that the low biological productivity in this region is mainly due to both iron (Fe)-limitation of phytoplankton growth (Boyd et al., 2000) and grazing (Pitchford and Brindley, 1999). However, in the core of the Southern Ocean, a massive bloom occurs annually above the Kerguelen plateau (Morris and Charette, 2013) with substantial differences between its northern and southern parts especially in the duration of the bloom (Schallenberg et al., in prep.). While the southernmost Kerguelen plateau bloom is sustained throughout the season by a combination of Fe-derived from an Antarctic shelf source and remineralisation of sinking material (Schallenberg et al., in prep.), the northernmost offshore bloom, located east of Kerguelen Islands feeds upon Fe laterally advected from the northern part of the plateau and/or Kerguelen coastal waters (Bowie et al., 2015), which have been shown to be derived from direct runoff, glacial melting and sedimentary inputs (Qu  rou   et al., 2015). Finally, in the midst of these two areas, another bloom, located on the northern plateau, which peaks around December and subsequently declines, uptakes Fe supplied from the sediments of the shallow plateau (Blain et al., 2008c; van der Merwe et al., 2015; Zhang et al., 2008) and from Fe regenerated from grazing (Sarhou et al., 2008). This ‘deep’-Fe reservoir is seeding surface waters through winter mixing and elevated vertical diffusivity (Blain et al., 2008c; Tagliabue et al., 2014b). However, on the northern part of the Kerguelen plateau, the influence of the two volcanically active islands (Coffin et al., 1986; Weis et al., 2002), i.e. Heard and McDonald islands, on the regional biogeochemistry of Fe is still not fully resolved (Bowie et al., 2015; Qu  rou   et al., 2015; van der Merwe et al., 2015). As Fe availability dictates the efficiency of the carbon pump, and controls about 50% of the worldwide ocean primary production (Blain et al., 2007; Le Qu  r   et al., 2013), any perturbation of Fe sources and sinks will lead to changes in

the carbon cycle with consequences on both other major nutrient cycles and the climate system. However, the extent to which both the chemical and the physical speciation of Fe are available and accessible for marine organisms, once it enters the ocean, remain uncertain. Iron is present in operationally defined particulate ($> 0.45 \mu\text{m}$, PFe) and dissolved (< 0.2 or $0.45 \mu\text{m}$, DFe) phases, the latter subdivided into colloidal ($0.02 - 0.2 \mu\text{m}$, CFe) and soluble ($< 0.02 \mu\text{m}$ or 10 kDa , SFe) fractions (Bruland et al., 1994; Gordon et al., 1998b; Martin et al., 1989; Wu et al., 2001). All these fractions have been shown to be bioavailable (Chen et al., 2003; Chen and Wang, 2001; Hassler et al., 2011b; Hawkings et al., 2014; Kuma and Matsunaga, 1995; van der Merwe et al., 2015; Wang and Dei, 2003). Therefore, it is the reactivity of Fe that makes Fe bioavailable rather than its physical speciation, although most of the bioavailable forms of Fe have been shown to be part of the dissolved Fe pool. The distribution of Fe within the dissolved pool appears to be related to the distribution of organic ligands, with more than 99.9% of Fe being bound to organic ligands, confirming their ubiquity in the water column (e.g. Boye et al., 2001; Gerringa et al., 2008; Rue and Bruland, 1995; Van den Berg, 1995) the rest being inorganic Fe (Fe^{3+}). Organic ligands are also present in both colloidal and soluble forms. Colloids have been shown to contribute from 0 to 90% of total DFe across the global ocean (e.g. Boye et al., 2010; Chever et al., 2010; Fitzsimmons and Boyle, 2014a; Kondo et al., 2008; Thuróczy et al., 2010). These Fe-binding organic ligands (Lt) help DFe to stabilize in ocean surface waters by increasing its solubility through a permanent equilibrium between free and complexed forms of Fe at the pH of seawater, thus limiting its precipitation, removal by scavenging and consequently, Fe export to deep ocean (e.g. Gledhill and Buck, 2012; Gledhill and Van Den Berg, 1994; Rue and Bruland, 1995). Therefore, Fe-binding organic ligands likely increase the residence time of Fe and enable enhanced DFe concentrations to persist way above its inorganic solubility in seawater (i.e. 10 pmol L^{-1} , Liu and Millero, 2002).

While Lt are present seemingly everywhere, from surface to deep waters of the coastal and open ocean, there are some distinguishable trends in their distributions and thermodynamic characteristics (Bundy et al., 2014; Gledhill and Buck, 2012). In most cases, ligand concentrations measured are in excess of DFe concentrations (Gledhill and Buck, 2012), with the highest and the most variable ligand concentrations relative to DFe observed in the surface ocean (e.g. Boyd and Tagliabue, 2015; Gledhill and Buck, 2012; Slagter et al., 2017; Völker and Tagliabue, 2015), often with stronger stability constants (Bruland and Rue, 2001; Hunter and Boyd, 2007). Within the surface layer, it has been shown that the highest Lt

concentrations were often associated with the chlorophyll biomass maxima (e.g. Boye et al., 2006; Buck and Bruland, 2007; Croot et al., 2004; Gerringa et al., 2008; Ibanmami et al., 2011; Tian et al., 2006; Van den Berg, 2006; Wagener, 2008) and to low DFe concentrations, consequently linking the production of Lt to biological uptake of Fe in Fe-limited areas (e.g. Buck and Bruland, 2007). The excess of Lt (L') without any chlorophyll biomass maxima, for its part, may alternatively be a result of the remnants of previous bloom as suggested by Sato et al. (2007) due to the presence of grazers. In some areas, it could also be the result of atmospheric inputs (Gerringa et al., 2007; Kieber et al., 2001, Cheize et al., 2012), though dust deposition can lead to a reduction in excess ligand (Rijkenberg et al., 2008). Lt have also been shown to be delivered to surface by sea ice melting (Lannuzel et al., 2015), river plumes (Buck et al., 2007; Bundy et al., 2015; Kondo et al., 2007; Powell and Wilson-Finelli, 2003; Slagter et al., 2017) and with bacteria through the release of siderophores and/or the remineralisation of particles regardless of their nature (Vraspir and Butler, 2009).

In contrast, the deep ocean exhibits more or less constant profiles often close to saturation (Boye et al., 2006; Boye et al., 2010; Boye et al., 2001; Ibanmami et al., 2011; Nolting et al., 1998), or even lower than the reported DFe concentrations in the core of a hydrothermal plume (Bennett et al., 2008; Buck et al., 2015). Anomalously high excess ligand concentrations have been observed in some specific environment such as shelf and bottom boundary layers (Batchelli et al., 2010; Buck et al., 2007; Bundy et al., 2014; Gerringa et al., 2008; Johnson et al., 2007; Kondo et al., 2007) have been reported and can even be higher than in surface waters.

In terms of conditional stability constants ($K_{FeL_i,Fe^{3+}}^{cond}$), the presence of L₁-type ($K_{FeL_i,Fe^{3+}}^{cond} > 22$) are more often observed in the top hundred meters of the water column, the L₂-type ($K_{FeL_i,Fe^{3+}}^{cond} = [21, 22]$) are found throughout the water column and the L₃-type ($K_{FeL_i,Fe^{3+}}^{cond} < 21$) in benthic boundary layer (Bundy et al., 2014; Cullen et al., 2006; Ibanmami et al., 2011; Rue and Bruland, 1995, 1997). Finally, it has been shown that DFe concentrations do not generally exceed the concentration of the stronger ligand class (L₁, Buck et al., 2007).

Consequently, it is essential to identify the various Fe species, assess their interconnections and understand how DFe speciation influences the accessibility of this essential element for marine phytoplankton, to understand Fe biogeochemistry in the ocean (Hatta et al., 2015). In the specific scope of the northern part of the Kerguelen plateau,

previous studies highlighted high primary productivity both on the northern plateau and in the wake of Heard and McDonald islands in contrast to surrounding open ocean waters. Although, the northern part of the Kerguelen plateau is a large source of both DFe and DLt likely feeding the phytoplankton bloom, Fe biogeochemistry and bioavailability are still poorly constrained in these two areas of the Kerguelen plateau. Therefore, the Heard Earth-Ocean-Biosphere Interaction (HEOBI) voyage (Fig. 5.1) proposed to 1) determine the identity of the specific sources and the reactivity of Lt in two fractions (soluble and dissolved phases), 2) determine which fraction (soluble or colloidal) drives the variability of DFe concentrations, 3) assess how organic ligands can modify the physical speciation of Fe and 4) assess if the ligands can explain the differences between the TChl-*a* biomasses observed at the B-transect and Heard and McDonald Islands.

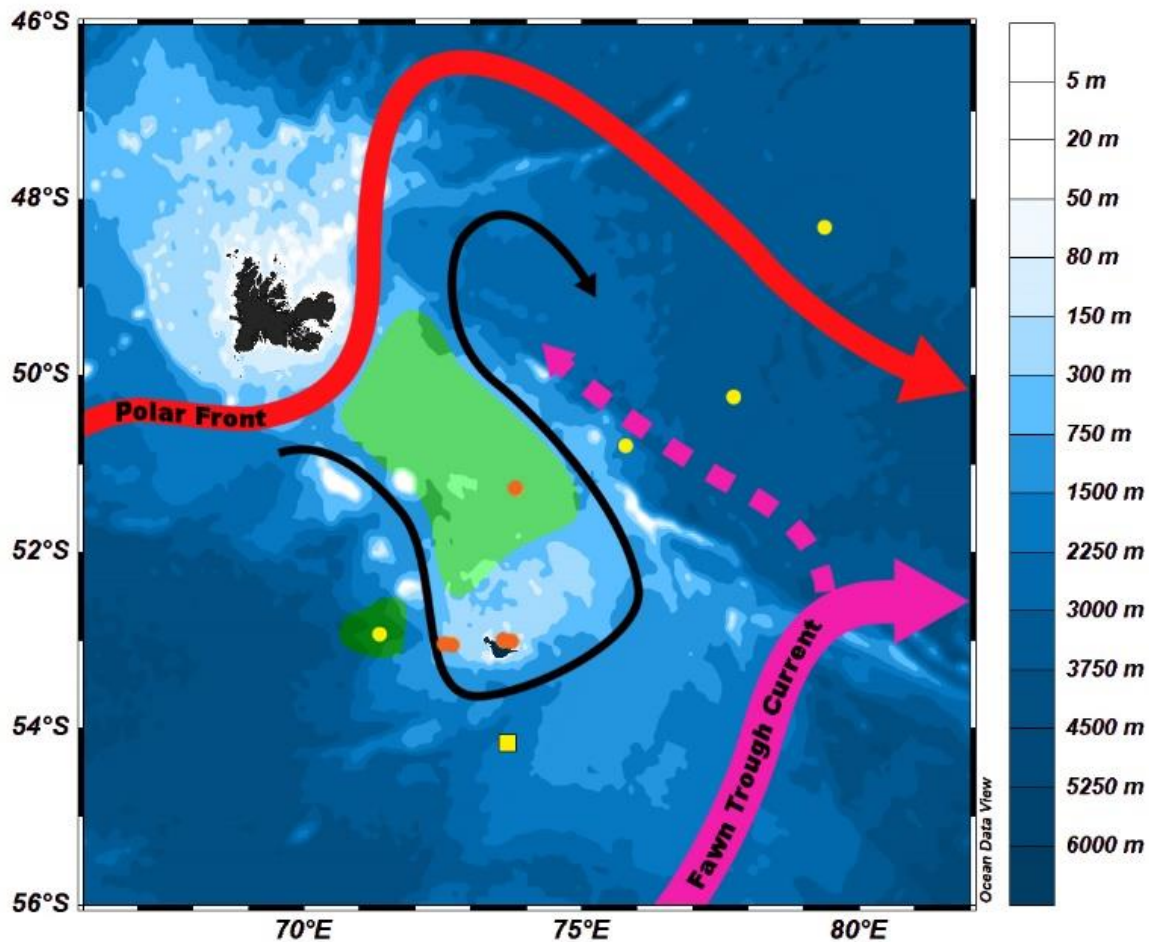


Figure 5.1: Schematic of total chlorophyll-*a* (TChl-*a*) concentrations (green) at the sampling period of the HEOBI voyage on top of the main circulation features as in Park et al. (2008b) (D. Alain and S. Hervé, IUEM). Note that the location of stations are represented as square for reference station R18 and dots for all other stations including B-transect and HIMI stations. Station colour coding refers to stations located on the Kerguelen plateau (orange) and to open ocean stations (yellow).

5.2 Material and method

(see Chapter 2)

5.3 Results

5.3.1 Hydrography

The general circulation occurring on the Kerguelen Plateau has been fully described in previous studies (Park et al., 2014; Park et al., 2008a; Park et al., 2008b; Park et al., 2009; Roquet et al., 2009; van Wijk et al., 2010). Overall, the main features and water masses identified in this study match those reported by Park et al. (2008b) during KEOPS. Briefly, the Antarctic Circumpolar Current (ACC) delineates the northern boundary of the Kerguelen Plateau. Within this area, the Polar Front separates the investigated area from the influence of Kerguelen Plateau on the north and the Fawn Trough Current splits the northern (i.e. the B-transect, Heard and McDonald Islands) and southern Kerguelen Plateau. The shallowest part of the northern Kerguelen Plateau is characterized by slow mean north-eastward currents ($\sim 6 \text{ cm s}^{-1}$; R. Roberston, pers. comm.). Over the B-transect five water masses were identified off-Plateau. From surface to depth these were the Antarctic Surface Water (AASW, surface θ maximum = 3.3°C), the Winter Water (WW, subsurface θ minimum = 2.1°C), the Upper Circumpolar Deep Water (UCDW, deep θ maximum = 2.7°C and O_2 minimum = $177 \mu\text{mol L}^{-1}$), Lower Circumpolar Deep Water (LCDW, salinity maximum = 34.8) and Antarctic Bottom Water (AABW, decreasing θ and salinity, i.e. down to 0.5°C and 34.7, respectively, increasing O_2 concentration, up to $222 \mu\text{mol L}^{-1}$) (Fig. 5.2). Above the Plateau only the AASW and the WW were present (Fig 2). AASW was encountered in surface waters ($< 100 \text{ m}$ depth) of the reference station (i.e. R18), followed by the WW ($\theta < 1^\circ\text{C}$, $100\text{-}200 \text{ m}$ depth) and deeper in the water column by the UCDW ($> 200 \text{ m}$ depth), which displayed decreasing temperature and increasing salinity. R18 had the typical characteristics of High-Nutrient, Low-Chlorophyll (HNLC) areas, with DFe concentrations below 0.11 nmol L^{-1} (except at $\sim 28 \text{ m}$ depth where $\text{DFe} = 0.27 \text{ nmol L}^{-1}$) and total chlorophyll-*a* (TChl-*a*) of 0.34 mg m^{-3} (for details see Holmes et al., in prep.). Finally, water surrounding the Heard and McDonald Islands (HIMI region) were well mixed as indicated by the very small gradients in temperature, salinity and O_2 from surface to depth (Fig. Fig. 5.2). At the HIMI stations, current velocity were primarily tidal.

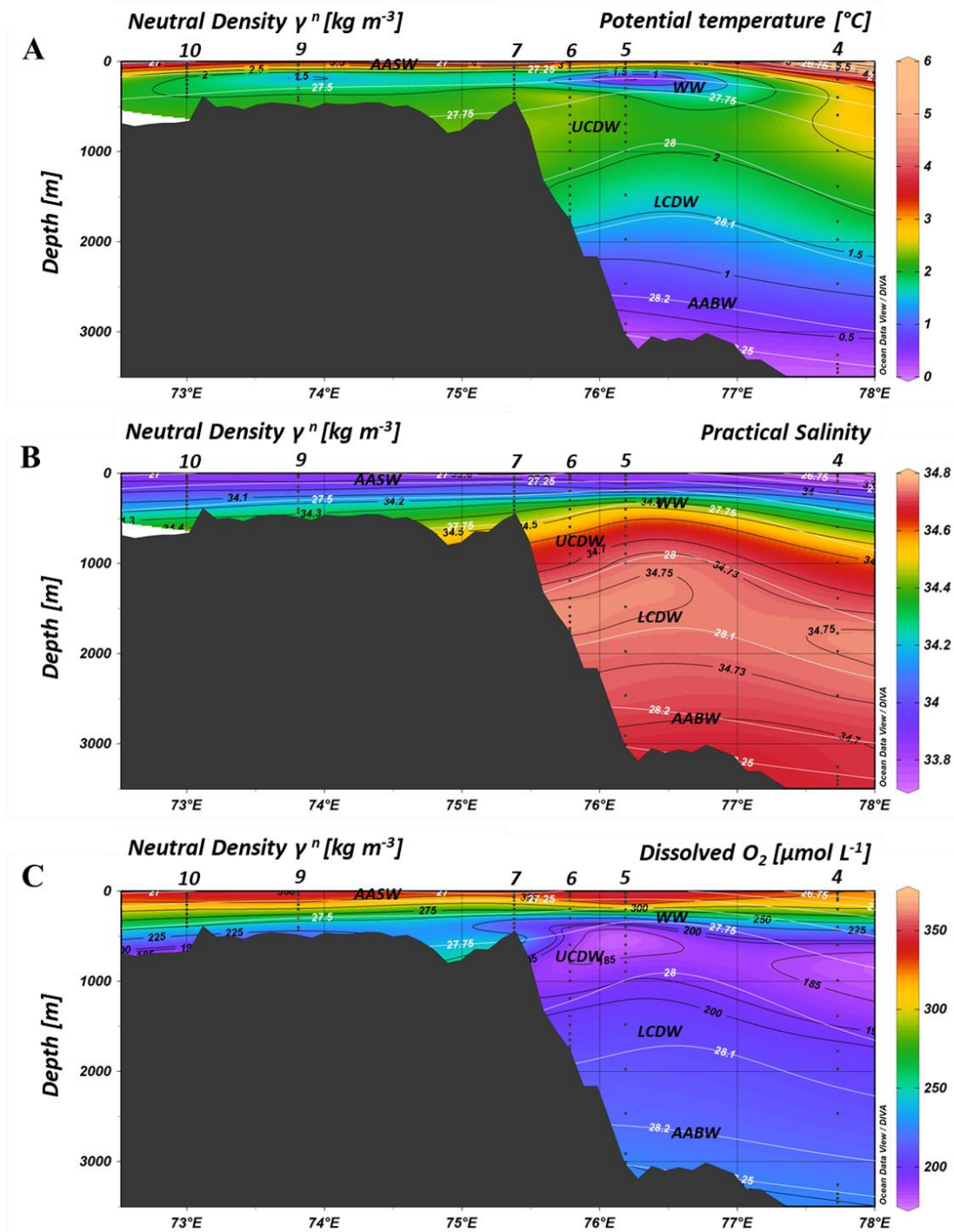


Figure 5.2: Section plots along the B-transect for A) potential temperature (θ), B) salinity and C) dissolved oxygen (O_2). Note that the neutral density is displayed on all section plots in white. Main water masses are also indicated as follows: Antarctic Surface Water (AASW), Winter Water (WW), Upper Circumpolar Deep Water (UCDW), Lower Circumpolar Deep Water (LCDW), and Antarctic Bottom Water (AABW).

5.3.2 Soluble Fe and dissolved and soluble Fe-binding organic ligands

In the following paragraphs, median values and ranges are presented per geographical region, the reference region (i.e. R18), B-transect stations (i.e. B2-B11), stations located in the vicinity of McDonald Island (i.e. M12, M14 and M25), stations under the influence of Heard Island (i.e. H23, H24 and H40). Medians with interquartile ranges were calculated instead of average because Fe and [Lt] had maxima in deep patches, which influenced the average values and increased the standard deviations, making median values more suitable.

5.3.2.1 Soluble Fe concentrations

In this paper, the DFe and PFe data sets will not be presented as they are fully described in Holmes et al. (in prep.) and van der Merwe et al. (in prep.), respectively. However, both data sets were used as a comparison with the SFe concentrations for the stations where SFe was sampled (Table 5.1) with lower depth resolution than for the DFe. Overall, SFe profiles followed DFe profiles but depending on the geographical region, SFe:DFe, SFe:CFe exhibited very different profiles (Fig. 5.3, Table 5.1).

Table 5.1: Concentrations of soluble iron (SFe), colloidal Fe (CFe), dissolved Fe (DFe, data from Holmes et al., in prep.), total particulate Fe (PFe, data from Van der Merwe et al., in prep.), and SFe:DFe, CFe:DFe, SFe:CFe, PFe labile:PFetotal, DFe:PFe ratios for the reference station and stations located nearby McDonald and Heard Islands. Note that median concentrations of SFe and CFe do not add to the median of DFe due to non-linearity of the median operation and that the ratios displayed are the median of the ratios.

	Reference			McDonald Island			Heard Island		
	Median	IQR	n	Median	IQR	n	Median	IQR	n
SFe	0.12	0.14	5	0.33	0.19	8	0.25	0.08	13
CFe	0.05	0.06	5	1.64	0.84	8	1.46	0.27	13
DFe	0.24	0.31	10	1.60	0.95	12	1.79	0.37	15
SFe:DFe	0.69	0.27	5	0.23	0.17	8	0.14	0.05	13
CFe:DFe	0.31	0.27	5	0.77	0.17	8	0.86	0.05	13
SFe:CFe	1.88	3.11	4	0.30	0.28	8	0.16	0.07	13
PFe total	0.07	0.04	6	662	131	8	615	166	9
PFe labile:PFetotal	0.21	0.29	6	0.11	0.01	8	0.18	0.04	9
DFe:PFe	1.24	1.35	6	0.002	0.002	8	0.003	0.001	9

Reference station R18

At the R18, SFe concentrations were lower in the upper 200 m depth of the water column (median 0.06 nmol L⁻¹ in the mixed layer and WW), and increased with depth to reach a maximum of 0.34 nmol L⁻¹ at ~500 m depth, after which depth, SFe concentration

decreased to 0.22 nmol L^{-1} . The soluble fraction of Fe was dominating the DFe pool as indicated by median SFe:DFe, and SFe:CFe ratio values of 0.69, and $1.88 \text{ mol mol}^{-1}$, respectively (Table 5.1, Fig. 5.3).

Heard (H) and McDonald (M) Islands

Both Heard and McDonald Islands exhibited similar median SFe, CFe concentrations (Table 5.1). SFe concentrations were overall homogenized throughout the water column of both Islands, however substantial differences were noticed between McDonald stations (M12 and M25) (Table 5.1). However, some patterns were distinguishable. Indeed, M12 exhibited slightly higher SFe concentrations at $\sim 50 \text{ m}$ depth followed by decreasing SFe concentrations, which close to the sediment interface, increased again (Fig. 5.3). SFe concentrations from H23 displayed an opposite trend in regards to DFe concentrations. From surface to $\sim 60 \text{ m}$ depth SFe concentrations increased from 0.28 nmol L^{-1} to reach a maximum value of 0.46 nmol L^{-1} and decreased from $\sim 60 \text{ m}$ depth to the bottom (0.25 nmol L^{-1} at the bottom sample; Fig. 5.3). CFe was dominating the DFe fraction for all the stations, but was considerably lower than the PFe fraction, which largely dominated the Fe pool (Table 5.1). The main difference between McDonald and Heard Islands was the higher proportion of CFe at Heard Island (Table 5.1).

5.3.2.2 Soluble and dissolved Fe-binding organic ligand concentrations and conditional stability constants

The ligand concentrations in the soluble fraction was lower than in the dissolved fraction. However, the ligands in both fractions were not always found in excess with respect to the Fe concentrations (Tables 5.1 and 5.2, Fig. 5.3). In addition to the organic complexation of Fe, the concentrations of inorganic Fe (Fe') and free Fe (Fe^{3+}) were calculated.

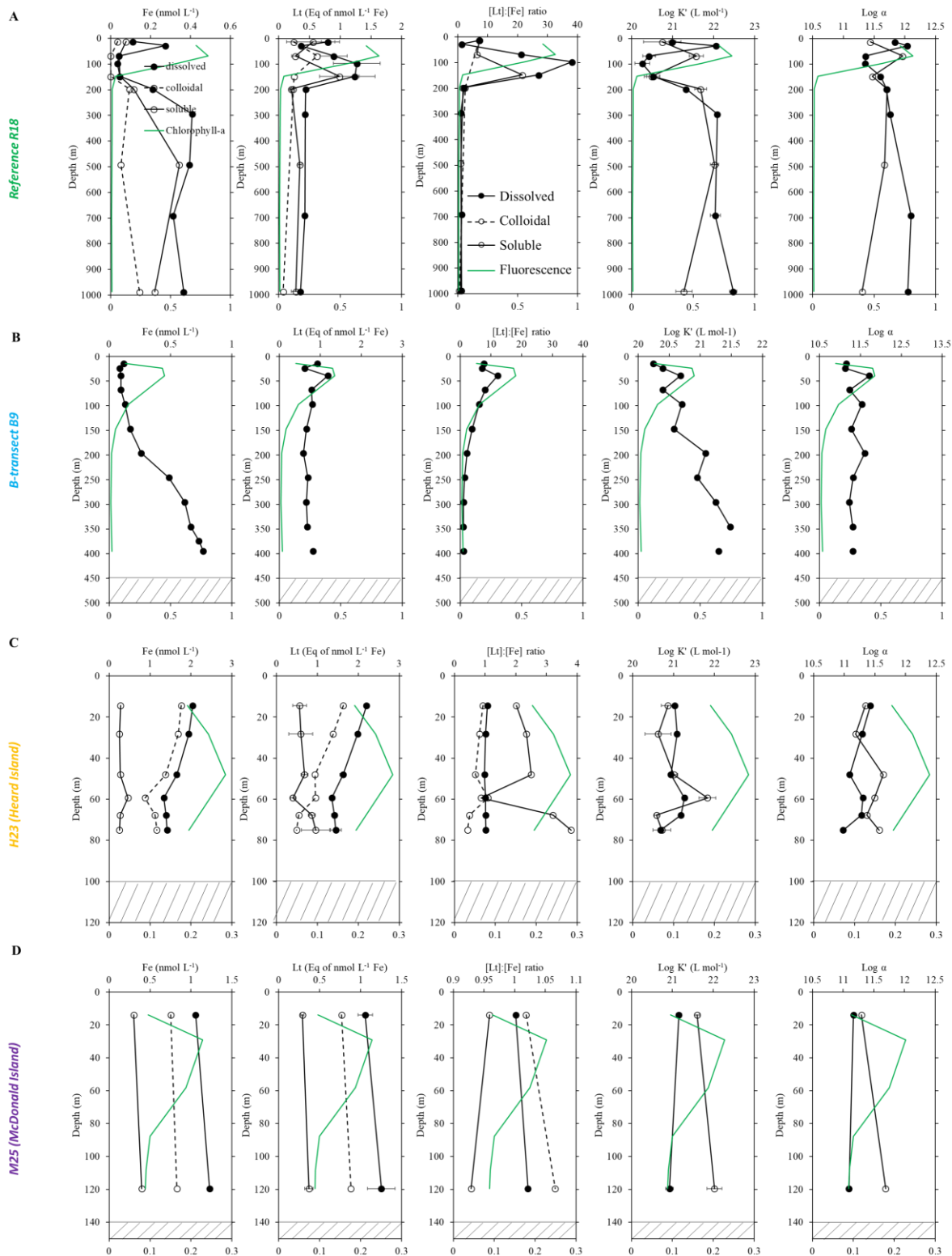


Figure 5.3: The partitioning (when available) of iron (Fe) and Fe-binding organic ligand characteristics in the dissolved (DFe, <0.2 μ m, solid circles and lines, data from Holmes et al., in prep.), soluble (SFe, <10 kDa, open circles, solid lines), and colloidal (CFE, 10 kDa – 0.2 μ m, open circles, dashed lines) as a function of depth for A) the reference R18, B) B-transect B9, C) Heard Island H23 and D) McDonald Island M25. Note that different scales are displayed for the different stations, that the fluorescence (in units of mg TChl-*a* m⁻³) is represented in green and that the shaded areas at the bottom of plots indicate the depth of the plateau.

Table 5.2: Median concentrations of soluble, colloidal and dissolved Fe, total Fe-binding organic ligands (Lt), [Lt]:[Fe] ratios, the conditional stability constant of Lt (log K', with respect to Fe³⁺), the reactivity of Lt (log α), inorganic Fe (Fe'), and the percentage of Fe bound to Lt for the reference, B-transect, Heard Island and McDonald Island stations and for different depth ranges.

	Fraction	Depth range	Fe (nmol L ⁻¹)			Lt (Eq. nM of Fe)		L' (Eq. nM of Fe)		[Lt]:[Fe]			Log K'		Log α		Fe' (pmol L ⁻¹)			FeL (%)		
			median	IQR	n	median	IQR	median	IQR	median	IQR	n	median	IQR	median	IQR	n	median	IQR	median	IQR	n
reference	soluble	full	0.1	0.2	6	0.31	0.3	0.16	0.423	4.1	6.01	6	21.43	0.9	11.57	0.27	6	15	31.37	86	9.67	6
		0-150	0.05	0.02	3	0.56	0.36	0.48	0.36	7.3	7.6	3	20.75	0.54	11.47	0.26	3	11	5	86	12	3
		150-500	0.23		2	0.28		0.05		1.4		2	21.85		11.69		2	30		86		2
		500-bottom	0.22		1	0.28		0.06		1.3		1	21.28		11.31		1	48		78		1
	colloidal	full	0.04	0.09	6	0.25	0.02	0.21	0.11	7.2	3.3	5										
		0-150	0.00	0.02	3	0.25	0.19	0.25	0.21	7.2		3										
		150-500	0.07		2	0.24		0.14		2.5		1										
		500-bottom	0.14		1	0.07		0.00		0.5		1										
	dissolved	full	0.24	0.32	10	0.44	0.47	0.23	0.76	2.1	19.9	9	21.33	1.54	11.76	0.44	9	4	3	96	5	9
		0-150	0.05	0.07	5	0.90	0.43	0.85	0.50	21.2	19.8	5	20.53	0.57	11.60	0.48	5	3	1	96	5	5
		150-500	0.39	0.10	3	0.44		0.13		1.6		2	21.71		11.73		2	14		96		2
		500-bottom	0.34		2	0.39		0.05		1.2		2	22.26		12.07		2	26		93		2
B-transect	dissolved	full	0.27	0.37	60	0.62	0.22	0.24	0.52	2.0	5.0	52	21.24	1.04	11.70	0.62	52	26	50	93	6	33
		0-150	0.10	0.10	24	0.71	0.56	0.57	0.59	7.3	5.3	18	20.83	0.61	11.90	0.47	18	3	5	97	5	14
		150-500	0.34	0.32	18	0.63	0.16	0.19	0.28	1.7	1.7	16	21.12	0.59	11.36	0.32	16	40	45	93	4	11
		500-bottom	0.48	0.18	18	0.52	0.18	0.00	0.02	1.0	0.0	18	21.86	0.34	11.83	0.41	18	55	112	90	4	8
Heard	soluble	full	0.25	0.08	13	0.58	0.40	0.31	0.44	2.2	1.6	8	20.83	0.40	11.36	0.41	8	18	32	93	14	8
	colloidal	full	1.50	0.28	13	1.17	0.87	-0.22	0.45	0.9	0.4	8										
McDonald	dissolved	full	1.83	0.38	13	1.68	0.35	0.02	0.02	1.0	0.0	13	21.18	0.22	11.29	0.17	13	104	46	93	2	13
	soluble	full	0.33	0.19	8	0.33		-0.02		0.9		2	21.82		11.50		2	68		81		2
	colloidal	full	1.69	0.86	8	0.83		0.03		1.0		2										
	dissolved	full	1.23	0.87	19	1.40	0.39	0.18	0.44	1.2	0.4	4	20.93	0.21	11.33	0.39	4	72	74	93	6	4

Reference station (R18)

At R18, soluble Fe-binding organic ligands (SLt), with a median (0.36, $n = 3$) of 0.56 nEq. of mol L⁻¹ Fe and dissolved Fe-binding organic ligands with a median (0.43, $n=5$) of 0.90 nEq. of nmol L⁻¹ Fe, $n = 5$) concentrations were higher within the first ~ 150 m depth of the water column and more variable than for deeper samples (median SLt = 0.28 nEq. of mol L⁻¹ Fe, $n = 3$; DLt = 0.41 nEq. of mol L⁻¹ Fe, $n = 4$, for depth deeper than 150 m) (Fig. 5.3A). The distribution of the excess ligand concentrations as a function of depth were relatively similar to the trends reported in the total ligand concentrations (Fig. 5.3A). Both the soluble ([SLt]:[SFe] = 1.35, $n = 3$) and dissolved ([DLt]:[DFe] = 1.4, $n = 4$) fractions were close to or at saturation from 150 m depth to the bottom of the water column (Fig. 5.3A, Table 5.2). However, within the first 150 m depth of the water column, SLt ranged from 0.27 to 0.99 nEq. of mol L⁻¹ Fe, while SFe ranged from 0.04 to 0.08 nmol L⁻¹ and DLt ranged from 0.37 to 1.27 nEq. of mol L⁻¹ Fe, while DFe ranged from 0.06 to 0.31 nmol L⁻¹ (Fig. 5.3A). At R18 the CLt concentrations were lower or similar than the SLt concentrations, except at 68 m depth. Conversely, closer to the bottom, the colloidal fraction was the most over-saturated with respect to Fe concentrations (Fig. 5.3A, Table 5.2). Interestingly, both SFe and CFe were depleted at depth coinciding with the chlorophyll-*a* maximum. Although, Fe-binding organic ligands were in excess of Fe for all Fe fractions in the first 150 m of the water column, the highest excess ligand (L') were found at the chlorophyll-*a* maximum and just below, in the upper nutricline (Fig. 5.3A). Within this depth range, Fe-binding organic ligands were mainly constituted of the colloidal fraction at the chlorophyll-*a* maximum, while in the upper nutricline, Fe organic ligands dominated in the soluble fraction. While the conditional stability constant (log K') was in the same range for the soluble (20.49 – 22.02) and the dissolved (20.26 – 22.48) fractions, they were different depending on the depth range considered (Table 5.2). At the maximum of fluorescence, the soluble fraction (log K' = 20.75) exhibited higher log K' than the dissolved fraction (log K' = 20.53). Conversely, at 1000 m depth, while dissolved log K' increased from 22.04 to 22.48, the soluble log K' decreased from 22.02 to 21.28 (Fig. 5.3, Table 5.2). The log α was higher for the dissolved than for the soluble fraction throughout the water column (Fig. 5.3A, Table 5.2), except at the peak of fluorescence (log α = 11.36 and 11.96, respectively). However, variations for both fractions were small (log α = 11.57, IQR = 0.27, $n = 6$ and 11.76, IQR = 0.44, $n = 9$; for the soluble and dissolved fractions, respectively). Finally, the percentage of Fe bound to organic

ligands was higher for the dissolved (median = 96, IQR = 5%) than for the soluble (median = 86, IQR = 10%) fractions (Fig. 5.3A, Table 5.2).

McDonald and Heard Islands (M12, M14, H23, H24, M25 and H40)

While for both Islands the ligands in the dissolved fraction were at saturation (i.e. [DLt]:[DFe] \sim 1, Table 5.2), only at Heard Island the soluble ligands were under-saturated in Fe (i.e. median [SLt]:[SFe] = 2.2, Table 5.2). The log K' were similar in the soluble and dissolved fraction at Heard Island (median log K' = 20.83 and 21.18, respectively), while at McDonald Island, the median log K' was higher in the soluble (log K' = 21.82) than in the dissolved (log K' = and 20.93) fractions (Table 5.2).

At H23, the DLt concentrations varied from 1.4 to 2.2 Eq of nmol L⁻¹ Fe (Fig. 5.3C). The highest concentrations were measured at the surface and progressively decreased until 60 m depth, then slightly increased (Fig. 5.3C). The colloidal ligands (median CLt = 0.95 Eq of nmol L⁻¹ Fe, n = 6) were overall higher than the one measured for the soluble (SLt = 0.64 Eq of nmol L⁻¹ Fe, n = 6) fraction, except for samples located closer to the sediment (i.e. below 65 m depth) in which there were more soluble than dissolved ligands (Fig. 5.3C). The log α were similar for the dissolved and soluble fractions, above 30 m depth while below this depth the SLt seemed to be more reactive (Fig. 5.3C). Similarly, there was more Fe bound to organic ligands in the dissolved than in the soluble fractions above 30 m depth, and vice versa below 30 m depth, except for the sample collected at \sim 60 m depth, which had the lowest percentage of soluble Fe bound to organic ligands (i.e. 77%). The median values for the SLt, CLt and DLt were 0.30, 1.8 and 2.1 Eq of nmol L⁻¹ Fe (n = 2), respectively for H24. The log α was higher for the dissolved (median log α = 11.27, n=2) than for the soluble (log α = 10.97, n = 2) fractions, and displayed a higher percentage of bound Fe (on a median base FeL = 93% and 82% for the dissolved and soluble fractions, respectively, Table 5.2). Although H40 was sampled for both dissolved and soluble Fe-binding organic ligands, we were not able to determine SLt concentrations nor their stability constants likely due to the ligand oversaturation by SFe.

Finally, at M25, located close to McDonald Island, the median concentrations for the SLt, CLt and DLt were 0.33, 0.83 and 1.2 Eq of nmol L⁻¹ Fe (n=2), respectively. For all fractions, the organic ligand concentrations were smaller in the surface than at depth (Fig. 5.3D). The log α was higher for the soluble (log α = 11.50) than for the dissolved (log α =

11.33) fractions (Table 5.2). There was more FeL in the dissolved (90%) than in the soluble (81%) fractions (Fig. 5.3D, Table 5.2).

B-transect (B2, B4, B6, B9, and B11)

The dissolved Fe-binding organic ligands had a median of 0.62 Eq of nmol L⁻¹ Fe (IQR = 0.22 Eq of nmol L⁻¹ Fe, n = 40, Fig. 5.3B, Table 5.2). Ligands were on a median base 0.24 Eq of nmol L⁻¹ Fe in excess of DFe and exhibited a median conditional stability constant (log K') of 21.24 L mol⁻¹ (IQR = 1.04, n = 40) (Fig. 5.3B, Table 5.2). The ligand concentrations were highest in surface waters, coinciding with fluorescence maxima, and close to the bottom (Fig. 5.3B, Table 5.2). A minimum of ligand concentrations was noticed at about 700 m depth for all the B-transect stations off the Plateau, while B9, located on the Plateau, had two minima located at about 200 and 300 m depth (Fig. 5.3B). The log K' was higher at depth than in surface waters for all the B-transect stations (Fig. 5.3B, Table 5.2). The dissolved [Lt]:[Fe] ratios were high in surface waters ranging from 2.5 to 38 and coinciding with the fluorescence maxima while ligands were closed to saturation below about 300 m depth and 500 m depth for stations located on and off the Plateau, respectively, down to the seafloor (Fig. 5.3B, Table 5.2). Only B6, located at the shelf break, constituted an exception with high excess ligand concentrations down to 1500 m depth. The log α was maximum at the fluorescence maximum for the B-transect stations (including station 2 and 11, for this study) and was minimum between 300 and 700 m depth. Finally, the percentage of Fe bound to organic ligands was higher in surface waters with up to 99% of Fe bound to ligands and decreased towards the seafloor with on a median base 90% of FeL (Table 5.2).

5.4 Discussion

During the HEOBI voyage, two distinct features were observed concerning the standing total Chlorophyll-*a* (TChl-*a*) inventories. Indeed, over and off the Southern Kerguelen Plateau of the B-transect, elevated integrated (from 0 to 80 m depth) TChl-*a* concentrations were measured (from 20 to 85 mg m⁻²), while around Heard and McDonald Islands integrated TChl-*a* concentrations barely reached 20 mg m⁻² (Wojtasiewicz et al., in prep.). In this context, this study focuses on Fe bioavailability from total Fe and Fe-binding organic ligand concentrations, characteristics and data to give insights on the unexpected lack of phytoplankton biomass around Heard and McDonald Islands while compared to B-transect.

5.4.1 Size partitioning of dissolved Fe and Fe-binding ligands

5.4.1.1 The reference station

At the reference R18, our results showed that SFe was depleted in surface waters, and then increased to a maximum at 500 m, resembling the profiles of the classic nutrients. Indeed, SFe was significantly correlated to all nutrients ($R^2 = 0.77$, $n = 6$, $p\text{-value} < 0.05$ and $R^2 = 0.71$, $n = 6$, $p\text{-value} < 0.05$ for nitrate and phosphate, respectively), especially to silicates ($R^2 = 0.79$, $n = 6$, $p\text{-value} < 0.05$) thus meaning that SFe was consumed in surface waters and remineralised at depth. In addition, the significant correlation between Si(OH)_4 and SFe suggested its uptake by diatoms. Indeed, Wojtasiewicz et al. (in prep.) reported that Fucoxanthin was 2 to 50 times more concentrated than other pigments and represented half of the total chlorophyll-*a* concentrations, thus confirming that they were dominating surface waters of R18 and were responsible for the depletion of SFe. Similarly, within the first 150 m of the water column, the CFe concentrations were positively correlated to SFe concentrations ($\text{SFe} = 0.76 \text{ CFe} + 0.05$, $R^2 = 0.99$, $n = 4$, $p\text{-value} < 0.01$), again highlighting that diatoms not only consumed the SFe but also the CFe. In contrast to what Wu et al. (2001) reported for the North Atlantic and North Pacific Oceans, but in agreement with Chen and Wang (2001), our results showed that CFe was directly bioavailable for diatom species present at R18, while bacteria remineralisation principally released Fe in the soluble fraction. Finally, at depth, although SFe was still dominating the dissolved Fe fraction ($\sim 68\%$), CFe concentrations increased towards the sediment reaching 0.14 nmol L^{-1} and representing 40% of the DFe fraction. (Fig. 5.3A, Table 5.2). These results clearly highlight, together with the comparison between the soluble and dissolved $\log \alpha = \log (K' \times L')$, that within surface waters, SFe was strongly bound to Fe-binding organic ligands, while at depth, the colloidal fraction was the one stabilised by Fe-binding organic ligands.

5.4.1.2 What controls DFe concentrations?

At R18, a significant relationship between DFe and SFe was observed ($\text{DFe} = 1.24 \text{ SFe} + 0.02$, $R^2 = 0.90$, $n = 5$, $p\text{-value} < 0.01$, Fig. 5.4A, in green). Such finding has already been reported by Fitzsimmons and Boyle (2014b) in the tropical North Atlantic Ocean. However, their data set showed a 50-50% DFe partitioning between SFe and CFe as well as similar DFe-SFe and DFe-CFe slopes, highlighting that both fractions contributed to the observed DFe variability, which in this study, was not the case. Indeed, the non-significant y-cut-off (i.e. the CFe concentration) demonstrates that the CFe concentrations did not play any

role in the determination of the DFe concentrations. Indeed, no significant relationship was found between DFe and CFe concentrations at R18 ($\text{DFe} = 2.08 \text{ CFe}$, $R^2 = 0.57$, $n = 5$). However, we must consider that any overestimation of the SFe fraction at R18, will be reflected in the CFe fraction and therefore underestimate this fraction by autocorrelation, as the CFe fraction is calculated from the difference between the DFe and the SFe. Since we found a significant correlation between the DFe and CFe fractions ($\text{DFe} = 1.07 \text{ CFe} + 0.19$, $R^2 = 0.57$, $n = 27$, $p\text{-value} <$) considering all the data, including the data from R18, we thus discarded systematic error in the estimation of both SFe and CFe fractions.

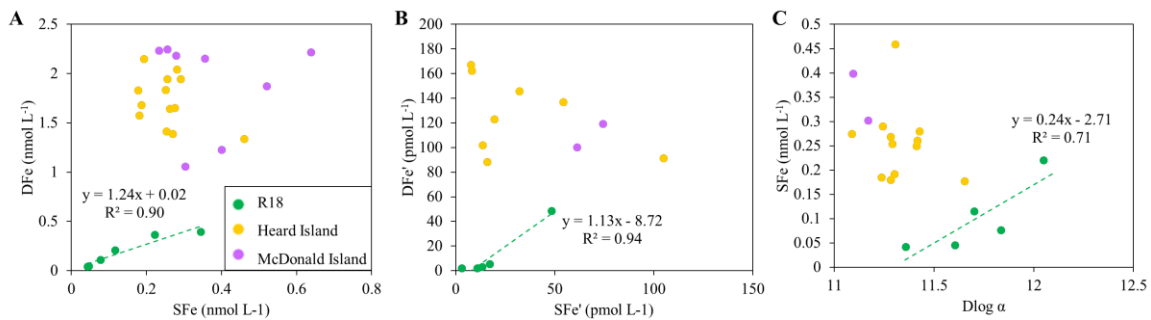


Figure 5.4: Linear relationships between A) dissolved iron (DFe, data from Holmes et al., in prep.) and soluble Fe (SFe) concentrations, B) inorganic DFe and SFe (DFe' and SFe', respectively) and C) SFe and the reactivity of DLt ($\log \alpha$). Note that the colour coding corresponds to the different areas with the reference station in green, Heard Island stations in yellow, and McDonald Island stations in purple.

Furthermore, a significant correlation was also found between DFe' and SFe' concentrations ($\text{DFe}' = 1.13 \text{ SFe}'$, $R^2 = 0.94$, $n = 5$, $p\text{-value} < 0.01$, Fig. 5.4B, in green), implying that the soluble fraction not only drives the total dissolved Fe fraction but also the inorganic and organic ($\% \text{DFeL} = 2 \% \text{SFeL}$, $R^2 = 0.98$, $n = 5$, $p\text{-value} < 0.01$) speciation of Fe, at R18. If the SFe fraction controls the organic and inorganic speciation of DFe, then we should find a positive relationship between the reactivity of SLt and the DFe concentrations and/or between DFe concentrations and SLt, as well as between SFe concentrations and the reactivity of SLt. Not only did we not find any relationship between these parameters but we found a counter-intuitive relationship between SFe and the reactivity of DLt ($\log \alpha$, $R^2 = 0.71$, $n = 5$; Fig. 5.4C, in green). This suggests that the SFe fraction is dependent of the reactivity of the ligands in both the soluble and the colloidal fraction and potentially that the SFe can only be present in seawater if the colloidal ligands are highly reactive preventing CFe from aggregation and therefore enabling it to experience disaggregation. The colloidal fraction should be seen as a temporary state whose fate, i.e. PFe vs. SFe, will depend on the reactivity of the colloidal ligands at R18. Conversely, at Heard and McDonald Islands that

lack of correlations between the soluble and the dissolved fractions suggests that the colloidal fraction is the one driving the dissolved fraction. Although we found a positive correlation between the DFe and the CFe fractions, the dependency of the two variable does not allow us to draw any conclusion.

5.4.2 Possible sources of dissolved and soluble Fe-binding organic ligands (B-transect and R18)

Aimed at tracking the different sources of Fe-binding organic ligands we separated stations from R18 and B-transect stations (except B2 as it was separated from the others by the Polar Front, Park et al., 2008b), according to the different water masses (Fig. 5.5). Despite large variations between DLt concentrations for the different stations, higher concentrations were measured in the upper 500 m, showed a minimum around 1500-2500 m depth and were higher again at the sediment interface (Figs 5.3 and 5.5), which broadly corresponded to the distributions and median values of DFe, DLt, Dlog α and DFe' within the six distinguished water types highlighted in figure 5.5. The highest DLt concentrations were found in the AASW, which was characterized by the highest fluorescence values, and to a lesser extent closer to the sediments within the shelf waters located above the Kerguelen Plateau and within the AABW (Fig. 5.5B). Therefore, potential sources of Fe-binding organic ligands that should be considered in this specific area are the biological component and the sediments. Minimum DLt concentrations were found within the LCDW where, remineralisation activity was low (Fig. 5.5B). Highest log K' were found within the UCDW and AABW where enhanced nitrate concentrations were observed (Fig. 5.5E and H), suggesting a regenerated source (bacterial or grazing). DFe' was minimum within the AASW and gradually increased with depth (Fig. 5.5D). Finally, ligand reactivity was maximal within AABW and minimal within the shelf waters where Mn inputs were relatively high (DMn data from Wuttig et al., in prep.) (Fig. 5.5C and I). The increasing DFe' and DMn concentrations towards the sediment points to a supply from the sediment and maybe an uptake of DFe' in surface waters (Fig. 5.5F), as previously reported by Gerringa et al. (2008). Gathering insights from R18 and B-transect stations we will, in the following sections, investigate the plausibility of these two sources in releasing Fe-binding organic ligands.

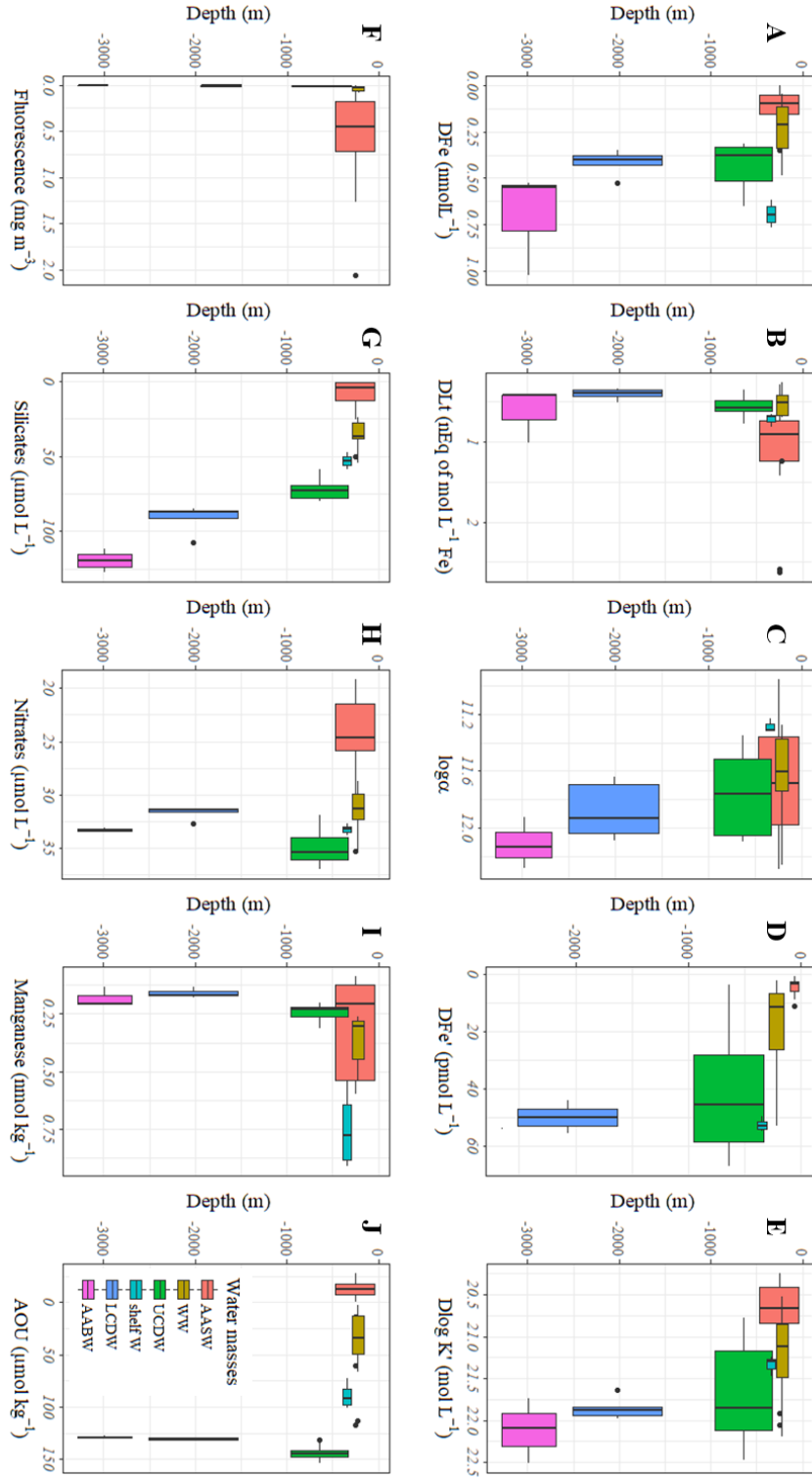


Figure 5.5: Box and whisker diagram of A) Fe concentrations (data from Holmes et al., in prep.), B) total Fe-binding organic ligand concentrations (Lt), C) the reactivity of Lt ($\log \alpha$), D) the inorganic Fe concentrations (Fe') and E) the conditional stability constant ($\log K'$, with respect to Fe^{3+}) for the dissolved Fe fraction, and F) the fluorescence (in units of $\text{mg TChl-}a \text{ m}^{-3}$), G) silicates ($\mu\text{mol L}^{-1}$), H) nitrates ($\mu\text{mol L}^{-1}$), I) dissolved manganese (in nmol kg^{-1}) data from Wuttig et al., in prep.) and J) Apparent Oxygen Utilization (AOU, ($\mu\text{mol kg}^{-1}$)), as a function of the different water masses determined at the B-transect. AASW: Antarctic Surface Water, WW: Winter Water, UCDW: Upper Circumpolar Deep Water, shelf W: deeper waters located within 70 m above the Kerguelen Plateau, LCDW: Lower Circumpolar Deep Water, and AABW: Antarctic Bottom Water.

5.4.2.1 Biological component as a source of Fe-binding organic ligands

Previous studies reported that under Fe deficient conditions, microorganisms are able to release Fe-binding organic ligands in order to facilitate the uptake of Fe. Such ligands have been shown to be siderophores that could be generated by autotrophic (i.e. *Synechococcus sp.* and *Prochlorococcus sp.*) and heterotrophic bacteria (Buck et al., 2018; Reid et al., 1993; Rue and Bruland, 1995; Wilhelm and Trick, 1994; Vaspur and Butler, 2005). Many studies also reported the possibility of grazing (e.g. Sato et al., 2007) and cell lysis (e.g. Mioni et al., 2005; Poorvin et al., 2004) to deliver Fe-binding organic ligands in solution (e.g. Rue and Bruland, 1995).

In our study, no direct relationship was found between phytoplankton (i.e. fluorescence) and dissolved Fe-binding organic ligands. However, a negative correlation was found between dissolved Fe-binding organic ligands and silicate concentrations ($R^2 = 0.25$, $n = 66$, $p\text{-value} < 0.001$) considering the whole water column, as well as a positive correlation between $\log K'$ and fluorescence ($R^2 = 0.82$, $n = 15$, $p\text{-value} < 0.001$) in AASW. The high ligand concentrations measured at low DFe concentrations (Fig. 5.5A and B) suggest that diatoms were able to exude dissolved ligands in response to Fe-limitation with high conditional stability constants (maximum $\log K' = 21.92$ Eq of nmol L^{-1} Fe within the AASW, see Section 5.2,) that fit in the range of siderophore-like substances. Such substances could be produced by diatoms (Meiners et al., 2008). The high concentrations of these ligands together with their high stability constants showed that these ligands were highly reactive, as indicated by the positive correlation found between dissolved $\log \alpha$ and fluorescence ($R^2 = 0.52$, $n = 15$, $p\text{-value} < 0.001$) within surface waters (fluorescence > 0.10 mg Chl-*a* m^{-3}).

Another possible source of ligands to surface waters could originate from bacterial activity either as free-living bacteria or as bacteria attached to diatoms (Amin et al., 2012). Despite the lack of bacterial abundance measurements, a weak but significant positive correlation was found between the reactivity of dissolved Fe-binding organic ligands and Apparent Oxygen Utilization ($\text{AOU} > 70 \mu\text{mol kg}^{-1}$, $R^2 = 0.32$, $n = 25$, $p\text{-value} < 0.01$), thus suggesting a possible link with bacterial production of highly reactive ligands (average $\log \alpha = 11.70 \pm 0.34$, median $\log \alpha = 11.74$). These ligands had an average $\log K'$ of 21.67 ± 0.52 L mol^{-1} ($n = 25$, median $\log K' = 21.67$ L mol^{-1}) and intermediate DLt concentrations with an average of 0.54 ± 0.16 Eq of nmol L^{-1} Fe ($n = 25$, median DLt = 0.53 Eq of nmol L^{-1} Fe). However, no relationship was found between dissolved $\log \alpha$ and nitrate concentrations, a

proxy of bacterial remineralisation. Although the DLt concentrations were relatively constant, the log K' displayed a strong variability in the water masses where AOU was higher than 70 $\mu\text{mol kg}^{-1}$, namely the shelf waters of the Kerguelen Plateau, the AABW, UCDW and LCDW off-plateau water masses. Indeed, within these water masses, both strong and intermediate ligand classes potentially bacteria-mediated were observed. The strongest class, observed in the AASW and the UCDW, exhibited average $\log K' = 22.26 \pm 0.21 \text{ L mol}^{-1}$ ($n = 7$), which could be of siderophore type (Gledhill and Buck, 2012), while the intermediate class, observed in the shelf waters LCDW and to a lesser extent in the UCDW had an average $\log K'$ equal to $21.53 \pm 0.38 \text{ L mol}^{-1}$ ($n = 16$), and could be a saccharide-type (Hassler et al., 2015; Hassler et al., 2011c), i.e. exopolysaccharids (EPS) or glucuronic acid (monosaccharide). Therefore, the lack of correlation between $\log \alpha$ and nitrate concentrations was not surprising and likely reflected the occurrence of different bacterial community. Our results are further supported by the study carried out by Obernosterer et al. (2008), who reported a three-fold more abundant heterotrophic bacterial community dominated by high-nucleic-acid-containing cells within the phytoplankton bloom and above the Kerguelen Plateau compared to surrounding HNLC waters.

The comparison between the results from Gerringa et al. (2008) and our B-transect stations are displayed in figure 5.6. Overall, there was a good agreement between the conditional stability constants ($\log K'$) determined during the two studies with no significant differences. However, a marked difference was noticed in the dissolved Fe-binding organic ligand concentrations with lower values for our study than for the study of Gerringa et al. (2008), resulting in much lower reactive ligands, especially at depths. The main differences between the two studies originated from higher DFe concentrations (Blain et al., 2008b; Holmes et al., in prep.) in our study and therefore ligands close to saturation, as indicated by the average dissolved $[\text{L}']:[\text{Fe}]$ ratios, i.e. 1.2 and 4.9 mol mol^{-1} , for HEOBI and KEOPS, respectively. However, for both studies, increasing DFe and Fe-binding organic ligand concentrations were noticed closer to the sediment, thus highlighting an important source of these two parameters from the Kerguelen Plateau.

Table 5.3: Comparison of median ligand characteristics for the different water masses determined for the B-transect (t-test). AASW: Antarctic Surface Water, WW: Winter Water, UCDW: Upper Circumpolar Deep Water, shelf W: deeper waters located within 70 m above the Kerguelen Plateau, LCDW: Lower Circumpolar Deep Water, and AABW: Antarctic Bottom Water.

Fe	AASW	WW	shelf W	UCDW	LCDW
WW	0.11				
shelf W	0.00	0.01			
UCDW	0.00	0.03	0.01		
LCDW	0.00	0.02	0.02	0.73	
AABW	0.00	0.01	0.70	0.09	0.02
Fe'	AASW	WW	shelf W	UCDW	LCDW
WW	0.04				
shelf W	0.01	0.13			
UCDW	0.00	0.24	0.55		
LCDW	0.00	0.00	0.17	0.01	
AABW	0.00	0.02	0.20	0.06	0.38
Lt	AASW	WW	shelf W	UCDW	LCDW
WW	0.01				
shelf W	0.26	0.28			
UCDW	0.00	0.97	0.02		
LCDW	0.00	0.23	0.02	0.01	
AABW	0.22	0.92	0.70	0.66	0.26
Log K'	AASW	WW	shelf W	UCDW	LCDW
WW	0.04				
shelf W	0.06	0.50			
UCDW	0.00	0.15	0.55		
LCDW	0.00	0.11	0.02	0.96	
AABW	0.01	0.08	0.10	0.29	0.38
Log α	AASW	WW	shelf W	UCDW	LCDW
WW	0.81				
shelf W	0.12	0.05			
UCDW	0.41	0.31	0.01		
LCDW	0.22	0.11	0.02	0.73	
AABW	0.06	0.05	0.10	0.06	0.17

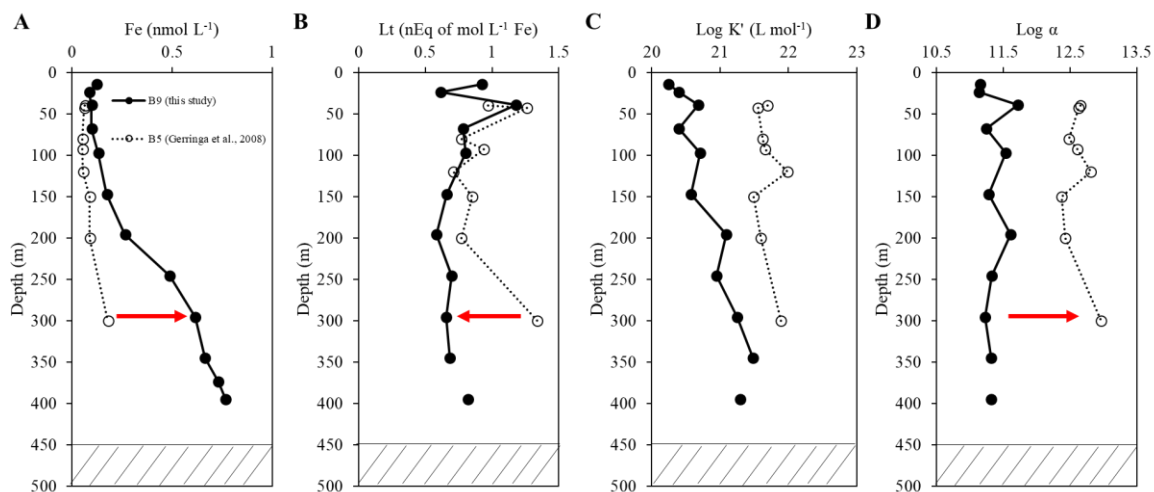


Figure 5.6: Plot of A) dissolved iron (DFe), B) Fe-binding organic ligand (Lt), C) conditional stability constant ($\log K'$) and D) reactivity of Lt ($\log \alpha$) as a function of depth for B9 from this study and B5 from Gerringa et al. (2008). Note that the shaded areas at the bottom of plots indicate the depth of the plateau for this study.

5.4.2.2 Sediment as a source of Fe-binding organic ligands

The higher DLt concentrations found near the sediments in our study could originate either from the upper ocean through accumulation of organic matter on the sediment floor and subsequent degradation or directly from the sediment.

A diffusive transfer of Fe-binding organic ligands from the Kerguelen Plateau sediments has previously been suggested by Gerringa et al. (2008), as indicated by higher DLt concentrations near the sediment. In their study, they sampled for sediment pore waters at station A3, which was not sampled during our study but which was a station located above the Kerguelen Plateau. Gerringa et al. (2008) were not able to report dissolved Fe-binding organic ligand concentrations since the DFe was largely in excess. However, they were able to measure the total DFe concentrations, which sharply increased at the sediment interface and especially within the sediment with up to $\sim 375 \text{ nmol L}^{-1}$ at 3 cm depth. It is thus undeniable that DFe originate from the sediments (Blain et al., 2007). In our study, we also found higher DLt concentrations close to the sediment above the Kerguelen Plateau coincident with higher DFe. However, our DLt concentrations were lower than the one reported by Gerringa et al. (2008) during KEOPS and the measured DFe was on average 2 times (Holmes et al., in prep.) higher than reported by Blain et al. (2008c) (Fig. 5.6). Therefore, it seems that the sources of DFe and Fe-binding organic ligands were not coupled, since we would have expected higher DLt concentrations for our study.

Another explanation of these enhanced DLt concentrations towards the sediment could be the degradation of organic matter on the sediment floor. Indeed, as reported above, the enhanced DLt concentrations found close to the sediment were associated to enhanced AOU and nitrate concentrations, thus potentially implying a bacteria-mediated production. In addition, during KEOPS, Armand et al. (2008) reported a greater number of phytoplankton cells preserved on the Kerguelen Plateau sediment and overlying deep waters than off-Plateau, thus supporting the accumulation of biogenic material on the sediment floor. This is also supported by the study of Sarthou et al. (2008) who reported that about half of the Fe demand is fulfilled by regenerated Fe from biogenic material in this area, thus implying organic matter accumulation on the sediment. Finally, our results together with the finding of Boyd et al. (2010) who pointed to the fact that the remineralization of biogenic PFe is likely the source of both DFe and Fe-binding organic ligands, supports the idea of a bacterial source rather than a sediment pore water source. Although the ligands measured in these waters were of intermediate class (median $\log K' = 21.29$), their conditional stability constant were higher than the one reported for surface waters (median $\log K' = 20.49$, Fig. 5.5). Thus in case of internal wave activity, as evidenced during KEOPS with the size-variation of the Benthic Boundary Layer over time (Blain et al., 2008c), the bacteria-mediated organically bound Fe will be resupplied in upper waters providing and sustaining DFe concentrations for phytoplankton.

5.4.3 Comparison between the different areas

5.4.3.1 Dissolved fraction

Within the dissolved fraction, there was no significant difference between R18 and B-transect stations for all the parameters displayed in Figure 5.7, except from DFe'. Consequently, we assume that the physical speciation of Fe and Fe-binding organic ligands were similar for the B-transect and R18 stations. However, clear significant differences (t-test, $p\text{-value} < 0.05$, Table 4) were noticed between Heard and McDonald Islands, as well as between both Islands, on one side and, R18 and B-transect stations on the other side (Fig. 5.7A-H). Although the highest DFe and DLt concentrations were measured at Heard Island compared to R18 and B-transect stations (Fig. 5.7A and B), most of these ligands were at saturation, as indicated by the distribution of excess ligands (Figs. 5.7E and F, Table 5.4), thus highlighting the instability of the DFe at both Islands compared to R18 and B-transect stations. Similarly, McDonald Island presented higher DFe and Fe-binding organic ligand

concentrations than at the B-transect and R18 stations (Table 5.4). However, excess ligand concentrations were not different from R18 and B-transect stations (Fig. 5.7A, B, E and F). However, when comparing $[L']:[Fe]$ ratios, no differences were found between Heard and McDonald Islands as well as between R18 and B-transect stations, which presented relatively higher free binding sites than for the two Islands (Fig. 5.7, Table 5.4). Although these differences could originate from the bacterial activity as we highlighted that bacterial activity was likely releasing Fe-binding organic ligands at R18 and B-transect stations, Obernosterer et al. (in prep.) highlighted that bacteria from Heard Island were very active. These differences were thus likely attributed to higher TChl-*a* concentrations measured at R18 and B-transect stations ($0.78 \pm 0.15 \text{ mg m}^{-3}$, $n = 12$, median = 0.65 mg m^{-3}) than for the Islands ($0.38 \pm 0.15 \text{ mg m}^{-3}$, $n = 3$, median = 0.40 mg m^{-3}) (Wojtasiewicz et al., in prep.), thus suggesting the higher potential for large diatoms to produce relatively high ligand concentrations in excess of Fe. This raises the question of why large diatoms produce ligands in excess of DFe. In a thermodynamic point of view; the only way to dissolve part of labile PFe is to have higher Fe-binding organic ligand concentrations than the DFe, particularly in case of weak ligands, to move the equilibrium between dissolved and particulate phases towards the dissolved phase. Therefore, large diatoms were likely producing high Fe-binding ligand concentrations to solubilize part of the PFe.

In terms of conditional stability constant, no difference was noticed between the B-transect, R18 and Heard Island stations ($p\text{-value} > 0.05$) but all these stations presented higher $\log K'$ than at McDonald Island stations (except for R18, Fig. 5.7C, Table 5.4A). The $\log K'$ together with the L' concentrations led to Fe-binding organic ligands significantly less reactive around the Islands than at R18 and B-transect stations (Table 5.4A), enabling higher DFe' concentrations around the Islands followed by the B-transect than at R18. Differences between the B-transect stations and R18 were likely due to the DFe' source from the sediment pore water above the Kerguelen Plateau (Gerringa et al., 2008). Similarly, we can assume that the high DFe' concentrations calculated around the Islands originated from the sediment resuspension (Fig. 5.7G). Indeed, waters around the Islands were more turbid than at R18 and B-transect stations (except for deeper samples above the Kerguelen plateau, Fig. 5.5).

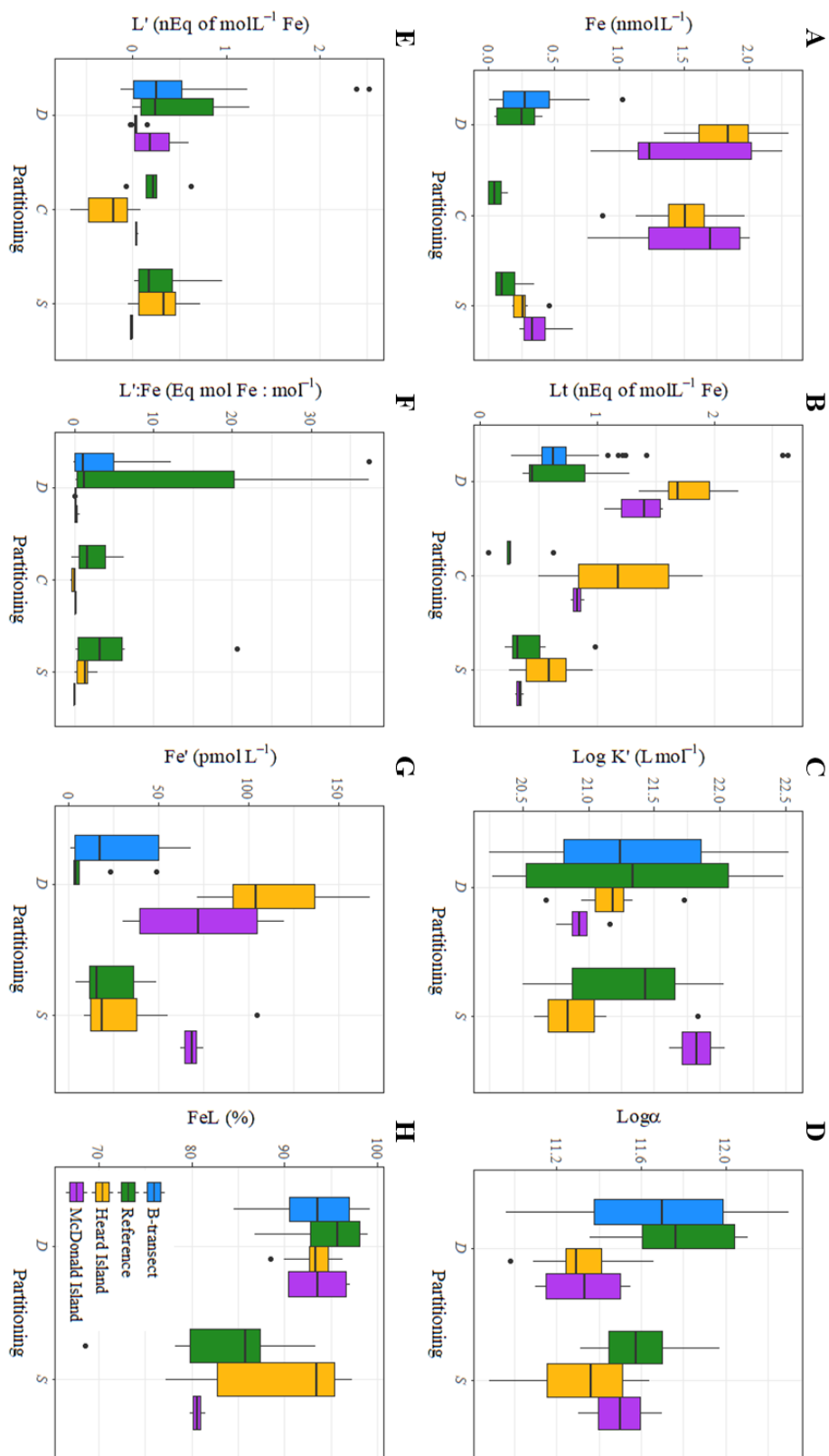


Figure 5.7: Box and whisker diagram of A) iron (Fe) concentrations, B) total Fe-binding organic ligand concentrations (Lt), C) conditional stability constants ($\log K'$, with respect to Fe^{3+}), D) the reactivity of ligands ($\log \alpha$), E) excess Fe-binding organic ligands (L'), F) $[\text{L}']:[\text{Fe}]$ ratio, G) inorganic Fe (Fe'), and H) the percentage of Fe bound to Fe-binding organic ligands, and G) as a function of Fe fractions D (dissolved) C (colloidal) and S (soluble) for the B-transect (in blue), the reference stations (in green), Heard Island (in yellow) and McDonald Island (in purple).

Table 5.4: Comparison of median ligand characteristics within A) the dissolved, B) the colloidal and C) the soluble fractions for the four different areas when data were available, i.e. the reference station, the B-transect stations, Heard Island stations and McDonald Island stations (t-test).

A

Dissolved fraction			
Fe	B-transect	Reference	McDonald
Reference	0.14		
McDonald	< 0.001	< 0.001	
Heard	< 0.001	< 0.001	0.03
Lt	B-transect	Reference	McDonald
Reference	0.83		
McDonald	0.006	0.004	
Heard	< 0.001	< 0.001	0.03
L'	B-transect	Reference	McDonald
Reference	0.6		
McDonald	0.38	0.27	
Heard	< 0.001	0.03	0.23
[L']:[Fe]	B-transect	Reference	McDonald
Reference	0.18		
McDonald	< 0.001	0.03	
Heard	< 0.001	0.03	0.23
Log K'	B-transect	Reference	McDonald
Reference	0.84		
McDonald	0.005	0.19	
Heard	0.22	0.52	0.04
Log α	B-transect	Reference	McDonald
Reference	0.58		
McDonald	0.04	0.02	
Heard	< 0.001	< 0.001	0.86
Fe'	B-transect	Reference	McDonald
Reference	0.01		
McDonald	0.06	0.03	
Heard	< 0.001	< 0.001	0.07
FeL (%)	B-transect	Reference	McDonald
Reference	0.22		
McDonald	0.74	0.56	
Heard	0.78	0.24	0.84

B

Colloidal fraction		
Fe	Reference	McDonald
McDonald	< 0.001	
Heard	< 0.001	0.78
Lt	Reference	McDonald
McDonald	0.005	
Heard	0.002	0.1
L'	Reference	McDonald
McDonald	0.08	
Heard	0.004	0.008
[L']: [Fe]	Reference	McDonald
McDonald	0.18	
Heard	0.16	0.01

C

Soluble fraction		
Fe	Reference	McDonald
McDonald	0.006	
Heard	0.07	0.06
Lt	Reference	McDonald
McDonald	0.41	
Heard	0.36	0.03
L'	Reference	McDonald
McDonald	0.08	
Heard	0.99	0.01
[L']: [Fe]	Reference	McDonald
McDonald	0.14	
Heard	0.23	0.01
Log K'	Reference	McDonald
McDonald	0.18	
Heard	0.24	0.07
Log α	Reference	McDonald
McDonald	0.71	
Heard	0.06	0.52
Fe'	Reference	McDonald
McDonald	0.01	
Heard	0.51	0.03
FeL (%)	Reference	McDonald
McDonald	0.5	
Heard	0.18	0.01

5.4.3.2 Impact for Fe physical and organic speciation

Aimed at understanding which fraction was responsible for the saturation of the dissolved Fe-binding organic ligands at the Islands compared to R18 and B-transect stations, we performed pairwise t-tests between the four areas and each parameters (when determined). Although some differences were noticed in the soluble fraction, it seems that the main differences originated from the colloidal fraction. Indeed, similarly as for the dissolved fraction, higher CFe and CLt were measured in the vicinity of the Islands compared to the R18 station (see Section 5.4.1, Table 5.4B), resulting in a saturated colloidal fraction for both Islands.

The indirect measurement of the colloidal fraction characteristics did not allowed us to determine the conditional stability constant nor the reactivity of the CLt. However, if no significant differences were found between the soluble $\log \alpha$ of the Islands and R18, significantly higher dissolved $\log \alpha$ were found at R18 compared to the Islands (Table 5.4A and C). Therefore, this suggests that the significantly lower reactivity of the dissolved fraction for Heard and McDonald Islands compared to R18, originated from the low reactive colloidal ligands at the Islands. This implies that PFe will account for a much higher fraction of the total iron pool at the Islands than at the B-transect and R18 stations. Indeed, the DFe:PFe ratios confirmed that PFe accounted for a much higher fraction at McDonald (median = 0.002 mol mol⁻¹) and Heard (median = 0.003 mol mol⁻¹) Islands than at the B-transect (median = 0.60 mol mol⁻¹) and R18 (median = 1.2 mol mol⁻¹) stations (DFe data from Holmes et al, in prep. and PFe data from van der Merwe et al., in prep.) (Table 5.1). It seemed therefore that the colloidal fraction is the one that determine the fate of Fe either experiencing scavenging, or remobilisation from the PFe pool.

The saturation of the dissolved Fe-binding organic ligands together with the high DFe concentrations point to an important source of DFe at Heard and McDonald Islands, enabling the DFe to reach concentrations higher than the concentrations of organic ligands with substantial DFe' concentrations. Such observations have previously been reported in areas with, for instance, hydrothermal activity (e.g. Buck et al., 2018; Buck et al., 2015; Gerringa et al., 2017). Although many studies (Fitzsimmons et al., 2017; Resing et al., 2015; Tagliabue et al., 2014a; Tagliabue et al., 2017) reported the transport of hydrothermal DFe over very long distances (~ 4,300 km), the low reactivity of the dissolved Fe-binding organic ligands measured in this study compared to those reported for other studies (i.e. strong ligand types, e.g. Buck et al., 2018; Buck et al., 2015) likely explained why high DFe concentrations were

only located around the Islands without a significant transport further to the north (see Fig. 7 from Holmes et al., in prep.), despite the broad circulation (Park et al., 2008b).

During the HEOBI voyage, on-board incubation experiments were performed with particles from McDonald Island added to reference station seawater. Obernosterer et al. (in prep.) reported that the particle-attached bacteria were highly active and that when comparing the control to the addition of McDonald Island particles this resulted in a production of Fe-binding organic ligands and higher DFe concentrations. However, although no statistical differences were noticed, higher conditional stability constants were measured at the end of the experiment with the addition of particles (average $\log K' = 11.90 \pm 0.46 \text{ L mol}^{-1}$) than in the control (average $\log K' = 11.40 \pm 0.16 \text{ L mol}^{-1}$). Therefore, there is evidence that McDonald Island bacteria were able to produce weak Fe-binding organic ligands and that the higher DFe concentration were either due to the stronger Fe-binding organic ligands present at the beginning of the experiment from R18 (see Section 5.4.1) or as the DLt concentration increased regardless of their reactivity.

To sum up, we found that the differences observed between the Islands and R18 and B-transect stations were likely due to the low reactivity of the colloidal fraction, resulting in substantial colloidal aggregation with no solubilisation of Fe from particles as the soluble ligands were not strong either.

5.4.3.3 Potential effects for the phytoplankton community

In addition to the differences in terms of TChl-*a* between the Islands and R18 and B-transect stations (Wojtasiewicz et al., in prep.), van der Merwe et al. (in prep.) reported significantly ($p\text{-value} < 0.05$) higher POC concentrations around the Islands (median POC = $77.4 \mu\text{g L}^{-1}$ and $54.5 \mu\text{g L}^{-1}$ for McDonald and Heard Islands, respectively) compared to R18 and B-transect stations (median POC = $9.6 \mu\text{g L}^{-1}$ and $29.8 \mu\text{g L}^{-1}$ for R18 and B-transect stations, respectively) for the full depth range. Furthermore, Wojtasiewicz et al. (in prep.) reported that most of the phytoplankton consisted of smaller cells around the Islands than at R18 and B-transect stations. This suggests that besides the phytoplankton cells, there was an additional POC source around the Islands. The low reactivity of dissolved Fe-binding organic ligands potentially suggests that they were of gel-like substances that are known to undergo fast aggregation (Baalousha et al., 2006; Verdugo et al., 2004). Passow (2002) reported that there was a significant relationship between TEP production and the growth phase of most of the diatoms (i.e. *Chatoceros affinis*, *C. neogracile*, *Thalassiosira weissflogii*, *Nitzschia angularis*, and mixed natural diatom community) as well as with dinoflagellates and

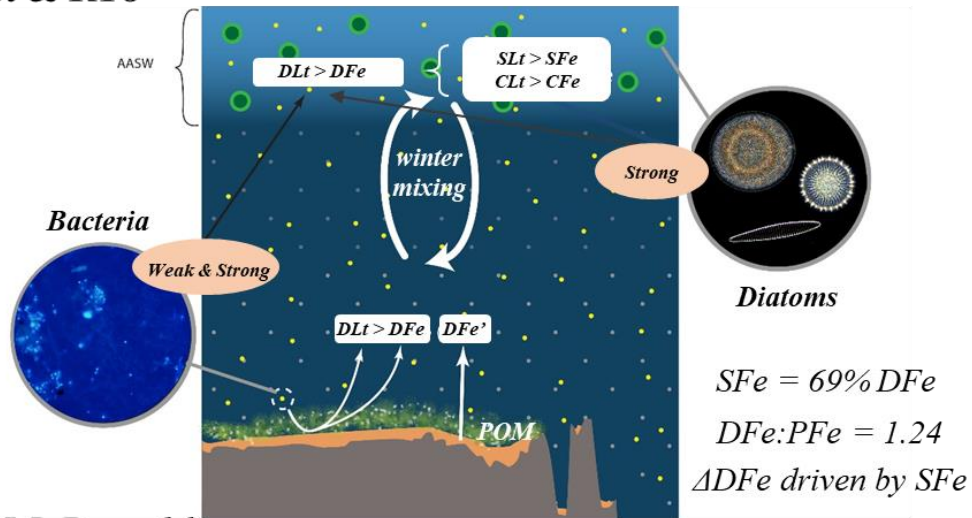
Haptophytes (i.e. *Phaeocystis* sp. and *Phaeocystis antarctica*). Although taxonomic determination of the phytoplankton community was not performed during our study, the pigment:TChl-*a* ratios suggested the presence of mainly small diatoms and type-8 Haptophytes (i.e. *Phaeocystis* sp.) (Wojtasiewicz et al., in prep.). Such functional group have been demonstrated to be more successful than diatoms in low Fe conditions (Verity et al., 2007) due to their better photosynthetic performance (Tagliabue and Arrigo, 2005) and their ability to form polysaccharide matrices able of Fe-sequestration, making them strong competitors for Fe at low Fe levels over diatoms (Pasquer et al., 2005), thus supporting the potential of an Fe-limitation of the diatom community despite the high DFe concentrations measured around Heard and McDonald Islands.

5.5 Conclusion

The physical speciation of the dissolved fraction seemed to be driven by the fraction (i.e. soluble or colloidal) that dominated the dissolved Fe pool. Both phytoplankton and bacteria might produce Fe-binding organic ligands with substantial differences in their conditional stability constants. Indeed, large diatoms that dominated surface waters of R18 and B-transect stations were likely able to produce strong Fe-binding organic ligands mainly within the colloidal fraction, which were largely in excess of the DFe, while bacteria located in the same region produced both strong and weak Fe-binding organic ligands likely within the soluble and colloidal fraction, respectively. This resulted in excess ligands in the first 200 m depth of the water column, increasing the Fe solubility and potentially its bioavailability (Fig. 5.8). The sediment from the B-transect were also a source of Fe, especially inorganic Fe, and Fe-binding organic ligands. However, it seems that these ligands were the result of particulate organic matter degradation, which accumulated on top of the sediment, rather than directly from the basaltic sediment. Therefore, it is very likely that winter mixing will fuel the surface waters of the B-transect with directly bioavailable DFe' and Fe bound to dissolved or particulate organic matter (POM). This POM will feed grazers and bacteria, which after degradation constitutes an additional source of DFe organically bound. That might be the triggering process of the phytoplankton bloom over the Kerguelen Plateau. We showed clear differences between R18 and B-transect stations and Heard and McDonald Island stations. Indeed, Heard and McDonald Island stations exhibited Fe-binding organic ligands over-saturated by Fe throughout the water column, thus highlighting an important source of Fe potentially inferred to cold seep features (Spain et al., in prep.). The water column of both

Islands was dominated by low reactive ligands resulting in higher proportions of PFe concentrations compared to R18 and B-transect stations. These weak ligands were potentially made of transparent exopolymer (TEP) or TEP precursors, which are gel-like substances known to trap living phytoplankton cells and could thus explain the lower Chlorophyll-*a* concentrations observed around both Islands. This hypothesis should be investigated in future cruises.

B-transect & R18



Heard & McDonald

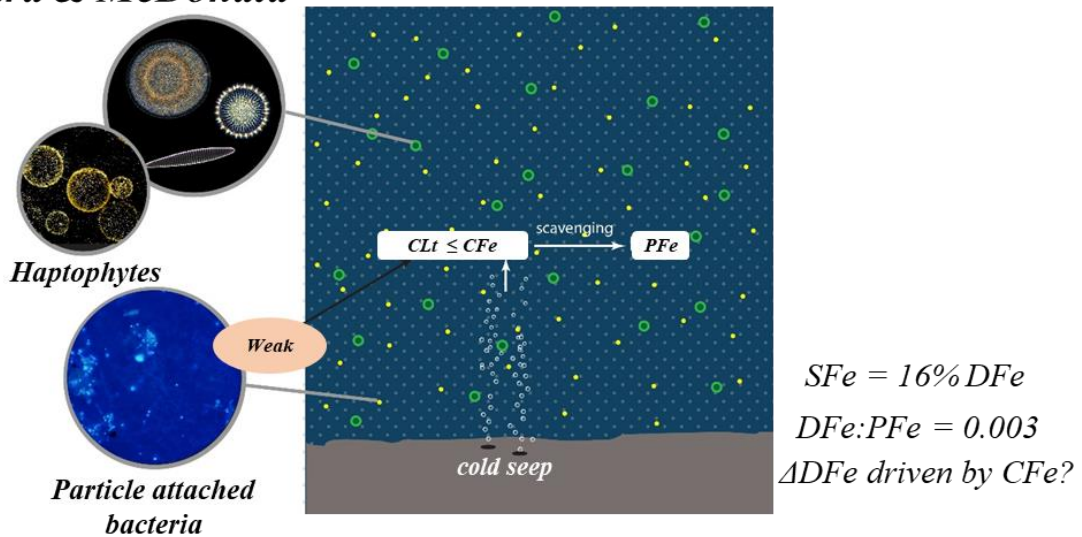


Figure 5.8: Conceptual schematic of the main finding at Heard and McDonald Islands stations and the B-transect and R18 stations (D. Alain and S. Hervé, IUEM). Note that yellow dots refer to bacteria, grey dots to particles, green dots to phytoplankton, the orange field on top of bathymetry refers to sediment and that the greenish material refers to Particulate Organic Matter (POM). (*DFe* data from Holmes et al., in prep., *PFe* data from van der Merwe et al., in prep.; pigment data from Wojtasiewicz et al., in prep., bacteria picture courtesy from S. Blain).

Chapter 6:

Conclusions and Perspectives

Chapter 6 – Conclusion and Perspectives

Table of Contents

6.1 Synthesis of the main results	290
6.1.1 The North Atlantic Ocean: DFe, macronutrient and pigment distribution	290
6.1.2 The Southern Ocean: Fe-binding organic ligands and primary production	295
6.1.3 Linking both study areas	298
6.2 Implications and perspectives	299

6.1 Synthesis of the main results

6.1.1 The North Atlantic Ocean: DFe, macronutrient and pigment distribution

In the framework of the GEOVIDE project, the dissolved iron (DFe), nutrient and pigment distributions provided interesting insights on the Fe sources and potential limitations of the phytoplankton.

The DFe concentrations measured during this study were in good agreement with previous studies that spanned the West European Basin, the Iceland Basin and the Labrador Sea (all references are summarized in Fig. 6.1).

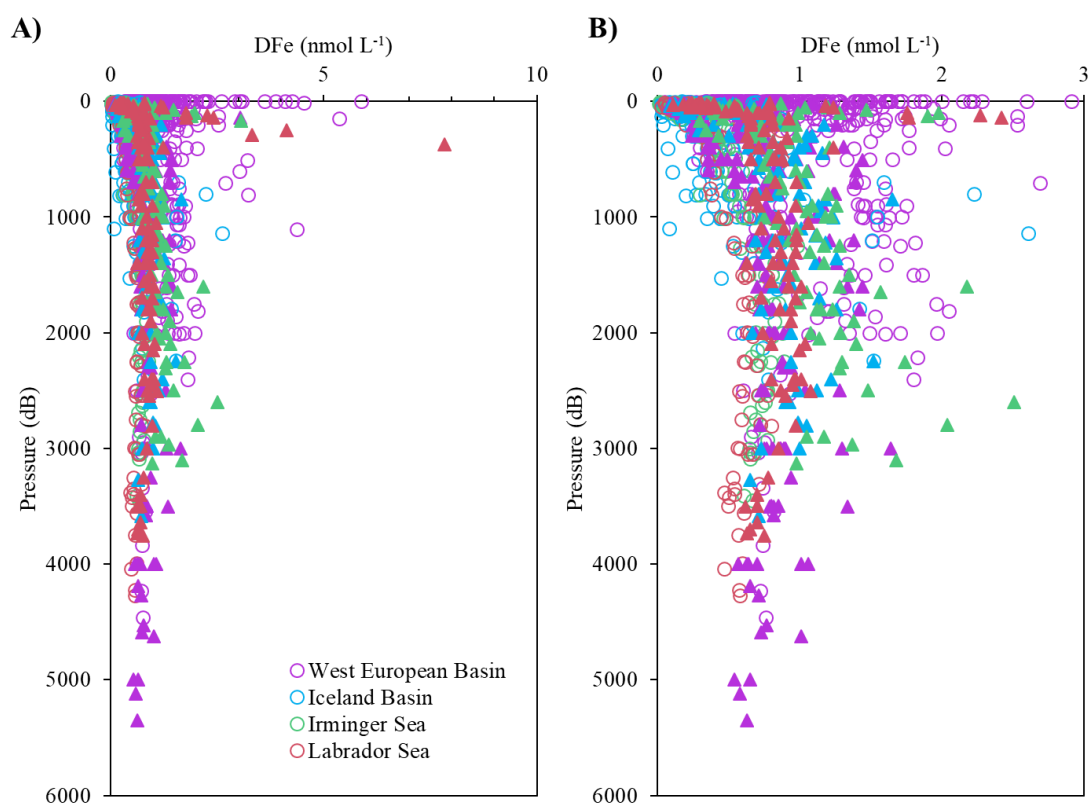


Figure 6.1 : Scatter plot of stations sampled in the West European Basin (purple), in the Iceland Basin (blue), in the Irminger Sea (green) and in the Labrador Sea (red) from past studies (Bergquist et al., 2007; Blain et al., 2004; Boye et al., 2006, 2003; de Jong et al., 2007; Gledhill et al., 1998; Hatta et al., 2015; Klunder et al., 2012; Laës et al., 2003; Martin et al., 1993; Measures et al., 2008; Mills et al., 2008; Mohamed et al., 2011; Nédélec et al., 2007; Nielsdóttir et al., 2009; Pohl et al., 2011; Rijkenberg et al., 2014; Sarthou et al., 2007, 2003; Sedwick et al., 2005; Ussher et al., 2013; Witter and Luther III, 1998; Wu and Boyle, 2002; Wu and Luther III, 1996, 1994; Wu et al., 2001, open circles) and this study (triangles).

However, within the Irminger Sea the DFe concentrations measured during this study were up to 3 times higher than the ones measured by Rijkenberg et al. (2014) in deep waters (> 1000 m depth) that was likely explained by the different water masses encountered (i.e. the Polar Intermediate Water, ~ 2800 m depth) and by a stronger signal of the Iceland Scotland Overflow Water (ISOW) from 1200 to 2300 m depth. This corresponded to the most striking feature of the whole section with DFe concentrations reaching up to 2.5 nmol L⁻¹ within the ISOW, Denmark Strait Overflow Water (DSOW) and Labrador Sea Water (LSW), three water masses that are part of the Deep Western Boundary Current. However, as these water masses reached the Labrador Sea, lower DFe concentrations were measured. These differences were explained by different processes occurring within the benthic nepheloid layers, where DFe was sometimes trapped onto particles due to Mn-oxide-sediment within the Labrador Sea ([1], Fig. 6.2; Gourain et al., 2018) and sometimes released from the sediment potentially as a result of interactions with dissolved organic matter. Fe-binding organic ligands could have been produced locally due to the intense remineralisation rate reported by Lemaître et al. (2017) of biogenic particles ([2], Fig. 6.2; Boyd et al., 2010; Gourain et al., 2018). The LSW exhibited increasing DFe concentrations along its flow path ([3], Fig. 6.2), likely resulting from sediment inputs at the Newfoundland Margin ([4], Fig. 6.2). Although DFe inputs through hydrothermal activity were expected at the slow spreading Reykjanes Ridge (Baker and German, 2004b; German et al., 1994), our data did not evidence this specific source as previously rated by Achterberg et al. (2018) further north (~60°N) from our section.

In surface waters several sources of DFe were highlighted especially close to land, with riverine inputs from the Tagus River at the Iberian margin as underlined by the negative correlation between DFe concentrations and salinity ([5], Fig. 6.2; Menzel Barraqueta et al., 2018) and meteoric inputs (including coastal runoff and glacial meltwater) at the Newfoundland and Greenland margins identified by $\delta^{18}\text{O}$ and macronutrient concentrations (Benetti et al., 2016) ([6], Fig. 6.2). Substantial sediment inputs were observed at all margins with increasing DFe concentrations moving towards the bottom of the water column but with different intensity. The highest DFe sediment input was located at the Newfoundland margin ([3], Fig. 6.2), while the lowest was observed at the eastern Greenland margin ([7], Fig. 6.2). These differences could be explained by the different nature of particles highlighted by the DFe:DAI, DFe:PFe and PFe:PAI ratios (dissolved aluminium, DAI, data from Menzel Barraqueta et al., 2018; particulate iron, PFe, and particulate aluminium, PAI, data from Gourain et al., 2018) with the most lithogenic located at the Iberian margin and the most

biogenic, at the Newfoundland margin (Gourain et al., 2018). Although previous studies (e.g. Jickells et al., 2005; Shelley et al., 2015) reported that atmospheric inputs substantially fertilized surface waters from the West European Basin, in our study only few stations exhibited enhanced surface DFe concentrations and thus atmospheric deposition appeared to be a minor source of Fe at the sampling period. Finally, there was evidence of convective inputs of the LSW identified by an extended Optimum Multi-Parameter (eOMP) analysis (García-Ibáñez et al., 2018) to surface seawater as underlined by enhanced dissolved oxygen concentrations. These convective inputs were caused by long tip jet event (Piron et al., 2016) that deepened the winter mixed layer down to ~ 1200 m depth (Zunino et al., 2017), in which Fe was depleted relative to nitrate ([8], Fig. 6.2).

In terms of potential nutrient limitations, three distinct areas could be distinguished within the North Atlantic Ocean via Canonical Correspondence Analysis (CCA) constraining phytoplankton size-classes determined by Uitz et al. (2006) and the main functional phytoplankton classes determined by the CHEMTAX program by significant environmental variables (i.e. physical and chemical):

1) The nitrogen-limited North Atlantic Subtropical East (NASTE) province led to the high abundance of diazotroph cyanobacteria (D. Fonseca Batista and F. Deman; unpublished data) in a potential symbiotic relationship with type-6 haptophytes (Cabello et al., 2016), the cyanobacteria providing nitrogen, and the type-6 haptophytes fixed carbon.

2) the North Atlantic Drift (NADR) province, where two sub-areas were distinguished : the surface waters of the southern branch of the North Atlantic Current (SNAC) were dominated by dinophytes that seemed to benefit from higher temperature, excess of DFe relative to nitrate (NO_3^-) and lower grazing pressure, while type-8 haptophytes and small diatoms were present deeper in the water column which would potentially experienced Fe-limitation and Si Fe-(co)-limitation, respectively. The northern part was clearly dominated by type-6 haptophytes that colonised the Si-impoverished waters as a result of a weakening of the Subpolar gyre and the intensification of the nutrient-poor Subtropical gyre, where there was no evidence of Fe-limitation.

3) the Atlantic Arctic (ARCT) province, where six areas depicted different levels of integrated total chlorophyll-*a* (TChl-*a*) that were explained by the broad circulation. Among

these areas the Greenland and Newfoundland margins were almost exclusively constituted of large neritic diatoms, which benefited from the simultaneous inputs of DFe and silicate (Si(OH)_4) from glacial meltwaters. In these turbulent high latitude waters, light is probably the most limiting factor (Harrison and Li, 2008; Harrison et al., 2013). Surface waters of the Labrador Sea seemed to be N-limited. Similarly, the Irminger gyre station seemed to be either light-limited or undergo enhanced grazing pressure.

Overall, the North Atlantic Ocean was dominated by two functional classes: diatoms and type-6 haptophytes that build biomineral skeleton known to enhance carbon export relative to other taxa.

A)

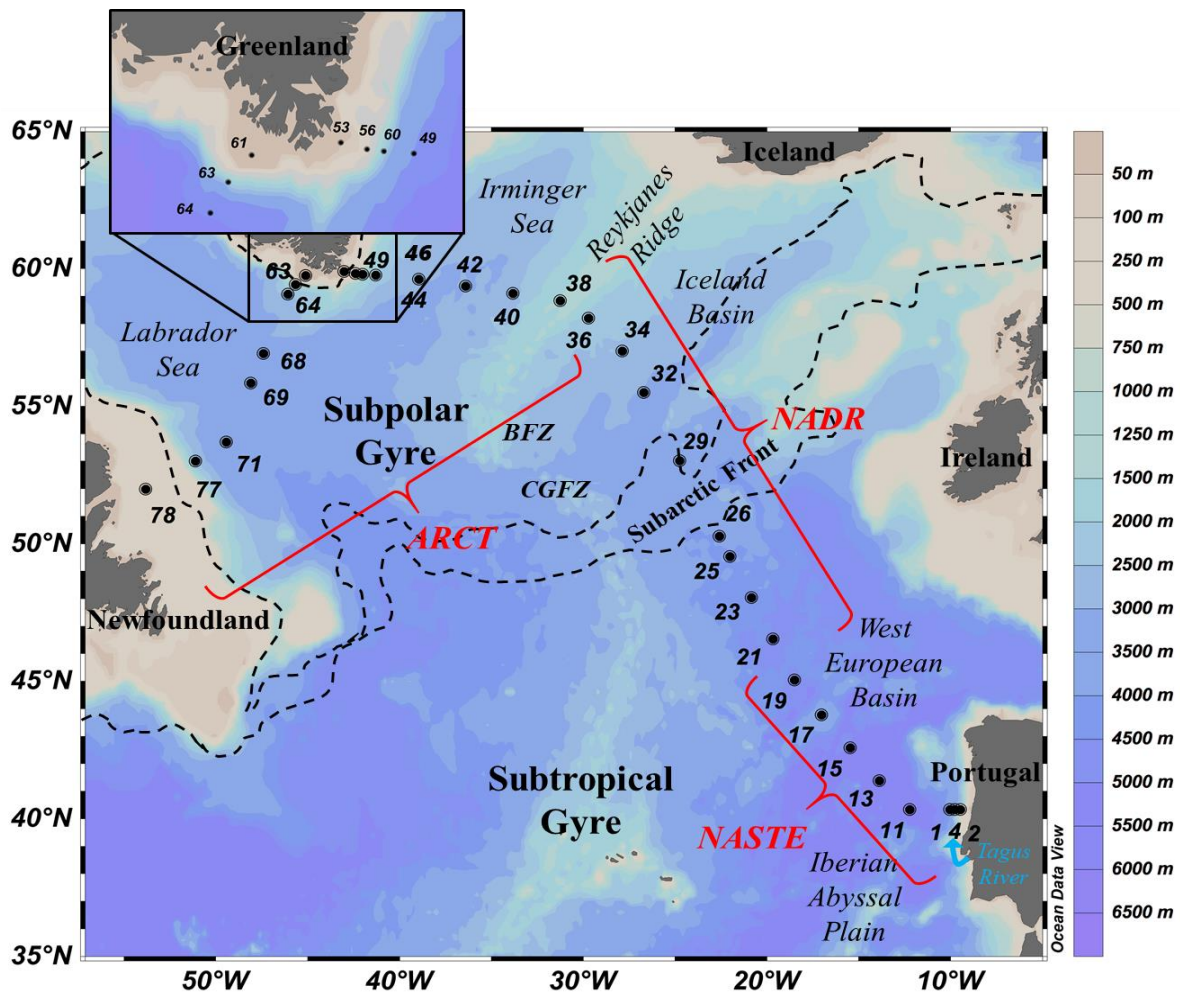
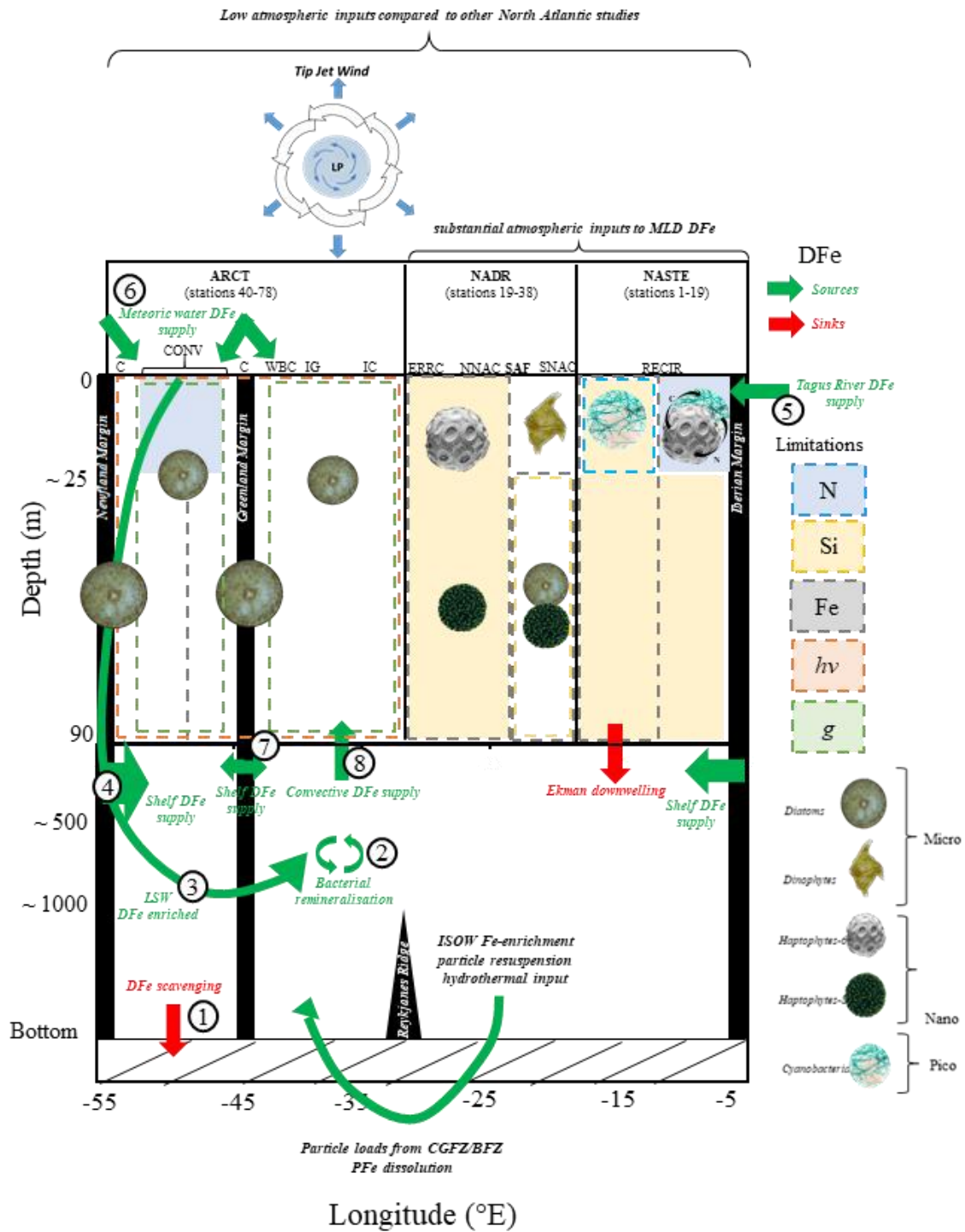


Figure 6.2: A) Map of the GEOTRACES GA01 voyage plotted on bathymetry as well as the major topographical features, main basins and corresponding Longhurst provinces. BFZ: Bight Fracture Zone, CGFZ: Charlie-Gibbs Fracture Zone, ARCT: Atlantic Arctic, NADR: North Atlantic Drift, NASTE: North Atlantic Subtropical East. B) Summary of DFe supplies, main phytoplankton classes and potential limitation(s) within the North Atlantic Ocean.

B)



6.1.2 The Southern Ocean: Fe-binding organic ligand and primary production

Over the northern part of the Kerguelen plateau, DFe, originating from the shallow Kerguelen plateau sediments brought to surface waters through winter mixing and vertical diffusivity (Blain et al., 2008b), has been highlighted as the main parameter controlling the phytoplankton bloom (Blain et al., 2008c) with minimum losses through advection due to weak currents (Park et al., 2008b) and high excess Fe-binding organic ligand concentrations (Gerringa et al., 2008). However, this phytoplankton bloom exhibits interannual variabilities in terms of magnitude and location, which might be inferred to the chemical and physical speciations of DFe that would prevent its bioavailability. Therefore, during the Heard Earth-Ocean-Biosphere Interaction (HEOBI) voyage, which took place in January – February 2016 towards the end of the phytoplankton bloom, the physical organic speciation of the DFe pool was investigated.

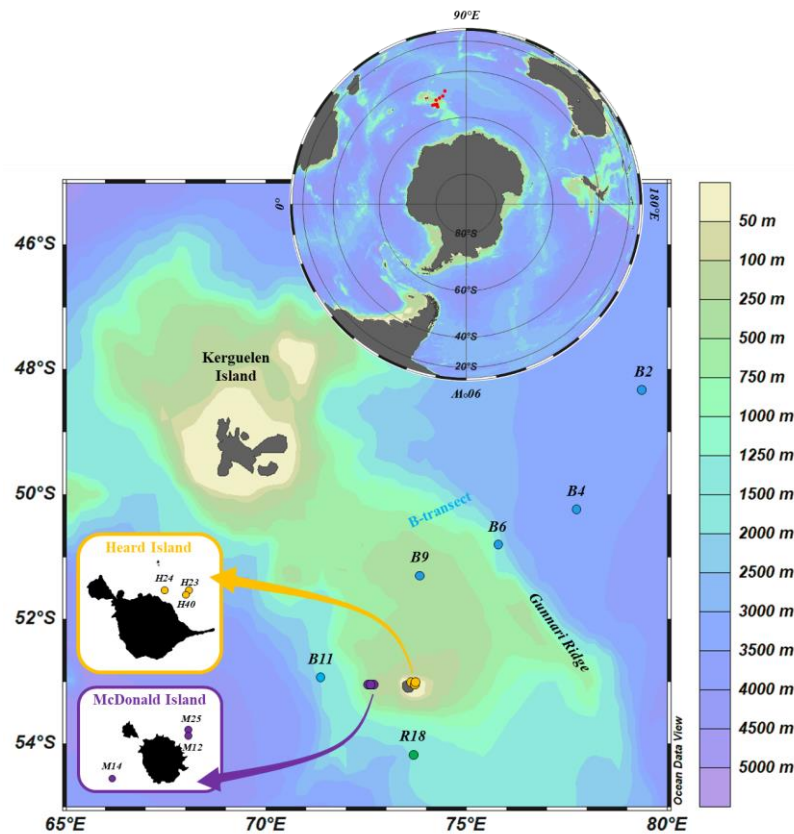
The investigation of dissolved, soluble and colloidal Fe-binding organic ligands (with the direct measurement of both the soluble and dissolved fractions and the indirect measurement of the colloidal fraction by subtracting the soluble fraction from the dissolved fraction) via competing ligand exchange adsorptive cathodic stripping voltammetry (CLE-AdCSV) revealed clear differences between the reference (R18) and the B-transect, and Heard and McDonald Islands stations (Fig. 6.3A).

Within surface waters of R18 and of the B-transect, the soluble iron (SFe) dominated the DFe pool. This SFe was likely sustained by strong soluble Fe-binding organic ligand (SLt) released through remineralisation as indicated by positive correlations between SLt and silicate concentrations. In addition, both phytoplankton, dominated by large diatoms, and bacteria seemed to produce strong Fe-binding organic ligands. This resulted in excess ligands relative to all physical Fe fractions, including the PFe (data from van der Merwe et al., in prep.) fraction. Deeper in the water column, there was evidence of a source of inorganic DFe (DFe') from the sediment through the comparison of the study carried out by Gerringa et al. (2008) during Kerguelen Ocean and Plateau Compared Study (KEOPS) against this study. This was highlighted by increasing DFe' concentrations moving towards the bottom of the water column. Similarly as for DFe', both DFe (data from Holmes et al., in prep.) and dissolved Fe-binding organic ligands seemed to have a deep source. However, they seemed to originate from the degradation of accumulated particulate organic matter, contrary to Gerringa et al. (2008)'s view.

Conversely, at Heard and McDonald Islands, the colloidal iron (CFe) dominated the DFe pool. There, Fe-binding organic ligands were over-saturated by Fe throughout the water column, thus highlighting an important source of Fe. The water column was dominated by low reactive colloidal ligands resulting in the scavenging of Fe to particles (Fig. 6.3B).

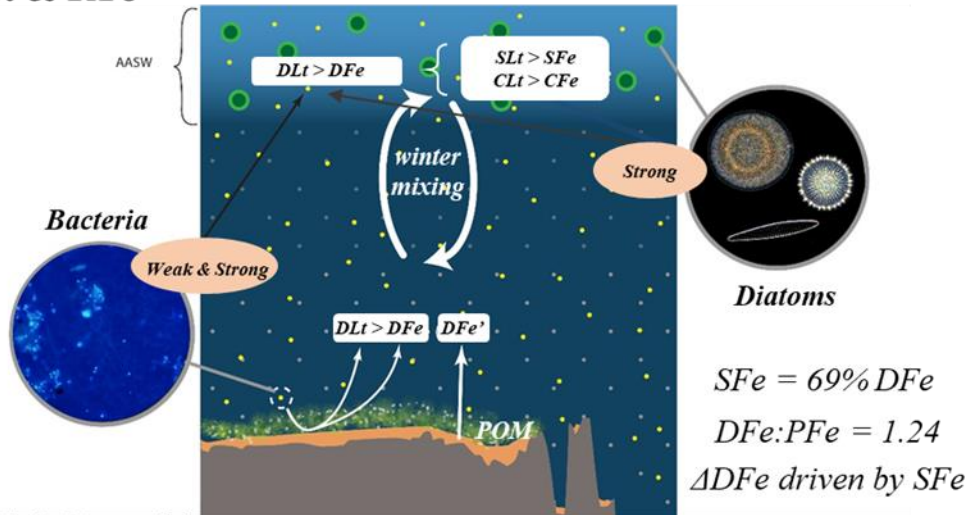
Finally, two distinct areas were noticed in terms of standing total chlorophyll-*a* (TChl-*a*) inventories, with on one side, the reference and B-transect stations, which exhibits elevated integrated TChl-*a* concentrations and on the other side, Heard and McDonald islands stations and their low integrated TChl-*a* concentrations (Wojtasiewicz et al., in prep.). These differences could potentially be explained by the physical and organic speciations of Fe as the TChl-*a* features matched those observed for dissolved, soluble and colloidal Fe-binding organic ligand concentrations, and dissolved, soluble, colloidal and particulate Fe concentrations.

A)



B)

B-transect & R18



Heard & McDonald

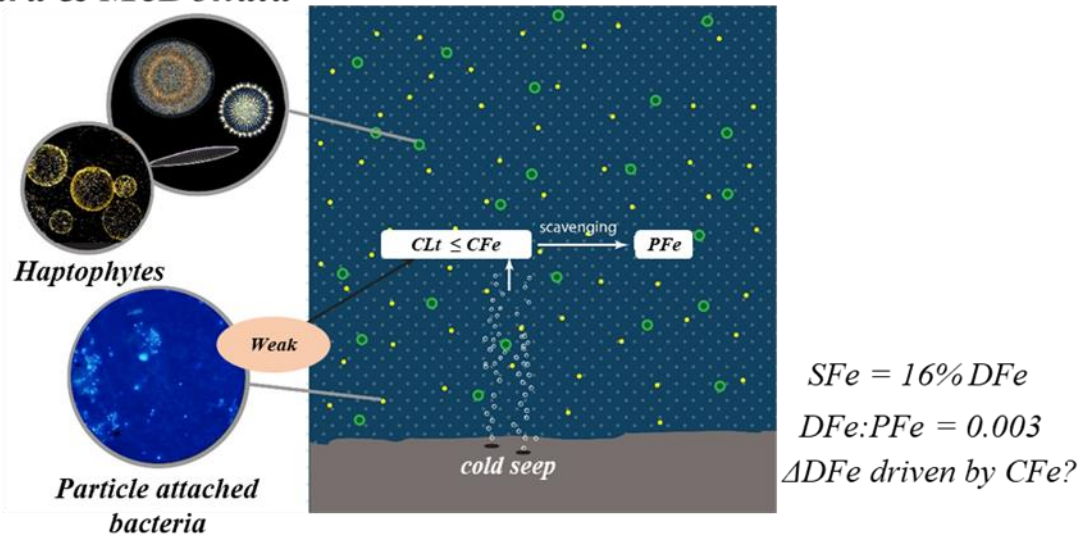


Figure 6.3: A) Location of the stations sampled during the HEOBI voyage using the Trace Metal Clean Rosette (modified from Thomas Holmes). Heard and McDonald Islands are shown in the inset, in yellow and purple, respectively, the reference station (R18) is represented in green. Transect B, in blue, follows the Kerguelen Ocean and Plateau Compared Study (KEOPS) transect B. B) Conceptual schematic of the main finding at Heard and McDonald Islands stations and the B-transect and R18 stations (D. Alain and S. Hervé, IUEM). Note that yellow dots refer to bacteria, grey dots to particles, green dots to phytoplankton, the orange field on top of bathymetry refers to sediment and that the greenish material refers to Particulate Organic Matter (POM). (DFe data from Holmes et al., in prep., PFe data from van der Merwe et al., in prep.; pigment data from Wojtasiewicz et al., in prep., bacteria picture courtesy from S. Blain).

6.1.3 Linking both study areas

This thesis improved the knowledge on Fe biogeochemical cycle combining two novel approaches i) the use of multiparameter statistical analyses gathering physical (salinity, temperature, pH), chemical (major nutrients and DFe) and biological (i.e. phytoplankton classes assessed from pigments via the CHEMTAX program) environmental variables and ii) the investigation of both the physical and organic speciations of Fe. This work allowed the determination of various DFe sources and sinks in both the North Atlantic Ocean and the Kerguelen plateau, and highlighted the complex relationship between the available forms of Fe and the response of the phytoplankton community structure. If Fe was not the main parameter responsible for the structure of the phytoplankton community in the high latitudes of the North Atlantic Ocean, i.e. within the Atlantic Arctic Longhurst province, it might co-limit with silicates diatoms within the Iceland Basin thus allowing type-6 haptophytes to bloom. This is probably due to the amount of external sources of DFe to surface waters in this geographic area of the world either brought through water mass circulation, atmospheric deposition, and coastal runoffs. Conversely, over the Kerguelen plateau, although Fe seemed to be ubiquitous, the organic speciation of Fe and more specifically the reactivity of colloidal Fe-binding organic ligands seemed to explain differences in both the standing total chlorophyll-*a* inventories and the phytoplankton community structure. Indeed, the reactivity of colloidal Fe-binding organic ligands seemed to determine the fate of Fe in the water column with either scavenging losses onto particles in case of unstability of the colloidal fraction or sustainability of the DFe fraction in case of excess colloidal ligands. Similarly, in the North Atlantic Ocean, although Fe organic speciation was not studied, it seems that Fe losses are linked to the amount of dissolved organic matter, namely the ligands that are able or not to remobilise Fe from particles.

The extrapolation of the results from these three studies highlights the central role of the organic speciation of Fe. Indeed, the long-range transport (~ 3,000 km) of DFe from Newfoundland shelf sediments to the Irminger Sea might also be due to the highly reactive colloidal fraction of Fe-binding organic ligands. Therefore, it seems crucial to investigate at the same resolution the physical and organic speciation of Fe to better constrain its fate in the water column and therefore its residence time. In addition, the phytoplankton community structure should be systematically assessed with CHEMTAX or even better with genomics and should be followed over the bloom duration in order to link it to macro- and micro-nutrient distributions. Finally, all these analyses should be done concomitantly with on-board

incubations to directly test for nutrient limitation by spiking natural phytoplankton communities by macro- and micro-nutrients to confirm or disprove limitation hypotheses arising from Si* and Fe* tracers.

6.2 Implications and perspectives

In the North Atlantic Ocean, the analyses of dissolved Fe-binding organic ligand concentrations and their characteristics have been performed, when they become available, these results will help to fully understand whether the identified external DFe sources are sustained in the water column. In addition to assessing the residence time and sustainability of DFe in the water column, it would have been interesting to directly test the bioavailability of the different sources of DFe. For example, the response of the natural phytoplankton community from the NASTE province in response to atmospheric dry and/or wet deposition could have been studied (Fig. 6.4). Indeed, despite numerous studies, the extent to which dust particles can be remobilized in the DFe pool and potentially bioavailable for the natural community remains uncertain. To do so, on board incubations amended with collected aerosols in order to follow through time the DFe concentrations in the different size spectrum, the Fe-binding organic ligands, the bacteria community, the potential shift within the natural phytoplankton community structure could be conducted. This type of experiment could help determining interactions between bacteria and phytoplankton and constrain the importance of atmospheric inputs and their broad impact in potentially favouring certain phytoplankton functional classes relative to others. Although Boyd et al. (2010) reported that the remineralisation of biogenic PFe is probably the main source of DFe and dissolved Fe-binding organic ligands compared to the one of lithogenic PFe using field experiments and modelling simulations, it will be valuable to further test this hypothesis for our voyage with particles from the four margins (i.e. the Iberian margin, the east and west Greenland margins and the Newfoundland margin), using the same type of experiments as for dust particles mentioned above (Fig. 6.4). That way, we could assess how phytoplankton respond to this potential source of regenerated Fe or if maybe the subsequent generated ligands will be too strong to be accessible for phytoplankton and if it induces a shift in the phytoplankton community.

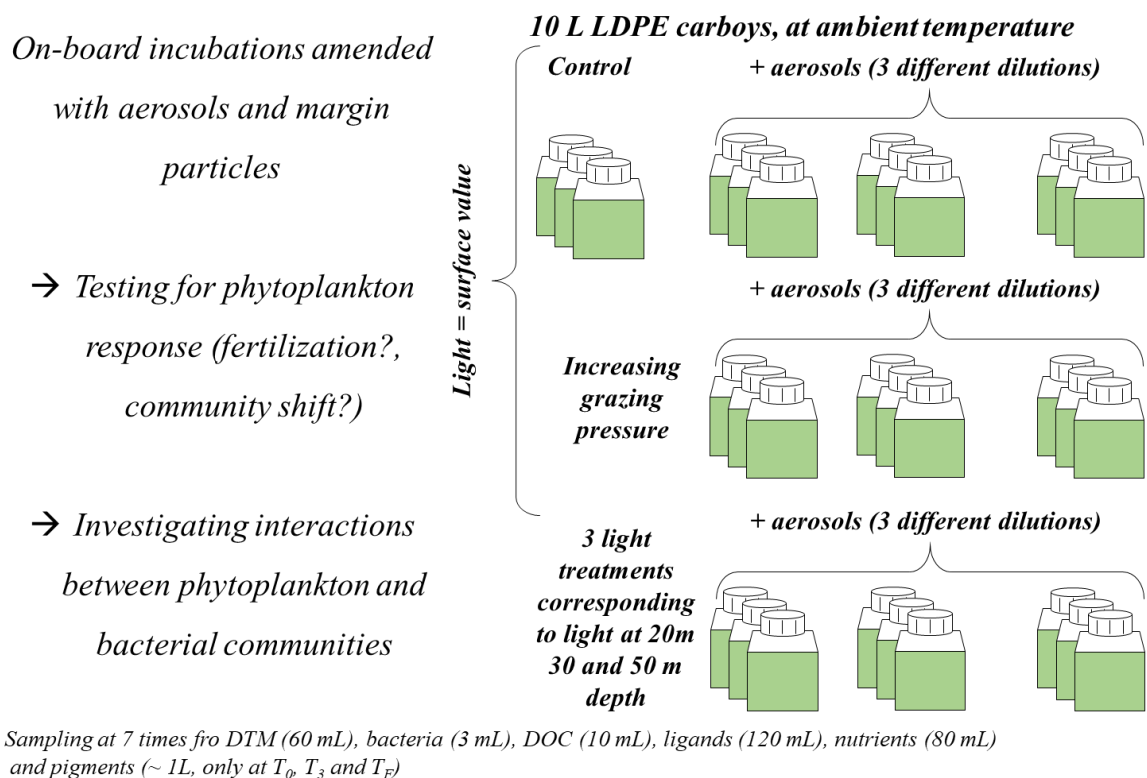


Figure 6.4: Idea of an experimental setup for on-board incubations amended with aerosols and margin particles.

It will also be important to build up the Fe budget along the GEOVIDE section. This is the first step to assess the relative importance of the external sources within the different basins prior to determine their variability through time. Although snapshots of oceanographic voyage allow the scientific community to determine specific sources, they do not allow the assessment of their temporal variability. Consequently, the repetition of such transect is essential to quantify and rank the sources by importance especially since there is evidence that our world is changing. Indeed, all the external sources reported for the North Atlantic Ocean are susceptible to increase or decrease in response to climate change with several impacts for the phytoplankton community. It has been reported for example that the Arctic has warmed more intensely than any other region on Earth during the past decades (Stroeve et al., 2014). Therefore, increased ice loss rate on the Greenland ice sheet (Nghiem et al., 2012; Stroeve et al., 2014) as well as sea ice retreat (Granskog et al., 2016) within the Arctic Ocean have been reported. If such trends are to continue, although we pointed to silicate (Si(OH)_4) and DFe inputs from glacial meltwater and runoff from the Greenland, the induced stratification would likely enhance the interactions between grazers and phytoplankton (Behrenfeld, 2010). Repeating the GA01 transect could help constrain biogeochemical

models and thus climatic models by determining impacts of long-term changes to the phytoplankton community.

Similarly, our study was the first conducted since the North Atlantic Oscillation shift towards positive values and it would be thus interesting to follow the associated changes in terms of macro- and micro-nutrient supply. In this study, although we assessed the potential for nitrate (NO_3^-), silicate (Si(OH)_4) and DFe limitation(s), investigating phosphate (PO_4^{3-}) to the global picture together with other bioactive metals could shed light on their interactions and biogeochemistry. In addition, testing for light limitation of high-latitude phytoplankton community could help to understand the factors controlling the decline of the spring phytoplankton bloom (Fig. 6.4). Additional parameters also include the grazing pressure that was only assessed in our study by the Chlorophyll-*a* degradation products and compared between the different provinces (Fig. 6.4).

During the GEOVIDE voyage, it was clear that the broad circulation directly translates into different total Chlorophyll-*a* integrated stocks. The area that is likely to be impacted by change in North Atlantic Oscillation (NAO) phases and external sources of nutrients is the transition zone between the Subtropical and Subpolar gyres, due to its remoteness, namely the Iceland basin. This area constitutes a wonderful laboratory to study the impact of mesoscale features such as eddy and fronts on phytoplankton community. The deployment of a mooring equipped with mesocosms and sediment traps would be of great value to understand the evolution of phytoplankton community and of the particles exported for different scenarios in this area impacted by two contrasting systems that will experience future change depending on the strength of the Atlantic Meridional Overturning Circulation (NASA EXport Processes in the Ocean from RemoTe Sensing, <http://oceanexports.org/>).

Regarding the HEOBI voyage, one of the biggest question that was previously raised by Gerringa et al. (2008) is the counter-effect of organic complexation as it inevitably decreases the amount of Fe'. Better constraining which chemical forms of Fe are more bioavailable will help the scientific community to draw more conclusive interpretations regarding the potential for Fe limitation.

Last but not least, the molecular structure and identification of ligands is a growing field of research and despite what is known of ligands so far, many are still unknown. Knowing the structure of ligands is of major importance. Indeed, microbial communities face selective pressures to develop uptake and utilization strategies that maximize access to organically-bound Fe which are sensitive to the molecular speciation of organic ligands.

Although new techniques are developed to identify the chemical structure of ligands (e.g. Mawji et al., 2008a; Repeta et al., 2017), these promising analyses that not only allow determination of the structure of ligands that bind Fe but also all other trace metals within one sample and their respective concentrations are not systematic yet. However, if it is assumed that ligands sustain DFe concentrations in surface waters, the study of their structural morphology will likely reveal their potential to undergo aggregation. We reported for the HEOBI voyage weak ligands with conditional stability constants that could fit in the range of saccharide-type substances (Hassler et al., 2015; Hassler et al., 2011c), i.e. exopolysaccharide (EPS) or glucuronic acid (monosaccharide). These gel-like substances might undergo fast organic matter aggregation in a time-scale of minutes to hours to move from the colloidal to the particulate phase as Transparent Exopolymer Particles (TEP) (e.g. Baalousha et al., 2006; Verdugo et al., 2004). These fast-settling particles are believed to bind particle reactive elements (e.g. Fe, Th; Engel et al., 2004) and can trap faecal pellets during their export to depth and even intact phytoplankton cells (Ebersbach et al., 2014). Although such compounds will increase the export of carbon they will concomitantly fix an upper limit to the concentrations that cells can achieve during a bloom (Dam and Drapeau, 1995). In addition, Berman-Frank et al. (2007) reported that the production of TEP is coupled with autocatalytic programmed cell death (PCD) process for some cyanobacteria. Similar observations were also reported for *Thalassiosira pseudonana* and *Emiliania huxleyi* (Bidle, 2015; Kahl et al., 2008; Vardi et al., 2012). Therefore, the occurrence of such substances could also be the reason of HNLC areas in the world trapping phytoplankton cells and scavenging DFe. With regards to the HEOBI voyage, although DFe concentrations were far from being limiting at our near shore stations, TChl-*a* concentrations were low compared to surrounding waters and TEP mediated Cell control, could be a hypothesis worth testing for future studies.

Étude du cycle biogéochimique du fer: distribution et spéciation en Océan Atlantique Nord (GA01) et en Océan Austral (GIpr05) (GEOTRACES)

A- Introduction

Le fer dissous (DFe) peut être délivré dans la colonne d'eau via divers processus sous forme nouvelle ou régénérée. Le DFe peut provenir de sources hydrothermales, des rivières, des glaciers, de la glace de mer, de la neige, de dépôts atmosphériques secs ou humides (incluant la pluie), des nuages ou encore des sédiments (incluant les couches néphéloïdes benthiques, les eaux interstitielles des sédiments et des processus de dissolution réductrice et non-réductrice). Les sources profondes enrichies en DFe jouent un rôle important dans le cycle du carbone du fait de leur entrainement potentiel, de leur remontée dans les eaux de surface à travers l'action des vents et/ou de la circulation thermohaline et/ou des tourbillons à méso-échelle. Elles peuvent donc fertiliser les communautés phytoplanctoniques présentes en surface. Le DFe peut également être régénéré dans la colonne d'eau par la re-minéralisation bactérienne ou encore le broutage du phytoplancton par le zooplancton. Toutes ces sources semblent non seulement libérer du fer dissous mais aussi des ligands organiques complexant le fer (Fig. A.1). Les perspectives sur la spéciation organique du Fe dans ces différentes phases permettront d'estimer le degré de disponibilité du Fe.

La dynamique des particules et leur tendance à se reminéraliser ajoutent un autre degré de complexité au cycle biogéochimique du fer. Dépendamment de leur nature (biogénique vs. lithogénique), les particules peuvent approvisionner les stocks de DFe et de ses ligands organiques ou bien l'adsorber et ballaster le fer particulaire (PFe) biogénique (Boyd et al., 2010). De plus, l'impact de ces particules dépend de la structure des communautés bactériennes (bactéries attachées aux particules vs. bactéries libres), les bactéries attachées aux particules jouant probablement un rôle crucial dans l'émission de DFe et de ses ligands (Obernosterer et al., en prép.). En outre, la fraction physique sous laquelle se trouve le DFe, c'est-à-dire sous forme de fer colloïdal (CFe) ou de fer soluble (SFe), va favoriser sa complexation avec certains ligands plutôt que d'autres. Ces ligands, en fonction

de leur origine, structure moléculaire et cinétique de complexation vont eux-mêmes impacter la façon dont le biote va acquérir le fer mais aussi déterminer le sort du DFe.

Bien que les connaissances au sujet du cycle biogéochimique du fer et de son lien avec les autres cycles biogéochimiques s'accroissent, les processus qui affectent les sources et les puits du DFe dans l'océan sont peu comprises. Il semble que ces processus dépendent eux-mêmes de la réactivité du fer, et que la réactivité du fer soit contrôlée par la concentration et la spéciation physique des ligands organiques du fer. La réactivité chimique va moduler la dissolution du PFe (Cheize et al., en révision) et la tendance des diverses formes de fer à être complexées organiquement ou transférées dans le pool particulaire via les processus d'adsorption ou d'agrégation colloïdale.

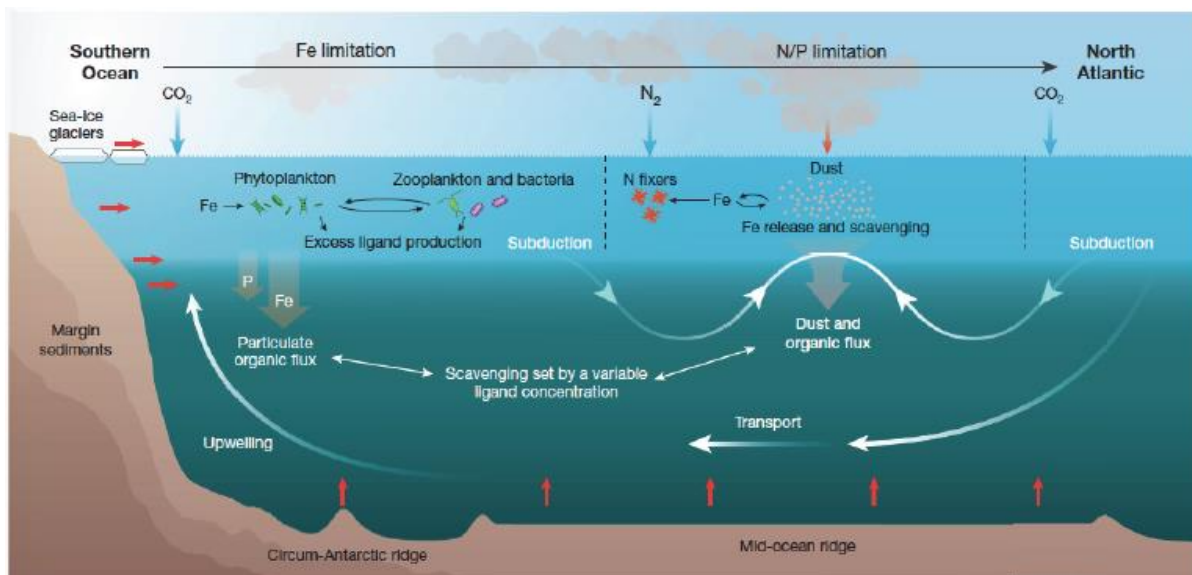


Figure A.1 : Représentation des processus majeurs du cycle océanique du fer, l'accent étant mis sur l'océan Atlantique (Tagliabue et al., 2017).

B-Présentations des zones d'études et des objectifs de la thèse

Le travail de cette thèse se concentre sur deux zones contrastées : l'océan Atlantique Nord et le plateau de Kerguelen localisé dans le secteur indien de l'océan Austral. Leurs principales caractéristiques sont décrites dans les sections suivantes mais détaillées dans les chapitres 3 et 4 en ce qui concerne l'océan Atlantique et le chapitre 5 pour le plateau de Kerguelen, enfin les objectifs de ce travail concluent cette introduction.

B.1-L'océan Atlantique Nord

Les propriétés des eaux de surface des océans mondiaux contrôlent la circulation thermohaline et impliquent un flux de surface d'eaux chaudes et salées depuis les régions subtropicales en direction du nord au sein de l'océan Atlantique nord via le courant nord Atlantique (NAC). Ces eaux se mélangent avec les eaux froides et peu salées de l'Arctique qui sont transportées par les courants est et ouest du Groenland (EGC et WGC, respectivement) puis par le courant du Labrador (LC) (Emery, 2001) (Fig. B.1). Le mélange de ces deux différentes masses d'eau provoque une augmentation de la densité engendrant leur convection profonde et leur transport immédiat vers le sud. Cela représente la circulation méridienne de retournement de l'Atlantique (AMOC) (Fig. B.1). L'AMOC est donc responsable du transport de larges quantités d'eau, de chaleur, de sel, de carbone, de nutriments et autres substances à travers le globe (Marshall et al., 2001). La variabilité de l'AMOC contribue de manière substantielle aux fluctuations des températures de surface (SST) et de la glace de mer en Atlantique nord (Junglaus et al., 2005). Sa force est liée à l'activité convective dans les régions de formation d'eaux profondes, notamment la mer du Labrador, et l'export d'eau douce de l'Arctique vers les sites de convection, lui-même variable dans le temps, module l'AMOC (Junglaus et al., 2005). Les fluctuations de l'un de ces composants pourraient donc affecter l'AMOC et donc la variabilité de l'exportation de carbone. En effet, Sabine et al. (2004) ont montré que l'Atlantique Nord, même s'il ne couvre que 15% de la surface de l'océan, constitue l'un des plus grands réservoirs de CO₂ anthropique, absorbant jusqu'à 23% du CO₂ anthropique mondial océanique en utilisant non seulement la pompe à carbone physique, mais également la pompe à carbone biologique. L'océan Atlantique Nord est connu pour ses proliférations phytoplanctoniques printanières prononcées en réponse à la stratification de la colonne d'eau ou de remontées d'eau froides et riches en nutriments (Bury et al., 2001; Henson et al., 2009; Savidge et al., 1995). Dans les eaux pauvres en éléments nutritifs du gyre subtropical, il a été démontré que la croissance du

phytoplancton était co-limitée par l'azote (N) et le phosphore (P) (e.g. Moore et al., 2008). Les études approfondies menées au moyen du « Continuous Plankton Recorder » (CPR) ont mis en évidence la relation existant entre l'oscillation nord-atlantique (NAO) et la dynamique du phytoplancton au centre de l'océan Atlantique nord (Barton et al., 2003). La NAO est associée à un changement des vents d'ouest, avec dans le cas d'une phase négative de la NAO une faiblesse des vents d'ouest entraînant un déplacement du front subarctique (SAF) vers le nord-ouest, et inversement (Bersch et al., 2007). Ainsi, selon l'emplacement du SAF, les communautés phytoplanctoniques du centre de l'Atlantique Nord seront plus ou moins limitées par les éléments nutritifs ou la lumière. Dans le gyre subpolaire, l'intense mélange hivernal alimente les eaux de surface en éléments nutritifs. Cependant, une fois la colonne d'eau stratifiée et le phytoplancton libéré de la limitation lumineuse, il a été démontré que le gyre subpolaire devenait N ou (et) Fe-(co)-limité dans le bassin islandais et la mer d'Irminger (e.g. Nielsdóttir et al., 2009; Painter et al., 2014; Sanders et al., 2005). Dans le cas d'une limitation par le Fe, il en résulte la formation de conditions saisonnières riches en nutriments et faibles en chlorophylle (HNLC) dans le gyre subpolaire, en particulier dans la mer d'Irminger et le bassin de l'Islande. Bien que de nombreuses études se soient penchées sur la répartition du DFe dans l'Atlantique Nord, la plupart de ces travaux ont été limités aux couches supérieures (moins de 1000 m de profondeur) ou à un bassin. Par conséquent, les voies par lesquelles le DFe est acheminé dans l'eau de mer et extrait de la colonne d'eau (cf. chapitre 3), la relation qui existe entre le Fe et les autres éléments nutritifs ainsi que la façon dont ils limitent la croissance des organismes phytoplanctoniques et, par conséquent, la façon dont ils structurent la communauté phytoplanctonique (cf. chapitre 4), sont encore peu contraintes dans cette région.

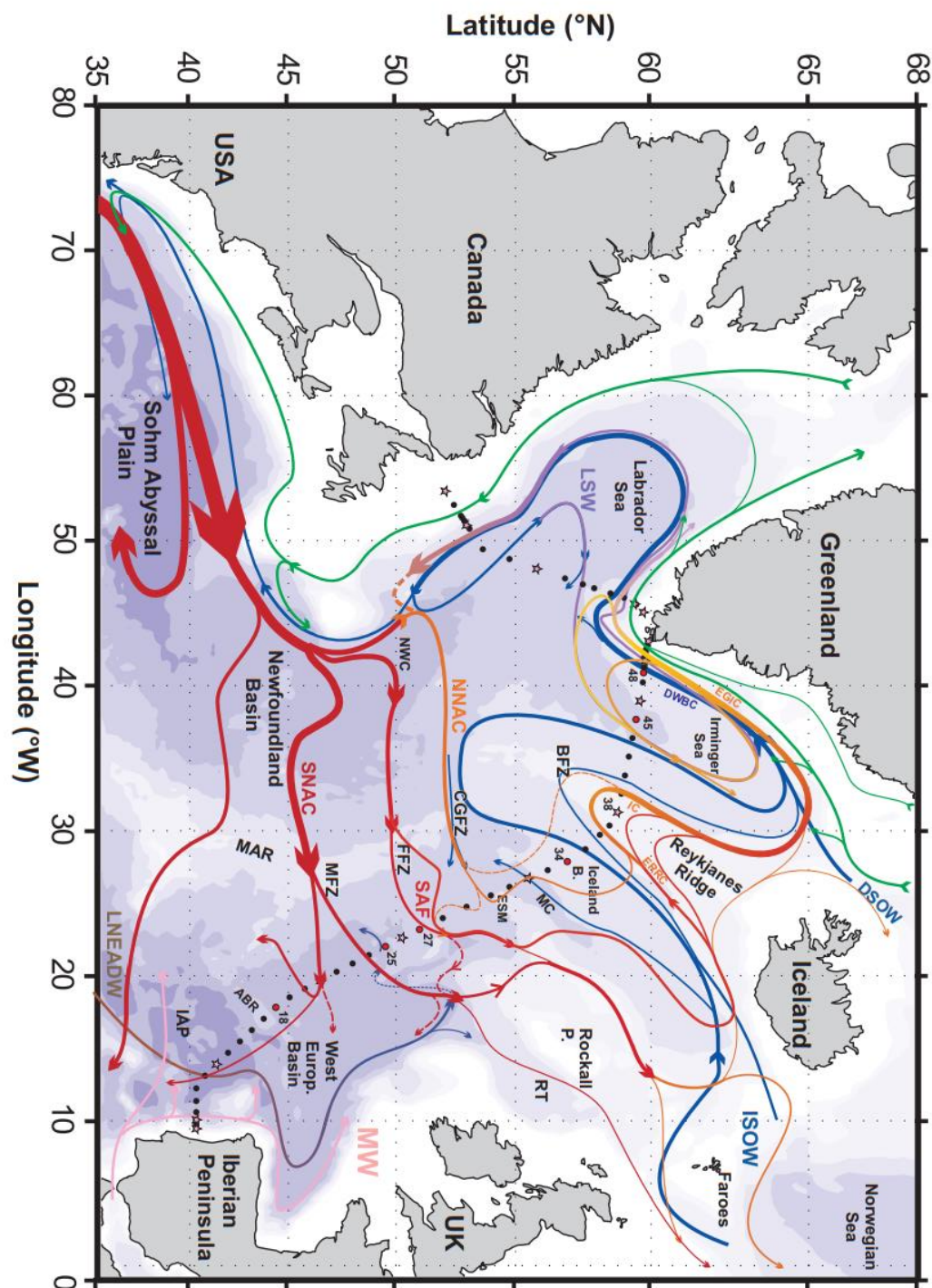


Figure B.1: Carte du schéma de circulation, des principales caractéristiques topographiques, des principaux bassins, courants et des principales masses d'eau de l'Atlantique Nord (Daniault et al., 2016).

B.2-Le plateau de Kerguelen (secteur indien de l'océan Austral)

L'océan Austral, comme l'océan Atlantique nord, s'est révélé être un important puits de CO₂ atmosphérique au niveau mondial (Gruber et al., 2009; Lenton et al., 2013; Sarmiento et al., 2010). Cependant, dans cette région, Pasquer et al. (2015) ont souligné que les échanges air-mer de CO₂ sont dictés par les conditions thermodynamiques, tandis que l'activité biologique n'est responsable que d'une fraction modeste du puits de carbone. En effet, l'océan Austral est la plus grande région HNLC des trois principaux systèmes océaniques. Bien qu'il s'agisse d'une région océanique globalement peu productive, certaines zones de l'océan Austral sont très productives. En effet, des niveaux élevés de biomasse vivante ont été observés dans le sillage des îles de l'océan Austral. La prolifération de phytoplancton au-dessus du plateau de Kerguelen (Fig. B.2) est l'une des plus importantes (Morris et Charette, 2013). Ce phénomène a été appelé « l'effet de masse d'île » par Hart (1942). Il a été le premier à mentionner l'éventualité que ces îles libéraient un oligo-élément tel que le Fe et que ce dernier était probablement la cause de la biomasse observée. Environ un demi-siècle plus tard, l'étude réalisée au cours de la campagne ANTARES3 / F-JGOFS a révélé une augmentation de la chlorophylle-*a* associée à une augmentation des concentrations de DFe, confirmant ainsi l'hypothèse d'une limitation par le Fe des communautés phytoplanctoniques de l'océan Austral soulagées par les apports insulaires (Blain et al., 2001; Bucciarelli et al., 2001). L'étude comparée de l'océan et du plateau de Kerguelen (KEOPS) a révélé une biomasse phytoplanctonique intense sur le plateau de Kerguelen (Uitz et al., 2009) et de très faibles concentrations de DFe ($\sim 0,1 \text{ nmol L}^{-1}$) dans l'ensemble des eaux de surface de la zone d'étude. Cependant, les stations situées sur le plateau étaient enrichies en DFe par rapport aux stations hors plateau (Blain et al., 2008c). Le processus responsable du transfert du DFe, depuis le plateau vers la couche de surface, était un mélange diapycnal renforcé par l'activité des vagues internes (Park et al., 2008a), fournissant ainsi du Fe à la communauté phytoplanctonique, mais pas assez pour répondre à sa demande. En effet, Sarthou et al. (2008) ont signalé qu'environ la moitié du fer particulaire (PFe) biogénique était régénérée au-dessus du plateau. De plus, Park et al. (2008b) ont mis en évidence un temps de résidence des masses d'eau de plusieurs mois au-dessus du plateau en raison de courants faibles, évitant ainsi la perte de DFe par advection. Les pertes de DFe par adsorption des particules ont été estimées comme étant minimales en raison des fortes concentrations de ligand mesurées en excès des concentrations de DFe, et ce, dans l'ensemble de la zone d'étude (Gerringa et al., 2008). Cependant, l'intensité et l'emplacement de la prolifération phytoplanctonique

présentaient des variabilités interannuelles. En effet, les concentrations de chlorophylle les plus élevées ne sont pas toujours associées aux plus faibles bathymétries et certaines régions du plateau présentent des concentrations résiduelles de chlorophylle toute l'année (Mongin et al., 2008). Bien que le DFe ait clairement été désigné comme le paramètre contrôlant la prolifération de phytoplancton sur le plateau de Kerguelen, sa biodisponibilité et donc ses spéciations chimiques et physiques ne sont toujours pas complètement comprises.

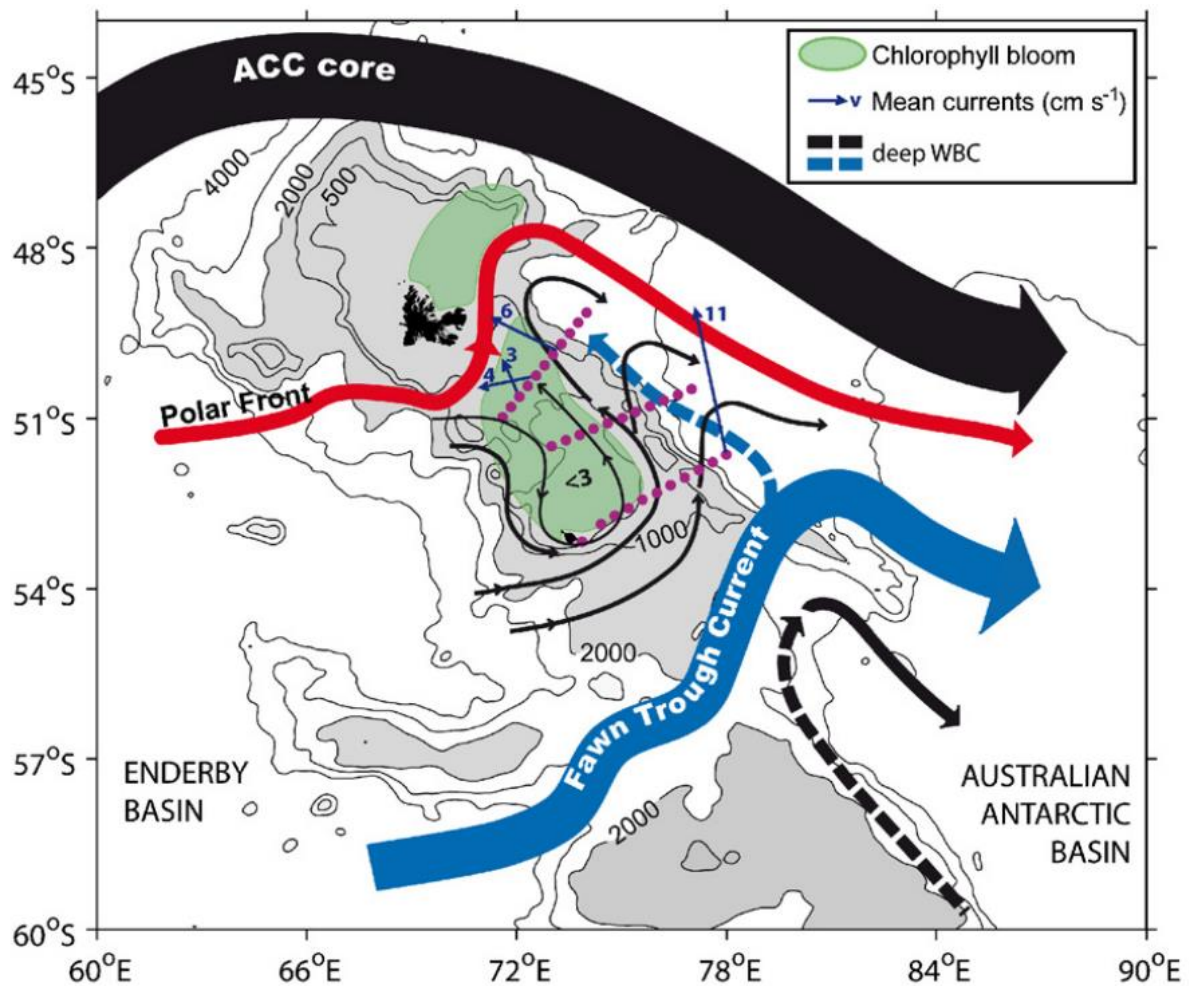


Figure B.2: Schéma de la circulation géostrophique sur et autour du plateau de Kerguelen pendant KEOPS (Park et al., 2008b).

C- Objectifs et plan de thèse

Le programme GEOTRACES a mis en évidence le fait que le cycle biogéochimique et la distribution du DFe sont uniques par rapport à ceux des autres nutriments (Tagliabue et al., 2016). Malgré les efforts récents de la communauté scientifique dans le cadre du programme GEOTRACES, le cycle du Fe est encore peu contraint. En effet, une grande disparité dans les temps de résidence du Fe a été constatée entre les différents modèles biogéochimiques, reflétant de ce fait la complexité à représenter correctement le cycle océanique du Fe. Les modèles qui reproduisent avec succès les données de terrain sont ceux incluant les nouvelles sources ainsi que les nouvelles voies de recyclage du Fe dans la colonne d'eau émergeant des avancées récentes. Cela montre clairement que, bien que 30 années de recherche aient été menées sur le cycle du Fe, il reste encore beaucoup à apprendre sur les sources de Fe et surtout sur l'ampleur des processus de piégeage du fer que ce soit au niveau qualitatif ou quantitatif. De bons exemples montrant qu'il reste encore beaucoup de questions à résoudre et qu'il est nécessaire de poursuivre les recherches sur le cycle du Fe sont les suivants: i) les récentes découvertes concernant les intenses sources de fer d'origine hydrothermales (e.g. Resing et al., 2015) remettant en cause la vision de longue date qui considérait ces sources comme négligeables (Elderfield et Schultz, 1996), ii) le débat persistant sur l'importance des ligands organiques pour expliquer le cycle biogéochimique du Fe avec le fait que, si les ligands organiques sont omniprésents, comment peuvent-ils expliquer les variations de concentrations en DFe. Des avancées récentes sur ce sujet ont montré que la modélisation pronostique de ligands organiques se liant au Fe, par opposition à une concentration uniforme de ces ligands, conduit à un profil de Fe plus proche des éléments nutritifs correspondant ainsi mieux aux données de terrain (Völker et Tagliabue, 2015). Cela indique que le temps de résidence des ligands organiques dans la colonne d'eau et les processus par lesquels ils sont enlevés de la colonne d'eau sont encore peu contraints et qu'il est nécessaire de continuer à approfondir les connaissances sur les sources, les puits et les caractéristiques des ligands organiques dans les océans (Lohan et al., 2015). Enfin, seuls quelques articles mentionnent le lien entre toutes les distributions de nutriments prises ensemble avec les assemblages de phytoplancton (e.g. Hassler et al., 2012). Cela devrait être fait systématiquement pour mieux comprendre leur potentiel à contrôler la biomasse phytoplanctonique et pour évaluer les principaux éléments nutritifs (i.e. macro- et micro-nutriments) limitants la croissance phytoplanctonique des océans mondiaux. Cela nous permettra de prédire potentiellement la classe de phytoplancton qui sera présente dans un

environnement spécifiquement (co)-limité en nutriments. Par conséquent, améliorer notre compréhension du cycle océanique du fer et de sa sensibilité aux conditions environnementales changeantes ainsi que le contrôle des macro et micro-nutriments sur les communautés de phytoplancton amélioreront les projections de la réponse des océans au changement climatique.

Afin de répondre à certaines de ces questions clés, les objectifs de cette thèse, dans le cadre du programme GEOTRACES, s'articulent autour de trois questions scientifiques : 1) Quels sont les distributions, les sources et les puits de fer dissous dans les deux régions d'étude spécifiées ? 2) Dans ces régions, quel est le lien entre la structure de la communauté phytoplanctonique et les concentrations de fer dissous ? 3) Comment la spéciation organique du fer dissous affecte-t-elle sa concentration et sa biodisponibilité pour la communauté phytoplanctonique ? Ces trois questions ont été examinées dans deux zones contrastées présentées ci-dessus : l'océan Atlantique Nord (GEOVIDE, GA01 GEOTRACES, IPG G. Sarthou et P. Lherminier) et l'océan Austral (HEOBI, GEOTRACES GIpr05, IPs A. Bowie, T. Trull, Z. Chase). Ces deux campagnes scientifiques ont été approuvées par le programme GEOTRACES.

Ce manuscrit se décompose de la manière suivante:

- Chapitre 2: Ce chapitre énumère les spécificités du travail sur les métaux traces. Les différentes méthodes analytiques utilisées dans cette thèse y sont présentées ainsi que les méthodes statistiques.
- Chapitre 3: Ce chapitre décrit les résultats du DFe dans l'océan Atlantique nord et dans la mer du Labrador le long de la section GEOVIDE. Ce chapitre se présente sous la forme d'un manuscrit soumis à « Biogeosciences Discussions ».
- Chapitre 4: Ce chapitre porte sur la répartition des assemblages phytoplanctoniques dans l'Atlantique Nord et la mer du Labrador le long de la section GEOVIDE déterminée par le modèle CHEMTAX à partir des données de pigments HPLC. Le présent manuscrit, en préparation, a pour objectif de comprendre le lien entre le forçage physique et les distributions de phytoplancton.

- Chapitre 5: Ce chapitre porte principalement sur les ligands organiques se complexant au Fe. Il explore le lien entre les ligands organiques et la biologie dans l'océan Austral et vise à mieux contraindre leurs caractéristiques. Ce chapitre sera soumis à « Marine Chemistry ».
- Chapitre 6: Le dernier chapitre de cette thèse résume les informations données dans les chapitres 3, 4 et 5. Le chapitre 6 suggère également de nouvelles perspectives et orientations des programmes internationaux futurs.

D- Résumé du chapitre 3

Les échantillons de Fe dissous provenant de la campagne océanographique GEOVIDE (GEOTRACES GA01, mai-juin 2014) qui s'est déroulée dans l'océan Atlantique nord, ont été analysés à l'aide d'un SeaFAST-picoTM couplé à un Element XR SF-ICP-MS. Ces échantillons ont fourni des informations intéressantes portant sur les sources de Fe dans cette zone. Dans l'ensemble, les concentrations de DFe allaient de $0,09 \pm 0,01 \text{ nmol L}^{-1}$ à $7,8 \pm 0,5 \text{ nmol L}^{-1}$. Des concentrations élevées de DFe ont été observées au-dessus des marges ibérique, du Groenland et de Terre-Neuve, probablement en raison des apports fluviaux du Tage, des apports d'eaux météoriques et des apports sédimentaires. L'intensification des interactions air-mer serait probablement responsable de l'augmentation des concentrations de DFe dans les eaux de subsurface de la mer d'Irminger en raison de la convection profonde survenue au cours de l'hiver précédent, ce qui a fourni des rapports fer/nitrate suffisants pour soutenir la croissance du phytoplancton. L'augmentation des concentrations de DFe le long de la voie d'écoulement de l'eau de la mer du Labrador (LSW) a été attribuée aux apports sédimentaires de la marge de Terre-Neuve. Les eaux de fond de la mer d'Irminger présentaient de fortes concentrations de DFe, probablement en raison de la dissolution de particules riches en Fe issues des eaux de débordement du détroit du Danemark (DSOW) et des eaux intermédiaires polaires (PIW). Enfin, les couches néphéloïdes situées dans les couches profondes des différents bassins et à la marge ibérique se sont avérées être des sources ou des puits de DFe en fonction de la nature des particules. Les particules organiques sont susceptibles de libérer du DFe alors que les particules constituées de manganèse (Mn) sont susceptibles de le piéger.

E- Résumé du chapitre 4

Cette étude examine la structure des tailles et la composition taxonomique de la prolifération printanière du phytoplancton dans l'Atlantique Nord et la mer du Labrador le long de la section GEOVIDE (du 15 mai 2014, de Lisbonne au 30 juin 2014, à St. John's). Une évaluation des principales limitations potentielles ainsi que la succession des principales classes de phytoplancton sont présentées dans un contexte d'un indice d'oscillation nord-atlantique (NAO) positif. L'analyse des rapports des nutriments a suggéré une variation du facteur contrôlant la croissance du phytoplancton avec, la plus intense limitation de la croissance du phytoplancton observée au sud de 50°N. La comparaison des taux de disparition des macronutriments (NO_3^- , Si(OH)_4) et du fer dissous (DFe), des distributions de nutriments, des pigments biomarqueurs utilisés pour identifier les groupes de phytoplancton dominants via le programme CHEMTAX, des rapports pigments photosynthétiques et photoprotecteurs et des pigments de dégradation ont démontré qu'au sud de 45°N, la prolifération phytoplanctonique, dominée par les diatomées, était globalement limitée par les concentrations de silicate et (co)-limitée en azote (N) plus près de la marge ibérique. Entre 45 et 50°N, les efflorescences de phytoplancton étaient dominées dans les eaux de surface par les haptophytes de type 8 et les dinophytes, tandis que les eaux plus profondes (de 50 à 90 m de profondeur) étaient dominées par les haptophytes de type 8 et les diatomées. Dans cette zone, la croissance phytoplanctonique était limitée par les silicates et éventuellement co-limitée par le Fe. La prolifération de phytoplancton dans le bassin islandais était dominée par les haptophytes de type 6 (i.e. les coccolithophoridés) et limitée par le Fe. La mer d'Irminger était dominée par les diatomées et affichait des concentrations accrues d'éléments nutritifs, suggérant un contrôle de la croissance phytoplanctonique par les niveaux trophiques supérieurs dans cette région et/ou une limitation par la lumière plutôt que des restrictions en éléments nutritifs. La mer du Labrador était potentiellement limitée par la lumière et co-limitée par l'azote et affichait une structure communautaire différente au sud et au nord de 55°N, probablement en raison du cycle de gel et de dégel. Bien que de nombreuses études aient signalé le passage des diatomées aux dinophytes en raison de l'augmentation de la température de la surface de la mer, ces résultats montrent que les diatomées dominaient largement l'Atlantique Nord, en particulier sous les hautes latitudes probablement du fait de la fonte de la glace arctique. La seule exception était le bassin de l'Islande dominé par les coccolithophoridés. Ces deux classes fonctionnelles de phytoplancton sont toutes deux connues pour améliorer l'export de carbone par rapport à d'autres taxons en raison de leur squelette biominéral.

F- Résumé du chapitre 5

Des échantillons de ligands organiques se liant au fer ($n = 86$) ont été recueillis de janvier à février 2016 pour l'étude de leurs fractions dissoutes ($<0,2 \mu\text{m}$) et solubles ($<0,02 \mu\text{m}$) dans les masses d'eau situées au-dessus et en dehors du plateau de Kerguelen (HEOBI, étude de processus GEOTRACES GIp05). La zone étudiée consistait en une répétition de la section B échantillonnée lors de la campagne océanographique KEOPS au cours de l'automne 2005 et de sites d'échantillonnage spécifiques autour des îles Heard et McDonald. Pour comprendre l'effet du plateau de Kerguelen, une station de référence située au sud des îles Heard et McDonald a été échantillonnée à des fins de comparaison. Une analyse voltammétrique inverse cathodique adsorbante à impulsions différentielles avec pour ligand de compétition du 2- (2-thiazolylazo) p-crésol a été utilisée pour mesurer les concentrations de ligands organiques complexant le Fe et leurs constantes de stabilité conditionnelle. Les concentrations de ligands organiques se complexant au Fe dissous allaient de 0,26 à 2,6 Eq de $\text{nmol L}^{-1} \text{ Fe}$, avec une concentration médiane de 0,70 Eq de $\text{nmol L}^{-1} \text{ Fe}$ et un logarithme médian de constante de stabilité conditionnelle de 21,24 L mol^{-1} . Nos résultats ont montré que les ligands organiques complexant du Fe dissous ne dépassaient les concentrations de DFe que dans les 200 premiers mètres des stations de référence et de la section B. Au-dessous de cette profondeur, les concentrations de ligands organiques étaient proches des concentrations mesurées en DFe ou saturées en DFe. En ce qui concerne les stations échantillonnées autour des îles Heard et McDonald, les ligands présentaient des concentrations proches de la saturation ou à saturation en DFe, et ce, sur l'intégralité de la colonne d'eau. Les sources de ligands semblent principalement d'origine biologique. Les ligands organiques colloïdaux semblent être produits par de grandes diatomées et par des bactéries au niveau des stations de référence et de la section B. Dans les environs des îles Heard et McDonald, seuls des ligands une faible capacité de complexation ont été mesurés et semblaient également être véhiculés par des bactéries. Ces caractéristiques ont entraîné des différences marquées dans la répartition des diverses fractions du Fe entre les stations de référence et de la section B d'un côté et des îles McDonald et Heard de l'autre. Bien que les eaux de l'île Heard présentaient des concentrations en ligands solubles en excès du SFe, la colonne d'eau des îles Heard et McDonald était dominée par des ligands à faible réactivité, tant en phase dissoute que soluble, contrairement aux stations de référence et de la section B.

G- Conclusions générales et perspectives

G.1- Synthèse des principaux résultats

G.1.1- Océan Atlantique Nord: distributions du DFe, des macronutriments et des pigments

Dans le cadre du projet GEOVIDE, les distributions du fer dissous (DFe), des éléments nutritifs et des pigments ont fourni des informations intéressantes sur les sources de Fe et les potentielles limitations de la croissance du phytoplancton.

Les concentrations de DFe mesurées au cours de cette étude étaient en bon accord avec les études précédentes couvrant le bassin ouest-européen, le bassin islandais et la mer du Labrador (Fig. G.1).

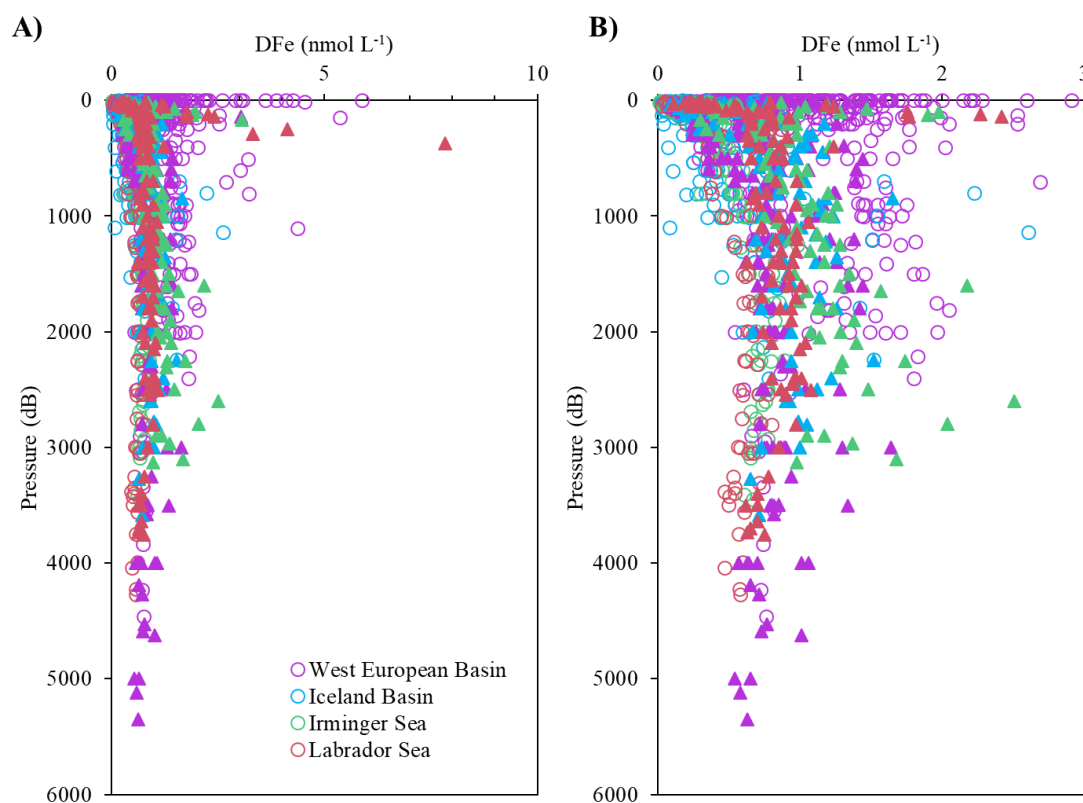


Figure G.1 : Nuage de points de stations échantillonnées dans le bassin ouest-européen (violet), dans le bassin islandais (en bleu), dans la mer d'Irminger (en vert) et dans la mer du Labrador (en rouge) au cours d'études antérieures (cercles ouverts) et de cette étude (triangles ombrés).

Cependant, dans la mer d'Irminger, les concentrations de DFe mesurées au cours de cette étude étaient jusqu'à trois fois plus élevées que celles mesurées par Rijkenberg et al. (2014) dans les eaux profondes (> 1000 m de profondeur) de la mer d'Irminger au cours de la campagne GA02. Cette dissemblance entre les campagnes GEOVIDE (GA01) et GA02 peut

éventuellement s'expliquer par l'intrusion de l'eau intermédiaire polaire (PIW) à environ 2800 m de profondeur et par un signal plus intense de l'eau de débordement islando-écossaise (ISOW) de 1200 à 2300 m de profondeur. Ce bassin océanique comporte la distribution des concentrations du DFe la plus marquée de l'ensemble de la section avec des concentrations de DFe atteignant jusqu'à $2,5 \text{ nmol L}^{-1}$ dans l'ISOW, les eaux de débordement du détroit du Danemark (DSOW) et l'eau de la mer du Labrador (LSW), trois masses d'eau faisant partie du courant profond de bord ouest. Cependant, lorsque ces masses d'eau atteignent la mer du Labrador, les concentrations du DFe décroissent. Ces différences ont été expliquées par divers processus intervenant dans les couches néphéloïdes benthiques. Au sein de ces couches, le DFe était parfois piégé dans des particules en raison des oxydes de manganèse qui composent les sédiments de la mer du Labrador ([1], Fig. G.2; Gourain et al., 2018) et parfois relâchés dans la colonne d'eau, potentiellement à la suite d'interactions entre les particules en suspension et la matière organique dissoute dans la bassin d'Irminger. En effet, des ligands organiques complexant le DFe auraient pu être produits localement en raison du fort taux de re-minéralisation (Lemaître et al., 2018) des particules biogéniques ([2], Fig. G.2; Boyd et al., 2010; Gourain et al., 2018). La LSW présentait des concentrations croissantes de DFe le long de son trajet d'écoulement ([3], Fig. G.2), probablement en raison de l'apport de sédiments depuis la marge canadienne ([4], Fig. G.2). Bien que des apports de DFe d'origine hydrothermale étaient attendus au niveau de la dorsale à propagation lente de Reykjanes (Baker et German, 2004b; German et al., 1994) telle que précédemment mentionnée par Achterberg et al. (2018) plus au nord ($\sim 60^\circ\text{N}$) de notre section, nos données n'ont pas mis en évidence cette source spécifique.

Dans les eaux de surface, plusieurs sources de DFe ont été mises en évidence, particulièrement près des masses continentales. Au niveau de la marge ibérique, les apports fluviaux du Tage ont été soulignés par une corrélation négative entre les concentrations de DFe et la salinité ([5], Fig. G.2; Menzel Barraqueta et al., 2018). Au niveau des marges de Terre-Neuve et du Groenland, les apports des eaux météoriques (comprenant les eaux de ruissellement côtières et les eaux glaciales de fonte) ont été identifiés par les concentrations de $\delta^{18}\text{O}$ et des macronutriments (Benetti et al., 2016) ([6], Fig. G.2). Toutes les marges continentales présentaient d'importants apports sédimentaires avec des concentrations croissantes en DFe de haut en bas de la colonne d'eau, toutefois, avec une intensité différente. L'apport le plus élevé en DFe et issu des sédiments se situait au niveau de la marge de Terre-Neuve ([3], Fig. G.2), tandis que le plus faible était observé dans la marge est du Groenland

([7], Fig. G.2). La différente nature des particules sédimentaires ainsi que la nature des particules en suspension dans la colonne d'eau seraient responsables des intensités contrastées en DFe. En effet, les rapports DFe:DAI, DFe:PFe et PFe:PAI (aluminium dissous, DAI, données issues de Menzel Barraqueta et al., 2018; particules de fer, PFe, et particules d'aluminium, PAI, issues de Gourain et al., 2018) ont mis en évidence une nature plus lithogénique de ces particules au niveau de la marge ibérique et plus biogénique au niveau de la marge de Terre-Neuve (Gourain et al., 2018). Bien que de précédentes études (e.g. Jickells et al., 2005; Shelley et al., 2015) aient révélé que les dépôts atmosphériques fertilisaient de façon substantielle les eaux de surface du bassin ouest-européen, dans notre étude, seules quelques stations présentaient des concentrations de DFe de surface accrues, de sorte que le dépôt atmosphérique semblait être une source mineure de Fe au moment de l'échantillonnage. Enfin, l'intrusion dans les eaux de surface de la mer d'Irminger de la LSW par convection a été identifiée par une analyse multi-paramètres optimale étendue (eOMP, García-Ibáñez et al., 2018) ainsi que par l'augmentation des concentrations en oxygène dissous (DO_2). La convection de la LSW par forçage atmosphérique (Piron et al., 2016) a approfondi la couche de mélange hivernale dans laquelle le DFe était appauvri par rapport aux nitrates ([8], Fig. 6.2) jusqu'à environ 1200 m de profondeur (Zunino et al., 2017).

En terme de potentielles limitations par les éléments nutritifs, trois principales zones se sont distinguées dans l'océan Atlantique Nord via une analyse canonique de correspondance qui visait à contraindre les classes de taille phytoplanctoniques déterminées par les équations de Uitz et al. (2006), ainsi que les principales classes fonctionnelles de phytoplancton déterminées par le programme CHEMTAX à l'aide de variables environnementales, à savoir des variables physiques et chimiques:

1. La province subtropicale est de l'Atlantique nord (NASTE) limitée en azote a entraîné une forte abondance de cyanobactéries diazotrophes (D. Fonseca Batista et F. Deman; données non publiées) subsistant potentiellement grâce à une relation symbiotique avec des haptophytes de type 6 (Cabello et al., 2016), les cyanobactéries fournissant de l'azote, les haptophytes de type 6 du carbone.
2. La province de la dérive nord-atlantique (NADR), dans laquelle deux sous-zones ont été distinguées à savoir les eaux de surface de la branche sud du courant

nord-atlantique (SNAC) dominées par des dinophytes semblant bénéficier de températures plus élevées, d'un excès de DFe relatif au nitrate (NO_3^-) et d'une moindre pression par les niveaux trophiques supérieurs, tandis que les haptophytes de type 8 et les petites diatomées étaient présents plus profondément dans la colonne d'eau. Dans cette zone, les haptophytes de type 8 pourraient être sujet à une limitation en Fe et les petites diatomées à une (co)-limitation en Silicate (Si(OH)_4) et Fe. La partie nord de la province NADR était clairement dominée par les haptophytes de type 6 qui ont colonisé les eaux appauvries en Si suite à un affaiblissement du gyre subpolaire et à l'intensification du gyre subtropical pauvre en nutriments. Les haptophytes de type 6 peuplant cette zone ne semblaient aucunement limités par le Fe.

3. Les six zones distinctes par des niveaux contrastés de chlorophylle-*a* totale intégrée sur les 200 premiers mètres (TChl-*a*) de la province de l'Arctique Atlantique (ARCT) étaient largement expliquées par la circulation à grande échelle. Parmi ces zones, les marges du Groenland et de Terre-Neuve étaient presque exclusivement constituées de grandes diatomées néritiques, qui bénéficiaient des apports simultanés de DFe et de silicate (Si(OH)_4) issus des eaux de fonte glaciaire. Dans ces eaux turbulentes de haute latitude, la lumière est probablement le facteur le plus limitant (Harrison et Li, 2008; Harrison et al., 2013). Les eaux de surface de la mer du Labrador semblaient être limitées en azote. De même, la station échantillonnée dans le gyre d'Irminger semblait être limitée soit par la disponibilité en lumière, soit soumise à un broutage accru.

Dans l'ensemble, l'Atlantique Nord était dominé par deux classes fonctionnelles : les diatomées et les haptophytes de type 6, deux classes phytoplanctoniques, construisant un squelette biominéral, susceptibles d'augmenter l'export de carbone.

A)

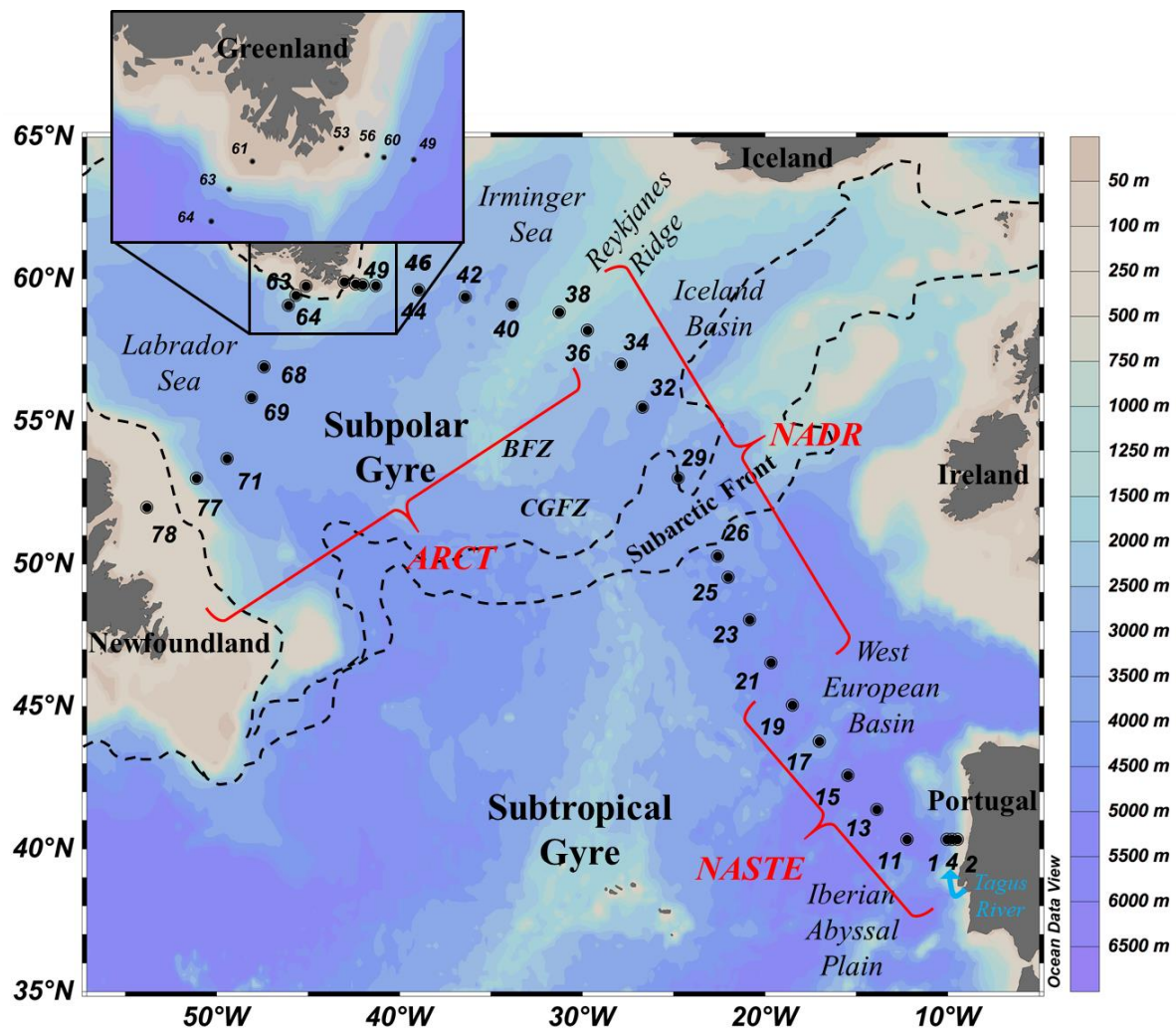
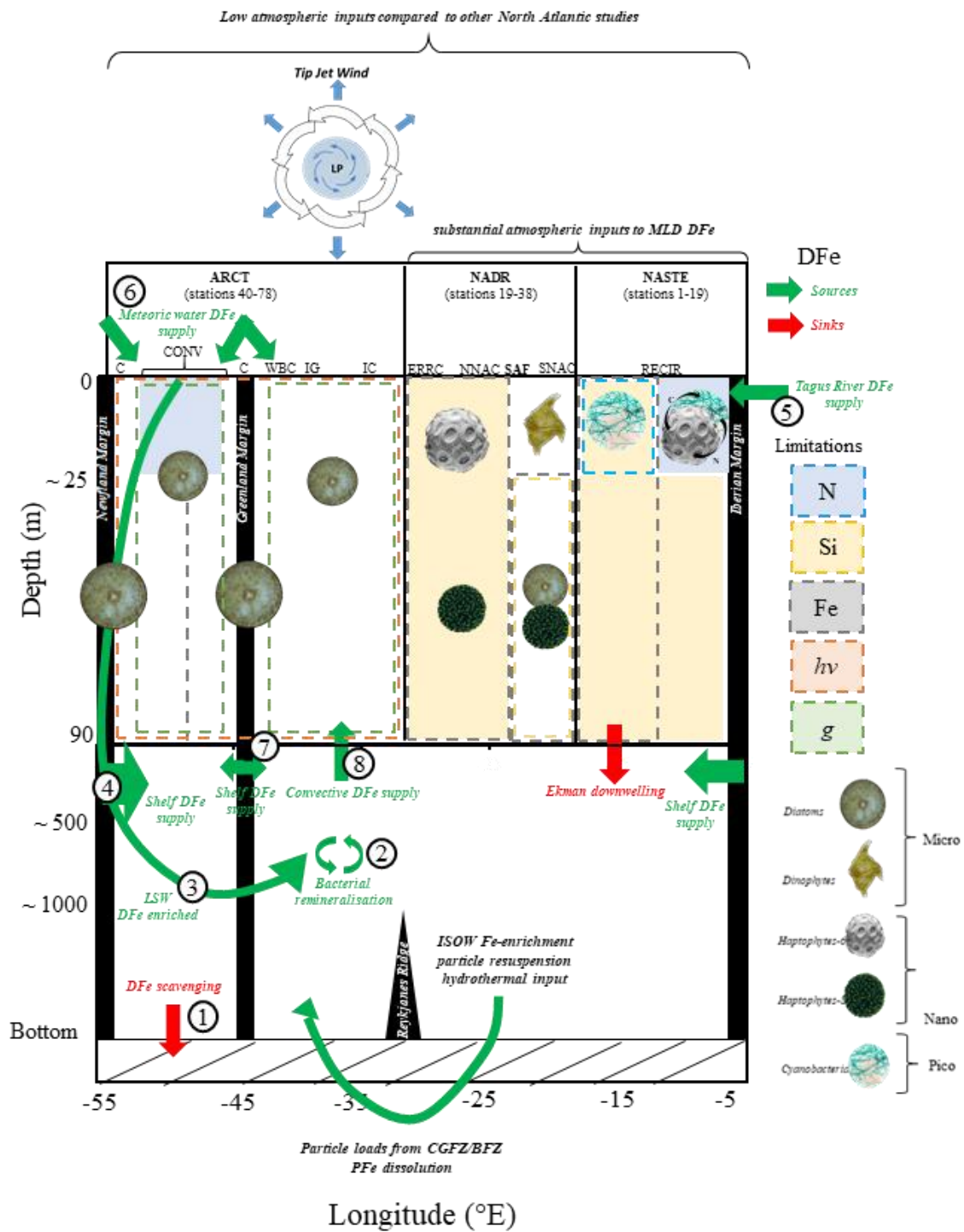


Figure G.2: A) Carte du voyage GEOTRACES GA01 avec en arrière fond la bathymétrie, ainsi que les principales caractéristiques topographiques, les principaux bassins et les provinces de Longhurst correspondantes. B) Récapitulatif des sources en DFe, des principales classes fonctionnelles de phytoplancton et des potentielles limitations de la croissance phytoplanctonique dans l'océan Atlantique nord.

B)



G.1.2- L'océan austral : les ligands organiques complexant le Fe et la production primaire

Sur la partie nord du plateau de Kerguelen, le DFe, provenant des sédiments du plateau peu profond de Kerguelen et apporté aux eaux de surface par brassage hivernal et diffusivité verticale (Blain et al., 2008b), a été mis en évidence comme étant le principal paramètre contrôlant la prolifération de phytoplancton (Blain et al., 2008c). Il a également été démontré que ce DFe subissait des pertes minimales par advection en raison de la présence de courants faibles (Park et al., 2008b) et de fortes concentrations de ligand organique complexant le Fe en excès des concentrations de DFe (Gerringa et al., 2008). Cependant, il existe une variabilité interannuelle en terme de magnitude et de localisation de la prolifération de phytoplancton. Ces différences spatio-temporelles pourraient éventuellement être dues aux formes chimiques et physiques du DFe dans cette zone empêchant ainsi sa biodisponibilité. Par conséquent, lors du voyage HEOBI (Interaction Terre-Océan-Biosphère Heard), qui s'est déroulé de janvier à février 2016 vers la fin de la prolifération de phytoplancton, les spéciations physiques et organiques du pool de DFe a été étudiée.

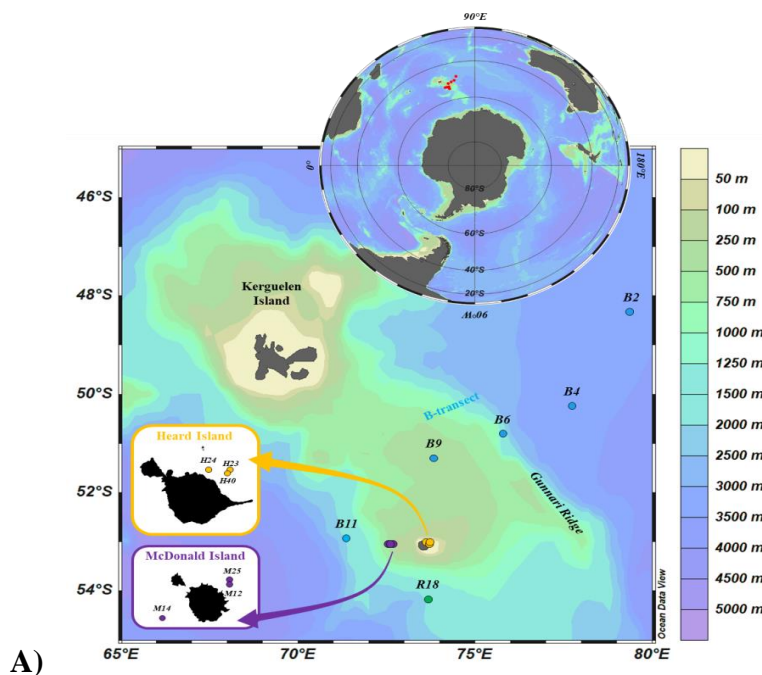
L'étude des ligands organiques complexant le fer dans les fractions dissoutes, solubles et colloïdales par analyse voltammétrique inverse cathodique et adsorbante à impulsion différentielle et compétition par échange de ligands (CLE-AdCSV) avec mesure directe des fractions solubles et dissoutes et mesure indirecte de la fraction colloïdale en soustrayant la fraction soluble de la fraction dissoute, a révélé de nettes différences entre les stations de référence (R18) et de la section B comparativement aux stations échantillonnées autour des îles Heard et McDonald (Fig. G.3A).

Dans les eaux de surface de R18 et de la section B, le fer soluble (SFe) dominait le pool de DFe. Ce SFe était probablement entretenu par un ligand organique présentant une forte capacité à complexer le fer (SLt) issu de la re-minéralisation, comme l'indiquent les corrélations positives entre les concentrations de SLt et de silicate. En outre, le phytoplancton, dominé par de grandes diatomées, et les bactéries semblaient produire de puissants ligands organiques complexant le Fe. Cela a entraîné un excès de ligands par rapport à toutes les fractions physiques de Fe, y compris la fraction particulaire (PFe, données de van der Merwe et al., en prép.). Plus en profondeur dans la colonne d'eau, la comparaison de l'étude réalisée lors de la campagne KEOPS par Gerringa et al. (2008) et de celle menée durant la campagne HEOBI a révélé la présence d'une source de DFe inorganique (DFe') issu des sédiments du plateau de Kerguelen. Cela a été mis en évidence par des concentrations

croissantes de DFe' de la surface vers l'interface sédimentaire. De la même manière que pour le DFe', les ligands organiques du DFe (DLt) ainsi que le DFe (données de Holmes et al., en prép.) semblaient avoir une source profonde. Cependant, ils semblaient provenir de la dégradation de la matière organique accumulée sur les couches sédimentaires, contrairement à ce qui avait été rapporté par Gerringa et al. (2008).

Inversement, aux îles Heard et McDonald, le fer colloïdal (CFe) dominait le pool de DFe. Dans cette région, les ligands organiques étaient saturés en Fe dans toute la colonne d'eau, mettant ainsi en évidence une source importante de Fe. La colonne d'eau était dominée par des ligands colloïdaux peu réactifs, ce qui entraînait le piégeage du Fe par les particules en suspension (Fig. G.3B).

Enfin, deux zones distinctes ont été observées en termes d'inventaires de chlorophylle-*a* totale (TChl-*a*), avec d'un côté, les stations de référence et de la section B présentant des concentrations élevées en TChl-*a* intégrées le long de la colonne d'eau et de l'autre côté, les stations des îles Heard et McDonald présentant de faibles concentrations en TChl-*a* intégrées le long de la colonne d'eau (Wojtasiewicz et al., en prép.). Ces différences en terme de TChl-*a* pourraient potentiellement être expliquées par les spéciations physiques et organiques du Fe du fait qu'elles correspondaient exactement aux différences observées dans les fractions dissoutes, solubles et colloïdales des concentrations de ligands organiques du Fe et des fractions dissoutes, solubles, colloïdales et particulaires du Fe.



B)

B-transect & R18

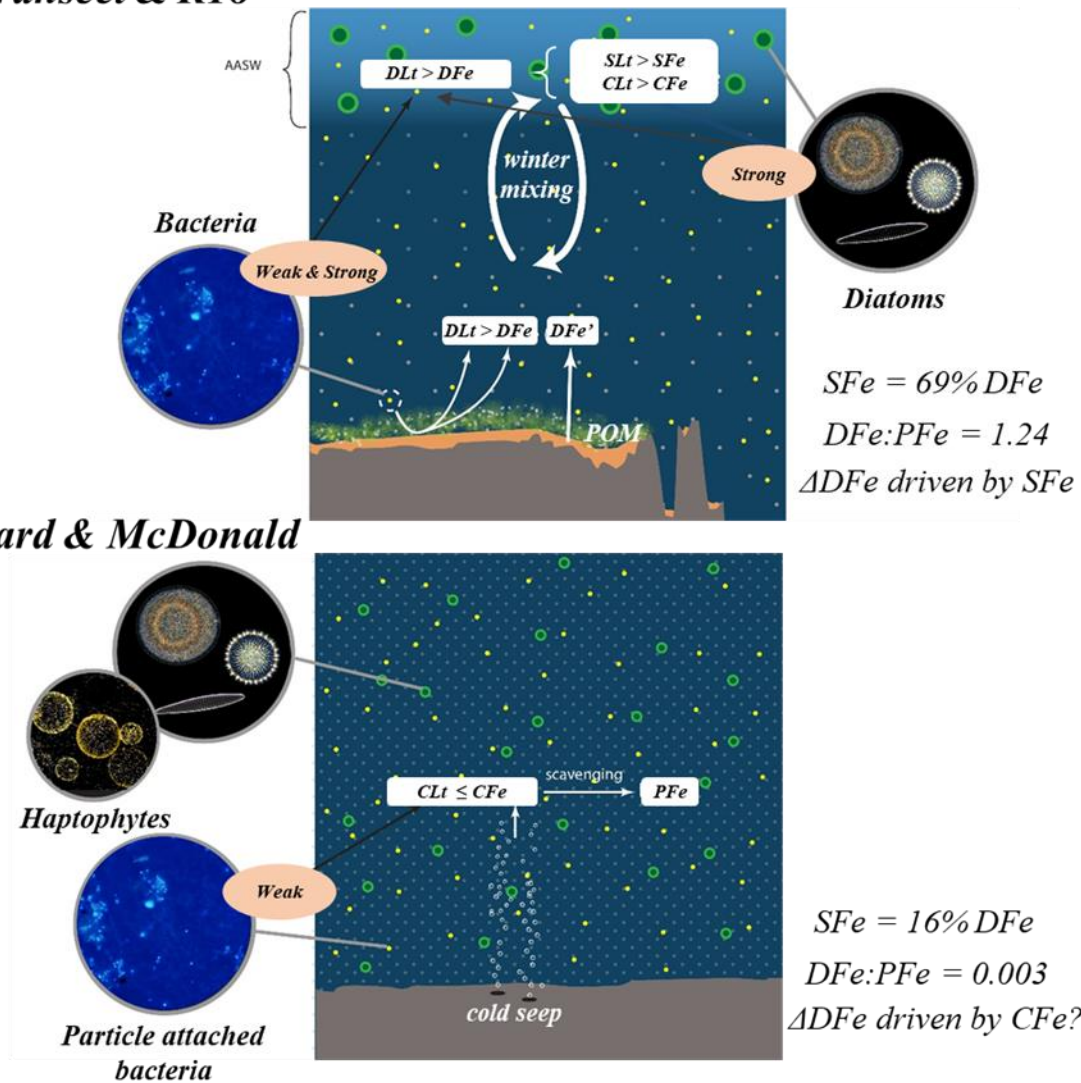


Figure G.3 : A) Emplacement des stations échantillonnées pendant le voyage HEOBI à l'aide de la rosette propre en métaux traces (Thomas Holmes). B) Schéma conceptuel des principales découvertes concernant les stations des îles Heard et McDonald et les stations de la section B et de la station de référence (R18) (D. Alain et S. Hervé, IUEM). (Données DFe de Holmes et al., en prép., données PFe de Van der Merwe et al., en prép.; données pigmentaires de Wojtasiewicz et al., en prép., Images de bactéries fournies par S. Blain).

G.1.3- rapprochement des deux zones d'étude

Cette thèse a permis d'améliorer les connaissances du cycle biogéochimique du Fe en combinant deux approches novatrices: i) l'utilisation d'analyses statistiques multi-paramètres rassemblant des variables environnementales physiques (salinité, température, pH), chimiques (éléments nutritifs principaux et DFe) et biologiques (classes de phytoplancton estimées à partir de pigments via le programme CHEMTAX) et ii) l'étude des spéciations physiques et organiques du Fe. Ces travaux ont permis de déterminer diverses sources et puits de DFe dans l'Atlantique Nord et sur le plateau de Kerguelen et ont mis en évidence la relation complexe entre les formes de Fe disponibles et la réponse de la structure de la communauté phytoplanctonique. Si le DFe n'était pas le paramètre responsable principalement de la structure de la communauté de phytoplancton dans les hautes latitudes de l'Atlantique Nord, c'est-à-dire dans la province ARCT de Longhurst, il se pourrait qu'il co-limite les diatomées avec les Si(OH)_4 dans le bassin islandais, permettant ainsi le développement d'efflorescence d'haptophytes de type 6. Cela est probablement dû à la quantité de sources externes de DFe affectant les eaux de surface dans cette région géographique du monde, que ce soit par la circulation des masses d'eau, les dépôts atmosphériques ou les eaux de ruissellement côtières. Inversement, sur le plateau de Kerguelen, bien que le Fe semble être ubiquiste, la spéciation organique du Fe et plus particulièrement la réactivité des ligands organiques colloïdaux complexant le Fe semblent expliquer les différences entre les inventaires de TChl-*a* et la structure de la communauté phytoplanctonique. En effet, la réactivité des ligands organiques colloïdaux semblait déterminer le devenir du Fe dans la colonne d'eau avec des pertes par adsorption sur les particules en suspension en cas d'instabilité de la fraction colloïdale ou de persistance de la fraction dissoute du Fe en cas de ligands colloïdaux présents en excès. De même, dans l'océan Atlantique Nord, bien que la spéciation organique du Fe n'ait pas été étudiée, il semble que les pertes en Fe ou le maintien du DFe dans la colonne d'eau soient modulées par la quantité de matière organique dissoute, à savoir les ligands capables ou non de remobiliser le Fe des particules.

L'extrapolation des résultats de ces trois études met en évidence le rôle central de la spéciation organique du Fe. En effet, le transport à longue distance (environ 3000 km) du DFe issu des sédiments de Terre-Neuve vers la mer d'Irminger pourrait également être dû à une haute réactivité de la fraction colloïdale des ligands organiques du Fe. Par conséquent, il semble crucial d'étudier avec la même résolution les spéciations physiques et organiques du

Fe afin de mieux contraindre son devenir dans la colonne d'eau et ainsi s'approcher du temps réel de résidence du Fe. De plus, la structure de la communauté phytoplanctonique devrait être systématiquement évaluée par le programme CHEMTAX ou mieux encore par une approche génomique et devrait être suivie sur toute la durée de la floraison afin de la relier aux distributions de macro et micro-nutriments. Enfin, toutes ces analyses doivent être effectuées de manière concomitante avec des incubations embarquées afin de tester directement la limitation en éléments nutritifs en enrichissant les assemblages naturels des communautés phytoplanctoniques en macro et micro-éléments nutritifs afin de confirmer ou d'infirmar les hypothèses de limitation issues des traceurs Si * et Fe *.

G.2 Implications et perspectives

Dans l'Atlantique Nord, l'analyse des concentrations de ligands organiques dissous complexant le Fe et de leurs caractéristiques ont été réalisées. Lorsqu'elles seront disponibles, elles permettront d'identifier si les sources externes de DFe peuvent être maintenues ou non dans la colonne d'eau. En plus d'évaluer le temps de résidence du DFe dans la colonne d'eau, il aurait été intéressant de tester directement la biodisponibilité des différentes sources de DFe. Par exemple, la réponse des assemblages de la communauté phytoplanctonique de la province NASTE en réponse aux dépôts atmosphériques secs et/ou humides aurait pu être étudiée (Fig. G.4). Malgré de nombreuses études, la mesure dans laquelle les particules de poussière peuvent être remobilisées sous forme de DFe et potentiellement biodisponibles pour les assemblages phytoplanctoniques naturels reste incertaine. Pour ce faire, des incubations embarquées enrichies avec les aérosols collectés lors de la campagne GEOVIDE auraient pu être conduites dans le but de suivre au cours du temps les concentrations de DFe et de ligands organiques complexant le Fe dans les diverses phases physiques, la communauté bactérienne, ainsi que les potentiels changements de la structure des communautés naturelles de phytoplancton. Ce type d'expérience pourrait aider à déterminer les interactions entre les bactéries et le phytoplancton et contraindre l'importance des apports atmosphériques et la façon dont ils favorisent certaines classes fonctionnelles de phytoplancton par rapport à d'autres. Bien que Boyd et al. (2010) aient rapporté, en utilisant des expériences sur le terrain et des simulations de modélisation, que la re-minéralisation du PFe biogénique était probablement la principale source de ligands organiques et de Fe dissous par rapport à la re-minéralisation du PFe lithogénique, il serait intéressant de vérifier cette hypothèse en utilisant le même type d'expériences que celles susmentionnées pour les particules de poussière

atmosphériques mais pour des particules issues des quatre marges continentales (i.e. la marge ibérique, les marges est et ouest du Groenland et la marge de Terre-Neuve) (Fig. G.4). De cette manière, nous pourrions évaluer la réponse du phytoplancton à cette source de Fe régénéré et la force de complexation des ligands organiques générés par la suite et le fait qu'ils soient accessibles ou non pour le phytoplancton et s'ils induisent un changement de la communauté phytoplanctonique.

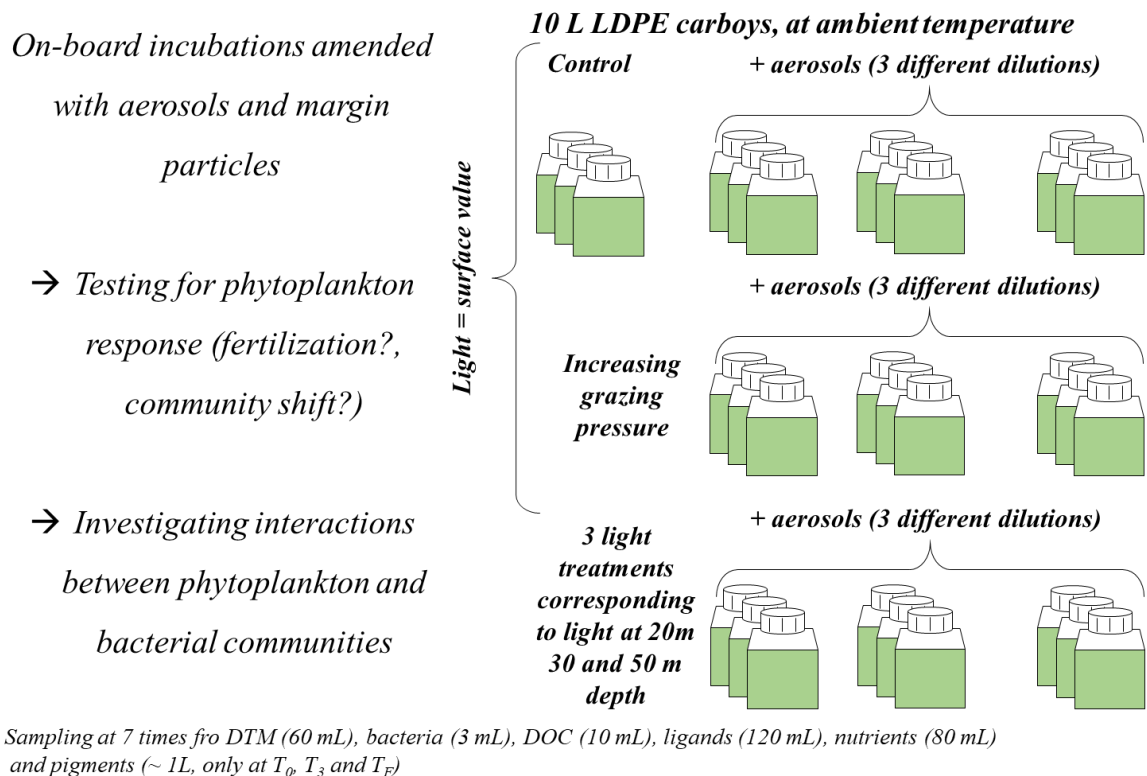


Figure G.4 : Idée d'un dispositif expérimental pour les incubations embarquées enrichies par des particules atmosphériques et des particules issues des marges continentales.

Il serait également important de construire les budgets du Fe le long de la section GEOVIDE. C'est une étape capitale permettant d'évaluer l'importance relative des sources externes dans les différents bassins océaniques s'effectuant avant de déterminer la variabilité de ces sources externes de DFe dans le temps. Bien que les voyages océanographiques soient figés dans le temps, ils permettent à la communauté scientifique de déterminer des sources spécifiques, mais ne permettent pas d'évaluer leur variabilité temporelle. Par conséquent, la répétition d'une telle section est essentielle pour quantifier et classer les sources par ordre

d'importance, d'autant plus qu'il est évident que notre monde est en train de changer. En effet, toutes les sources externes recensées à ce jour pour l'Atlantique Nord sont susceptibles d'augmenter ou de diminuer en fonction du changement climatique, ce qui aura plusieurs incidences sur les communautés phytoplanctoniques. Il a, par exemple, été signalé que l'Arctique s'était réchauffé plus intensément que toute autre région de la Terre au cours des dernières décennies (Stroeve et al., 2014). Ainsi, une augmentation du taux de perte de la calotte glaciaire groenlandaise (Nghiem et al., 2012; Stroeve et al., 2014), et le retrait de la glace de mer (Granskog et 2016,) dans l'océan Arctique ont été rapportés. Si de telles tendances devaient se maintenir, bien que nous ayons signalé des apports de Si(OH)_4 et de DFe provenant des eaux de fonte des glaciers et des eaux de ruissellement du Groenland, la stratification induite renforcerait probablement les interactions entre les organismes brouteurs et le phytoplancton (Behrenfeld, 2010). Répéter la section GA01 pourrait aider à contraindre les modèles biogéochimiques et donc les modèles climatiques en déterminant les impacts des changements à long terme sur les communautés phytoplanctoniques.

Par ailleurs, notre étude est la première à avoir été réalisée depuis le basculement vers des valeurs positives de l'oscillation nord-atlantique en 2013. Il serait donc intéressant de suivre les changements liés aux apports en macro et en micro-nutriments. Dans cette étude, bien que nous ayons évalué les limitations potentielles de la croissance phytoplanctonique en terme de nitrate (NO_3^-), de silicate (Si(OH)_4) et de DFe, inclure les concentrations de phosphate (PO_4^{3-}) ainsi que celles des autres métaux bioactifs (e.g. Mn, Co, Zn, ...) à l'analyse multi-variée aurait permis de révéler les interactions de tous ces nutriments avec le phytoplancton et les interactions des cycles biogéochimiques de ces nutriments. Des tests visant à estimer la limitation de la croissance des communautés phytoplanctoniques des hautes latitudes par la lumière pourraient aider à comprendre les facteurs contrôlant le déclin des efflorescences printanières de phytoplancton (Fig. G.4). En plus des paramètres évoqués plus haut, l'estimation de la pression exercée par les niveaux trophiques supérieurs sur le phytoplancton, qui n'a été évaluée dans notre étude que par les produits de dégradation de la chlorophylle-*a* suivie d'une comparaison entre les différentes provinces, devrait être mise en balance avec les autres paramètres contrôlant la croissance phytoplanctonique (Fig. G.4).

Au cours de la campagne océanographique GEOVIDE, il était clair que la circulation grande-échelle impactait les stocks intégrés de chlorophylle-*a* totale. La zone susceptible d'être la plus touchée par le changement des phases de l'oscillation nord-atlantique (NAO) et par des changements au niveau des sources externes d'éléments nutritifs, est la zone de

transition entre les gyres subtropicaux et subpolaires, en raison de son éloignement, à savoir, le bassin islandais. Cette zone constitue un laboratoire merveilleux pour étudier l'impact des structures océaniques de moyenne échelle telles que les tourbillons et les fronts sur les communautés phytoplanctoniques. Le déploiement d'un mouillage équipé de mésocosmes et de pièges à sédiments serait très utile pour comprendre l'évolution de la communauté phytoplanctonique et l'export des particules dans cette zone impactée par deux systèmes contrastés qui subiront des changements futurs dépendamment de la force de l'AMOC (programme d'étude de la NASA par télédétection des processus d'export dans l'océan, <http://oceanexports.org/>).

En ce qui concerne la campagne océanographique HEOBI, l'une des questions les plus importantes soulevée précédemment par Gerringa et al. (2008) est le contre-effet de la complexation organique car elle diminue inévitablement la quantité de fer inorganique (Fe'). Une meilleure estimation des formes chimiques biodisponibles du Fe aiderait la communauté scientifique à tirer des interprétations plus concluantes concernant le pouvoir limitant du Fe.

Enfin et surtout, la structure moléculaire et l'identification des ligands organiques constituent un domaine de recherche en pleine expansion. Malgré ce que l'on sait des ligands jusqu'à présent, beaucoup d'entre eux sont encore inconnus. Connaître la structure des ligands est d'une importance majeure. En effet, les communautés microbiennes développent des stratégies d'absorption et d'utilisation optimisant l'accès au Fe lié à la matière organique qui sont sensibles à la spéciation moléculaire des ligands organiques. Bien que de nouvelles techniques soient développées pour identifier la structure chimique des ligands (par exemple, Mawji et al., 2008a; Repeta et al., 2017), ces analyses prometteuses permettant non seulement de déterminer la structure des ligands organiques du Fe, mais également celles de tous les autres métaux traces dans au sein d'un même échantillon ainsi que leurs concentrations respectives, ne sont pas encore systématiques. Cependant, si l'on suppose que les ligands maintiennent les concentrations de DFe dans les eaux de surface, l'étude de leur morphologie structurale révélera probablement leur potentiel d'agrégation. Au cours de la campagne HEOBI, des ligands présentant de faibles constantes de stabilité conditionnelle pouvant correspondre à la gamme de substances de type saccharide (Hassler et al., 2015; Hassler et al., 2011c), à savoir, exopolysaccharide (EPS) ou acide glucuronique (monosaccharide) ont été mis en évidence. Ces substances de type gel peuvent subir une agrégation rapide faisant passer cette matière organique de la phase colloïdale à la phase particulaire sous forme de particules transparentes d'exopolymère (TEP) sur des échelles de temps allant de quelques

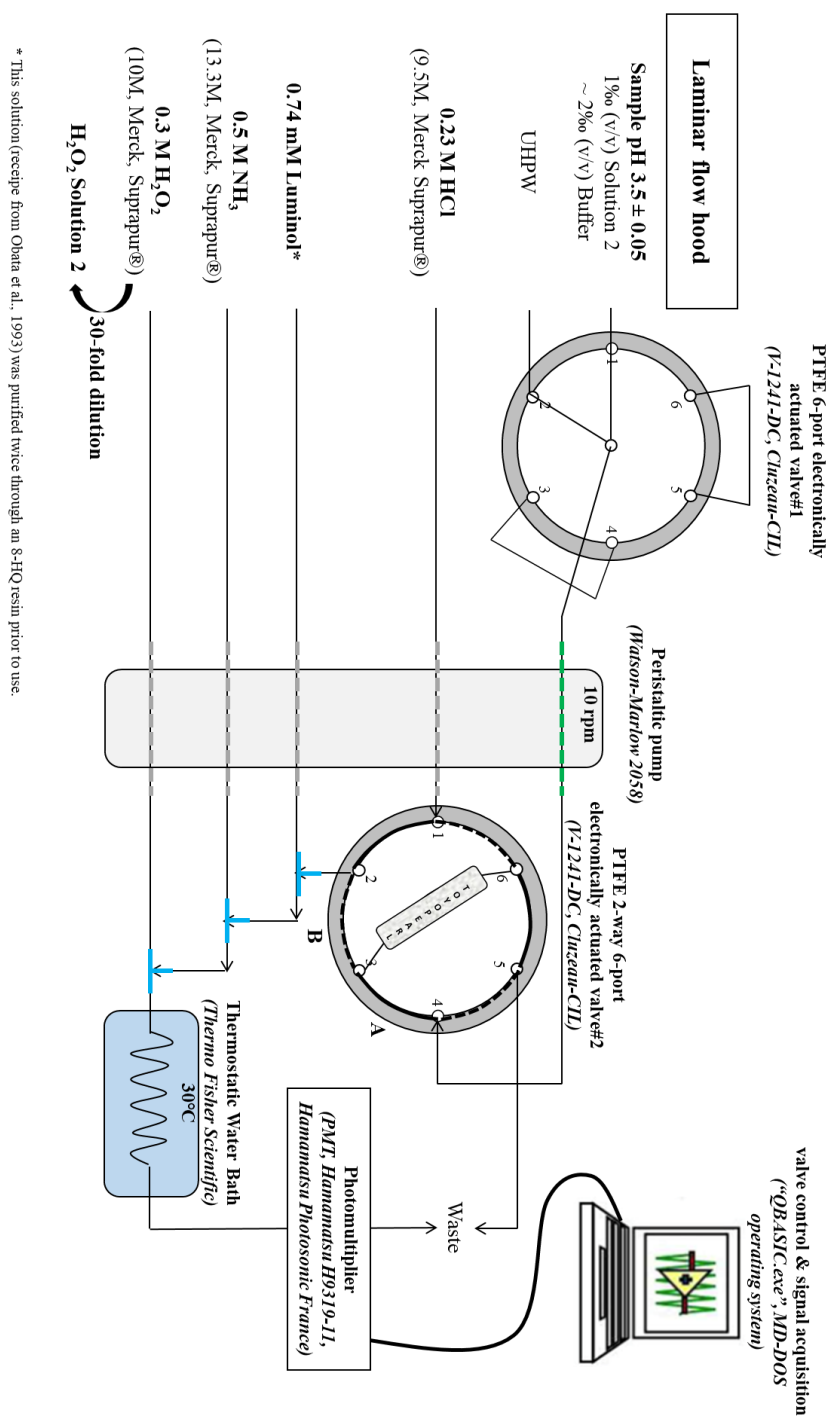
minutes à quelques heures (e.g. Baalousha et al., 2006; Verdugo et al., 2004). Ces particules à sédimentation rapide seraient capables de se lier aux éléments réactifs aux particules (Fe, Th; Engel et al., 2004) et peuvent piéger les pelotes fécales lors de leur export en profondeur ainsi que des cellules phytoplanctoniques intactes (Ebersbach et al., 2014). Bien que ces composés augmentent les exports de carbone, ils fixent simultanément une limite supérieure aux concentrations que les organismes phytoplanctoniques peuvent atteindre lors d'une efflorescence (Dam et Drapeau, 1995). De plus, Berman-Frank et al. (2007) ont rapporté que la production de TEP est couplée à un processus de mort cellulaire auto-catalytique programmée (PCD) pour certaines cyanobactéries. Des observations similaires ont également été rapportées pour *Thalassiosira pseudonana* et *Emiliania huxleyi* (Bidle, 2015; Kahl et al., 2008; Vardi et al., 2012). Par conséquent, la présence de ces substances capturant des cellules de phytoplancton et piégeant le DFe pourrait également expliquer l'occurrence de zones HNLC dans le monde. En ce qui concerne le voyage HEOBI, bien que les concentrations de DFe aient été loin d'être limitantes au niveau des stations côtières, les concentrations de TChl-a étaient faibles comparées aux eaux environnantes et le contrôle cellulaire à médiation par le TEP pourrait expliquer les distributions de TChl-a. Cette hypothèse mériterait d'être explorée au cours de prochaines expéditions.

Appendices

A – Chapter 2	329
B – Chapter 3.....	345
C – Chapter 4	348
D – Chapter 5	358

Appendix A (Chapter 2): Flow Injection Analysis with Chemiluminescence detection (FIA-CL) method development

The FIA-CL-analyser was initially chosen for the GEOVIDE DFe samples because it allows the determination of total DFe [Fe(II), Fe(III)], the use of a commercially available resin, it is portable and has a relatively low cost. The construction of the analyser is based on the manifold described in Bucciarelli et al. (2001), Obata et al. (1993) and Sarthou et al. (2003) with optimisation of various parameters. At the LEMAR, the 8-hydroxyquinoline (8-HQ) resin was used in routine to analyze DFe samples. However, the 8-HQ resin is not commercially available and needs to be synthesized (Dierssen et al., 2001). Therefore, a method-development was performed as part of this thesis using two commercially available resins, i.e. the Nobias-chelate-PA1 with ethylenediaminetriacetic acid (EDTriA) and iminodiacetic acid (IDA) functional groups (Hitachi High Technologies[®], VWR France) – Nobias hereafter- and Toyopearl-AF-chelate-650M with IDA functional group (65 µm particle size, Sigma-Aldrich[®]) –Toyopearl hereafter, The aim was to obtain the most sensitive resin without any interference from other metals in the detection of DFe by the FIA-CL analyser. However, the lack of reproducibility of the FIA-CL system using the toyopearl resin, leads us re-analysing the full DFe data set with the seaFAST-pico[™] SF-ICP-MS analytical technique. In the following section, each step of method development is quickly described. Note that the FIA-CL manifold used for the method development is described in Figure A.1.



* This solution (recipe from Obara et al., 1993) was purified twice through an 8-HQ resin prior to use.

Figure 2.7: Schematic of the FIA-CL system used for the determination of DFe concentrations in seawater. The 2-way 6-port-switching valve#2 setups in position A and B are presented in continuous and dashed black lines, respectively. Note that this schematic does not include the preconditioning step in which case the buffered UHPW will be set in position 1 on the 6-port valve#1, sample in position 2 and UHPW in position 3 (see Tables 2.2 and 2.3). All continuous thin black lines represent PTFE tubing (inner diameter, i.d., 0.8 mm), dashed thick lines represent peristaltic tubing 2-stop PVC Phthalate Free Tygon® (Lab Unlimited, Carl Stuart Group) for the reagents in grey (grey-grey Tygon®, i.d. 1.30 mm) and for the sample in green (green-green Tygon®, i.d. 1.85 mm). The detector (i.e. the photomultiplier) contained a Teflon® chemiluminescence flow cell (Global FIA, GloCel™) and were both stored in a black box to avoid light interaction. Three PTFE “T” pieces used to connect the reagent lines are represented in light blue. Finally note that the thermostatic water bath contained a 2m PTFE reaction loop.

A1 Calibration seawater

Two different seawater samples were collected and used for the FIA-CL method development and for the calibration curve of DFe sample analysis. These samples corresponded to low-level Fe seawater matrices and are referred hereafter as SW0. Both seawater matrices were filtered at sea and were acidified (2‰ HCl v/v, Merck, Ultrapur[®]) in the land-based laboratory (LEMAR) at least 2 days prior to use.

Table A.1: Characteristic of the GEOVIDE#4 and DYFAMED calibration seawater matrices. Note that DFe concentrations were determined by FIA-CL with 8-HQ resin routinely used at the LEMAR.

Sample name	GEOVIDE#4 seawater	DYFAMED seawater	
		Old (2008)	New (2015)
Collection location	North Atlantic Ocean	Mediterranean Sea	
Latitude, Longitude	53.00°N, -51.10°E	~ 43.42°N, 7.87°E	
Depth	~ 40 m and 2-3 m	~ 20-40 m	
Filtration	0.2 µm pore size filter capsule (Sartorius SARTOBRAN® 300)		
Acidification	2‰ HCl (v/v, Ultrapur®, Merck), final pH ~ 1.7		
DFe (nmol L ⁻¹)	0.10 ± 0.02	0.35 ± 0.02	0.59 ± 0.02
UV-digested	0.38 ± 0.06	0.40 ± 0.02	NA
Ligands (nmol L ⁻¹)	~ 5	~1	NA
References	(Aridane G. Gonzalez and Marie Cheize, pers. comm.)	(Cheize, 2012; Chever, 2009; Wagener, 2008)	

A1.1 GEOVIDE standard reference seawater

The GEOVIDE#4 seawater was filtered through 0.2 µm pore size filters (Sartorius SARTOBRAN[®] 300) during the GEOVIDE voyage in the Labrador Sea at station 77 (53.00°N and -51.10°E, see Chapter 2) in the surface (40 m depth) and was stored in 20-30L acid-cleaned LDPE carboys (Nalgene[™], see Section 2.1.2.3 for cleaning procedure). All the carboys (Nalgene[™]) were pre-rinsed with 6 to 9 L of seawater before sampling. These seawater samples have a DFe concentration of ~ 0.10 ± 0.02 nmol L⁻¹ (Table A1).

A1.2 DYFAMED standard reference seawater

In June 2015, natural seawater from the Ligurian Sea has been sampled nearby the DYFAMED (Atmospheric Flux DYnamic in MEDditerranée) station, 55 km far from Nice, along the radial Nice-Calvi (43°25'N, 7°52'E; Fig. 2.6) aboard the INSU ship N.O. Téthys II

in collaboration with Laurent Coppola, Justine Louis, Emilie Diamond, Grigor Obolensky, Foucaut Tachon, Vincenzo Vellucci and the captain Joël Perrot and his crew from the Laboratory of Oceanography of Villefranche-sur-mer (LOV). The particularity of this area is to be isolated from the coastal inputs thanks to the Ligurian stream (Béthoux and Prieur, 1983). This sampling period allows the seawater to have low Fe concentrations, low nutrient salt concentrations and acceptable ligand concentrations (Wagener et al., 2008).

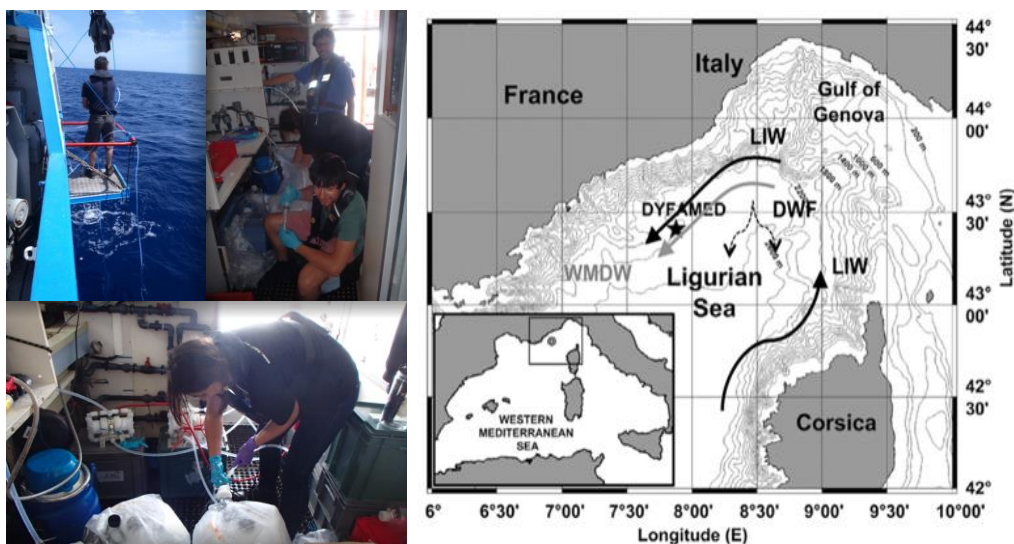


Figure A.2: Pictures of water sampling aboard *Téthys II*: top left, mechanical arm and PTFE tubing; top right, chemical lab; bottom picture, PFA pumps (Asti) filter cartridges and double bagged carboys; right hand-side, DYFAMED site mapping and streams (<http://www.obs-vlfr.fr/sodyf/img/Map2014.png>)

The seawater was collected in surface waters (~ 20-40 m deep) thanks to two double-bellows pumps (Asti, PFA) driven by filtered (Aervent-50 mm 0.2 μm hydrophobic PTFE filters, Merck Millipore) compressed air and linked to PTFE tubing attached to a rope ballasted by epoxy coated lead weights (Fig. A.2). The PTFE tubing and ballasted rope were moved away from the boat thanks to a mechanical arm. While sampling for this seawater, the boat water outlet was closed, and the boat was positioned in a way that the sampling gear was upstream of the boat to avoid contamination. The water was directly filtered through 0.2 μm pore size filters (Sartorius SARTOBRAN[®] 300) and collected in 20-30 LDPE carboys (Nalgene[™], Fig. A.1) in the *Téthys II* chemical laboratory. This laboratory is not equipped with any laminar flow hood and consequently the filter cartridges (Sartorius SARTOBRAN[®] 300) were connected to the 20-30 L carboys (Nalgene[™]) in a way that they were covering the whole neck of the carboys. All the carboys (Nalgene[™]) were acid-cleaned the same way as for the sampling bottles of DFe (see Section 1.2.3) and were pre-rinsed with 6 to 9 L of seawater before sampling. The DFe concentration determined for this seawater is $0.59 \pm 0.02 \text{ nmol L}^{-1}$ (see Table A.2).

Note that the DYFAMED calibration seawater has already been sampled in the same area and conditions (Chever, 2009; Wagener, 2008) and is referred in this chapter to the old (2008) DYFAMED seawater, which has a DFe concentration of $0.35 \pm 0.02 \text{ nmol L}^{-1}$ (see Table A.2).

A2 Procedure

At the beginning of an analytical session, the elution solution and UHPW were loaded as a sample for 10 and 5 cycles during 120s of load, respectively. The former 10 cycles allowing the elution of the resin in both sides. Then, a low-Fe seawater (SW0) was run for at least 15 cycles and 120s aimed at stabilising the signal. Once the signal was stabilised a fresh seawater without any spike of Fe(III) (SW0) was prepared and load for 10s and 5 cycles on the resin. Finally, as recommended by Floor et al. (2015), a 8 point calibration curve was used with standard additions (0, 0.07, 0.17, 0.24, 0.34, 0.50, 0.75, 1 nM Fe(III), all spiked with H_2O_2 1‰ (v/v), solution 2) to the acidified SW0 (2‰ HCl v/v, Merck, Ultrapur[®]) and were allowed to equilibrate for 30 minutes before run to oxidise Fe(II) into Fe(III), and were loaded for 120s. Since measurements were repeated three times for each calibration point, a total of $8 \times 3 = 24$ results were obtained. Note that acidified seawater standards and samples were buffered off-line just before their run to avoid Fe lost on the wall of the LDPE bottles.

Before and after each extraction session, the manifold was cleaned with UHPW for 30 mins. Once cleaned, all lines were filled with dedicated reagents except the sample line which was filled with 0.23 M HCl (Merck, Suprapur[®]). The timing parameters for the different steps and the position of the two six port valves are presented in Tables A.2 and A.3.

Table A.2: Extraction timing parameters and 6-port valve line number and 2-way valve position during a run without pre-conditioning step

Process	Cleaning	Loading	Matrix removal	Eluting
Timing	30 minutes	120s	60s	120s
6-port	1	1	2	2
2-way	A	A	A	B

Table A.3: extraction timing parameters and 6-way valves position during a run with a pre-conditioning step

Process	Cleaning	Conditioning	Loading	Matrix removal	Eluting
Timing	30 minutes	60s	120s	60s	120s
6-port	1	3	1	2	2
2-way	A	A	A	A	B

A3 Method development

A3.1 Reagents and column preparation

Reagent and diluted samples were prepared or stored in LDPE bottles (Nalgene), Polytetrafluoroethylene (PTFE) vials (Savillex®) or polypropylene (PP) tubes (Technoplas) (see Section 2.1.2.3 for cleaning procedure). All reagents (hydrogen peroxide, ammonia solution and eluent) were prepared on a daily basis. Only the luminol solution was prepared at least two days prior to use to allow good dissolution of the luminol grainy crystals, which has a low solubility in water at room temperature ($< 0.1 \text{ g } 100 \text{ mL}^{-1}$, Barni et al., 2007).

A3.1.1 Fe standard solutions

The preparation of the Fe standards is common to all the FIA-CL system regardless the resin used. Iron calibration solutions were prepared by dilution of a commercial solution of $\text{FeCl}_3 \cdot 6\text{H}_2\text{O}$ (Carlo Erba Reagenti) into UHPW acidified at 0.1 % (v/v) with HCl Suprapur® (Merck). A first dilution, F1, was prepared gravimetrically by adding 280 μL of the commercial solution to 50 mL of acidified UHPW with a final concentration of 0.1 M. Then F2 and F3 dilutions were prepared by adding respectively 500 and 50 μL of the F1 solution to 50 mL of acidified UHPW for a final concentration of 1 μM and 100 nM, respectively. These standard solutions were prepared weekly.

A3.1.2 Homemade resin columns

Column – The column was made as described in Qu  rou   et al. (2014) (Fig. A.3). To reduce excessive backpressures of the Nobias and Toyopearl resins, the smallest resin beads were first excluded by gravimetric size fractionation (see Qu  rou   et al., 2014) in 15 mL PP tubes (Technoplas) in a 3 M HNO_3 (Merck, Ultrapur®) repeated 10 times over a week (Conway et al., 2013) before loading into the column.

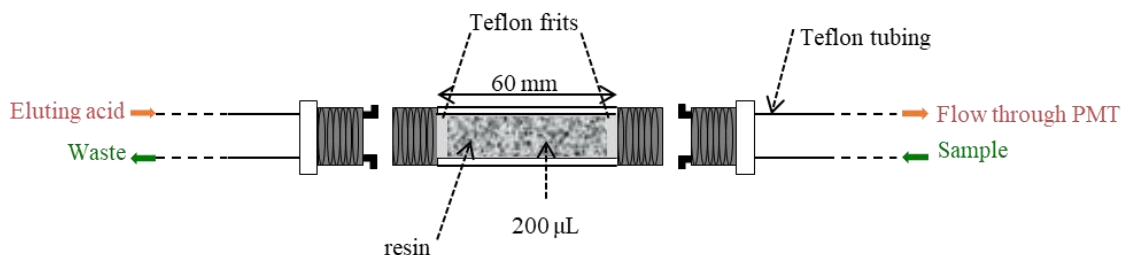


Figure A.3: Schematic of the pre-concentration column used in the system (from Planquette, 2008).

A3.1.3 Reagent preparation

Nobias resin

Luminol solution – A 0.74 mM of luminol solution was made by mixing 0.13 g of luminol ($\text{C}_8\text{H}_7\text{O}_2\text{N}_3$) 97% (Merck), 0.53 g of potassium carbonate-1.5-hydrate Suprapur[®] ($\text{K}_2\text{CO}_3 \cdot 1.5 \text{ H}_2\text{O}$) (Merck), and 60 μL of triethylenetetramine (TETA) 60% (Sigma) in an acid-washed 1L LDPE volumetric flask. Then, ultrapure water (UHPW) was added to a final volume of 1L. This solution was purified twice through an 8-hydroxyquinoline (8-HQ) resin prior to use.

Hydrogen peroxide – A 0.7 M hydrogen peroxide solution (H_2O_2) was made by adding 72 mL of H_2O_2 30% (9.8 M, Suprapur[®], Merck) to UHPW to a final volume of 1 L in LDPE volumetric flask (solution 1). This solution was diluted 30-fold with UHPW (solution 2), in a PTFE vial (Saville[®]). This latter solution was used to spike samples and standards in order to oxidise any Fe(II) present into Fe(III).

Nitric acid – 1 M HNO_3 solution was prepared by adding 62.5 mL of concentrated (16 M, Suprapur[®] Merck) HNO_3 to UHPW to a final volume of 1 L in LDPE volumetric flask and was used as an eluent.

Ammonia solution – A 2 M NH_4OH solution was prepared by adding 150 mL of NH_3 25% (11 M, Suprapur[®], Merck) to UHPW to a final volume of 1L in LPDE volumetric flask.

Ammonium acetate buffer – An acetic acid-ammonium acetate buffer (CH_3COO^- and NH_4^+) was prepared in 125mL LDPE bottle by mixing 25 mL of concentrated (18 M, Suprapur[®] Merck) CH_3COOH and 51 mL of concentrated NH_3 25% (11 M, Suprapur[®], Merck) and UHPW to a final volume of 125 mL. The pH of this solution was then adjusted to 9.0 ± 0.2 with either CH_3COOH or NH_3 . This solution was purified five-times off-line the FIA-CL system on 8-HQ resin prior to use.

Toyopearl resin

The same reagents as in Obata et al. (1993) were used except that they were less concentrated to decrease the reagent background Fe concentration and contribution to the baseline.

Hydrogen peroxide – A 0.3 M hydrogen peroxide solution (H_2O_2) was made by adding 30.5 mL of H_2O_2 30% (9.8 M, Suprapur[®], Merck) to UHPW to a final volume of 1 L in LDPE volumetric flask (solution 1). This solution was diluted 30-fold with UHPW (solution 2), in a PTFE vial (Savillex[®]). This latter solution was used to spike samples and standards in order to oxidise any Fe(II) present into Fe(III).

Ammonia solution – A 0.5 M ammonia solution (NH_4OH) was prepared in a 1L LDPE volumetric flask by mixing 38 mL of ammonia 25% (13.3 M, Suprapur[®], Merck) with UHPW up to a final volume of 1L.

Hydrochloric acid – 0.23 M hydrochloric acid (HCl) was prepared in 1L LDPE volumetric flask by mixing 24 mL of HCl (9.5 M, Suprapur[®], Merck) with UHPW up to a final volume of 1L in LDPE volumetric flask and was used as an eluent.

A3.2 Tested parameters

A3.2.1 8-HQ resin

The 8-HQ resin that was used routinely to analyze DFe samples at the LEMAR (see Obata et al., 1993, for reagent preparation and procedure) with DYFAMED calibration seawater was sensitive enough (slope = 319 ± 97 , $n = 5$) to give suitable R^2 (on average $R^2 = 0.98 \pm 0.02$, $n = 5$, from linear regression curve), a low detection limit ($\text{DL} = 0.02 \pm 0.01 \text{ nmol L}^{-1}$, $n = 5$) and good accuracy of the method.

As the DYFAMED seawater was running out, the calibration seawater had to be changed toward the GEOVIDE#4 seawater, which has the particularity to be highly concentrated in Fe-binding organic ligands (at least, 5 Eq of nmol L^{-1} Fe, voltammetry, Aridane G. Gonzalez and Marie Cheize pers. comm.). Using the GEOVIDE#4 seawater for the calibration resulted in a sensitivity decrease and concomitantly an overestimation of all the reference material ($\text{KEOPS2} = 0.67 \pm 0.05 \text{ nmol L}^{-1}$ and $\text{GEOVIDE} = 0.36 \pm 0.03 \text{ nmol L}^{-1}$) that was likely due to the presence of Fe-binding organic ligands remained in solution, despite the acidification of the GEOVIDE#4 calibration seawater. Therefore, different pre-treatments of the GEOVIDE#4 calibration seawater (after acidification and before analysis) were tested to allow linearity of the calibration curve and good recoveries of reference and

certified material using the 8-HQ resin. These different pre-treatments included the UV-digestion between 2h00 and 6h00 (Guéguen et al., 1999; Ndung'u et al., 2003), the microwaving (by either a standard microwave, Weeks and Bruland, 2002; or a Milestone ETHOS ONE microwave, used in collaboration with Claire Bassoullet and Marie-Laure Rouget) or the retention of the GEOVIDE seawater on a Sep-Pak[®] C18 classic cartridges (WAT051910, 360 mg sorbent per cartridge, 55-105 µm particle size, Waters SA, France; Elbaz-Poulichet et al., 1994; Mills et al., 1987; Mills and Quinn, 1981). Among all the treatment tested, 4h00 UV-digestion of GEOVIDE#4 seawater was the only one presenting consistent repeatability of measurements and was chosen to continue the development with the Nobias resin.

A3.2.2 Nobias resin

According to literature, a pH ranging from 5.0 to 6.2 (e.g. 5.0, Minami et al., 2015; 6.15, Conway et al., 2013; 6.2, Biller and Bruland, 2012; Quérroué et al., 2014) was successfully extracting on- or off-line dissolved trace metals (including Fe) with a Nobias resin that were quantified using an ICP-MS. Three-extraction pH (i.e. 5.0, 5.5, 6.2) were tested two-by-two within the same day to avoid reagent effect, which can play on the sensitivity (especially the luminol) of the FIA-CL device using the Nobias resin. Among the three pH tested, no significant differences were observed in the linearity of the calibration curve (p-value > 0.1, t-test), but significantly higher sensitivity was observed with a pH of 5.5 compared to the two other pH tested (p-value < 0.001, t-test). In addition, the comparison of the DFe concentrations determined for KEOPS2 seawater with GEOVIDE#4 UV-digested 4h00 calibration seawater presented no significant differences using either the Nobias resin (retention pH = 5.5) or the 8-HQ resin (p-value > 0.2, t-test).

Similarly as for the pH, three UV-digestion times (i.e. 0h00, 2h00 and 4h00) were tested on the Nobias resin using a retention pH of 5.5. Results highlighted significantly lower linearity and sensitivity of the calibration curve for no irradiation compared to 4h00 of UV-digestion (p-value < 0.001, t-test) and no significant difference between 2h00 and 4h00 of UV-digestion (p-value > 0.2). A MANOVA was also performed to test together the UV-digestion times of the GEOVIDE#4 seawater and the pH of extraction that gave similar results. Therefore, a pH of 5.5 and a UV-digestion of 2h00 were used to test for interferences with other metals.

The effect of other metals on the Nobias resin was investigated by multiple additions (one, two and three additions) of CASS-4 certified material, a standard solution gravimetrically prepared containing Cu and Mn but not Fe (from H. Planquette) into the GEOVIDE#4 seawater UV-digested for 2h00. The results highlighted positive interferences of Cu and Mn (Fig. A.4, SAFe S, CASS-4 and standard solution) and a negative interference of an unknown metal (potentially Zn; Fig. A.4, SAFe D2) with the oxidation reaction of luminol. Therefore, due to interferences in the Fe FIA-CL reaction with other metals, the Nobias resin was replaced with the Toyopearl resin.

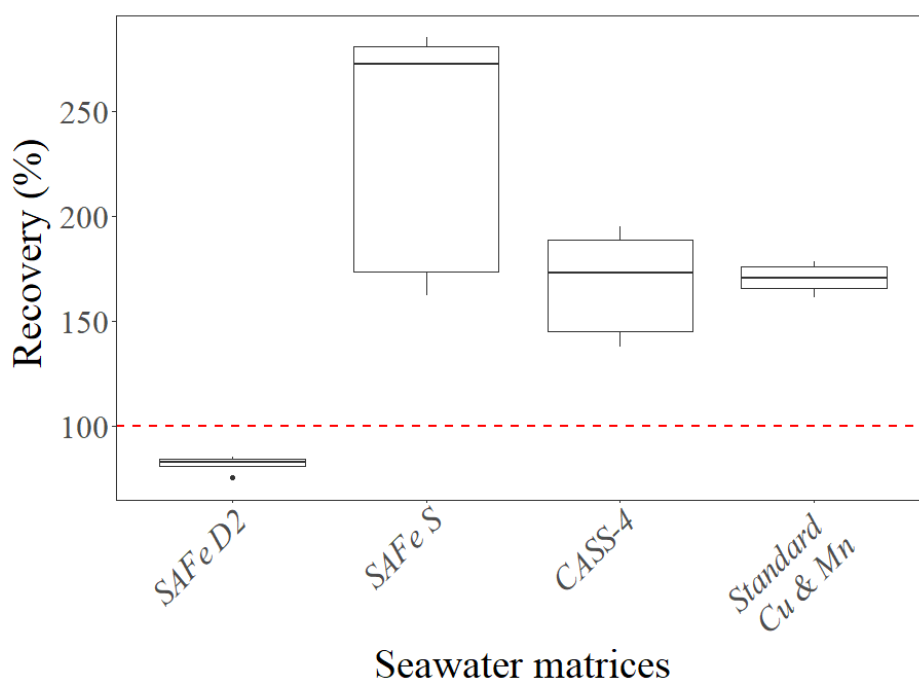


Figure A.4: Box and whisker diagram of dissolved iron (DFe) concentration recoveries from SAFe D2 and S, CASS-4 and the standard solution containing Cu and Mn as determined with a calibration curve performed on GEOVIDE seawater UV-digested 2h00 and a retention pH of 5.5 on the Nobias resin.

A3.2.3 Toyopearl resin

Similarly to Lohan et al., 2000, the pre-concentration step was performed at $\text{pH} = 3.50 \pm 0.05$ with a pre-conditioning step, prior to pre-concentrate the seawater onto the resin, using UHPW buffered at pH 3.5. There was no significant difference ($p\text{-value} > 0.05$, t-tests) between the recoveries of the reference material using either the 8-HQ resin with DYFAMED seawater for the calibration or the toyopearl resin with GEOVIDE seawater for the calibration without any UV-digestion of the calibration seawater matrices (Fig. A.5). Different reagent (i.e. H_2O_2 , NH_4OH and HCl) concentrations were compared using a MANOVA to evaluate their effect on SAFe seawater recovery. The MANOVA showed no significant differences (p -

value > 0.05) between the reagent used whether concentrated by a factor of 2 or not. Therefore, to reduce the costs, the less concentrated reagents were chosen.

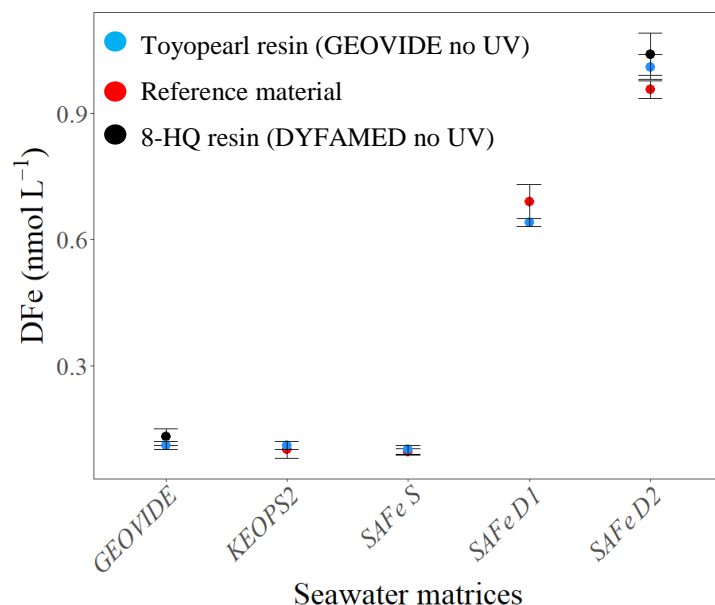


Figure A.5: Plot of average dissolved iron (DFe) concentrations determined by FIA-CL for the GEOVIDE, KEOPS2, SAFe S, D1 and D2 seawater samples. Note that the blue dots correspond to the average DFe concentration determined with the toyopearl resin without UV-digestion of the GEOVIDE calibration seawater, the red dots correspond to the reference DFe concentration of each of the different seawater samples previously reported using the same technique (KEOPS2, [Cheize, 2012](#)) and many different techniques (SAFe S, D1 and D2, [Johnson et al., 2007](#)) and the black dots correspond to the DFe concentration determined with the 8-HQ resin without UV-digestion of the DYFAMED calibration seawater.

We next investigated the preconditioning of the resin prior to DFe load (see Table A.3 details on valves and times). No preconditioning, preconditioning with UHPW buffered at pH 3.5 and preconditioning with a weak acid ($0.011 \text{ mol L}^{-1} \text{ HCl}$, Suprapur[®], Merck) were tested with regard to the recovery of the reference material SAFe S, D1 and D2. The results highlighted no significant difference (p-value > 0.05, t-test) between the reference and the measured DFe concentrations of all seawater matrices for both no preconditioning and a preconditioning step with UHPW buffered at pH 3.5. Therefore, to reduce the time of analysis, no preconditioning step was chosen. Finally, the effect of the time between the preparation of the calibration seawater (i.e. standard additions of Fe(III) and H_2O_2 1‰ (v/v), solution 2) and the analysis of the calibration seawater was investigated. The results highlighted no significant difference (p-value > 0.05, t-test) between the reference and the measured DFe concentrations of SAFe D1 and D2 seawater matrices when the calibration seawater was prepared 30 minutes before analysis, while a significant difference was noticed for the DFe concentrations of SAFe S (p-value ~ 0.001, t-test). Conversely, no significant difference (p-value > 0.05, t-test) was noticed between the reference and the measured DFe concentrations of SAFe S when the calibration seawater was prepared 24h before analysis, while a significant difference was noticed for the DFe concentrations of SAFe D1 and D2 seawater matrices (p-value ~ 0.001, t-tests). As two reference material were validated and

that the SAFe S presented an increase of 22% ($\text{SAFe S} = 0.14 \pm 0.01 \text{ nmol L}^{-1}$) while preparing the calibration 30 minutes before analysis, this parameter was selected.

Using no preconditioning and preparing the calibration 30 minutes before analysis, no metal interaction was observed. Indeed, all the certified and reference SAFe seawater matrices were validated with respect to standard deviations (Fig. A.6) and the standard additions of the solution containing Cu and Mn did not show any positive nor negative interaction with the oxidation reaction of luminol, in contrast to the Nobias resin.

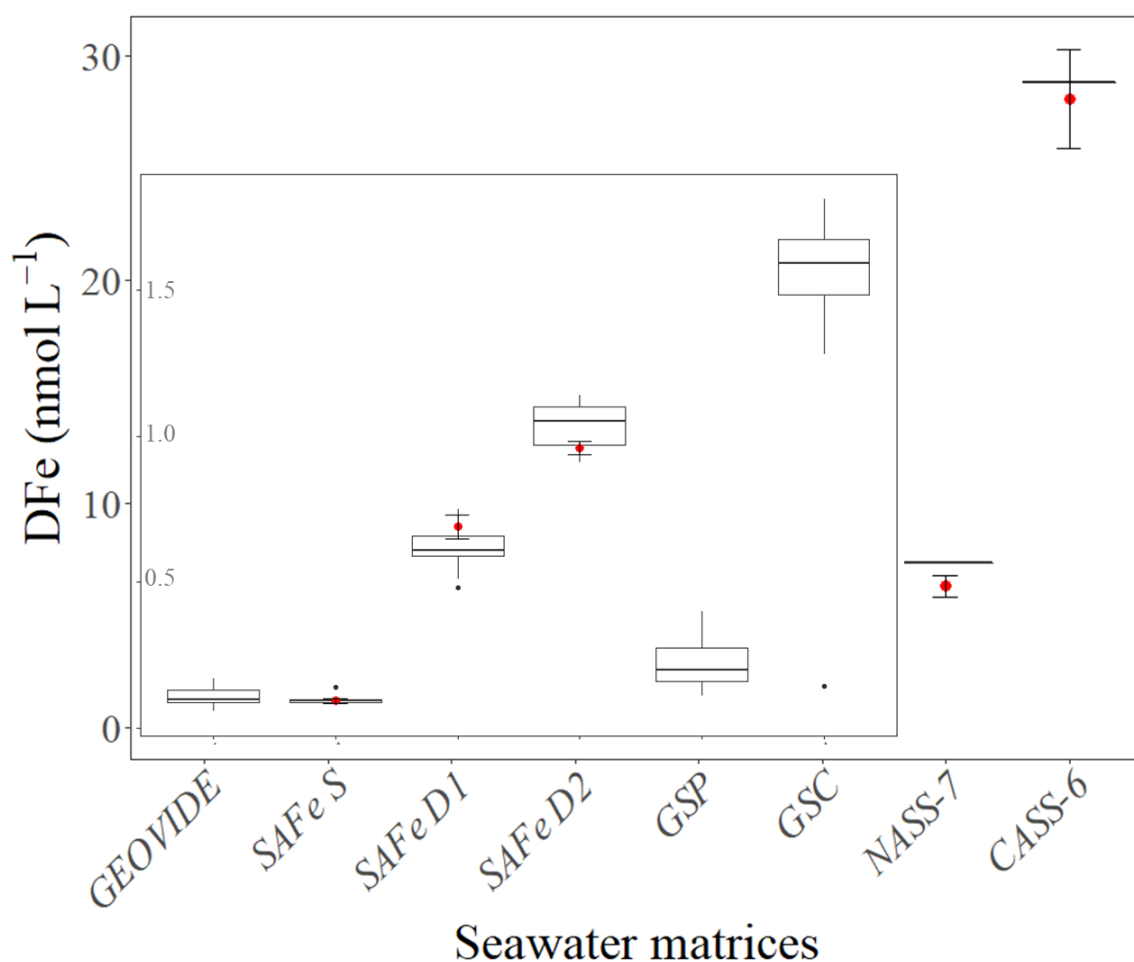


Figure A.6: Box and whisker diagram of dissolved iron (DFe) concentrations determined by FIA-CL using Toyopearl resin for the GEOVIDE, SAFe S, SAFe D1, SAFe D2, GSP, GSC, NASS-7 and CASS-6 seawaters. Note that the red dots represent the DFe concentration of each of the different seawaters previously reported (SAFe S, SAFe D1 and SAFe D2, Johnson et al., 2007; [NASS-7 and CASS-6, https://www.nrc-cnrc.gc.ca/](https://www.nrc-cnrc.gc.ca/)).

A4 Precision, accuracy and reproducibility

When concentrations exceeded $\text{SW0} + 1 \text{ nmol L}^{-1}$ standard, samples were diluted with acidified (HCl 2%, v/v) calibration seawater (SW0). The detection limit, defined as three

times the standard deviation (σ) of the blank (blank in SW0, $0.02 \pm 0.01 \text{ nmol L}^{-1} \text{ DFe}$, $n = 55$) was on average $0.01 \pm 0.01 \text{ nmol L}^{-1}$ ($n = 55$). The GEOVIDE seawater used for the calibrations was on average $0.11 \pm 0.02 \text{ nmol L}^{-1}$ ($n = 55$) (Fig. A.6). The accuracy of the method was checked using SAFe S, D1 and D2 GEOTRACES consensus seawater samples³. $S = 0.10 \pm 0.02 \text{ nmol L}^{-1}$ ($n = 10$), $D1 = 0.62 \pm 0.06 \text{ nmol L}^{-1}$ ($n = 55$), $D2 = 1.04 \pm 0.08 \text{ nmol L}^{-1}$ ($n = 9$) (Fig. 2.14), for consensus values equal to $S = 0.095 \pm 0.008 \text{ nmol L}^{-1}$, $D1 = 0.69 \pm 0.04 \text{ nmol L}^{-1}$, $D2 = 0.96 \pm 0.02 \text{ nmol L}^{-1}$. The GSP and GSC seawater matrices averaged 0.22 ± 0.08 ($n=27$) and 1.59 ± 0.14 ($n=17$), respectively (Fig. A.6). All the reported values correspond to days of GEOVIDE samples analysis.

Although the above-mentioned DFe concentrations were in the range of the values reported for reference and certified seawater matrices, many calibrations were not good enough to allow the analysis of GEOVIDE samples, thus highlighting a low reproducibility of the FIA-CL system using the toyopearl resin.

In addition to the DFe concentrations reported for the reference and certified seawater matrices, the reproducibility of the FIA-CL system was also investigated with forty-one GEOVIDE samples analysed during two different days of analysis. The results showed that there was a variation of 1 to 34% between the two DFe concentrations for the same sample with in average $16 \pm 10\%$ of difference between the two values considering the forty-one samples. Note that the highest variations corresponded to the same sample analysed without dilution and diluted. The lack of reproducibility of the FIA-CL system using the toyopearl resin, leads us re-analysing the full DFe data set with the *seaFAST-pico*TM HR-ICP-MS analytical technique.

A5 Comparison between FIA-CL and *seaFAST-pico*TM HR-ICP-MS

In the following section, a comparison between the two DFe data sets from the GEOVIDE voyage generated by the FIA-CL system using the Toyopearl resin and the *seaFAST-pico*TM SF-ICP-MS using the Nobias resin is discussed.

³ <http://www.geotraces.org/science/intercalibration/322-standards-and-reference-materials>; Johnson, K. S., Boyle, E., Bruland, K., Coale, K., Measures, C., Moffett, J., Aguilar-Islas, A., Barbeau, K., Bergquist, B., Bowie, A., Buck, K., Cai, Y., Chase, Z., Cullen, J., Doi, T., Elrod, V., Fitzwater, S., Gordon, M., King, A., Laan, P., Laglera-Baquer, L., Landing, W., Lohan, M., Mendez, J., Milne, A., Obata, H., Osslander, L., Plant, J., Sarthou, G., Sedwick, P., Smith, G. J., Sohst, B., Tanner, S., Van den Berg, S., and Wu, J.: Developing standards for dissolved iron in seawater, Eos, Transaction American Geophysical Union, 88, 131-132, 2007.

The comparison between the two data sets only included seawater matrices originating from the exact same sampling bottle to avoid accounting for the differences that could arise from the cleaning of the sampling bottles, the subsampling of the seawater or from sample handling in general. While comparing the DFe concentrations of this sample subset, there was a good agreement between the FIA-CL system and the seaFAST-picoTM SF-ICP-MS ($\text{DFe}_{\text{FIA}} = 0.93 \text{ DFe}_{\text{seaFAST}}$, $R^2 = 0.76$, $p\text{-value} < 0.001$, $n = 96$, Fig. 2.18A). However, the absolute variation between the DFe concentrations generated by the two analytical methods for each sample was ranging from 0 to 94% with overall higher DFe concentrations for the seaFAST-picoTM SF-ICP-MS than for the FIA-CL system. Such differences could arise from the amounts and/or the strength of the Fe-binding organic ligands present within the seawater matrix as mentioned in Section 3.2.1.5, which would compete with the resin. Indeed, among the samples for which there was both the DFe concentration generated by the two analytical techniques and the total Fe-binding organic ligand (Lt) concentrations ($n = 21$), we found a significant linear relationship between the percentage of DFe variation and the Lt concentration ($\Delta\text{DFe} = 23\text{Lt} - 42$, $R^2 = 0.49$, $p\text{-value} < 0.001$, $n = 21$, Fig. 2.18B). Note that no relationship was found between ΔDFe and the logarithm of the conditional stability constant ($\log K_{\text{FeL}_i, \text{Fe}^{3+}}^{\text{cond}}$) nor with the reactivity of the ligands ($\log \alpha_{\text{FeL}}$). This thus suggests that despite the overall good recovery of reference and certified seawater matrices from the FIA-CL system using the toyopearl resin (see Section 3.2.1.6), there was interactions between the Lt concentration and the toyopearl resin, with higher DFe concentrations for the seaFAST-picoTM HR-ICP-MS than for the FIA-CL system when Lt concentrations were higher, and vice versa. In addition to these interactions, the seaFAST-picoTM HR-ICP-MS had a much better reproducibility than the FIA-CL system (see Sections 3.2.1.6 and 3.2.2.3 for the FIA-CL system and the seaFAST-picoTM HR-ICP-MS, respectively). Therefore, the DFe data set from the FIA-CL system was discarded and instead the DFe data set from the seaFAST-picoTM HR-ICP-MS was used to investigate DFe sources and sinks from the GEOVIDE voyage that are discussed in Chapter 3.

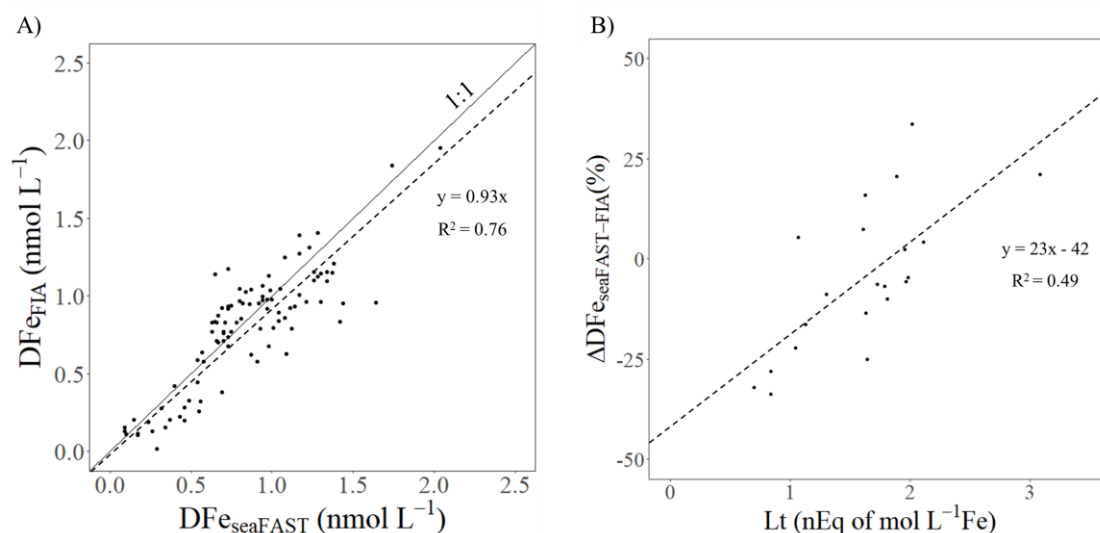


Figure 2.18: Scatter plot of A) dissolved iron (DFe) concentrations analysed with the FIA-CL system as a function of the DFe concentrations analysed with the seaFAST-pico™ SF-ICP-MS for samples from the GEOVIDE voyage coming from the same sampling bottle ($n = 96$) and B) dissolved total Fe-binding organic ligand (Lt) concentrations as a function of the percentage of variation between the DFe data generated with the two analytical techniques ($n = 21$).

A6 Conclusion

A wide range of techniques using pre-concentration resins, from the FIA-CL system to the seaFAST-pico™-HR-ICP-MS, is employed by the worldwide laboratories working on the accurate determination of DFe concentrations in seawater. Although big inter-comparison efforts are more and more systematic especially within the frame of the GEOTRACES programme, these comparisons highlighted substantial differences between data set generated by two different labs were often inferred to the use of the different techniques, which have their own limits, and/or contamination issues. As a result, and likely due to past contamination issues that the scientific community has experienced in determining ‘accurate’ DFe concentration, if high variability is noticed between two DFe data sets, generally the one presenting the lowest DFe concentrations will be preferred as considered more ‘trustable’ (i.e. less contamination) with variability likely explained by the different steps of sample processing. However, none of these inter-comparisons really explored the reason of such differences other than contamination issues.

In Chapter 3 of this thesis, a succinct comparison was made between the FIA-CL system and the seaFAST-pico™-HR-ICP-MS using two different resins, i.e. the Toyopearl-AF-chetale-650M and the Nobias-chelate-PA1, respectively, that were used to analyse the DFe samples from the GEOVIDE voyage. Although only a few samples ($n = 96$) originating from the exact same sampling bottle were analysed by the two techniques, there was evidence

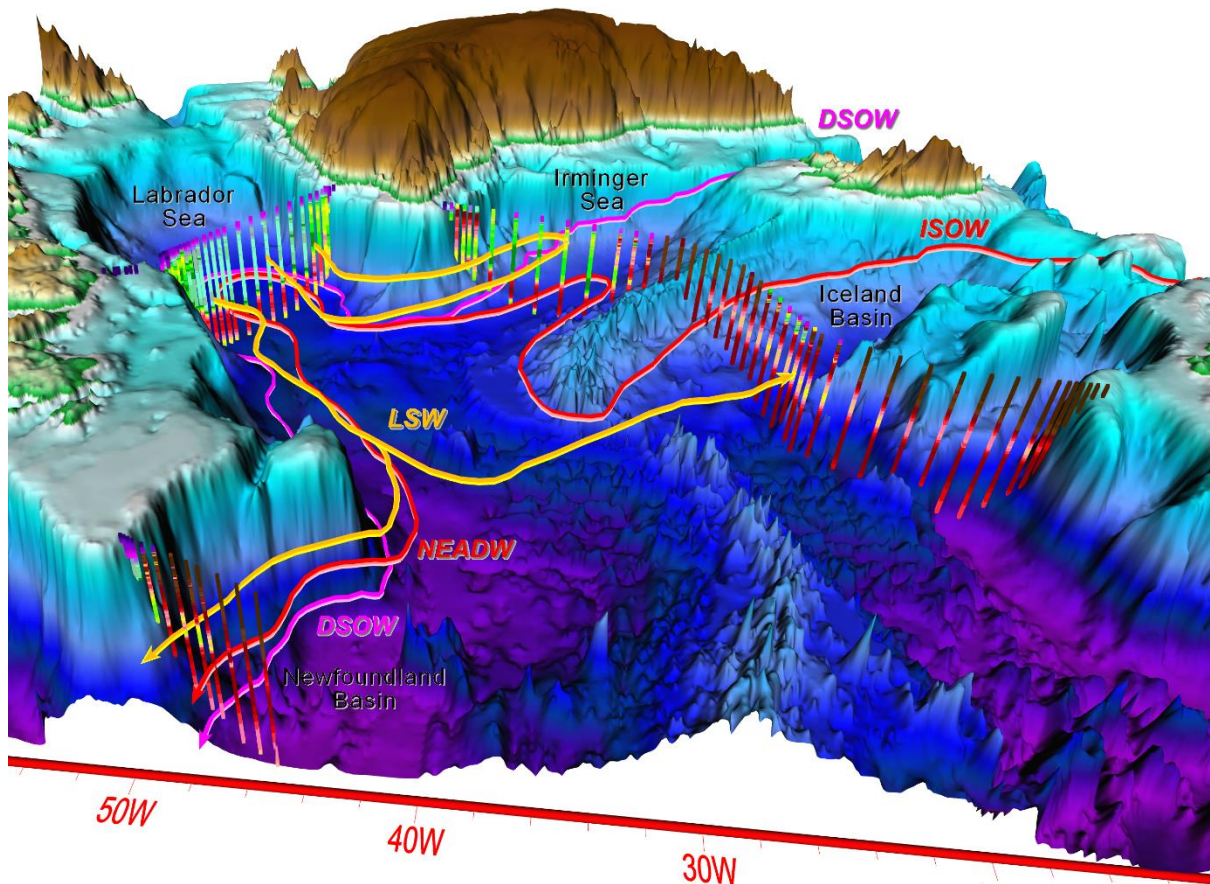
of different sensitivities relative to Fe-binding organic ligand concentrations and not to their strength ($n = 21$) between the two resins. The results highlighted that the Toyopearl resin was more likely to be prone to organic interactions with competition between the resin and the organic ligand Fe-binding sites despite long-term acidification (> 6 months). However, both techniques were able to give accurate measurement of SAFe consensus reference material, thus highlighting the need of characterizing associated parameters of the investigated element such as the amount of organic matter within these seawater matrices. In addition, over the past 14 years SAFe consensus reference values have remained the same despite the analytical technique advancement and the age of the seawater matrices (i.e. freshness of the material vs. long-term acidification). The underlying issue of these constant values are more likely a result of biased validation of new analytical techniques rather than true constant values through ages. Indeed, the validation of analytical techniques and method development that are constantly improved is achieved by good recoveries or replicable recoveries of consensus reference material (e.g. SAFe seawater matrices), namely that they are calibrated by these matrices, thus converging toward the same values. Therefore, the values of these reference seawater matrices should be updated together with the improvement of analytical techniques and discoveries related to Fe cycle that could explain differences.

It is undeniable that to compare two analytical techniques they must measure the same thing. Although this statement is trivial, the FIA-CL system used in this thesis has already been used by others (e.g. Floor et al., 2015) with similar chemical reactions, procedure, same pre-concentration pH and same resin but is unlikely to be comparable to systems using the Nobias resin due to different sensitivities to Fe-binding organic ligand concentrations. Finally, in voltammetry the DFe concentration used as a starting point of the titration is often the one determined by either the FIA-CL system or the seaFAST-picoTM-HR-ICP-MS rather than the one determined by voltammetry due to higher limit of detection, lower accuracy and bigger volume of seawater. Therefore, better constraining DFe analytical techniques and understanding what is really measured will also help improving other techniques.

Appendix B (Chapter 3)

B1 Schematic representation of the main North Atlantic water masses

Map with schematic representations of the pathways of Denmark Strait Overflow Water (DSOW, purple), North East Atlantic Deep Water (NEADW, red) and Iceland Scotland Overflow Water (ISOW, red) and LSW (yellow) which are the primary water masses carried by the DWBC (from <http://www.bio.gc.ca>).



B2 Reykjanes Ridge: Hydrothermalism and/or resuspension of particles

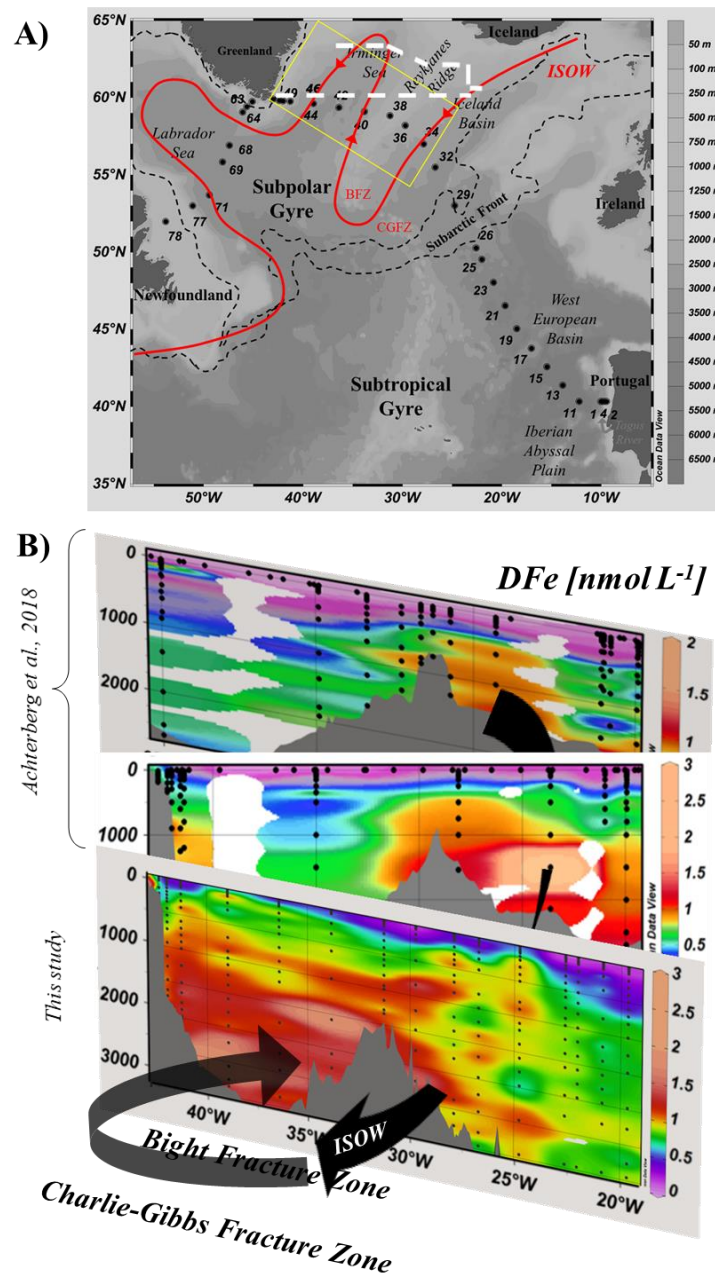
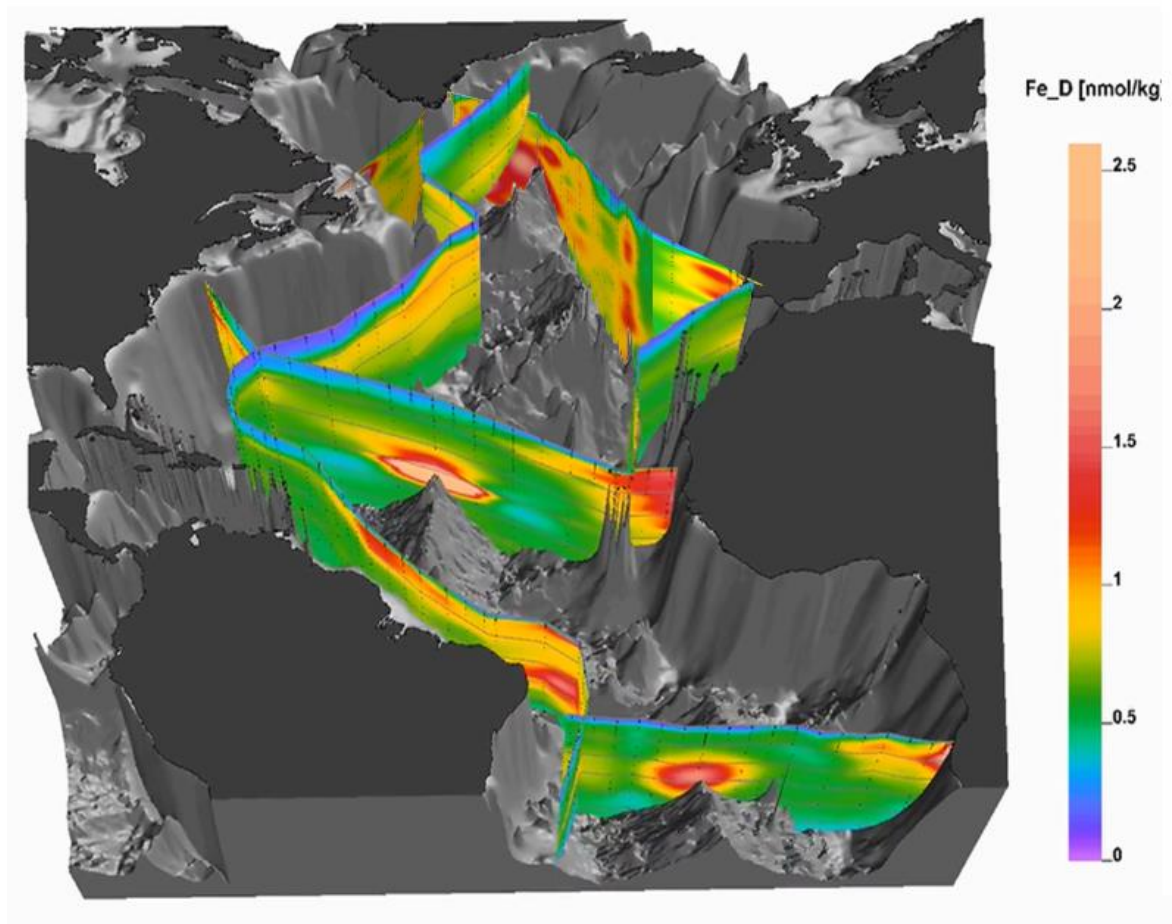


Figure B2: A) surface plot of the GEOVIDE voyage with location of the D364 voyage represented as a white dashed line (Achterberg et al., 2018), the circulation path of the Iceland Scotland Overflow Water (ISOW, in red). Note that the yellow box shows the orientation of the sections as displayed on panel B. B) Section plots of dissolved Fe (DFe) concentrations for the D354 voyage (Achterberg et al., 2018) and for the GEOVIDE voyage. Note that the black arrow represents the circulation path of the ISOW.

B3 3-Dimension representation of the GEOVIDE section

3D-representation of the dissolved iron (DFe) concentration for the GEOVIDE voyage and previous scientific voyages, which occurred in the North Atlantic Ocean in the frame of the GEOTRACES program (data from Ken Bruland, Tim Conway, Hein de Baar, Fanny Chever, Seth John, Maarten Klunder, Patrick Laan, Francois Lacan, Rob Middag, Abigail Noble, Micha Rijkenberg, Mak Saito, Geraldine Sarthou, Jingfeng Wu, graphic modified after Reiner Schlitzer, Schlitzer et al., 2018). .



Appendix C (Chapter 4)

C1 Pigment distribution along the GEOVIDE transect (GEOTRACES, GA01) – (Fig. C1)

The highest fucoxanthin concentrations, were observed north of the Subarctic Front and more interestingly around the Greenland and Newfoundland margins with maximum value of fucoxanthin pigment above the Newfoundland margin at 30 m depth (4.9 mg.m^{-3} , station 78). Zeaxanthin pigment was mainly found south of the Subarctic Front with maximum values in surface waters (0.1 mg.m^{-3} at station 13). In surface waters and north of the Subarctic Front, zeaxanthin was detected in very low concentrations (0.03 mg.m^{-3}). The highest BChl*a* concentrations, a proxy of photoheterotrophic bacteria, were found in surface waters south of the Subarctic Front (up to 0.004 mg.m^{-3} at station 23). Peridinin, showed highest concentrations in surface waters (above 30 m depth) south of the Subarctic Front from stations 19 to 26 (0.3 mg.m^{-3} at station 23), east of the Greenland margin (0.1 and 0.2 mg.m^{-3} , stations 49 and 60, respectively) and east of the Newfoundland margin (0.2 mg.m^{-3} , stations 71 and 77). Total chlorophyll-*b* (TChl*b*), showed minimum concentrations at depth (less than 0.0005 mg.m^{-3}). Minor pigments such as prasinoxanthin associated to chlorophyll-*b*, as well as neoxanthin, violaxanthin and lutein were found in significant concentrations at the same stations. Alloxanthin pigment showed highest values north of the Subarctic Front and around the Greenland and Newfoundland margins. 19'-hexanoyloxyfucoxanthin (19HF) and 19'-butanoyloxyfucoxanthin (19BF) pigments show similar patterns. 19HF was detected in surface waters between stations 21 and 40 and in the Labrador basin (stations 71 and 77). 19BF pigment concentrations showed highest values in the surface waters (less than 80 m depth) from stations 11 to 38 with a maximum value at station 15 (0.2 mg.m^{-3} at 60 m depth) and at stations 71 and 77 localised in the Labrador basin. Concentrations of the two photoprotective pigments diadinoxanthin and diatoxanthin significantly increased in surface waters localised north of the Subarctic Front. Chlorophyllide-*a* was observed nearby Greenland margin with extent to station 44 east of Greenland above 30m depth. Similarly, phaeophorbide-*a* and phaeophytine-*a* were found in significant concentrations around Greenland and Newfoundland margins (stations 71, 77 and 78) and at stations 40.

Overall, the selected pigments and from 0 to 200 m depth, the correlation matrix showed that TChl-*a* is highly correlated to fucoxanthin and ($R^2=0.96$). *c3* and alloxanthin presented correlation coefficient higher than 0.50 with TChl-*a*. All the nine other pigments

were poorly correlated to TChl-*a*, highlighting the fact that the taxon represented by those pigments were in minority. TChl-*b*, neoxanthin, prasinoxanthin and violaxanthin displayed correlation coefficient higher than 0.75 with respect to each other highlighting the presence of the chlorophytes and prasinophytes. Interestingly, lutein pigment was not correlated to prasinoxanthin and was poorly ($R^2 < 0.40$) correlated to TChl-*b*, violaxanthin and neoxanthin emphasizing the absence of type-1- prasinophytes and the presence of type-3-prasinophytes. Lutein and zeaxanthin were highly correlated ($R^2 > 0.75$), underlining the presence of type-1- chlorophytes and cyanobacteria.

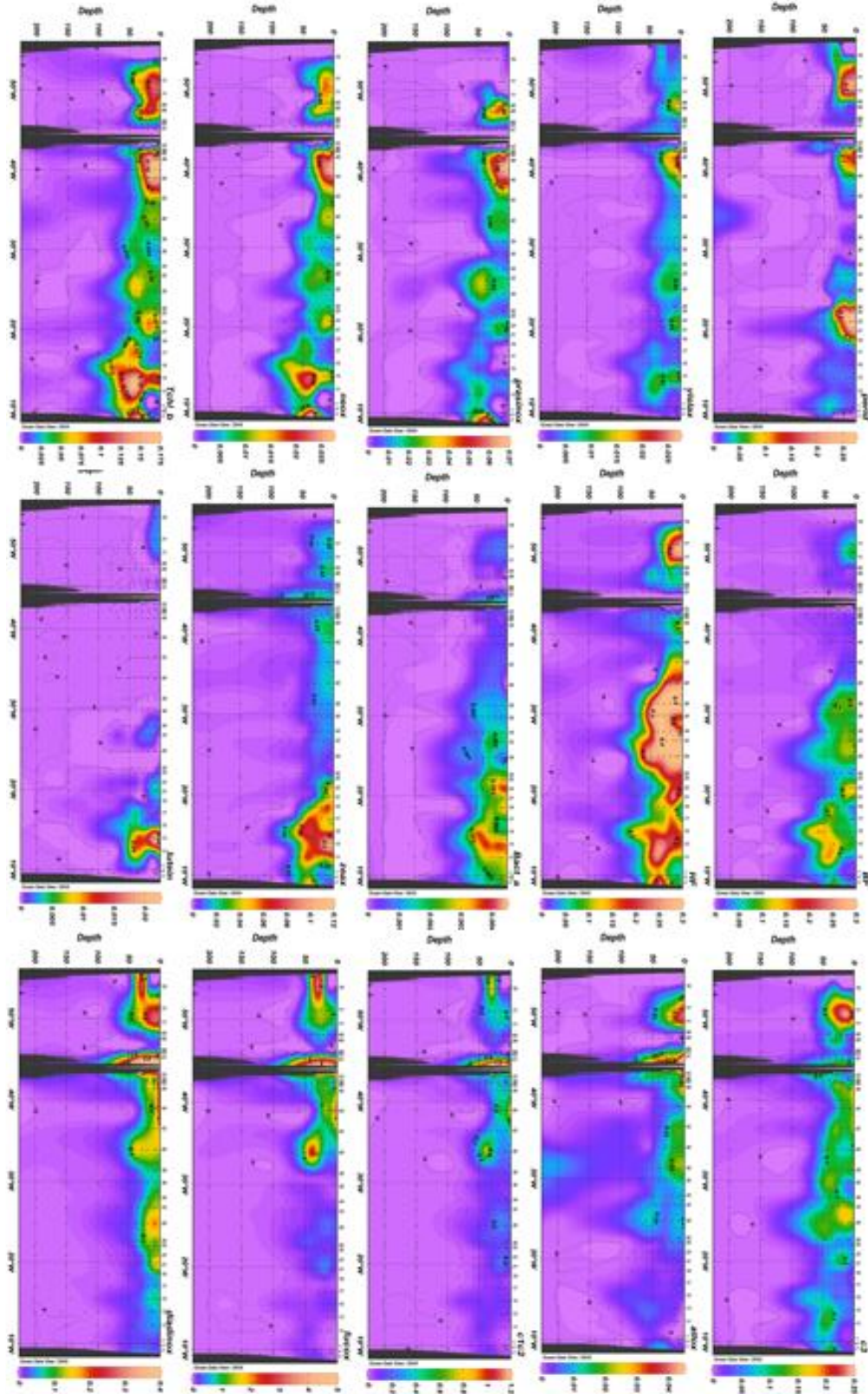
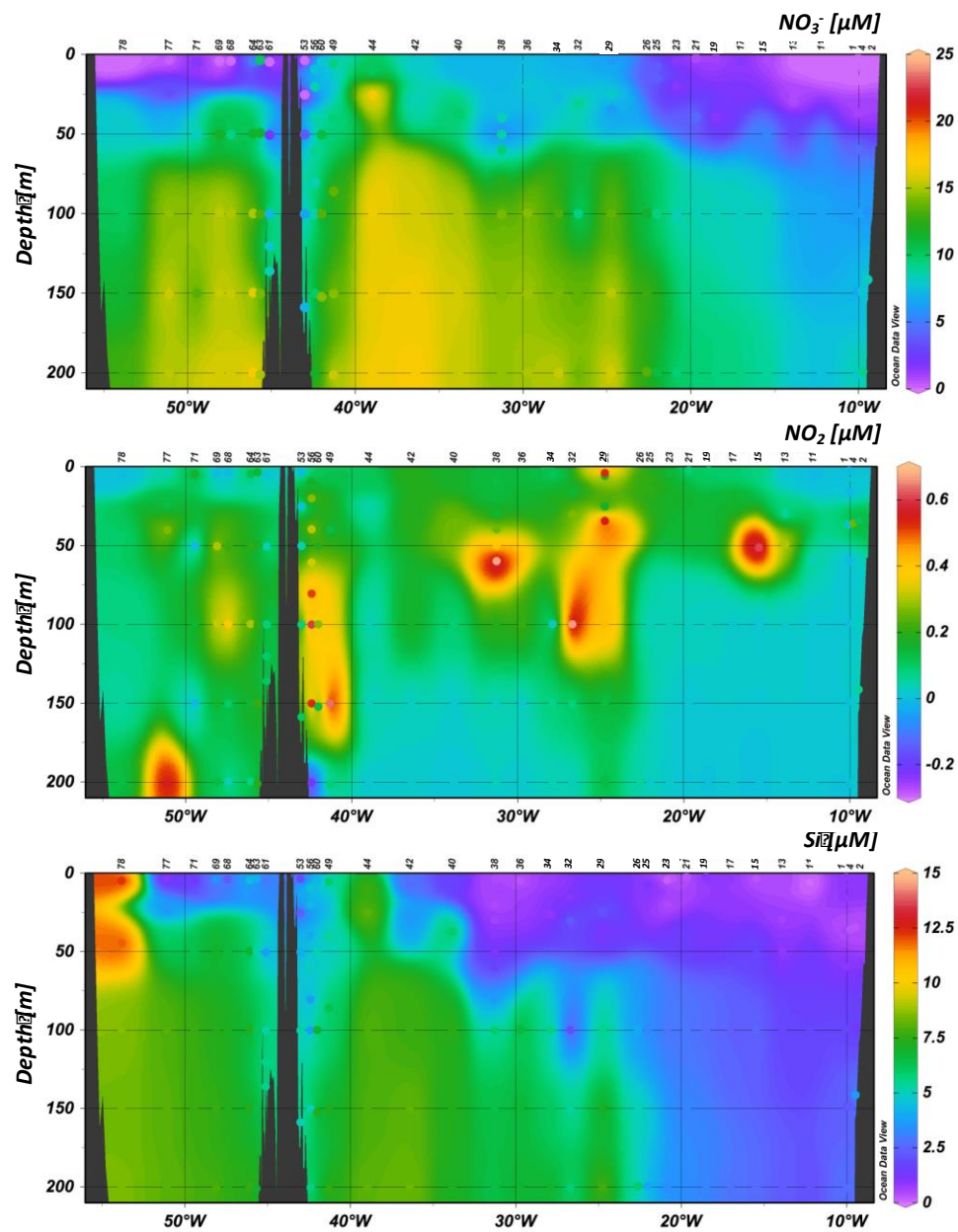


Figure C1: Vertical cross sections for biomarker pigment concentrations (mg.m^{-3}) across the GA01 voyage transect. (a) zeaxanthin, (b) bacteriochlorophyll-a, (c) 19'-hexanoyloxyfucoxanthin, (d) 19'-butanoyloxyfucoxanthin, (e) total chlorophyll-b, (f) peridinin, (g) fucoxanthin, (h) alloxanthin, degradation products: (i) phaeophorbide-a + phaeophytin-a, (j) chlorophyllid-a. Small black dots represent collected water samples at each sampling station.

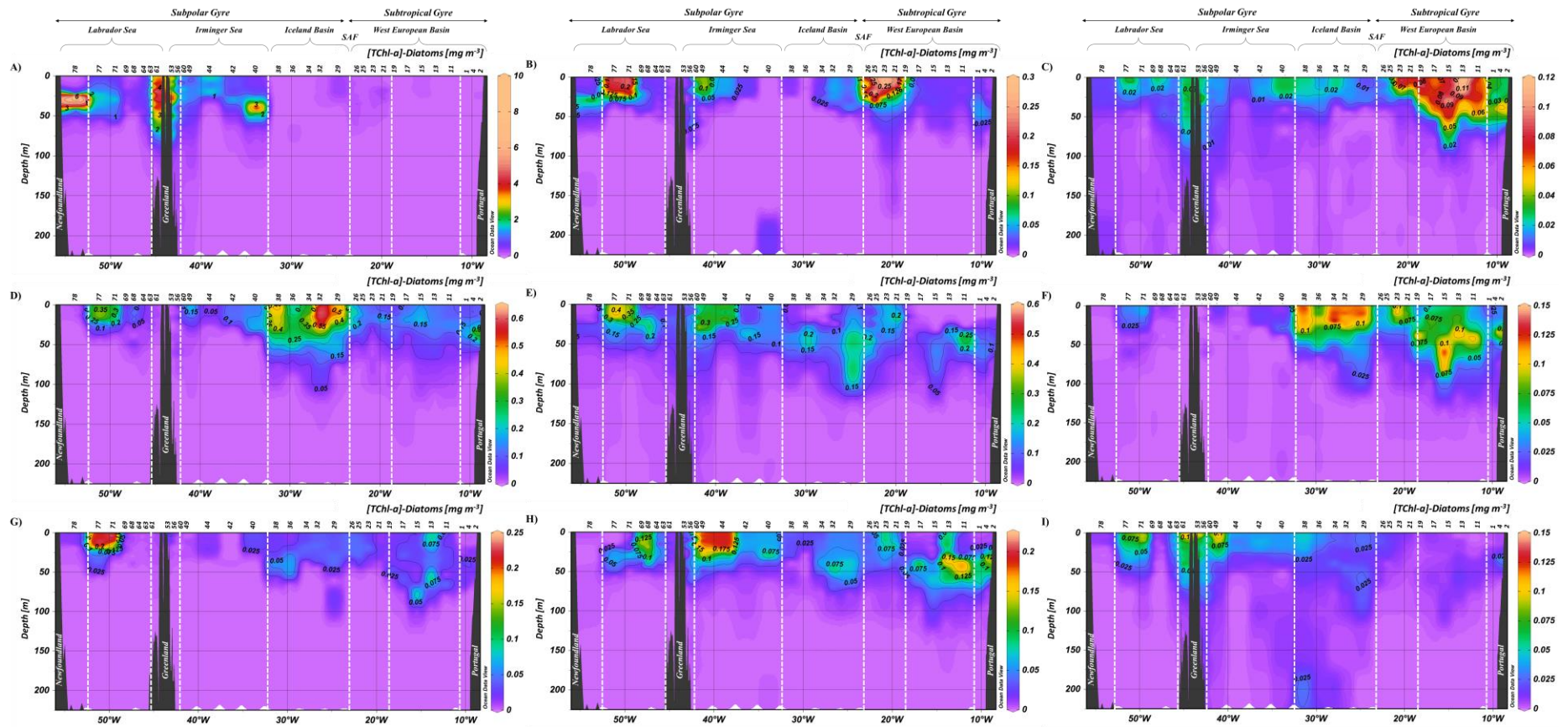
C2 Interpolated nutrient data

Macronutrients interpolated data as background and measured data as dot points for NO_3^- (A), NO_2^- (B), and Si (C) represented as a function of depth along the whole section.



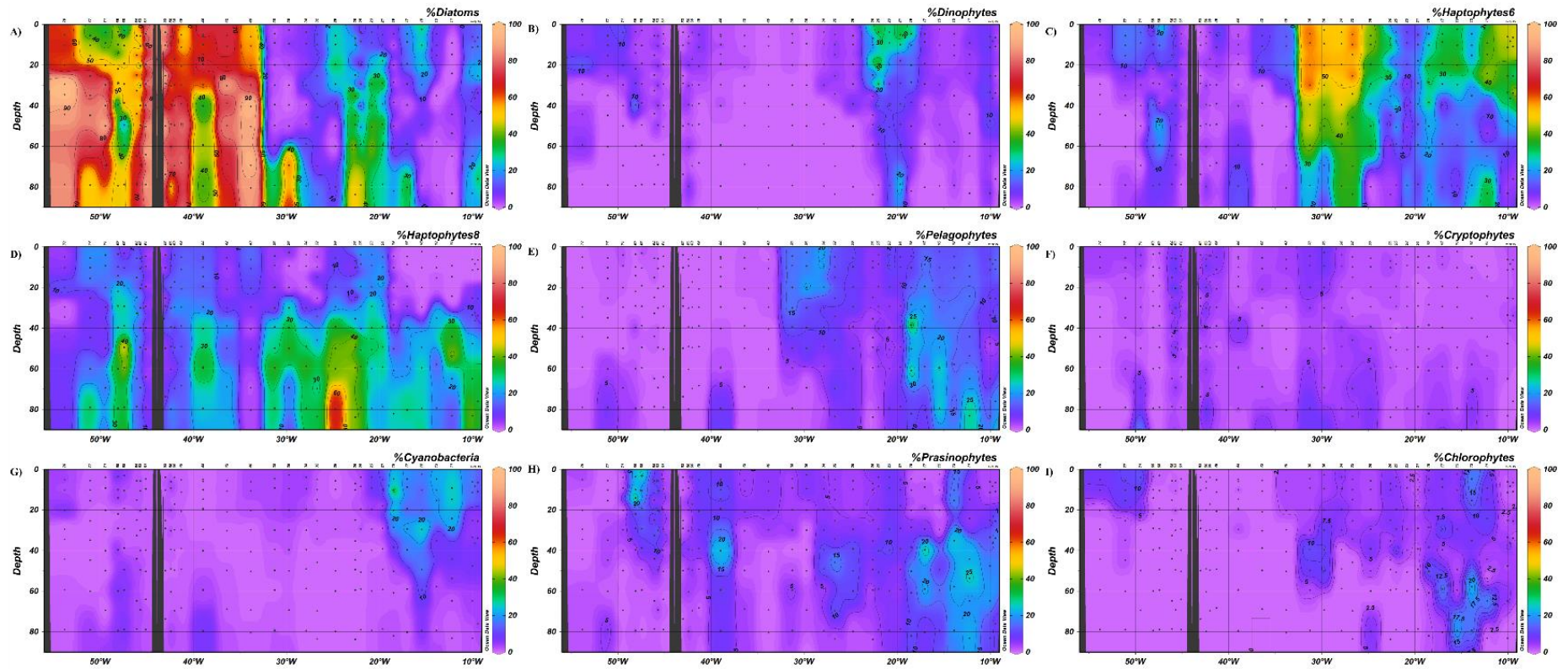
C3 Taxa (mg m^{-3}) distributions along the GEOVIDE (GEOTRACES, GA01) section

Vertical cross sections for the main phytoplankton classes (mg.m^{-3}) as determined by CHEMTAX across the GEOVIDE voyage transect for (A) Diatoms, (B) Dinophytes, (C) Cyanobacteria, (D) Haptophytes type 6, (E) Haptophytes types 8, (F) Pelagophytes, (G) Chlorophytes, (H) Prasinophytes and (I) Cryptophytes as a function of depth. Note that the scale is different from one plot to another.



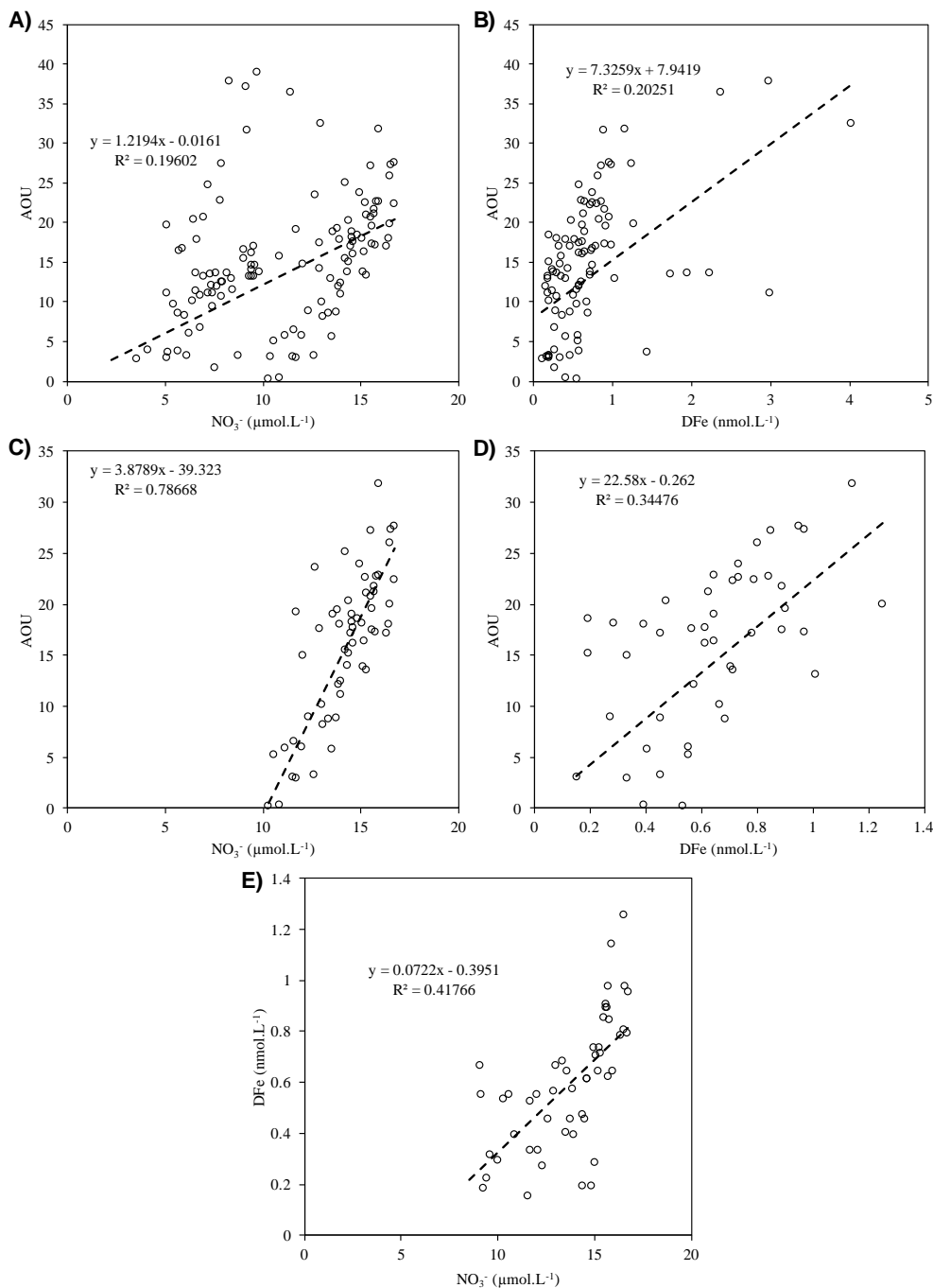
C4 Taxa (%) distributions along the GEOVIDE (GEOTRACES, GA01) section

Vertical cross sections for the percentage of the different phytoplankton functional-classes across the GA01 voyage transect for A) Diatoms, B) Dinophytes, C) Haptophytes-6, D) Haptophytes-8, E) Pelagophytes, F) Cryptophytes, G) Cyanobacteria, H) Prasinophytes and I) Chlorophytes. Small black dots represent collected water samples at each sampling station.



C5 Apparent Oxygen Utilization (AOU) and nutrients

Apparent Oxygen Utilization (AOU) as a function of (A) nitrate concentration (NO_3^-) and (B) dissolved Fe concentration (DFe) considering all stations and below 50 m depth. AOU as a function of (C) NO_3^- and (D) DFe considering stations from the Subpolar gyre without margins influence and (E) DFe as a function of NO_3^- for the same subset of stations.



C6 Tables summarizing the statistics behind the different Canonical Correspondence Analysis (CCA) performed.

Location	all Stations above 90 m depth (n=79)		Stations 1-19 (n=26)		Stations 19-38 (n=27)		Stations 40-78 (n=30)	
Axis	1	2	1	2	1	2	1	2
Sum of all eigenvalues		0.2628		0.522		0.62		0.3952
Sum of all canonical eigenvalues		0.148		0.276		0.3048		0.2312
Variance explained (%)		56		53		49		58
p-value		0.001		0.001		0.002		0.002
eigenvalues	0.1051	0.03961	0.196	0.055	0.2048	0.06891	0.1593	0.05811
species-environment correlations	0.81	0.74	0.95	0.72	0.97	0.87	0.96	0.93
cumulative percentage variance								
of species data	26	11	17	12	27	11	22	8
of species-environment relation	71	27	71	20	67	23	69	25

	all Stations above 90 m depth (n=79)		Stations 1-19 (n=26)		Stations 19-38 (n=27)		Stations 40-78 (n=30)	
Variables	F-value	significance	F-value	significance	F-value	significance	F-value	significance
Nitrates (NO ₃ ⁻)			16.27	***			8.8367	***
Nitrite (NO ₂ ⁻)					3.1574	*		
Silicic acid (Si)					4.3349	*		
Dissolved iron (DFe)								
Salinity	51.73	***					5.781	**
Temperature	13.43	***	2.14	.	12.8193	***	4.2984	**
pH	0.69				0.2497		0.8322	
z:Z _{eu}			3.04	*	1.9185		0.9362	
Si*			2.10				2.4012	.
Fe*			5.45	**	0.524		3.1855	*
NOx:Si					0.7598			
TChl- <i>a</i> ^{micro}	1.59							
TChl- <i>a</i> ^{nano}	13.13	***						
TChl- <i>a</i> ^{pico}	9.31	***						

significativity codes *** (p-value < 0.001) ** (p-value = [0.001, 0.01]) * (p-value = [0.01, 0.05]) . (p-value = [0.05, 0.1])

All stations			
	Axis	CCA1	CCA2
Constraining variable scores	Salinity	0.26	0.75
	Temperature	-0.14	0.82
	pH	-0.36	0.61
	TChl- <i>a</i> ^{micro}	-0.27	-0.73
	TChl- <i>a</i> ^{nano}	0.03	0.65
	TChl- <i>a</i> ^{pico}	-0.20	0.20
Species scores	Nitrates (NO ₃ ⁻)	0.20	0.09
	Nitrite (NO ₂ ⁻)	-0.05	0.36
	Silicic acid (Si)	0.16	0.29
	Dissolved iron (DFe)	-1.00	0.32

Stations 1-19			
	Axis	CCA1	CCA2
Constraining variable scores	Nitrates (NO ₃ ⁻)	-0.81	0.41
	Temperature	0.73	-0.55
	z:Z _{eu}	-0.58	-0.40
	Si*	0.84	-0.37
	Fe*	0.11	-0.94
	Chlorophytes	0.07	0.33
Species scores	Diatoms	-0.24	-0.62
	Prasinophytes	-0.28	0.13
	Pelagophytes	0.02	0.15
	Haptophytes type-8	-0.81	0.06
	Haptophytes type-6	0.38	0.10
	Cyanobacteria	0.62	0.08

Stations 19-38			
	Axis	CCA1	CCA2
Constraining variable scores	Nitrites (NO ₂ ⁻)	-0.28	-0.67
	Temperature	0.86	0.49
	z:Z _{eu}	0.48	-0.76
	Si	0.33	-0.57
	Fe*	-0.06	0.44
	NOx:Si	-0.77	-0.13
	pH	0.72	0.66
Species scores	Chlorophytes	-0.24	0.43
	Diatoms	0.55	-0.13
	Dinophytes	0.59	0.40
	Pelagophytes	-0.15	0.26
	Cryptophytes	-0.43	-0.32
	Haptophytes type-8	0.19	-0.29
	Haptophytes type-6	-0.56	-0.03
	Cyanobacteria	0.22	0.76

Stations 40-78			
	Axis	CCA1	CCA2
Constraining variable scores	Nitrates (NO ₃ ⁻)	-0.04	0.73
	Temperature	-0.81	0.17
	Salinity	-0.74	0.35
	pH	-0.66	-0.27
	z:Z _{eu}	0.61	0.15
	Si*	0.38	-0.63
	Fe*	0.67	-0.51
Species scores	Chlorophytes	-1.24	-0.85
	Diatoms	0.18	-0.03
	Dinophytes	-1.12	-0.31
	Prasinophytes	-0.59	1.01
	Pelagophytes	-1.10	-0.39
	Cryptophytes	-0.52	0.17
	Haptophytes type-8	-0.58	0.43
	Haptophytes type-6	-1.21	-0.48
	Cyanobacteria	-0.22	0.22

Appendix D (Chapter 5)

Details of station location and Fe-contaminated samples with TAC (for which no DFe' was reported).

Index	TMR	Latitude	Longitude	Bottom Depth	TAC	Niskin	Depth	DLt			Log K'			DFe'		
	#	(°S)	(°E)	(m)	(nmol L ⁻¹)	#	(m)	(Eq of nmol L ⁻¹ Fe)			(L mol ⁻¹)			(pmol L ⁻¹)		
B-transect	2	-48.31	79.37	3303	0.09	12	14	0.69	±	0.11	21.23	±	0.10	2	±	0
						11	29	0.69	±	0.26	21.12	±	0.25		±	
						10	49	0.55	±	0.14	21.28	±	0.23	2	±	0
						9	69	0.67	±	0.05	21.47	±	0.05	3	±	0
						8	99	0.62	±	0.11	20.84	±	0.16	3	±	0
						7	148	0.58	±	0.25	21.00	±	0.33	3	±	0
						6	198	0.61	±	0.11	21.08	±	0.11	4	±	0
						5	298	0.56	±	0.16	20.81	±	0.16	17	±	0
						4	498	0.54	±	0.07	21.17	±	0.11	30	±	0
						3	698	0.47	±	0.05	21.72	±	0.09	49	±	0
						2	999	0.56	±	0.05	21.86	±	0.10	53	±	0
						1	1598	0.62	±	0.04	22.06	±	0.08	48	±	0
	4	-50.24	77.73	3520	0.15	10	68	2.63	±	0.72	20.62	±	0.16			
						9	97	1.24	±	0.30	20.86	±	0.16			
						8	197	1.09	±	0.57	20.45	±	0.31			
						7	296	1.21	±	0.41	20.65	±	0.24			
						6	493	0.68	±	0.32	20.35	±	0.29			
						5	591	0.58	±	0.13	20.93	±	0.14			
						4	987	0.57	±	0.08	21.85	±	0.18			
						3	1971	0.43	±	0.10	21.63	±	0.23			
						2	2951	0.41	±	0.08	22.10	±	0.39			
						1	3317	0.42	±	0.04	21.73	±	0.08			
						7	295	0.44	±	0.13	21.15	±	0.25			
	6	-50.79	75.78	1759	0.15	6	493	0.64	±	0.11	20.78	±	0.12			
						5	690	0.58	±	0.10	21.25	±	0.11			
						4	986	0.77	±	0.17	21.10	±	0.14			
						3	1479	0.35	±	0.05	21.90	±	0.18			
						2	1578	0.34	±	0.03	21.86	±	0.08			
						1	1628	0.38	±	0.05	21.84	±	0.18			
	9	-51.29	73.81	446	0.15	12	14	0.93	±	0.68	20.24	±	0.46	11	±	0
						11	24	0.62	±	0.33	20.40	±	0.29	9	±	0
						10	39	1.18	±	0.21	20.68	±	0.10	3	±	0
						9	67	0.79	±	0.28	20.40	±	0.23	7	±	0
						8	97	0.80	±	0.22	20.70	±	0.16	5	±	0
						7	147	0.66	±	0.55	20.58	±	0.79	11	±	0
						6	196	0.59	±	0.10	21.09	±	0.19	8	±	0
						5	246	0.70	±	0.14	20.95	±	0.12	27	±	0
						4	295	0.66	±	0.15	21.25	±	0.17	55	±	0
						3	345	0.68	±	0.05	21.48	±	0.06	50	±	0
						1	395	0.82	±	0.14	21.29	±	0.14	53	±	0

(continued)

Index	TMR	Latitude	Longitude	Bottom Depth	TAC	Niskin	Depth	DLt			Log K'			DFe'		
	#	(°S)	(°E)	(m)	(nmol L ⁻¹)	#	(m)	(Eq of nmol L ⁻¹ Fe)			(L mol ⁻¹)			(pmol L ⁻¹)		
B-transect	11	-52.93	71.36	2850	0.09	12	13	1.42	±	0.26	20.82	±	0.12	3	±	0
						11	29	2.59	±	0.39	20.81	±	0.12	1	±	0
						10	68	0.72	±	0.22	21.31	±	0.25	3	±	0
						9	98	0.28	±	0.01	21.92	±	0.04			
						8	197	0.26	±	0.02	21.95	±	0.10	26	±	0
						7	295	0.33	±	0.03	22.20	±	0.09	53	±	0
						6	493	0.53	±	0.06	21.58	±	0.08	62	±	0
						5	689	0.65	±	0.04	22.45	±	0.14	42	±	0
						4	987	0.53	±	0.05	22.16	±	0.12	67	±	0
						3	1578	0.51	±	0.03	21.98	±	0.07	56	±	0
						2	2560	0.41	±	0.04	21.95	±	0.11	44	±	0
						1	2658	1.01	±	0.06	22.52	±	0.14	54	±	0
Reference	18	-54.17	73.67	2152		12	13	0.80	±	0.11	20.99	±	0.09	2	±	0
						11	28	0.37	±	0.02	22.06	±	0.06	4	±	0
						10	68	0.90	±	0.22	20.43	±	0.16	3	±	0
						9	97	1.27	±	0.38	20.26	±	0.18	3	±	0
						8	148	1.24	±	0.33	20.53	±	0.16	2	±	0
						7	197	0.44	±	0.04	21.33	±	0.05	5	±	0
						6	294	0.43	±	0.01	22.09	±	0.05	23	±	0
						4	691	0.42	±	0.03	22.04	±	0.13	4	±	0
						3	987	0.35	±	0.02	22.48	±	0.09	49	±	0
McDonald	14	-53.03	72.55	219		7	13	1.56	±	0.11	20.75	±	0.05	29	±	0
						1	172	1.53	±	0.08	20.92	±	0.04	43	±	0
	25	-53.03	72.66	139		6	14	1.06	±	0.09	21.16	±	0.07	100	±	0
Heard	23	-53.01	73.72	98		1	120	1.25	±	0.17	20.93	±	0.09	119	±	0
						6	14	2.20	±	0.07	21.04	±	0.03	89	±	0
						5	28	1.98	±	0.06	21.09	±	0.03	123	±	0
						4	48	1.63	±	0.08	20.94	±	0.04	167	±	0
						3	59	1.35	±	0.06	21.27	±	0.03	91	±	0
						2	68	1.41	±	0.07	21.18	±	0.04	102	±	0
						1	75	1.45	±	0.13	20.68	±	0.06	162	±	0
	24	-53.00	73.61	58		4	14	2.14	±	0.08	21.18	±	0.03	146	±	0
						1	35	1.96	±	0.09	21.05	±	0.04	137	±	0
	40	-53.01	73.72	94		5	14	1.66	±	0.13	21.18	±	0.06	136	±	0
						4	29	1.85	±	0.08	21.73	±	0.06	71	±	0
						3	49	1.87	±	0.13	21.32	±	0.07	94	±	0
						2	63	1.61	±	0.07	21.15	±	0.04	104	±	0
						1	72	1.68	±	0.07	21.33	±	0.04	87	±	0

References

- Abadie, C., Lacan, F., Radic, A., Pradoux, C., and Poitrasson, F.: Iron isotopes reveal distinct dissolved iron sources and pathways in the intermediate versus deep Southern Ocean, *Proc Natl Acad Sci U S A*, 114, 858-863, 10.1073/pnas.1603107114, 2017.
- Achterberg, E. P., Moore, C. M., Henson, S. A., Steigenberger, S., Stohl, A., Eckhardt, S., Avendano, L. C., Cassidy, M., Hembury, D., and Klar, J. K.: Natural iron fertilization by the Eyjafjallajökull volcanic eruption, *Geophysical Research Letters*, 40, 921-926, 2013.
- Achterberg, E. P., Steigenberger, S., Marsay, C. M., LeMoigne, F. A., Painter, S. C., Baker, A. R., Connelly, D. P., Moore, C. M., Tagliabue, A., and Tanhua, T.: Iron Biogeochemistry in the High Latitude North Atlantic Ocean, *Scientific reports*, 8, 1-15, 10.1038/s41598-018-19472-1, 2018.
- Alderkamp, A.-C., Mills, M. M., van Dijken, G. L., Laan, P., Thuróczy, C.-E., Gerringa, L. J. A., de Baar, H. J. W., Payne, C. D., Visser, R. J. W., Buma, A. G. J., and Arrigo, K. R.: Iron from melting glaciers fuels phytoplankton blooms in the Amundsen Sea (Southern Ocean): Phytoplankton characteristics and productivity, *Deep Sea Research Part II: Topical Studies in Oceanography*, 71-76, 32-48, 10.1016/j.dsr2.2012.03.005, 2012.
- Aldredge, A. L., and Silver, M. W.: Characteristics, dynamics and significance of marine snow, *Progress in Oceanography*, 20, 41-82, 1988.
- Amin, S. A., Parker, M. S., and Armbrust, E. V.: Interactions between diatoms and bacteria, *Microbiol Mol Biol Rev*, 76, 667-684, 10.1128/MMBR.00007-12, 2012.
- Aminot, A., and Kerouel, R.: Dosage automatique des nutriments dans les eaux marines, Quae ed., 2007.
- Anderson, L. A., and Sarmiento, J. L.: Redfield ratios of remineralization determined by nutrient data-analysis, *Global Biogeochemical Cycle*, 8, 65-80, 1994.
- Anderson, R. F., Mawji, E., Cutter, G. A., Measures, C. I., and Jeandel, C.: GEOTRACES Changing the Way We Explore Ocean Chemistry, *Oceanography*, 27, 50-61, 2014.
- Annett, A. L., Skiba, M., Henley, S. F., Venables, H. J., Meredith, M. P., Statham, P. J., and Ganeshram, R. S.: Comparative roles of upwelling and glacial iron sources in Ryder Bay, coastal western Antarctic Peninsula, *Marine Chemistry*, 176, 21-33, 10.1016/j.marchem.2015.06.017, 2015.
- Armand, L. K., Crosta, X., Quéguiner, B., Mosseri, J., and Garcia, N.: Diatoms preserved in surface sediments of the northeastern Kerguelen Plateau, *Deep Sea Research Part II: Topical Studies in Oceanography*, 55, 677-692, 10.1016/j.dsr2.2007.12.032, 2008.
- Arrigo, K. R., Robinson, D. H., Worthen, D. L., Dunbar, R. B., DiTullio, G. R., VanWoert, M., and Lizotte, M. P.: Phytoplankton Community Structure and the Drawdown of Nutrients and CO₂ in the Southern Ocean, *Science* 283, 365-367, 1999.
- Arrigo, K. R., Worthen, D. L., and Robinson, D. H.: A coupled ocean-ecosystem model of the Ross Sea: 2. Iron regulation of phytoplankton taxonomic variability and primary production, *Journal of Geophysical Research-Oceans*, 108, 10.1029/2001jc000856, 2003.
- Arteaga, L., Pahlow, M., and Oschlies, A.: Global patterns of phytoplankton nutrient and light colimitation inferred from an optimality-based model, *Global Biogeochemical Cycles*, 28, 648-661, 10.1002/2013gb004668, 2014.

Baalousha, M., Motelica-Heino, M., and Le Coustumer, P.: Conformation and size of humic substances: Effect of major cation concentration and type, pH, salinity, and residence time, *Colloids and Surfaces A: Physicochemical and Engineering Aspects*, 272, 48-55, 10.1016/j.colsurfa.2005.07.010, 2006.

Bacon, S., Gould, W. J., and Jia, Y.: Open-ocean convection in the Irminger Sea, *Geophysical Research Letters*, 30, 1246, doi:10.1029/2002GL016271, 2003.

Baker, A. R., and Croot, P. L.: Atmospheric and marine controls on aerosol iron solubility in seawater, *Marine Chemistry*, 120, 4-13, 10.1016/j.marchem.2008.09.003, 2010.

Baker, A. R., Adams, C., Bell, T. G., Jickells, T. D., and Ganzeveld, L.: Estimation of atmospheric nutrient inputs to the Atlantic Ocean from 50°N to 50°S based on large-scale field sampling: Iron and other dust-associated elements, *Global Biogeochemical Cycles*, 27, 755-767, 10.1002/gbc.20062, 2013.

Baker, A. T., and German, C. R.: On the Global Distribution of Hydrothermal vent Fields, in: *Mid-Ocean Ridges*, edited by: German, C. R., Lin, J., and Parson, L. M., 2004a.

Baker, E. T., and German, C. R.: Hydrothermal Interactions Between the Lithosphere and Oceans, in: *Mid-Ocean Ridges*, edited by: German, C. R., Lin, J., and Parson, L. M., *Geophysical Monograph Series*, AGU, 245-266, 2004b.

Bakker, D. C. E., Bozec, Y., Nightingale, P. D., Goldson, L., Messias, M.-J., de Baar, H. J. W., Liddicoat, M., Skjelvan, I., Strass, V., and Watson, A. J.: Iron and mixing affect biological carbon uptake in SOIREE and EisenEx, two Southern Ocean iron fertilisation experiments, *Deep Sea Research Part I: Oceanographic Research Papers*, 52, 1001-1019, 10.1016/j.dsr.2004.11.015, 2005.

Barbeau, K., Moffett, J. W., Caron, D. A., Croot, P. L., and Erdner, D. L.: Role of protozoan grazing in relieving iron limitation of phytoplankton, *Nature*, 380, 61-64, 1996.

Barbeau, K., Rue, E. L., Bruland, K. W., and Butler, A.: Photochemical cycling of iron in the surface ocean mediated by microbial iron(III)-binding ligands, *Nature*, 413, 409-413, 2001.

Barbeau, K., Rue, E. L., Trick, C. G., Bruland, K. T., and Butler, A.: Photochemical reactivity of siderophores produced by marine heterotrophic bacteria and cyanobacteria based on characteristic Fe(III) binding groups, *Limnology and Oceanography*, 48, 1069-1078, 2003.

Barcelos E Ramos, J., Schulz, K. G., Voss, M., Narciso, Á., Müller, M. N., Reis, F. V., Cachão, M., and Azevedo, E. B.: Nutrient-specific responses of a phytoplankton community: a case study of the North Atlantic Gyre, Azores, *Journal of Plankton Research*, 39, 744-761, 10.1093/plankt/fbx025, 2017.

Barlow, R. G., Mantoura, R. F. C., Gough, M. A., and Fileman, T. W.: Pigment signatures of the phytoplankton composition in the northeastern Atlantic during the 1990 spring bloom, *Deep-Sea Research II*, 40, 459-477, 1993.

Barni, F., Lewis, S. W., Berti, A., Miskelly, G. M., and Lago, G.: Forensic application of the luminol reaction as a presumptive test for latent blood detection, *Talanta*, 72, 896-913, 10.1016/j.talanta.2006.12.045, 2007.

Barton, A. D., Greene, C. H., Monger, B. C., and Pershing, A. J.: The Continuous Plankton Recorder survey and the North Atlantic Oscillation: Interannual- to Multidecadal-scale patterns of phytoplankton variability in the North Atlantic Ocean, *Progress in Oceanography*, 58, 337-358, 10.1016/j.pocean.2003.08.012, 2003.

Barton, A. D., Lozier, M. S., and Williams, R. G.: Physical controls of variability in North Atlantic phytoplankton communities, *Limnology and Oceanography*, 60, 181-197, 10.1002/lno.10011, 2015.

Batchelli, S., Muller, F. L. L., Chang, K. C., and Lee, C. L.: Evidence for Strong but Dynamic Iron-Humic Colloidal Associations in Humic-Rich Coastal Waters., *Environmental Science & Technology*, 44, 8485-8490, 2010.

- Behrenfeld, M. J.: Abandoning Sverdrup's Critical Depth Hypothesis on phytoplankton blooms
 Author(s): Michael J. Source: Ecology, Vol. 91, No. 4 (April 2010), pp. 977-989, Ecology, 91, 977-989, 2010.
- Belcher, A., Iversen, M., Manno, C., Henson, S. A., Tarling, G. A., and Sanders, R.: The role of particle associated microbes in remineralization of fecal pellets in the upper mesopelagic of the Scotia Sea, Antarctica, *Limnology and Oceanography*, 61, 1049-1064, 10.1002/lno.10269, 2016.
- Benetti, M., Reverdin, G., Pierre, C., Khatiwala, S., Tournadre, B., Olafsdottir, S., and Naamar, A.: Variability of sea ice melt and meteoric water input in the surface Labrador Current off Newfoundland, *Journal of Geophysical Research Oceans*, 121, 2841-2855, doi:10.1002/2015JC011302., 2016.
- Benetti, M., Reverdin, G., Lique, C., Yashayaev, I., Holliday, N. P., Tynan, E., Torres-Valdes, S., Lherminier, P., Tréguer, P., and Sarthou, G.: Composition of freshwater in the spring of 2014 on the southern Labrador shelf and slope, *Journal of Geophysical Research: Oceans*, 122, 1102-1121, 10.1002/2016jc012244, 2017.
- Benitez-Nelson, C. R.: The biogeochemical cycling of phosphorus in marine systems, *Earth-Science Reviews*, 51, 109-135, 2000.
- Benitez-Nelson, C. R., Buesseler, K. O., and Crossin, G.: Upper ocean carbon export, horizontal transport, and vertical eddy diffusivity in the southwestern Gulf of Maine, *Continental Shelf Research*, 20, 707-736, 2000.
- Bennett, S. A., Achterberg, E. P., Connelly, D. P., Statham, P. J., Fones, G. R., and German, C. R.: The distribution and stabilisation of dissolved Fe in deep-sea hydrothermal plumes, *Earth and Planetary Science Letters*, 270, 157-167, 10.1016/j.epsl.2008.01.048, 2008.
- Berg, G. M., Balode, M., Purina, I., Bekere, S., Bechemin, C., and Meaestrini, S. Y.: Plankton community composition in relation to availability and uptake of oxidized and reduced nitrogen, *Aquatic Microbial Ecology*, 30, 263-274, 2003.
- Berger, C. J. M., Lippiatt, S. M., Lawrence, M. G., and Bruland, K. W.: Application of a chemical leach technique for estimating labile particulate aluminum, iron, and manganese in the Columbia River plume and coastal waters off Oregon and Washington, *Journal of Geophysical Research-Oceans*, 113, 10.1029/2007jc004703, 2008.
- Bergquist, B. A., Wu, J., and Boyle, E. A.: Variability in oceanic dissolved iron is dominated by the colloidal fraction, *Geochimica Et Cosmochimica Acta*, 71, 2960-2974, 10.1016/j.gca.2007.03.013, 2007.
- Berman-Frank, I., Cullen, J. T., Shaked, Y., Sherrell, R. M., and Falkowski, P. G.: Iron availability, cellular iron quotas, and nitrogen fixation in *Trichodesmium*, *Limnology and Oceanography*, 46, 1249-1260, 2001.
- Berman-Frank, I., Rosenberg, G., Levitan, O., Haramaty, L., and Mari, X.: Coupling between autocatalytic cell death and transparent exopolymeric particle production in the marine cyanobacterium *Trichodesmium*, *Environ Microbiol*, 9, 1415-1422, 10.1111/j.1462-2920.2007.01257.x, 2007.
- Bersch, M., Yashayaev, I., and Koltermann, K. P.: Recent changes of the thermohaline circulation in the subpolar North Atlantic, *Ocean Dynamics*, 57, 223-235, 10.1007/s10236-007-0104-7, 2007.
- Bertrand, E. M., Saito, M. A., Rose, J. M., Riesselman, C. R., Lohan, M. C., Noble, A. E., Lee, P. A., and DiTullio, G. R.: Vitamin B-12 and iron colimitation of phytoplankton growth in the Ross Sea, *Limnology and Oceanography*, 52, 1079-1093, 2007.
- Béthoux, J. P., and Prieur, L.: Hydrologie et circulation en Méditerranée Nord-Occidentale, *Pétroles et Techniques*, 299, 25-34, 1983.

Bhatia, M. P., Kujawinski, E. B., Das, S. B., Breier, C. F., Henderson, P. B., and Charette, M. A.: Greenland meltwater as a significant and potentially bioavailable source of iron to the ocean, *Nature Geoscience*, 2013, 274-278, 10.1038/ngeo1746, 2013.

Bidle, K. D.: The molecular ecophysiology of programmed cell death in marine phytoplankton, *Ann Rev Mar Sci*, 7, 341-375, 10.1146/annurev-marine-010213-135014, 2015.

Bienfang, B. K.: SETCOL - A Technologically Simple and Reliable Method for Measuring Phytoplankton Sinking Rates, *Canadian Journal of Fish and Aquaculture Science*, 38, 1289-1294, 1981.

Billier, D. V., and Bruland, K. W.: Analysis of Mn, Fe, Co, Ni, Cu, Zn, Cd, and Pb in seawater using the Nobias-chelate PA1 resin and magnetic sector inductively coupled plasma mass spectrometry (ICP-MS), *Marine Chemistry*, 130-131, 12-20, 2012.

Bintanja, R., and van de Wal, R. S.: North American ice-sheet dynamics and the onset of 100,000-year glacial cycles, *Nature*, 454, 869-872, 10.1038/nature07158, 2008.

Biscaye, P. E., and Eitrem, S. L.: Suspended particulate loads and transports in the nepheloid layer of the abyssal Atlantic Ocean, *Marine Geology*, 23, 155-172, 1977.

Bishop, J. K. B., Edmond, J. M., Ketten, D. R., Bacon, M. P., and Silker, W. B.: Chemistry, Biology, and Vertical Flux of Particulate Matter from Upper 400 m of Equatorial Atlantic Ocean, *Deep-Sea Research*, 24, 511-548, 1977.

Bishop, J. K. B., Ketten, D. R., and Edmond, J. M.: Chemistry, Biology and Vertical Flux of Particulate Matter from the Upper 400 m of the Cape Basin in the Southeast Atlantic Ocean, *Deep-Sea Research*, 25, 1121-1161, 1978.

Bishop, J. K. B., Schupack, D., Sherrell, R. M., and Conte, M. H.: A Multiple Unit Large Volume in-situ Filtration System (MULVFS) for sampling oceanic particulate matter in mesoscale environments, in: *Mapping strategies in Chemical Oceanography*, edited by: Zirino, A., 155-175, 1985.

Bishop, J. K. B., Stepien, J. C., and Wiebe, P. H.: Particulate Matter Distributions, Chemistry and Flux in the Panama Basin - Response to Environmental Forcing, *Progress in Oceanography*, 17, 1-59, 1986.

Bishop, J. K. B., and Wood, T. J.: Particulate matter chemistry and dynamics in the twilight zone at VERTIGO ALOHA and K2 sites, *Deep Sea Research Part I: Oceanographic Research Papers*, 55, 1684-1706, 2008.

Bjørnland, T., Liaaen-Jensen, S., and Throndsen, J.: Carotenoids of the marine chrysophyte *Pelagococcus subviridis*, *Phytochemistry*, 28, 3347-3353, 1989.

Blain, S., Treguer, P., Belviso, S., Bucciarelli, E., Denis, M., Desabre, S., Fiala, M., Jezequel, V. M., Le Fevre, J., Mayzaud, P., Marty, J. C., and Razouls, S.: A biogeochemical study of the island mass effect in the context of the iron hypothesis: Kerguelen Islands, Southern Ocean, *Deep-Sea Research Part I-Oceanographic Research Papers*, 48, 163-187, 10.1016/s0967-0637(00)00047-9, 2001.

Blain, S., Queguiner, B., Armand, L., Belviso, S., Bombled, B., Bopp, L., Bowie, A., Brunet, C., Brussaard, C., Carlotti, F., Christaki, U., Corbiere, A., Durand, I., Ebersbach, F., Fuda, J. L., Garcia, N., Gerringa, L., Griffiths, B., Guigue, C., Guillerm, C., Jacquet, S., Jeandel, C., Laan, P., Lefevre, D., Lo Monaco, C., Malits, A., Mosseri, J., Obernosterer, I., Park, Y. H., Picheral, M., Pondaven, P., Remenyi, T., Sandroni, V., Sarthou, G., Savoye, N., Scouarnec, L., Souhaut, M., Thuiller, D., Timmermans, K., Trull, T., Uitz, J., van Beek, P., Veldhuis, M., Vincent, D., Viollier, E., Vong, L., and Wagener, T.: Effect of natural iron fertilization on carbon sequestration in the Southern Ocean, *Nature*, 446, 1070-1074, 10.1038/nature05700, 2007.

Blain, S., Bonnet, S., and Guieu, C.: Dissolved iron distribution in the tropical and sub tropical South Eastern Pacific, *Biogeosciences*, 5, 269-280, 2008a.

- Blain, S., Quéguiner, B., and Trull, T.: The natural iron fertilization experiment KEOPS (Kerguelen Ocean and Plateau compared Study): An overview, *Deep Sea Research Part II: Topical Studies in Oceanography*, 55, 559-565, 10.1016/j.dsr2.2008.01.002, 2008b.
- Blain, S., Sarthou, G., and Laan, P.: Distribution of dissolved iron during the natural iron-fertilization experiment KEOPS (Kerguelen Plateau, Southern Ocean), *Deep Sea Research Part II: Topical Studies in Oceanography*, 55, 594-605, 10.1016/j.dsr2.2007.12.028, 2008c.
- Blain, S., and Tagliabue, A.: *Iron Cycle in Oceans*, Focus Series, edited by: Treguer, P., ISTE Ltd John Wiley & Sons, Inc., London, U.K.; Hoboken, U.S.A., 124 pp., 2016.
- Blais, M., Ardyna, M., Gosselin, M., Dumont, D., Bélanger, S., Tremblay, J.-É., Gratton, Y., Marchese, C., and Poulin, M.: Contrasting interannual changes in phytoplankton productivity and community structure in the coastal Canadian Arctic Ocean, *Limnology and Oceanography*, 62, 2480-2497, 10.1002/lno.10581, 2017.
- Boccaletti, G., Ferrari, R., and Fox-Kemper, B.: Mixed Layer Instabilities and Restratification, *Journal of Physical Oceanography*, 37, 2228-2250, 10.1175/jpo3101.1, 2007.
- Boiteau, R. M., Fitzsimmons, J. N., Repeta, D. J., and Boyle, E. A.: Detection of Iron Ligands in Seawater and Marine Cyanobacteria Cultures by High-Performance Liquid Chromatography–Inductively Coupled Plasma–Mass Spectrometry, *Analytical Chemistry*, 85, 4357-4362, 2013.
- Bonnet, S., and Guieu, C.: Dissolution of atmospheric iron in seawater, *Geophysical Research Letters*, 31, 10.1029/2003gl018423, 2004.
- Bonnet, S., and Guieu, C.: Atmospheric forcing on the annual iron cycle in the western Mediterranean Sea: A 1-year survey, *Journal of Geophysical Research*, 111, 10.1029/2005jc003213, 2006.
- Bopp, L., and Le Quéré, C.: The ocean carbon cycle, in: *Surface Ocean Lower Atmosphere Processes*, edited by: Le Quéré, C., and Saltzman, E., AGU Geophysical Monographs, Washington, D.C., US, 2009.
- Boutorh, J., Sarthou, G., Gonzalez, A. G., Cheize, M., Planquette, H., Bucciarelli, E., Vaïtilingom, M., Deguillaume, L., Vinatier, V., Delort, A. M., and Mailhot, G.: Iron organic Complexation in Cloud Water Samples from the Puy De Dôme Station (France), *International Conference on Atmospheric Chemical and Biological Processes: Interactions and Impacts (ATMOCHEMBIO)*, Clermont-Ferrand (France), 2017.
- Bowie, A., Maldonado, M. T., Frew, R. D., Croot, P., Achterberg, E. P., Mantoura, F. C., Worsfold, P. J., Law, C. S., and Boyd, P. W.: The fate of added iron during a mesoscale fertilisation experiment in the Southern Ocean, *Deep Sea Research Part II: Topical Studies in Oceanography*, 48, 2703-2743, 2001.
- Bowie, A. R., Achterberg, E. P., Croot, P. L., de Baar, H. J. W., Laan, P., Moffett, J. W., Ussher, S., and Worsfold, P. J.: A community-wide intercomparison exercise for the determination of dissolved iron in seawater, *Marine Chemistry*, 98, 81-99, 10.1016/j.marchem.2005.07.002, 2006.
- Bowie, A. R., van der Merwe, P., Quéroué, F., Trull, T., Fourquez, M., Planchon, F., Sarthou, G., Chever, F., Townsend, A. T., Obernosterer, I., Sallée, J. B., and Blain, S.: Iron budgets for three distinct biogeochemical sites around the Kerguelen Archipelago (Southern Ocean) during the natural fertilisation study, KEOPS-2, *Biogeosciences*, 12, 4421-4445, 10.5194/bg-12-4421-2015, 2015.
- Boyd, P. W., Watson, A. J., Law, C. S., Abraham, E. R., Trull, T., Murdoch, R., Bakker, D. C. E., Bowie, A. R., Buesseler, K. O., Chang, H., Charette, M., Croot, P., Downing, K., Frew, R., Gall, M., Hadfield, M., Hall, J., Harvey, M., Jameson, G., LaRoche, J., Liddicoat, M., Ling, R., Maldonado, M. T., McKay, R. M., Nodder, S., Pickmere, S., Pridmore, R., Rintoul, S., Safi, K., Sutton, P., Strzepek, R., Tanneberger, K., Turner, S., Waite, A., and Zeldis, J.: A mesoscale phytoplankton bloom in the polar Southern Ocean stimulated by iron fertilization, *Nature*, 407, 695-702, 2000.
- Boyd, P. W., Law, C. S., Hutchins, D. A., Abraham, E. R., Croot, P. L., Ellwood, M., Frew, R. D., Hadfield, M., Hall, J., Handy, S., Hare, C., Higgins, J., Hill, P., Hunter, K. A., LeBlanc, K., Maldonado, M. T., McKay, R. M., Mioni, C., Oliver, M., Pickmere, S., Pinkerton, M., Safi, K., Sander, S., Sanudo-Wilhelmy, S.

A., Smith, M., Strzepek, R., Tovar-Sanchez, A., and Wilhelm, S. W.: FeCycle: Attempting an iron biogeochemical budget from a mesoscale SF6 tracer experiment in unperturbed low iron waters, *Global Biogeochemical Cycles*, 19, n/a-n/a, 10.1029/2005gb002494, 2005.

Boyd, P. W., Jickells, T., Law, C. S., Blain, S., Boyle, E. A., Buesseler, K. O., Coale, K. H., Cullen, J. J., de Baar, H. J., Follows, M., Harvey, M., Lancelot, C., Levasseur, M., Owens, N. P., Pollard, R., Rivkin, R. B., Sarmiento, J., Schoemann, V., Smetacek, V., Takeda, S., Tsuda, A., Turner, S., and Watson, A. J.: Mesoscale iron enrichment experiments 1993-2005: synthesis and future directions, *Science*, 315, 612-617, 10.1126/science.1131669, 2007.

Boyd, P. W., and Ellwood, M. J.: The biogeochemical cycle of iron in the ocean, *Nature Geoscience*, 3, 675-682, 10.1038/ngeo964, 2010.

Boyd, P. W., Iribanmi, E., Sander, S. G., Hunter, K. A., and Jackson, G. A.: Remineralization of upper ocean particles: Implications for iron biogeochemistry, *Limnology and Oceanography*, 55, 1271-1288, 10.4319/lm.2010.55.3.1271, 2010.

Boyd, P. W.: Toward quantifying the response of the oceans' biological pump to climate change, *Frontiers in Marine Science*, 2, 10.3389/fmars.2015.00077, 2015.

Boyd, P. W., Strzepek, R. F., Ellwood, M. J., Hutchins, D. A., Nodder, S. D., Twining, B. S., and Wilhelm, S. W.: Why are biotic iron pools uniform across high- and low-iron pelagic ecosystems?, *Global Biogeochemical Cycles*, 29, 1028-1043, 10.1002/2014gb005014, 2015.

Boyd, P. W., and Tagliabue, A.: Using the L* concept to explore controls on the relationship between paired ligand and dissolved iron concentrations in the ocean, *Marine Chemistry*, 173, 52-66, 10.1016/j.marchem.2014.12.003, 2015.

Boye, M., van den Berg, C. M. G., de Jong, J. T. M., Leach, H., Croot, P., and de Baar, H. J. W.: Organic complexation of iron in the Southern Ocean, *Deep Sea Research Part I: Oceanographic Research Papers*, 48, 1477-1497, 2001.

Boye, M., Aldrich, A. P., van den Berg, C. M. G., de Jong, J. T. M., Veldhuis, M., and de Baar, H. J. W.: Horizontal gradient of the chemical speciation of iron in surface waters of the northeast Atlantic Ocean, *Marine Chemistry*, 80, 129-143, 2003.

Boye, M., Aldrich, A., van den Berg, C. M. G., de Jong, J. T. M., Nirmaier, H., Veldhuis, M., Timmermans, K. R., and de Baar, H. J. W.: The chemical speciation of iron in the north-east Atlantic Ocean, *Deep Sea Research Part I: Oceanographic Research Papers*, 53, 667-683, 10.1016/j.dsr.2005.12.015, 2006.

Boye, M., Nishioka, J., Croot, P., Laan, P., Timmermans, K. R., Strass, V. H., Takeda, S., and de Baar, H. J. W.: Significant portion of dissolved organic Fe complexes in fact is Fe colloids, *Marine Chemistry*, 122, 20-27, 10.1016/j.marchem.2010.09.001, 2010.

Boyle, E. A., Bergquist, B. A., Kayser, R. A., and Mahowald, N.: Iron, manganese, and lead at Hawaii Ocean Time-series station ALOHA: Temporal variability and an intermediate water hydrothermal plume, *Geochimica et Cosmochimica Acta*, 69, 933-952, 10.1016/j.gca.2004.07.034, 2005.

Brand, L. E., Sunda, W. G., and Guillard, R. R. L.: Reduction in marine phytoplankton reproduction rates by copper and cadmium, *Journal of Experimental Marine Biology and Ecology*, 96, 225-250, 1986.

Breitbarth, E., Achterberg, E. P., Ardelan, M. V., Baker, A. R., Bucciarelli, E., Chever, F., Croot, P. L., Duggen, S., Gledhill, M., Hassellöv, M., Hassler, C., Hoffmann, L. J., Hunter, K. A., Hutchins, D. A., Ingri, J., Jickells, T., Lohan, M. C., Nielsdóttir, M. C., Sarthou, G., Schoemann, V., Trapp, J. M., Turner, D. R., and Ye, Y.: Iron biogeochemistry across marine systems at changing times – conclusions from the workshop held in Gothenburg, Sweden (14–16 May 2008), *Biogeosciences Discussions*, 7, 1075-1097, 2010.

Bressac, M., and Guieu, C.: Post-depositional processes: What really happens to new atmospheric iron in the ocean's surface?, *Global Biogeochemical Cycles*, 27, 859-870, 10.1002/gbc.20076, 2013.

Bressac, M., Guieu, C., Doxaran, D., Bourrin, F., Desboeufs, K., Leblond, N., and Ridame, C.: Quantification of the lithogenic carbon pump following a simulated dust-deposition event in large mesocosms, *Biogeosciences*, 11, 1007-1020, 10.5194/bg-11-1007-2014, 2014.

Brewer, P. G., Spencer, D. W., Biscaye, P. E., Hanley, A., Sachs, P. L., Smith, C. L., Kadar, S., and Fredericks, J.: The distribution of particulate matter in the Atlantic Ocean, *Earth and Planetary Science Letters*, 32, 393-402, 1976.

Brewin, R. J. W., Sathyendranath, S., Hirata, T., Lavender, S. J., Barciela, R. M., and Hardman-Mountford, N. J.: A three-component model of phytoplankton size class for the Atlantic Ocean, *Ecological Modelling*, 221, 1472-1483, 10.1016/j.ecolmodel.2010.02.014, 2010.

Brotas, V., Brewin, R. J. W., Sá, C., Brito, A. C., Silva, A., Mendes, C. R., Diniz, T., Kaufmann, M., Tarran, G., Groom, S. B., Platt, T., and Sathyendranath, S.: Deriving phytoplankton size classes from satellite data: Validation along a trophic gradient in the eastern Atlantic Ocean, *Remote Sensing of Environment*, 134, 66-77, 10.1016/j.rse.2013.02.013, 2013.

Bruland, K. W., Orians, K. J., and Cowen, J. P.: Reactive trace metals in the stratified central North Pacific, *Geochimica Et Cosmochimica Acta*, 58, 3171-3182, 1994.

Bruland, K. W., and Lohan, M. C.: The oceans and marine geochemistry, in: *Treatise on Geochemistry*, edited by: Elderfield, H., Elsevier, Amsterdam, 23-47, 2004.

Bruland, K. W., and Rue, E. L.: Analytical methods for the determination of concentrations and speciation of iron, in: *The biogeochemistry of iron in seawater*, edited by: Turner, D. R., and Hunter, K. A., John Wiley & Sons Ltd., 255-289, 2001.

Brzezinski, M. A., Jones, J. L., and Demarest, M. S.: Control of silica production by iron and silicic acid during the Southern Ocean Iron Experiment (SOFeX), *Limnology and Oceanography*, 50, 810-824, 2005.

Bucciarelli, E., Blain, S., and Treguer, P.: Iron and manganese in the wake of the Kerguelen Island (southern Ocean), *Marine Chemistry*, 73, 21-36, 2001.

Buck, C. S., Landing, W. M., Resing, J. A., and Measures, C. I.: The solubility and deposition of aerosol Fe and other trace elements in the North Atlantic Ocean: Observations from the A16N CLIVAR/CO2 repeat hydrography section, *Marine Chemistry*, 120, 57-70, 10.1016/j.marchem.2008.08.003, 2010.

Buck, K. N., and Bruland, K. W.: The physicochemical speciation of dissolved iron in the Bering Sea, Alaska, *Limnology and Oceanography*, 52, 1800-1808, 10.4319/lo.2007.52.5.1800, 2007.

Buck, K. N., Lohan, M. C., Berger, C. J. M., and Bruland, K. W.: Dissolved iron speciation in two distinct river plumes and an estuary: Implications for riverine iron supply, *Limnology and Oceanography*, 52, 843-855, 2007.

Buck, K. N., Moffett, J., Barbeau, K. A., Bundy, R. M., Kondo, Y., and Wu, J.: The organic complexation of iron and copper: an intercomparison of competitive ligand exchange-adsorptive cathodic stripping voltammetry (CLE-ACSV) techniques, *Limnology and Oceanography-Methods*, 10, 496-515, 10.4319/lom.2012.10.496, 2012.

Buck, K. N., Sohst, B., and Sedwick, P. N.: The organic complexation of dissolved iron along the U.S. GEOTRACES (GA03) North Atlantic Section, *Deep Sea Research Part II: Topical Studies in Oceanography*, 116, 152-165, 10.1016/j.dsr2.2014.11.016, 2015.

Buck, K. N., Bonnain, C., and Bundy, R. M.: Biogeochemical cycling of organic iron-binding ligands: Insights from GEOTRACES data in the Atlantic Ocean, *OCB NEWS*, 9, 6-11, 2016.

Buck, K. N., Sedwick, P. N., Sohst, B., and Carlson, C. A.: Organic complexation of iron in the eastern tropical South Pacific: Results from US GEOTRACES Eastern Pacific Zonal Transect (GEOTRACES cruise GP16), *Marine Chemistry*, 201, 229-241, 10.1016/j.marchem.2017.11.007, 2018.

Buffle, J.: The analytical challenge posed by fulvic and humic compounds, *Analytica Chimica Acta*, 232, 1-2, 1990.

Buffle, J., Wilkinson, K. J., Stoll, S., Filella, M., and Zhang, J.: A Generalized Description of Aquatic Colloidal Interactions: The Three-colloidal Component Approach, *Environmental Science & Technology*, 32, 2887-2899, 10.1021/es980217h, 1998.

Buitenhuis, E. T., Pangerc, T., Franklin, D. J., Le Quere, C., and Malin, G.: Growth rates of six coccolithophorid strains as a function of temperature, *Limnology and Oceanography*, 53, 1181-1185, 2008.

Bundy, R. M., Biller, D. V., Buck, K. N., Bruland, K. W., and Barbeau, K. A.: Distinct pools of dissolved iron-binding ligands in the surface and benthic boundary layer of the California Current, *Limnology and Oceanography*, 59, 769-787, 10.4319/lo.2014.59.3.0769, 2014.

Bundy, R. M., Abdulla, H. A. N., Hatcher, P. G., Biller, D. V., Buck, K. N., and Barbeau, K. A.: Iron-binding ligands and humic substances in the San Francisco Bay estuary and estuarine-influenced shelf regions of coastal California, *Marine Chemistry*, 173, 183-194, 10.1016/j.marchem.2014.11.005, 2015.

Bundy, R. M., Jiang, M., Carter, M., and Barbeau, K. A.: Iron-Binding Ligands in the Southern California Current System: Mechanistic Studies, *Frontiers in Marine Science*, 3, 10.3389/fmars.2016.00027, 2016.

Burd, A. B., Hansell, D. A., Steinberg, D. K., Anderson, T. R., Arístegui, J., Baltar, F., Beaupré, S. R., Buesseler, K. O., DeHairs, F., Jackson, G. A., Kadko, D. C., Koppelman, R., Lampitt, R. S., Nagata, T., Reinthaler, T., Robinson, C., Robison, B. H., Tamburini, C., and Tanaka, T.: Assessing the apparent imbalance between geochemical and biochemical indicators of meso- and bathypelagic biological activity: What the @\$#! is wrong with present calculations of carbon budgets?, *Deep Sea Research Part II: Topical Studies in Oceanography*, 57, 1557-1571, 10.1016/j.dsr2.2010.02.022, 2010.

Burd, A. B., Buchan, A., Church, M., Landry, M., McDonnell, A., Passow, U., Steinberg, D., and Benway, H.: Towards a transformative understanding of the biology of the ocean's biological pump: Priorities for future research, Report of the NSF Biology of the Biological Pump Workshop, Hyatt Place New Orleans, New Orleans, LA, 67, 2016.

Bury, S. J., Boyd, P. W., Preston, T., Savidge, G., and Owens, N. J. P.: Size-fractionated primary production and nitrogen uptake during a North Atlantic phytoplankton bloom: implications for carbon export estimates, *Deep sea research Part 1 Oceanographic research papers*, 48, 689-720, 10.1016/S0967-0637(00)00066-2, 2001.

Cabello, A. M., Cornejo-Castillo, F. M., Raho, N., Blasco, D., Vidal, M., Audic, S., de Vargas, C., Latasa, M., Acinas, S. G., and Massana, R.: Global distribution and vertical patterns of a prymnesiophyte-cyanobacteria obligate symbiosis, *ISME J*, 10, 693-706, 10.1038/ismej.2015.147, 2016.

Cáceres, C., Rivera, A., González, S., and Anadón, R.: Phytoplankton community structure and dynamics in the North Atlantic subtropical gyre, *Progress in Oceanography*, 151, 177-188, 10.1016/j.pocean.2016.12.003, 2017.

Caldeira, K., and Wickett, M. E.: Anthropogenic carbon and ocean pH, *Nature*, 425, 365, 10.1038/425365a, 2003.

Canário, J., Vale, C., Caetano, M., and Madureira, M. J.: Mercury in contaminated sediments and pore waters enriched in sulphate (Tagus Estuary, Portugal), *Environmental Pollution*, 126, 425-433, 10.1016/S0269-7491(03)00234-3, 2003.

Carpenter, J. H.: The accuracy of the Winkler method for dissolved oxygen analysis, *Limnology and Oceanography*, 10, 10.4319/lo.1965.10.1.0135, 1965.

Castellani, C., Irigoien, X., Mayor, D. J., Harris, R. P., and Wilson, D.: Feeding of *Calanus finmarchicus* and *Oithona similis* on the microplankton assemblage in the Irminger Sea, North Atlantic, *Journal of Plankton Research*, 30, 1095-1116, 10.1093/plankt/fbn074, 2008.

Charette, M. A., Morris, P. J., Henderson, P. B., and Moore, W. S.: Radium isotope distributions during the US GEOTRACES North Atlantic cruises, *Marine Chemistry*, 177, 184-195, 10.1016/j.marchem.2015.01.001, 2015.

Chase, Z., and Anderson, R. F.: Comment on "On the importance of opal, carbonate, and lithogenic clays in scavenging and fractionating Th-230, Pa-231 and Be-10 in the ocean" by S. Luo and T.-L. Ku, *Earth and Planetary Science Letters*, 220, 213-222, 2004.

Chase, Z., Johnson, K. S., Elrod, V. A., Plant, J. N., Fitzwater, S. E., Pickell, L., and Sakamoto, C. M.: Manganese and iron distributions off central California influenced by upwelling and shelf width, *Marine Chemistry*, 95, 235-254, 10.1016/j.marchem.2004.09.006, 2005.

Cheize, M.: Cycle biogéochimique du fer à l'interface Océan-Atmosphère : Spéciation organique du fer dans l'eau de pluie et son devenir après dépôt dans l'eau de mer, Doctorat de Chimie Marine, UMR 6539 - Institut Universitaire Européen de la Mer (IUEM) - Laboratoire de l'Environnement MARin (LEMAR), Université de Bretagne Occidentale (UBO), Ecole doctorale des Sciences de la Mer (EDSM), 2012.

Cheize, M., Sarthou, G., Croot, P. L., Bucciarelli, E., Baudoux, A. C., and Baker, A. R.: Iron organic speciation determination in rainwater using cathodic stripping voltammetry, *Anal Chim Acta*, 736, 45-54, 10.1016/j.aca.2012.05.011, 2012.

Cheize, M., Planquette, H. F., Fitzsimmons, J. N., Pelleter, E., Sherrell, R. M., Lambert, C., Bucciarelli, E., Sarthou, G., Le Goff, M., Liorzou, C., Chéron, S., Viollier, E., and Gayet, N.: Contribution of resuspended sedimentary particles to dissolved iron and manganese in the ocean: an experimental study, *Chemical Geology*, under review.

Chen, M., and Wang, W. X.: Bioavailability of natural colloid-bound iron to marine plankton: Influences of colloidal size and aging, *Limnology and Oceanography*, 46, 1956-1967, 2001.

Chen, M., Dei, R. C. H., Wang, W. X., and Guo, L. D.: Marine diatom uptake of iron bound with natural colloids of different origins, *Marine Chemistry*, 81, 177-189, 10.1016/S0304-4203(03)00032-X, 2003.

Chen, Y. J.: Influence of the Iceland mantle plume on crustal accretion at the inflated Reykjanes Ridge: Magma lens and low hydrothermal activity, *Journal of Geophysical Research*, 108, 2524, 2003.

Chester, R., Murphy, K. J. T., Lin, F. J., Berry, A. S., Bradshaw, G. A., and Corcoran, P. A.: Factors controlling the solubilities of trace-metals from nonremote aerosols deposited to the sea-surface by the dry deposition mode, *Marine Chemistry*, 42, 107-126, 10.1016/0304-4203(93)90241-f, 1993.

Chester, R., and Jickells, T. D.: *Marine Geochemistry*, 3rd ed., Wiley-Blackwell, 420 pp., 2012.

Chever, F.: Spéciation du fer en milieu océanique, interactions avec le phytoplancton, Doctorat de Chimie Marine, UMR 6539 - Institut Universitaire Européen de la Mer (IUEM) - Laboratoire de l'Environnement MARin (LEMAR), Université de Bretagne Occidentale (UBO), Ecole doctorale des Sciences de la Mer (EDSM), 186 pp., 2009.

Chever, F., Bucciarelli, E., Sarthou, G., Speich, S., Arhan, M., Penven, P., and Tagliabue, A.: Physical speciation of iron in the Atlantic sector of the Southern Ocean, along a transect from the subtropical domain to the Weddell Sea Gyre, *Journal of Geophysical Research*, 115, 1-15, 2010.

Chisholm, S. W.: Phytoplankton Size, in: *Primary Productivity and Biogeochemical Cycles in the Sea*, edited by: Falkowski, P. G., Woddedhead, A. D., and Vivirito, K., Environmental Science research, Springer, Boston, MA, 213-237, 1992.

Claustre, H.: The trophic status of various oceanic provinces as revealed by phytoplankton pigment signatures, *Limnology and Oceanography*, 39, 1206-1210, 1994.

Coale, K. H., Johnson, K. S., Chavez, F. P., Buesseler, K. O., Barber, R. T., Brzezinski, M. A., Cochlan, W. P., Millero, F. J., Falkowski, P. G., Bauer, J. E., Wanninkhof, R. H., Kudela, R. M., Altabet, M. A., Hales, B. E., Takahashi, T., Landry, M. R., Bidigare, R. R., Wang, X., Chase, Z., Strutton, P. G., Friederich, G. E., Gorbunov, M. Y., Lance, V. P., Hiltling, A. K., Hiscock, M. R., Demarest, M. S., Hiscock, W. T., Sullivan, K. F., Tanner, S. J., Gordon, R. M., Hunter, C. N., Elrod, V. A., Fitzwater, S. E., Jones, J. L., Tozzi, S., Koblizek, M., Roberts, A. E., Herndon, J., Brewster, J., Ladizinsky, D., Smith, G. J., Cooper, D., Timothy, D. A., Brown, S. L., Selph, K. E., Sheridan, C. C., Twining, B. S., and Johnson, Z. I.: Southern Ocean Iron Enrichment Experiment: carbon cycling in high- and low-Si waters, *Science*, 304, 408-414, 2004.

Cochlan, W. P., Wikner, J., Steward, G. F., Smith, D. C., and Azam, F.: Spatial distribution of viruses, bacteria and chlorophyll a in neritic, oceanic and estuarine environments, *Marine Ecology Progress Series*, 92, 77-87, 1993.

Coffin, M., Davies, H., and Haxby, W.: Structure of the Kerguelen Plateau province from SEASAT altimetry and seismic reflection data, *Nature*, 324, 134-136, 1986.

Coleman, M. L., Hedrick, D. B., Lovley, D. R., White, D. C., and Pye, K.: Reduction of Fe(III) in sediments by sulphate-reducing bacteria, *Nature*, 361, 436-438, 10.1038/361436a0, 1993.

Collier, R., and Edmond, J.: The Trace Element Geochemistry of marine Biogenic Particulate Matter, *Progress in Oceanography*, 13, 113-199, 1984.

Collos, Y.: Nitrate uptake, nitrite release and uptake, and new production estimates, *Marine Ecology Progress Series*, 171, 293-301, 1998.

Conway, T. M., Rosenberg, A. D., Adkins, J. F., and John, S. G.: A new method for precise determination of iron, zinc and cadmium stable isotope ratios in seawater by double-spike mass spectrometry, *Anal Chim Acta*, 793, 44-52, 10.1016/j.aca.2013.07.025, 2013.

Conway, T. M., and John, S. G.: Quantification of dissolved iron sources to the North Atlantic Ocean, *Nature*, 511, 212-215, 10.1038/nature13482, 2014.

Cooper, L. W., Whitledge, T. E., Grebmeier, J. M., and Weingartner, T.: The nutrient, salinity, and stable oxygen isotope composition of Bering and Chukchi Seas waters in and near the Bering Strait, *Journal of Geophysical Research*, 102, 512,563-512,573, 1997.

Cooper, L. W., McClelland, J. W., Holmes, R. M., Raymond, P. A., Gibson, J. J., Guay, C. K., and Peterson, B. J.: Flow-weighted values of runoff tracers ($\delta^{18}\text{O}$, DOC, Ba, alkalinity) from the six largest Arctic rivers, *Geophysical Research Letters*, 35, 1-5, 10.1029/2008GL035007, 2008.

Cota, G. F., Smith Jr., W. O., and Mitchell, B. G.: Photosynthesis of *Phaeocystis* in the Greenland Sea, *Limnology and Oceanography*, 39, 948-953, 1994.

Cota, G. F., Harrison, W. G., Platt, T., Sathyendranath, S., and Stuart, V.: Bio-optical properties of the Labrador Sea, *Journal of Geophysical Research*, 108, 1-21, 10.1029/2000jc000597, 2003.

Crane, K., Johnson, L., Appelgate, B., Nishimura, C., Buck, R., Jones, C., Vogt, P., and Kos'yan, R.: Volcanic and Seismic Swarm Events on the Reykjanes Ridge and Their Similarities to Events on Iceland: Results of a Rapid Response Mission, *Marine Geophysical Researches*, 19, 319-338, 1997.

Croft, M. T., Lawrence, A. D., Raux-Deery, E., Warren, M. J., and Smith, A. G.: Algae acquire vitamin B12 through a symbiotic relationship with bacteria, *Nature*, 438, 90-93, 10.1038/nature04056, 2005.

Croot, P. L., and Johansson, M.: Determination of iron speciation by Cathodic Stripping Voltammetry in seawater using the competing ligand 2-(2-Thiazolylazo)-*p*-cresol (TAC), *Electroanalysis*, 12, 565-576, 2000.

Croot, P. L., Andersson, K., Öztürk, M., and Turner, D. R.: The distribution and speciation of iron along 6°E in the Southern Ocean, Deep Sea Research Part II: Topical Studies in Oceanography, 51, 2857-2879, 10.1016/j.dsr2.2003.10.012, 2004.

Cullen, J. T., Bergquist, B. A., and Moffett, J. W.: Thermodynamic characterization of the partitioning of iron between soluble and colloidal species in the Atlantic Ocean, Marine Chemistry, 98, 295-303, 10.1016/j.marchem.2005.10.007, 2006.

Culley, A. I., and Welschmeyer, N. A.: The abundance, distribution, and correlation of viruses, phytoplankton, and prokaryotes along a Pacific Ocean transect, Limnology and Oceanography, 47, 1508-1513, 10.4319/lm.2002.47.5.1508 2002.

Cupp, E. E.: Marine Plankton Diatoms of the West Coast of North America, Bulletin of the scripps institution of oceanography, edited by: Sverdrup, H. U., Fleming, R. H., Miller, L. H., and ZoBell, C. E., University of California Press; Cambridge University Press, Berkeley, California; London, England, 1-238 pp., 1943.

Cutter, G., Casciotti, K., Croot, P., Geibert, W., Heimbürger, L. E., Lohan, M., Planquette, H., and van de Fliedert, T.: Sampling and the Sample-handling Protocols for GEOTRACES Cruises, 2017.

Cutter, G. A., and Bruland, K. W.: Rapid and noncontaminating sampling system for trace elements in global ocean surveys, Limnology and Oceanography-Methods, 10, 425-436, 10.4319/lom.2012.10.425, 2012.

d'Ovidio, F., De Monte, S., Alvain, S., Dandonneau, Y., and Levy, M.: Fluid dynamical niches of phytoplankton types, Proc Natl Acad Sci U S A, 107, 18366-18370, 10.1073/pnas.1004620107, 2010.

Dalbec, A. A., and Twining, B. S.: Remineralization of bioavailable iron by a heterotrophic dinoflagellate, Aquatic Microbial Ecology, 54, 279-290, 10.3354/ame01270, 2009.

Dam, H. G., and Drapeau, D. T.: Coagulation efficiency, organic-matter glues and the dynamics of particles during a phytoplankton bloom in a mesocosm study, Deep-sea Research II 42, 111-123, 1995.

Daniault, N., Mercier, H., Lherminier, P., Sarafanov, A., Falina, A., Zunino, P., Pérez, F. F., Ríos, A. F., Ferron, B., Huck, T., Thierry, V., and Gladyshev, S.: The northern North Atlantic Ocean mean circulation in the early 21st century, Progress in Oceanography, 146, 142-158, 10.1016/j.pocean.2016.06.007, 2016.

de Baar, H. J. W., de Jong, J. T. M., Bakker, D. C. E., Löscher, B. M., Veth, C., Bathmann, U., and Smetacek, V.: Importance of iron for plankton blooms and carbon dioxide drawdown in the Southern Ocean, Nature, 373, 412-415, 1995.

de Baar, H. J. W., Van Leeuwe, M. A., Scharek, R., Goeyens, L., Bakker, K. M. J., and Fritsche, P.: Nutrient anomalies in *Fragilariopsis kerguelensis* blooms, iron deficiency and the nitrate/phosphate ratio (A. C. Redfield) of the Antarctic Ocean, Deep-Sea Research Part II-Topical Studies in Oceanography, 44, 229+, 10.1016/s0967-0645(96)00102-6, 1997.

de Baar, H. J. W., de Jong, J. T. M., Nolting, R. F., Timmermans, K. R., Van Leeuwe, M. A., Bathmann, U., Van der Loeff, M. R., and Sildam, J.: Low dissolved Fe and the absence of diatom blooms in remote Pacific waters of the Southern Ocean, Marine Chemistry, 66, 1-34, 1999.

de Baar, H. J. W., and de Jong, J. T. M.: Distributions, Sources and Sinks of Iron in Seawater, in: The Biogeochemistry of Fe in Seawater, edited by: Turner, D. R., and Hunter, K. A., John Wiley & Sons Ltd, Baltimore, 2001.

de Baar, H. J. W., Boyd, P. W., Coale, K. H., Landry, M. R., Tsuda, A., Assmy, P., Bakker, D. C. E., Bozec, Y., Barber, R. T., Brzezinski, M. A., Buesseler, K. O., Boye, M., Croot, P. L., Gervais, F., Gorbunov, M. Y., Harrison, P. J., Hiscock, W. T., Laan, P., Lancelot, C., Law, C. S., Levasseur, M., Marchetti, A., Millero, F. J., Nishioka, J., Nojiri, Y., van Oijen, T., Riebesell, U., Rijkenberg, M. J. A., Saito, H., Takeda, S., Timmermans, K. R., Veldhuis, M. J. W., Waite, A. M., and Wong, C. S.: Synthesis of iron fertilization

experiments: From the iron age in the age of enlightenment, *Journal of Geophysical Research-Oceans*, 110, 10.1029/2004jc002601, 2005.

de Barros, M. C.: A case study of waste inputs in the Tagus estuary, in: *The role of the Oceans as a Waste Disposal Option*, edited by: Kullenberg, G., NATO ASI Series; Series C: Mathematical and Physical Sciences, 172, Springer Netherlands, 307-324, 1986.

de Jong, J., Schoemann, V., Maricq, N., Mattielli, N., Langhorne, P., Haskell, T., and Tison, J.-L.: Iron in land-fast sea ice of McMurdo Sound derived from sediment resuspension and wind-blown dust attributes to primary productivity in the Ross Sea, Antarctica, *Marine Chemistry*, 157, 24-40, 10.1016/j.marchem.2013.07.001, 2013.

de Jong, M. F., van Aken, H. M., Våge, K., and Pickart, R. S.: Convective mixing in the central Irminger Sea: 2002–2010, *Deep Sea Research Part I: Oceanographic Research Papers*, 63, 36-51, 10.1016/j.dsr.2012.01.003, 2012.

De La Rocha, C. L., and Passow, U.: Factors influencing the sinking of POC and the efficiency of the biological carbon pump, *Deep Sea Research Part II: Topical Studies in Oceanography*, 54, 639-658, 10.1016/j.dsr2.2007.01.004, 2007.

Dehairs, F., Shopova, D., Ober, S., Veth, C., and Goeyens, L.: Particulate barium stocks and oxygen consumption in the Southern Ocean mesopelagic water column during spring and early summer: Relationship with export production, *Deep Sea Research II*, 44, 497-516, 10.1016/S0967-0645(96)00072-0, 1997.

Demers, S., Roy, S., Gagnon, R., and Vignault, C.: Rapid light-induced changes in cell fluorescence and in xanthophyll-cycle pigments of *Alexandrium excavatum* (Dinophyceae) and *Thalassiosira pseudonana* (Bacillariophyceae): a photo-protection mechanism, *Marine Ecology Progress Series*, 76, 185-193, 1991.

Deng, F., Henderson, G. M., Castrillejo, M., and Perez, F. F.: Evolution of ²³¹Pa and ²³⁰Th in overflow waters of the North Atlantic, *Biogeosciences*, 1-24, 10.5194/bg-2018-191, 2018.

Deng, W., Cruz, B. N., and Neuer, S.: Effects of nutrient limitation on cell growth, TEP production and aggregate formation of marine *Synechococcus*, *Aquatic Microbial Ecology*, 78, 39-49, 10.3354/ame01803, 2016.

Denman, K. L., Brasseur, G., Chidthaisong, A., Ciais, P., Cox, P. M., Dickinson, R. E., Hauglustaine, D., Heinze, C., Holland, E., Jacob, D., Lohmann, U., Ramachandran, S., da Silva Dias, P. L., Wofsy, S. C., and Zhang, X.: Couplings between changes in the climate system and biogeochemistry, in: *Climate Change 2007: The Physical Science Basis. Contribution of Working Group I to the Fourth Assessment Report of the Intergovernmental Panel on Climate Change*, edited by: Solomon, S., Qin, D., Manning, M., Chen, Z., Marquis, M., Averyt, K. B., Tignor, M., and Miller, H. L., Cambridge University Press, Cambridge, United Kingdom and New York, NY, USA 2007.

Desboeufs, K., Leblond, N., Wagener, T., Bon Nguyen, E., and Guieu, C.: Chemical fate and settling of mineral dust in surface seawater after atmospheric deposition observed from dust seeding experiments in large mesocosms, *Biogeosciences*, 11, 5581-5594, 10.5194/bg-11-5581-2014, 2014.

Desboeufs, K. V., Sofikitis, A., Losno, R., Colin, J. L., and Ausset, P.: Dissolution and solubility of trace metals from natural and anthropogenic aerosol particulate matter, *Chemosphere*, 58, 195-203, 10.1016/j.chemosphere.2004.02.025, 2005.

Deutsch, C., Sarmiento, J. L., Sigman, D. M., Gruber, N., and Dunne, J. P.: Spatial coupling of nitrogen inputs and losses in the ocean, *Nature*, 445, 163–167, 2007.

Dierssen, H., Balzer, W., and Landing, W. M.: Simplified synthesis of an 8-hydroxyquinoline chelating resin and a study of trace metal profiles from Jellyfish Lake, Palau, *Marine Chemistry*, 73, 173-192, 10.1016/s0304-4203(00)00107-9, 2001.

Droop, M. R.: Auxotrophy and Organic Compounds in the Nutrition of Marine Phytoplankton, *Journal of general Microbiology*, 16, 286-293, 1957.

Duce, R. A., Liss, P. S., Merrill, J. T., Atlas, E. L., Buat-Menard, P., Hicks, B. B., Miller, J. M., Prospero, J. M., Arimoto, R., Church, T. M., Ellis, W., Galloway, J. N., Hansen, L., Jickells, T. D., Knap, A. H., Reinhardt, K. H., Schneider, B., Soudine, A., Tokos, J. J., Tsunogai, S., Wollast, R., and Zhou, M.: The atmospheric input of trace species to the world ocean, *Global Biogeochemical Cycle*, 5, 193-259, 10.1029/91GB01778, 1991.

Duce, R. A., and Tindale, N. W.: Atmospheric transport of iron and its deposition in the ocean, *Limnology and Oceanography*, 36, 1715-1726, 1991.

Ebersbach, F., Assmy, P., Martin, P., Schulz, I., Wolzenburg, S., and Nöthig, E.-M.: Particle flux characterisation and sedimentation patterns of protistan plankton during the iron fertilisation experiment LOHAFEX in the Southern Ocean, *Deep Sea Research Part I: Oceanographic Research Papers*, 89, 94-103, 10.1016/j.dsr.2014.04.007, 2014.

Egge, J. K., and Aksnes, G. L.: Silicate as regulating nutrient in phytoplankton competition, *Marine Ecology Progress Series*, 83, 281-289, 1992.

Elbaz-Poulichet, F., Cauwet, G., Guan, D. M., Faguet, D., Barlow, R., and Mantoura, R. F. C.: C18 Sep-Pak extractable trace metals in waters from the Gulf of Lions, *Marine Chemistry*, 46, 67-75, 10.1016/0304-4203(94)90046-9, 1994.

Elderfield, H., and Schultz, A.: Mid-Ocean Ridge Hydrothermal Fluxes and the Chemical Composition of the Ocean, *Annual Review of Earth and Planetary Sciences*, 24, 191-224, 10.1146/annurev.earth.24.1.191, 1996.

Ellwood, M. J.: Wintertime trace metal (Zn, Cu, Ni, Cd, Pb and Co) and nutrient distributions in the Subantarctic Zone between 40–52°S; 155–160°E, *Marine Chemistry*, 112, 107-117, 10.1016/j.marchem.2008.07.008, 2008.

Elrod, V. A., Berelson, W. M., Coale, K. H., and Johnson, K. S.: The flux of iron from continental shelf sediments: A missing source for global budgets, *Geophysical Research Letters*, 31, 1-4, 10.1029/2004GL020216, 2004.

Emery, W. J.: Water Types And Water Masses, in: *Encyclopedia of Ocean Sciences*, 3179-3187, 2001.

Engel, A., Thoms, S., Riebesell, U., Rochelle-Newall, E., and Zondervan, I.: Polysaccharide aggregation as a potential sink of marine dissolved organic carbon, *Nature*, 428, 929-932, 10.1038/nature02506, 2004.

Eppley, R. W., Rogers, J. N., and McCarthy, J. J.: Half-saturation constants for uptake of nitrate and ammonium by marine phytoplankton, *Limnology and Oceanography* 14, 912-920, 1969.

Eppley, R. W., and Thomas, W. H.: Comparison of half-saturation constants for growth and nitrate uptake of marine phytoplankton, *Journal of Phycology*, 5, 375-379, 1969.

Eppley, R. W., and Peterson, B. J.: Particulate organic matter flux and planktonic new production in the deep ocean *Nature*, 282, 677-680, 1979.

Eppley, R. W.: Chlorophyll, photosynthesis and new production in the Southern California Bight, *Progress in Oceanography*, 30, 117-150, 1992.

Fagel, N., Robert, C., and Hilaire-Marcel, C.: Clay mineral signature of the NW Atlantic Boundary Undercurrent, *Marine Geology*, 130, 19-28, 1996.

Fagel, N., Robert, C., Preda, M., and Thorez, J.: Smectite composition as a tracer of deep circulation: the case of the Northern North Atlantic, *Marine Geology*, 172, 309-330, 2001.

Falkowski, P. G., Laws, E. A., Barber, R. T., and Murray, J. W.: Phytoplankton and Their Role in Primary, New and Export Production, in: *Ocean Biogeochemistry. The Role of the Ocean Carbon Cycle in Global Change*, edited by: Fasham, M. J. R., Springer, Berlin, Germany, 99-121, 2003.

Falkowski, P. G., Katz, M. E., Knoll, A. H., Quigg, A., Raven, J. A., Schofield, O., and Taylor, F. J.: The evolution of modern eukaryotic phytoplankton, *Science*, 305, 354-360, 10.1126/science.1095964, 2004.

Fan, S.-M., Moxim, W. J., and Levy, H.: Aeolian input of bioavailable iron to the ocean, *Geophysical Research Letters*, 33, 10.1029/2005gl024852, 2006.

Feng, Y., Hare, C. E., Leblanc, K., Rose, J. M., Zhang, Y., DiTullio, G. R., Lee, P. A., Wilhelm, S. W., Rowe, J. M., Sun, J., Nemcek, N., Gueguen, C., Passow, U., Benner, I., Brown, C., and Hutchins, D. A.: Effects of increased pCO₂ and temperature on the North Atlantic spring bloom. I. The phytoplankton community and biogeochemical response, *Marine Ecology Progress Series*, 388, 13-25, 10.3354/meps08133, 2009.

Ferron, B., Kokoszka, F., Mercier, H., Lherminier, P., Huck, T., Rios, A., and Thierry, V.: Variability of the Turbulent Kinetic Energy Dissipation along the A25 Greenland–Portugal Transect Repeated from 2002 to 2012, *Journal of Physical Oceanography*, 46, 1989-2003, 10.1175/jpo-d-15-0186.1, 2016.

Figueres, G., Martin, J. M., Meybeck, M., and Seyler, P.: A comparative study of mercury contamination in the Tagus estuary (Portugal) and major French estuaries (Gironde, Loire, Rhone), *Estuarine, Coastal and Shelf Science*, 20, 183-203, 1985.

Fischer, H., Siggaard-Andersen, M.-L., Ruth, U., Röthlisberger, R., and Wolff, E.: Glacial/interglacial changes in mineral dust and sea-salt records in polar ice cores: Sources, transport, and deposition, *Reviews of Geophysics*, 45, 10.1029/2005rg000192, 2007.

Fishwick, M. P., Sedwick, P. N., Lohan, M. C., Worsfold, P. J., Buck, K. N., Church, T. M., and Ussher, S. J.: The impact of changing surface ocean conditions on the dissolution of aerosol iron, *Global Biogeochemical Cycles*, 28, 1235-1250, 10.1002/2014gb004921, 2014.

Fitzsimmons, J. N., and Boyle, E. A.: Assessment and comparison of Anopore and cross flow filtration methods for the determination of dissolved iron size fractionation into soluble and colloidal phases in seawater, *Limnology and Oceanography-Methods*, 12, 246-263, 10.4319/lom.2014.12.246, 2014a.

Fitzsimmons, J. N., and Boyle, E. A.: Both soluble and colloidal iron phases control dissolved iron variability in the tropical North Atlantic Ocean, *Geochimica et Cosmochimica Acta*, 125, 539-550, 10.1016/j.gca.2013.10.032, 2014b.

Fitzsimmons, J. N., Boyle, E. A., and Jenkins, W. J.: Distal transport of dissolved hydrothermal iron in the deep South Pacific Ocean, *Proc Natl Acad Sci U S A*, 111, 16654-16661, 10.1073/pnas.1418778111, 2014.

Fitzsimmons, J. N., John, S. G., Marsay, C. M., Hoffman, C., Nicholas, S., Toner, B. M., German, C. R., and Sherrell, R. M.: Iron persistence in a distal hydrothermal plume supported by dissolved-particulate exchange, *Nature Geoscience*, 10, 195-201, 10.1038/ngeo2900, 2017.

Fiuza, A.: Hidrologia e dinamica das aguas costeiras de Portugal, Ph. D., Universidade de Lisboa, Lisboa, Portugal, unpublished, 1984.

Floor, G. H., Clough, R., Lohan, M. C., Ussher, S. J., Worsfold, P. J., and Quetel, C. R.: Combined uncertainty estimation for the determination of the dissolved iron amount content in seawater using flow injection with chemiluminescence detection, *Limnology and Oceanography-Methods*, 13, 673-686, 10.1002/lom3.10057, 2015.

Fogg, G. E.: Tansley Review No. 30 The phytoplanktonic ways of life, *New Phytologist*, 118, 191-232, 1991.

Follows, M., and Dutkiewicz, S.: Meteorological modulation of the North Atlantic Spring Bloom, *Deep Sea Research Part II: Topical Studies in Oceanography*, 49, 321-344, 2001.

- Fowler, S. W., and Knauer, G. A.: Role of large particles in the transport of elements and organic compounds through the oceanic water column, *Progress in Oceanography*, 16, 147-194, 1986.
- Fox-Kemper, B., Ferrari, R., and Hallberg, R.: Parameterization of Mixed Layer Eddies. Part I: Theory and Diagnosis, *Journal of Physical Oceanography*, 38, 1145-1165, 10.1175/2007jpo3792.1, 2008.
- Francois, R., Honjo, S., Krishfield, R., and Manganini, S.: Factors controlling the flux of organic carbon to the bathypelagic zone of the ocean, *Global Biogeochemical Cycles*, 16, 34-31-34-20, 10.1029/2001gb001722, 2002.
- Frankignoulle, M., Canon, C., and Gattudo, J.-P.: Marine calcification as a source of carbon dioxide : Positive deedback of increasing atmospheric CO₂, *Limnology and Oceanography*, 39, 458-462, 1994.
- Frew, R. D., Hutchins, D. A., Nodder, S., Sanudo-Wilhelmy, S., Tovar-Sanchez, A., Leblanc, K., Hare, C. E., and Boyd, P. W.: Particulate iron dynamics during FeCycle in subantarctic waters southeast of New Zealand, *Global Biogeochemical Cycles*, 20, n/a-n/a, 10.1029/2005gb002558, 2006.
- Fung, I. Y., Meyn, S. K., Tegen, I., Doney, S. C., John, J. G., and Bishop, J. K. B.: Iron supply and demand in the upper ocean, *Global Biogeochemical Cycles*, 14, 281-295, 10.1029/1999gb900059, 2000.
- Gaillardet, J., Viers, J., and Dupre, B.: 7.7 – Trace elements in river waters, in: *Treatise on Geochemistry*, 2nd ed., edited by: Turekian, H. D. H. K., Elsevier, Oxford, 195-235, 2014.
- Gallant, R. M., and Von Damm, K. L.: Geochemical controls on hydrothermal fluids from the Kairei and Edmond Vent Fields, 23°-25°S, Central Indian Ridge, *Geochemistry, Geophysics, Geosystems*, 7, n/a-n/a, 10.1029/2005gc001067, 2006.
- García-Ibáñez, M. I., Pardo, P. C., Carracedo, L. I., Mercier, H., Lherminier, P., Ríos, A. F., and Pérez, F. F.: Structure, transports and transformations of the water masses in the Atlantic Subpolar Gyre, *Progress in Oceanography*, 135, 18-36, 10.1016/j.pocean.2015.03.009, 2015.
- García-Ibáñez, M. I., Pérez, F. F., Lherminier, P., Zunino, P., Mercier, H., and Tréguer, P.: Water mass distributions and transports for the 2014 GEOVIDE cruise in the North Atlantic, *Biogeosciences*, 15, 2075-2090, 10.5194/bg-15-2075-2018, 2018.
- García-Ibáñez, M. I., Pérez, F. F., Lherminier, P., Zunino, P., and Tréguer, P.: Water mass distributions and transports for the 2014 GEOVIDE cruise in the North Atlantic, *Biogeosciences*, this issue.
- Garçon, V. C., Oschlies, A., Doney, S. C., McGillicuddy, D., and Waniek, J.: The role of mesoscale variability on plankton dynamics in the North Atlantic, *Deep-Sea Research II*, 48, 2199-2226, 2001.
- Gartman, A., Findlay, A. J., and Luther III, G. W.: Nanoparticulate pyrite and other nanoparticles are a widespread component of hydrothermal vent black smoker emissions, *Chemical Geology*, 366, 32-41, 2014.
- Gaudencio, M. J., Guerra, M. T., and Glemarec, M.: Recherches biosédimentaires sur la zone maritime de l'estuaire du Tage, Portugal: donnees sedimentaires preliminaires. , in: *Estuaries and Coasts: Spatial and Temporal Intercomparisons*, edited by: Elliot, M., and Ducrottoy, J. C., Olsen and Olsen, Fredensborg, 11-16, 1991.
- Geider, R., and La Roche, J.: Redfield revisited: variability of C:N:P in marine microalgae and its biochemical basis, *European Journal of Phycology*, 37, 1-17, 10.1017/s0967026201003456, 2002.
- Geider, R. J., Laroche, J., Greene, R. M., and Olaizola, M.: Response of the photosynthetic apparatus of *Phaeodactylum tricornutum* (Bacillariophyceae) to nitrate, phosphate, or iron starvation, *Journal of Phycology*, 29, 755-766, 1993.
- Genovese, C., Grotti, M., Pittaluga, J., Ardini, F., Janssens, J., Wuttig, K., Moreau, M., and Lannuzel, D.: Influence of organic complexation on dissolved iron distribution in East Antarctic pack ice, *Marine Chemistry*, 10.1016/j.marchem.2018.04.005, 2018.

German, C. R., Campbell, A. C., and Edmond, J. M.: Hydrothermal scavenging at the Mid-Atlantic Ridge: modification of trace element dissolved fluxes, *Earth and Planetary Science Letters*, 107, 101-114, 1991.

German, C. R., Briem, J., Chin, C. S., Danielsen, M., Holland, S., James, R. H., Jonsdottir, A., Ludford, E., Moser, C., Olafsson, J., Palmer, M. R., and Rudnicki, M. D.: Hydrothermal activity on the Reykjanes Ridge: the Steinahóll vent-field at 63°06'N, *Earth and Planetary Science Letters*, 121, 647-654, 1994.

German, C. R., and Seyfried, W. E.: 8.7 – Hydrothermal processes, in: *Treatise on Geochemistry*, edited by: Turekian, H. D. H. K., Elsevier, Oxford, 191-233, 2014.

German, C. R., Casciotti, K. A., Dutay, J. C., Heimbürger, L. E., Jenkins, W. J., Measures, C. I., Mills, R. A., Obata, H., Schlitzer, R., Tagliabue, A., Turner, D. R., and Whitby, H.: Hydrothermal impacts on trace element and isotope ocean biogeochemistry, *Philos Trans A Math Phys Eng Sci*, 374, 10.1098/rsta.2016.0035, 2016.

Gerringa, L. J. A., Herman, P. M. J., and Poortvliet, T. C. W.: Comparison of the linear Van den Berg/Ruzic transformation and a non-linear fit of the Langmuir isotherm applied to Cu speciation data in the estuarine environment, *Marine Chemistry*, 48, 131-142, 1995.

Gerringa, L. J. A., Veldhuis, M. J. W., Timmermans, K. R., Sarthou, G., and de Baar, H. J. W.: Co-variance of dissolved Fe-binding ligands with phytoplankton characteristics in the Canary Basin, *Marine Chemistry*, 102, 276-290, 10.1016/j.marchem.2006.05.004, 2006.

Gerringa, L. J. A., Rijkenberg, M. J. A., Wolterbeek, H. T., Verburg, T. G., Boye, M., and de Baar, H. J. W.: Kinetic study reveals weak Fe-binding ligand, which affects the solubility of Fe in the Scheldt estuary, *Marine Chemistry*, 103, 30-45, 10.1016/j.marchem.2006.06.002, 2007.

Gerringa, L. J. A., Blain, S., Laan, P., Sarthou, G., Veldhuis, M. J. W., Brussaard, C. P. D., Viollier, E., and Timmermans, K. R.: Fe-binding dissolved organic ligands near the Kerguelen Archipelago in the Southern Ocean (Indian sector), *Deep Sea Research Part II: Topical Studies in Oceanography*, 55, 606-621, 10.1016/j.dsr2.2007.12.007, 2008.

Gerringa, L. J. A., Alderkamp, A.-C., Laan, P., Thuroczy, C.-E., De Baar, H. J. W., Mills, M. M., van Dijken, G. L., van Haren, H., and Arrigo, K. R.: Iron from melting glaciers fuels the phytoplankton blooms in Amundsen Sea (Southern Ocean): Iron biogeochemistry, *Deep-Sea Research Part II-Topical Studies in Oceanography*, 71-76, 16-31, 10.1016/j.dsr2.2012.03.007, 2012.

Gerringa, L. J. A., Rijkenberg, M. J. A., Schoemann, V., Laan, P., and de Baar, H. J. W.: Organic complexation of iron in the West Atlantic Ocean, *Marine Chemistry*, 177, 434-446, 10.1016/j.marchem.2015.04.007, 2015.

Gerringa, L. J. A., Slagter, H. A., Bown, J., van Haren, H., Laan, P., de Baar, H. J. W., and Rijkenberg, M. J. A.: Dissolved Fe and Fe-binding organic ligands in the Mediterranean Sea – GEOTRACES G04, *Marine Chemistry*, 194, 100-113, 10.1016/j.marchem.2017.05.012, 2017.

Gibb, S. W., Cummings, D. G., Irigoien, X., Barlow, R. G., Fauzi, R., and Montoura, C.: Phytoplankton pigment chemotaxonomy of the northeastern Atlantic, *Deep-Sea Research II*, 48, 795-823, 2001.

Giering, A. L. C., Sanders, R., Lampitt, R. S., Anderson, T. R., Tamburini, C., Boutrif, M., Zubkov, M. V., Marsay, C. M., Henson, S. A., Saw, K., Cook, K., and Mayor, D. J.: Reconciliation of the carbon budget in the ocean's twilight zone, *Nature*, 507, 480-483, 2014.

Giering, S. L. C., Steigenberger, S., Achterberg, E. P., Sanders, R., and Mayor, D. J.: Elevated iron to nitrogen recycling by mesozooplankton in the Northeast Atlantic Ocean, *Geophysical Research Letters*, 39, n/a-n/a, 10.1029/2012gl051776, 2012.

Gieskes, W. W. C., Kraay, G. W., Nontji, A., Setiapermana, D., and Sutomo: Moosoonal alternation of a mixed and a layered structure in the phytoplankton of the euphotic zone of the banda sea (Indonesia): a mathematical analysis of algal pigment fingerprints, *Netherlands Journal of Sea Research*, 22, 123-137, 1988.

Ginoux, P., Prospero, J. M., Gill, T. E., Hsu, N. C., and Zhao, M.: Global-scale attribution of anthropogenic and natural dust sources and their emission rates based on MODIS Deep Blue aerosol products, *Reviews of Geophysics*, 50, 10.1029/2012rg000388, 2012.

Giraudeau, J., Hulot, V., Hanquiez, V., Devaux, L., Howa, H., and Garlan, T.: A survey of the summer coccolithophore community in the western Barents Sea, *Journal of Marine Systems*, 158, 93-105, 10.1016/j.jmarsys.2016.02.012, 2016.

Gledhill, M., and Van Den Berg, C. M. G.: Determination of complexation of iron(III) with natural organic complexing ligands in seawater using cathodic stripping voltammetry, *Marine Chemistry*, 47, 41-54, 10.1016/0304-4203(94)90012-4, 1994.

Gledhill, M., and van den Berg, C. M. G.: Measurement of the redox speciation of iron in seawater by catalytic cathodic stripping voltammetry, *Marine Chemistry*, 50, 51-61, 1995.

Gledhill, M., and Buck, K. N.: The organic complexation of iron in the marine environment: a review, *Front Microbiol*, 3, 69, 10.3389/fmicb.2012.00069, 2012.

Gobler, C. J., Donat, J. R., Consolvo III, J. A., and Sanudo-Wilhelmy, S. A.: Physicochemical speciation of iron during coastal algal blooms, *Marine Chemistry*, 77, 71-89, 2002.

Gonzalez-Davila, M., Santana-Casiano, J. M., and Millero, F. J.: Oxidation of iron(II) nanomolar with H₂O₂ in seawater, *Geochimica Et Cosmochimica Acta*, 69, 83-93, 10.1016/j.gca.2004.05.043, 2005.

Gordon, R. M., Martin, J. H., and Knauer, G. A.: Iron in northeast Pacific waters, *Nature*, 299, 611-612, 10.1038/299611a0, 1982.

Gordon, R. M., Johnson, K. S., and Coale, K. H.: The behaviour of iron and other trace elements during the IronEx-I and PlumEx experiments in the Equatorial Pacific, *Deep Sea Research Part II: Topical Studies in Oceanography*, 45, 995-1041, 1998a.

Gordon, R. M., Johnson, K. S., and Coale, K. H.: The behaviour of iron and other trace elements during the IronEx-I and PlumEx experiments in the Equatorial Pacific, *Deep-Sea Research Part II-Topical Studies in Oceanography*, 45, 995-1041, 10.1016/s0967-0645(98)00012-5, 1998b.

Gourain, A., Planquette, H., Cheize, M., Menzel-Barraqueta, J. L., Boutorh, J., Shelley, R. U., Pereira-Contreira, L., Lemaitre, N., Lacan, F., Lherminier, P., and Sarthou, G.: particulate trace metals along the GEOVIDE section, *Biogeosciences*, 2018.

Arctic Research on Thin Ice: Consequences of Arctic Sea Ice Loss:
<https://eos.org/project-updates/arctic-research-on-thin-ice-consequences-of-arctic-sea-ice-loss>, access: June 4th, 2016.

Gregg, W. W., and Casey, N. W.: Modeling coccolithophores in the global oceans, *Deep Sea Research Part II: Topical Studies in Oceanography*, 54, 447-477, 10.1016/j.dsr2.2006.12.007, 2007.

Grotti, M., Soggia, F., Ianni, C., and Frache, R.: Trace metals distributions in coastal sea ice of Terra Nova Bay, Ross Sea, Antarctica, *Antarctic Science*, 17, 289-300, 10.1017/s0954102005002695, 2005.

Gruber, N., and Sarmiento, J. L.: Global patterns of marine nitrogen fixation and denitrification, *Global Biogeochemical Cycles*, 11, 235-266, 10.1029/97gb00077, 1997.

Gruber, N., Gloor, M., Mikaloff Fletcher, S. E., Doney, S. C., Dutkiewicz, S., Follows, M. J., Gerber, M., Jacobson, A. R., Joos, F., Lindsay, K., Menemenlis, D., Mouchet, A., Müller, S. A., Sarmiento, J. L., and Takahashi, T.: Oceanic sources, sinks, and transport of atmospheric CO₂, *Global Biogeochemical Cycles*, 23, n/a-n/a, 10.1029/2008gb003349, 2009.

Guéguen, C., Belin, C., Thomas, B. A., Monna, F., Favarger, P.-Y., and Dominik, J.: The effect of freshwater UV-irradiation prior to resin preconcentration of trace metals, *Analytica Chimica Acta*, 386, 155-159, 1999.

Guerzoni, S., Chester, R., Dulac, F., Herut, B., Loye-Pilot, M.-D., Measures, C., Migon, C., Molinaroli, E., Moulin, C., Rossini, P., Saydam, C., Soudine, A., and Ziveri, P.: The role of atmospheric deposition in the biogeochemistry of the Mediterranean Sea, *Progress in Oceanography*, 44, 147-190, 1999.

Guidi, L., Steadman, L., Jackson, G. A., Inabaz, F., Claustre, H., Legendre, L., Picheral, M., and Gorsky, G.: Effects of phytoplankton community on production, size and export of large aggregates: A world-ocean analysis, *Limnology and Oceanography*, 54, 1951-1963, 2009.

Guieu, C.: Vertical particle flux in the northeast Atlantic Ocean (POMME experiment), *Journal of Geophysical Research*, 110, 10.1029/2004jc002672, 2005.

Guieu, C., Loye-Pilot, M. D., Benyahya, L., and Dufour, A.: Spatial variability of atmospheric fluxes of metals (Al, Fe, Cd, Zn and Pb) and phosphorus over the whole Mediterranean from a one-year monitoring experiment: Biogeochemical implications, *Marine Chemistry*, 120, 164-178, 10.1016/j.marchem.2009.02.004, 2010.

Guieu, C., Aumont, O., Paytan, A., Bopp, L., Law, C. S., Mahowald, N., Achterberg, E. P., Marañón, E., Salihoglu, B., Crise, A., Wagener, T., Herut, B., Desboeufs, K., Kanakidou, M., Olgun, N., Peters, F., Pulido-Villena, E., Tovar-Sanchez, A., and Völker, C.: The significance of the episodic nature of atmospheric deposition to Low Nutrient Low Chlorophyll regions, *Global Biogeochemical Cycles*, 28, 1179-1198, 10.1002/2014gb004852, 2014.

Hand, J. L., Mahowald, N. M., Chen, Y., Siefert, R. L., and Luo, C.: Estimates of atmospheric processed soluble iron from observations and a global mineral aerosol model: biogeochemical implications, *Journal of Geophysical Research: Atmospheres*, 109, D17205, 2004.

Hansell, D.: Marine Dissolved Organic Matter and the Carbon Cycle, *Oceanography*, 14, 41-49, 10.5670/oceanog.2001.05, 2001.

Harrison, W. G., and Li, W. K. W.: Phytoplankton growth and regulation in the Labrador Sea: light and nutrient limitation, *Journal of Northwest Atlantic Fishery Science*, 39, 71-82, 10.2960/J.v39.m592, 2008.

Harrison, W. G., Yngve Børshheim, K., Li, W. K. W., Maillet, G. L., Pepin, P., Sakshaug, E., Skogen, M. D., and Yeats, P. A.: Phytoplankton production and growth regulation in the Subarctic North Atlantic: A comparative study of the Labrador Sea-Labrador/Newfoundland shelves and Barents/Norwegian/Greenland seas and shelves, *Progress in Oceanography*, 114, 26-45, 10.1016/j.pocean.2013.05.003, 2013.

Hart, T. J.: Phytoplankton periodicity in Antarctic surface water, University of California, 1-268, 1942.

Hassler, C. S., and Schoemann, V.: Discriminating between intra- and extracellular metals using chemical extractions: an update on the case of iron, *Limnology and Oceanography-Methods*, 7, 479-489, 2009.

Hassler, C. S., Alasonati, E., Mancuso Nichols, C. A., and Slaveykova, V. I.: Exopolysaccharides produced by bacteria isolated from the pelagic Southern Ocean: role in Fe binding, chemical reactivity, and bioavailability, *Marine Chemistry*, 123, 88-98, 2011a.

Hassler, C. S., Alasonati, E., Mancuso Nichols, C. A., and Slaveykova, V. I.: Exopolysaccharides produced by bacteria isolated from the pelagic Southern Ocean — Role in Fe binding, chemical reactivity, and bioavailability, *Marine Chemistry*, 123, 88-98, 10.1016/j.marchem.2010.10.003, 2011b.

Hassler, C. S., Schoemann, V., Nichols, C. M., Butler, E. C., and Boyd, P. W.: Saccharides enhance iron bioavailability to Southern Ocean phytoplankton, *Proc Natl Acad Sci U S A*, 108, 1076-1081, 10.1073/pnas.1010963108, 2011c.

Hassler, C. S., Schoemann, V., Nichols, C. M., Butler, E. C. V., and Boyd, P. W.: Saccharides enhance iron availability to Southern Ocean phytoplankton, *Proceedings of the National Academy of Sciences of the United States of America*, 108, 1076-1081, 2011d.

Hassler, C. S., Sinoir, M., Clementson, L. A., and Butler, E. C.: Exploring the Link between Micronutrients and Phytoplankton in the Southern Ocean during the 2007 Austral Summer, *Front Microbiol*, 3, 202, 10.3389/fmicb.2012.00202, 2012.

Hassler, C. S., Norman, L., Mancuso Nichols, C. A., Clementson, L. A., Robinson, C., Schoemann, V., Watson, R. J., and Doblin, M. A.: Iron associated with exopolymeric substances is highly bioavailable to oceanic phytoplankton, *Marine Chemistry*, 173, 136-147, 10.1016/j.marchem.2014.10.002, 2015.

Hatta, M., Measures, C. I., Wu, J., Roshan, S., Fitzsimmons, J. N., Sedwick, P., and Morton, P.: An overview of dissolved Fe and Mn distributions during the 2010-2011 US GEOTRACES north Atlantic cruises: GEOTRACES GA03, Deep-Sea Research Part II-Topical Studies in Oceanography, 116, 117-129, 10.1016/j.dsr2.2014.07.005, 2015.

Hatun, H., Azetsu-Scott, K., Somavilla, R., Rey, F., Johnson, C., Mathis, M., Mikolajewicz, U., Coupel, P., Tremblay, J. E., Hartman, S., Pacariz, S. V., Salter, I., and Olafsson, J.: The subpolar gyre regulates silicate concentrations in the North Atlantic, *Scientific Reports*, 7, 1-9, 10.1038/s41598-017-14837-4, 2017.

Hawkings, J., Wadham, J., Tranter, M., Telling, J., Bagshaw, E., Beaton, A., Simmons, S.-L., Chandler, D., Tedstone, A., and Nienow, P.: The Greenland Ice Sheet as a hot spot of phosphorus weathering and export in the Arctic, *Global Biogeochemical Cycles*, 30, 191-210, 10.1002/2015gb005237, 2016.

Hawkings, J. R., Wadham, J. L., Tranter, M., Raiswell, R., Benning, L. G., Statham, P. J., Tedstone, A., Nienow, P., Lee, K., and Telling, J.: Ice sheets as a significant source of highly reactive nanoparticulate iron to the oceans, *Nature communications*, 5, 1-8, 10.1038/ncomms4929, 2014.

Hawkings, J. R., Wadham, J. L., Tranter, M., Lawson, E., Sole, A., Cowton, T., Tedstone, A. J., Bartholomew, I., Nienow, P., Chandler, D., and Telling, J.: The effect of warming climate on nutrient and solute export from the Greenland Ice Sheet, *Geochemical Perspectives Letters*, 94-104, 10.7185/geochemlet.1510, 2015.

Hegarty, S. G., and Villareal, T. A.: Effects of light level and N:P supply ratio on the competition between *Pheocystis* cf. *pouchetii* (Hariot) Lagerheim (Prymnesiophyceae) and five diatom species, *Journal of Experimental Marine Biology and Ecology*, 226, 241-258, 1998.

Heller, M. I., Lam, P. J., Moffett, J. W., Till, C. P., Lee, J.-M., Toner, B. M., and Marcus, M. A.: Accumulation of Fe oxyhydroxides in the Peruvian oxygen deficient zone implies non-oxygen dependent Fe oxidation, *Geochimica et Cosmochimica Acta*, 211, 174-193, 10.1016/j.gca.2017.05.019, 2017.

Henson, S. A., Sanders, R., Holeton, C., and Allen, J. T.: Timing of nutrient depletion, diatom dominance and a lower-boundary estimate of export production for Irminger Basin, North Atlantic, *Marine Ecology Progress Series*, 313, 73-84, 10.3354/meps313073, 2006.

Henson, S. A., Dunne, J. P., and Sarmiento, J. L.: Decadal variability in North Atlantic phytoplankton blooms, *Journal of Geophysical Research*, 114, 10.1029/2008jc005139, 2009.

Ho, T.-Y., Quigg, A., Finkel, Z. V., Milligan, A. J., Wyman, K., Falkowski, P. G., and Morel, F. M. M.: The elemental composition of some marine phytoplankton, *Journal of Phycology*, 39, 1145-1159, 2003.

Ho, T.-Y.: Nickel limitation of nitrogen fixation in *Trichodesmium*, *Limnology and Oceanography*, 58, 112-120, 10.4319/lo.2013.58.1.0112, 2013.

Hoffmann, L. J., Peeken, I., Lochte, K., Assmy, P., and Veldhuis, M.: Different reactions of Southern Ocean phytoplankton size classes to iron fertilization, *Limnology and Oceanography*, 51, 1217-1229, 2006.

Hoffmann, L. J., Peeken, I., and Lochte, K.: Iron, silicate, and light co-limitation of three Southern Ocean diatom species, *Polar Biology*, 31, 1067-1080, 10.1007/s00300-008-0448-6, 2008.

Holmes, T. M., Chase, Z., van der Merwe, P., Townsend, A. T., and Bowie, A. R.: Detection, dispersal and biogeochemical contribution of hydrothermal iron in the ocean, *Marine and Freshwater Research*, 68, 10.1071/mf16335, 2017.

Holmes, T. M., Wuttig, K., Chase, Z., van der Merwe, P., Townsend, A. T., Schallenberg, C., Tonnard, M., and Bowie, A. R.: Iron availability influences nutrient drawdown in the Heard and McDonald Island region, Southern Ocean, in prep.

Homann, V., Edwards, K., Webb, E., and Butler, A.: Siderophores of *Marinobacter aquaeolei*: petrobactin and its sulfonated derivatives, *BioMetals*, 22, 565-571, 2009.

Homoky, W. B., Hembury, D. J., Hepburn, L. E., Mills, R. A., Statham, P. J., Fones, G. R., and Palmer, M. R.: Iron and manganese diagenesis in deep sea volcanogenic sediments and the origins of pore water colloids, *Geochimica Et Cosmochimica Acta*, 75, 5032-5048, 10.1016/j.gca.2011.06.019, 2011.

Homoky, W. B., John, S. G., Conway, T. M., and Mills, R. A.: Distinct iron isotopic signatures and supply from marine sediment dissolution, *Nature Communications*, 4, 10.1038/ncomms3143, 2013.

Homoky, W. B., Weber, T., Berelson, W. M., Conway, T. M., Henderson, G. M., van Hulten, M., Jeandel, C., Severmann, S., and Tagliabue, A.: Quantifying trace element and isotope fluxes at the ocean-sediment boundary: a review, *Philos Trans A Math Phys Eng Sci*, 374, 10.1098/rsta.2016.0246, 2016.

Honeyman, B. D., and Santschi, P. H.: A Brownian-pumping model for oceanic trace metal scavenging: Evidence from Th isotopes, *Journal of Marine Research*, 47, 951-992, 10.1357/002224089785076091, 1989.

Honjo, S.: Fluxes of particles to the interior of the open oceans, in: *Particle Flux in the Ocean*, edited by: Ittekkot, V., Schaefer, P., Honjo, S., and Depetris, P. J., John Wiley & Sons, New York, 91-154, 1996.

Hooks, C. E., Bidigare, R. R., Keller, M. D., and Guillard, R. R. L.: Coccolid eukaryotic marine ultraplankters with four different HPLC pigment signatures, *Journal of Phycology*, 24, 571-580, 1988.

Hudson, R. J. M., Covault, D. T., and Morel, F. M. M.: Investigations of iron coordination and redox reactions in seawater using Fe-59 radiometry and ion-pair solvent-extraction of amphiphilic iron complexes, *Marine Chemistry*, 38, 209-235, 10.1016/0304-4203(92)90035-9, 1992.

Humphreys, M. P., Griffiths, A. M., Achterberg, E. P., Holliday, N. P., Rérolle, V., Menzel Barraqueta, J. L., Coudrey, M. P., Oliver, K. I., Hartman, S. E., and Esposito, M.: Multidecadal accumulation of anthropogenic and remineralized dissolved inorganic carbon along the Extended Ellett Line in the northeast Atlantic Ocean, *Global Biogeochemical Cycles*, 30, 293-310, doi: 10.1002/2015GB005246, 2016.

Hunke, E. C., Notz, D., Turner, A. K., and Vancoppenolle, M.: The multiphase physics of sea ice: a review for model developers, *The Cryosphere*, 5, 989-1009, 10.5194/tc-5-989-2011, 2011.

Hunter, K. A., and Boyd, P. W.: Iron-binding ligands and their role in the ocean biogeochemistry of iron, *Environmental Chemistry*, 4, 221, 10.1071/en07012, 2007.

Hutchins, D. A., and Bruland, K. W.: Grazer-mediated regeneration and assimilation of Fe, Zn and Mn from planktonic prey, *Marine Ecology Progress Series*, 110, 259-269, 10.3354/meps110259, 1994.

Hutchins, D. A., and Bruland, K. W.: Iron-limited diatom growth and Si:N uptake ratios in a coastal upwelling regime, *Nature*, 393, 561-564, 1998.

Hutchins, D. A., Witter, A. E., Butler, A., and Luther III, G. W.: Competition among marine phytoplankton for different chelated iron species, *Nature*, 400, 858-861, 1999.

Ibisanmi, E., Sander, S. G., Boyd, P. W., Bowie, A. R., and Hunter, K. A.: Vertical distributions of iron-(III) complexing ligands in the Southern Ocean, Deep-Sea Research Part II-Topical Studies in Oceanography, 58, 2113-2125, 10.1016/j.dsr2.2011.05.028, 2011.

Iglesias-Rodríguez, M. D., Brown, C. W., Doney, S. C., Kleypas, J., Kolber, D., Kolber, Z., Hayes, P. K., and Falkowski, P. G.: Representing key phytoplankton functional groups in ocean carbon cycle models: Coccolithophorids, Global Biogeochemical Cycles, 16, 1-47, 10.1029/2001gb001454, 2002.

Irigoien, X., Harris, R. P., Verheye, H. M., Joly, P., Runge, J., Starr, M., Pond, D., Campbell, R., Shreeve, R., Ward, P., Smith, A. N., Damq, H. G., Peterson, W., Tirelli, V., Koski, M., Smith, T., Harbour, D., and Davidson, R.: Copepod hatching success in marine ecosystems with high diatom concentrations, Nature, 419, 387-389, 10.1038/nature01072, 2002.

Irigoien, X., Titelman, J., Harris, R. P., Harbour, D., and Castellani, C.: Feeding of *Calanus finmarchicus* nauplii in the Irminger Sea, Marine Ecology Progress Series, 262, 193-200, 2003.

Ito, Y., and Butler, A.: Structure of Synechobactins, New Siderophores of the Marine Cyanobacterium *Synechococcus* sp. PCC 7002, Limnology and Oceanography, 50, 1918-1923, 2005.

Jacobson, D. M., and Anderson, D. M.: Thecate heterotrophic dinoflagellates: feeding behavior and mechanisms, Journal of Phycology, 22, 249-258, 10.1111/j.1529-8817.1986.tb00021.x, 1986.

Janssens, J., Meiners, K. M., Tison, J.-L., Dieckmann, G., Delille, B., and Lannuzel, D.: Incorporation of iron and organic matter into young Antarctic sea ice during its initial growth stages, Elementa: Science of the Anthropocene, 4, 000123, 10.12952/journal.elementa.000123, 2016.

Jeandel, C., Van der Loeff, M. R., Lam, P. J., Roy-Barman, M., Sherrell, R. M., Kretschmer, S., German, C., and Dehairs, F.: What did we learn about ocean particle dynamics in the 1 GEOSECS-JGOFS era?, Progress in Oceanography, 133, 6-16, 10.1016/j.pocean.2014.12.018, 2015.

Jeffrey, S. W.: Algal Pigment Systems, in: Primary Productivity in the Sea, edited by: Falkowski, P. G., Environmental Science Research, Springer, Boston, MA, 1980.

Jeffrey, S. W., Veski, M., and Mantoura, R. F. C.: Phytoplankton pigments: windows into the pastures of the sea, Nature and Resources, 33, 14-29, 1997.

Jickells, T., and Moore, C. M.: The importance of atmospheric deposition for ocean productivity, Annual Review of Ecology, Evolution, and Systematics, 46, 481-501, 10.1146/annurev-ecolsys-112414-054118, 2015.

Jickells, T. D., An, Z. C., Andersen, K. K., Baker, A. R., Bergametti, G., Brooks, N., Cao, J. J., Boyd, P. W., Duce, R. A., Hunter, K. A., Kawahata, H., Kubilay, N., laRoche, J., Liss, P. S., Mahowald, N., Prospero, J. M., Ridgwell, A. J., Tegen, I., and Torres, R.: Global iron connections between desert dust, ocean biogeochemistry, and climate, Science, 308, 67-71, 2005.

Jochem, F. J., and Zeitzschel, B.: Productivity regime and phytoplankton size structure In the tropical and subtropical North Atlantic in spring 1989, Deep-Sea Research, 40, 495-519, 1993.

Johnson, K. S., Gordon, R. M., and Coale, K. H.: What controls dissolved iron concentrations in the world ocean?, Marine Chemistry, 57, 137-161, 10.1016/s0304-4203(97)00043-1, 1997a.

Johnson, K. S., Gordon, R. M., and Coale, K. H.: What controls dissolved iron concentrations in the world ocean? Authors' closing comments, Marine Chemistry, 57, 181-186, 1997b.

Johnson, K. S., Boyle, E., Bruland, K., Coale, K., Measures, C., Moffett, J., Aguilar-Islas, A., Barbeau, K., Bergquist, B., Bowie, A., Buck, K., Cai, Y., Chase, Z., Cullen, J., Doi, T., Elrod, V., Fitzwater, S., Gordon, M., King, A., Laan, P., Laglera-Baquer, L., Landing, W., Lohan, M., Mendez, J., Milne, A., Obata, H., Osslander, L., Plant, J., Sarthou, G., Sedwick, P., Smith, G. J., Sohst, B., Tanner, S., Van den Berg, S., and Wu,

J.: Developing standards for dissolved iron in seawater, *Eos, Transaction American Geophysical Union*, 88, 131-132, 2007.

Jonasdottir, S. H., Visser, A. W., Richardson, K., and Heath, M. R.: Seasonal copepod lipid pump promotes carbon sequestration in the deep North Atlantic, *Proc Natl Acad Sci U S A*, 112, 12122-12126, 10.1073/pnas.1512110112, 2015.

Jones, E. P., Anderson, L. G., and Swift, J. H.: Distribution of Atlantic and Pacific waters in the upper Arctic Ocean: Implications for circulation, *Geophysical Research Letters*, 25, 765-768, 1998.

Jungclauss, J. H., Haak, H., Latif, M., and Mikolajewicz, U.: Arctic–North Atlantic Interactions and Multidecadal Variability of the Meridional Overturning Circulation, *Journal of Climate*, 18, 4013-4031, 10.1175/JCLI3462.1, 2005.

Junge, K., Eicken, H., and Deming, J. W.: Bacterial Activity at -2 to -20 C in Arctic Wintertime Sea Ice, *Applied and Environmental Microbiology*, 70, 550-557, 10.1128/aem.70.1.550-557.2004, 2004.

Kahl, L. A., Vardi, A., and Schofield, O.: Effects of phytoplankton physiology on export flux, *Marine Ecology Progress Series*, 354, 3-19, 10.3354/meps07333, 2008.

Kallos, G., Papadopoulos, A., Katsafados, P., and Nickovic, S.: Transatlantic Saharan dust transport: Model simulation and results, *Journal of Geophysical Research*, 111, 10.1029/2005jd006207, 2006.

Kan, C. C., Chen, W. H., Wan, M. W., Phatai, P., Wittayakun, J., and Li, K. F.: The preliminary study of iron and manganese removal from groundwater by NaOCl oxidation and MF filtration, *Sustain. Environ. Res.*, 22, 25-30, 2012.

Kara, A. B., Rochford, P. A., and Hurlburt, H. E.: An optimal definition for ocean mixed layer depth, *Journal of Geophysical Research*, 105, 16,803-816, 10.1029/2000JC900072, 2000.

Karl, D. M., Michaels, A. F., Bergman, B., Capone, D., Carpenter, E. J., Letelier, R., Lipschultz, F., Paerl, H., Sigman, D., and Stal, L.: Dinitrogen fixation in the world's oceans, *Biogeochemistry*, 57/58, 47-98, 2002.

Karleskind, P., Lévy, M., and Memery, L.: Subduction of carbon, nitrogen, and oxygen in the northeast Atlantic, *Journal of Geophysical Research*, 116, 10.1029/2010jc006446, 2011.

Kieber, R. J., Williams, K., Willey, J. D., Skrabal, S., and Avery, G. B.: Iron speciation in coastal rainwater: concentration and deposition to seawater, *Marine Chemistry*, 73, 83-95, 10.1016/s0304-4203(00)00097-9, 2001.

Kieber, R. J., Willey, J. D., and Avery, G. B.: Temporal variability of rainwater iron speciation at the Bermuda Atlantic time series station, *Journal of Geophysical Research-Oceans*, 108, 10.1029/2001jc001031, 2003.

Kissel, C., Laj, C., Mulder, T., Wandres, C., and Cremer, M.: The magnetic fraction: A tracer of deep water circulation in the North Atlantic, *Earth and Planetary Science Letters*, 288, 444-454, 10.1016/j.epsl.2009.10.005, 2009.

Klaas, C., and Archer, D. E.: Association of sinking organic matter with various types of mineral ballast in the deep sea: Implications for the rain ratio, *Global Biogeochemical Cycles*, 16, 63-61-63-14, 10.1029/2001gb001765, 2002.

Klaveness, D.: Biology and Ecology of the Cryptophyceae: Status and Challenges, *Biological Oceanography*, 6, 257-270, 10.1080/01965581.1988.10749530, 1989.

Klunder, M. B., Laan, P., Middag, R., De Baar, H. J. W., and van Ooijen, J. C.: Dissolved iron in the Southern Ocean (Atlantic sector), *Deep-Sea Research Part II-Topical Studies in Oceanography*, 58, 2678-2694, 10.1016/j.dsr2.2010.10.042, 2011.

- Klunder, M. B., Bauch, D., Laan, P., de Baar, H. J. W., van Heuven, S. M. A. C., and Ober, S.: Dissolved iron in the Arctic shelf seas and surface waters of the Central Arctic Ocean: impact of Arctic river water and ice-melt, *Journal of Geophysical Research*, 117, 1-18, 2012.
- Kondo, Y., Takeda, S., and Furuya, K.: Distribution and speciation of dissolved iron in the Sulu Sea and its adjacent waters, *Deep-Sea Research Part II-Topical Studies in Oceanography*, 54, 60-80, 10.1016/j.dsr2.2006.08.019, 2007.
- Kondo, Y., Takeda, S., Nishioka, J., Obata, H., Furuya, K., Johnson, W. K., and Wong, C. S.: Organic iron(III) complexing ligands during an iron enrichment experiment in the western subarctic North Pacific, *Geophysical Research Letters*, 35, 10.1029/2008gl033354, 2008.
- Kondo, Y., and Moffett, J. W.: Iron redox cycling and subsurface offshore transport in the eastern tropical South Pacific oxygen minimum zone, *Marine Chemistry*, 168, 95-103, 10.1016/j.marchem.2014.11.007, 2015.
- Kostka, J. E., Haeefe, E., Viehweger, R., and Stucki, J. W.: Respiration and Dissolution of Iron(III)-Containing Clay Minerals by Bacteria, *Environmental Science & Technology*, 33, 3127-3133, 1999.
- Krachler, R., Jirsa, F., and Ayromlou, S.: Factors influencing the dissolved iron input by river water to the open ocean, *Biogeosciences*, 2, 311-315, 2005.
- Krachler, R., Krachler, R. F., Wallner, G., Hann, S., Laux, M., Recalde, M. F. C., Jirsa, F., Neubauer, E., von der Kammer, F., Hofmann, T., and Keppler, B. K.: River-derived humic substances as iron chelators in seawater, *Marine Chemistry*, 174, 85-93, 10.1016/j.marchem.2015.05.009, 2015.
- Krembs, C., Eicken, H., Junge, K., and Deming, J. W.: High concentrations of exopolymeric substances in Arctic winter sea ice: implications for the polar ocean carbon cycle and cryoprotection of diatoms, *Deep-Sea Research I*, 49, 2163-2181, 2002.
- Kremling, K.: The behavior of Zn, Cd, Cu, Ni, Co, Fe, and Mn in anoxic baltic waters, *Marine Chemistry*, 13, 87-108, 10.1016/0304-4203(83)90019-1, 1983.
- Kuma, K., and Matsunaga, K.: Availability of colloidal ferric oxides to coastal marine phytoplankton, *Marine Biology*, 122, 1-11, 1995.
- Kuma, K., Nishioka, J., and Matsunaga, K.: Controls on iron(III) hydroxide solubility in seawater: The influence of pH and natural organic chelators, *Limnology and Oceanography*, 41, 396-407, 1996.
- Kustka, A., Sanudo-Wilhelmy, S., Carpenter, E. J., Capone, D. G., and Raven, J. A.: A revised estimate of the iron use efficiency of nitrogen fixation, with special reference to the marine cyanobacterium *Trichodesmium* spp. (Cyanophyta), *Journal of Phycology*, 39, 12-25, 2003.
- Kustka, A. B., Shaked, Y., Milligan, A. J., King, D. W., and Morel, F. M. M.: Extracellular production of superoxide by marine diatoms: Contrasting effects on iron redox chemistry and bioavailability, *Limnology and Oceanography*, 50, 1172-1180, 2005.
- Kwon, E. Y., Primeau, F., and Sarmiento, J. L.: The impact of remineralization depth on the air-sea carbon balance, *Nature Geoscience*, 2, 630-635, 10.1038/ngeo612, 2009.
- Kwon, E. Y., Kim, G., Primeau, F., Moore, W. S., Cho, H.-M., DeVries, T., Sarmiento, J. L., Charette, M. A., and Cho, Y.-K.: Global estimate of submarine groundwater discharge based on an observationally constrained radium isotope model, *Geophysical Research Letters*, 41, 8438-8444, 10.1002/2014gl061574, 2014.
- Lackschewitz, K. S., Endler, R., Gehrke, B., Wallrabe-Adams, H.-J., and Thiede, J.: Evidence for topography- and current-controlled deposition on the reykjanes Ridge between 59°N and 60°N, *Deep-Sea Research I*, 43, 1683-1711, 1996.

Lacour, L., Claustre, H., Prieur, L., and D'Ortenzio, F.: Phytoplankton biomass cycles in the North Atlantic subpolar gyre: A similar mechanism for two different blooms in the Labrador Sea, *Geophysical Research Letters*, 42, 5403-5410, 10.1002/2015gl064540, 2015.

Lacour, L., Ardyna, M., Stec, K. F., Claustre, H., Prieur, L., Poteau, A., D'Alcala, M. R., and Iudicone, D.: Unexpected winter phytoplankton blooms in the North Atlantic subpolar gyre, *Nature Geoscience*, 10, 836-839, 10.1038/ngeo3035, 2017.

Lacour, L., Claustre, H., Briggs, N., Ardyna, M., and Dall'Olmo, G.: Intra-seasonal dynamics of the mixed layer pump in the North Atlantic Subpolar Gyre : a BGC-Argo approach, *Journal of Geophysical Research*, in prep.

Laes, A., Blain, S., Laan, P., Achterberg, E. P., Sarthou, G., and de Baar, H. J. W.: Deep dissolved iron profiles in the eastern North Atlantic in relation to water masses, *Geophysical Research Letters*, 30, 10.1029/2003gl017902, 2003.

Laes, A., Blain, S., Laan, P., Ussher, S. J., Achterberg, E. P., Treguer, P., and de Baar, H. J. W.: Sources and transport of dissolved iron and manganese along the continental margin of the Bay of Biscay, *Biogeosciences*, 4, 181-194, 2007.

Lagerström, M. E., Field, M. P., Seguret, M., Fischer, L., Hann, S., and Sherrell, R. M.: Automated on-line flow-injection ICP-MS determination of trace metals (Mn, Fe, Co, Ni, Cu and Zn) in open ocean seawater: Application to the GEOTRACES program, *Marine Chemistry*, 155, 71-80, 10.1016/j.marchem.2013.06.001, 2013.

Laglera, L. M., Battaglia, G., and van den Berg, C. M. G.: Determination of humic substances in natural waters by cathodic stripping voltammetry of their complexes with iron, *Analytica Chimica Acta*, 599, 58-66, 2007.

Laglera, L. M., and van den Berg, C. M. G.: Evidence for geochemical control of iron by humic substances in seawater, *Limnology and Oceanography*, 54, 610-619, 10.4319/lo.2009.54.2.0610, 2009.

Lam, P. J., and Bishop, J. K. B.: High Biomass Low Export regimes in the Southern Ocean, *Deep Sea Research Part II: Topical Studies in Oceanography*, 54, 601-638, 2007.

Lam, P. J., and Bishop, J. K. B.: The continental margin is a key source of iron to the HNLC North Pacific Ocean, *Geophysical Research Letters*, 35, L07608, 10.1029/2008GL033294, 2008.

Lam, P. J., and Marchal, O.: Insights into Particle Cycling from Thorium and Particle Data, *Annual Review of Marine Science*, 7, 159-184, 10.1146/annurev-marine-010814-015623, 2015.

Lam, P. J., Ohnemus, D. C., and Auro, M. E.: Size fractionated major particle composition and mass from the US GEOTRACES North Atlantic Zonal Transect, *Deep-Sea Research Part II-Topical Studies in Oceanography*, 116, 303-320, 10.1016/j.dsr2.2014.11.020, 2015.

Lambelet, M., van de Flierdt, T., Crockett, K., Rehkamper, M., Katharina, K., Coles, B., Rijkenberg, M. J. A., Gerringa, L. J. A., de Baar, H. J. W., and Steinfeldt, R.: Neodymium isotopic composition and concentration in the western North Atlantic Ocean: Results from the GEOTRACES GA02 section, *Geochimica Et Cosmochimica Acta*, 177, 1-29, 2016.

Lampert, L.: Chémotaxonomie pigmentaire – Initiation aux calculs appliqués au phytoplancton, Ifremer, Département « DYNamiques de l'Environnement CÔtier"
Brest, 2014.

Lampert, W.: Release of dissolved organic carbon by grazing zooplankton, *Limnology and Oceanography*, 23, 831-834, 1978.

Lancelot, C.: The mucilage phenomenon in the continental coastal waters of the North Sea, *The Science of the Total Environment*, 165, 83-102, 1995.

Landry, M. R., Barber, R. T., Bidigare, R. R., Chai, F., Coale, K. H., Dam, H. G., Lewis, M. R., Lindley, S. T., McCarthy, J. J., Roman, M. R., Stoecker, D. K., verity, P. G., and White, J. R.: Iron and grazing constraints on primary production in the central equatorial Pacific: An EqPac synthesis, *Limnology and Oceanography*, 42, 405-418, 1997.

Lannuzel, D., Schoemann, V., de Jong, J., Chou, L., Delille, B., Becquevort, S., and Tison, J.-L.: Iron study during a time series in the western Weddell pack ice, *Marine Chemistry*, 108, 85-95, 10.1016/j.marchem.2007.10.006, 2008.

Lannuzel, D., Schoemann, V., de Jong, J., Pasquer, B., van der Merwe, P., Masson, F., Tison, J.-L., and Bowie, A.: Distribution of dissolved iron in Antarctic sea ice: Spatial, seasonal, and inter-annual variability, *Journal of Geophysical Research-Biogeosciences*, 115, 10.1029/2009jg001031, 2010.

Lannuzel, D., van der Merwe, P. C., Townsend, A. T., and Bowie, A. R.: Size fractionation of iron, manganese and aluminium in Antarctic fast ice reveals a lithogenic origin and low iron solubility, *Marine Chemistry*, 161, 47-56, 10.1016/j.marchem.2014.02.006, 2014.

Lannuzel, D., Grotti, M., Abelmoschi, M. L., and van der Merwe, P.: Organic ligands control the concentrations of dissolved iron in Antarctic sea ice, *Marine Chemistry*, 174, 120-130, 10.1016/j.marchem.2015.05.005, 2015.

Lannuzel, D., Chever, F., van der Merwe, P. C., Janssens, J., Roukaerts, A., Cavagna, A.-J., Townsend, A. T., Bowie, A. R., and Meiners, K. M.: Iron biogeochemistry in Antarctic pack ice during SIPEX-2, *Deep Sea Research Part II: Topical Studies in Oceanography*, 131, 111-122, 10.1016/j.dsr2.2014.12.003, 2016a.

Lannuzel, D., Vancoppenolle, M., van der Merwe, P., de Jong, J., Meiners, K. M., Grotti, M., Nishioka, J., and Schoemann, V.: Iron in sea ice: Review and new insights, *Elementa: Science of the Anthropocene*, 4, 000130, 10.12952/journal.elementa.000130, 2016b.

LaRoche, J., and Breitbarth, E.: Importance of the diazotrophs as a source of new nitrogen in the ocean, *Journal of Sea Research*, 53, 67-91, 10.1016/j.seares.2004.05.005, 2005.

Laurenceau-Cornec, E. C., Trull, T. W., Davies, D. M., Bray, S. G., Doran, J., Planchon, F., Carlotti, F., Jouandet, M. P., Cavagna, A. J., Waite, A. M., and Blain, S.: The relative importance of phytoplankton aggregates and zooplankton fecal pellets to carbon export: insights from free-drifting sediment trap deployments in naturally iron-fertilised waters near the Kerguelen Plateau, *Biogeosciences*, 12, 1007-1027, 10.5194/bg-12-1007-2015, 2015.

Lazier, J., Hendry, R., Clarke, A., Yashayaev, I., and Rhines, P.: Convection and restratification in the Labrador Sea, 1990–2000, *Deep-Sea Research I*, 49, 1819–1835, 10.1016/S0967-0637(02)00064-X, 2002.

Le Quéré, C., Andres, R. J., Boden, T., Conway, T., Houghton, R. A., House, J. I., Marland, G., Peters, G. P., van der Werf, G. R., Ahlström, A., Andrew, R. M., Bopp, L., Canadell, J. G., Ciais, P., Doney, S. C., Enright, C., Friedlingstein, P., Huntingford, C., Jain, A. K., Jourdain, C., Kato, E., Keeling, R. F., Klein Goldewijk, K., Levis, S., Levy, P., Lomas, M., Poulter, B., Raupach, M. R., Schwinger, J., Sitch, S., Stocker, B. D., Viovy, N., Zaehle, S., and Zeng, N.: The global carbon budget 1959–2011, *Earth System Science Data*, 5, 165-185, 10.5194/essd-5-165-2013, 2013.

Le Roy, E., Sanial, V., Charette, M. A., van Beek, P., Lacan, F., Jacquet, S. H. M., Henderson, P. B., Souhaut, M., García-Ibáñez, M. I., Jeandel, C., Pérez, F. F., and Sarthou, G.: The ²²⁶Ra–Ba relationship in the North Atlantic during GEOTRACES-GA01, *Biogeosciences*, 15, 3027-3048, 10.5194/bg-15-3027-2018, 2018.

Lead, J. R., and Wilkinson, K. J.: Environmental colloids and particles: current knowledge and future developments, in: *Environmental Colloids and Particles*, edited by: Wilkinson, K. J., and Lead, J. R., Analytical and Physical Chemistry of Environmental Systems, John Wiley & Sons, 1-16, 2007.

Leblanc, K.: A seasonal study of diatom dynamics in the North Atlantic during the POMME experiment (2001): Evidence for Si limitation of the spring bloom, *Journal of Geophysical Research*, 110, 10.1029/2004jc002621, 2005.

Lee, Z., Weidemann, A., Kindle, J., Arnone, R., Carder, K. L., and Davis, C.: Euphotic zone depth: Its derivation and implication to ocean-color remote sensing, *Journal of Geophysical Research*, 112, 1-11, 10.1029/2006jc003802, 2007.

Legendre, L., Rivkin, R. B., Weinbauer, M. G., Guidi, L., and Uitz, J.: The microbial carbon pump concept: Potential biogeochemical significance in the globally changing ocean, *Progress in Oceanography*, 134, 432-450, 10.1016/j.pocean.2015.01.008, 2015.

Lemaitre, N., Planchon, F., Planquette, H., Dehairs, F., Fonseca-Batista, D., Roukaerts, A., Deman, F., Tang, Y., Mariez, C., and Sarthou, G.: High variability of export fluxes along the North Atlantic GEOTRACES section GA01: Particulate organic carbon export deduced from the ^{234}Th method *Biogeosciences*, 1-38, 10.5194/bg-2018-190, 2018.

Lemaître, N., planquette, H., Planchon, F., Sarthou, G., Jacquet, S., Garcia-Ibanez, M. I., Gourain, A., Cheize, M., Monin, L., Andre, L., Laha, P., Terryn, H., and Dehairs, F.: Particulate barium tracing significant mesopelagic carbon remineralisation in the North Atlantic *Biogeosciences Discussions*, 2017.

Lenton, A., Tilbrook, B., Law, R., Bakker, D., Doney, S. C., Gruber, N., Hoppema, M., Ishii, M., Lovenduski, N. S., Matear, R. J., McNeil, B. I., Metzl, N., Mikaloff Fletcher, S. E., Monteiro, P., Rödenbeck, C., Sweeney, C., and Takahashi, T.: Sea-air CO_2 fluxes in the Southern Ocean for the period 1990–2009, *Biogeosciences Discussions*, 10, 285-333, 10.5194/bgd-10-285-2013, 2013.

Leonardos, N., and Geider, R. J.: Elevated Atmospheric Carbon Dioxide Increases Organic Carbon Fixation by *Emiliana Huxleyi* (Haptophyta), under Nutrient-Limited High-Light Conditions, *Journal of Phycology*, 41, 1196-1203, 10.1111/j.1529-8817.2005.00152.x, 2005.

Leterme, S. C., Edwards, M., Seuront, L., Attrill, M. J., Reid, P. C., and John, A. W. G.: Decadal basin-scale changes in diatoms, dinoflagellates, and phytoplankton color across the North Atlantic, *Limnology and Oceanography*, 50, 1244-1253, 2005.

Li, W. K. W., Jellett, J. F., and Dickie, P. M.: DNA distributions in planktonic bacteria stained with TOTO or TO-PRO *Limnology and Oceanography*, 40, 1485-1495, 1995.

Li, W. K. W., and Harrison, W. G.: Chlorophyll, bacteria and picophytoplankton in ecological provinces of the North Atlantic, *Deep-sea Research Part II*, 48, 2271-2293, 2001.

Li, W. K. W.: Macroecological patterns of phytoplankton in the northwestern North Atlantic Ocean, *Nature*, 419, 154-157, 10.1038/nature00994, 2002.

Lin, H., Rauschenberg, S., Hexel, C. R., Shaw, T. J., and Twining, B. S.: Free-drifting icebergs as sources of iron to the Weddell Sea, *Deep-Sea Research Part II-Topical Studies in Oceanography*, 58, 1392-1406, 10.1016/j.dsr2.2010.11.020, 2011.

Lin, H., and Twining, B. S.: Chemical speciation of iron in Antarctic waters surrounding free-drifting icebergs, *Marine Chemistry*, 128-129, 81-91, 10.1016/j.marchem.2011.10.005, 2012.

Lindemann, C., and St. John, M. A.: A seasonal diary of phytoplankton in the North Atlantic, *Frontiers in Marine Science*, 1, 10.3389/fmars.2014.00037, 2014.

Litchman, E., Klausmeier, C. A., Schofield, O. M., and Falkowski, P. G.: The role of functional traits and trade-offs in structuring phytoplankton communities: scaling from cellular to ecosystem level, *Ecol Lett*, 10, 1170-1181, 10.1111/j.1461-0248.2007.01117.x, 2007.

Liu, X. W., and Millero, F. J.: The solubility of iron hydroxide in sodium chloride solutions, *Geochimica Et Cosmochimica Acta*, 63, 3487-3497, 1999.

Liu, X. W., and Millero, F. J.: The solubility of iron in seawater, *Marine Chemistry*, 77, 43-54, 10.1016/s0304-4203(01)00074-3, 2002.

Lochte, K., Ducklow, H. W., Fasham, M. J. R., and Stienen, C.: Plankton succession and carbon cycling at 47°N 20°W during the JGOFS North Atlantic Bloom Experiment, *Deep-Sea Research II: Topical Studies in Oceanography*, 40, 91-114, 1993.

Lohan, M. C., Statham, P. J., and Crawford, D. W.: Total dissolved zinc in the upper water column of the subarctic North East Pacific, *Deep-Sea Research Part II-Topical Studies in Oceanography*, 49, 5793-5808, 10.1016/s0967-0645(02)00215-1, 2002.

Lohan, M. C., Aguilar-Islas, A. M., and Bruland, K. W.: Direct determination of iron in acidified (pH 1.7) seawater samples by flow injection analysis with catalytic spectrophotometric detection: Application and intercomparison, *Limnology and Oceanography-Methods*, 4, 164-171, 2006.

Lohan, M. C., and Bruland, K. W.: Elevated Fe(II) and Dissolved Fe in Hypoxic Shelf Waters off Oregon and Washington: An Enhanced Source of Iron to Coastal Upwelling Regimes, *Environmental Science & Technology*, 42, 6462-6468, 10.1021/es800144j, 2008.

Lohan, M. C., Buck, K. N., and Sander, S. G.: Organic ligands — A key control on trace metal biogeochemistry in the oceans, *Marine Chemistry*, 173, 1-2, 10.1016/j.marchem.2015.03.017, 2015.

Long, R. A., and Azam, F.: Abundant protein-containing particles in the sea, *Aquatic Microbial Ecology*, 10, 213-221, 1996.

Longhurst, A. R.: *Ecological geography of the Sea*, Second Edition ed., Elsevier Academic Press publications, Burlington, 542 pp., 2007.

Louanchi, F., and Najjar, R. G.: Annual cycles of nutrients and oxygen in the upper layers of the North Atlantic Ocean, *Deep Sea Research Part II: Topical Studies in Oceanography*, 48, 2155-2171, 2001.

Luo, Y. W., Doney, S. C., Anderson, L. A., Benavides, M., Berman-Frank, I., Bode, A., Bonnet, S., Boström, K. H., Böttjer, D., Capone, D. G., Carpenter, E. J., Chen, Y. L., Church, M. J., Dore, J. E., Falcón, L. I., Fernández, A., Foster, R. A., Furuya, K., Gómez, F., Gundersen, K., Hynes, A. M., Karl, D. M., Kitajima, S., Langlois, R. J., LaRoche, J., Letelier, R. M., Marañón, E., McGillicuddy, D. J., Moisander, P. H., Moore, C. M., Mouriño-Carballido, B., Mulholland, M. R., Needoba, J. A., Orcutt, K. M., Poulton, A. J., Rahav, E., Raimbault, P., Rees, A. P., Riemann, L., Shiozaki, T., Subramaniam, A., Tyrrell, T., Turk-Kubo, K. A., Varela, M., Villareal, T. A., Webb, E. A., White, A. E., Wu, J., and Zehr, J. P.: Database of diazotrophs in global ocean: abundance, biomass and nitrogen fixation rates, *Earth System Science Data*, 4, 47-73, 10.5194/essd-4-47-2012, 2012.

Luther III, G. W., and Wu, J.: What controls dissolved iron concentrations in the world ocean? - a comment, *Marine Chemistry*, 57, 173-179, 1997.

Lutz, V. A., Sathyendranath, S., Head, E. J. H., and Li, W. K. W.: Variability in pigment composition and optical characteristics of phytoplankton in the Labrador Sea and the Central North Atlantic, *Marine Ecology Progress Series*, 260, 1-18, 2003.

Mackey, D. J., O'Sullivan, J. E., Watson, R. J., and Dal Pont, G.: Interference effects in the extraction of trace metals from estuarine waters, *Marine Chemistry*, 59, 113-126, 10.1016/s0304-4203(97)00066-2, 1997.

Mackey, K. R., Chien, C. T., Post, A. F., Saito, M. A., and Paytan, A.: Rapid and gradual modes of aerosol trace metal dissolution in seawater, *Frontiers in Microbiology*, 5, 1-11, 10.3389/fmicb.2014.00794, 2015.

Mackey, M. D., Mackey, D. J., Higgins, H. W., and Wright, S. W.: CHEMTAX - a program for estimating class abundances from chemical markers: application to HPLC measurements of phytoplankton, *Marine Ecology Progress Series*, 144, 265-283, 1996.

Mahadevan, A., Tandon, A., and Ferrari, R.: Rapid changes in mixed layer stratification driven by submesoscale instabilities and winds, *Journal of Geophysical Research*, 115, 10.1029/2008jc005203, 2010.

Mahadevan, A., D'Asaro, E., Lee, C., and Perry, M. J.: Eddy-Driven Stratification Initiates North Atlantic Spring Phytoplankton Blooms, *Science*, 337, 54-58, 2012.

Mahadevan, A.: Eddy effects on biogeochemistry, *Nature*, 506, 168-169, 2014.

Mahowald, N. M., Baker, A. R., Bergametti, G., Brooks, N., Duce, R. A., Jickells, T. D., Kubilay, N., Prospero, J. M., and Tegen, I.: Atmospheric global dust cycle and iron inputs to the ocean, *Global Biogeochemical Cycles*, 19, n/a-n/a, 10.1029/2004gb002402, 2005.

Mahowald, N. M., Engelstaedter, S., Luo, C., Sealy, A., Artaxo, P., Benitez-Nelson, C., Bonnet, S., Chen, Y., Chuang, P. Y., Cohen, D. D., Dulac, F., Herut, B., Johansen, A. M., Kubilay, N., Losno, R., Maenhaut, W., Paytan, A., Prospero, J. M., Shank, L. M., and Siefert, R. L.: Atmospheric iron deposition: global distribution, variability, and human perturbations, *Ann Rev Mar Sci*, 1, 245-278, 10.1146/annurev.marine.010908.163727, 2009.

Maldonado, M. T., and Price, N. M.: Utilization of iron bound to strong organic ligands by plankton communities in the subarctic Pacific Ocean, *Deep Sea Research Part II: Topical Studies in Oceanography*, 46, 2447-2473, 10.1016/s0967-0645(99)00071-5, 1999.

Maldonado, M. T., Boyd, P. W., LaRoche, J., Strzepek, R. F., Waite, A. M., Bowie, A. R., Croot, P. L., Frew, R. D., and Price, N. M.: Iron uptake and physiological response of phytoplankton during a mesoscale Southern Ocean iron enrichment, *Limnology and Oceanography*, 46, 1802-1808, 2001.

Maldonado, M. T., and Price, N. M.: Reduction and transport of organically bound iron by *Thalassiosira oceanica* (Bacillariophyceae), *Journal of Phycology*, 37, 298-310, 2001.

Maldonado, M. T., Strzepek, R. F., Sander, S., and Boyd, P. W.: Acquisition of iron bound to strong organic complexes, with different Fe binding groups and photochemical reactivities, by plankton communities in Fe-limited subantarctic waters, *Global Biogeochemical Cycles*, 19, n/a-n/a, 10.1029/2005gb002481, 2005.

Malone, T. C., Neale, P. J., and Boardman, D.: Influences of Estuarine Circulation on the Distribution and Biomass of Phytoplankton Size Fractions, in: *Estuarine Perspectives*, edited by: Kennedy, V. S., Academic Press, Inc.; a subsidiary of Harcourt Brace Jovanovich, Publishers, New York, USA

San Francisco, USA, 249-262, 1980.

Mantoura, R. F. C., and Riley, J. P.: The use of gel filtration in the study of metal binding by humic acids and related compounds, *Analytica Chimica Acta*, 78, 193-200, 1975.

Maranger, R., Bird, D. F., and Price, N. M.: Iron acquisition by photosynthetic marine phytoplankton from ingested bacteria, *Nature*, 396, 248-251, 10.1038/24352, 1998.

Margalef, R.: Life-forms of phytoplankton as survival alternatives in an unstable environment, *Oceanologica Acta*, 1, 493-509, 1978.

Mari, X., Rassoulzadegan, F., Brussaard, C. P. D., and Wassmann, P.: Dynamics of transparent exopolymeric particles (TEP) production by *Phaeocystis globosa* under N- or P-limitation: a controlling factor of the retention/export balance, *Harmful Algae*, 4, 895-914, 10.1016/j.hal.2004.12.014, 2005.

Mari, X., Passow, U., Migon, C., Burd, A. B., and Legendre, L.: Transparent exopolymer particles: Effects on carbon cycling in the ocean, *Progress in Oceanography*, 151, 13 - 37, 2016.

Maring, H., Savoie, D. L., Izaguirre, M. A., Custals, L., and Reid, J. S.: Mineral dust aerosol size distribution change during atmospheric transport, *Journal of Geophysical Research*, 108, 1-8, 10.1029/2002jd002536, 2003.

Markus, T., Stroeve, J. C., and Miller, J.: Recent changes in Arctic sea ice melt onset, freezeup, and melt season length, *Journal of Geophysical Research*, 114, 10.1029/2009jc005436, 2009.

Marshall, J., and Schott, F.: Open-ocean convection: observations, theory, and models, *Reviews of Geophysics*, 37, 1-64, doi: 10.1029/98RG02739, 1999.

Marshall, J., Kushnir, Y., Battisti, D., Chang, P., Czaja, A., Dickson, R., Hurrell, J., McCartney, M., Saravanan, R., and Visbeck, M.: North Atlantic climate variability: phenomena, impacts and mechanisms, *International Journal of Climatology*, 21, 1863-1898, 10.1002/joc.693, 2001.

Martin-Jézéquel, V., Hildebrand, M., and Brzezinski, M. A.: Silicon metabolism in diatoms: implications for growth, *Journal of Phycology*, 36, 821-840, 2000.

Martin, J.-M., Elbaz-Poulichet, F., Guieu, C., Loÿe-Pilot, M.-D., and Han, G.: River versus atmospheric input of material to the Mediterranean Sea: an overview*, *Marine Chemistry*, 28, 159-182, 1989.

Martin, J. D., and Fitzwater, S. E.: Iron deficiency limits phytoplankton growth in the north-east Pacific subarctic, *Nature*, 331, 341-343, 1988.

Martin, J. H., and Gordon, R. M.: Northeast Pacific iron distribution in relation to phytoplankton productivity, *Deep Sea Research*, 35, 177-196, 1988.

Martin, J. H.: Glacial-interglacial CO₂ change: the iron hypothesis, *Paleoceanography*, 5, 1-13, 1990.

Martin, J. H., Fitzwater, S. E., and Gordon, R. M.: Iron deficiencies limits phytoplankton growth in Antarctic waters, *Global Biogeochemical Cycles*, 4, 5-12, 1990.

Martin, J. H., Gordon, R. M., and Fitzwater, S. E.: THE CASE FOR IRON, *Limnology and Oceanography*, 36, 1793-1802, 1991.

Martin, J. H., Coale, K. H., Johnson, K. S., Fitzwater, S. E., Gordon, R. M., Tanner, S. J., Hunter, C. N., Elrod, V. A., Nowicki, J. L., Coley, T. L., Barber, R. T., Lindley, S., Watson, A. J., Van Scoy, K., Law, C. S., Liddicoat, M. I., Ling, R., Stanton, T., Stockel, J., Collins, C., Anderson, A., Bidigare, R., Ondrusek, M., Latasa, M., Millero, F. J., Lee, K., Yao, W., Zhang, J. Z., Friederich, G., Sakamoto, C., Chavez, F., Buck, K., Kolber, Z., Greene, R., Falkowski, P., Chisholm, S. W., Hoge, F., Swift, R., Yungel, J., Turner, S., Nightingale, P., Hatton, A., Liss, P., and Tindale, N. W.: Testing the Iron Hypothesis in Ecosystems of the Equatorial Pacific Ocean, *Nature*, 371, 123-129, 10.1038/371123a0, 1994.

Martin, P., Lampitt, R. S., Jane Perry, M., Sanders, R., Lee, C., and D'Asaro, E.: Export and mesopelagic particle flux during a North Atlantic spring diatom bloom, *Deep Sea Research Part I: Oceanographic Research Papers*, 58, 338-349, 10.1016/j.dsr.2011.01.006, 2011.

Martin, P., van der Loeff, M. R., Cassar, N., Vandromme, P., d'Ovidio, F., Stemmann, L., Rengarajan, R., Soares, M., González, H. E., Ebersbach, F., Lampitt, R. S., Sanders, R., Barnett, B. A., Smetacek, V., and Naqvi, S. W. A.: Iron fertilization enhanced net community production but not downward particle flux during the Southern Ocean iron fertilization experiment LOHAFEX, *Global Biogeochemical Cycles*, 27, 871-881, 10.1002/gbc.20077, 2013.

Martinez, J. S., Zhang, G. P., Holt, P. D., Jung, H.-T., Carrano, C. J., Haygood, M. G., and Butler, A.: Self-Assembling Amphiphilic Siderophores from Marine Bacteria, *Science*, 287, 1245-1247, 2000.

Martinez, J. S., Carter-Franklin, J. N., Mann, E. L., Martin, J. D., Haygood, M. G., and Butler, A.: Structure and membrane affinity of a suite of amphiphilic siderophores produced by a marine bacterium, *PNAS*, 100, 3754-3759, 10.1073/pnas.0637444100, 2003.

Martinez, J. S., and Butler, A.: Marine amphiphilic siderophores: Marinobactin structure, uptake, and microbial partitioning, *Journal of Inorganic Biochemistry*, 101, 1692-1698, 2007.

- Mawji, E., Gledhill, M., Milton, J. A., Tarran, G. A., Ussher, S., Thompson, A., Wolff, G. A., Worsfold, P. J., and Achterberg, E. P.: Hydroxamate Siderophores: Occurrence and Importance in the Atlantic Ocean, *Environmental Science & Technology*, 42, 8675-8680, 10.1021/es801884r, 2008a.
- Mawji, E., Gledhill, M., Worsfold, P. J., and Achterberg, E. P.: Collision-induced dissociation of three groups of hydroxamate siderophores: ferrioxamines, ferrichromes and coprogens/fusigens, *Rapid Commun Mass Spectrom*, 22, 2195-2202, 10.1002/rcm.3604, 2008b.
- Mawji, E., Gledhill, M., Milton, J. A., Zubkov, M. V., Thompson, A., Wolff, G. A., and Achterberg, E. P.: Production of siderophore type chelates in Atlantic Ocean waters enriched with different carbon and nitrogen sources, *Marine Chemistry*, 124, 90-99, 10.1016/j.marchem.2010.12.005, 2011.
- McGillicuddy, D. J., Anderson, L. A., Doney, S. C., and Maltrud, M. E.: Eddy-driven sources and sinks of nutrients in the upper ocean: Results from a 0.1° resolution model of the North Atlantic, *Global Biogeochemical Cycles*, 17, n/a-n/a, 10.1029/2002gb001987, 2003.
- Measures, C. I., Landing, W. M., Brown, M. T., and Buck, C. S.: High-resolution Al and Fe data from the Atlantic Ocean CLIVAR-CO2 Repeat Hydrography A16N transect: Extensive linkages between atmospheric dust and upper ocean geochemistry, *Global Biogeochemical Cycles*, 22, 1-10, 10.1029/2007gb003042, 2008.
- Measures, C. I., Brown, M. T., Selph, K. E., Apprill, A., Zhou, M., Hatta, M., and Hiscock, W. T.: The influence of shelf processes in delivering dissolved iron to the HNLC waters of the Drake Passage, Antarctica, *Deep Sea Research Part II: Topical Studies in Oceanography*, 90, 77-88, 10.1016/j.dsr2.2012.11.004, 2013.
- Meiners, K., Krembs, C., and Gradinger, R.: Exopolymer particles: microbial hotspots of enhanced bacterial activity in Arctic fast ice (Chukchi Sea), *Aquatic Microbial Ecology*, 52, 195-207, 10.3354/ame01214, 2008.
- Meire, L., Meire, P., Struyf, E., Krawczyk, D. W., Arendt, K. E., Yde, J. C., Juul Pedersen, T., Hopwood, M. J., Rysgaard, S., and Meysman, F. J. R.: High export of dissolved silica from the Greenland Ice Sheet, *Geophysical Research Letters*, 43, 9173-9182, 10.1002/2016gl070191, 2016.
- Melling, H., and Moore, R. M.: Modification of halocline source waters during freezing on the Beaufort Sea shelf: Evidence from oxygen isotopes and dissolved nutrients, *Continental Shelf Research*, 15, 89-113, 1995.
- Menzel Barraqueta, J. L., Schlosser, C., Planquette, H., Gourain, A., Cheize, M., Boutorh, J., Shelley, R. U., Pereira Contreira, L., Gledhill, M., Hopwood, M. J., Lherminier, P., Sarthou, G., and Achterberg, E. P.: Aluminium in the North Atlantic Ocean and the Labrador Sea (GEOTRACES GA01 section): roles of continental inputs and biogenic particle removal, *Biogeosciences Discussions*, 1-28, 10.5194/bg-2018-39, 2018.
- Mercier, H., Lherminier, P., Sarafanov, A., Gaillard, F., Daniault, N., Desbruyères, D., Falina, A., Ferron, B., Gourcuff, C., Huck, T., and Thierry, V.: Variability of the meridional overturning circulation at the Greenland–Portugal OVIDE section from 1993 to 2010, *Progress in Oceanography*, 132, 250-261, 10.1016/j.pocean.2013.11.001, 2015.
- Meskhidze, N., Hurley, D., Royalty, T. M., and Johnson, M. S.: Potential effect of atmospheric dissolved organic carbon on the iron solubility in seawater, *Marine Chemistry*, 194, 124-132, 10.1016/j.marchem.2017.05.011, 2017.
- Mil-Homens, M., Branco, V., Lopes, C., Vale, C., Abrantes, F., Boer, W., and Vicente, M.: Using factor analysis to characterise historical trends of trace metal contamination in a sediment core from the Tagus Prodelta, Portugal, *Water, Air, and Soil Pollution*, 197, 277-287, 2009.
- Millero, F. J., Sotolongo, S., and Izaguirre, M.: The oxidation kinetics of Fe(II) in seawater, *Geochimica et Cosmochimica Acta*, 51, 793-801, 1987.
- Millero, F. J., and Izaguirre, M.: Effect of ionic strength and ionic interactions on the oxidation of Fe(II), *Journal of Solution Chemistry*, 18, 585-599, 1989.

- Millero, F. J., and Sotolongo, S.: The oxidation of Fe(II) with H₂O₂ in seawater, *Geochimica et Cosmochimica Acta*, 53, 1867-1873, 1989.
- Millero, F. J.: Solubility of Fe(III) in seawater, *Earth and Planetary Science Letters*, 154, 323-329, 1998.
- Mills, G. L., and Quinn, J. G.: Isolation of dissolved organic matter and copper-organic complexes from estuarine waters using reverse-phase liquid chromatography, *Marine Chemistry*, 10, 93-102, 10.1016/0304-4203(81)90025-6, 1981.
- Mills, G. L., McFadden, E., and Quinn, J. G.: Chromatographic studies of dissolved organic matter and copper-organic complexes isolated from estuarine waters, *Marine Chemistry*, 20, 313-325, 10.1016/0304-4203(87)90065-X, 1987.
- Mills, M. M., Ridame, C., Davey, M., La Roche, J., and Geider, R. J.: Iron and phosphorus co-limit nitrogen fixation in the eastern tropical North Atlantic, *Nature*, 429, 2004.
- Minami, T., Konagaya, W., Zheng, L., Takano, S., Sasaki, M., Murata, R., Nakaguchi, Y., and Sohrin, Y.: An off-line automated preconcentration system with ethylenediaminetriacetate chelating resin for the determination of trace metals in seawater by high-resolution inductively coupled plasma mass spectrometry, *Analytica Chimica Acta*, 854, 183-190, 2015.
- Mioni, C., Poorvin, L., and Wihelm, S. W.: Virus and siderophore-mediated transfer of available Fe between heterotrophic bacteria: characterization using an Fe-specific bioreporter, *Aquatic Microbial Ecology*, 41, 233-245, 2005.
- Mitchell, B. G.: Predictive bio-optical relationships for polar oceans and marginal ice zones, *Journal of Marine Systems*, 3, 91-105, 1992.
- Mochizuki, N., Tanaka, R., Grimm, B., Masuda, T., Moulin, M., Smith, A. G., Tanaka, A., and Terry, M. J.: The cell biology of tetrapyrroles: a life and death struggle, *Trends in Plant Science*, 15, 488-498, 2010.
- Mock, T., and Thomas, D. N.: Microalgae in Polar Regions: Linking Functional Genomics and Physiology with Environmental Conditions, in: *Psychrophiles: from Biodiversity to Biotechnology*, edited by: al., R. M. e., Springer, Verlag Berlin Heidelberg 285-312, 2008.
- Moeslund, L., Thamdrup, B., and Jorgensen, B. B.: Sulfur and iron cycling in a coastal sediment: radiotracer studies and seasonal dynamics, *Biogeochemistry*, 27, 129-152, 1994.
- Mongin, M., Molina, E., and Trull, T. W.: Seasonality and scale of the Kerguelen plateau phytoplankton bloom: A remote sensing and modeling analysis of the influence of natural iron fertilization in the Southern Ocean, *Deep Sea Research Part II: Topical Studies in Oceanography*, 55, 880-892, 10.1016/j.dsr2.2007.12.039, 2008.
- Moore, C. M., Mills, M. M., Milne, A., Langlois, R., Achterberg, E. P., Lochte, K., Geider, R. J., and La Roche, J.: Iron limits primary productivity during spring bloom development in the central North Atlantic, *Global Change Biology*, 12, 626-634, 10.1111/j.1365-2486.2006.01122.x, 2006.
- Moore, C. M., Mills, M. M., Langlois, R., Milne, A., Achterberg, E. P., La Roche, J., and Geider, R. J.: Relative influence of nitrogen and phosphorus availability on phytoplankton physiology and productivity in the oligotrophic sub-tropical North Atlantic Ocean, *Limnology and Oceanography*, 53, 291-205, 2008.
- Moore, C. M., Mills, M. M., Achterberg, E. P., Geider, R. J., LaRoche, J., Lucas, M. I., McDonagh, E. L., Pan, X., Poulton, A. J., Rijkenberg, M. J. A., Suggett, D. J., Ussher, S. J., and Woodward, E. M. S.: Large-scale distribution of Atlantic nitrogen fixation controlled by iron availability, *Nature Geoscience*, 2, 867-871, 10.1038/ngeo667, 2009.
- Moore, C. M., Mills, M. M., Arrigo, K. R., Berman-Frank, I., Bopp, L., Boyd, P. W., Galbraith, E. D., Geider, R. J., Guieu, C., Jaccard, S. L., Jickells, T. D., La Roche, J., Lenton, T. M., Mahowald, N. M., Marañón,

E., Marinov, I., Moore, J. K., Nakatsuka, T., Oschlies, A., Saito, M. A., Thingstad, T. F., Tsuda, A., and Ulloa, O.: Processes and patterns of oceanic nutrient limitation, *Nature Geoscience*, 6, 701-710, 10.1038/ngeo1765, 2013.

Moore, G. W. K.: Gale force winds over the Irminger Sea to the east of Cape Farewell, Greenland, *Geophysical Research Letters*, 30, n/a-n/a, 10.1029/2003gl018012, 2003.

Moore, J. K., Doney, S. C., Glover, D. M., and Fung, I. Y.: Iron cycling and nutrient limitation patterns in surface waters of the World Ocean, *Deep Sea Research Part II: Topical Studies in Oceanography*, 49, 463-507, 2001.

Moore, J. K., and Braucher, O.: Sedimentary and mineral dust sources of dissolved iron to the world ocean, *Biogeosciences*, 5, 631-656, 10.5194/bg-5-631-2008, 2008.

Moore, W. S.: The effect of submarine groundwater discharge on the ocean, *Ann Rev Mar Sci*, 2, 59-88, 10.1146/annurev-marine-120308-081019, 2010.

Morel, F. M., and Price, N. M.: The biogeochemical cycles of trace metals in the oceans, *Science*, 300, 944-947, 10.1126/science.1083545, 2003.

Morel, F. M. M., Reinfelder, J. R., Roberts, S. B., Chamberlain, C. P., Lee, J. G., and Yee, D.: Zinc and carbon co-limitation of marine phytoplankton, *Nature*, 369, 740-742, 10.1038/369740a0, 1994.

Morel, F. M. M., Milligan, A. J., and Saito, M. A.: Marine Bioinorganic Chemistry: the role of trace metals in the oceanic cycles of major nutrients, in: *The Oceans and Marine Geochemistry*, Elsevier ed., edited by: Elderfield, H., Treatise on Geochemistry, Princeton University, New Jersey, U.S.A., 113-143., 2003.

Morris, P. J., and Charette, M. A.: A synthesis of upper ocean carbon and dissolved iron budgets for Southern Ocean natural iron fertilization studies, *Deep Sea Research Part II: Topical Studies in Oceanography*, 90, 147-157, 10.1016/j.dsr2.2013.02.001, 2013.

Muller, M. N., Trull, T. W., and Hallegraeff, G. M.: Independence of nutrient limitation and carbon dioxide impacts on the Southern Ocean coccolithophore *Emiliania huxleyi*, *ISME J*, 11, 1777-1787, 10.1038/ismej.2017.53, 2017.

Ndung'u, K., Franks, R. P., Bruland, K. W., and Flegal, A. R.: Organic complexation and total dissolved trace metal analysis in estuarine waters: comparison of solvent-extraction graphite furnace atomic absorption spectrometric and chelating resin flow injection inductively coupled plasma-mass spectrometric analysis, *Analytica Chimica Acta*, 481, 127-138, 2003.

Nghiem, S. V., Hall, D. K., Mote, T. L., Tedesco, M., Albert, M. R., Keegan, K., Shuman, C. A., DiGirolamo, N. E., and Neumann, G.: The extreme melt across the Greenland ice sheet in 2012, *Geophysical Research Letters*, 39, 10.1029/2012gl053611, 2012.

Nielsdóttir, M. C., Moore, C. M., Sanders, R., Hinz, D. J., and Achterberg, E. P.: Iron limitation of the postbloom phytoplankton communities in the Iceland Basin, *Global Biogeochemical Cycles*, 23, n/a-n/a, 10.1029/2008gb003410, 2009.

Nishioka, J., Takeda, S., Wong, C. S., and Johnson, W. K.: Size-fractionated iron concentrations in the northeast Pacific Ocean: distribution of soluble and small colloidal iron, *Marine Chemistry*, 74, 157-179, 10.1016/s0304-4203(01)00013-5, 2001.

Nolting, R. F., Gerringa, L. J. A., Swagerman, M. J. W., Timmermans, K. R., and de Baar, H. J. W.: Fe(III) speciation in the high nutrient, low chlorophyll Pacific region of the Southern Ocean, *Marine Chemistry*, 62, 335-352, 10.1016/s0304-4203(98)00046-2, 1998.

Nuester, J., Vogt, S., Newville, M., Kustka, A. B., and Twining, B. S.: The unique biogeochemical signature of the marine diazotroph *trichodesmium*, *Front Microbiol*, 3, 150, 10.3389/fmicb.2012.00150, 2012.

- Nuester, J., Shema, S., Vermont, A., Fields, D. M., and Twining, B. S.: The regeneration of highly bioavailable iron by meso- and microzooplankton, *Limnology and Oceanography*, 59, 1399-1409, 10.4319/lso.2014.59.4.1399, 2014.
- O'Sullivan, D. W., Hanson, A. K., Miller, W. L., and Kester, D. R.: Measurement of Fe(II) in surface water of the equatorial Pacific, *Limnology and Oceanography*, 36, 1727-1741, 1991.
- Obata, H., Karatani, H., and Nakayama, E.: Automated determination of iron in seawater by chelating resin concentration and chemiluminescence detection, *Anal. Chem.*, 65, 1524-1528, 1993.
- Obernosterer, I., Christaki, U., Lefèvre, D., Catala, P., Van Wambeke, F., and Lebaron, P.: Rapid bacterial mineralization of organic carbon produced during a phytoplankton bloom induced by natural iron fertilization in the Southern Ocean, *Deep Sea Research Part II: Topical Studies in Oceanography*, 55, 777-789, 10.1016/j.dsr2.2007.12.005, 2008.
- Ohnemus, D. C., and Lam, P. J.: Cycling of lithogenic marine particles in the US GEOTRACES North Atlantic transect, *Deep Sea Research Part II: Topical Studies in Oceanography*, 116, 283-302, 10.1016/j.dsr2.2014.11.019, 2015.
- Community Ecology Package - Package 'vegan': <http://vegan.r-forge.r-project.org/>, access: 28th May, 2010.
- Olafsson, J., Thors, K., and Cann, J. R.: A sudden cruise off Iceland, *RIDGE Events*, 2, 35-28, 1991.
- Omanović, D., Garnier, C., and Pižeta, I.: ProMCC: An all-in-one tool for trace metal complexation studies, *Marine Chemistry*, 173, 25-39, 10.1016/j.marchem.2014.10.011, 2015.
- Oschlies, A.: Nutrient supply to the surface waters of the North Atlantic: A model study, *Journal of Geophysical Research*, 107, 10.1029/2000jc000275, 2002.
- Paasche, E.: Silicon and the Ecology of Marine Plankton Diatoms. I. *Thalassiosira pseudonana* (*Cyclotella nana*) Grown in a Chemostat with Silicate as Limiting Nutrient, *Marine Biology*, 19, 117-126, 1973.
- Paasche, E.: Roles of nitrogen and phosphorus in coccolith formation in *Emiliania huxleyi* (Prymnesiophyceae), *European Journal of Phycology*, 33, 33-42, 10.1080/09670269810001736513, 1998.
- Padisák, J., Soróczki-Pintér, É., and Reznér, Z.: Sinking properties of some phytoplankton shapes and the relation of form resistance to morphological diversity of plankton – an experimental study, *Hydrobiologia*, 500, 243-257, 10.1023/a:1024613001147, 2003.
- Page, S., Hipkin, C. R., and Flynn, K. J.: Interactions between nitrate and ammonium in *Emiliania huxleyi*, *Journal of Experimental Marine Biology and Ecology*, 236, 307-319, 1999.
- Painter, S. C., Henson, S. A., Forryan, A., Steigenberger, S., Klar, J., Stinchcombe, M. C., Rogan, N., Baker, A. R., Achterberg, E. P., and Moore, C. M.: An assessment of the vertical diffusive flux of iron and other nutrients to the surface waters of the subpolar North Atlantic Ocean, *Biogeosciences*, 11, 2113-2130, 10.5194/bg-11-2113-2014, 2014.
- Pakhomova, S. V., Hall, P. O. J., Kononets, M. Y., Rozanov, A. G., Tengberg, A., and Vershinin, A. V.: Fluxes of iron and manganese across the sediment–water interface under various redox conditions, *Marine Chemistry*, 107, 319-331, 2007.
- Palmer, M. R., Ludford, E. M., German, C. R., and Lilley, M. D.: Dissolved methane and hydrogen in the Steinahóll hydrothermal plume, 63°N, Reykjanes Ridge, in: *Hydrothermal Vents and Processes*, edited by: Parson, L. M., Walker, C. L., and Dixon, D. R., Special Publications, Geological Society, London, 111-120, 1995.

- Palter, J. B., Sarmiento, J. L., Gnanadesikan, A., Simeon, J., and Slater, R. D.: Fueling export production: nutrient return pathways from the deep ocean and their dependence on the Meridional Overturning Circulation, *Biogeosciences*, 7, 3549-3568, 10.5194/bg-7-3549-2010, 2010.
- Parekh, P., Follows, M. J., and Boyle, E. A.: Decoupling of iron and phosphate in the global ocean, *Global Biogeochemical Cycles*, 19, 1-16, 10.1029/2004gb002280, 2005a.
- Parekh, P., Follows, M. J., and Boyle, E. A.: Decoupling of iron and phosphate in the global ocean, *Global Biogeochemical Cycle*, 19, 2005b.
- Parekh, P., Dutkiewicz, S., Follows, M. J., and Ito, T.: Atmospheric carbon dioxide in a less dusty world, *Geophysical Research Letters*, 33, 10.1029/2005gl025098, 2006.
- Paris, R., and Desboeufs, K. V.: Effect of atmospheric organic complexation on iron-bearing dust solubility, *Atmospheric Chemistry and Physics*, 13, 4895-4905, 10.5194/acp-13-4895-2013, 2013.
- Park, Y.-H., Fuda, J.-L., Durand, I., and Naveira Garabato, A. C.: Internal tides and vertical mixing over the Kerguelen Plateau, *Deep Sea Research Part II: Topical Studies in Oceanography*, 55, 582-593, 10.1016/j.dsr2.2007.12.027, 2008a.
- Park, Y.-H., Roquet, F., Durand, I., and Fuda, J.-L.: Large-scale circulation over and around the Northern Kerguelen Plateau, *Deep Sea Research Part II: Topical Studies in Oceanography*, 55, 566-581, 10.1016/j.dsr2.2007.12.030, 2008b.
- Park, Y.-H., Vivier, F., Roquet, F., and Kestenare, E.: Direct observations of the ACC transport across the Kerguelen Plateau, *Geophysical Research Letters*, 36, 10.1029/2009gl039617, 2009.
- Park, Y.-H., Durand, I., Kestenare, E., Rougier, G., Zhou, M., d'Ovidio, F., Cotté, C., and Lee, J.-H.: Polar Front around the Kerguelen Islands: An up-to-date determination and associated circulation of surface/subsurface waters, *Journal of Geophysical Research: Oceans*, 119, 6575-6592, 10.1002/2014jc010061, 2014.
- Parra, M., Delmont, P., Ferragne, A., Latouche, C., Pons, J. C., and Puechmaille, C.: Origin and evolution of smectites in recent marine sediments of the NE Atlantic, *Clay Minerals*, 20, 335-346, 1985.
- Pasquer, B., Laruelle, G., Becquevort, S., Schoemann, V., Goosse, H., and Lancelot, C.: Linking ocean biogeochemical cycles and ecosystem structure and function: results of the complex SWAMCO-4 model, *Journal of Sea Research*, 53, 93-108, 10.1016/j.seares.2004.07.001, 2005.
- Pasquer, B., Metzl, N., Goosse, H., and Lancelot, C.: What drives the seasonality of air-sea CO₂ fluxes in the ice-free zone of the Southern Ocean: A 1D coupled physical-biogeochemical model approach, *Marine Chemistry*, 177, 554-565, 10.1016/j.marchem.2015.08.008, 2015.
- Passow, U.: Production of transparent exopolymer particles (TEP) by phyto- and bacterioplankton, *Marine Ecology Progress Series*, 236, 1-12, 2002.
- Paytan, A., and McLaughlin, K.: The oceanic phosphorus cycle, *Chem Rev*, 107, 563-576, 10.1021/cr0503613, 2007.
- Peers, G., and Price, N. M.: A role for manganese in superoxide dismutases and growth of iron-deficient diatoms, *Limnology and Oceanography*, 49, 1774-1783, 2004.
- Pérez, F. F., Mercier, H., Vázquez-Rodríguez, M., Lherminier, P., Velo, A., Pardo, P. C., Rosón, G., and Ríos, A. F.: Atlantic Ocean CO₂ uptake reduced by weakening of the meridional overturning circulation, *Nature Geoscience*, 6, 146-152, 10.1038/ngeo1680, 2013.
- Pérez, F. F., Treguer, P., Branellec, P., García-Ibáñez, M. I., Lherminier, P., and Sarthou, G.: The 2014 Greenland-Portugal GEOVIDE bottle data (GO-SHIP A25 and GEOTRACES GA01). SEANOE (Ed.), 2018.

- Petrich, C., and Eicken, H.: Growth, structure and properties of sea ice, in: *Sea Ice*. 2nd ed., edited by: Thomas, D. N., and Dieckmann, G. S., Wiley-Blackwell, Oxford, U.K., 23-77, 2010.
- Pickart, R. S., Straneo, F., and Moore, G. W. K.: Is Labrador Sea Water formed in the Irminger basin?, *Deep Sea Research Part I*, 50, 23-52, 2003.
- Piron, A., Thierry, V., Mercier, H., and Caniaux, G.: Argo float observations of basin-scale deep convection in the Irminger sea during winter 2011–2012, *Deep Sea Research Part I: Oceanographic Research Papers*, 109, 76-90, 10.1016/j.dsr.2015.12.012, 2016.
- Pitchford, J. W., and Brindley, J.: Iron limitation, grazing pressure and oceanic high nutrient–low chlorophyll (HNLC) regions, *Journal of Plankton Research*, 21, 525-547, 1999.
- Planquette, H.: Iron biogeochemistry in the waters surrounding the Crozet Islands, Southern Ocean, 2008.
- Poorvin, L., Rinta-Kanto, J. M., Hutchins, D. A., and Wilhelm, S. W.: Viral release of iron and its bioavailability to marine plankton, *Limnology and Oceanography*, 49, 1734-1741, 2004.
- Poulton, S. W., and Raiswell, R.: The low-temperature geochemical cycle of iron: from continental fluxes to marine sediment deposition, *American Journal of Science*, 302, 774–805, 2002.
- Powell, R. T., and Wilson-Finelli, A.: Photochemical degradation of organic iron complexing ligands in seawater, *Aquatic Sciences - Research Across Boundaries*, 65, 367-374, 10.1007/s00027-003-0679-0, 2003.
- Prézelin, B. B., Hofmann, E. E., Mengelt, C., and Klinck, J. M.: The linkage between Upper Circumpolar Deep Water (UCDW) and phytoplankton assemblages on the west Antarctic Peninsula continental shelf, *Journal of Marine Research*, 58, 165-202, 10.1357/002224000321511133, 2000.
- Price, N. M., and Morel, F. M. M.: Cadmium and cobalt substitution for zinc in a marine diatom, *Nature*, 344, 658-660, 1990.
- Prospero, J. M.: Environmental characterization of global sources of atmospheric soil dust identified with the NIMBUS 7 Total Ozone Mapping Spectrometer (TOMS) absorbing aerosol product, *Reviews of Geophysics*, 40, 10.1029/2000rg000095, 2002.
- Quéroué, F., Townsend, A., van der Merwe, P., Lannuzel, D., Sarthou, G., Bucciarelli, E., and Bowie, A.: Advances in the offline trace metal extraction of Mn, Co, Ni, Cu, Cd, and Pb from open ocean seawater samples with determination by sector field ICP-MS analysis, *Analytical Methods*, 6, 2837, 10.1039/c3ay41312h, 2014.
- Quéroué, F., Sarthou, G., Planquette, H. F., Bucciarelli, E., Chever, F., van der Merwe, P., Lannuzel, D., Townsend, A. T., Cheize, M., Blain, S., d'Ovidio, F., and Bowie, A. R.: High variability in dissolved iron concentrations in the vicinity of the Kerguelen Islands (Southern Ocean), *Biogeosciences*, 12, 3869-3883, 10.5194/bg-12-3869-2015, 2015.
- Quigg, A., Finkel, Z. V., Irwin, A. J., Rosenthal, Y., Ho, T. Y., Reinfelder, J. R., Schofield, O., Morel, F. M. M., and Falkowski, P. G.: The evolutionary inheritance of elemental stoichiometry in marine phytoplankton, *Nature*, 425, 291-294, 2003.
- Quigg, A., Irwin, A. J., and Finkel, Z. V.: Evolutionary inheritance of elemental stoichiometry in phytoplankton, *Proceedings Biological sciences*, 278, 526-534, 10.1098/rspb.2010.1356, 2011.
- Radic, A., Lacan, F., and Murray, J. W.: Iron isotopes in the seawater of the equatorial Pacific Ocean: New constraints for the oceanic iron cycle, *Earth and Planetary Science Letters*, 306, 1-10, 10.1016/j.epsl.2011.03.015, 2011.
- Ragueneau, O., Treguer, P., Leynaert, A., Anderson, R. F., Brzezinski, M. A., DeMaster, D. J., Dugdale, R. C., Dymond, J., Fischer, G., Francois, R., Heinze, C., Maier-Reimer, E., Martin-Jezequel, V.,

Nelson, D. M., and Queguiner, B.: A review of the Si cycle in the modern ocean: recent progress and missing gaps in the application of biogenic opal as a paleoproductivity proxy, *Global and Planetary Change*, 26, 317-365, 2000.

Raiswell, R., Tranter, M., Benning, L. G., Siebert, M., De'ath, R., Huybrechts, P., and Payne, T.: Contributions from glacially derived sediment to the global iron (oxyhydr)oxide cycle: Implications for iron delivery to the oceans, *Geochimica et Cosmochimica Acta*, 70, 2765-2780, 10.1016/j.gca.2005.12.027, 2006.

Raiswell, R., Benning, L. G., Tranter, M., and Tulaczyk, S.: Bioavailable iron in the Southern Ocean: the significance of the iceberg conveyor belt, *Geochem Trans*, 9, 1-9, 10.1186/1467-4866-9-7, 2008.

Raiswell, R.: Iceberg-hosted nanoparticulate Fe in the Southern Ocean: Mineralogy, origin, dissolution kinetics and source of bioavailable Fe, *Deep-Sea Research Part II-Topical Studies in Oceanography*, 58, 1364-1375, 10.1016/j.dsr2.2010.11.011, 2011.

Rapp, I., Schlosser, C., Rusiecka, D., Gledhill, M., and Achterberg, E. P.: Automated preconcentration of Fe, Zn, Cu, Ni, Cd, Pb, Co, and Mn in seawater with analysis using high-resolution sector field inductively-coupled plasma mass spectrometry, *Anal Chim Acta*, 976, 1-13, 10.1016/j.aca.2017.05.008, 2017.

Ras, J., Claustre, H., and Uitz, J.: Spatial variability of phytoplankton pigment distribution in the Subtropical South Pacific Ocean: comparison between *in situ* and predicted data, *Biogeosciences*, 5, 353-369, 2008.

Raven, J. A.: The Iron and Molybdenum use Efficiencies of Plant Growth with Different Energy, Carbon and Nitrogen sources, *New Phytologist*, 109, 279-287, 1988.

Raven, J. A., Evans, M. C. W., and Korb, R. E.: The role of trace metals in photosynthetic electron transport in O₂-evolving organisms, *Photosynthesis Research*, 60, 111-150, 1999.

Redfield, A. C.: On the Proportions of Organic Derivatives in Sea Water and Their Relation to the Composition of Plankton, in: *James Johnstone Memorial Volume*, University Press of Liverpool, 176-192, 1934.

Redfield, A. C.: The biological control of chemical factors in the environment, *American Scientist*, 46, 205-221, 1958.

Reid, P. C., Johns, D. G., Edwards, M., Starr, M., Poulin, M., and Snoeijs, P.: A biological consequence of reducing Arctic ice cover: arrival of the Pacific diatom *Neodenticula seminiae* in the North Atlantic for the first time in 800 000 years, *Global Change Biology*, 13, 1910-1921, 10.1111/j.1365-2486.2007.01413.x, 2007.

Reid, R. T., Livet, D. H., Faulkner, D. J., and Butler, A.: A siderophore from a marine bacterium with an exceptional ferric ion affinity constant, *Nature*, 366, 455-458, 10.1038/366455a0, 1993.

Repeta, D. J., Boiteau, R. M., Till, C. P., and Bundy, R. M.: Molecular speciation of trace metal organic ligands in the Pacific Ocean, *Goldschmidt*, Paris, France, 2017.

Resing, J. A., Sedwick, P. N., German, C. R., Jenkins, W. J., Moffett, J. W., Sohst, B. M., and Tagliabue, A.: Basin-scale transport of hydrothermal dissolved metals across the South Pacific Ocean, *Nature*, 523, 200-U140, 10.1038/nature14577, 2015.

Revels, B. N., Ohnemus, D. C., Lam, P. J., Conway, T. M., and John, S. G.: The isotopic signature and distribution of particulate iron in the North Atlantic Ocean, *Deep-Sea Research Part II-Topical Studies in Oceanography*, 116, 321-331, 10.1016/j.dsr2.2014.12.004, 2015.

Rich, H. W., and Morel, F. M. M.: Availability of well-defined iron colloids to the marine diatom *Thalassiosira weissflogii*, *Limnology and Oceanography*, 35, 652-662, 1990.

- Riebesell, U., Schloss, I., and Smetacek, V.: Aggregation of algae released from melting sea ice: implications for seeding and sedimentation, *Polar Biology*, 11, 239-248, 1991.
- Riegman, R., Noordeloos, A. A. M., and Cadée, G. C.: Phaeocystis blooms and eutrophication of the continental coastal zones of the North Sea, *Marine Biology*, 112, 479-484, 1992.
- Riegman, R., and Van Boekel, W.: The ecophysiology of *Pheacystis globosa*: A review, *Journal of Sea Research*, 35, 235-242, 1996.
- Riegman, R., Stolte, W., Noordeloos, A. A. M., and Slezak, D.: Nutrient uptake and alkaline phosphatase (EC 3:1:3:1) activity of *Emiliania huxleyi* (Prymnesiophyceae) during growth under N and P limitation in continuous cultures, *Journal of Phycology*, 36, 87-96, 2000.
- Rijkenberg, M. J., Middag, R., Laan, P., Gerringa, L. J., van Aken, H. M., Schoemann, V., de Jong, J. T., and de Baar, H. J.: The distribution of dissolved iron in the West Atlantic Ocean, *PLoS One*, 9, e101323, 10.1371/journal.pone.0101323, 2014.
- Rijkenberg, M. J. A., Gerringa, L. J. A., Velzeboer, I., Timmermans, K. R., Buma, A. G. J., and de Baar, H. J. W.: Iron-binding ligands in Dutch estuaries are not affected by UV induced photochemical degradation, *Marine Chemistry*, 100, 11-23, 10.1016/j.marchem.2005.10.005, 2006.
- Rijkenberg, M. J. A., Powell, C. F., Dall'Osto, M., Nielsdottir, M. C., Patey, M. D., Hill, P. G., Baker, A. R., Jickells, T. D., Harrison, R. M., and Achterberg, E. P.: Changes in iron speciation following a Saharan dust event in the tropical North Atlantic Ocean, *Marine Chemistry*, 110, 56-67, 10.1016/j.marchem.2008.02.006, 2008.
- Rodellas, V., Garcia-Orellana, J., Tovar-Sanchez, A., Basterretxea, G., Lopez-Garcia, J. M., Sanchez-Quiles, D., Garcia-Solsona, E., and Masque, P.: Submarine groundwater discharge as a source of nutrients and trace metals in a Mediterranean bay (Palma Beach, Balearic Islands), *Marine Chemistry*, 160, 56-66, 10.1016/j.marchem.2014.01.007, 2014.
- Roquet, F., Park, Y.-H., Guinet, C., Bailleul, F., and Charrassin, J.-B.: Observations of the Fawn Trough Current over the Kerguelen Plateau from instrumented elephant seals, *Journal of Marine Systems*, 78, 377-393, 10.1016/j.jmarsys.2008.11.017, 2009.
- Rose, A. L., Salmon, T. P., Lukondeh, T., Neilan, B. A., and Waite, T. D.: Use of Superoxide as an Electron Shuttle for Iron Acquisition by the Marine Cyanobacterium *Lyngbya majuscula*, *Environmental Science & Technology*, 39, 3708 -3715, 10.1021/es048766c, 2005.
- Rost, B., and Riebesell, U.: Coccolithophores and the biological pump: responses to environmental changes, in: *Coccolithophores: from molecular processes to global impact*, edited by: Thierstein, H. R., and Young, J. R., Springer, Berlin, 99-125, 2004.
- Roy, S., Llewellyn, C., Egeland, E. S., and Johnsen, G.: *Phytoplankton Pigments - Characterization, Chemotaxonomy and Applications in Oceanography*, Cambridge Environmental Chemistry Series, edited by: Campbell, P. G. C., Harrison, R. M., and de Mora, S. J., Cambridge University Press, New York, 2011.
- Rubin, M., Berman-Frank, I., and Shaked, Y.: Dust- and mineral-iron utilization by the marine dinitrogen-fixer *Trichodesmium*, *Nature Geoscience*, 4, 529-534, 10.1038/ngeo1181, 2011.
- Rue, E., and Bruland, K.: Domoic acid binds iron and copper: a possible role for the toxin produced by the marine diatom *Pseudo-nitzschia*, *Marine Chemistry*, 76, 127-134, 10.1016/s0304-4203(01)00053-6, 2001.
- Rue, E. L., and Bruland, K. W.: Complexation of iron(III) by natural organic-ligands in the central North Pacific as determined by a new competitive ligand equilibration adsorptive cathodic stripping voltammetric method, *Marine Chemistry*, 50, 117-138, 10.1016/0304-4203(95)00031-1, 1995.

Rue, E. L., and Bruland, K. W.: The role of organic complexation on ambient iron chemistry in the equatorial Pacific Ocean and the response of a mesoscale iron addition experiment, *Limnology and Oceanography*, 42, 901-910, 1997.

Rueter, J. G., Hutchins, D. A., Smith, R. W., and Unsworth, N.: Iron nutrition of *Trichodesmium*, in: *Marine Pelagic Cyanobacteria: Trichodesmium and Other Diazotrophs*, edited by: Carpenter, E. J., Capone, D. G., and Rueter, J. G., Kluwer Academic Publication, Dordrecht, 289-306, 1992.

Ruzic, I.: Theoretical aspects of the direct titration of natural waters and its information yield for trace metal speciation, *Analytica Chimica Acta*, 140, 99-113, 1982.

Ryan-Keogh, T. J., Macey, A. I., Nielsdóttir, M. C., Lucas, M. I., Steigenberger, S. S., Stinchcombe, M. C., Achterberg, E. P., Bibby, T. S., and Moore, C. M.: Spatial and temporal development of phytoplankton iron stress in relation to bloom dynamics in the high-latitude North Atlantic Ocean, *Limnology and Oceanography*, 58, 533-545, 10.4319/lo.2013.58.2.0533, 2013.

Sabine, C. L., Feely, R. A., Gruber, N., Key, R. M., Lee, K., Bullister, J. L., Wanninkhof, R., Wong, C. S., Wallace, D. W. R., Tilbrook, B., Millero, F. J., Peng, T.-H., Kozyr, A., Ono, T., and Rios, A. F.: The Oceanic sink for anthropogenic CO₂, *Science*, 305, 367-371, 2004.

Saito, M. A., Goepfert, T. J., and Ritt, J. T.: Some thoughts on the concept of colimitation: Three definitions and the importance of bioavailability, *Limnology and Oceanography*, 53, 276-290, 2008.

Saito, M. A., Goepfert, T. J., Noble, A. E., Bertrand, E. M., Sedwick, P. N., and DiTullio, G. R.: A seasonal study of dissolved cobalt in the Ross Sea, Antarctica: micronutrient behavior, absence of scavenging, and relationships with Zn, Cd, and P, *Biogeosciences*, 7, 4059-4082, 10.5194/bg-7-4059-2010, 2010.

Sallée, J.-B., Matear, R. J., Rintoul, S. R., and Lenton, A.: Localized subduction of anthropogenic carbon dioxide in the Southern Hemisphere oceans, *Nature Geoscience*, 5, 579-584, 10.1038/ngeo1523, 2012.

Salter, I., Lampitt, R. S., Sanders, R., Poulton, A., Kemp, A. E. S., Boorman, B., Saw, K., and Pearce, R.: Estimating carbon, silica and diatom export from a naturally fertilised phytoplankton bloom in the Southern Ocean using PELAGRA: A novel drifting sediment trap, *Deep-Sea Research Part II-Topical Studies in Oceanography*, 54, 2233-2259, 10.1016/j.dsr2.2007.06.008, 2007.

Sambrotto, R. N., Savidge, G., Robinson, C., Boyd, P., Takahashi, T., Karl, D. M., Langdon, C., Chipman, D., Marra, J., and Codispoti, L.: Elevated consumption of carbon relative to nitrogen in the surface ocean, *Nature*, 363, 248-250, 1993.

Sander, S. G., and Koschinsky, A.: Metal flux from hydrothermal vents increased by organic complexation, *Nature Geoscience*, 4, 145-150, 10.1038/ngeo1088, 2011.

Sanders, R., Brown, L., Henson, S., and Lucas, M.: New production in the Irminger Basin during 2002, *Journal of Marine Systems*, 55, 291-310, [http:// dx.doi.org/10.1016/j.jmarsys.2004.09.002](http://dx.doi.org/10.1016/j.jmarsys.2004.09.002), 2005.

Sanders, R., Henson, S. A., Koski, M., De La Rocha, C. L., Painter, S. C., Poulton, A. J., Riley, J., Salihoglu, B., Visser, A., Yool, A., Bellerby, R., and Martin, A. P.: The Biological Carbon Pump in the North Atlantic, *Progress in Oceanography*, 129, 200-218, 10.1016/j.pocean.2014.05.005, 2014.

Santana-Casiano, J. M., Gonzalez-Davila, M., and Millero, F. J.: The oxidation of Fe(II) in NaCl-HCO₃⁻ and seawater solutions in the presence of phthalate and salicylate ions: a kinetic model, *Marine Chemistry*, 85, 27-40, 10.1016/j.marchem.2003.09.001, 2004.

Santana-Casiano, J. M., Gonzalez-Davila, A., and Millero, F. J.: The role of Fe(II) species on the oxidation of Fe(II) in natural waters in the presence of O₂ and H₂O₂, *Marine Chemistry*, 99, 70-82, 10.1016/j.marchem.2005.03.010, 2006.

Santos-Echeandia, J., Vale, C., Caetano, M., Pereira, P., and Prego, R.: Effect of tidal flooding on metal distribution in pore waters of marsh sediments and its transport to water column (Tagus estuary, Portugal), *Mar Environ Res*, 70, 358-367, 10.1016/j.marenvres.2010.07.003, 2010.

Sarmiento, J. L., Gruber, N., Brzezinski, M. A., and Dunne, J. P.: High-latitude controls of thermocline nutrients and low latitude biological productivity, *Nature*, 427, 56-60, 2004.

Sarmiento, J. L., Gloor, M., Gruber, N., Beaulieu, C., Jacobson, A. R., Mikaloff Fletcher, S. E., Pacala, S., and Rodgers, K.: Trends and regional distributions of land and ocean carbon sinks, *Biogeosciences*, 7, 2351-2367, 10.5194/bg-7-2351-2010, 2010.

Sarthou, G., and Jeandel, C.: Seasonal variations of iron concentrations in the Ligurian Sea and iron budget in the Western Mediterranean Sea, *Marine Chemistry*, 74, 115-129, 10.1016/S0304-4203(00)00119-5, 2001.

Sarthou, G., Baker, A. R., Blain, S., Achterberg, E. P., Boye, M., Bowie, A. R., Croot, P., Laan, P., de Baar, H. J. W., Jickells, T. D., and Worsfold, P. J.: Atmospheric iron deposition and sea-surface dissolved iron concentrations in the eastern Atlantic Ocean, *Deep Sea Research Part I: Oceanographic Research Papers*, 50, 1339-1352, 10.1016/S0967-0637(03)00126-2, 2003.

Sarthou, G., Timmermans, K. R., Blain, S., and Tréguer, P.: Growth physiology and fate of diatoms in the ocean: a review, *Journal of Sea Research*, 53, 25-42, 10.1016/j.seares.2004.01.007, 2005.

Sarthou, G., Baker, A. R., Kramer, J., Laan, P., Laës, A., Ussher, S., Achterberg, E. P., de Baar, H. J. W., Timmermans, K. R., and Blain, S.: Influence of atmospheric inputs on the iron distribution in the subtropical North-East Atlantic Ocean, *Marine Chemistry*, 104, 186-202, 10.1016/j.marchem.2006.11.004, 2007.

Sarthou, G., Vincent, D., Christaki, U., Obernosterer, I., Timmermans, K. R., and Brussaard, C. P. D.: The fate of biogenic iron during a phytoplankton bloom induced by natural fertilisation: Impact of copepod grazing, *Deep Sea Research Part II: Topical Studies in Oceanography*, 55, 734-751, 10.1016/j.dsr2.2007.12.033, 2008.

Sarthou, G., Lherminier, P., Achterberg, E. P., Alonso-Pérez, F., Bucciarelli, E., Boutorh, J., Bouvier, V., Boyle, E. A., Branellec, P., Carracedo, L. I., Casacuberta, N., Castrillejo, M., Cheize, M., Contreira Pereira, L., Cossa, D., Daniault, N., De Saint-Léger, E., Dehairs, F., Deng, F., Desprez de Gésincourt, F., Devesa, J., Foliot, L., Fonseca-Batista, D., Gallinari, M., García-Ibáñez, M. I., Gourain, A., Grossteffan, E., Hamon, M., Heimbürger, L. E., Henderson, G. M., Jeandel, C., Kermabon, C., Lacan, F., Le Bot, P., Le Goff, M., Le Roy, E., Lefebvre, A., Leizour, S., Lemaitre, N., Masqué, P., Ménage, O., Menzel Barraqueta, J.-L., Mercier, H., Perault, F., Pérez, F. F., Planquette, H. F., Planchon, F., Roukaerts, A., Sanial, V., Sauzède, R., Shelley, R. U., Stewart, G., Sutton, J. N., Tang, Y., Tisnérat-Laborde, N., Tonnard, M., Tréguer, P., van Beek, P., Zurbrick, C. M., and Zunino, P.: Introduction to the French GEOTRACES North Atlantic Transect (GA01): GEOVIDE cruise, *Biogeosciences Discussions*, 1-24, 10.5194/bg-2018-312, 2018.

Sathyendranath, S., Cota, G., Stuart, V., Maass, H., and Platt, T.: Remote sensing of phytoplankton pigments: A comparison of empirical and theoretical approaches, *International Journal of Remote Sensing*, 22, 249-273, 10.1080/014311601449925, 2001.

Sato, M., Takeda, S., and Furuya, K.: Iron regeneration and organic iron(III)-binding ligand production during in situ zooplankton grazing experiment, *Marine Chemistry*, 106, 471-488, 10.1016/j.marchem.2007.05.001, 2007.

Savidge, G., Boyd, P. W., Pomroy, A., Harbour, D., and Joint, I.: Phytoplankton production and biomass estimates in the northeast Atlantic Ocean, May-June 1990, *Deep Sea Research Part I: Oceanographic Research Papers*, 42, 599-617, 1995.

Scatchard, G., Coleman, J. S., and Shen, A. L.: Physical Chemistry of Protein Solutions. VII. The binding of Some Small Anions to Serum Albumin, *Journal of the American Chemical Society*, 79, 12-20, 1957.

Schallenberg, C., Bestley, S., Klocker, A., Trull, T. W., Davies, D. M., Gault-Ringold, M., Eriksen, R., Roden, N. P., Sander, S., Sumner, M., Townsend, A. T., Merwe, P. v. d., Westwood, K., Wuttig, K., and Bowie, A.: Sustained upwelling of subsurface iron supplies seasonally persistent phytoplankton blooms around the southern Kerguelen plateau, Southern Ocean, in prep.

Schindler, D. W.: Evolution of Phosphorus Limitation in Lakes, *Science*, 195, 260-262, 10.1126/science.195.4275.260, 1977.

Ocean Data View, <https://odv.awi.de> ODV4, version 4.7.6 (23 March 2016), access: 6 April, 2016.

Schlitzer, R., Anderson, R. F., Dodas, E. M., Lohan, M., Geibert, W., Tagliabue, A., Bowie, A., Jeandel, C., Maldonado, M. T., Landing, W. M., Cockwell, D., Abadie, C., Abouchami, W., Achterberg, E. P., Agather, A., Aguiar-Islas, A., Aken, H. M. v., Andersen, M., Archer, C., Auro, M., Baar, H. J. d., Baars, O., Baker, A. R., Bakker, K., Basak, C., Baskaran, M., Bates, N. R., Bauch, D., Beek, P. v., Behrens, M. K., Black, E., Bluhm, K., Bopp, L., Bouman, H., Bowman, K., Bown, J., Boyd, P., Boye, M., Boyle, E. A., Branellec, P., Bridgestock, L., Brissebrat, G., Browning, T., Bruland, K. W., Brumsack, H.-J., Brzezinski, M., Buck, C. S., Buck, K. N., Buesseler, K., Bull, A., Butler, E., Cai, P., Mor, P. C., Cardinal, D., Carlson, C., Carrasco, G., Casacuberta, N., Casciotti, K. L., Castrillejo, M., Chamizo, E., Chance, R., Charette, M. A., Chaves, J. E., Cheng, H., Chever, F., Christl, M., Church, T. M., Closset, I., Colman, A., Conway, T. M., Cossa, D., Croot, P., Cullen, J. T., Cutter, G. A., Daniels, C., Dehairs, F., Deng, F., Dieu, H. T., Duggan, B., Dulaquais, G., Dumousseaud, C., Echegoyen-Sanz, Y., Edwards, R. L., Ellwood, M., Fahrbach, E., Fitzsimmons, J. N., Flegal, A. R., Fleisher, M. Q., Flierdt, T. v. d., Frank, M., Friedrich, J., Fripiat, F., Fröllje, H., Galer, S. J. G., Gamo, T., Ganeshram, R. S., Garcia-Orellana, J., Garcia-Solsona, E., Gault-Ringold, M., George, E., Gerringa, L. J. A., Gilbert, M., Godoy, J. M., Goldstein, S. L., Gonzalez, S. R., Grissom, K., Hammerschmidt, C., Hartman, A., Hassler, C. S., Hathorne, E. C., Hatta, M., Hawco, N., Hayes, C. T., Heimbürger, L.-E., Helgoe, J., Heller, M., Henderson, G. M., Henderson, P. B., Heuven, S. v., Ho, P., Horner, T. J., Hsieh, Y.-T., Huang, K.-F., Humphreys, M. P., Isshiki, K., Jacquot, J. E., Janssen, D. J., Jenkins, W. J., John, S., Jones, E. M., Jones, J. L., Kadko, D. C., Kayser, R., Kenna, T. C., Khondoker, R., Kim, T., Kipp, L., Klar, J. K., Klunder, M., Kretschmer, S., Kumamoto, Y., Laan, P., Labatut, M., Lacan, F., Lam, P. J., Lambelet, M., Lamborg, C. H., Moigne, F. A. C. L., Roy, E. L., Lechtenfeld, O. J., Lee, J.-M., Lherminier, P., Little, S., López-Lora, M., Lu, Y., Masque, P., Mawji, E., McClain, C. R., Measures, C., Mehic, S., Barraqueta, J.-L. M., Merwe, P. v. d., Middag, R., Mieruc, S., Milne, A., Minami, T., Moffett, J. W., Moncoiffe, G., Moore, W. S., Morris, P. J., Morton, P. L., Nakaguch, Y., Nakayama, N., Niedermiller, J., Nishioka, J., Nishiuchi, A., Noble, A., Obata, H., Ober, S., Ohnemus, D. C., Ooijen, J. v., O'Sullivan, J., Owens, S., Pahnke, K., Paul, M., Pavia, F., Pena, L. D., Peters, B., Planchon, F., Planquette, H., Pradoux, C., Puigcorbé, V., Quay, P., Queroue, F., Radic, A., Rauschenberg, S., Rehkämper, M., Rember, R., Remenyi, T., Resing, J. A., Rickli, J., Rigaud, S., Rijkenberg, M. J. A., Rintoul, S., Robinson, L. F., Roca-Martí, M., Rodellas, V., Roeske, T., Rolison, J. M., Rosenberg, M., Roshan, S., Loeff, M. M. R. v. d., Ryabenko, E., Saito, M. A., Salt, L. A., Sanial, V., Sarthou, G., Schallenberg, C., Schauer, U., Scher, H., Schlosser, C., Schnetger, B., Scott, P., Sedwick, P. N., Semiletov, I., Shelley, R., Sherrell, R. M., Shiller, A. M., Sigman, D. M., Singh, S. K., Slagter, H. A., Slater, E., Smethie, W. M., Snaith, H., Sohrin, Y., Sohst, B., Sonke, J. E., Speich, S., Steinfeldt, R., Stewart, G., Stichel, T., Stirling, C. H., Stutsman, J., Swarr, G. J., Swift, J. H., Thomas, A., Thorne, K., Till, C. P., Till, R., Townsend, A. T., Townsend, E., Tuerena, R., Twining, B. S., Vance, D., Velazquez, S., Venchiarutti, C., Villa-Alfageme, M., Vivancos, S. M., Voelker, A. H. L., Wake, B., Warner, M. J., Watson, R., Weerlee, E. v., Weigand, M. A., Weinstein, Y., Weiss, D., Wisotzki, A., Woodward, E. M. S., Wu, J., Wu, Y., Wuttig, K., Wyatt, N., Xiang, Y., Xie, R. C., Xue, Z., Yoshikawa, H., Zhang, J., Zhang, P., Zhao, Y., Zheng, L., Zheng, X.-Y., Zieringer, M., Zimmer, L. A., Ziveri, P., Zunino, P., and Zurbick, C.: The GEOTRACES Intermediate Data Product 2017, *Chemical Geology*, 493, 210-223, 10.1016/j.chemgeo.2018.05.040, 2018.

Schlosser, C., and Croot, P. L.: Application of cross-flow filtration for determining the solubility of iron species in open ocean seawater, *Limnology and Oceanography: Methods*, 6, 630-642, 2008.

Schlüter, L., and Møhlenberg, F.: Detecting presence of phytoplankton groups with non-specific pigment signatures, *Journal of Applied Phycology*, 15, 465-476, 2003.

Schoemann, V., Becquevort, S., Stefels, J., Rousseau, V., and Lancelot, C.: Phaeocystis blooms in the global ocean and their controlling mechanisms: a review, *Journal of Sea Research*, 53, 43-66, 10.1016/j.seares.2004.01.008, 2005.

- Schoof, C.: Marine ice-sheet dynamics. Part 1. The case of rapid sliding, *Journal of Fluid Mechanics*, 573, 10.1017/s0022112006003570, 2007.
- Schroth, A. W., Crusius, J., Hoyer, I., and Campbell, R.: Estuarine removal of glacial iron and implications for iron fluxes to the ocean, *Geophysical Research Letters*, 41, 3951-3958, 10.1002/2014GL060199, 2014.
- Sedwick, P. N., Edwards, P. R., Mackey, D. J., Griffiths, F. B., and Parslow, J. S.: Iron and manganese in surface waters of the Australian subantarctic region, *Deep-Sea Research Part I-Oceanographic Research Papers*, 44, 1239-1253, 10.1016/s0967-0637(97)00021-6, 1997.
- Severmann, S., McManus, J., Berelson, W. M., and Hammond, D. E.: The continental shelf benthic iron flux and its isotope composition, *Geochimica et Cosmochimica Acta*, 74, 3984-4004, 10.1016/j.gca.2010.04.022, 2010.
- Shaked, Y., Kustka, A. B., and Morel, F. M. M.: A general kinetic model for iron acquisition by eukaryotic phytoplankton, *Limnology and Oceanography*, 50, 872-882, 2005.
- Shaked, Y., Xu, Y., Leblanc, K., and Morel, F. M. M.: Zinc availability and alkaline phosphatase activity in *Emiliania huxleyi*: Implications for Zn-P co-limitation in the ocean, *Limnology and Oceanography*, 51, 299-309, 2006.
- Shaw, T. J., Raiswell, R., Hexel, C. R., Vu, H. P., Moore, W. S., Dudgeon, R., and Smith, K. L., Jr.: Input, composition, and potential impact of terrigenous material from free-drifting icebergs in the Weddell Sea, *Deep-Sea Research Part Ii-Topical Studies in Oceanography*, 58, 1376-1383, 10.1016/j.dsr.2010.11.012, 2011.
- Shelley, R. U., Morton, P. L., and Landing, W. M.: Elemental ratios and enrichment factors in aerosols from the US-GEOTRACES North Atlantic transects, *Deep Sea Research*, 116, 262-272, 2015.
- Shelley, R. U., Roca-Martí, M., Castrillejo, M., Sanial, V., Masqué, P., Landing, W. M., van Beek, P., Planquette, H., and Sarthou, G.: Quantification of trace element atmospheric deposition fluxes to the Atlantic Ocean (>40°N; GEOVIDE, GEOTRACES GA01) during spring 2014, *Deep Sea Research Part I: Oceanographic Research Papers*, 119, 34-49, 10.1016/j.dsr.2016.11.010, 2017.
- Shelley, R. U., Landing, W. M., Ussher, S. J., Planquette, H., and Sarthou, G.: Characterisation of aerosol provenance from the fractional solubility of Fe (Al, Ti, Mn, Co, Ni, Cu, Zn, Cd and Pb) in North Atlantic aerosols (GEOTRACES cruises GA01 and GA03) using a two stage leach, *Biogeosciences*, 2018.
- Sholkovitz, E. R.: Flocculation of dissolved Fe, Mn, Al, Cu, Ni, Co and Cd during estuarine mixing, *Earth and Planetary Science Letters*, 41, 77-86, 10.1016/0012-821X(78)90043-2, 1978.
- Shor, A., Lonsdale, P., Hollister, D., and Spencer, D.: Charlie-Gibbs fracture zone: bottom-water transport and its geological effects, *Deep Sea Research*, 27A, 325-345, 1980.
- Sieracki, M. E., Verity, P. G., and Stoecker, D. K.: Plankton community response to sequential silicate and nitrate depletion during the 1989 North Atlantic spring bloom, *Deep-Sea Research*, 40, 213-225, 1993.
- Sinha, M. C., Navin, D. A., MacGregor, L. M., Constable, S., Peirce, C., White, A., Heinson, G., and Inglis, M. A.: Evidence for accumulated melt beneath the slow-spreading Mid-Atlantic Ridge, *Philosophical Transactions of the Royal Society A*, 355, 233-253, 1997.
- Slagter, H. A., Reader, H. E., Rijkenberg, M. J. A., Rutgers van der Loeff, M., de Baar, H. J. W., and Gerringa, L. J. A.: Organic Fe speciation in the Eurasian Basins of the Arctic Ocean and its relation to terrestrial DOM, *Marine Chemistry*, 197, 11-25, 10.1016/j.marchem.2017.10.005, 2017.
- Smallwood, J. R., and White, R. S.: Crustal accretion at the Reykjanes Ridge, 61°-62°N, *Journal of Geophysical Research: Solid Earth*, 103, 5185-5201, 10.1029/97jb03387, 1998.

Smetacek, V., Klaas, C., Strass, V. H., Assmy, P., Montresor, M., Cisewski, B., Savoye, N., Webb, A., d'Ovidio, F., Arrieta, J. M., Bathmann, U., Bellerby, R., Berg, G. M., Croot, P., Gonzalez, S., Henjes, J., Herndl, G. J., Hoffmann, L. J., Leach, H., Losch, M., Mills, M. M., Neill, C., Peeken, I., Rottgers, R., Sachs, O., Sauter, E., Schmidt, M. M., Schwarz, J., Terbruggen, A., and Wolf-Gladrow, D.: Deep carbon export from a Southern Ocean iron-fertilized diatom bloom, *Nature*, 487, 313-319, 10.1038/nature11229, 2012.

Smetacek, V. S.: Role of sinking in diatom life-history cycles: ecological, evolutionary and geological significance, *Marine Biology*, 84, 239-251, 1985.

Smith Jr., K. L., Robinson, B. H., Helly, J. J., Kaufmann, R. S., Ruhl, H. A., Shaw, T. J., Twining, B. S., and Vernet, M.: Free-Drifting Icebergs: Hot Spots of Chemical and Biological Enrichment in the Weddell Sea, *Science*, 317, 478-482, 10.1126/science.1142834, 2007.

Sohm, J. A., Webb, E. A., and Capone, D. G.: Emerging patterns of marine nitrogen fixation, *Nat Rev Microbiol*, 9, 499-508, 10.1038/nrmicro2594, 2011.

Spain, E., Johnson, S., Hutton, B., Whittaker, J., Lucieer, V., Watson, S., Fox, J., and Coffin, M. F.: Shallow seafloor gas emissions near Heard and McDonald islands on the Kerguelen Plateau, Southern Indian Ocean, in prep.

Statham, P. J., German, C. R., and Connelly, D. P.: Iron(II) distribution and oxidation kinetics in hydrothermal plumes at the Kairei and Edmond vent sites, Indian Ocean, *Earth and Planetary Science Letters*, 236, 588-596, 10.1016/j.epsl.2005.03.008, 2005.

Statham, P. J., Skidmore, M., and Tranter, M.: Inputs of glacially derived dissolved and colloidal iron to the coastal ocean and implications for primary productivity, *Global Biogeochemical Cycles*, 22, 1-11, 10.1029/2007GB003106, 2008.

Stauber, J. L., and Jeffrey, S. W.: Photosynthetic pigments in fifty-one species of marine diatoms, *Journal of Phycology*, 24, 158-172, 1988.

Steinberg, D. K., Carlson, C. A., Bates, N. R., Goldthwait, S. A., Madin, L. P., and Michaels, A. F.: Zooplankton vertical migration and the active transport of dissolved organic and inorganic carbon in the Sargasso Sea, *Deep Sea Research*, 47, 137-158, 2000.

Steinberg, D. K., Van Mooy, B. A. S., Buesseler, K. O., Boyd, P. W., Kobari, T., and Karl, D. M.: Bacterial vs. zooplankton control of sinking particle flux in the ocean's twilight zone, *Limnology and Oceanography*, 53, 1327-1338, 2008.

Sterner, R. W., and Elser, J. J.: *Ecological Stoichiometry: Biology of Elements from Molecules to the Biosphere*, Princeton University Press, Princeton, NJ, USA, 2002.

Stintzi, A., Barnes, C., Xu, J., and Raymond, K. N.: Microbial iron transport via a siderophore shuttle: A membrane ion transport paradigm, *PNAS*, 97, 10691-10696, 2000.

Stolpe, B., Guo, L., Shiller, A. M., and Hasselov, M.: Size and composition of colloidal organic matter and trace elements in the Mississippi River, Pearl River and the northern Gulf of Mexico, as characterized by flow field-flow fractionation, *Marine Chemistry*, 118, 119-128, 10.1016/j.marchem.2009.11.007, 2010.

Stroeve, J. C., Markus, T., Boisvert, L., Miller, J., and Barrett, A.: Changes in Arctic melt season and implications for sea ice loss, *Geophysical Research Letters*, 41, 1216-1225, 10.1002/2013gl058951, 2014.

Strzepek, R. F., Maldonado, M. T., Higgins, J. L., Hall, J., Safi, K., Wilhelm, S. W., and Boyd, P. W.: Spinning the "Ferrous Wheel": The importance of the microbial community in an iron budget during the FeCycle experiment, *Global Biogeochemical Cycles*, 19, n/a-n/a, 10.1029/2005gb002490, 2005.

Stuart, V., Sathyendranath, S., Head, E. J. H., Platt, T., Irwin, B., and Maass, H.: Bio-optical characteristics of diatom and prymnesiophyte populations in the Labrador Sea, *Marine Ecology Progress Series*, 201, 91-106, 2000.

Stumm, W.: Chemistry of the solid-water interface: processes at the mineral-water and particle-water interface in natural systems, John Wiley & Son Inc., New York, U.S.A., 1992.

Stumm, W., and Morgan, J. J.: Chemical Equilibria and Rates in Natural Waters, in: Aquatic Chemistry, John Wiley & Son Inc., New York, U.S.A., 1996.

Sunda, W., and Huntsman, S.: Effect of pH, light, and temperature on Fe-EDTA chelation and Fe hydrolysis in seawater, *Marine Chemistry*, 84, 35-47, 10.1016/s0304-4203(03)00101-4, 2003.

Sunda, W. G.: Trace metal interactions with marine phytoplankton, *Biological oceanography*, 6, 411-442, 10.1080/01965581.1988.10749543, 1989.

Sunda, W. G., and Huntsman, S. A.: Iron uptake and growth limitation in oceanic and coastal phytoplankton, *Marine Chemistry*, 50, 189-206, 10.1016/0304-4203(95)00035-p, 1995a.

Sunda, W. G., and Huntsman, S. A.: Cobalt and zinc interreplacement in marine phytoplankton: Biological and geochemical implications, *Limnology and Oceanography*, 40, 1404-1417, 1995b.

Sunda, W. G.: Feedback Interactions between Trace Metal Nutrients and Phytoplankton in the Ocean, *Front Microbiol*, 3, 204, 10.3389/fmicb.2012.00204, 2012.

Sutherland, D. A., Pickart, R. S., Peter Jones, E., Azetsu-Scott, K., Jane Eert, A., and Ólafsson, J.: Freshwater composition of the waters off southeast Greenland and their link to the Arctic Ocean, *Journal of Geophysical Research*, 114, 10.1029/2008jc004808, 2009.

Sverdrup, H. U.: On conditions for the vernal blooming of phytoplankton, *ICES Journal of Marine Science*, 18, 287-295, 1953.

Tagliabue, A., and Arrigo, K. R.: Iron in the Ross Sea: 1. Impact on CO₂ fluxes via variation in phytoplankton functional group and non-Redfield stoichiometry, *Journal of Geophysical Research: Oceans*, 110, 1-15, 10.1029/2004jc002531, 2005.

Tagliabue, A., Bopp, L., Aumont, O., and Arrigo, K. R.: Influence of light and temperature on the marine iron cycle: From theoretical to global modeling, *Global Biogeochemical Cycles*, 23, n/a-n/a, 10.1029/2008gb003214, 2009.

Tagliabue, A., Bopp, L., Dutay, J.-C., Bowie, A. R., Chever, F., Jean-Baptiste, P., Bucciarelli, E., Lannuzel, D., Remenyi, T., Sarthou, G., Aumont, O., Gehlen, M., and Jeandel, C.: Hydrothermal contribution to the oceanic dissolved iron inventory, *Nature Geoscience*, 3, 252-256, 10.1038/ngeo818, 2010.

Tagliabue, A., and Volker, C.: Towards accounting for dissolved iron speciation in global ocean models, *Biogeosciences*, 8, 2011.

Tagliabue, A., Mtshali, T., Aumont, O., Bowie, A. R., Klunder, M. B., Roychoudhury, A. N., and Swart, S.: A global compilation of dissolved iron measurements: focus on distributions and processes in the Southern Ocean, *Biogeosciences*, 9, 2333-2349, 10.5194/bg-9-2333-2012, 2012.

Tagliabue, A., Aumont, O., and Bopp, L.: The impact of different external sources of iron on the global carbon cycle, *Geophysical Research Letters*, 41, 920-926, 10.1002/2013gl059059, 2014a.

Tagliabue, A., Sallée, J.-B., Bowie, A. R., Lévy, M., Swart, S., and Boyd, P. W.: Surface-water iron supplies in the Southern Ocean sustained by deep winter mixing, *Nature Geoscience*, 7, 314-320, 10.1038/ngeo2101, 2014b.

Tagliabue, A., Aumont, O., DeAth, R., Dunne, J. P., Dutkiewicz, S., Galbraith, E., Misumi, K., Moore, J. K., Ridgwell, A., Sherman, E., Stock, C., Vichi, M., Völker, C., and Yool, A.: How well do global ocean biogeochemistry models simulate dissolved iron distributions?, *Global Biogeochemical Cycles*, 30, 149-174, 10.1002/2015gb005289, 2016.

Tagliabue, A., Bowie, A. R., Boyd, P. W., Buck, K. N., Johnson, K. S., and Saito, M. A.: The integral role of iron in ocean biogeochemistry, *Nature*, 543, 51-59, 2017.

Takahashi, T., Sutherland, S. C., Sweeney, C., Poisson, A., Metzl, N., Tilbrook, B., Bates, N., Wanninkhof, R., Feely, R. A., Sabine, C., Olafsson, J., and Nojiri, Y.: Global sea-air CO₂ flux based on climatological surface ocean pCO₂, and seasonal biological and temperature effects, *Deep Sea Research Part II: Topical Studies in Oceanography*, 49, 10.1016/S0967-0645(02)00003-6, 2002.

Takeda, S.: Influence of iron availability on nutrient consumption ratio of diatoms in oceanic waters, *Nature*, 393, 774-777, 1998.

Tanhua, T., Olsson, K. A., and Jeansson, E.: Formation of Denmark Strait overflow water and its hydro-chemical composition, *Journal of Marine Systems*, 57, 264-288, 10.1016/j.jmarsys.2005.05.003, 2005.

Tebo, B. M., Bargar, J. R., Clement, B. G., Dick, G. J., Murray, K. J., Parker, D., Verity, R., and Webb, S. M.: Biogenic Manganese Oxides: Properties and Mechanisms of Formation, *Annual Review of Earth and Planetary Sciences*, 32, 287-328, 10.1146/annurev.earth.32.101802.120213, 2004.

Teng, Z., Huang, J. Y., Fujito, K., and Takizawa, S.: Manganese removal by hollow fiber micro-filter. Membrane separation for drinking water, *European Conference on Desalination and the Environment*, Amsterdam, 28 May, 2001.

Ternon, E., Guieu, C., Loÿe-Pilot, M. D., Leblond, N., Bosc, E., Gasser, B., and Miquel, J. C.: The impact of Saharan dust on the particulate export in the water column of the North Western Mediterranean Sea, *Biogeosciences Discussions*, 6, 10737-10773, 10.5194/bgd-6-10737-2009, 2009.

Thompson, A. W., Foster, R. A., Krupke, A., Carter, B. J., Musat, N., Vulot, D., Kuypers, M. M. M., and Zehr, J. P.: Unicellular Cyanobacterium Symbiotic with a Single-Celled Eukaryotic Alga, *Science*, 337, 1546-1550, 10.1126/science.1222700, 2012.

Thuróczy, C. E., Gerringa, L. J. A., Klunder, M. B., Middag, R., Laan, P., Timmermans, K. R., and de Baar, H. J. W.: Speciation of Fe in the Eastern North Atlantic Ocean, *Deep Sea Research Part I: Oceanographic Research Papers*, 57, 1444-1453, 10.1016/j.dsr.2010.08.004, 2010.

Tian, F., Frew, R. D., Sander, S., Hunter, K. A., and Ellwood, M. J.: Organic iron(III) speciation in surface transects across a frontal zone: the Chatham Rise, New Zealand, *Marine and Freshwater Research*, 57, 533-544, 10.1071/mf05209, 2006.

Timmermans, K. R., van Leeuwel, M. A., de Jong, J. T. M., McKay, R. M. L., Nolting, R. F., Witte, H. J., van Ooyen, J., Swagerman, M. J. W., Kloosterhuis, H., and de Baar, H. J. W.: Iron stress in the Pacific region of the Southern Ocean: Evidence from enrichment bioassays, *Marine Ecology Progress Series*, 166, 27-41, 1998.

Tonnard, M., Donval, A., Lampert, L., Tréguer, P., Bowie, A. R., van der Merwe, P., planquette, H., Claustre, H., Dimier, C., Ras, J., and Sarthou, G.: Phytoplankton assemblages in the North Atlantic Ocean and in the Labrador Sea along the GEOVIDE section (GEOTRACES section GA01) determined by CHEMTAX analysis from HPLC pigment data, *Biogeosciences*, in prep.

Tonnard, M., Planquette, H., Bowie, A. R., van der Merwe, P., Gallinari, M., Desprez de Gésincourt, F., Germain, Y., Gourain, A., Benetti, M., Reverdin, G., Tréguer, P., Boutorh, J., Cheize, M., Menzel Barraqueta, J. L., Pereira Contreira, L., Shelley, R. U., Lherminier, P., and Sarthou, G.: Dissolved iron in the North Atlantic ocean and in the Labrador Sea along the GEOVIDE section (GEOTRACES section GA01), *Biogeosciences Discussions*, submitted.

Torondel, B., Ensink, J. H. J., Gundogdu, O., Ijaz, U. Z., Parkhill, J., Abdelahi, F., Nguyen, V.-A., Sudgen, S., Gibson, Walker, A. W., and Quince, C.: Assessment of the influence of intrinsic environmental and geographical factors on the bacterial ecology of pit latrines, *Microbial Biotechnology*, 9, 209-223, 10.1111/1751-7915.12334, 2016.

Torres-Valdés, S., Tsubouchi, T., Bacon, S., Naveira-Garabato, A. C., Sanders, R., McLaughlin, F. A., Petrie, B., Kattner, G., Azetsu-Scott, K., and Whitley, T. E.: Export of nutrients from the Arctic Ocean, *Journal of Geophysical Research: Oceans*, 118, 1625-1644, 10.1002/jgrc.20063, 2013.

Tovar-Sanchez, A., Duarte, C. M., Alonso, J. C., Lacorte, S., Tauler, R., and Galban-Malagon, C.: Impacts of metals and nutrients released from melting multiyear Arctic sea ice, *Journal of Geophysical Research-Oceans*, 115, 10.1029/2009jc005685, 2010.

Tréguer, P. J., and De La Rocha, C. L.: The world ocean silica cycle, *Ann Rev Mar Sci*, 5, 477-501, 10.1146/annurev-marine-121211-172346, 2013.

Tremblay, J. É., Gratton, Y., Carmack, E. C., Payne, C. D., and Price, N. M.: Impact of the large-scale Arctic circulation and the North Water Polynya on nutrient inventories in Baffin Bay, *Journal of Geophysical Research*, 107, 1-26, 10.1029/2000jc000595, 2002.

Turley, C. M., and Mackie, P. J.: Biogeochemical significance of attached and free-living bacteria and the flux of particles in the NE Atlantic Ocean *Marine Ecology Progress Series*, 115, 191-203, 1994.

Turner, J. T.: Zooplankton fecal pellets, marine snow and sinking phytoplankton blooms, *Aquatic Microbial Ecology*, 27, 57-102, 2002.

Turner, J. T.: Zooplankton fecal pellets, marine snow, phytodetritus and the ocean's biological pump, *Progress in Oceanography*, 130, 205-248, 10.1016/j.pocean.2014.08.005, 2015.

Twining, B. S., Baines, S. B., and Fisher, N. S.: Element stoichiometries of individual plankton cells collected during the Southern Ocean Iron Experiment (SOFEX), *Limnology and Oceanography*, 49, 2115-2128, 2004a.

Twining, B. S., Baines, S. B., Fisher, N. S., and Landry, M. R.: Cellular iron contents of plankton during the Southern Ocean Iron Experiment (SOFEX), *Deep Sea Research Part I: Oceanographic Research Papers*, 51, 1827-1850, 10.1016/j.dsr.2004.08.007, 2004b.

Twining, B. S., and Baines, S. B.: The trace metal composition of marine phytoplankton, *Ann Rev Mar Sci*, 5, 191-215, 10.1146/annurev-marine-121211-172322, 2013.

Tyrell, T., Maranon, E., Poulton, A. J., Bowie, A. R., Harbour, D. S., and Woodward, E. M. S.: Large-scale latitudinal distribution of *Trichodesmium* spp. in the Atlantic Ocean, *Journal of Plankton Research*, 25, 405-416, 2003.

Uitz, J., Claustre, H., Morel, A., and Hooker, S. B.: Vertical distribution of phytoplankton communities in open ocean: An assessment based on surface chlorophyll, *Journal of Geophysical Research*, 111, 1-23, 2006.

Uitz, J., Claustre, H., Griffiths, F. B., Ras, J., Garcia, N., and Sandroni, V.: A phytoplankton class-specific primary production model applied to the Kerguelen Islands region (Southern Ocean), *Deep Sea Research Part I: Oceanographic Research Papers*, 56, 541-560, 10.1016/j.dsr.2008.11.006, 2009.

Ussher, S. J., Achterberg, E. P., Sarthou, G., Laan, P., de Baar, H. J. W., and Worsfold, P. J.: Distribution of size fractionated dissolved iron in the Canary Basin, *Marine Environmental Research*, 70, 46-55, 2010.

Ussher, S. J., Achterberg, E. P., Powell, C., Baker, A. R., Jickells, T. D., Torres, R., and Worsfold, P. J.: Impact of atmospheric deposition on the contrasting iron biogeochemistry of the North and South Atlantic Ocean, *Global Biogeochemical Cycles*, 27, 1096-1107, 10.1002/gbc.20056, 2013.

Van Beusekom, J. E. E.: Distribution of aluminium in surface waters of the North Sea: influence of suspended matter., in: *Biogeochemistry and Distribution of Suspended Matter in the North Sea and Implications to fisheries Biology*, edited by: Kempe, S., Mittleitungen aus dem Geologisch-Paläontologischen Institut der Universität Hamburg, SCOPE/UNEP Sonderband, 117-136, 1988.

van de Poll, W. H., Kulk, G., Timmermans, K. R., Brussaard, C. P. D., van der Woerd, H. J., Kehoe, M. J., Mojica, K. D. A., Visser, R. J. W., Rozena, P. D., and Buma, A. G.: Phytoplankton chlorophyll *a* biomass, composition, and productivity along a temperature and stratification gradient in the northeast Atlantic Ocean, *Biogeosciences*, 10, 4227-4240, 2013.

Van den Berg, C. M. G.: Detremination of the complexing capacity and conditional stability constants of complexes of copper(II) with natural organic ligands in seawater by cathodic stripping voltammetry of copper - Catechol complex ions, *Marine Chemistry*, 15, 1-18, 1984.

Van den Berg, C. M. G.: Evidence for organic complexation of iron in seawater, *Marine Chemistry*, 50, 139-157, 10.1016/0304-4203(95)00032-m, 1995.

Van den Berg, C. M. G.: Chemical Speciation of Iron in Seawater by Cathodic Stripping Voltammetry with Dihydroxynaphthalene, *Analytical Chemistry*, 78, 156-163, 2006.

van der Merwe, P., Lannuzel, D., Nichols, C. A. M., Meiners, K., Heil, P., Norman, L., Thomas, D. N., and Bowie, A. R.: Biogeochemical observations during the winter-spring transition in East Antarctic sea ice: Evidence of iron and exopolysaccharide controls, *Marine Chemistry*, 115, 163-175, 10.1016/j.marchem.2009.08.001, 2009.

van der Merwe, P., Lannuzel, D., Bowie, A. R., and Meiners, K. M.: High temporal resolution observations of spring fast ice melt and seawater iron enrichment in East Antarctica, *Journal of Geophysical Research-Biogeosciences*, 116, 10.1029/2010jg001628, 2011.

van der Merwe, P., Bowie, A. R., Quéroué, F., Armand, L., Blain, S., Chever, F., Davies, D., Dehairs, F., Planchon, F., Sarthou, G., Townsend, A. T., and Trull, T. W.: Sourcing the iron in the naturally fertilised bloom around the Kerguelen Plateau: particulate trace metal dynamics, *Biogeosciences*, 12, 739-755, 10.5194/bg-12-739-2015, 2015.

van Heukelem, L., and Thomas, C. S.: Computer-assisted high performance liquid chromatography method development with applications to the isolation and analysis of phytoplankton pigments, *Journal of Chromatography A*, 910, 31-49, 2001.

Van Oostende, N., Fawcett, S. E., Marconi, D., Lueders-Dumont, J., Sabadel, A. J. M., Woodward, E. M. S., Jönsson, B. F., Sigman, D. M., and Ward, B. B.: Variation of summer phytoplankton community composition and its relationship to nitrate and regenerated nitrogen assimilation across the North Atlantic Ocean, *Deep Sea Research Part I: Oceanographic Research Papers*, 121, 79-94, 10.1016/j.dsr.2016.12.012, 2017.

van Wijk, E. M., Rintoul, S. R., Ronai, B. M., and Williams, G. D.: Regional circulation around Heard and McDonald Islands and through the Fawn Trough, central Kerguelen Plateau, *Deep Sea Research Part I: Oceanographic Research Papers*, 57, 653-669, 10.1016/j.dsr.2010.03.001, 2010.

Vardi, A., Haramaty, L., Van Mooy, B. A., Fredricks, H. F., Kimmance, S. A., Larsen, A., and Bidle, K. D.: Host-virus dynamics and subcellular controls of cell fate in a natural coccolithophore population, *Proc Natl Acad Sci U S A*, 109, 19327-19332, 10.1073/pnas.1208895109, 2012.

Vedamati, J., Goepfert, T., and Moffett, J. W.: Iron speciation in the eastern tropical South Pacific oxygen minimum zone off Peru, *Limnology and Oceanography*, 59, 1945-1957, 10.4319/lo.2014.59.6.1945, 2014.

Velasquez, I., Nunn, B. L., Ibisani, E., Goodlett, D. R., Hunter, K. A., and Sander, S. G.: Detection of hydroxamate siderophores in coastal and Sub-Antarctic waters off the South Eastern Coast of New Zealand, *Marine Chemistry*, 126, 97-107, 10.1016/j.marchem.2011.04.003, 2011.

Veldhuis, M. J. W., and Kraay, G. W.: Phytoplankton in the subtropical Atlantic Ocean: towards a better assessment of biomass and composition, *Deep-Sea Research I*, 51, 507-530, 2004.

Verdugo, P., Alldredge, A. L., Azam, F., Kirchman, D. L., Passow, U., and Santschi, P. H.: The oceanic gel phase: a bridge in the DOM–POM continuum, *Marine Chemistry*, 92, 67-85, 10.1016/j.marchem.2004.06.017, 2004.

verity, P. G., Brussaard, C. P., Nejstgaard, J. C., van Leeuwe, M. A., Lancelot, C., and Medlin, L. K.: Current understanding of *Phaeocystis* ecology and biogeochemistry, and perspectives for future research, *Biogeochemistry*, 83, 311-330, 10.1007/s10533-007-9090-6, 2007.

Vidussi, F., Claustre, H., Manca, B. B., Luchetta, A., and Marty, J.-C.: Phytoplankton pigment distribution in relation to upper thermocline circulation in the eastern Mediterranean Sea during winter, *Journal of Geophysical Research: Oceans*, 106, 19939-19956, 10.1029/1999jc000308, 2001.

Volk, T., and Hoffert, M. I.: Ocean carbon pumps: Analysis of relative strengths and efficiencies in ocean-driven atmospheric CO₂ changes, in: *The Carbon Cycle and atmospheric CO₂: Natural Variations Archean to Present*, edited by: Sundquist, E. T., and Broecker, W. S., *Geophysical Monograph*, American Geophysical Union, Washington, DC, 99-110, 1985.

Völker, C., and Tagliabue, A.: Modeling organic iron-binding ligands in a three-dimensional biogeochemical ocean model, *Marine Chemistry*, 173, 67-77, 10.1016/j.marchem.2014.11.008, 2015.

von Appen, W.-J., Koszalka, I. M., Pickart, R. S., Haine, T. W. N., Mastropole, D., Magaldi, M. G., Valdimarsson, H., Garton, J., Jochumsen, K., and Krahmann, G.: The East Greenland Spill Jet as an important component of the Atlantic Meridional Overturning Circulation, *Deep Sea Research Part I: Oceanographic Research Papers*, 92, 75-84, 10.1016/j.dsr.2014.06.002, 2014.

Vraspir, J. M., and Butler, A.: Chemistry of Marine Ligands and Siderophores, *Annual Review of Marine Science*, 1, 43-63, 10.1146/annurev.marine.010908.163712, 2009.

Wadham, J. L., Tranter, M., Skidmore, M., Hodson, A. J., Priscu, J., Lyons, W. B., Sharp, M., Wynn, P., and Jackson, M.: Biogeochemical weathering under ice: Size matters, *Global Biogeochemical Cycles*, 24, n/a-n/a, 10.1029/2009gb003688, 2010.

Wadhams, P.: *Ice in the Ocean*, Gordon and Breach Science Publishers, London, UK, 2000.

Wagener, T.: *Le fer a l'interface ocean-atmosphere: flux et processus de dissolution dans l'eau de mer*, Docteur de l'Universite Aix-Marseille II, Centre d'Océanologie de Marseille, Université de la Méditerranée, Aix-Marseille II, 213 pp., 2008.

Wagener, T., Pulido-Villena, E., and Guieu, C.: Dust iron dissolution in seawater: Results from a one-year time-series in the Mediterranean Sea, *Geophysical Research Letters*, 35, 10.1029/2008gl034581, 2008.

Wagener, T., Guieu, C., and Leblond, N.: Effects of dust deposition on iron cycle in the surface Mediterranean Sea: results from a mesocosm seeding experiment, *Biogeosciences Discussions*, 7, 2799-2830, 2010.

Waite, A. M., Stemann, L., Guidi, L., Calil, P. H. R., Hogg, A. M. C., Feng, M., Thompson, P. A., Picheral, M., and Gorsky, G.: The wineglass effect shapes particle export to the deep ocean in mesoscale eddies, *Geophysical Research Letters*, 43, 9791-9800, 10.1002/2015gl066463, 2016.

Wang, J., and Mahmoud, J.: Chelate adsorption for trace voltammetric measurements of iron(III), *Frenesius' Journal of Analytical Chemistry*, 327, 789-793, 1987.

Wang, W. X., and Dei, R. C. H.: Bioavailability of iron complexed with organic colloids to the cyanobacteria *Synechococcus* and *Trichodesmium*, *Aquatic Microbial Ecology*, 33, 247-259, 2003.

Ward, B. A., and Waniek, J. J.: Phytoplankton growth conditions during autumn and winter in the Irminger Sea, North Atlantic, *Marine Ecology Progress Series*, 334, 47-61, 2007.

Weeks, D. A., and Bruland, K. W.: Improved method for shipboard determination of iron in seawater by flow injection analysis, *Analytica Chimica Acta*, 453, 21-32, 2002.

Weis, D., Frey, F. A., Schlich, R., Schaming, M., Montigny, R., Damasceno, D., Mattielli, N., Nicolaysen, K. E., and Scoates, J. S.: Trace of the Kerguelen mantle plume: Evidence from seamounts between the Kerguelen Archipelago and Heard Island, Indian Ocean, *Geochemistry, Geophysics, Geosystems*, 3, 1-27, 10.1029/2001GC000251, 2002.

Weiss, R. F.: Carbon dioxide in water and seawater: the solubility of a non-ideal gas, *Marine Chemistry*, 2, 203–215, 10.1016/0304-4203(74)90015-2, 1974.

Wells, M. L., Zorkin, N. G., and Lewis, A. G.: The role of colloid chemistry in providing a source of iron to phytoplankton, *Journal of Marine Research*, 41, 731-746, 10.1357/002224083788520478, 1983.

Wells, M. L., and Mayer, L. M.: Variations in the chemical lability of iron in estuarine, coastal and shelf waters and its implications for phytoplankton, *Marine Chemistry*, 32, 195-210, 10.1016/0304-4203(91)90038-x, 1991a.

Wells, M. L., and Mayer, L. M.: The photoconversion of colloidal iron oxyhydroxides in seawater, *Deep-Sea Research Part a-Oceanographic Research Papers*, 38, 1379-1395, 10.1016/0198-0149(91)90012-5, 1991b.

Welschmeyer, N. A., and Hoeffner, N.: Rapid xanthophyll cycling: an in situ tracer for mixing in the upper ocean, *EOS Trans. Am. Geophys. Union*, 67, 969, 1986.

Whitby, H., Planquette, H., Cheize, M., Menzel Barraqueta, J. L., Shelley, R. U., Boutorh, J., Pereira Contreira, L., Tonnard, M., Gonzalez, A. G., Bucciarelli, E., and Sarthou, G.: Iron-binding Humic Substances Along the GEOVIDE Transect in the North Atlantic (GEOTRACES, GA01, 2014), *Ocean Science Meeting*, Portland, Oregon, USA, 2018.

Whitfield, M., and Turner, D. R.: *Aquatic surface chemistry*, edited by: Stumm, W., John Wiley & Son Inc., New York, U.S.A, 1987.

Wilhelm, S. W., and Trick, C. G.: Iron-limited growth of cyanobacteria: Multiple siderophore production is a common response, *Limnology and Oceanography*, 39, 1979-1984, 1994.

Winter, A., Henderiks, J., Beaufort, L., Rickaby, R. E. M., and Brown, C. W.: Poleward expansion of the coccolithophore *Emiliana huxleyi*, *Journal of Plankton Research*, 36, 316-325, 10.1093/plankt/fbt110, 2014.

Witter, A. E., and Luther, G. W., 3rd: Variation in Fe-organic complexation with depth in the Northwestern Atlantic Ocean as determined using a kinetic approach, *Marine Chemistry*, 62, 241-258, 10.1016/s0304-4203(98)00044-9, 1998.

Witter, A. E., Lewis, B. L., and Luther, G. W.: Iron speciation in the Arabian Sea, *Deep-Sea Research Part II-Topical Studies in Oceanography*, 47, 1517-1539, 10.1016/s0967-0645(99)00152-6, 2000.

Wojtasiewicz, B., Trull, T. W., Davies, D. M., Schallenberg, C., Clementson, L., and Hardman-Mountford, N. J.: Possible explanations for the unexpected lack of phytoplankton biomass in naturally iron fertilized waters near Heard and McDonald islands in the Southern Ocean. (In preparation), in prep.

Wolf-Gladrow, D. A., Riebesell, U., Burkhardt, S., and Buma, J.: Direct effects of CO₂ concentration on growth and isotopic composition of marine plankton, *Tellus B: Chemical and Physical Meteorology*, 51, 461-476, 10.3402/tellusb.v51i2.16324, 1999.

Wolfe-Simon, F., Grzebyk, D., Schofield, O., and Falkowski, P. G.: The Role and Evolution of Superoxide Dismutases in Algae1, *Journal of Phycology*, 41, 453-465, 10.1111/j.1529-8817.2005.00086.x, 2005.

- Wolfe-Simon, F., Starovoytov, V., Reinfelder, J. R., Schofield, O., and Falkowski, P. G.: Localization and role of manganese superoxide dismutase in a marine diatom, *Plant Physiol*, 142, 1701-1709, 10.1104/pp.106.088963, 2006.
- Wolfe, G. V., Levasseur, M., Cantin, G., and Michaud, S.: DMSP and DMS dynamics and microzooplankton grazing in the Labrador Sea: application of the dilution technique, *Deep Sea Research I*, 47, 2243-2264, 2000.
- Woodgate, R. A., and Aagaard, K.: Revising the Bering Strait freshwater flux into the Arctic Ocean, *Geophysical Research Letters*, 32, 10.1029/2004GL021747., 2005.
- Wright, S. W., and Jeffrey, S. W.: Fucoxanthin pigment markers of marine phytoplankton analysed by HPLC and HPTLC, *Marine Ecology Progress Series*, 38, 259-266, 1987.
- Wright, S. W., and Jeffrey, S. W.: Pigment markers for phytoplankton production, in: *Marine organic matter: Biomarkers, isotopes and DNA*, edited by: Volkman, J. K., *The Handbook of Environmental Chemistry*, Springer-Verlag, Berlin, 71-104, 2006.
- Wright, S. W., Ishikawa, A., Marchant, H. J., Davidson, A. T., van den Enden, R. L., and Nash, G. V.: Composition and significance of picophytoplankton in Antarctic waters, *Polar Biology*, 32, 797-808, 2009.
- Wu, J., Boyle, E., Sunda, W., and Wen, L.-S.: Soluble and colloidal iron in the oligotrophic North Atlantic and North Pacific, *Science*, 293, 847-849, 2001.
- Wu, J., and Boyle, E.: Iron in the Sargasso Sea: Implications for the processes controlling dissolved Fe distribution in the ocean, *Global Biogeochemical Cycles*, 16, 33-31-33-38, 10.1029/2001gb001453, 2002.
- Wu, J. F., and Luther, G. W.: Size-fractionated iron concentrations in the water column of the western North-Atlantic Ocean, *Limnology and Oceanography*, 39, 1119-1129, 1994.
- Wu, J. F., and Luther, G. W.: Complexation of Fe(III) by natural organic-ligands in the northwest Atlantic Ocean by a competitive ligand equilibration method and a kinetic approach, *Marine Chemistry*, 50, 159-177, 10.1016/0304-4203(95)00033-n, 1995.
- Wurl, O., Miller, L., and Vagle, S.: Production and fate of transparent exopolymer particles in the ocean, *Journal of Geophysical Research*, 116, 10.1029/2011jc007342, 2011.
- Wuttig, K., Wagener, T., Bressac, M., Dammschäuser, A., Streu, P., Guieu, C., and Croot, P. L.: Impacts of dust deposition on dissolved trace metal concentrations (Mn, Al and Fe) during a mesocosm experiment, *Biogeosciences*, 10, 2583-2600, 10.5194/bg-10-2583-2013, 2013.
- Wuttig, K., Merwe, P. v. d., Gault-Ringold, M., Schallenberg, C., Holmes, T., Rijkenberg, M. J. A., Lannuzel, D., Townsend, A. T., and Bowie, A. R.: Recommendations for the optimization of a SeaFAST system for the analysis of trace metals in a wide range of marine samples, *Analytica Chimica Acta*, in prep.
- Wuttig, K., Townsend, A. T., Merwe, P. v. d., Gault-Ringold, M., Holmes, T., Schallenberg, C., Latour, P., Tonnard, M., Rijkenberg, M. J., Lannuzel, D., and Bowie, A. R.: Critical evaluation of a seaFAST system for the analysis of trace metals in marine samples, *Talanta*, subm.
- Yee, D., and Morel, F. M. M.: In vivo substitution of zinc by cobalt in carbonic anhydrase of a marine diatom, *Limnology and Oceanography*, 41, 573-577, 1996.
- Yucel, M., Gartman, A., Chan, C. S., and Luther III, G. W.: Hydrothermal vents as a kinetically stable source of iron-sulphide-bearing nanoparticles to the ocean, *Nature Geoscience*, 4, 367-371, 2011.
- Yücel, N.: Variability in Phytoplankton Pigment Composition in Mersin Bay, *Turkish Journal of Aquatic Sciences*, 49-70, 10.18864/tjas201705, 2017.

Zapata, M., Jeffrey, S. W., Wright, S. W., Rodriguez, F., Garrido, J. L., and Clementson, L.: Photosynthetic pigments in 37 species (65 strains) of Haptophyta: implications for oceanography and chemotaxonomy, *Marine Ecology Progress Series*, 270, 83-102, 2004.

Zhang, Y., Lacan, F., and Jeandel, C.: Dissolved rare earth elements tracing lithogenic inputs over the Kerguelen Plateau (Southern Ocean), *Deep-Sea Research Part II-Topical Studies in Oceanography*, 55, 638-652, 10.1016/j.dsr2.2007.12.029, 2008.

Zhuang, G., Yi, Z., and Wallace, G. T.: Iron(II) in rainwater, snow, and surface seawater from a coastal environment, *Marine Chemistry*, 50, 41-50, 1995.

Zou, S., Lozier, S., Zenk, W., Bower, A., and Johns, W.: Observed and modeled pathways of the Iceland Scotland Overflow Water in the eastern North Atlantic, *Progress in Oceanography*, 159, 211-222, 10.1016/j.pocean.2017.10.003, 2017.

Zunino, P., Lherminier, P., Mercier, H., Daniault, N., García-Ibáñez, M. I., and Pérez, F. F.: The GEOVIDE cruise in may-June 2014 revealed an intense MOC over a cold and fresh subpolar North Atlantic, *Biogeosciences*, 2017.



Titre : Etude du Cycle Biogéochimique du Fer : Distribution et spéciation dans l'Océan Atlantique Nord (GA01) et l'Océan Austral (Glpr05) (GEOTRACES).

Mots clés : Fer, Cycle biogéochimique, Limitation de la croissance du phytoplancton, Spéciation organique du Fe

Résumé : Il est désormais établi que la disponibilité en fer (Fe) contrôle environ 50% de la production primaire des océans du monde. Cependant, les processus régissant l'intensité des puits et des sources du Fe ainsi que la prédominance relative de ces sources au sein des divers bassins océaniques, sont elles-mêmes peu contraintes. Par ailleurs, une fois entrées dans le système océanique, la disponibilité et l'accessibilité des diverses formes de Fe pour les organismes marins restent incertaines. La réactivité du Fe au sein de l'environnement marin dépend de son état d'oxydoréduction et de complexation. Le fer dissous (DFe) est souvent considéré comme la fraction la plus biodisponible pour le phytoplancton et les ligands organiques du Fe augmentent vraisemblablement le temps de résidence du Fe et permettent des concentrations de DFe bien plus élevées que sa solubilité inorganique ne le permet dans l'eau de mer (10 pmol L^{-1}).

Dans ce contexte et s'inscrivant dans le programme international GEOTRACES, cette thèse a pour but principal d'implémenter notre savoir du cycle biogéochimique du Fe dans l'océan et ses interactions avec la structure des communautés phytoplanctoniques, en particulier afin de mieux contraindre les formes biodisponibles du Fe. Ainsi, les objectifs de cette thèse reposent sur trois questions scientifiques : 1) Quelles sont les distributions, sources, et puits de Fe ? 2) Quel est le lien entre la structure des communautés phytoplanctoniques et les concentrations en DFe ? 3) Comment la spéciation organique du DFe impacte ses concentrations et sa biodisponibilité ? Ces trois questions ont été explorées sur de deux zones d'études contrastées : l'océan Nord Atlantique (GEOVIDE, GA01 GEOTRACES voyage, Pls G. Sarthou and P. Lherminier) étant occasionnellement et saisonnièrement appauvri en Fe et l'océan Austral (HEOBI, Glpr05 GEOTRACES voyage, Pls A. Bowie, T. Trull, Z. Chase) l'étant de manière permanente.

Title: Biogeochemical cycle of Iron: distribution and speciation in the North Atlantic Ocean (GA01) and the Southern Ocean (Glpr05) (GEOTRACES).

Keywords : Iron, Biogeochemical cycle, Phytoplankton growth limitation, Organic speciation

Abstract: It is now recognized that iron (Fe) availability dictates the efficiency of the global biological carbon pump such that any perturbation of Fe sources will lead to changes in the carbon cycles with consequences on both other major nutrient cycles and the climate system, controlling about 50% of the worldwide ocean primary production. However, the underlying processes themselves that affect the pathways releasing and trapping Fe, and the relative predominance of Fe sources among the different ocean basins are still poorly constrained. More importantly, the extent to which both the chemical and the physical speciation of Fe are available and accessible for marine organisms, once it enters the ocean, remains uncertain. The reactivity of Fe within the marine environment will depend on its redox and complexation state, with DFe generally considered the most bioavailable form for phytoplankton and Fe-binding organic ligands likely increasing the residence time of Fe that enables enhanced DFe concentrations way above its inorganic solubility in seawater (c.a. 10 pmol L^{-1}).

In this context and as part of the international GEOTRACES program, this thesis aims at improving our knowledge on Fe biogeochemical cycle in the ocean and its interactions with the phytoplankton community structure to better constrain the bioavailable forms of Fe. The objectives of this thesis revolve around three scientific questions: 1) What are the distributions, sources, and sinks of dissolved iron? 2) What is the link between the phytoplankton community structure and dissolved iron concentrations? 3) How the organic speciation of dissolved iron affects its concentrations and bioavailability for the phytoplankton community? These three questions were investigated through two contrasted areas: the North Atlantic Ocean (GEOVIDE, GA01 GEOTRACES voyage, Pls G. Sarthou and P. Lherminier) and the Southern Ocean (HEOBI, Glpr05 GEOTRACES voyage, Pls A. Bowie, T. Trull, Z. Chase) the former being occasionally seasonally depleted in Fe, the latter permanently.